Technical Assistance in Support of Biomass Co-firing Demonstration

Summary Report provided to Pacificorp/Rocky Mountain Power

March 15, 2022

Andrew Fry
Associate Professor
Chemical Engineering
Brigham Young University

Eric Eddings
Professor and Chair
Chemical Engineering
University of Utah

Klas Andersson
Professor
Department of Space, Earth and Environment, Energy Technology
Chalmers University

Project Overview

The health of national forests in Utah has been strongly impacted by bark beetles, with areas of up to 70% mortality. The abundance of dead trees poses a significant environmental challenge if left to decay in place or in the case of a wildland fire. Additionally, operators of coal-fired utility boilers are facing increasing pressure to reduce their CO_2 emissions. These environmental conditions suggest an obvious solution to offset the utilization of coal in power plants by burning dead trees, which are carbon neutral in their life cycle. The objective of this project was to evaluate the technical feasibility of firing these dead trees in a coal-fired utility boiler, without modifications to the plant hardware or operating conditions, hopefully culminating in a demonstration at full-scale. To satisfy this objective, woody biomass would have to be prepared, to be more like coal, to minimize the impacts on the plant. Two preparation processes were investigated. Torrefied biomass was prepared and delivered for both pilot-scale testing and for demonstration by Amaron Energy. Steam Exploded biomass was provided for pilot-scale testing by Active Energy Group.

The key technical challenges identified were fuel preparation and ash behavior. It is known that the lignin in biomass poses a challenge to milling equipment designed for coal. It is also known that the mineral chemistry in fuel blends can negatively impact ash deposition rate. To elucidate these effects pilot-scale milling and combustion tests were performed at the University of Utah in 2016 through 2018 and subsequently at the San Rafael Energy Research Center using the same equipment in 2021. A full-scale demonstration was performed at PacifiCorp's Hunter, Unit 3 in 2019. This report provides a summary of these tests and acts as an index to the publications that were generated by this project where all details of the testing and results are provided. This report is split into sections which provide an overview of the milling tests, the combustion tests, the demonstration, and supporting modeling and then a summary of conclusions is provided. In each section, references to the publications are provided and then each of the publications appear in the Appendix in order of reference. There were two presentations that provide an overview of the entire project. [1] [2]

Biomass Milling

The first mill trials were performed in November of 2016. These tests were executed in a CE 321 Raymond Bowl Mill at the University of Utah. The objective of the testing was to determine the impact of processing a 15% woody biomass / 85% Sufco coal blend on mill power requirement and product particle size distribution. Multiple biomass samples were prepared through torrefaction at a range of temperatures from 210 to 325 °C and through steam explosion. All fuel blends were run at the same volumetric flow irrespective of heating value. Conclusions from these tests were:

1) The power requirement to mill the torrefied fuel blends was dependent on torrefaction temperatures, where the 210 °C material required a 39% increase in power compared to the pure coal and caused the mill to fault, but the 325 °C required 17% less power than pure coal.
2) The steam exploded biomass blends milled with a power requirement 29% lower than was required for pure coal.
3) The product particle size distribution was similar for the steam exploded blend and the pure coal, but the product from the torrefied blends contained more large particles than the pure coal.

The results of these experiments are detailed in the journal article entitled, "Investigation of co-milling Utah bituminous coal with prepared woody biomass materials in a Raymond Bowl Mill" [3] and in a conference presentation [4].

Additional mill testing was performed in October of 2021. These tests were performed in the same equipment as the previous testing. The equipment was in a new location at the San Rafael Energy Research Center (SRERC) in Orangeville, UT. The new objective was to evaluate the mill performance (power requirement and product particle size distribution) when milling blends of Sufco coal with steam exploded biomass at concentrations ranging from pure coal to pure biomass. Prior to these tests the roller / bowl spacing was adjusted by mill mechanics from the Hunter Power Plant. Conclusions from these tests were:

1) Mill power requirement increased as a liner function of biomass concentration with an approximate 70% increase in required power for the bure biomass when compared to the pure coal. In addition, the mill faulted at the pure biomass condition.
2) The pure biomass was milled again after moving the rollers closer to the bowl and the mill requirement was approximately 12% less for the pure biomass than for the pure coal.
3) Mill tuning (roller spacing) is necessary when milling steam exploded biomass to achieve optimal performance.
4) As observed in the first round of mill trials, the biomass blend fuels produced a product with larger particles in the size distribution than the pure coal.
5) Tuning the roller spacing significantly improved the particle size distribution of the milled material from the pure biomass.

The results of these experiments have not yet been published. Details of the experiments and the results can be found in the summary presentation entitled, "Mill performance and combustion testing of blends of coal and steam exploded biomass" [5].

Additional information about milling of biomass blends was generated during the demonstration testing at Hunter, Unit 3. This information will be presented in a section below.

Pilot-scale Combustion

Combustion tests were performed in 1.5 MWth entrained flow furnace (L1500) at the University of Utah in November of 2018 using the 15/85% (mass) blended material milled in the 2016 mill trials. The objective of these tests was to evaluate the combustion performance, emissions and ash behavior when combusting the steam exploded biomass blend, and the 325 °C torrefied biomass blend along with pure Sufco coal. Measurements of aerosol and deposited ash were performed at conditions that were expected to promote deposition through fouling mechanisms, similar to the vertical reheat section of the Hunter, Unit 3 boiler. Conclusions from these tests were:

1) Ash deposition rates were similar for the coal and two biomass blend fuels.
2) There were some differences in the entrained ash particle size distribution in the submicron range between the three fuels, but generally the PSD's were also very similar.
3) The aerosol particles generated from the biomass blends were slightly enriched in sodium, potassium, calcium and sulfur at all size fractions.
4) The NO_x emission was reduced approximately 28% when firing the torrefied blend fuel when compared to the pure coal, but there was little difference in the NOx emission when firing the steam exploded blend.
5) SO_2 emissions were very low and similar for all three fuels.
6) Heat release profile as measured by radiometer was similar for all three fuels, but the biomass blends burned out more quickly than the pure coal.

These experimental results are detailed in a journal article entitled, "Ash aerosol and deposit formation from combustion of coal and its blend with woody biomass at two combustion scales: part 1 – 1.5 MWth pilot-scale combustor tests" [6] and in the summary presentation entitled, "Technical assistance in support of biomass co-firing demonstration, pilot-scale combustion testing, November 2018" [7] and in multiple conference presentations [8] [9] [10] and [11].

Additional combustion tests were performed in the L1500 in October of 2021 after it had been moved to the SRERC. The objective of these tests was to evaluate the combustion performance, emissions and ash behavior while firing the blends ranging from pure steam exploded biomass to pure Sufco coal prepared in the 2021 mill trials. The same measurements were taken as the previous combustion trials. Conclusions from these tests were:

1) The ash deposition for the pure biomass was 5 times lower than for the pure coal, which is consistent with the parent fuel ash content.
2) There did not appear to be any synergistic ash chemistry effects on deposition from the fuel blends.
3) Small particles were enriched in sodium, potassium, phosphorus, chlorine and sulfur, and there were more small particles in the heavy biomass blends and pure biomass than in pure coal.
4) NOx emission was about 19% lower for the biomass case than the pure coal case, but the NOx information was difficult to interpret because of varying O_2 concentrations.
5) Radiation intensity was influenced by the amount of biomass in the blend, with lower intensities for pure biomass.

The results from these tests have not yet been published or presented. Details concerning these tests are provided in the summary presentation entitled, "Mill performance and combustion testing of blends of coal and steam exploded biomass" [5].

Demonstration at Hunter, Unit 3

Demonstration tests were performed in Hunter, Unit 3 in August of 2019. For these tests, 724 tons of torrefied wood were delivered to the plant and fired in Unit 3 over the course of approximately a 24-hour period. The biomass cofiring was preceded and followed by baseline testing, all performed at approximately 90% full load. During the testing, special measurements were performed to: evaluate the deposition rate at the vertical reheater, determine the PSD and composition of the entrained ash particles, measure the flue gas composition at various locations in the boiler by FTIR and to evaluate the heat release profile of the flame using radiometers. Major conclusions from the testing were:

1) A 15/85% (mass) biomass/coal blend was targeted. Postmortem analysis of the data suggested that the blend was close to 20/80% (mass), likely due to poor calibration of the truck scale.
2) Boiler load, excess O_2, turbine throttle pressure and flue gas pressure drop were held constant through the baseline and demonstration testing.
3) There was a 6.6% increase in fuel mass flow to account for the decrease in heating value.
4) The NO_x concentration in the flue gas averaged over the entire demonstration indicated a 11.4% decrease when compared to the baseline, but trended down throughout the test and was 35% lower than baseline at the end of the test.
5) The SO_2 concentration in the flue gas averaged over the entire demonstration indicated a 28.1% decrease when compared to the baseline but trended down throughout the test and was 38% lower than baseline at the end of the test.
6) CO concentrations were 4 times higher during the blend test.
7) The mills were negatively impacted by the blend testing. There was a 15 -40% increase in mill current during the test. Pyrite flow increased and the proportion of fuel in the pyrites increased during the blend test.
8) The blended fuel generally pushed the PSD to larger sizes, but the PSD was more impacted by classifier pipe outlet geometry than by fuel blend.
9) There was little impact of the fuel blend on entrained ash PSD and composition.
10) Deposition rate in the region of the vertical reheater decreased during the demonstration test and there was no observable impact to the deposited particle morphology during the demonstration test.
11) Heat release profile was similar during the demonstration test when compared to the baseline, with an increase in flame intensity just below the nose.

The ash behavior results from these tests were detailed in a journal article entitled, “Ash aerosol and deposit formation from combustion of coal and its blend with woody biomass at two combustion scales: part 2 – tests on a 471 Mwe full-scale boiler.” [12] The broader results of this testing were reported in a summary presentation entitled, “Firing of torrefied biomass in PacifiCorp’s Hunter, Unit 3.” [13] Additional information concerning this test has been detailed in various presentations. [2] [8] [9] [10] [14] [15]

Modeling

To help understand the influence of biomass/coal blends on particle behavior in the mills, CFD modeling was performed using CPFD’s Barracuda software. The objective of the modeling was to determine if there were small changes that could be made to the mills that would reduce the number of large particles leaving the classifier when milling biomass blends and was based on the November 2016 milling test data. Major conclusions from this effort include:

1) Large biomass particles may leave the classifier with the products due to differences in particle density and aspect ratio.

2) Simple tuning of the classifier vane angles could reduce the volume of particles (greater than 300 µm) from 5% to 4%.
3) When vane angle tuning was combined with modifications to the vortex finder length the volume of large particles could be reduced to less than 0.5%.

Results of this modeling effort have been detailed in a journal article entitled, "Analysis of particle behavior inside the classifier of a Raymond Bowl Mill wile co-milling biomass with coal." [16] and in a presentation [17].

Another modeling effort was focused on the configuration and evaluation of a mechanistic deposition model that could predict the influence of blended fuel mineral matter chemistry on relative deposition rate without the incorporation of CFD modeling. This model was tuned and tested on data generated in this program and in other biomass combustion projects at the University of Utah. Major conclusions from this work are:

1) Melt fraction stickiness model can accurately predict deposition rate for a variety of fuels if the model is informed of condensation propensity as a function of temperature from a thermodynamic model like FactSage to determine sticking efficiency.
2) The model was validated against 12 different biomass and coal fuel blends.

This modeling effort has been detailed in the journal article, "Modeling ash deposit growth rates for a wide range of solid fuels in a 100 kW combustor." [18]

CFD simulations were performed by Reaction Engineering International (REI) to further evaluate the data generated at multiple experimental scales from this project and from other data available from the University of Utah at smaller scales and to determine mechanisms and commonalities. The CFD analysis was performed using REI's Glacier software which has been previously used on other projects to simulate each of the pilot-scale furnaces and PacifiCorp's Hunter, Unit 3. Additionally, the model has unique capabilities to predict ash deposition. Major conclusions from this effort include:

1) Predicted ash deposition rates generally agreed with experiments at all three scales and the trend when firing biomass blends relative to pure coal was well captured in the model.
2) CFD modeling can utilize discrete deposit measurements to validate the model and then offer a broader picture of particle behavior throughout the boiler.
3) Comparison of predicted and measured NOx were in good agreement.
4) Comparison of predicted gas composition with discretely measured gas constituents is difficult because of flue gas stratification and accuracy in achieving and reporting discrete location.

Details of this effort were presented at the Clearwater Clean Energy Conference in 2021. [19]

Conclusions

Pilot scale milling and combustion tests were performed to support the eventual demonstration of the firing of a blend of prepared woody biomass with coal in PacifiCorp's Hunter, Unit 3. Pre-demonstration tests were focused on a 15/85% (mass) blend of biomass/coal. Biomass was evaluated that was prepared using a torrefaction process and a steam explosion process. The pilot-scale tests consisted of both milling and combustion trials. The mill tests verified that it was possible to mill a 15/85 blend of biomass with minimal impacts to the equipment and the product fuel. It was determined that the temperature of biomass torrefaction strongly influenced the power required to mill the blended fuel. The steam exploded material was milled with a slightly reduced mill power requirement. Both biomass preparation methods resulted in an increase in large particles in the milled product. The combustion trials showed that flame stability and emissions would not be a concern and that NO_x emissions were expected to reduce when firing the biomass blend. Additionally, the deposition rate when firing the biomass blend was similar or slightly lowered when firing the blend. All data provided confidence in proceeding to the demonstration tests.

The demonstration of biomass cofiring at Hunter Plant in August of 2019 was very successful. During this test 724 tons of torrefied biomass were burned in Unit 3. The unit was able to maintain steady operation in terms of unit load, flue gas excess O_2, turbine throttle pressure and flue gas pressure drop. The ash deposition rate was decreased. NOx and SO_2 emission decreased and the lime utilization in the wet FGDs was significantly reduced. The mill operation was observed to be negatively impacted when milling the biomass blend in terms of power consumption and reject rate including fuel material. This adverse effect is likely the result of 1) firing the torrefied biomass at a ratio higher than was tested in the pilot-scale trials, and 2) possibly control of the torrefaction process at the required temperature and residence time, which was shown during the pilot-scale milling trials to be critical parameters during fuel preparation for mill performance.

Originally, a separate demonstration test was planned to fire the steam exploded biomass. This test was not performed because the fuel supplier was not able to provide enough material for demonstration testing. As an alternative, additional pilot-scale testing was performed to investigate the impact of steam exploded biomass blend ratio on milling and combustion performance. This test was performed in October of 2021. A range of blending ratios from pure coal to pure biomass were investigated. The milling tests showed that the there was a linear increase in mill power requirement with increasing biomass content of the blend. However, after adjusting the roller spacing closer to the bowl, even pure biomass was milled with no impact on mill power requirement. Combustion testing showed that biomass decreased the intensity of the flame in the near burner region. The deposition rate decreased as a function of biomass content with no synergistic effects of blending with coal.

Publications and Presentations

[1] A. Fry, Z. Dobó, E. G. Eddings, K. Andersson and K. Clark, "Demonstration of the Co-firing of Modified Biomass with Pulverized Coal at the Hunter Plant," in *Clearwater Clean Energy Conference*, Clearwater Beach, FL, 2018.

[2] E. G. Eddings, A. Fry and K. Andersson, "Overview of a Comprehensive Program to Assess the Impact of Co-firing Biomass with Coal in a 471 MWe Power Plant," in *Clearwater Clean Energy Conference*, Clearwater Beach, FL, 2021.

[3] Z. Dobó and A. Fry, "Investigation of co-milling Utah bituminous coal with prepared woody," *Fuel,* vol. 222, pp. 343-349, 2018.

[4] A. Fry, S. Fakourian, E. Eddings and Z. Dobó, "Milling of Utah, Sufco Coal with 15% Prepared Manti-La Sal Woody Biomass with a Raymond Bowl Mill," in *Clearwater Clean Energy Conference*, Clearwater Beach, FL, 2017.

[5] R. Roy, B. Schooff, A. Fry, X. Li, T. Draper, A. Prlina, J. Wendt, E. G. Eddings, S. Montgomery and J. Tuttle, "Mill Performance and Combustion Testing of Blends of Coal and Steam Exploded Biomass," University of Utah, Salt Lake City, UT, 2022.

[6] S. Fakourian, X. Li, Y. Wang, J. O. Wendt and A. Fry, "Ash Aerosol and Deposit Formation from Combustion of Coal and its blend with woody biomass at two combustion scales: part 1 - 1.5 mwth pilot-scale combustor tests," *Energy & Fuels,* vol. 36, p. 554−564, 2021.

[7] A. Fry, S. Fakourian, E. Eddings, J. O. Wendt, Y. Wang, X. Li, M. Backman, T. Draper, K. Scheib, S. Harding, K. Andersson, T. Allgurén, A. Gunnarsson and D. Gall, "Technical Assistance in Support of Biomass Co-firing Demonstration, Pilot-scale Combustion Testing, November 2018," University of Utah, Salt Lake City, UT, 2019.

[8] X. Li, Y. Wang, S. Fakourian, A. Fry and J. O. Wendt, "Ash Aerosol Characteristics from Combustion of Coal/Woody Biomass Blends and Laboratory, Pilot, and Industrial Scales," in *Clearwater Cean Energy Conference*, Clearwater Beach, FL, 2021.

[9] A. Fry, S. Fakourian, X. Li and J. Wendt, "Mineral Matter Deposition Behavior whicl Firing a Woody Biomass/Coal Blend at Lab, Pilot and Industrial Scales," in *Clearwater Clean Energy Conference*, Clearwater Beach, FL, 2021.

[10] T. Allgurén, K. Andersson, A. Fry and E. G. Eddings, "NOx Formation During Co-combustion of Coal and Biomass in a 480 MWe Power Plant," in *Clearwater Clean Energy Conference*, Clearwater Beach, FL, 2021.

[11] T. Allgurén, R. Edland, K. Andersson, A. Fry, E. G. Eddings and F. Normann, "NO Formation During Co-combustion of Coal with Two Thermally Treated Biomasses," in *Clearwater Clean Energy Conferec*, Clearwater Beach, FL, 2019.

[12] X. Li, S. Fakourian, B. Moyer, J. O. Wendt and A. Fry, "Ash Aerosol and Deposit Formation from Combustion of Coal and Its Blend with Woody Biomass at Two Combustion Scales: Part 2–Tests on a 471 MWe Full-Scale Boiler," *Energy & Fuels,* vol. 36, pp. 565-574, 2021.

[13] A. Fry, S. Fakourian, E. Eddings, J. Wendt, S. Harding, T. Draper, X. Li, A. Prlina, K. Andersson, T. Allgurén, D. Gall and A. Gunnarsson, "Firing of Torrefied Biomass in PacifiCorp's Hunter, Unit 3," University of Utah, Salt Lake City, UT, 2019.

[14] A. Fry and L. Huntsman, "Demonstration of Torrefied Woody Biomass and Coal Co-firing at PacifiCorp's Hunter, Unit 3 (Plant Impacts)," in *Clearwater Clean Energy Conference*, Clearwater Beach, FL, 2021.

[15] T. Draper, A. Prlina, T. Ring, E. G. Eddings, A. Gunnarsson, T. Allgurén, D. Gall, K. Andersson, S. Harding and A. Fry, "A Comparison of Industrial-scale (471 MWe) Radiometer Heat Flux Measurements Between Pulverized-coal and 85% Coal/15% Biuomass Co-firing Combustion," in *Clearwater Clean Energy Conference*, Clearwater Beach, FL, 2021.

[16] S. Fakourian, A. Fry and T. Jasperson, "Analysis of particle behavior inside the classifier of a raymond bowl mill while co-milling woody biomass with coal," *Fuel Processing Technology,* vol. 182, pp. 95-103, 2018.

[17] A. Fry, S. Fakourian and T. Jasperson, "Elucidating the Behavior of a Blend of Prepared Woody Biomass and Utah Bituminous Coal in a Raymond Bowl Mill," in *Clearwater Clean Energy Conference*, Clearwater Beach, FL, 2018.

[18] S. Fakourian, Z. McAllister, A. Fry, Y. Wang, X. Li, J. O. Wendt and J. Dai, "Modeling ash deposit growth rates for a wide range of solid fuels in a 100 kW combustor," *Fuel Processing Technology,* vol. 2017, 2021.

[19] H.-S. Shim, A. Chiodo, Z. Zhan, K. Davis, J. Wendt and A. Fry, "CFD and Process Model Simulations of Woody Biomass/Coal Co-firing at Lab, Pilot and Industrial Scales," in *Clearwater Clean Energy Conference*, Clearwater Beach, FL, 2021.

Appendix (Referenced Papers & Presentations)

Demonstration of the Co-firing of Modified Biomass with Pulverized Coal at the Hunter Plant

Andrew Fry
Brigham Young University

Zsolt Dobó, Eric Eddings
University of Utah

Klas Andersson
Chalmers University

Ken Clark
PacifiCorp/Rocky Mountain Power

Clearwater Clean Energy Conference
June 3 – 8, 2018
Sheraton Sand Key Resort, Clearwater FL

Utah Sustainable Transportation & Energy Plan (STEP)

- Utah state legislation (SB 115) – five-year pilot program with Rocky Mountain Power to provide funding for
  - Electric vehicle infrastructure
  - Clean coal research
  - Solar development
  - Utility-scale battery storage
  - Other innovative technologies
  - Economic development
  - Air quality initiatives

Providing support for biomass co-firing demonstration

THE UNIVERSITY OF UTAH

BRIGHAM YOUNG UNIVERSITY · FOUNDED 1875 · PROVO, UTAH

Introduction: Beetle Kill, Manti – La Sal National Forest

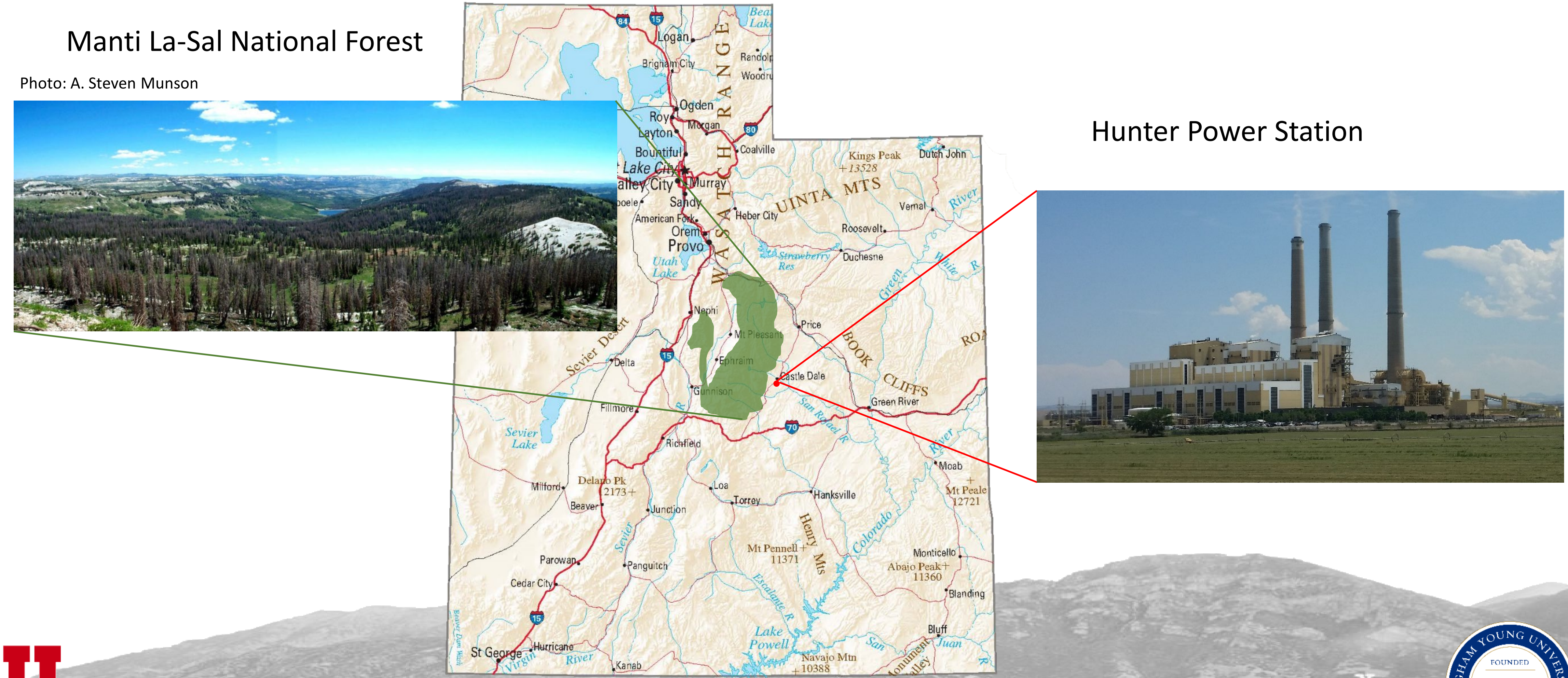

Manti La-Sal National Forest

Photo: A. Steven Munson

Hunter Power Station

Introduction: Beetle Kill, Manti – La Sal National Forest

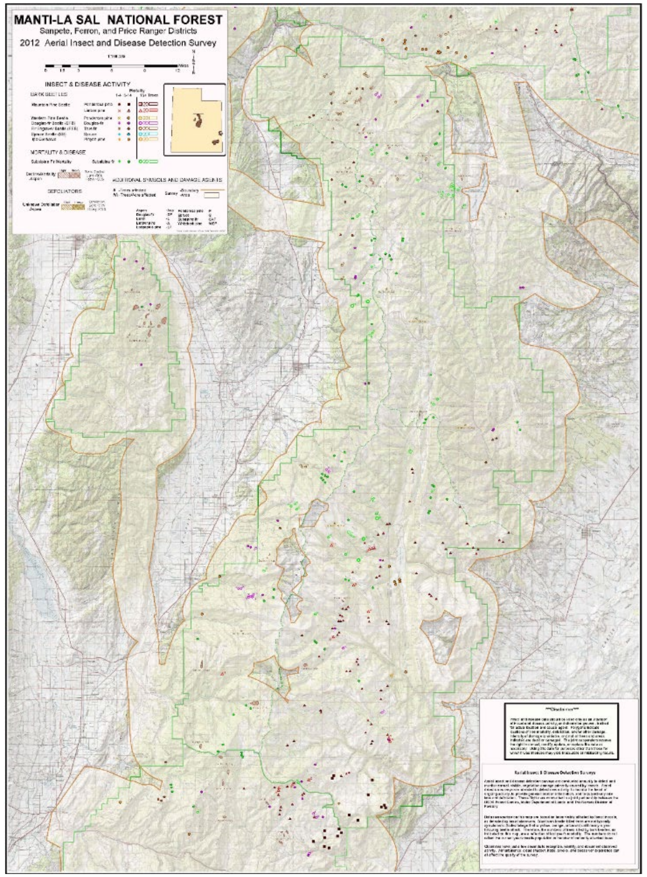

Map: US Department of Agriculture

- ~75,000 acres of beetle kill
  - Ponderosa, Douglas-fir, Spruce and Pinyon
- Indicator of unhealthy forest
- Increased potential wildland fires and particulate matter emissions
- Releases greenhouse gases while deadfall decays
  - CO_2 & CH_4

THE UNIVERSITY OF UTAH

BRIGHAM YOUNG UNIVERSITY FOUNDED BYU 1875 PROVO, UTAH

Introduction: Coal / Biomass Co-firing

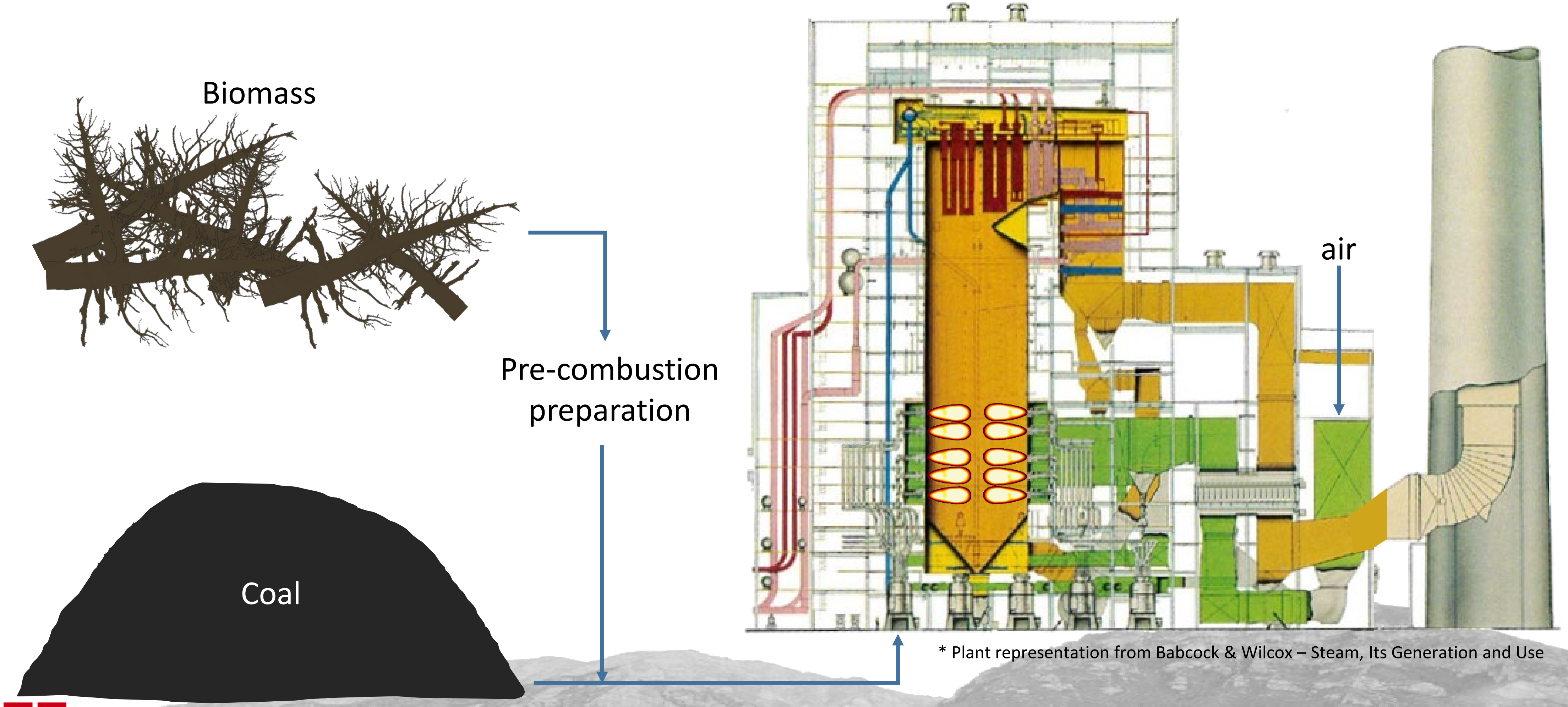

Biomass

Pre-combustion preparation

Coal

air

* Plant representation from Babcock & Wilcox – Steam, Its Generation and Use

THE UNIVERSITY OF UTAH

BRIGHAM YOUNG UNIVERSITY
FOUNDED
BYU
1875
PROVO, UTAH

Introduction: Raw Woody Biomass

- Low energy density
- Too much moisture
- Non-uniform shape = difficult material handling
- Cannot use existing coal handling and milling equipment

We fix these by pre-processing the woody biomass

Introduction: Biomass Preparation

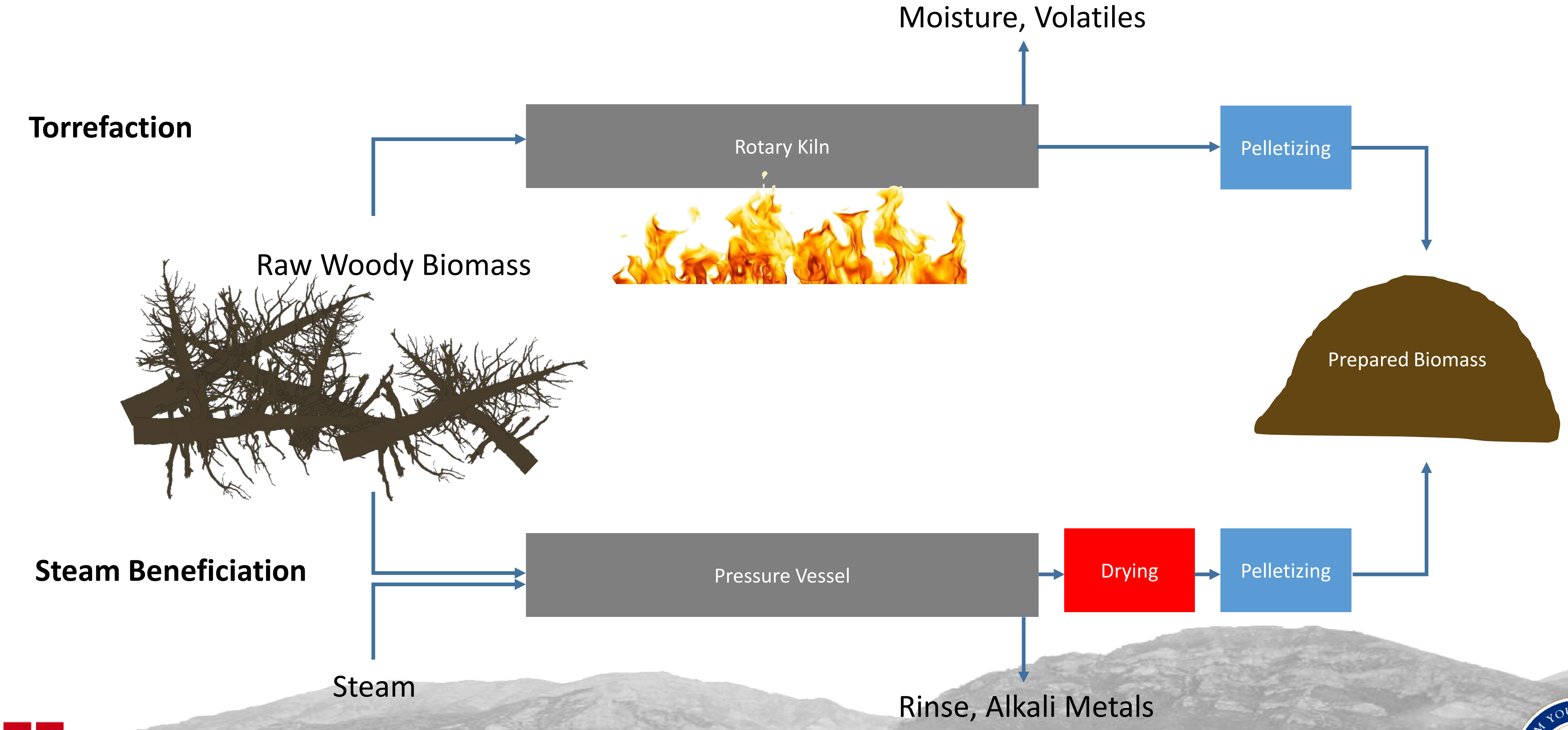

Torrefaction

Raw Woody Biomass

Moisture, Volatiles

Rotary Kiln

Pelletizing

Prepared Biomass

Steam Beneficiation

Pressure Vessel

Drying

Pelletizing

Steam

Rinse, Alkali Metals

THE
UNIVERSITY
OF UTAH

BRIGHAM YOUNG UNIVERSITY
FOUNDED
BYU
1875
PROVO, UTAH

Hunter Plant Biomass Co-firing Demonstration Project

- Rocky Mountain Power – Hunter Plant Unit No. 3 – 500 MW_e
  - Located near Castle Dale, UT
  - 500 MW_e – firing pulverized Utah bituminous coal
  - Wet lime scrubber, cloth filter baghouse
- Use of two sources of modified biomass at ~10% of thermal input
  - AEG CoalSwitch – Steam Beneficiated Biomass
  - Amaron Energy – Torrefied Biomass
- Planned operation of ~12 hours on each biomass fuel
- UofU/BYU team provide research and technical support

Program Objective #1

Technical Demonstration of Co-firing

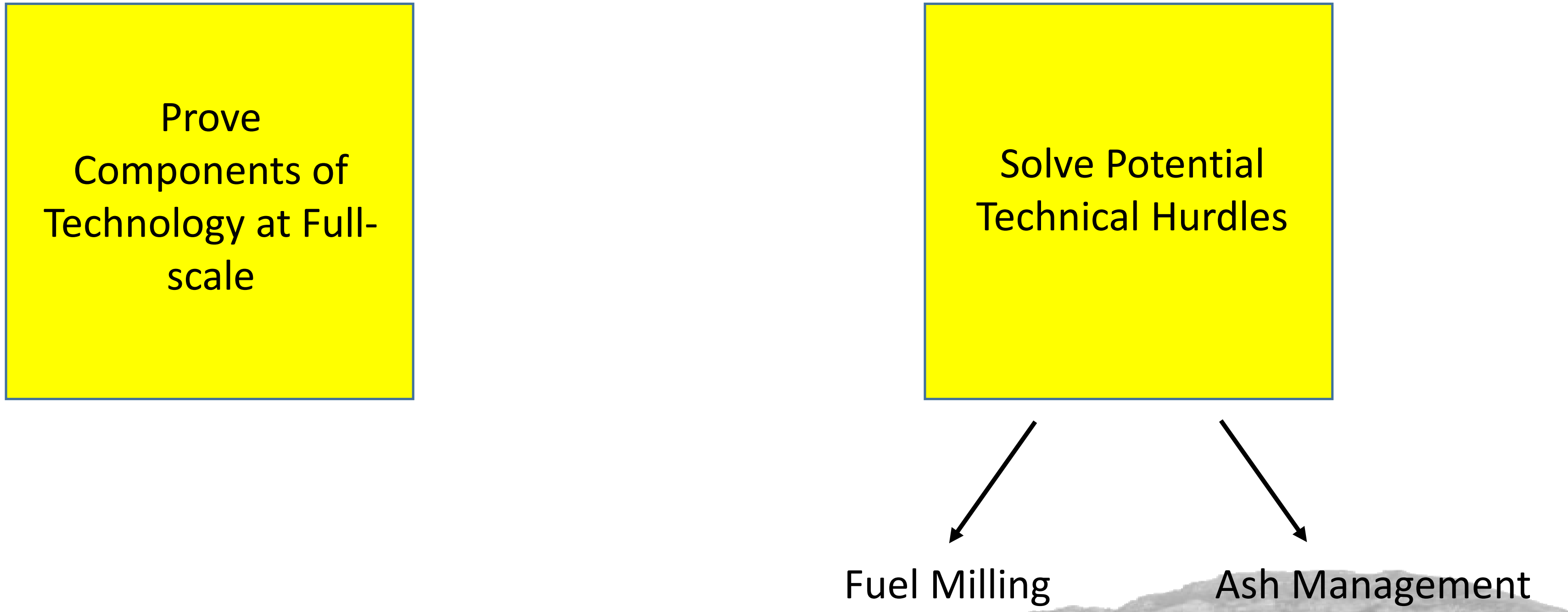

Prove Components of Technology at Full-scale

Solve Potential Technical Hurdles

- Fuel Milling
- Ash Management

Program Objective #2

Multi-Scale Ash Behavior Data

100 kW_{th}
Oxy-Fuel Combustor (OFC)
University of Utah

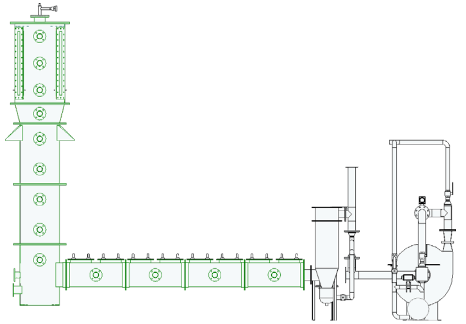

→

1.5 MW_{th}
L1500
University of Utah

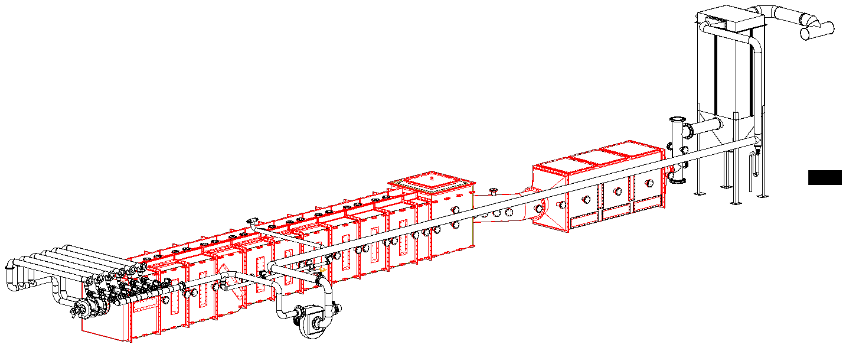

→

500 MW_e
Hunter, Unit 3
PacifiCorp

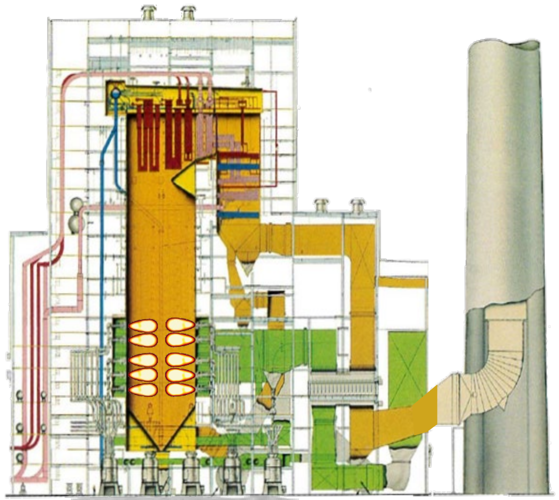

* Plant representation from Babcock & Wilcox – Steam, Its Generation and Use

Program Objective #2

Multi-Scale Ash Behavior Data

Entrained Particle Size Distribution

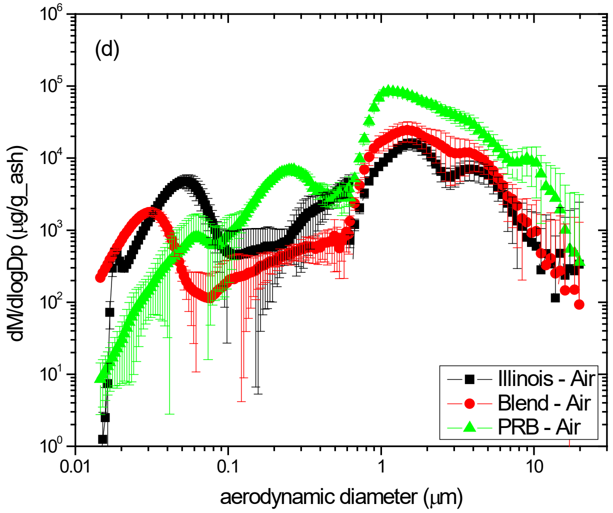

Entrained Particle Composition

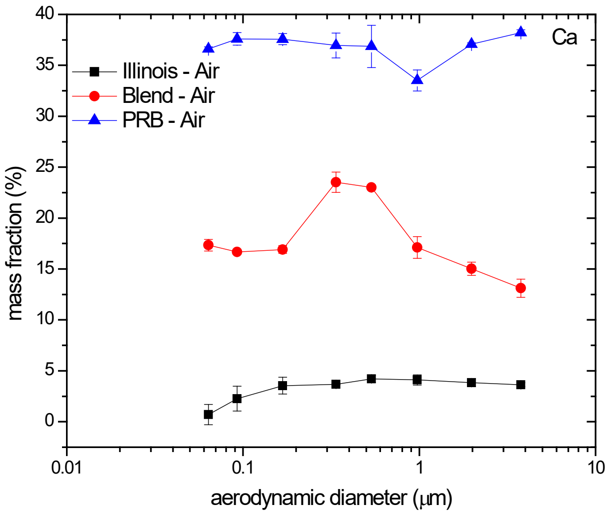

Deposited Particle Composition

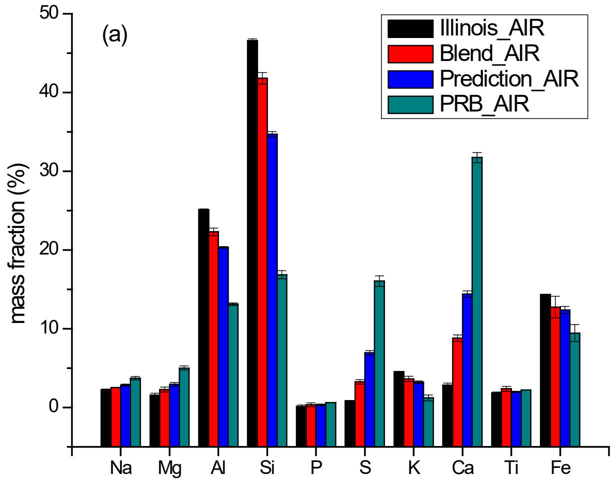

Deposition Rate

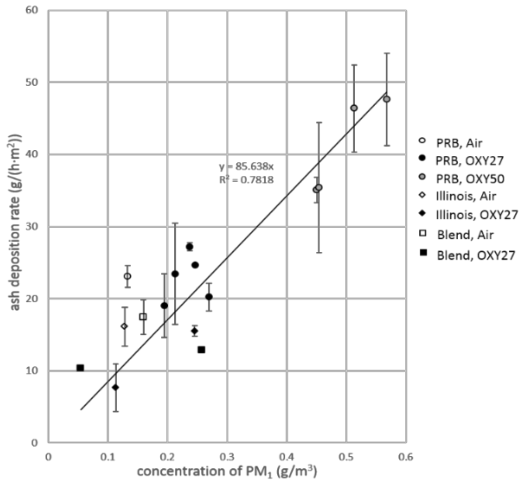

100 kW Pilot-scale Furnace (OFC)

UofU/BYU Support of Hunter Plant Biomass Co-firing Demonstration

- Task 0 – Pilot-scale Milling Trials
- Task 1 – Biomass Fuel Handling and Stability (UofU)
- Task 2 – Source Material Evaluations (UofU)
- Task 3 – Protocol for the Hunter Plant Co-firing Burn Test (BYU)
- Task 4 – On-site (Hunter Plant) Measurements During Co-firing Demonstration (UofU and BYU)
- Task 5 – Analysis of Boiler Operating, Emissions and Performance Data (BYU)
- Task 6 – Combustion Performance Evaluations (UofU)
- Task 7 – Air Quality Assessment of Biomass Co-firing (UofU)

Task 0 – Pilot-scale Milling Trials

Facilities: Mill at the University of Utah

Particle Filter

Blower & Heater

Hopper & Conveyor

Raymond Bowl Mill

Crusher

Experimental: Coal and Biomass Properties

		Sufco Coal	Torrefied 210 °C	Torrefied 248 °C	Torrefied 290 °C	Torrefied 325 °C	Steam Beneficiated
Ultimate, As Received (Wt, %)	**Carbon**	61.48	49.41	51.22	55.18	54.98	59.59
	Hydrogen	4.94	6.15	5.85	5.81	5.41	5.81
	Nitrogen	0.91	0.55	0.54	0.59	0.59	0.59
	Sulfur	0.58	BDL	BDL	BDL	BDL	BDL
	Oxygen	15.90	41.21	36.71	35.49	31.59	30.49
	Ash	16.20	2.68	5.67	2.94	7.44	3.52
Proximate (Wt, %)	**Moisture**	4.15	3.43	1.98	0.89	2.24	2.76
	FC	37.6	14.4	15.9	21.9	26	28.6
	VM	42	79.5	76.4	74.3	64.3	65.1
Btu/lb	**HHV**	10551	8924	8871	9494	9703	10246

Experimental: Measurements

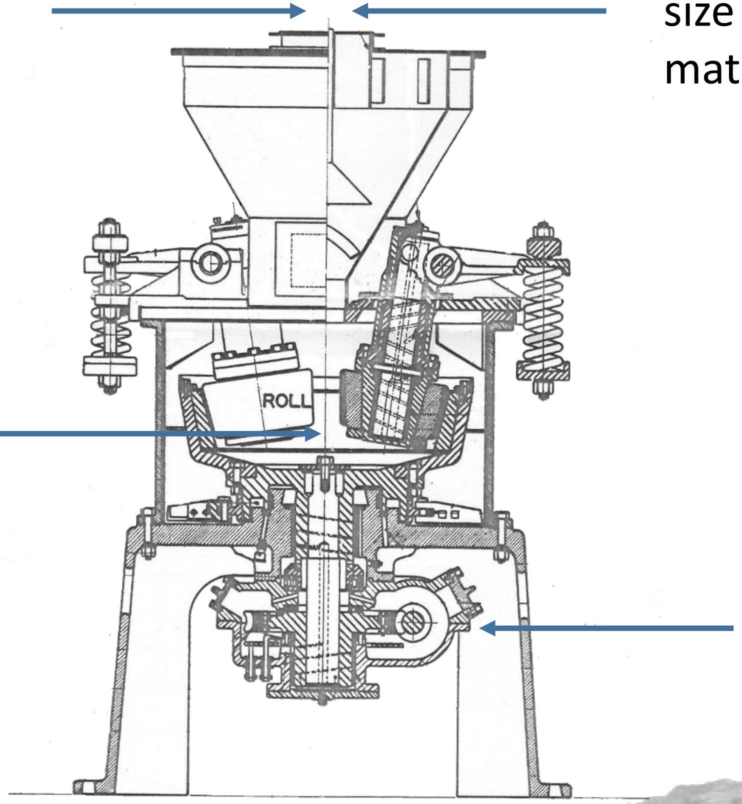

Measure the mill exit temperature

Measure the particle size distribution of the material exiting the mill

Visually inspect the bowl after milling each material

Measure the power requirement of the motor driving the rotating bowl

Task 4 – On-site (Hunter Plant) Measurements During Co-firing Demonstration

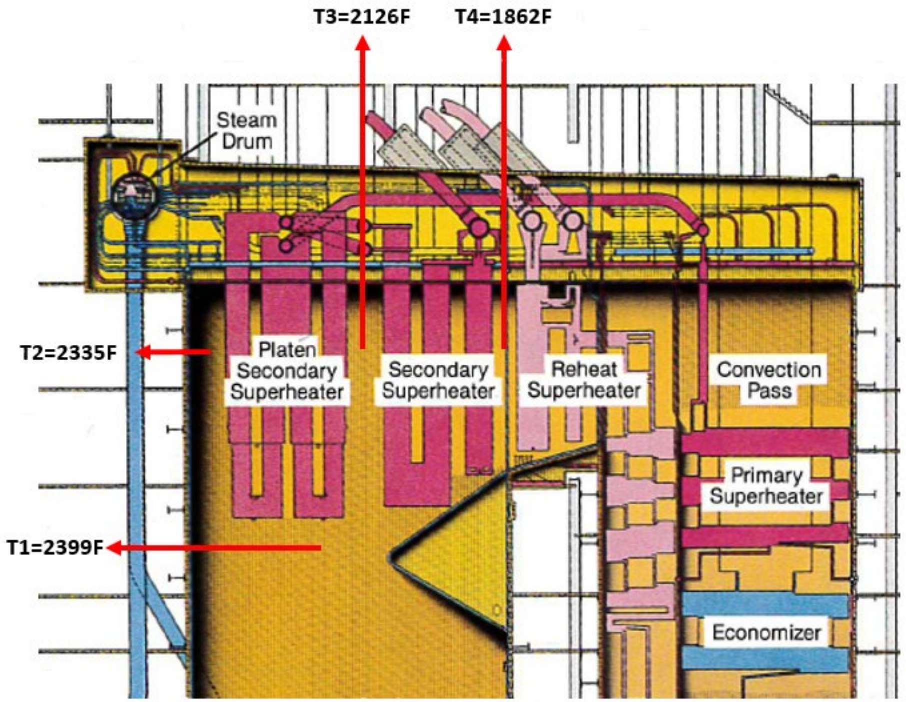

- UofU and BYU students and staff will be on-site during co-firing demonstration
- Will use/adapt existing instruments and hardware for PSD and deposition rate measurements
- Develop new isokinetic probe for particulate sampling
- Additional gas sampling provided by PacifiCorp

Task 5 – Analysis of Boiler Operating, Emissions and Performance Data

- Obtain operational data from Hunter Unit 3
  - Before and during the biomass co-firing demonstration
- Build process model of Hunter Unit 3
  - Baseline operation
  - Biomass co-firing
- Use model to evaluate differences in operation in baseline vs. co-firing

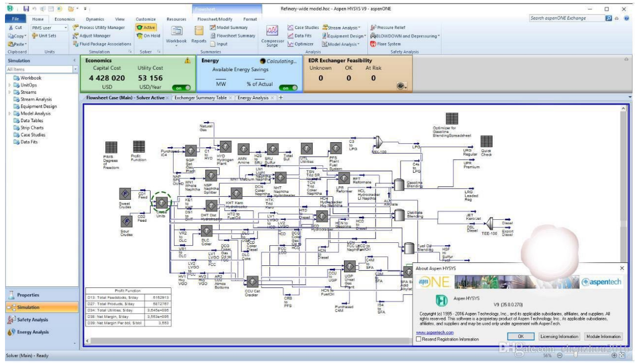

THE UNIVERSITY OF UTAH

BRIGHAM YOUNG UNIVERSITY FOUNDED BYU 1875 PROVO, UTAH

Task 6 – Combustion Performance Evaluations

- Pilot-scale (1.5 MW) investigations of pollutant emissions levels and ash-deposit properties
- Two biomass co-fire blends
  - Use material prepared during Task 0 Milling Trials
- Measurements to include
  - Suite of particle and deposit analysis
  - NOx, SO2, CO and CO2
  - SO3 and HCl
- Test campaign schedule for June 25, 2018

Task 7 – Air Quality Assessment of Biomass Co-firing

- Environmental impact of
    - Harvesting biomass from forest thinning operations, and burning biomass with coal in controlled manner at Hunter Plant
    - *versus* uncontrolled burns due to forest fire or slash pile burns

- Assessments to include
    - Particulate matter emissions
    - Regional haze
    - CO2 emissions
    - VOC and NOx emissions
    - Air toxics
    - Overall evaluation of greenhouse gas emissions and net energy return
- Will consider following life-cycle stages
    - Extraction, transport and combustion of the coal
    - Harvesting, transporting, processing and combustion of the biomass
    - Combustion of biomass by controlled burns

THE UNIVERSITY OF UTAH

BRIGHAM YOUNG UNIVERSITY FOUNDED BYU 1875 PROVO, UTAH

Acknowledgements

The authors gratefully acknowledge financial support provided by PacifiCorp/Rocky Mountain Power and the State of Utah through the Utah Sustainable Transportation and Energy Plan (STEP).

Conflict of Interest Management: Eric Eddings has financial interest in Amaron Energy

Questions?

Overview of a Comprehensive Program to Assess the Impact of Co-firing Biomass with Coal in a 471 MWe Power Plant

Eric Eddings
University of Utah

Andrew Fry
Brigham Young University

Klas Andersson
Chalmers University

Clearwater Clean Energy Conference
June 3 – 8, 2018
Virtual Conference & Sheraton Sand Key Resort, Clearwater FL

THE UNIVERSITY OF UTAH

PACIFICORP

ROCKY MOUNTAIN POWER

REACTION ENGINEERING INTERNATIONAL

AVANCEZ

BYU

Background – Biomass Co-firing with Coal

- Potential approach for reducing net CO_2 emissions from coal-fired power generation
- Challenges with raw woody biomass use
  - Low energy density
  - Too much moisture
  - Non-uniform shape = difficult material handling
  - Cannot use existing coal handling and milling equipment
- We can address these challenges by pre-processing the woody biomass

THE UNIVERSITY OF UTAH

BRIGHAM YOUNG UNIVERSITY FOUNDED 1875 PROVO, UTAH BYU

Biomass Pre-processing – Two Approaches

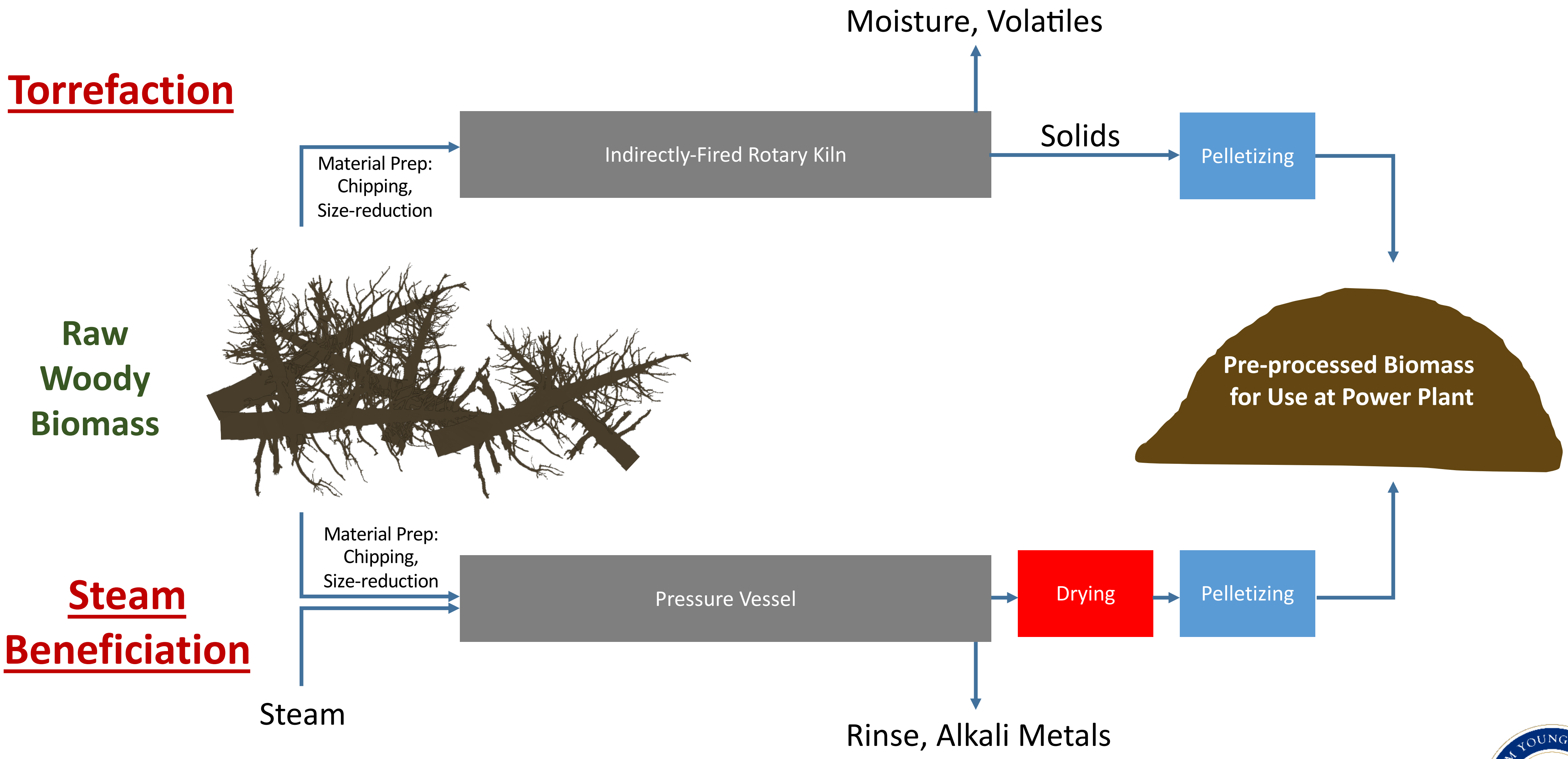

Torrefaction

Material Prep:
Chipping,
Size-reduction

Indirectly-Fired Rotary Kiln

Moisture, Volatiles

Solids

Pelletizing

Raw Woody Biomass

Pre-processed Biomass for Use at Power Plant

Steam Beneficiation

Material Prep:
Chipping,
Size-reduction

Steam

Pressure Vessel

Rinse, Alkali Metals

Drying

Pelletizing

THE UNIVERSITY OF UTAH

BRIGHAM YOUNG UNIVERSITY
FOUNDED
BYU
1875
PROVO, UTAH

Beetle Kill, Manti – La Sal National Forest

Photo: A. Steven Munson

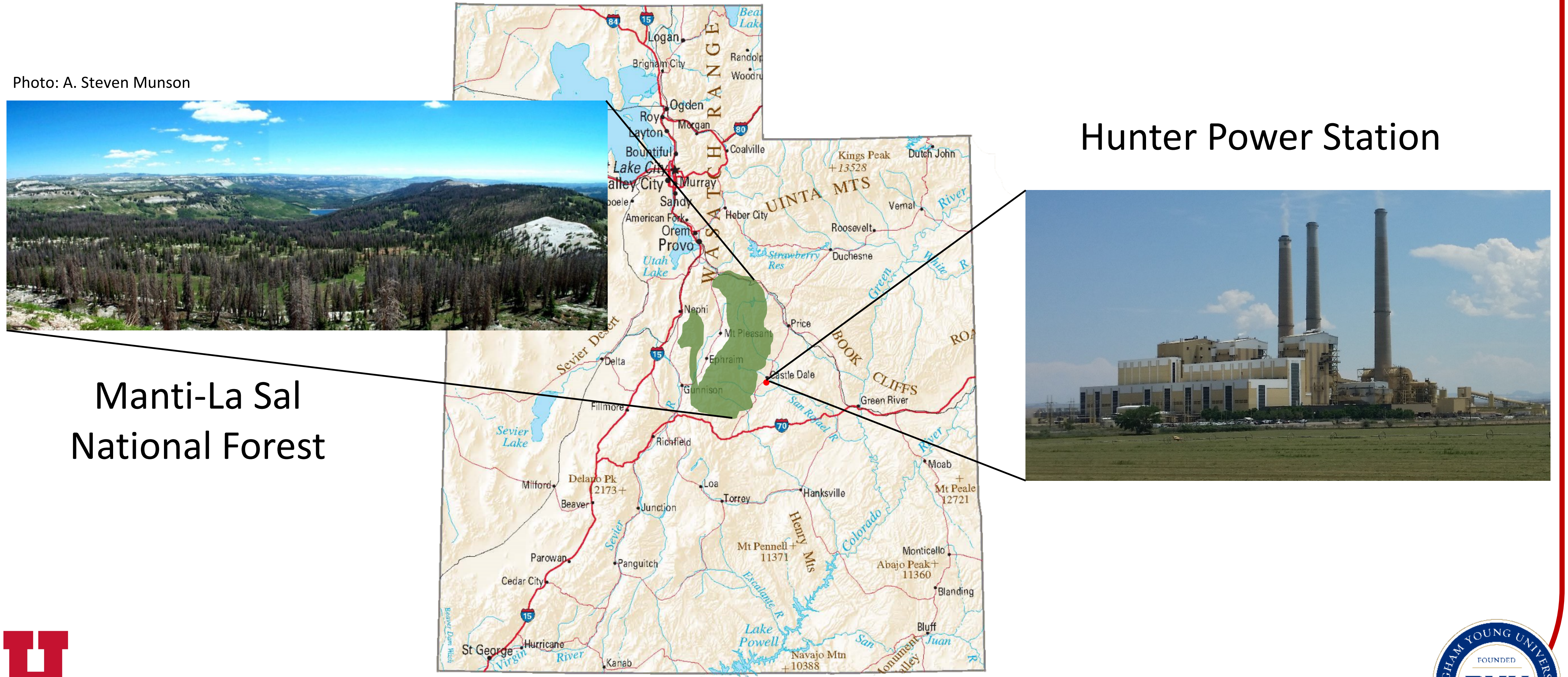

Hunter Power Station

Manti-La Sal National Forest

Beetle Kill, Manti – La Sal National Forest

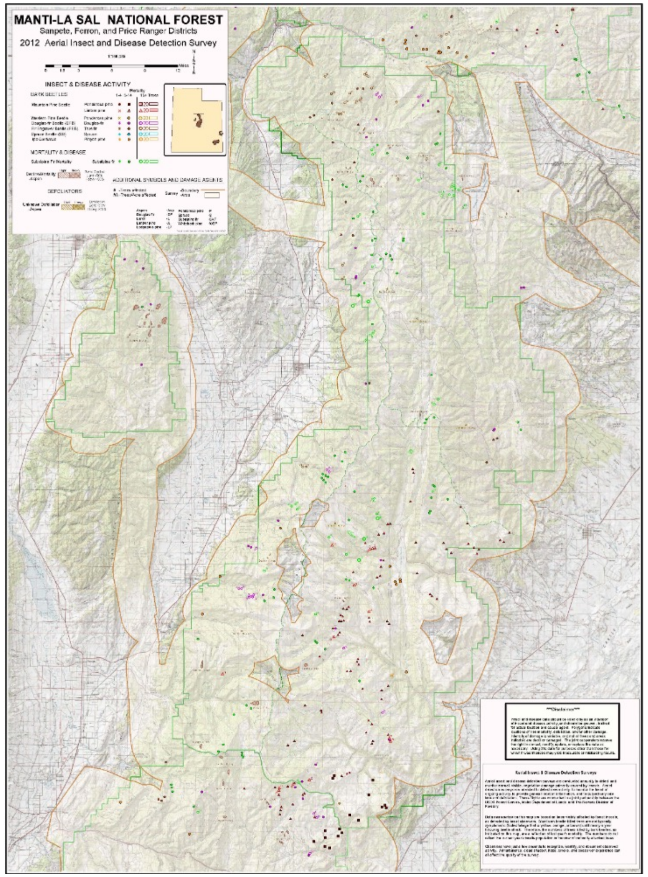

Map: US Department of Agriculture

- ~75,000 acres of beetle kill
  - Ponderosa, Douglas-fir, Spruce and Pinyon
- Indicator of unhealthy forest
- Increased potential wildland fires and particulate matter emissions
- Releases greenhouse gases while deadfall decays
  - CO_2 & CH_4

Utah Sustainable Transportation & Energy Plan (STEP)

- Utah state legislation (SB 115) – five-year pilot program with Rocky Mountain Power/PacifiCorp to provide funding for
  - Electric vehicle infrastructure
  - Clean coal research
  - Solar development
  - Utility-scale battery storage
  - Other innovative technologies
  - Economic development
  - Air quality initiatives

Provided support for a biomass co-firing demonstration

Hunter Plant Biomass Co-firing Demonstration: *Summary*

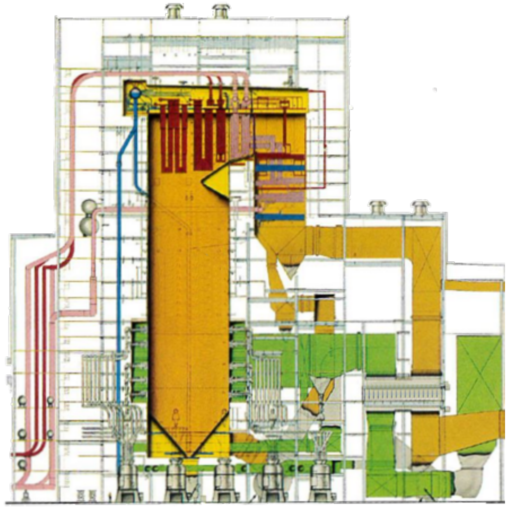

- Site: Rocky Mountain Power – Hunter Plant Unit No. 3 – 471 MW_e
  - Located near Castle Dale, UT
  - Firing pulverized Utah bituminous coal
  - Wet lime scrubber, cloth filter baghouse
- Proposed use of two sources of modified biomass at ~10% of thermal input
  - *Steam Beneficiated Biomass* - Active Energy Renewable Power (AERP - AEG CoalSwitch)
  - *Torrefied Biomass* - Amaron Energy
- Planned operation of ~12 hours on each biomass fuel
- UofU/BYU team contracted to provide research and technical support for the demonstration
  - Additional technical support provided by Chalmers University and Reaction Engineering International

* Plant representation from Babcock & Wilcox – Steam, Its Generation and Use

Hunter Plant Biomass Co-firing Demonstration: *Study Overview*

- Milling trials to assess the impact of co-feeding modified biomass and coal on pulverizer operation
- Study of the mechanical stability of the biomass fuels
- Life-cycle analysis of harvesting wood for use in co-firing
- Bench- and pilot-scale firing of the coal and biomass blends
- Full-scale demonstrations of the co-firing of coal and biomass blends at the Hunter power plant.
  - Production of ~750 tons each of torrefied and steam-beneficiated biomass pellets by two different commercial suppliers
  - Torrefied biomass demo – completed Summer 2019
  - Steam-beneficiated biomass demo – scheduled for Summer 2021
- Detailed data analysis and boiler/process modeling

THE UNIVERSITY OF UTAH

Hunter Plant Biomass Co-firing Workshop

- Presentations today will cover the following topics:
  - Project Overview *(Eddings)*
    - Background
    - Summary of milling trials
    - Summary of mechanical durability testing
  - Plant Impacts *(Fry)*
  - Aerosol Behavior *(Li)*
  - Mineral Matter Deposition *(Fry)*
  - Heat Flux Measurements *(Draper)*
  - NOx Formation *(Andersson)*
  - CFD and Process Model Simulations *(Shim)*
- Panel Discussion and Q&A

Pilot-scale Milling Trials*

*Results previously presented at the 2018 Clearwater Clean Energy Conference and details are published in:

Z. Dobo and A. Fry, "Investigation of co-milling Utah bituminous coal with prepared woody biomass materials in a Raymond Bowl Mill," *Fuel*, 222 (2018), 343-349.

Facility Used: Mill at the University of Utah*

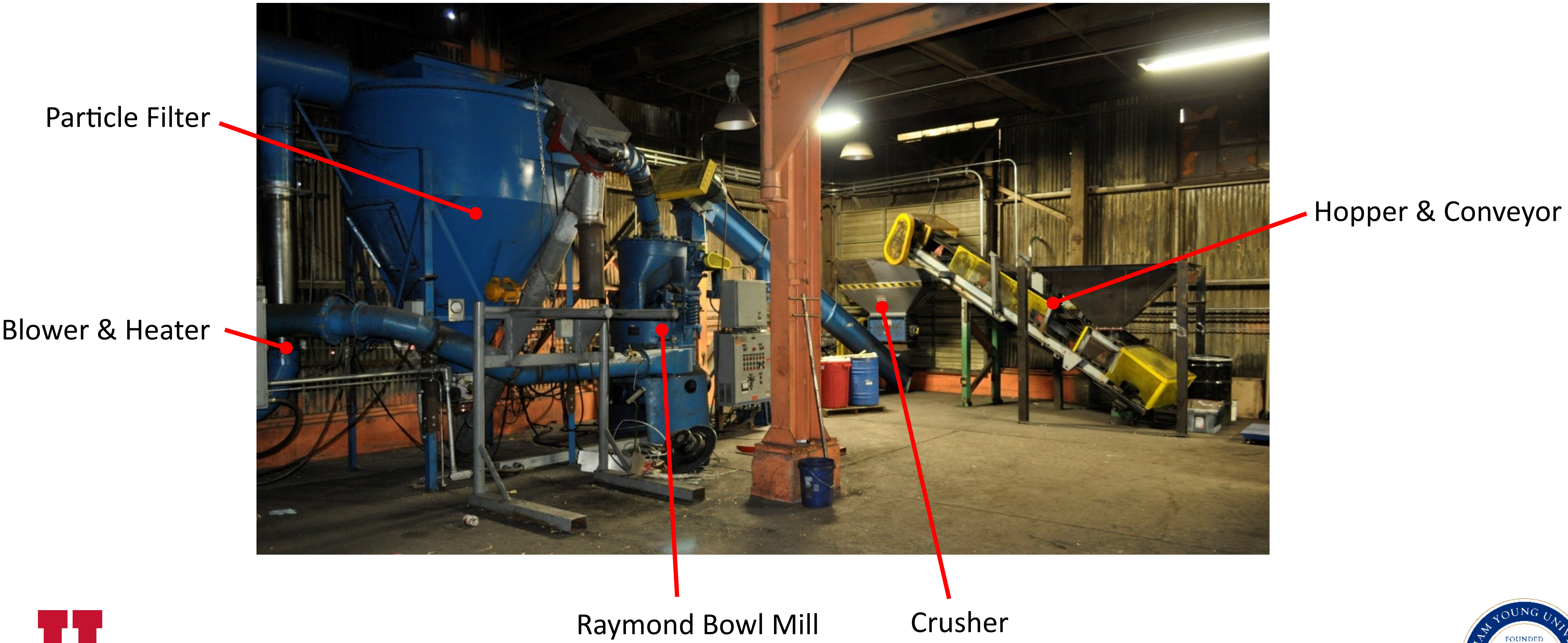

*Mill is now located at the San Rafael Energy Research Center, Emery County, Utah

Experimental: Coal and Biomass Properties

		Utah Coal	Torrefied 210 °C	Torrefied 248 °C	Torrefied 290 °C	Torrefied 325 °C	Steam Beneficiated
Ultimate, As Received (Wt, %)	**Carbon**	61.48	49.41	51.22	55.18	54.98	59.59
	Hydrogen	4.94	6.15	5.85	5.81	5.41	5.81
	Nitrogen	0.91	0.55	0.54	0.59	0.59	0.59
	Sulfur	0.58	BDL	BDL	BDL	BDL	BDL
	Oxygen	15.90	41.21	36.71	35.49	31.59	30.49
	Ash	16.20	2.68	5.67	2.94	7.44	3.52
Proximate (Wt, %)	**Moisture**	4.15	3.43	1.98	0.89	2.24	2.76
	FC	37.6	14.4	15.9	21.9	26	28.6
	VM	42	79.5	76.4	74.3	64.3	65.1
Btu/lb	**HHV**	10551	8924	8871	9494	9703	10246

Experimental: Measurements

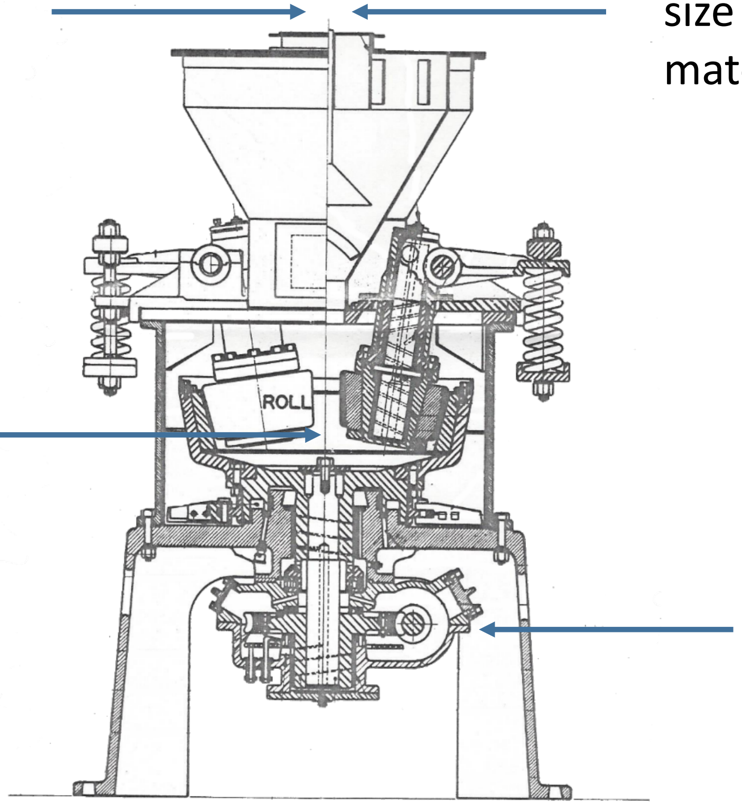

Measure the mill exit temperature

Measure the particle size distribution of the material exiting the mill

Visually inspect the bowl after milling each material

Measure the power requirement of the motor driving the rotating bowl

Results: Mill Current

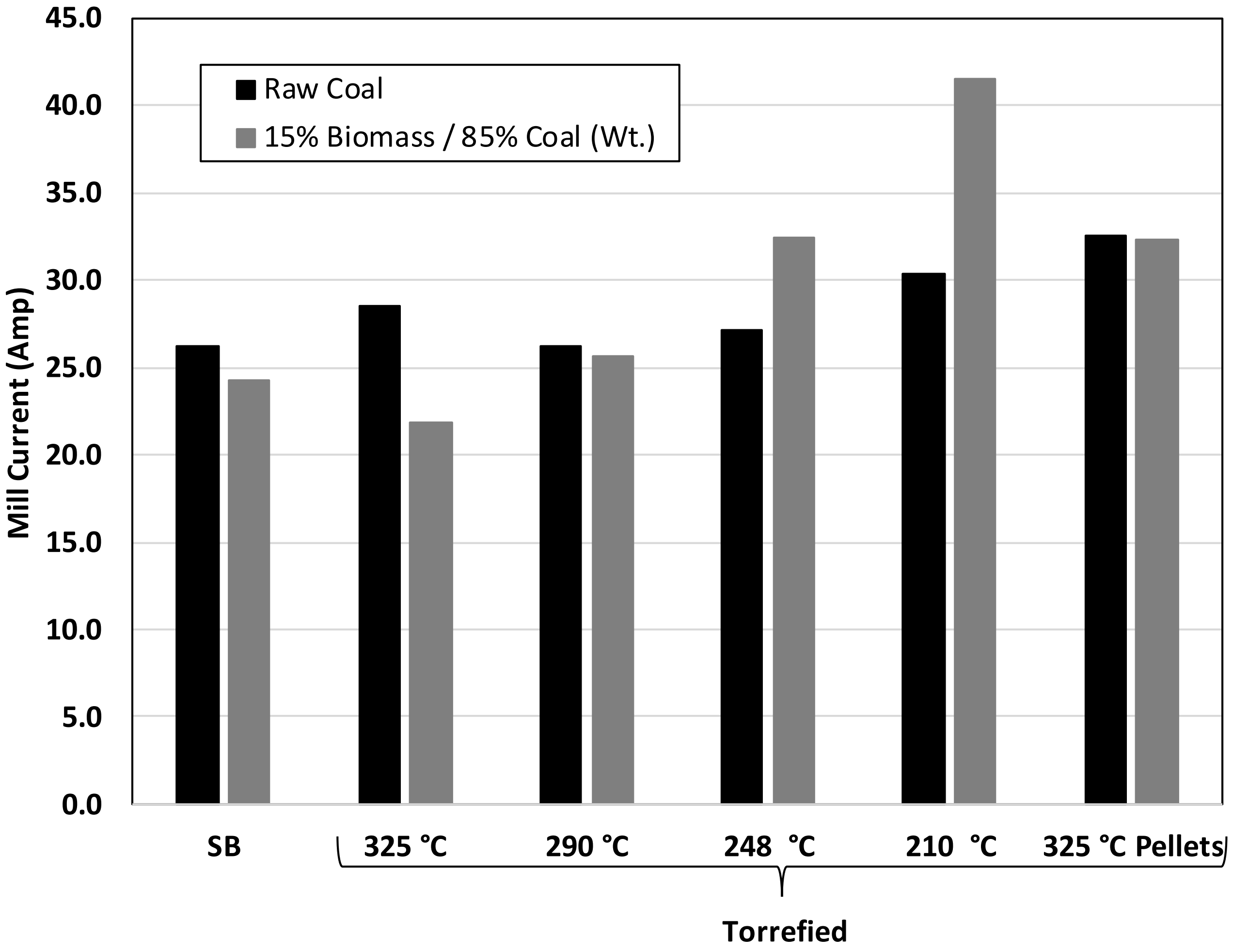

- Mill current is inversely proportional to the temperature at which biomass is torrefied
    - An indicator of the degree to which the fibrous structure has deteriorated
- Pelletizing increases the power requirement
- Torrefaction at 325 °C and steam beneficiation both with pelletization do not increase the mill power requirements
- All testing was at approximately the same mass flow rate.

Results: Particle Size

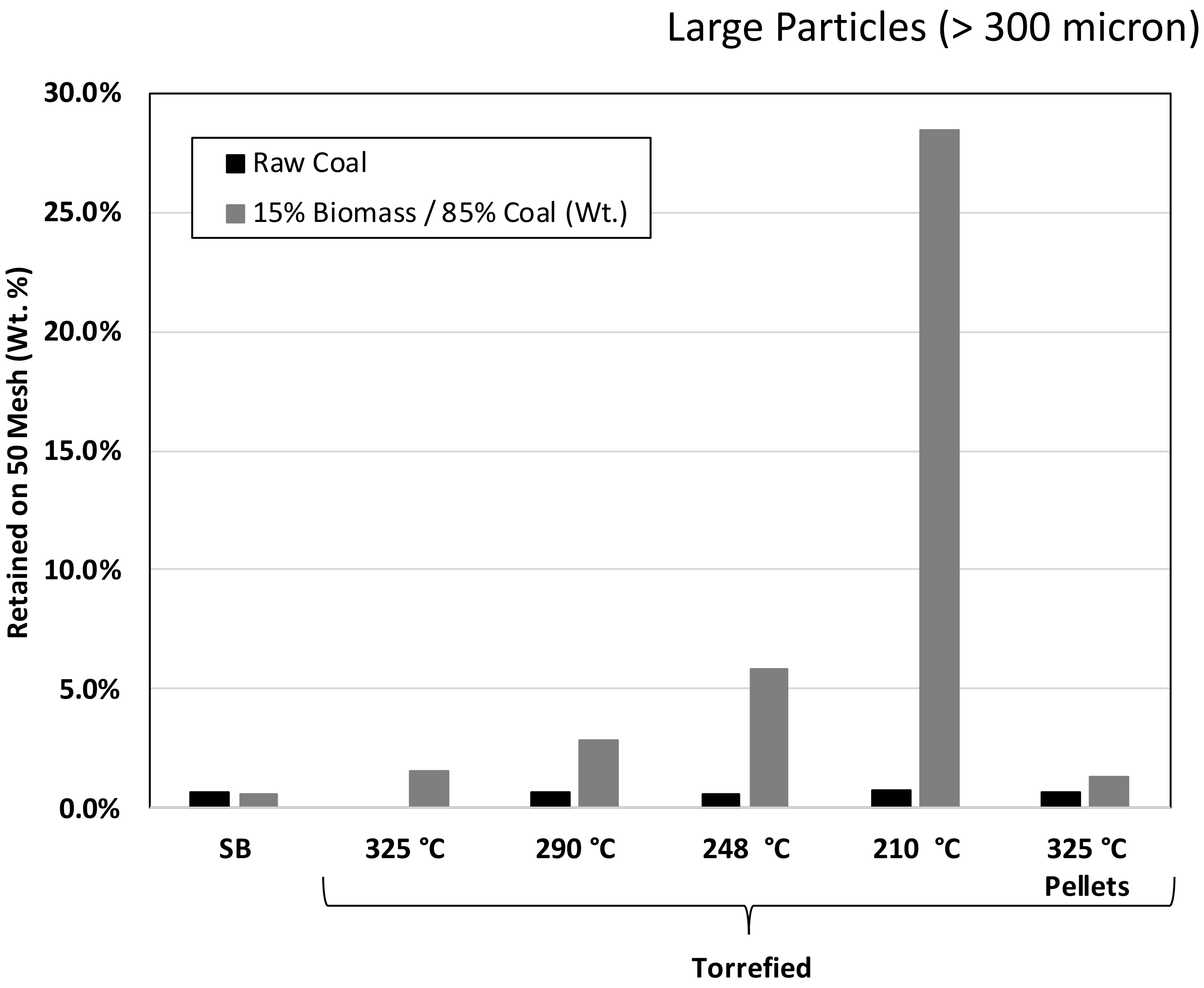

- All torrefied material resulted in an increase in fraction of large particles when compared to pure coal
- Fraction of large particles is reduced from torrefied materials when processing temperature is increased
- Large particle effect is minimized with a processing temperature of 325 °C
- Steam beneficiated biomass does not increase the fraction of large particles when compared to pure coal

Results: Particle Size

Small Particles (< 70 micron)

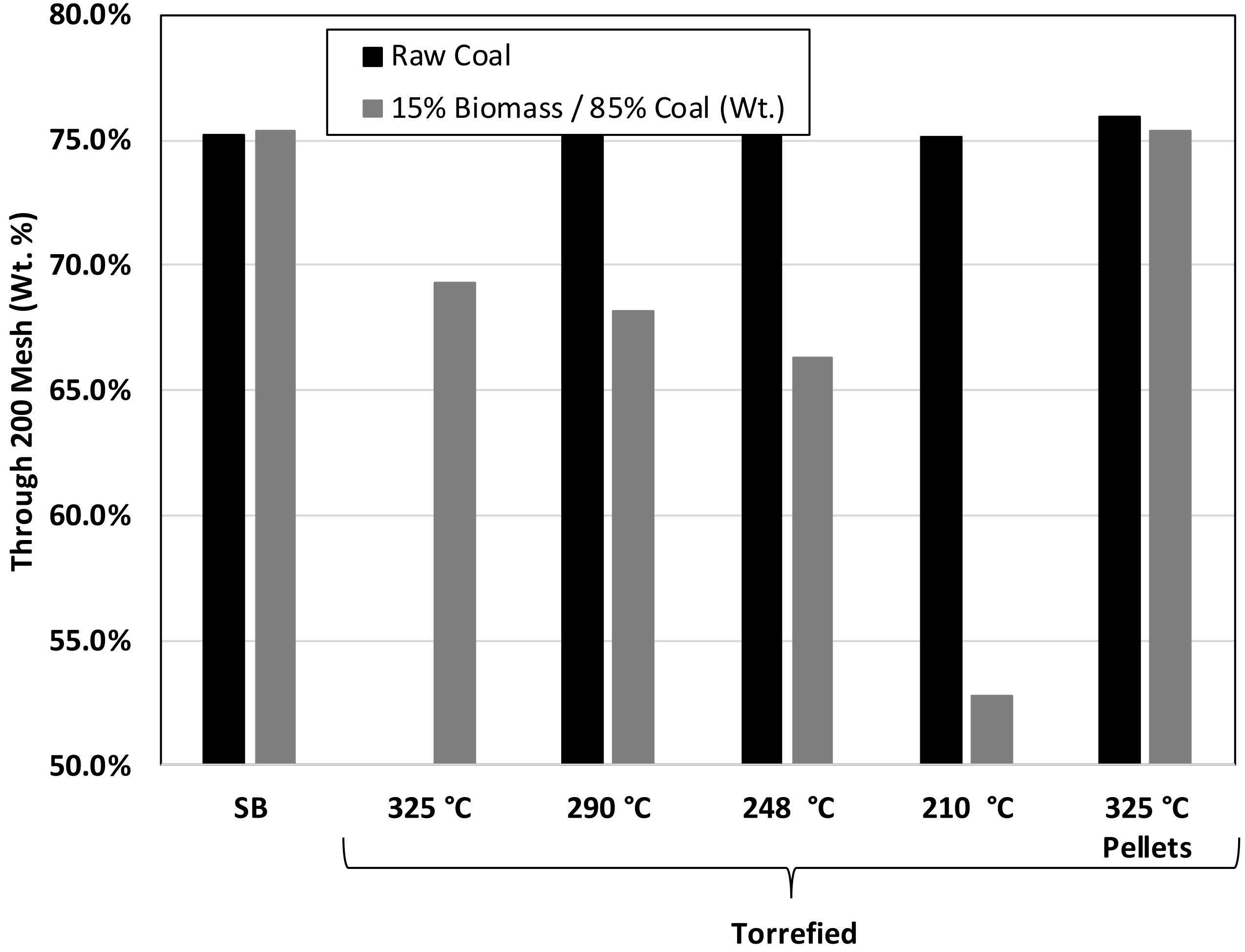

- The requirement of 70% through 200 mesh was achieved by biomass coal blends where the biomass was beneficiated or torrefied at 325 °C and pelletized
- Pelletizing appeared to have an added benefit to the millability of the torrefied material
- Pelletizing needed for long term storage, handling, and to minimize dust

THE UNIVERSITY OF UTAH

BYU

Summary Comments

- **Mill Performance**
  - Torrefaction at 325 °C and steam beneficiation, *both with pelletization*, do not increase the mill power requirements
- **Particle Size Behavior**
  - Steam beneficiated biomass does not increase the fraction of large particles when compared to pure coal
  - All torrefied material resulted in an increase in fraction of large particles when compared to pure coal
    - Large particle effect is minimized with a torrefaction processing temperature of 325 °C
  - The requirement of 70% through 200 mesh was achieved by biomass/coal blends where the biomass was either steam beneficiated or torrefied at 325 °C *and pelletized*
- **Mill Outlet Temperature**
  - Mill outlet temperatures were only slightly higher for the coal biomass blends, indicating no unwanted reaction in the mill

Biomass Durability Testing*

*Results previously presented at the 2019 Clearwater Clean Energy Conference

THE UNIVERSITY OF UTAH

BYU

Biomass Fuel Handling and Stability

- Key issues for use of modified biomass at the plant
  - Grindability – mill performance
  - Material handling during transport and survivability in the fuel yard
    - Moisture uptake
    - Mechanical durability/dust production
- Pellet performance assessed via the following three test methods
  - Moisture uptake
    - Immersion Test
    - Humidity Exposure Test
  - Mechanical durability
    - Tumbling Test (w/ and w/o grinding balls)

Types of Prepared Biomass Used in Study

- Torrefied pellets (pelletized then torrefied)
- Torrefied pellets (torrefied then pelletized)
- Steam exploded pellets (Company A)
- Steam exploded pellets (Company B)
- *Raw wood pellets (not torrefied)*
- *Torrefied wood chips*

Immersion Test Procedure*

- Pellet samples were sieved with a sieve mesh # 6 (sieve opening 3.35 mm)
- Sieved samples were submerged in sufficient water and kept at constant temperature (25 °C)during the testing period (1, 8, 12 , 24 , 48 and 72 hours)
- After each testing time, pellets and water were separated leaving the sample dripping in a strainer for two hours, then the samples were weighed
- Wet pellets were dried at 105 °C for 24 hours, left at ambient temperature for two hours and weighed

**C. Göbl and U. Wolfesberger-Schwabl, "Report on test methods and properties of torrefied biomass," Deliverable No. D8.5, Production of Solid Sustainable Energy Carriers from Biomass by Means of Torrefaction, GA No. 282826, European Commission, 2015.*

Results - Water Immersion Test

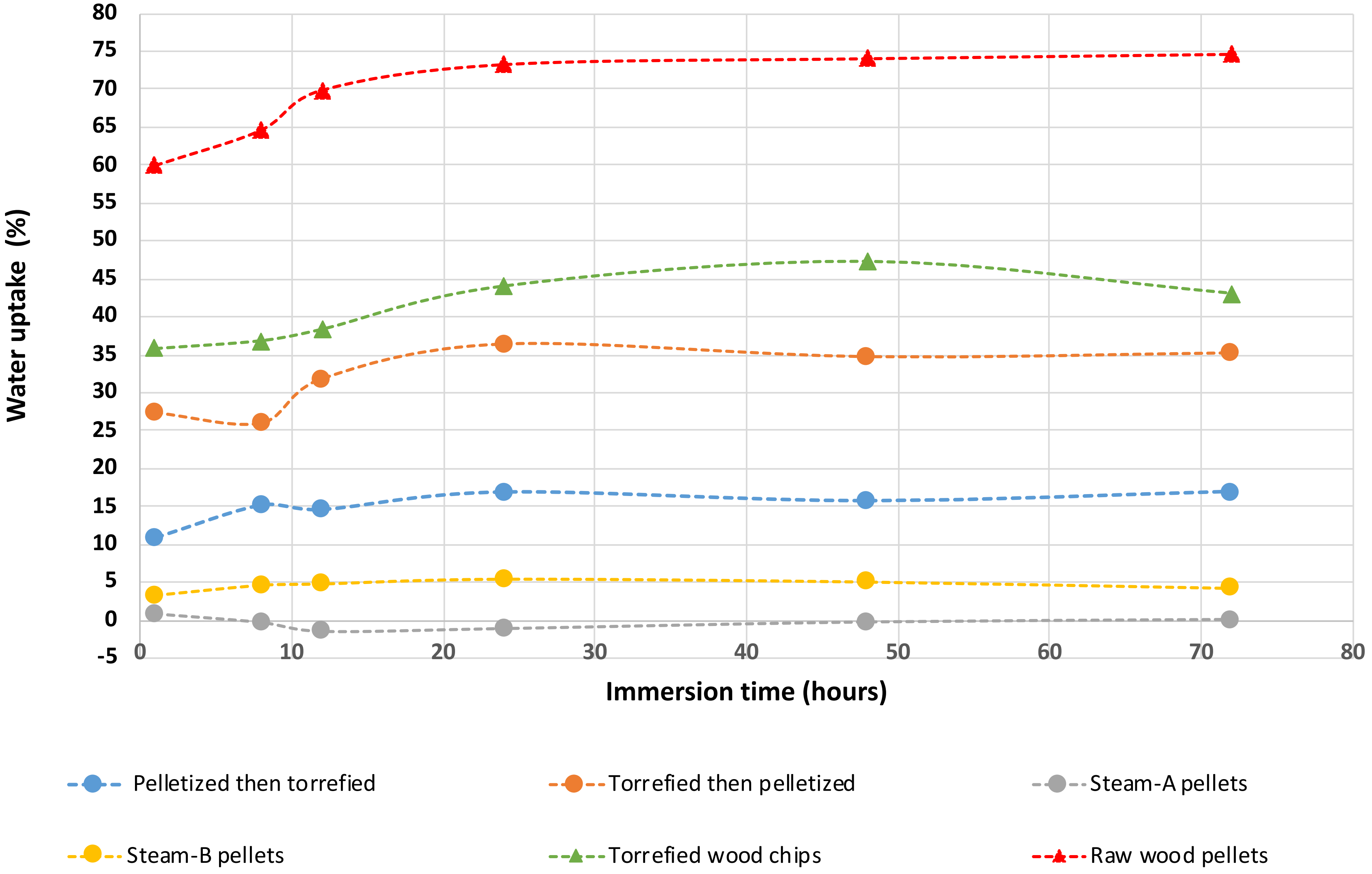

Samples Before and After Immersion Test

Top: as received - Middle: after 48 hours - Bottom: after 72 hours

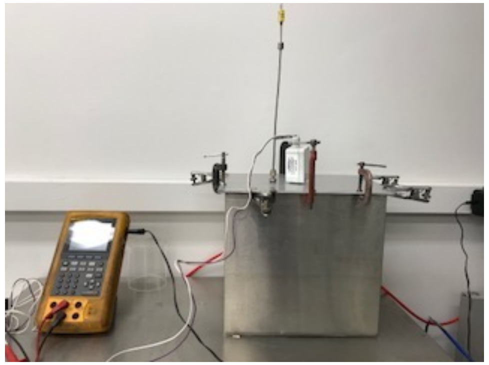

High Humidity Exposure Test*

- Pellet samples were sieved with a #6 sieve mesh (sieve opening 3.35 mm)
- Pellets were exposed to high humidity environment (92-95%) at ambient temperature (30 °C) for two weeks (336 hours).
- High humidity condition generated using saturated solution of Potassium Sulfate in a sealed container. Hot plates were used to keep the temperature at 30 °C.
- Each sample was reweighed every 24 hours and the water absorption was calculated

S. Graham, C. Eastwick, C. Snape, and W. Quick, "Mechanical degradation of biomass wood pellets during long term stockpile storage," Fuel Processing Technology, **160, 143–151, 2017.*

THE UNIVERSITY OF UTAH

BYU

Results – High Humidity Exposure (2 wks)

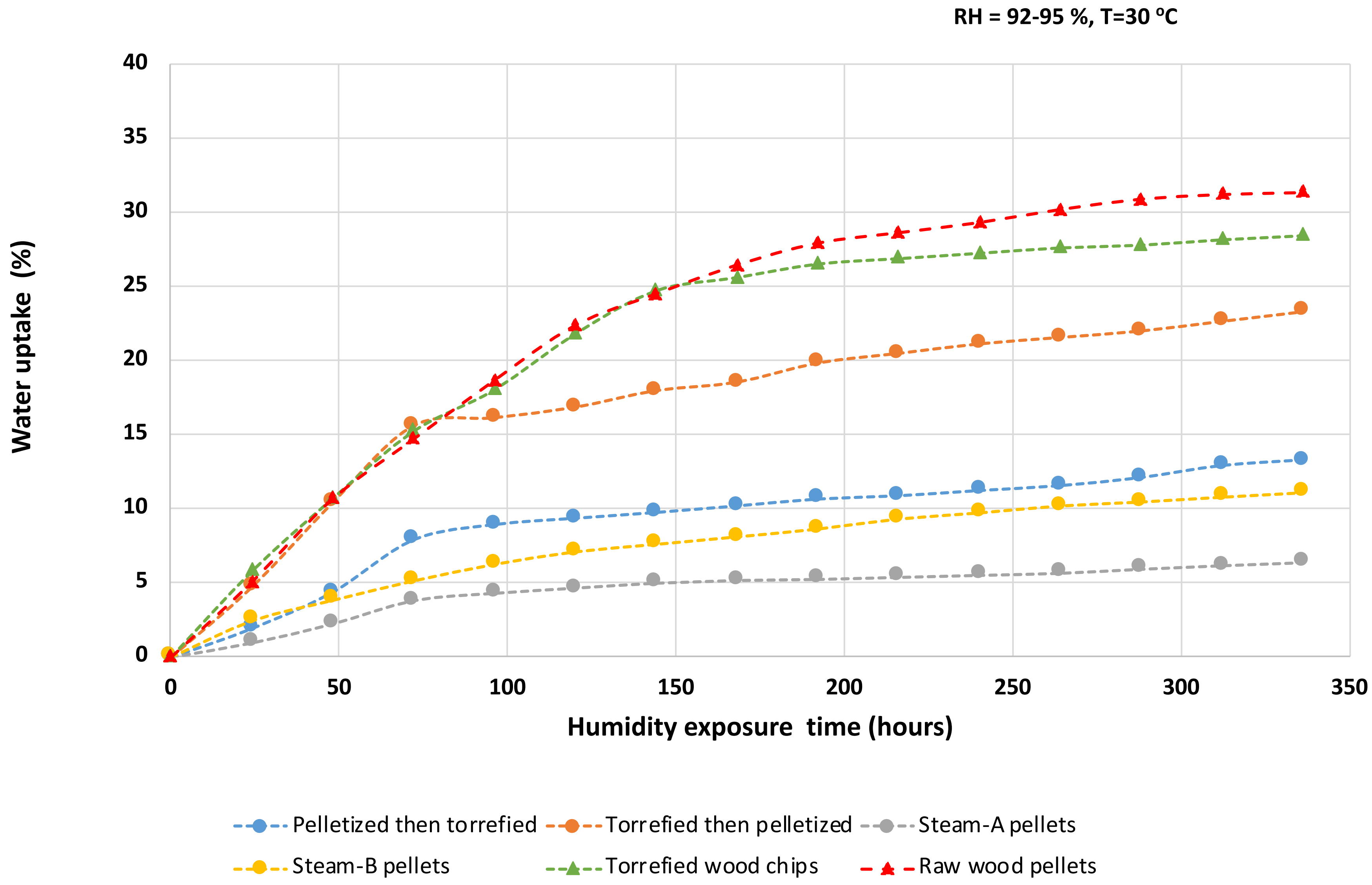

Samples before and after two-week humidity test

Top: as received - Middle: after 1 week - Bottom: after 2 weeks

Steam-A pellets

Steam-B pellets

Pelletized then torrefied

Torrefied then pelletized

As Rec'd

1 Wk

2 Wks

THE UNIVERSITY OF UTAH

Mechanical Durability Test*

- Durability tests were performed on degraded pellets at the end of the humidity exposure test
  - Durability test performed every 24 hours up to 1-week exposure.
  - Durability test also performed at end of the 2-week exposure.
- Samples were poured into a ceramic container and rotated at a speed of 100 rpm on a rotary tumbler for 3, 6 and 9 minutes
  - Durability tests performed with and without steel grinding balls
- After rotation, samples were sieved (sieve opening 3.35 mm), hand-shaken for 1 minute and the durability was calculated as the weight percentage retained on mesh

$$Durability\ (\%) = \left(\frac{M_{sample}\ larger\ than\ 3.35\ mm\ \boldsymbol{after}\ rotation}{M_{sample}\ larger\ than\ 3.35\ mm\ \boldsymbol{before}\ rotation}\right) \times 100$$

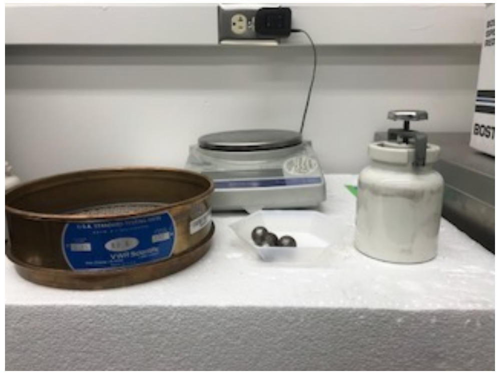

*S. Graham et al., "Changes in mechanical properties of wood pellets during artificial degradation in a laboratory environment," Fuel Processing Technology, **148**, 395–402, 2016.*

Durability Test Results* after 14 Days of Exposure to High Humidity Environment

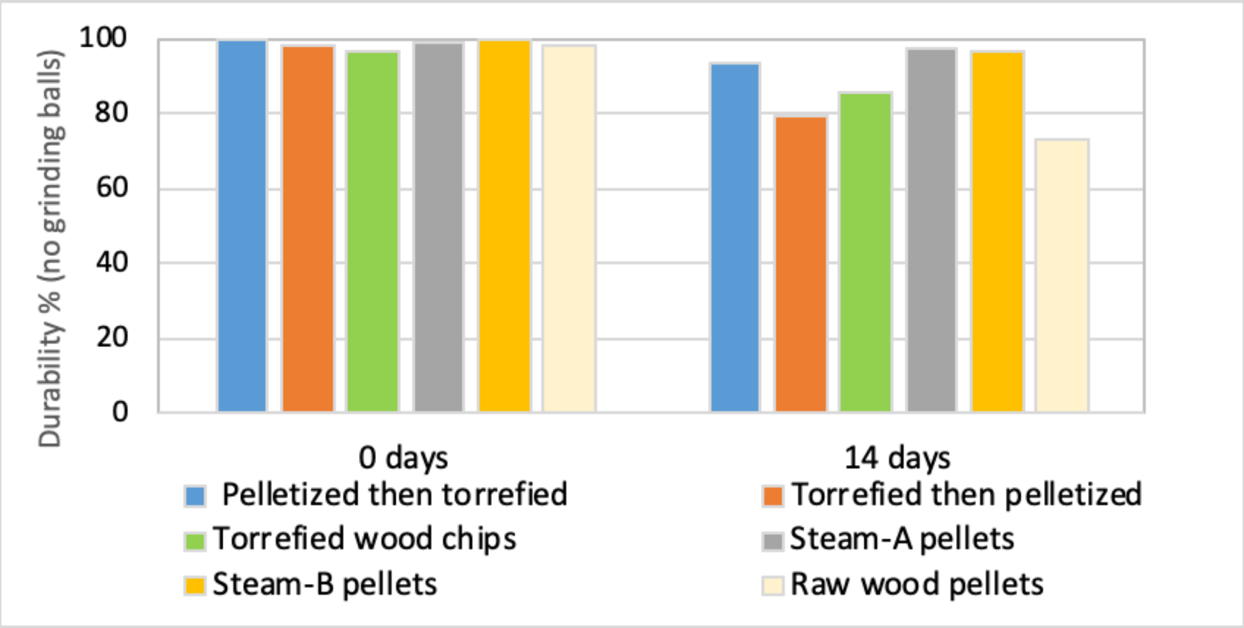

No Grinding Balls

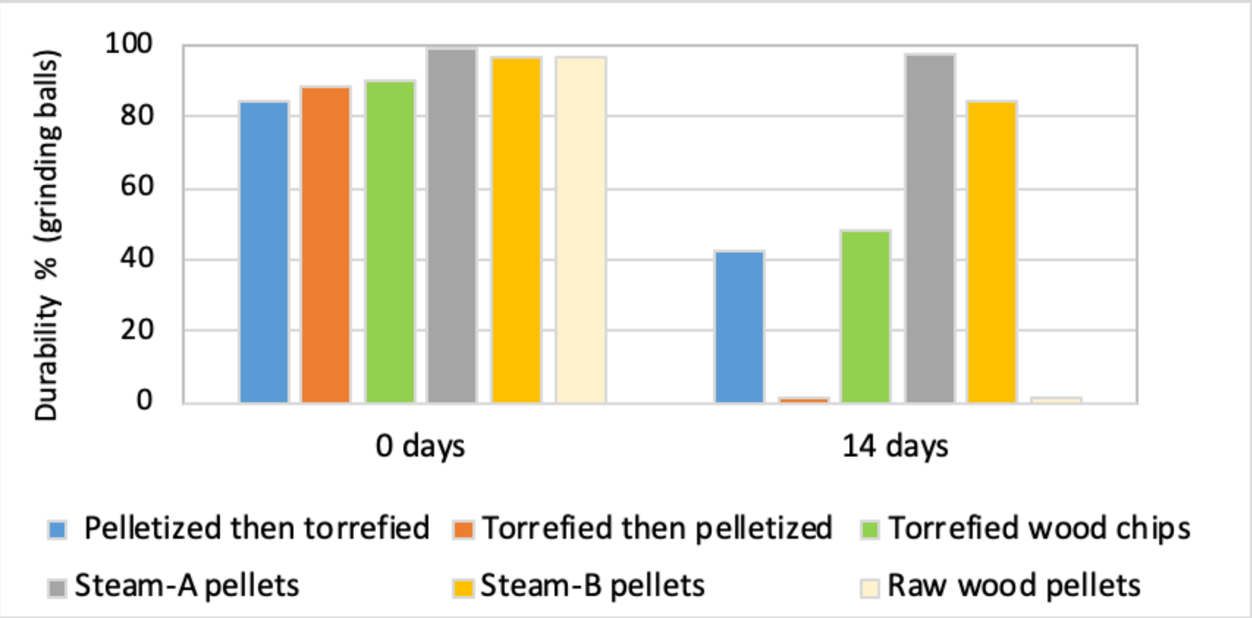

With Grinding Balls

*after 9 minutes of tumbling

Summary Comments

- **Immersion & Humidity Exposure Tests**
    - Steam exploded pellets exhibited lowest moisture uptake
    - Torrefied pellets exhibited a higher moisture uptake, but lower than raw wood
        - **pelletizing followed by torrefaction yielded much lower water uptake than torrefaction followed by pelletizing**
- **Mechanical Durability (Tumbling) Tests**
    - ***Without** grinding balls*, essentially all pellet samples (Torrefied, Steam-A, Steam-B) behaved well during tumbling, with little attrition
        - Steam exploded pellets had less attrition than torrefied pellets
    - ***With** grinding balls*, the Torrefied pellets exhibited much lower durability than the Steam-A and Steam-B pellets.
        - Especially after lengthy exposure to high humidity or immersion
- For torrefied wood pellets, best performance overall found when wood is pelletized first and then torrefied

Acknowledgements

The authors gratefully acknowledge financial support provided by Rocky Mountain Power/ PacifiCorp and the State of Utah through the Utah Sustainable Transportation and Energy Plan (STEP). We are grateful to Ken Clark, Program Manager for this project for Rocky Mountain Power/PacifiCorp.

Conflict of Interest Management:
Eric Eddings discloses a minority financial interest in Amaron Energy

Questions?

Facility Description: Mill Operation

312 Combustion Engineering Raymond Bowl Mill

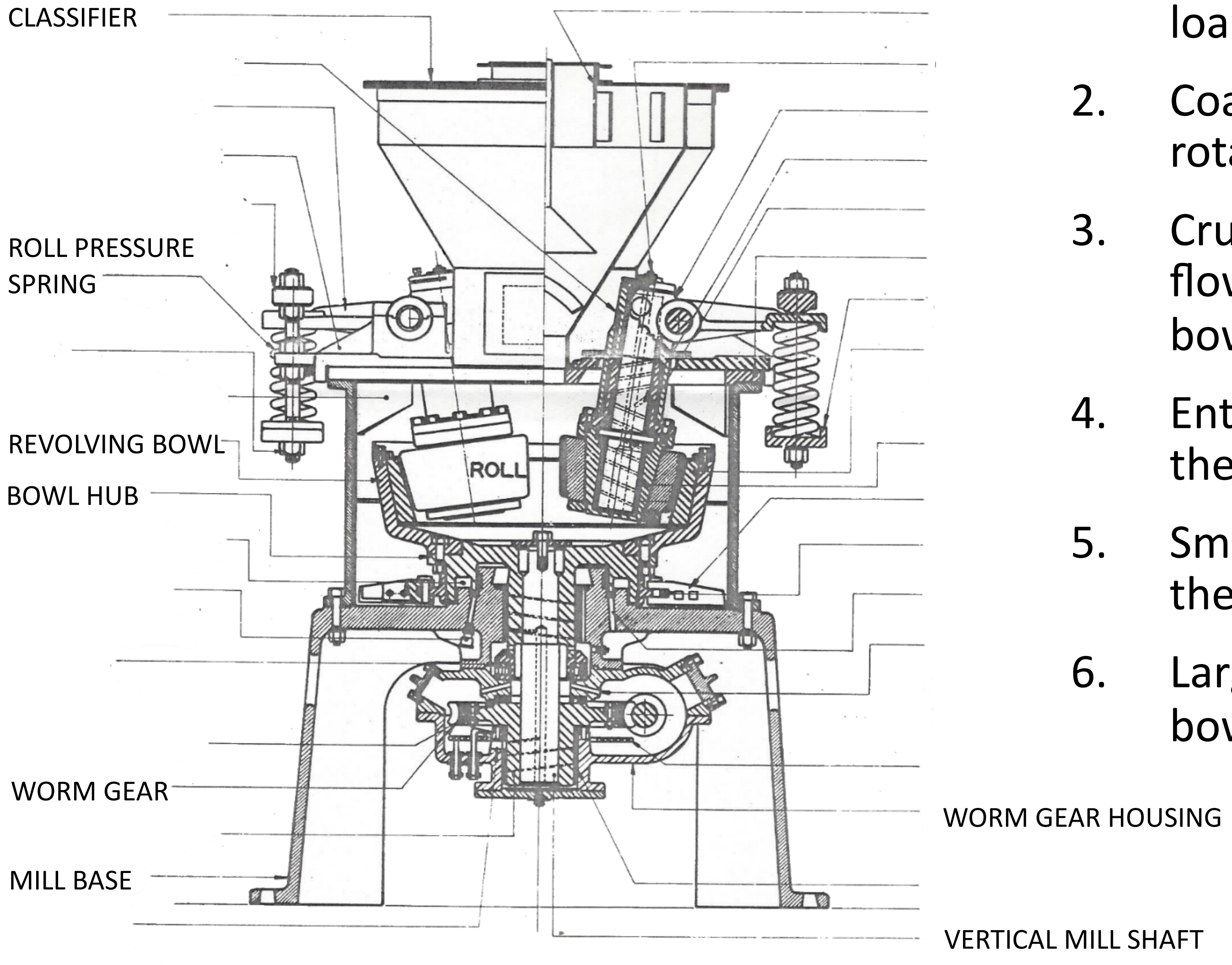

1. 2” minus coal is continuously loaded into the rotating bowl
2. Coal is crushed between the rotating bowl and the rolls
3. Crushed coal is entrained by air flowing around the outside of the bowl
4. Entrained coal is introduced into the top of the classifier (cyclone)
5. Small particles are carried out of the classifier
6. Large particles are returned to the bowl

Fuel 222 (2018) 343–349

Contents lists available at ScienceDirect

Fuel

journal homepage: www.elsevier.com/locate/fuel

Full Length Article

Investigation of co-milling Utah bituminous coal with prepared woody biomass materials in a Raymond Bowl Mill

Zsolt Dobó[a,*], Andrew Fry[b]

[a] University of Utah, Institute for Clean and Secure Energy, 84112 Salt Lake City, UT, USA
[b] Brigham Young University, Department of Chemical Engineering, 84602 Provo, UT, USA

ARTICLE INFO

Keywords:
Co-milling
Biomass
Torrefaction
Steam explosion
Bituminous coal

ABSTRACT

The operational performance of a Combustion Engineering 312 Raymond Bowl Mill has been investigated while milling a blend of Utah bituminous coal and prepared Manti-La Sal woody biomass. The research focuses on identifying the differences between the various biomass pretreatment methods regarding to co-milling behavior in a pilot scale bowl mill. Torrefied chips, torrefied pellets and steam exploded pellets were evaluated with a mass ratio of 15% biomass and 85% coal and compared to the measured pure coal mill performance. The milling process was monitored by recording the mill power requirement, inlet and outlet temperatures, fluidization air flow rates, fuel moisture content, milled product particle size distribution and SEM analysis of the particles. It was found that the blend with steam exploded pellets is the most suitable for co-milling due to it shows particle size distribution (PSD) close to the case of 100% coal while the grinding energy significantly decreased. A decreased power requirement was also noticeable when milling the blend with wood chips torrefied at 325 °C and pellets torrefied at 325 °C when compared with pure coal, but the mass fraction of large particles in the product increased for these blends. Co-milling coal with wood chips torrefied at 210 °C was not possible in these experiments. The pretreatment of woody biomass materials has the potential of co-firing at higher biomass rates in existing pulverized coal fired power plants without performing significant modifications.

1. Introduction

Co-firing beetle kill wood, or any dead woody biomass in coal-fired boilers is an attractive method for utilities to manage their carbon footprint and to help maintain the health of forests. This technology is being pursued by many groups as a viable power production alternative, with applications ranging from biomass-coal blends to a complete conversion to biomass firing [1–4]. Ideally, biomass can be prepared and utilized as a coal replacement. In this simplest of scenarios, the biomass would be blended with coal upstream of the mill and would be processed by existing conveying and milling equipment associated with the coal power station [5,6]. Since the fibrous nature of raw wood materials does not behave well in traditional coal mills [7], the main goal of this experimental study is to evaluate the co-milling of differently treated dead woody biomass materials blended with Utah bituminous (Sufco) coal at pilot scale (1 t/h) and select the most desirable pretreatment method for a full scale co-firing tests in utility boilers.

Various woody biomass pretreatment methods have been developed [8]. One advantage of the physical upgrade of a biomass material is that it significantly improves its characteristics for both feeding and grinding [9,10], both of which impact the milling process. Torrefaction is a thermal process which removes moisture, densifies the material and breaks down the cellulose cell wall structure [9]. This process typically takes place at relatively low temperatures of 200–300 °C in an anaerobic environment [9]. Several studies describe biomass torrefaction [8–16] as well as the subsequent pelletization process [16,17] in depth. Steam explosion [8,18–20] is a pretreatment method where the biomass undergoes a sudden decompression from an equilibrium state at high pressure, resulting in the rupture of the cellulose cell wall structure. The medium for pressurizing the biomass is steam. The resulting cake of biomass must then be rinsed (potentially removing alkali metals) and dried. Pelletizing steam exploded material is a common process which further increases the energy density.

The grindability of different raw and pretreated biomass materials have been investigated by several researchers [21–30]. However, there is limited information available concerning the milling behavior of treated woody biomass materials blended with coal at pilot or full scale. Gil at al. [10] published a study where chestnut woodchips torrefied at 280 °C was selected for co-milling with coal at lab scale. The biomass ratio in blends ranged from 0 to 100%. Based on the particle size

---

* Corresponding author.
E-mail addresses: zsolt.dobo@utah.edu (Z. Dobó), afry@byu.edu (A. Fry).

https://doi.org/10.1016/j.fuel.2018.02.181
Received 11 November 2017; Received in revised form 23 February 2018; Accepted 28 February 2018

distribution of different cases the authors concluded that the grindability of blends up to 15% biomass is similar to that of 100% coal. Savolainen [31] published a study concerning co-firing coal and sawdust in a 315 MW_{th} power plant. In this study it was shown that grinding coal and wood in the form of sawdust had negative effects on the coal fineness. It was concluded that only sawdust or other biofuels with small particle sizes can be utilized when applying simultaneous feeding of coal and biofuels. Zuwala at al. [32] described a trial test carried out in a 1532 MW_{th} power plant. Coal blended with 9.5% (mass basis) sawdust was sent through an unmodified bowl mill. They concluded that energy efficiency and emission levels of the boiler were not significantly impacted. However, grinding the fuel blend impacted the coal fineness, shifting the size distribution towards larger particles, negatively impacting the burn-out efficiency of the fuel. Tillman [6] reviewed the influences of co-firing on the combustion process including the scenario of blending biomass with coal on the fuel pile. It was observed that the most significant impact of the biomass coal blend was to the pulverizer, increasing the mill power consumption and affecting feeder speeds. In fact performance of the mill limited the maximum concentration of biomass that could be processed. It was also observed that co-firing 5% (mass basis) wood waste blended with coal resulted in less than acceptable particle size distribution of the milled product.

To the best of the authors' knowledge, no detailed reports are available investigating the co-milling of bituminous coal blended with pretreated dead woody biomass materials at pilot or full scale. This paper investigates the co-milling of Utah bituminous (Sufco) coal blended with differently treated dead woody biomass materials by utilizing a pilot scale (1 t/h) bowl mill for a purpose of selecting the most desirable pretreatment method for a full scale co-firing tests in utility boilers.

2. Equipment

The Industrial Combustion and Gasification Research Facility (ICGRF) at the University of Utah (USA) has industrial-scale equipment used to mill solid fuels for pilot-scale combustion and gasification experiments. The milling equipment includes: a crusher (capacity: 1 t/h, motor power: 11 kW), a 312 Combustion Engineering Raymond Bowl Mill (capacity: 1 t/h, motor power: 19 kW), a static classifier, a cyclone, a baghouse filter, an air recycle fan (power: 15 kW) and an electric heater (power: 105 kW). The equipment configuration and points of measurement relevant for this study are detailed in Fig. 1. Typically mills of this variety are used in direct-fired configuration, where the material being processed by the mill is continuously delivered to the boiler and immediately fired. The configuration used for this research differs as it is used for pulverizing and storing the fuel for later use in combustion systems.

Air is circulated in a closed loop through the mill, cyclone/filter, fan and heater and can be preheated up to 120 °C before entering the mill. A portion of the air in the closed loop circuit comes out of the system just before entering the mill and is replaced by fresh air in the mill classifier overturning the air in the system over time. This "refreshing" of the air impacts its moisture content by carrying out water evaporated during the milling process. The particle size distribution can be tuned by manually adjusting the air flow rate in the loop and/or the position of the vanes at the inlet to the classifier. The system is typically adjusted to produce a particle size distribution where 70% (mass basis) of the sampled product passes through a 200 mesh (75 μm) sieve.

The maximum capacity of the mill system is 1 t/h of pulverized coal. The milled product is loaded into a plastic lined super sack using a screw auger. The bag is purged with nitrogen during the operation in order to inert the product. Bags that are typically used have the dimensions of 90 × 90 × 90 cm with a maximum storage capacity of 1 t.

3. Measurement and materials

Woody biomass representative of beetle kill, deadfall and slash piles was collected in cooperation with the U.S. Forest Service [33]. The biomass was sourced in the Wasatch Mountains near Tibble Fork in American Fork Canyon and the main species were pinyon pine (Pinus edulis), juniper (Juniperus) and spruce (Picea). The material was shredded to a particle size of about 12 mm minus. The shredded material was separated into 6 portions and each portion was prepared using specific conditions, resulting in 6 configurations of prepared biomass. These are detailed in Table 1, where each is provided a descriptive name for future reference and the preparation conditions and methods are summarized. The 210°C, 248 °C, 290 °C and 325 °C samples were torrefied in rotary kiln with a residence time of 10 min at temperatures found in the sample name. Pellet 1 sample represents a configuration where the shredded biomass was first pelletized without using any additives and then torrefied at 325 °C. Pellet 2 sample represents a configuration where the shredded biomass was first steam exploded (conditions: 20 bar saturated steam, ≈15 min residence time), then the exploded product was rinsed, dried and pelletized. Typically, both type of pellets are 10 to 20 mm long with a diameter of 6.5 mm. The biomass handling and preparation was done by individual companies. Proximate and ultimate analysis was performed on the 6 prepared biomass materials and the raw coal. The results of these analyses are presented in Table 2, where the higher heating value (HHV) of each material is also listed. The composition of Pellet 1 was assumed to be the same as the wood chips torrefied at 325 °C. The temperature of the materials fed into the crusher was ambient.

Each configuration of prepared biomass was mixed with a Utah

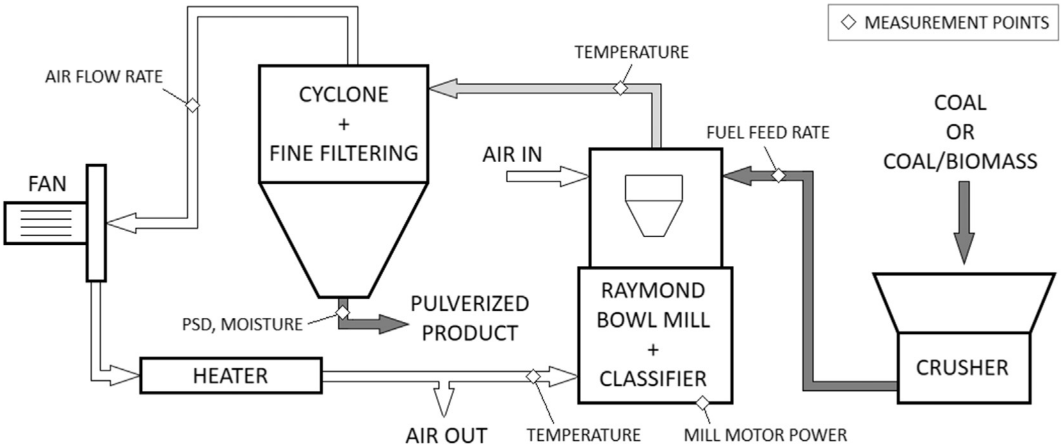

Fig. 1. Schematic illustration of the milling system including the measurement points.

Table 1
List of prepared biomass configurations used in this research.

Sample Name	Description of Preparation Conditions
210 °C	Torrefied in rotary kiln at 210 °C
245 °C	Torrefied in rotary kiln at 245 °C
290 °C	Torrefied in rotary kiln at 290 °C
325 °C	Torrefied in rotary kiln at 325 °C
Pellet 1	Pellet preparation then torrefaction at 325 °C
Pellet 2	Steam exploded treatment then pelletization

bituminous (Sufco) coal using a mass ratio of 85% coal and 15% biomass. The fuel blending was performed on a concrete slab using a Kubota tractor. Each mixture was milled using the following procedure:

1. Turn on the air recirculation and adjust the mill input temperature to 120 °C;
2. After reaching thermal equilibrium, 100% coal was introduced into the mill. The system was manually adjusted to produce a particle size distribution where 70% (mass basis) of the sampled product passes through a 200 mesh (75 µm) sieve;
3. Start performing measurements with pure coal input. Measurements include (refer to Fig. 1):

a. Particle size distribution of the product;
b. Mill motor power;
c. Mill input and mill output air temperatures;
d. Air recirculation flow rate;
e. Fuel feed rate;
f. Moisture content of the product;

4. Switch feed to the coal-biomass mixture at the same volumetric feed rate, and continue measurements until approximately 1 ton of blended product is produced;
5. Shut down the milling system and wait at least 12 h to cool down.

This process was repeated for each of the six mixtures of prepared biomass and coal. Following each milling experiment a sample was taken from the super sack containing the pulverized fuel blend product using a grain probe. The representative sample was used to perform PSD and scanning electron microscopy (SEM) analyses. The PSD was measured using two different techniques: a traditional sieve system and an optical analyzer. The sieve shaker (manufacturer: W.S. Tyler; model: RX-29) contained standard sieves with hole sizes of 75, 150 and 300 µm. A 100 g sample was shook each time for a 15 min period. The sample for the optical analyzer (manufacturer: Beckman Coulter; model: LS-230) was prepared as following: a 50 ml of ethanol was used to dissolve 50 mg of pulverized product and the resulting suspension was stirred into a homogeneous sample, then 5 ml of the suspension was fed into the analyzer. The optical analyzer is based on a laser diffraction theory and the instrument includes a Fourier lens optics. Volume distribution was used for data evaluation. The comparison of different particle size measurement techniques for biomass particle characterization was discussed by Trubetskaya et al. [34]. The SEM images of the different products were produced using a FEI Quanta 600 FEG. The mill is equipped with a 3 phase asynchronous motor (460 V, 19 kW) with delta connection. The electric current provided to the motor was measured using Fluke 3000 FC amp meters. Power was computed using the following formula:

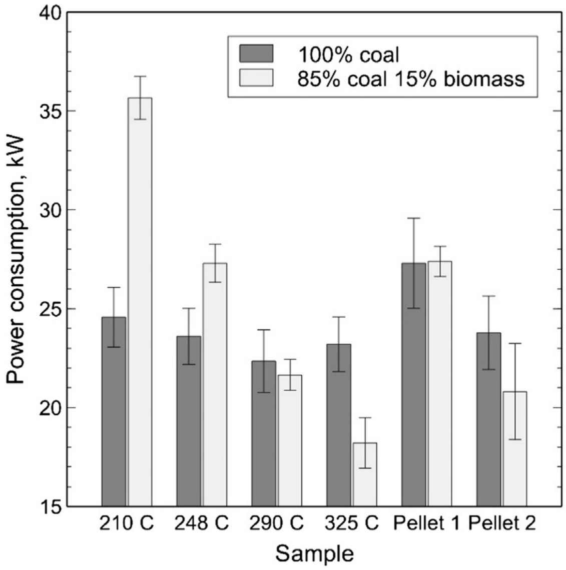

Fig. 2. Power consumption of the 312 Combustion Engineering Raymond Bowl Mill for each of the 6 biomass blend configurations and their corresponding pure coal baselines. Note, that the power consumption of the mill when idling and no material is fed into it is 15 kW.

$$P = \sqrt{3}\cdot U\cdot I\cdot cos\varphi,$$

where U is the measured line voltage, I is the measured line current, and cosφ is the power factor. The air recirculation rate was measured using a Dwyer 641RM hot wire anemometer. The moisture content of the product was determined using a Mettler Toledo HB43-S moisture analyzer.

4. Results and discussion

4.1. Mill power consumption

The mill power requirement was computed for all six biomass blend configurations and for the corresponding pure coal baseline. These results have been compared and presented in Fig. 2. It is important to compare the performance of the mill while processing the biomass blend with its own baseline for pure coal. The plot indicates that the pure coal baseline could be different for each material dependent on operating parameters that were not well controlled between days of operation, primarily fuel feed rate.

The power consumption of the mill using 100% coal was in range 22.4–24.6 kW excluding the Pellet 1 case, where the power was

Table 2
Analysis of the differently treated biomass materials and the coal. BDL means before detection limit, what was 0.05% in case of Sulphur. The analysis was performed by following ASTM standards: D5373 for Carbon, Hydrogen and Nitrogen, D3176 for Oxygen, D4239 for Sulphur, D7582 for Proximate, D5865 for HHV.

	Ultimate, % by weight					Proximate, % by weight				HHV, MJ/kg
	C	H	N	S	O	Fixed Carbon	Volatile	Moisture	Ash	
Coal	61.5	4.94	0.91	0.58	15.9	37.6	42.0	4.15	16.2	24.54
210 °C	49.4	6.15	0.55	BDL	41.2	14.4	79.5	3.43	2.68	20.76
248 °C	51.2	5.85	0.54	BDL	36.7	15.9	76.4	1.98	5.67	20.63
290 °C	55.2	5.81	0.59	BDL	35.5	21.9	74.3	0.89	2.94	22.08
325 °C & Pellet1	55.0	5.41	0.59	BDL	31.6	26.0	64.3	2.24	7.44	22.57
Pellet 2	59.6	5.81	0.59	BDL	30.5	28.6	65.1	2.76	3.52	23.83

unusually high. The coal mixed with biomass torrefied at 210 °C gave the highest power consumption. The high power requirement for this condition indicates the mill cannot completely break down the fibrous cell structure of the biomass in a given period of time and a portion of this material is retained in the bowl and on other internal mill surfaces. Retention of particles is due to the size and the weight of the particle exceeding that which can be entrained by the air flow into the classifier. The biomass accumulation in the mill caused operational problems and it was necessary to stop the milling process. This was the only case when the experiment was interrupted. The 248 °C fuel configuration also required an increase in power compared to the baseline operation (i.e. 100% coal input). However, for this fuel configuration it was possible to run the mill continuously, indicating that there is no biomass accumulation in the mill bowl but the power required to break down the structure is still higher than the baseline. The power requirement in 290 °C was lower than the baseline, and the 325 °C case showed the lowest power requirement of all of the fuel configurations tested. There was almost no change in required power for Pellet 1, however, a significant power reduction was observed for Pellet 2. These results should be interpreted with the understanding that the volumetric flow rate was maintained between the baseline and biomass mixture test. Therefore the total thermal flow was lower for the biomass mixtures than for the baseline.

The error bars in Fig. 2 represent the standard deviation of the mill power during the entire operation with each fuel configuration. The variability in power requirement provides an indication of how smooth the milling process is for a given fuel configuration. The standard deviation is lower for cases 210 °C, 248 °C, 290 °C, 325 °C and Pellet 1 when compared to the pure coal baseline. Pellet 2 resulted in a higher value of the standard deviation of the power requirement. Generally the hardness of the biomass particles is much lower than coal, resulting in smoother operation. The decreased power fluctuation may help to protect the mill resulting in longer lifetime. Fig. 3 better illustrates the decreasing power fluctuation when there is a change in the feeding from coal to coal-biomass.

The grinding energy in each case was calculated based on the mass flow rates of the fuel introduced into the mill and the mill power consumption. Table 3 contains the results, where the R ratio of the grinding energies is also listed for better comparison. If the value of R = 1, the mill is expected to utilize the same amount of grinding energy as when processing 100% coal. When R < 1 less power should be consumed when milling the biomass blend than pure coal and when R greater than 1 more power will likely be required. As seen in the table, there are 3 cases where R < 1. When utilizing the preparation methods for the biomass blends in these cases, it is expected for the mill power requirement to be lower than for pure coal in a utility boiler, while maintaining the boiler heat input. These results may only be used to infer full scale operational behavior as observed behavior at full-scale may vary. The energy required for producing either torrefied or steam exploded biomass have not been considered in this calculation and should be considered when determining the economic benefit of the process.

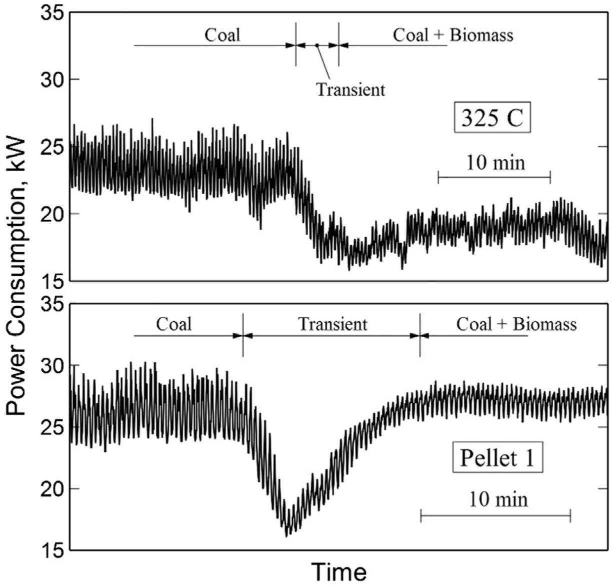

Fig. 3. Mill power consumption at the time of transition from coal to coal-biomass mixture.

Table 3
Comparison of grinding energy requirements for each fuel configuration and the corresponding baseline. R is the ratio of blend to the pure coal grinding energies.

	Grinding energy, kWh/t		R
	100% Coal	85% Coal – 15% Biomass	
210 °C	35.10	48.85	1.39
248 °C	34.30	44.25	1.29
290 °C	31.93	33.50	1.05
325 °C	33.14	27.41	0.83
Pellet 1	30.27	25.99	0.86
Pellet 2	33.24	23.42	0.70

As seen in the Table 3 the biomass pretreatment method significantly impacts the energy requirement, what is coincident with the literature. For example, Repellin et al. [22] found that natural beech or spruce requires as high as 750–850 kWh/t energy and as the torrefaction temperature increases the grinding energy significantly decreases: the wood torrefied at 280 °C required only 100–150 kWh/t grinding energy. Ultra centrifugal mill was used in this research. Authors also noted that typical coal grinding energy range between 7 kWh/t and 36 kWh/t.

4.2. Particle size distribution

The PSD of the different product materials was measured using a sieve shaker. A comparison of the fuel fineness for each of the 6 fuel configurations compared with a pure coal baseline is presented in Fig. 4. The target for the pure coal cases was 70 ± 5% through 200 mesh (75 µm), and the operating conditions for the mill were not adjusted when moving from baseline to the biomass blend. The fraction of mass in the large particle size (greater than 300 µm) was 13.4% in the 210 °C case. This indicates that at low torrefaction temperatures the

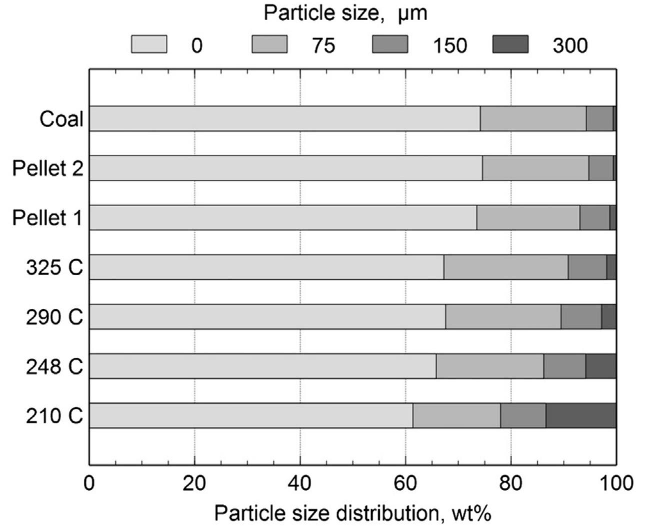

Fig. 4. PSD of the product materials determined using a traditional shaking equipment.

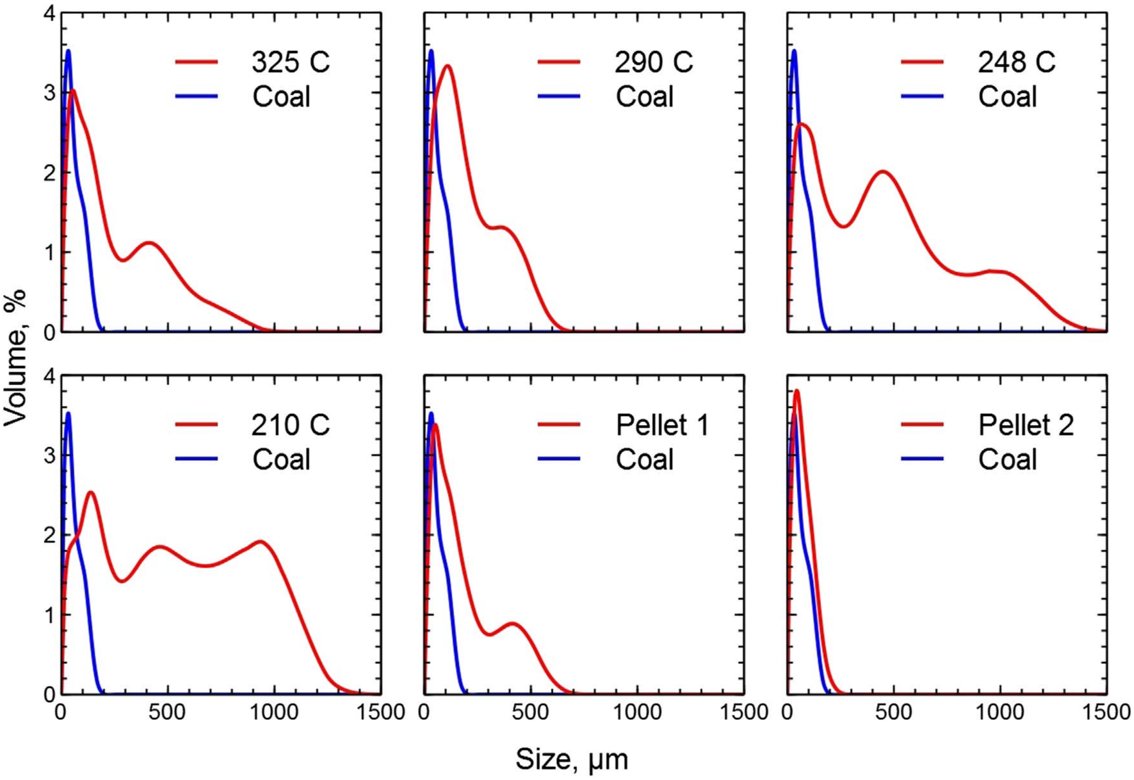

Fig. 5. Beckman Coulter LS-230 PSD analysis.

mill cannot break up the fibrous structure of the wood, but the weight and the aerodynamic properties of these particles enable them to travel through the cyclone and exit as product. These data also indicate that increasing the wood torrefaction temperature significantly decreases the 300 µm particles suggesting more efficient destruction of the fibrous material in the wood. Similar observations were published by other researchers at lab scale [22,23]. Pellet 1 slightly increases the amount of particles greater than 300 µm and there is almost no change in PSD using Pellet 2.

The PSD was also measured using a Beckman Coulter LS-230 analyzer which can provide more details. These results are presented in Fig. 5, where each fuel blend configuration is compared to a 100% coal case. Based on this measurement the maximum particle size found in the sample in cases of 210 °C and 248 °C is approximately 1.5 mm. By increasing the torrefaction temperature the maximum particle size decreases. Pellet 2 has the most similar PSD compared to pure coal, while the PSD for Pellet 1 and 325 °C is likely also acceptable. Pure coal displays a simple unimodal distribution, however the coal-biomass blends show bimodal and trimodal distributions except Pellet 2. Generally, the second peak appears between 400 and 450 µm, and only the 210 °C and the 248 °C sample showed trimodal distribution, which appears around 1000 µm. Comparison between sieve and optical results can be difficult. Sieve methods have greater error for the smallest particle sizes and optical methods error increases for particles that are larger. However, these data provide valuable insight into the relationship between preparation configuration and PSD.

4.3. SEM analysis

The objective of performing the SEM analysis was to characterize the shape of biomass particles in the product. Fig. 6 shows an SEM image for each fuel blend configuration and for the pure coal. Particles with a high aspect ratio are typical of biomass due to its fibrous nature. These are apparent in the images even though the length and the diameter varies over a broad range. It is also apparent that higher torrefaction temperature resulted in a shorter and thinner biomass particles. Needle shaped biomass particles cannot be found in case of Pellet 1 or Pellet 2, and these images are similar to the pure coal image. The dimensions of the particles in the 210 °C are extremely large as suggested by the optical PSD measurement.

4.4. Other parameters

The temperature of the air introduced into the mill was set to 120 ± 0.5 °C in each case. Since the temperature of the solid fuel was ambient and because the solid fuel contains moisture that partially evaporates, the outlet temperature of the mill was significantly lower in both coal and coal-biomass blends. Using pure coal the outlet temperature decreased to 60 ± 3 °C, while using the coal biomass mixture the outlet temperature was 70 ± 3 °C.

A small difference in moisture content between the milled product and feed was observed: the moisture of pure coal product was 4.8–5.8%, while the moisture of milled blends was 3.4–4.5%. The final moisture content of the blended materials is due to the lower moisture content of the pretreated biomass materials than the raw coal.

Typically, the air flow rate was adjusted to be between 31.6 and 32.3 Nm^3/min at 100% coal. However, as seen on Fig. 7, a noticeable flow rate increase was observed in a case of the coal-biomass blends, indicative of a lower overall system pressure drop.

5. Conclusions

The main goal of this experimental study is to evaluate the co-milling of differently treated dead woody biomass materials blended with Utah bituminous (Sufco) coal at pilot scale (1 t/h) and select the most desirable pretreatment method for a full scale co-firing tests in utility boilers. A total of six fuel configurations were investigated using different preparation conditions. The mass ratio of blends were fixed at 85% coal and 15% biomass. Based on the grinding energy, PSD and SEM analysis the steam exploded pellet, the pellet torrefied at 325 °C

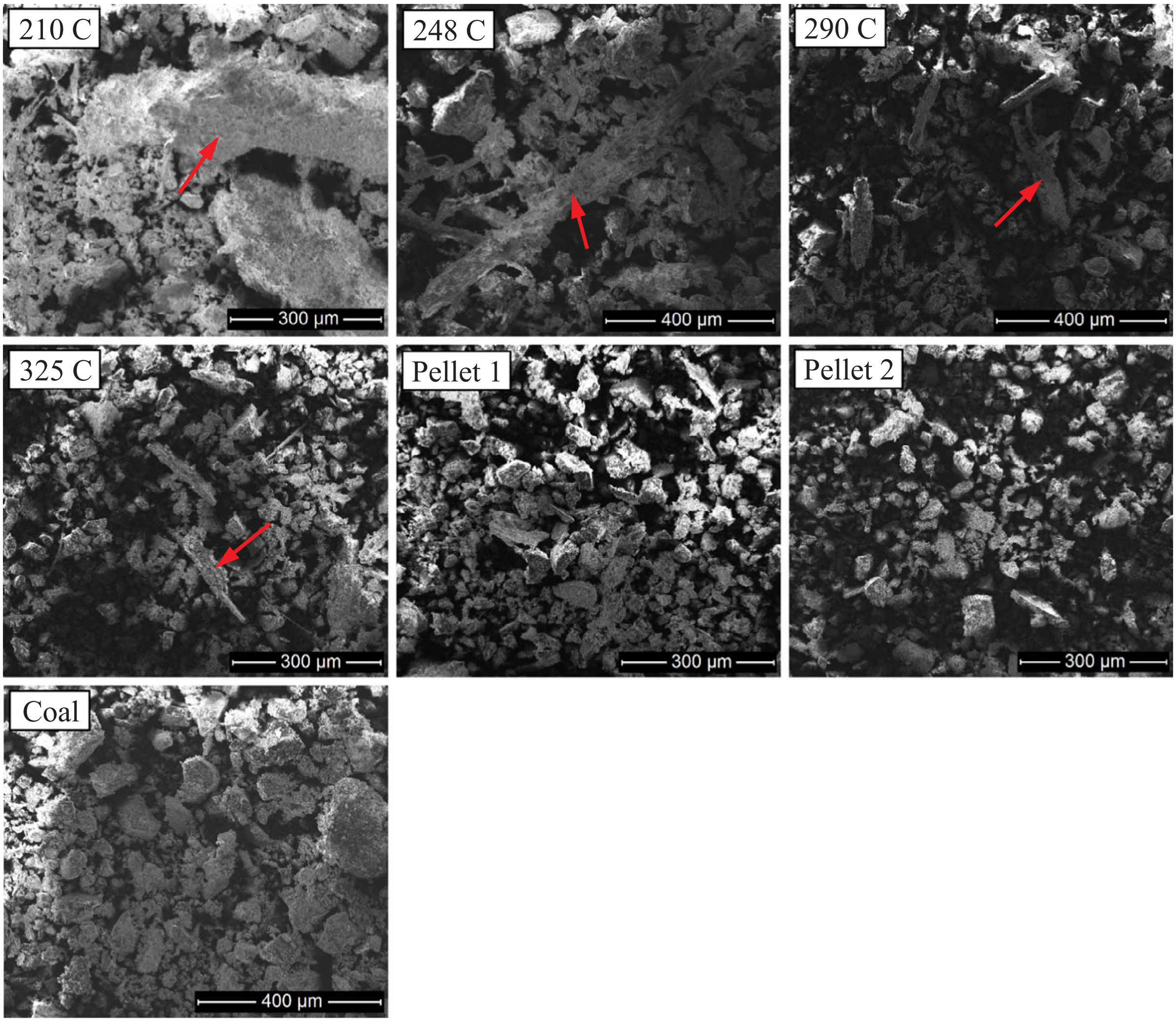

Fig. 6. SEM images taken on representative samples of the milled products for each fuel configuration. Biomass particles can be clearly found in the case of 210 °C, 245 °C, 290 °C and 325 °C blends, as indicated with arrows. The Coal picture represents the baseline, or pure coal.

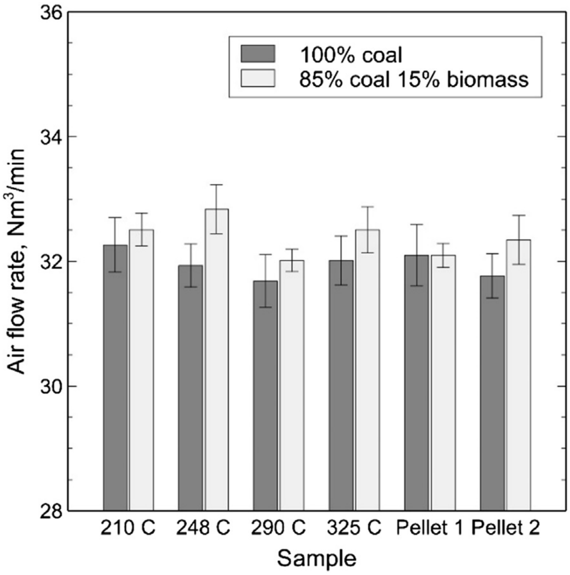

Fig. 7. Comparison of air flow rates recirculated in the milling system.

and the wood chips torrefied at 325 °C are the most promising options for a full scale co-firing tests. In these cases the mill power consumption was less compared to 100% coal, while the PSD was similar. Interrupt the milling process was necessary due to overloading in case of 210 °C sample, where the mill was not able to completely break down the fibrous structure of the biomass. Torrefaction temperatures of 290 °C or greater were necessary in order to achieve mill power what equals or is less than that required for pure coal. A blend of steam exploded biomass pellets and coal was milled with a grinding energy of 23.42 kWh/t what was the lowest in the investigated blends.

When milling the torrefied biomass coal blends, the mass fraction of particles with a diameter of 300 μm or greater was an inverse function of the torrefaction temperature, with the range between 13.4 and 1.9 mass percent for the 210 °C through the 325 °C respectively. Pure coal has less than one mass percent particles greater than 300 μm in the milled product. The milled product of the blend of steam exploded biomass pellets and coal had a particle sized distribution nearly identical to the pure coal milled product. Optical analysis of the particle size distribution of the milled products indicates that milling the torrefied biomass coal blends results a bimodal or even trimodal size distribution. Conversely the pure coal and steam exploded biomass have only one mode in the size distribution.

Based on these observed results either biomass torrefied at temperatures of 325 °C or greater, or steam exploded pellets mixed with coal should produce satisfactory performance in the mill for use as a coal replacement (up to 15%) in a full-scale utility boiler.

References

[1] Beagle E, Belmont E. Technoeconomic assessment of beetle kill biomass co-firing in existing coal fired power plants in the Western United States. Energy Policy 2016;97:429–38.
[2] Economic use of beetle-killed trees. USDA Forest Service, Status Report; 2011.
[3] Co-firing as part of the solution to dead biomass in the west (January 9, 2018). < http://www.eesi.org/articles/view/co-firing-as-part-of-the-solution-to-dead-biomass-in-the-west > .
[4] Project aims to turn beetle-ravaged trees into electricity (January 9, 2018). < https://www.eenews.net/stories/1059991961 > .
[5] Basu Prabir, Butler James, Leon Mathias A. Biomass co-firing options on the emission reduction and electricity generation costs in coal-fired power plants. Renewable Energy 2011;36:282–8.
[6] Tillman DA. Biomass cofiring: the technology, the experience, the combustion consequences. Biomass Bioenergy 2000;19:365–84.
[7] Altawell Najib. The selection process of biomass materials for the production of biofuels and co-firing. Wiley-IEEE Press; 2014.
[8] Pandey Ashok, Negi Sangeeta, Binod Parameswaran, Larroche Christian. Pretreatment of biomass: processes and technologies. Elsevier; 2015.
[9] Agbor Ezinwa, Zhang Xiaolei, Kumar Amit. A review of biomass co-firing in North America. Renewable Sustainable Energy Rev 2014;40:930–43.
[10] Gil MV, García R, Pevida C, Rubiera F. Grindability and combustion behavior of coal and torrefied biomass blends. Bioresour Technol 2015;191:205–12.
[11] Acharya Bimal, Sule Idris, Dutta Animesh. A review on advances of torrefaction technologies for biomass processing. Biomass Convers Biorefin 2012;2:349–69.
[12] Batidzirai B, Mignot APR, Schakel WB, Junginger HM, Faaij APC. Biomass torrefaction technology: techno-economic status and future prospects. Energy 2013;62:196–214.
[13] Tran Kha-Quang, Trinh Trung Ngoc, Bach Quang-Vu. Development of a biomass torrefaction process integrated with oxy-fuel combustion. Bioresour Technol 2016;199:408–13.
[14] van der Stelt MJC, Gerhauser H, Kiel JHA, Ptasinski KJ. Biomass upgrading by torrefaction for the production of biofuels: a review. Biomass Bioenergy 2011;35:3748–62.
[15] Chew JJ, Doshi V. Recent advances in biomass pretreatment – torrefaction fundamentals and technology. Renewable Sustainable Energy Rev 2011;15:4212–22.
[16] Chen W-Hsin, Peng Jianghong, Xiaotao TBi. A state-of-the-art review of biomass torrefaction, densification and applications. Renewable Sustainable Energy Rev 2015;44:847–66.
[17] Nunes LJR, Matias JCO, Catalao JPS. A review on torrefied biomass pellets as a sustainable alternative to coal in power generation. Renewable Sustainable Energy Rev 2014;40:153–60.
[18] Steam explosion for biomass pre-treatment. Energy & Climate, Centre for Renewable Energy and Transport, Section for Biomass.
[19] Lam Pak Sui. Steam explosion of biomass to produce durable wood pellets (Thesis) Vancouver: The University of British Columbia; 2011.
[20] Saeed Muhammad Azam, Anez Nieves Fernandez, Andrews Gordon E, Phylaktou Herodotos N, Gibbs Bernard M. Steam exploded pine wood burning properties with particle size dependence. Fuel 2017;194:527–32.
[21] Gong Chunxiao, Huang Jing, Feng Chen, Wang Guanghui, Tabil Lope, Wang Decheng. Effects and mechanism of ball milling on torrefaction of pine sawdust. Bioresour Technol 2016;214:242–7.
[22] Repellin Vincent, Govin Alexandre, Rolland Matthieu, Guyonnet René. Energy requirement for fine grinding of torrefied wood. Biomass Bioenergy 2010;34:923–30.
[23] Phanphanich Manunya, Mani Sudhagar. Impact of torrefaction on the grindability and fuel characteristics of forest biomass. Bioresour Technol 2011;102:1246–53.
[24] Wang Liang, Barta-Rajnai Eszter, Skreiberg Øyvind, Khalil Roger, Czégény Zsuzsanna, Jakab Emma, et al. Impact of torrefaction on woody biomass properties. Energy Procedia 2017;105:1149–54.
[25] Williams Orla, Newbolt Gary, Eastwick Carol, Kingman Sam, Giddings Donald, Lormor Stephen, et al. Influence of mill type on densified biomass comminution. Appl Energy 2016;182:219–31.
[26] Arias B, Pevida C, Fermoso J, Plaza MG, Rubiera F, Pis JJ. Influence of torrefaction on the grindability and reactivity of woody biomass. Fuel Process Technol 2008;89:169–75.
[27] Colin B, Dirion J-L, Arlabosse P, Salvador S. Quantification of the torrefaction effects on the grindability and the hygroscopicity of wood chips. Fuel 2017;197:232–9.
[28] Tamura Masato, Watanabe Shinji, Kotake Naoya, Hasegawa Masahiro. Grinding and combustion characteristics of woody biomass for co-firing with coal in pulverised coal boilers. Fuel 2014;134:544–53.
[29] Trubetskaya Anna, Poyraz Yunus, Weber Roman, Wadenbäck Johan. Secondary comminution of wood pellets in power plant and laboratory-scale mills. Fuel Process Technol 2017;160:216–27.
[30] Williams Orla, Eastwick Carol, Kingman Sam, Giddings Donald, Lormor Stephen, Lester Edward. Investigation into the applicability of Bond Work Index (BWI) and Hardgrove Grindability Index (HGI) tests for several biomasses compared to Colombian La Loma coal. Fuel 2015;158:379–87.
[31] Savolainen Kati. Co-firing of biomass in coal-fired utility boilers. Appl Energy 2003;74:369–81.
[32] Zuwala Jaroslaw, Sciazko Marek. Full-scale co-firing trial tests of sawdust and biowaste in pulverized coal-fired 230 t/h steam boiler. Biomass Bioenergy 2010;34:1165–74.
[33] U.S. Forest Service (January 30, 2018). < https://www.fs.fed.us/ > .
[34] Trubetskaya Anna, Beckmann Gert, Wadenbäck Johan, Holm Jens Kai, Velaga Sitaram P, Weber Roman. One way of representing the size and shape of biomass particles in combustion modeling. Fuel 2017;206:675–83.

Milling of Utah, Sufco Coal with 15% Prepared Manti-La Sal Woody Biomass in a Raymond Bowl Mill

Andrew Fry, Seyedhassan Fakourian
Brigham Young University

Eric Eddings, Zsolt Dobó
University of Utah

Clearwater Clean Energy Conference
June 11 – 15, 2017
Sheraton Sand Key Resort, Clearwater FL

Institute for
CLEAN AND SECURE ENERGY
THE UNIVERSITY OF UTAH

Introduction: Beetle Kill, Manti – La Sal National Forest

Manti La-Sal National Forest

Photo: A. Steven Munson

Hunter Power Station

Introduction: Beetle Kill, Manti – La Sal National Forest

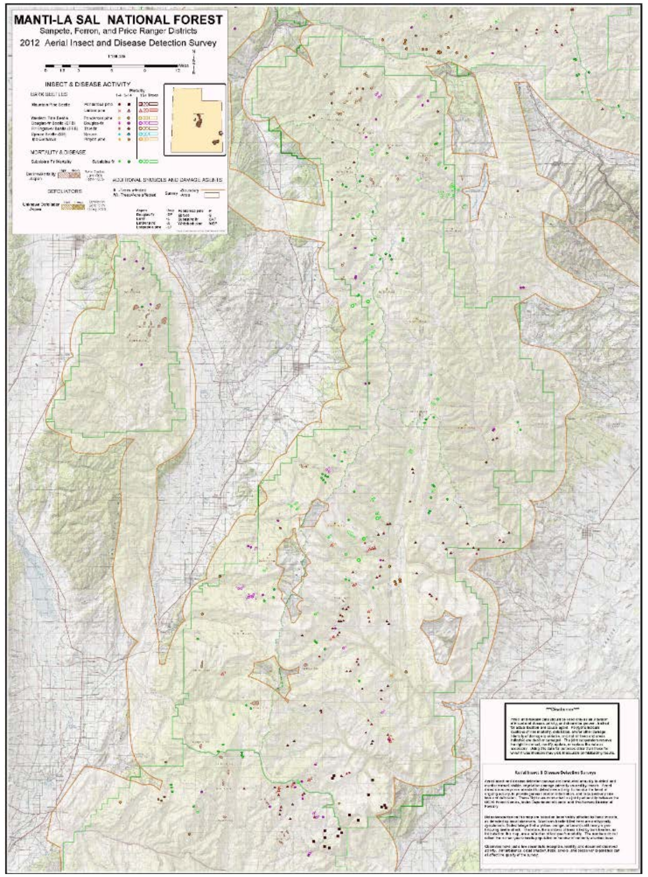

Map: US Department of Agriculture

- ~75,000 acres of beetle kill
  - Ponderosa, Douglas-fir, Spruce and Pinyon
- Indicator of unhealthy forest
- Increased potential wildland fires and particulate matter emissions
- Releases greenhouse gases while deadfall decays
  - CO_2 & CH_4

Introduction: Coal / Biomass Co-firing

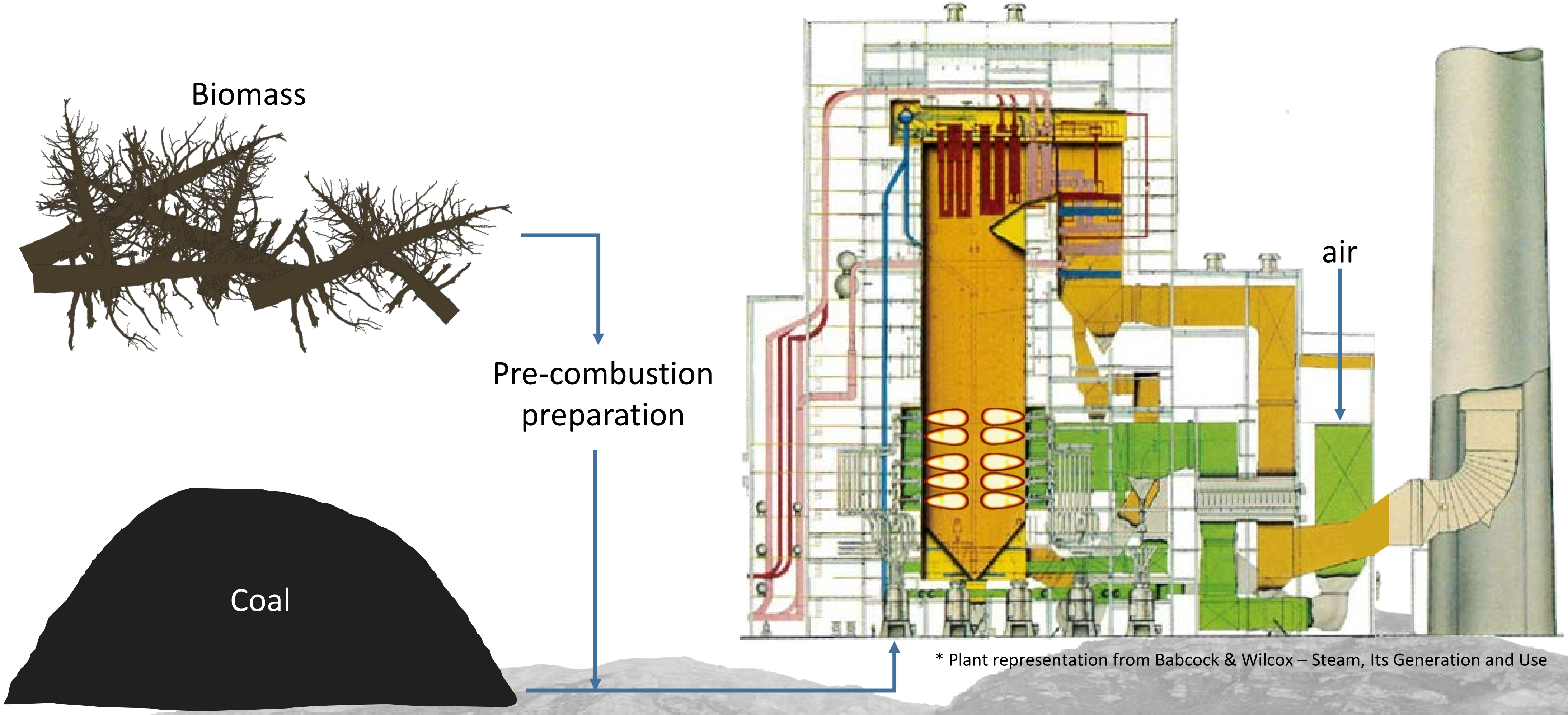

Biomass

Pre-combustion preparation

air

Coal

* Plant representation from Babcock & Wilcox – Steam, Its Generation and Use

Introduction: Raw Woody Biomass

- Low energy density
- Too much moisture
- Non-uniform shape = difficult material handling
- Cannot use existing coal handling and milling equipment

We fix these by pre-processing the woody biomass

Introduction: Biomass Preparation

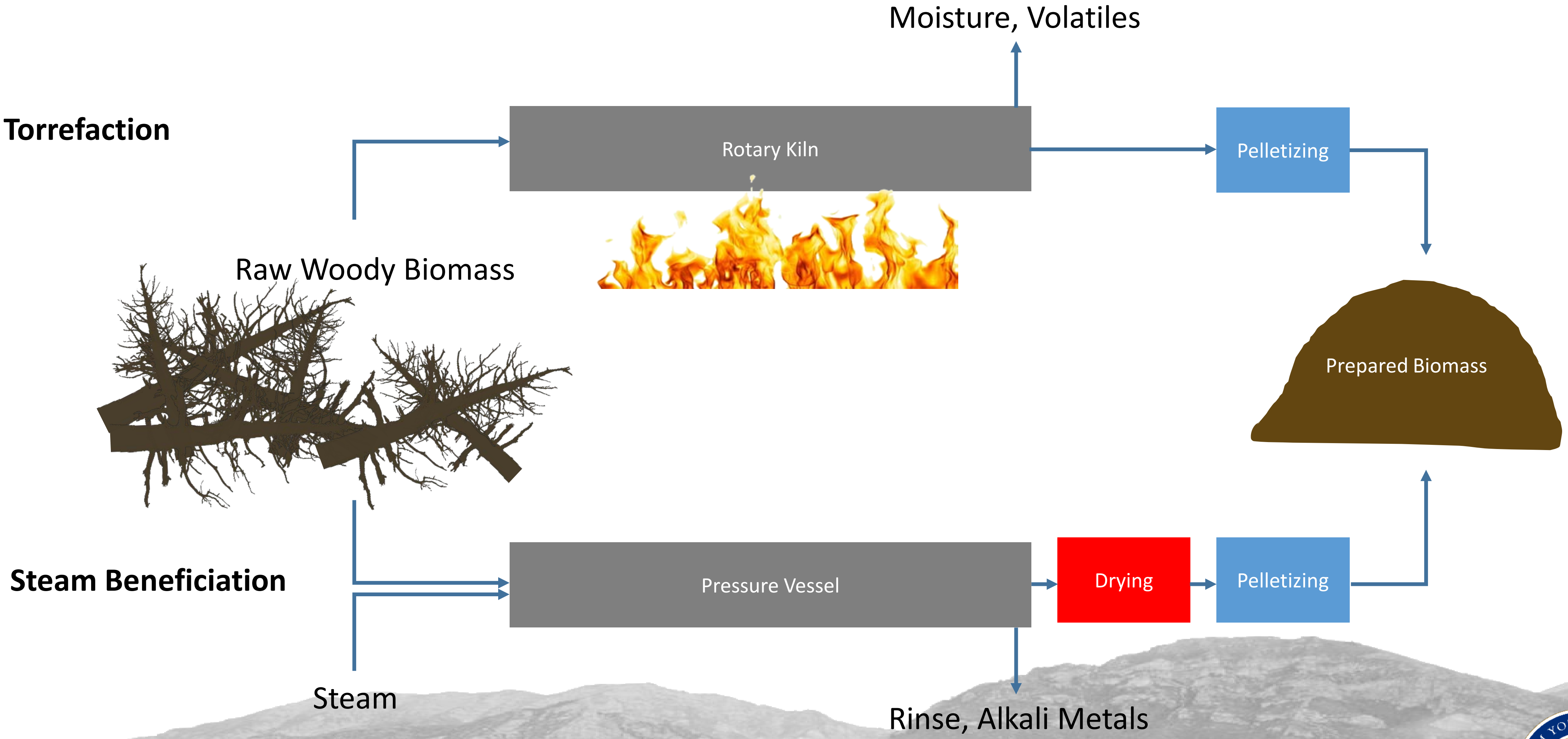

Torrefaction

Moisture, Volatiles

Rotary Kiln

Pelletizing

Raw Woody Biomass

Prepared Biomass

Steam Beneficiation

Pressure Vessel

Drying

Pelletizing

Steam

Rinse, Alkali Metals

Facilities: Mill at the University of Utah

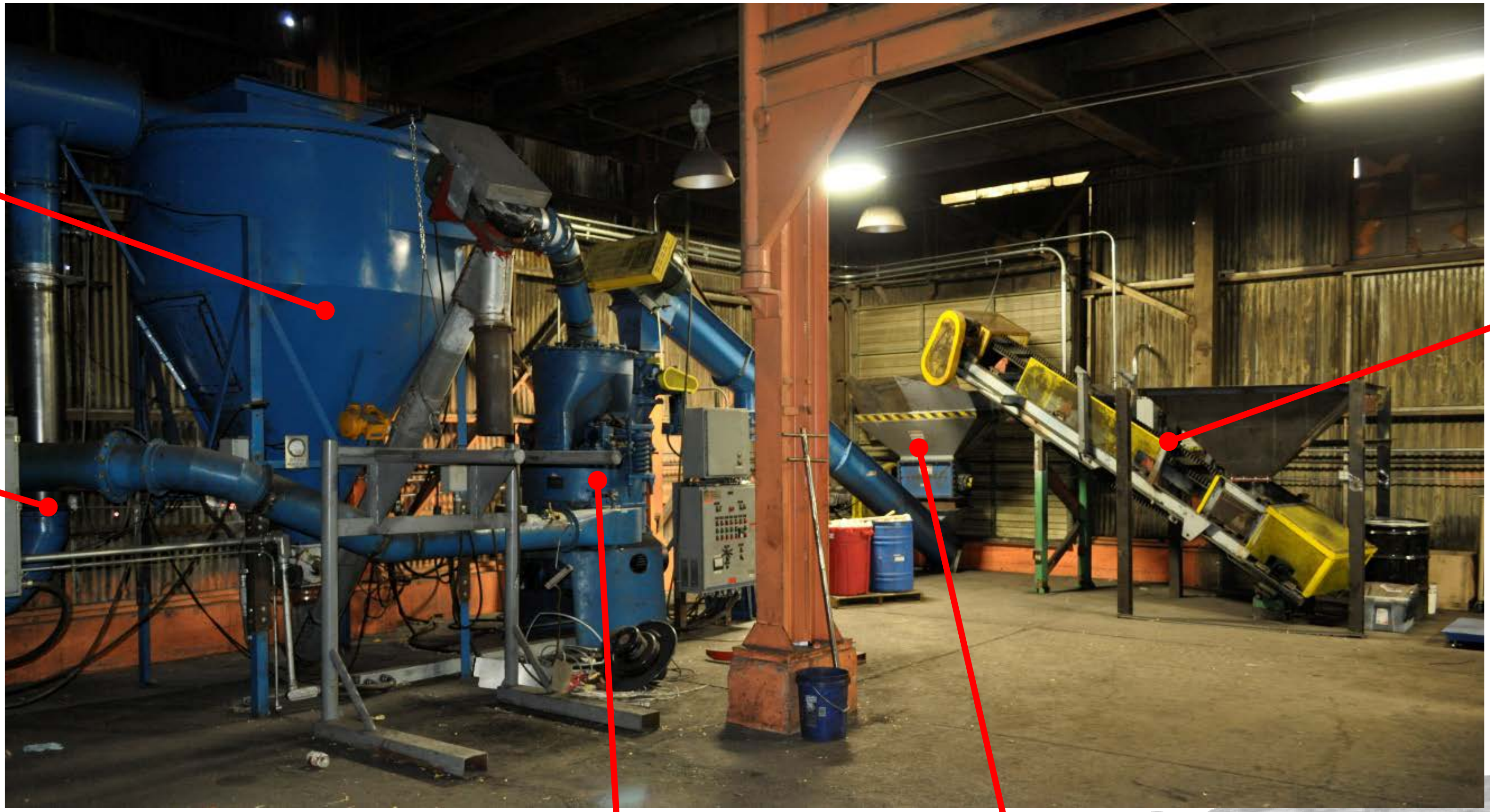

Particle Filter

Blower & Heater

Hopper & Conveyor

Raymond Bowl Mill

Crusher

Facilities: Mill Operation

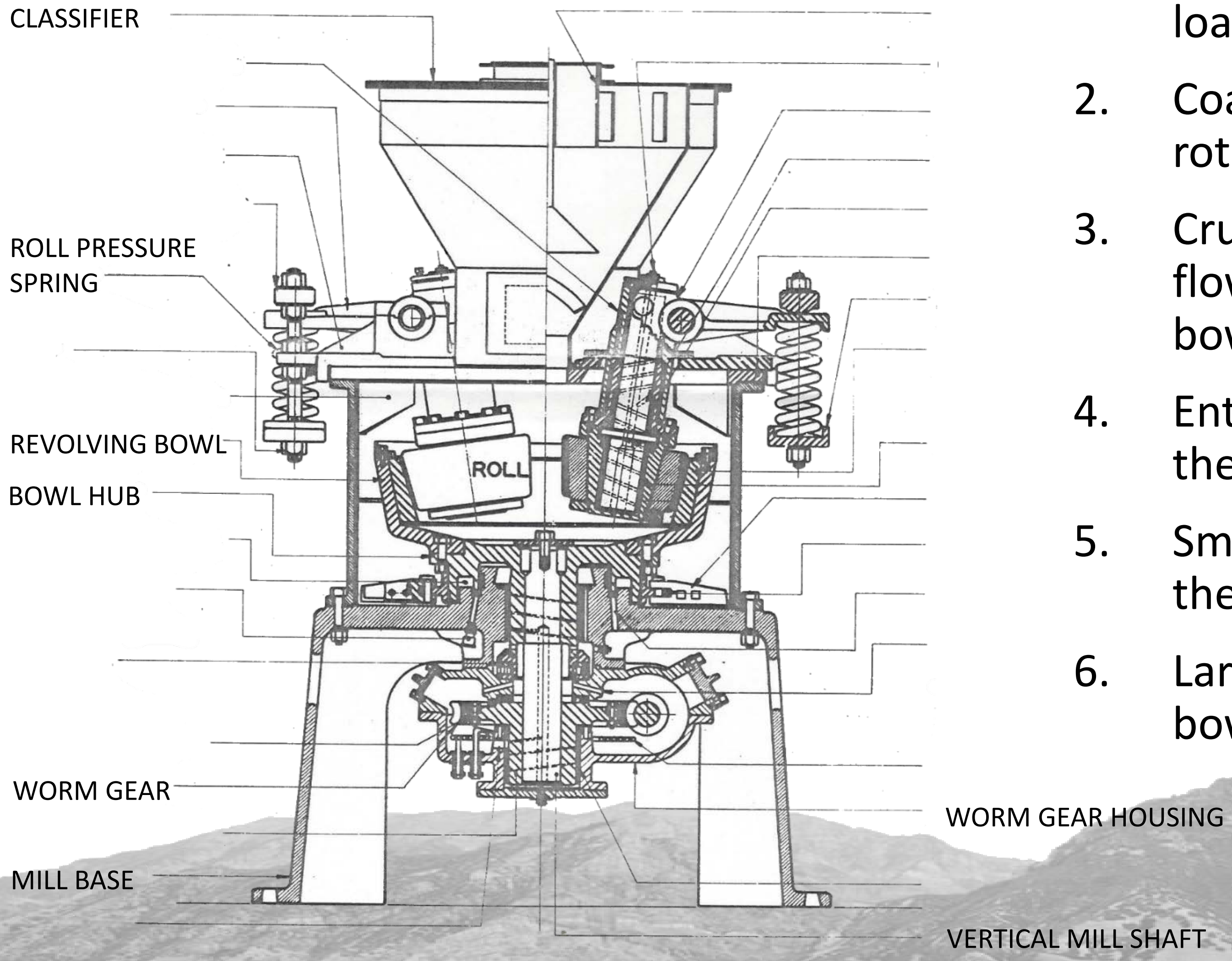
312 Combustion Engineering Raymond Bowl Mill

1. 2" minus coal is continuously loaded into the rotating bowl
2. Coal is crushed between the rotating bowl and the rolls
3. Crushed coal is entrained by air flowing around the outside of the bowl
4. Entrained coal is introduced into the top of the classifier (cyclone)
5. Small particles are carried out of the classifier
6. Large particles are returned to the bowl

Experimental: Coal and Biomass Properties

		Sufco Coal	Torrefied 210 °C	Torrefied 248 °C	Torrefied 290 °C	Torrefied 325 °C	Steam Beneficiated
Ultimate, As Received (Wt, %)	**Carbon**	61.48	49.41	51.22	55.18	54.98	59.59
	Hydrogen	4.94	6.15	5.85	5.81	5.41	5.81
	Nitrogen	0.91	0.55	0.54	0.59	0.59	0.59
	Sulfur	0.58	BDL	BDL	BDL	BDL	BDL
	Oxygen	15.90	41.21	36.71	35.49	31.59	30.49
	Ash	16.20	2.68	5.67	2.94	7.44	3.52
Proximate (Wt, %)	**Moisture**	4.15	3.43	1.98	0.89	2.24	2.76
	FC	37.6	14.4	15.9	21.9	26	28.6
	VM	42	79.5	76.4	74.3	64.3	65.1
Btu/lb	**HHV**	10551	8924	8871	9494	9703	10246

Experimental: Measurements

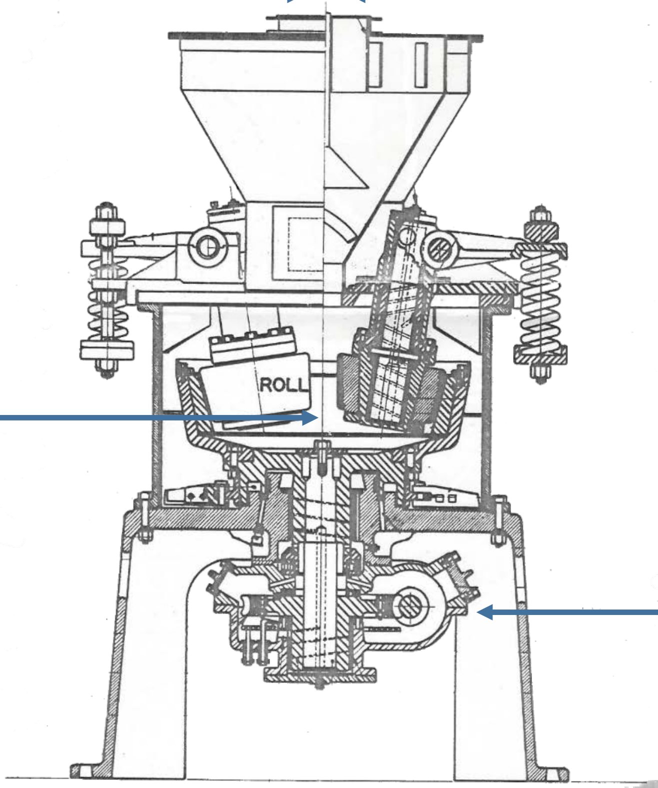

Measure the mill exit temperature

Measure the particle size distribution of the material exiting the mill

Visually inspect the bowl after milling each material

Measure the power requirement of the motor driving the rotating bowl

Results: Mill Current

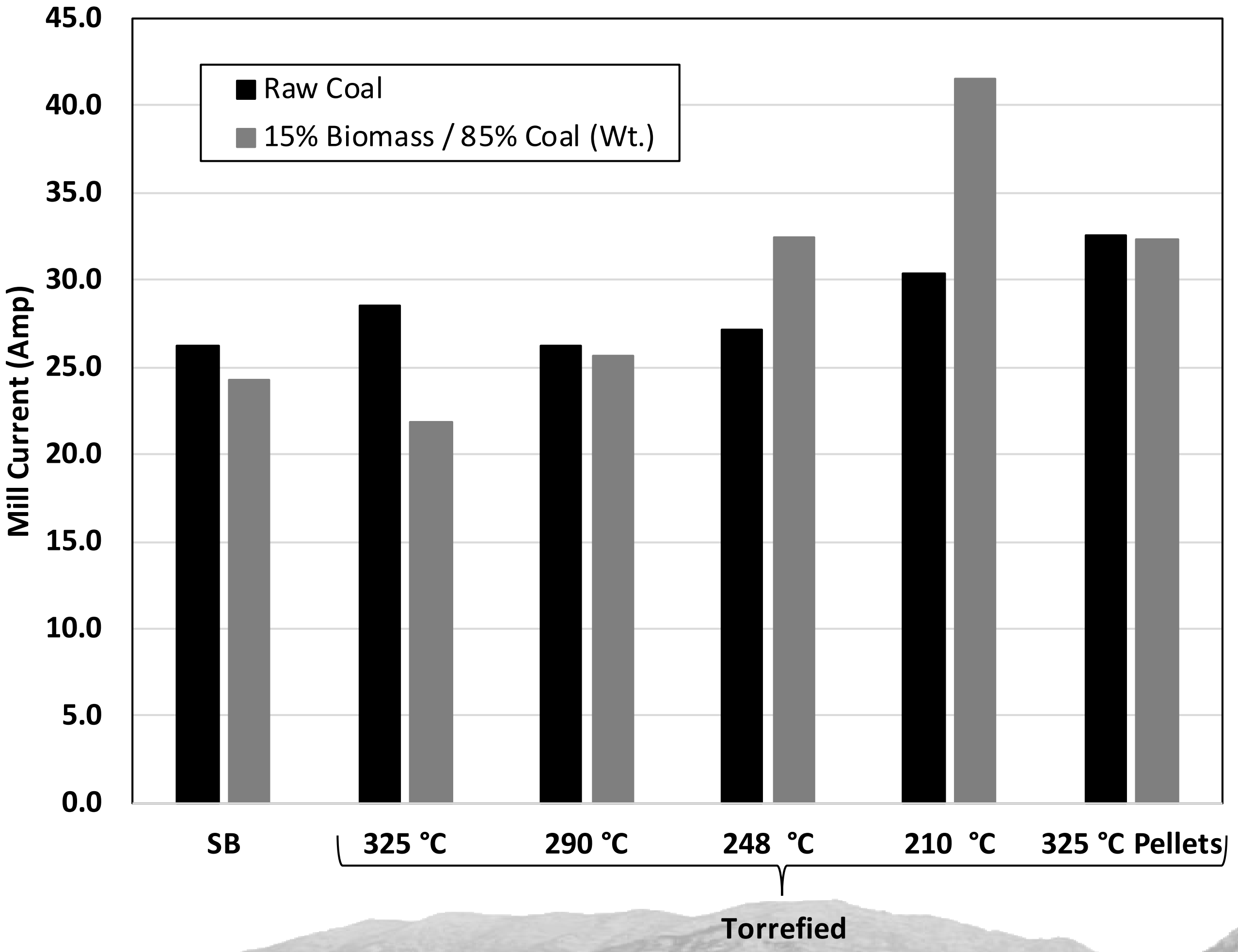

- Mill current is inversely proportional to the temperature at which biomass is torrefied
  - An indicator of the degree to which the fibrous structure has deteriorated
- Pelletizing increases the power requirement
- 325 °C torrefaction and steam beneficiation both with pelletization do not increase the mill power requirements
- All testing was at approximately the same mass flow rate.

Results: Particle Size

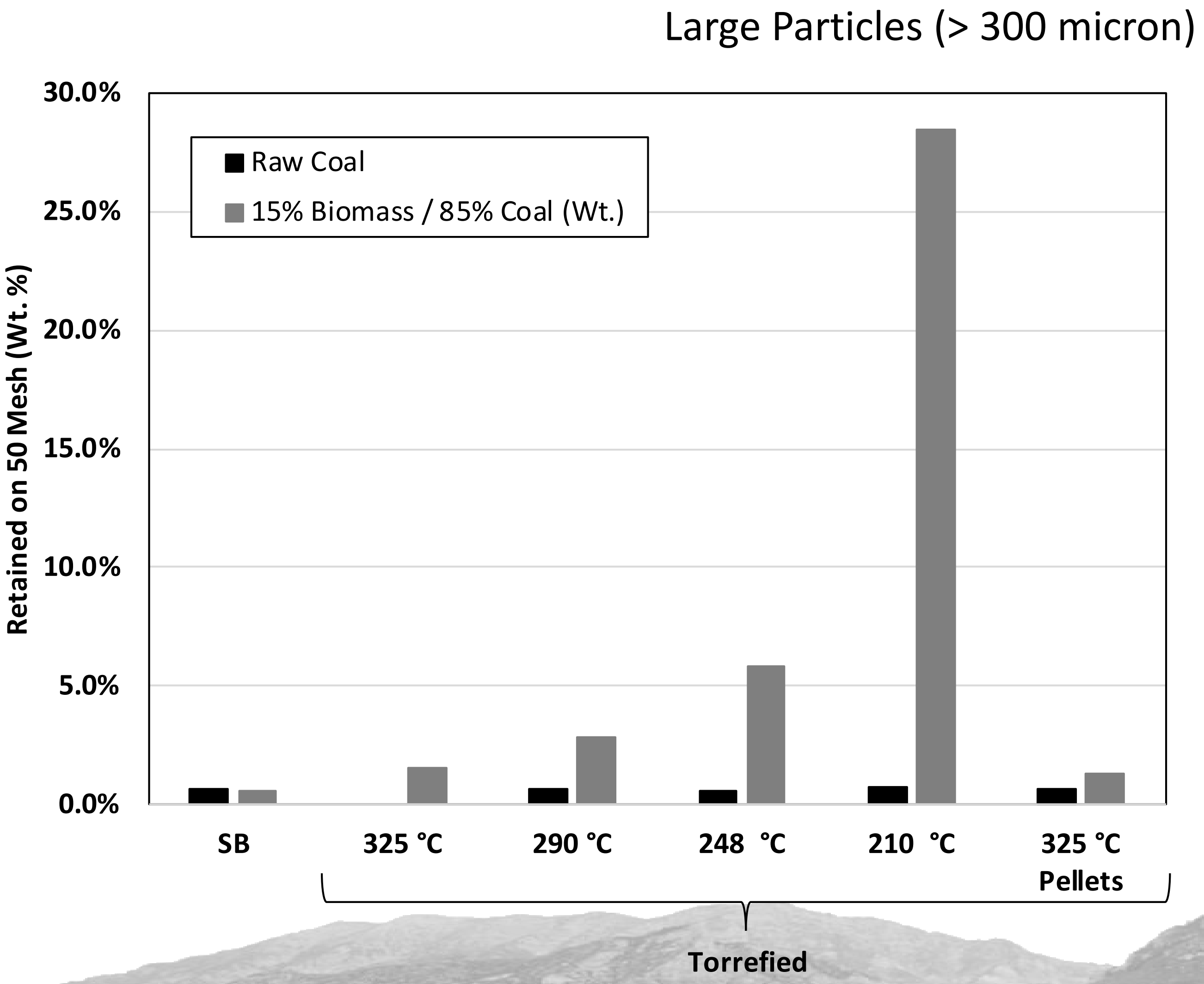

Large Particles (> 300 micron)

- All torrefied material resulted in an increase in fraction of large particles when compared to pure coal
- Fraction of large particles is reduced from torrified materials when processing temperature is increased
- Large particle effect is minimized with a processing temperature of 325 °C
- Steam beneficiated biomass does not increase the fraction of large particles when compared to pure coal

Results: Particle Size

Small Particles (< 70 micron)

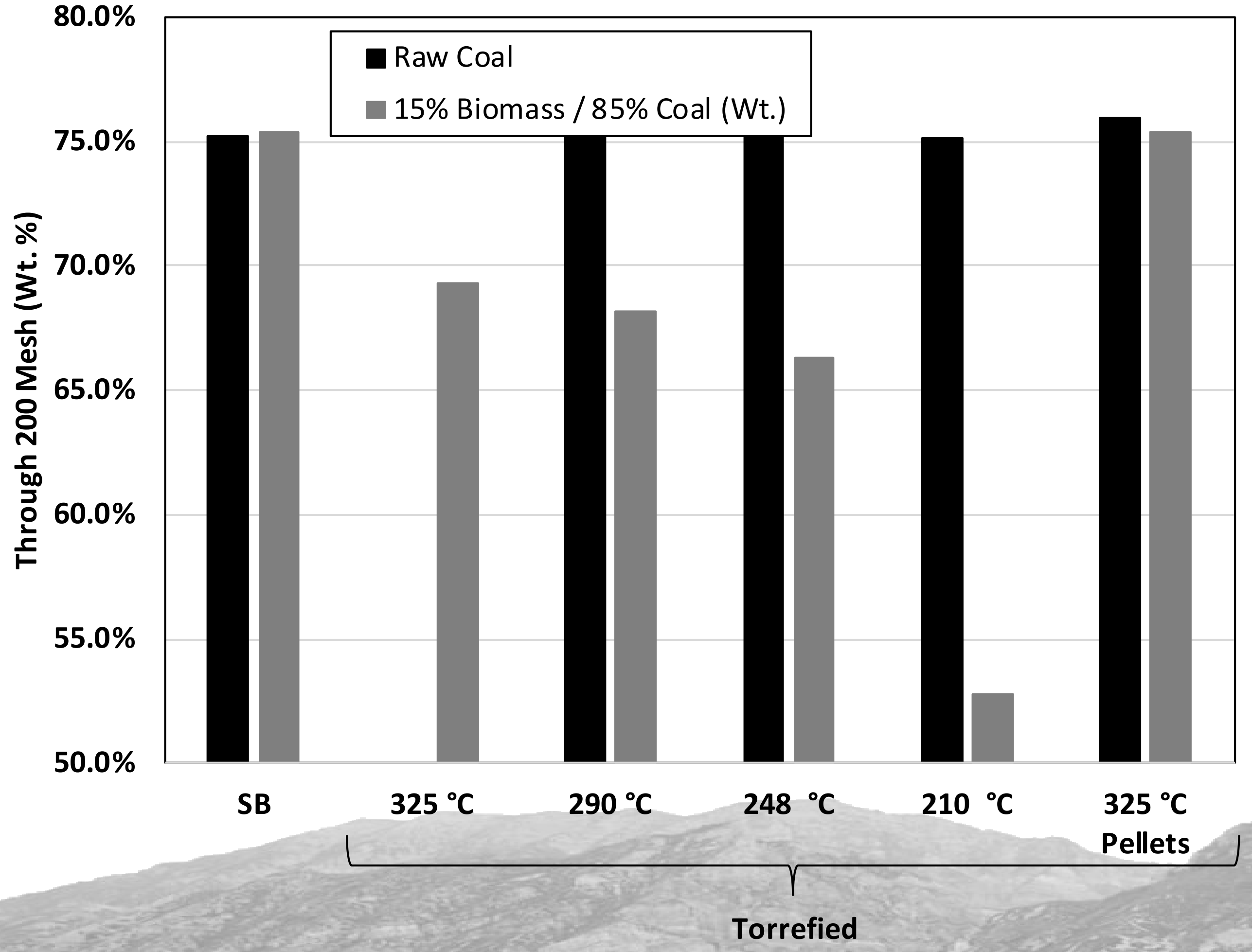

- The requirement of 70% through 200 mesh was achieved by biomass coal blends where the biomass was beneficiated or torrefied at 325 °C and pelletized
- Pelletizing appeared to have an added benefit to the millability of the torrefied material
- Pelletizing needed for long term storage, handling, and to minimize dust

Results: Mill Outlet Temperature

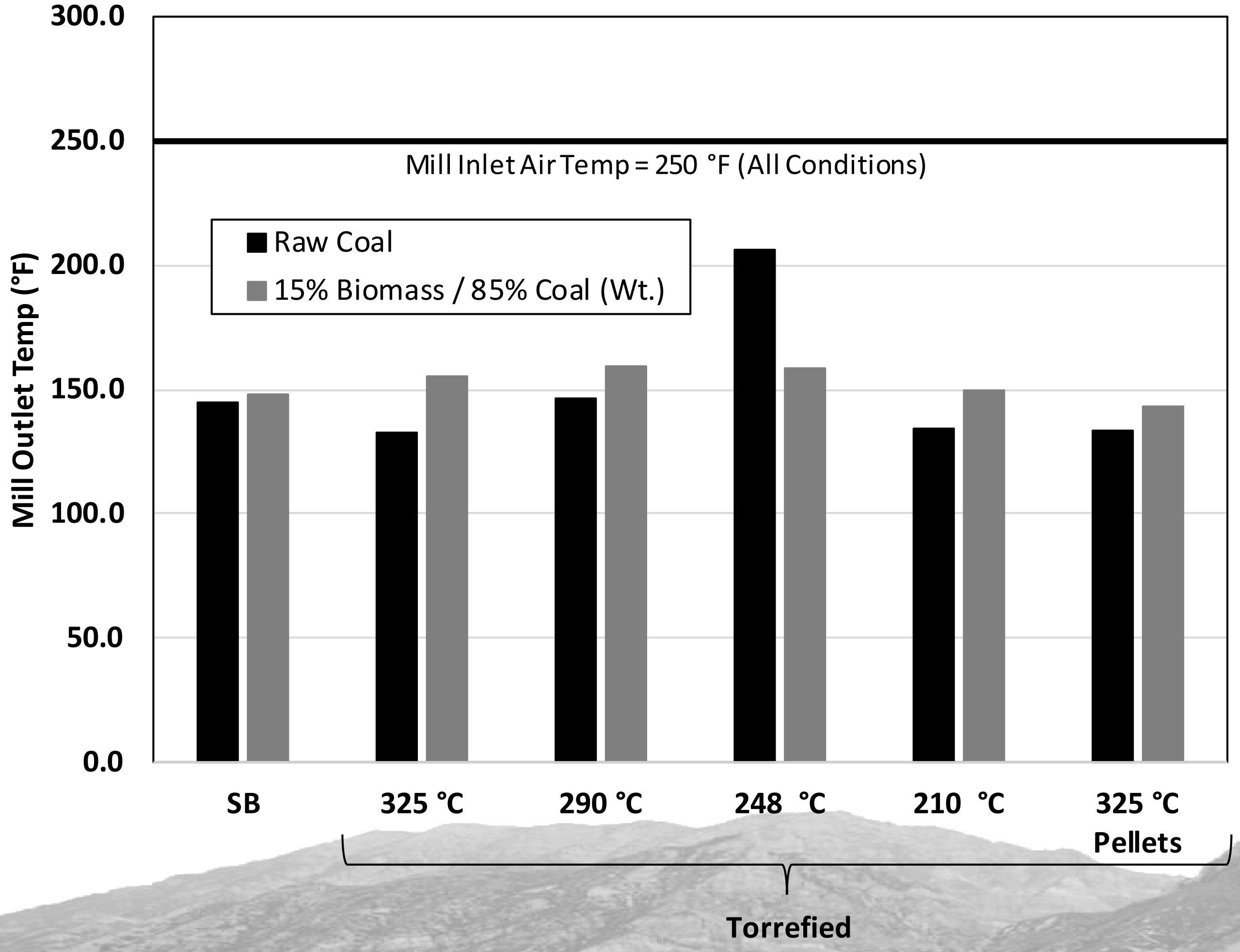

- Mill outlet temperatures were only slightly higher for the coal biomass blends, indicating no unwanted reaction in the mill

Results: Remaining Material in the Bowl
Torrefied

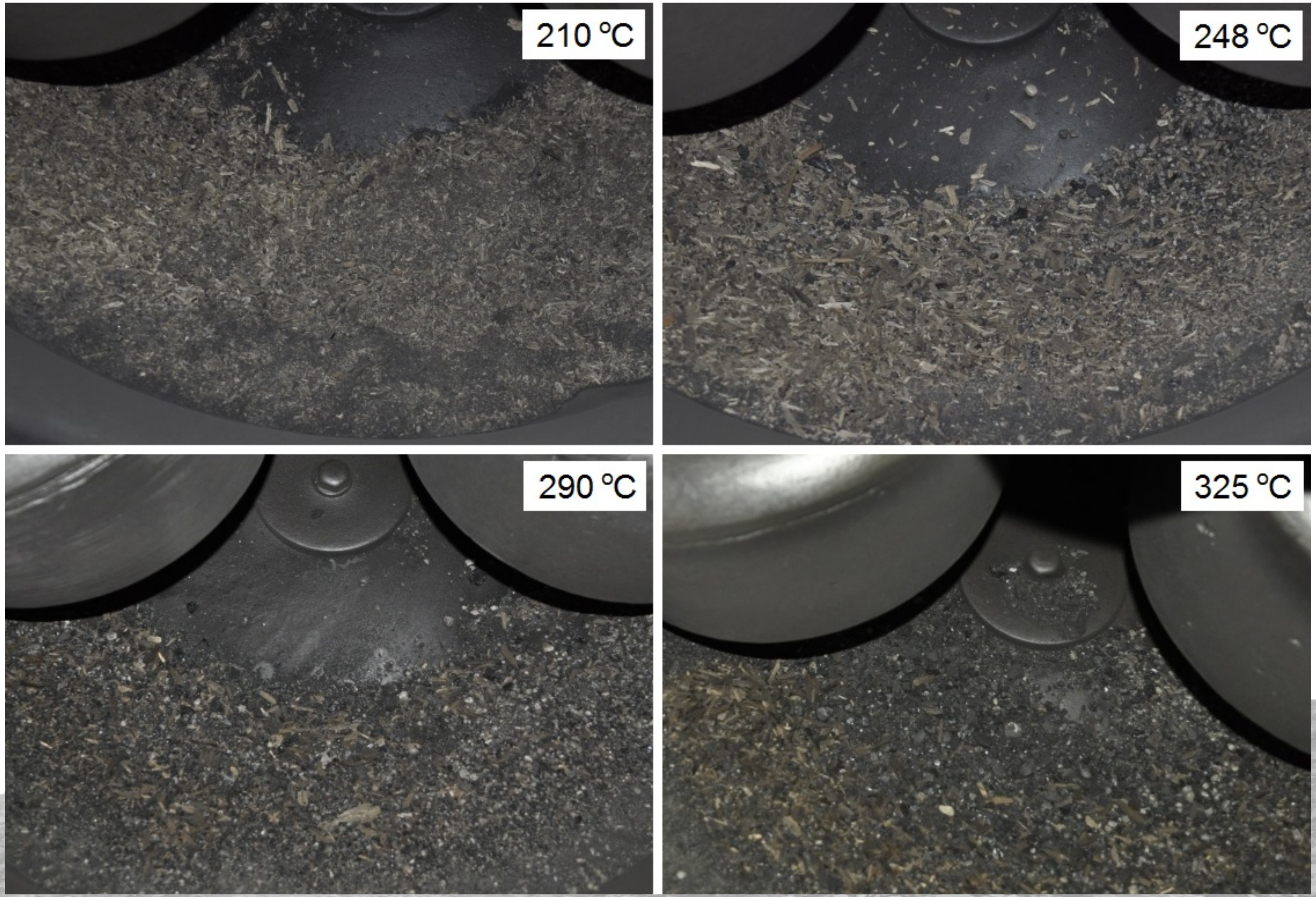

Results: Remaining Material in the Bowl

Steam Beneficiated

Results: Remaining Material in the Bowl
Torrefied and Pelletized

Summary

- Woody biomass was collected that is representative of the beetle kill material in the Manti-La Sal National Forest in Utah
- Woody biomass was prepared for milling tests using a torrefaction process at several torrefaction temperatures and using a steam beneficiation process
- Coal / biomass blends were prepared in an 85% / 15% (mass) mixture with Utah Sufco Coal
- Coal / Biomass lends were milled in a 1 ton per hour CE Raymond Bowl Mill
- The mill power requirement, outlet particle size distribution and outlet temperature were measured and compared to pure coal conditions

Conclusions

- 15% mixtures of both steam beneficiated biomass and torrefied biomass at 325 °C exhibited similar mill power requirements and outlet particle size distributions to the pure coal
- Torrefaction at temperatures below 325 °C resulted in an increase in mill power and an increase in the large particle fraction
- Pelletizing appeared to improve the performance of the torrefied biomass in the mill

Questions

Mill Performance and Combustion Testing of Blends of Coal and Steam Exploded Biomass

Rajarshi Roy, Brian Schooff, Andrew Fry
Brigham Young University

Xiaolong Li, Teri Draper, Alex Prlina, Jost Wendt, Eric Eddings
University of Utah

Scott Montgomery, Jake Tuttle
San Rafael Energy Research Center

Coal Mill Experiments

Coal Mill: Layout

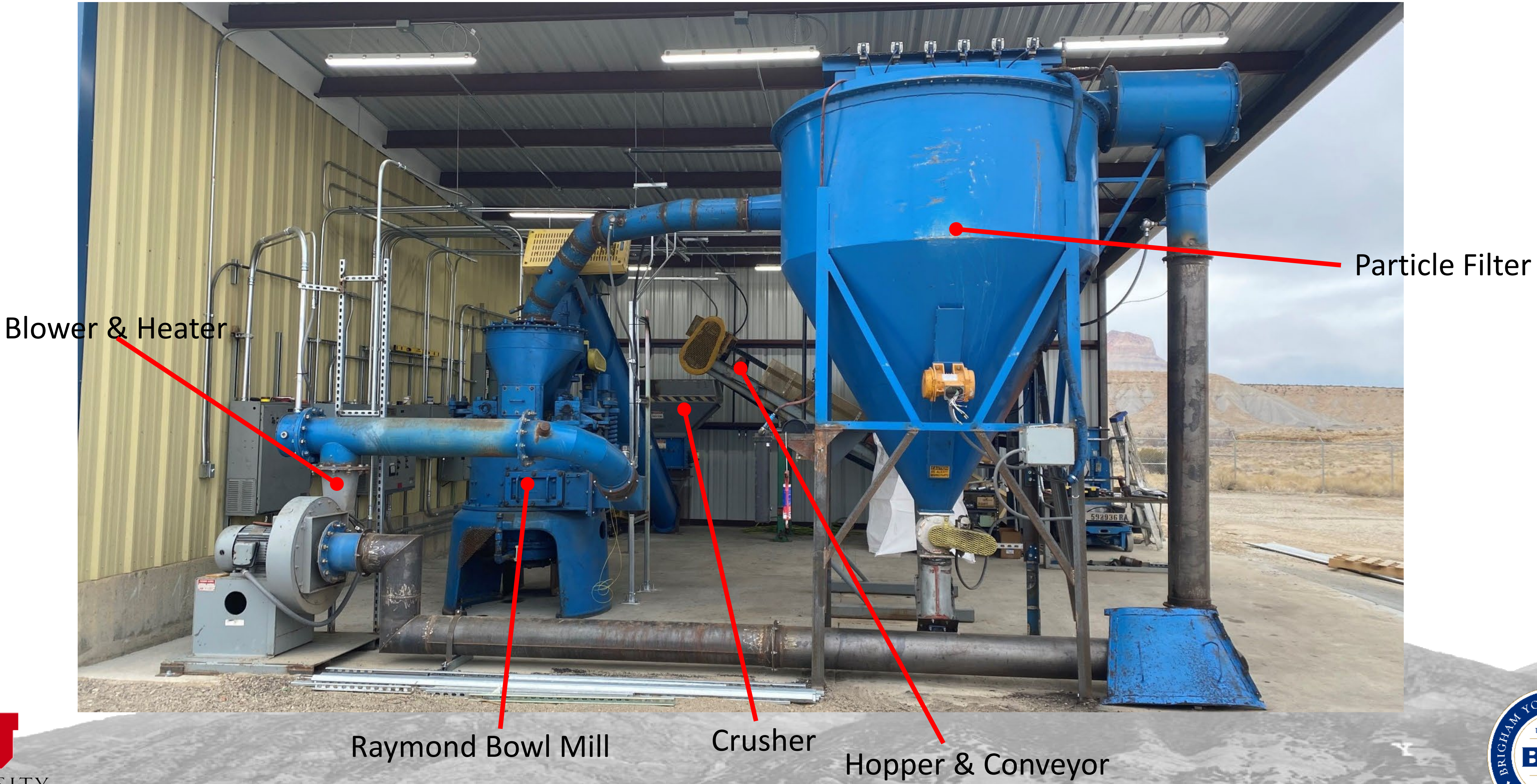

Coal Mill: Configuration

312 Combustion Engineering Raymond Bowl Mill

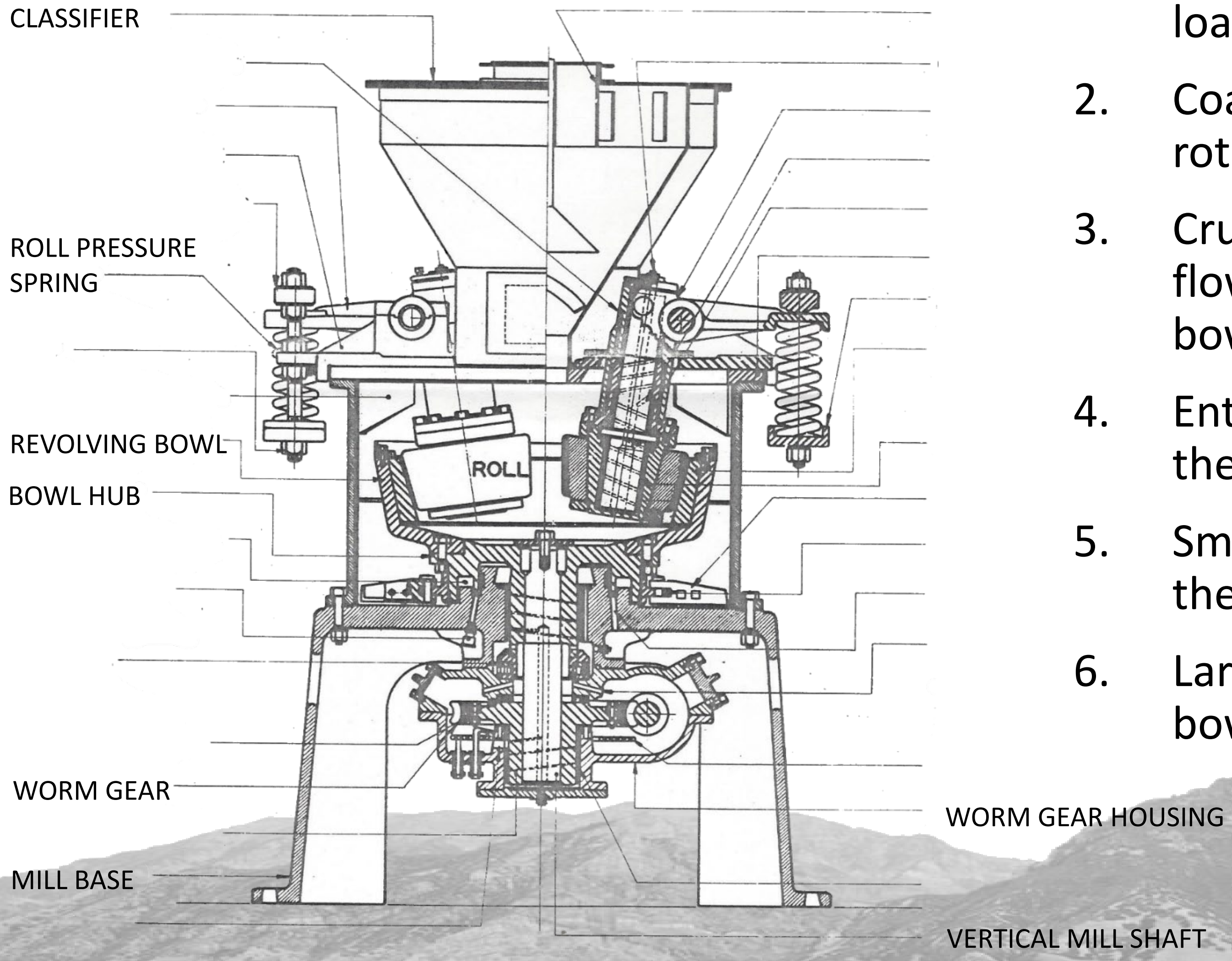

1. 2” minus coal is continuously loaded into the rotating bowl
2. Coal is crushed between the rotating bowl and the rolls
3. Crushed coal is entrained by air flowing around the outside of the bowl
4. Entrained coal is introduced into the top of the classifier (cyclone)
5. Small particles are carried out of the classifier
6. Large particles are returned to the bowl

THE UNIVERSITY OF UTAH

Coal Mill: Milling Objective & Method

- Determine mill behavior of various blends of coal/SX biomass.
  - Continuously measure mill power usage
  - Measure particle size distribution (PSD) of milled coal/biomass
- Milling conditions were kept constant throughout the milling testing
  - Feed rate into the mill
  - Mill temperature
  - Air flowrate

Coal Mill: Measurements

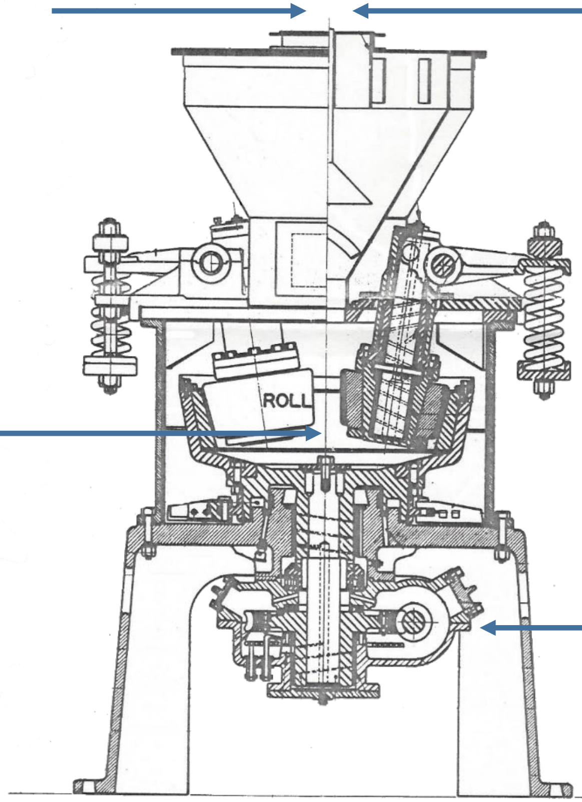

Measure the mill exit temperature

Measure the particle size distribution of the material exiting the mill
Sieve Shaker and Beckman Coulter LS230

These two issues are very important!

Visually inspect the bowl after milling each material

Measure the power requirement of the motor driving the rotating bowl
E-Mon Power Meter @ 1 Hz measurement

Coal Mill: Measurements

- Prior to experiments, the mill rollers were adjusted for coal (typical settings) by mill mechanics from a nearby power station.
- Before milling a new blend, we milled pure coal for about 20 minutes to get a baseline to try to account for changes in ambient conditions.
- Weather conditions during the mill testing were very wet, with rain and snow, which impacted the testing due to wet feed stock.
- To get the pure SX biomass to mill, the mill rollers had to be moved closer to the bowl. The baseline coal associated with the SX biomass run was also milled with the adjusted rollers.

Coal Mill: Bowl Motor Current

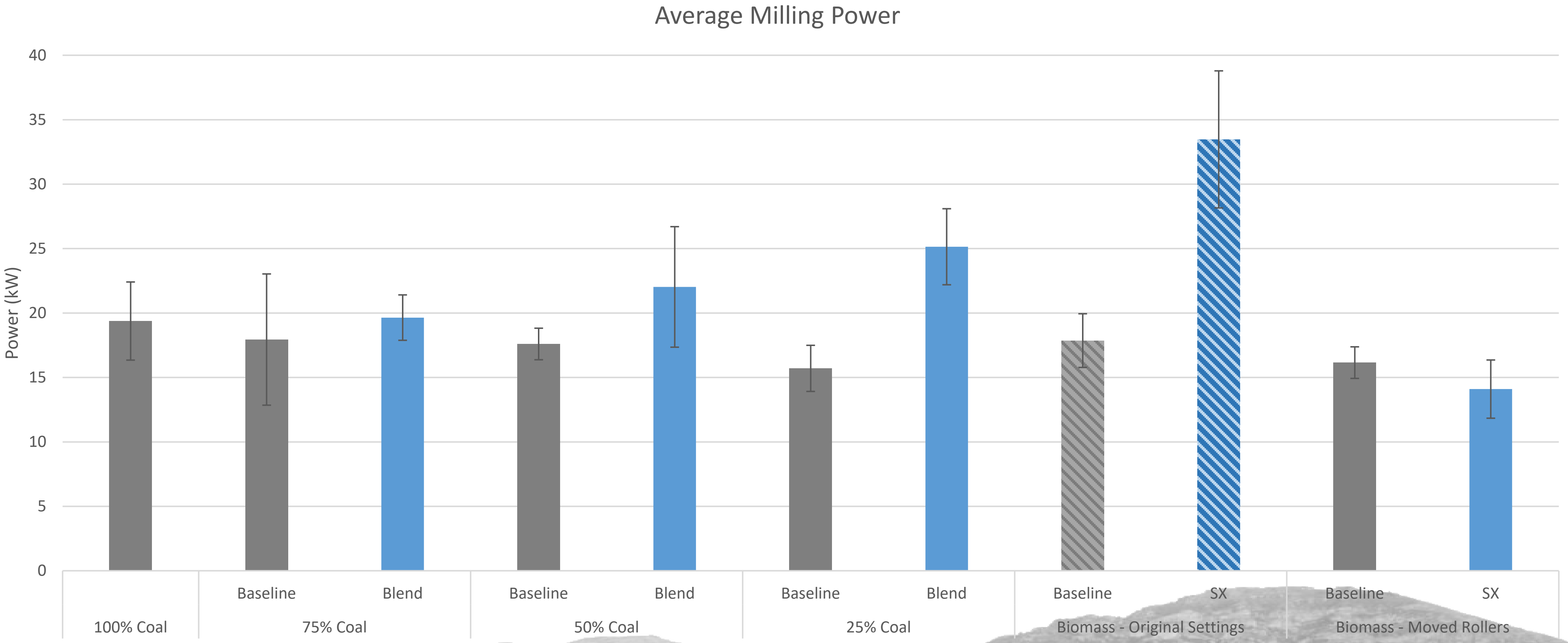

- Mill current increased with increasing biomass, until rollers were adjusted for 100% biomass

Coal Mill: Bowl Motor Current

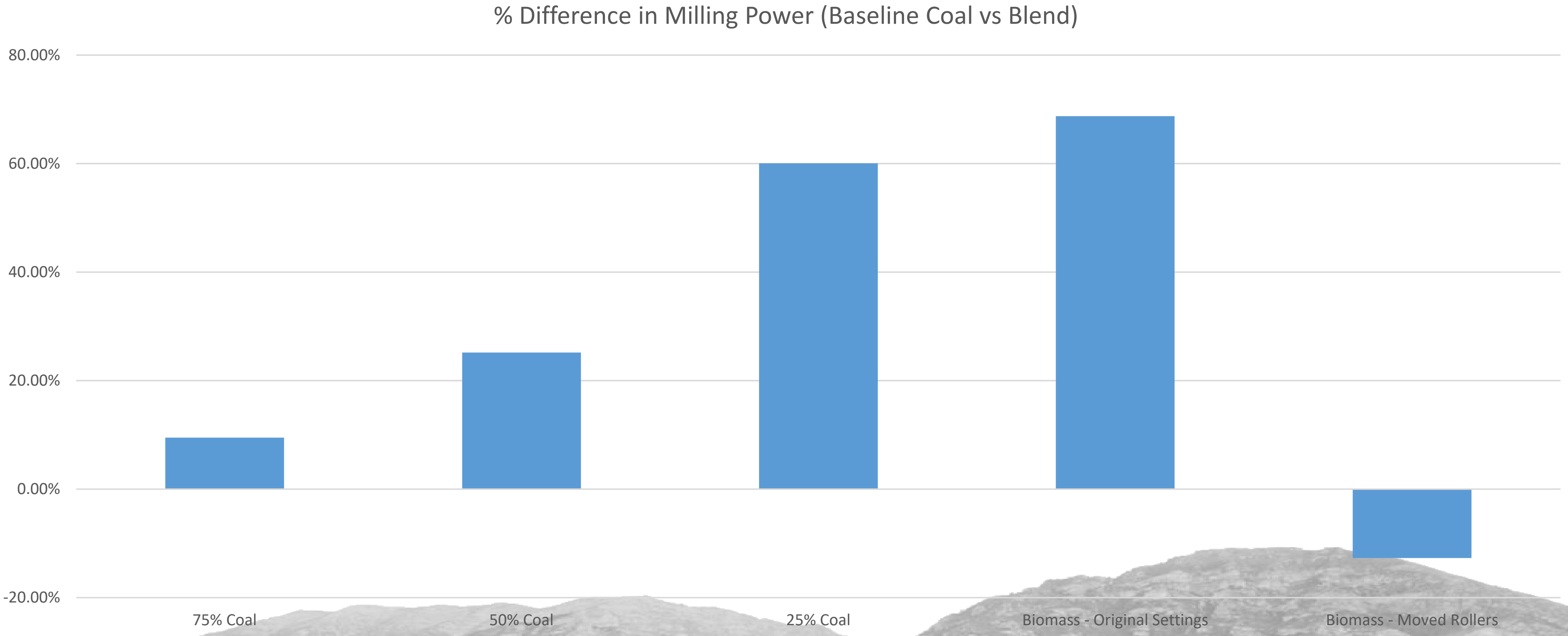

- Mill current increased with increasing biomass, until rollers were adjusted for 100% biomass

Coal Mill: Particle Size

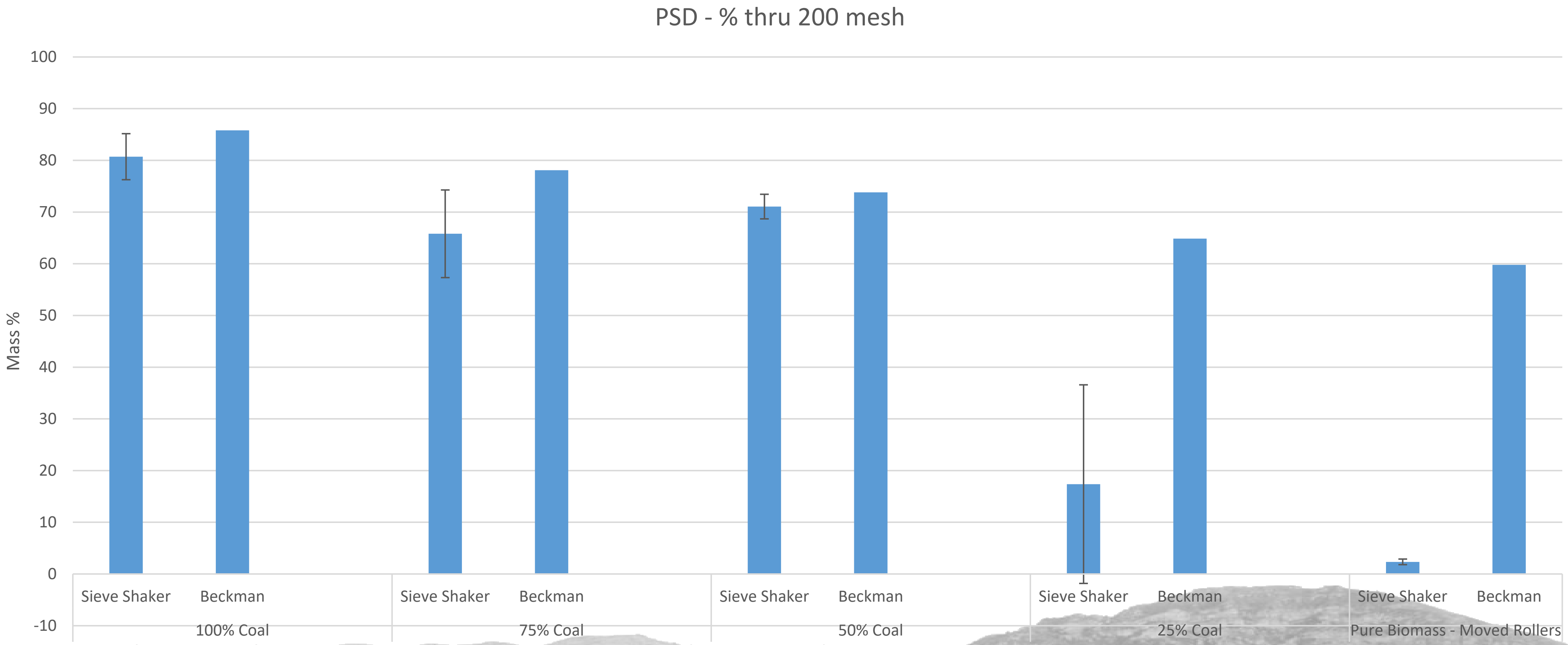

- Blending biomass with coal increases the particle size
- Sieve Shaker methodology was unreliable (likely due to wet weather conditions causing particles to agglomerate)

Coal Mill: Particle Size (Beckman Coulter LS230)

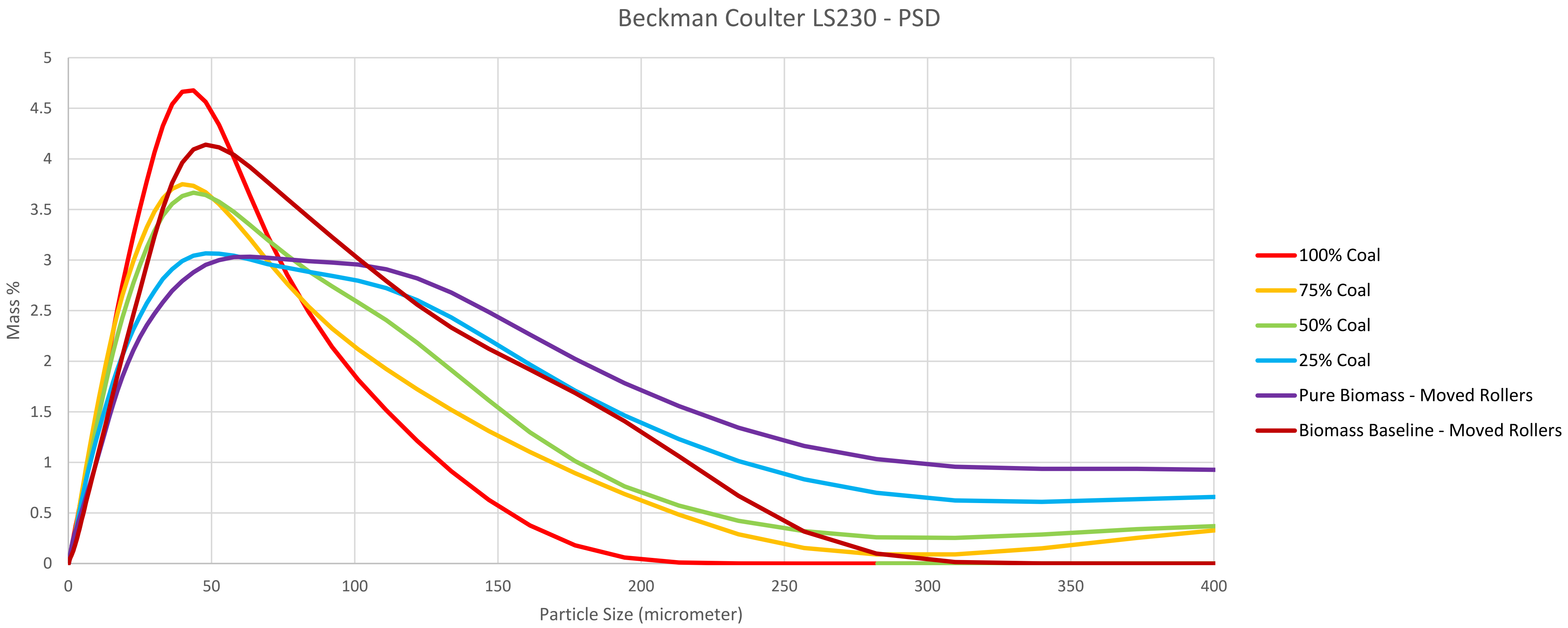

- Blends are bimodal and tend towards larger particle sizes

L1500

Particle Deposition & Combustion Behavior Experiments

L1500: Overview

Unique L1500 Capabilities:

- Realistic Burner Turbulent Mixing Scale
- Realistic Radiative Conditions
- Realistic Time – Temperature Profile

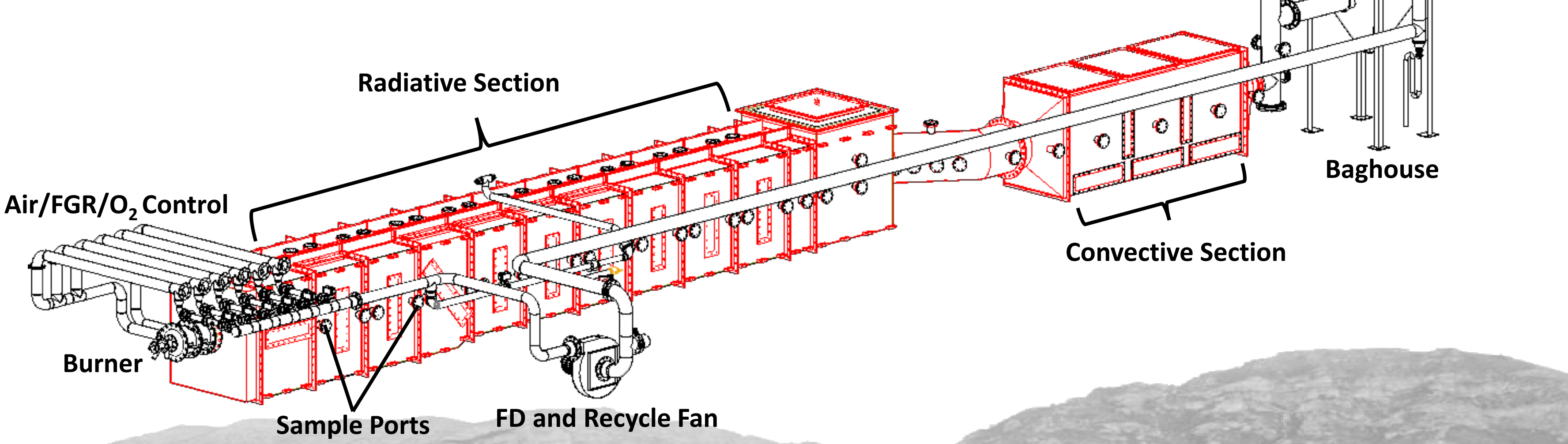

L1500: Coal Flame

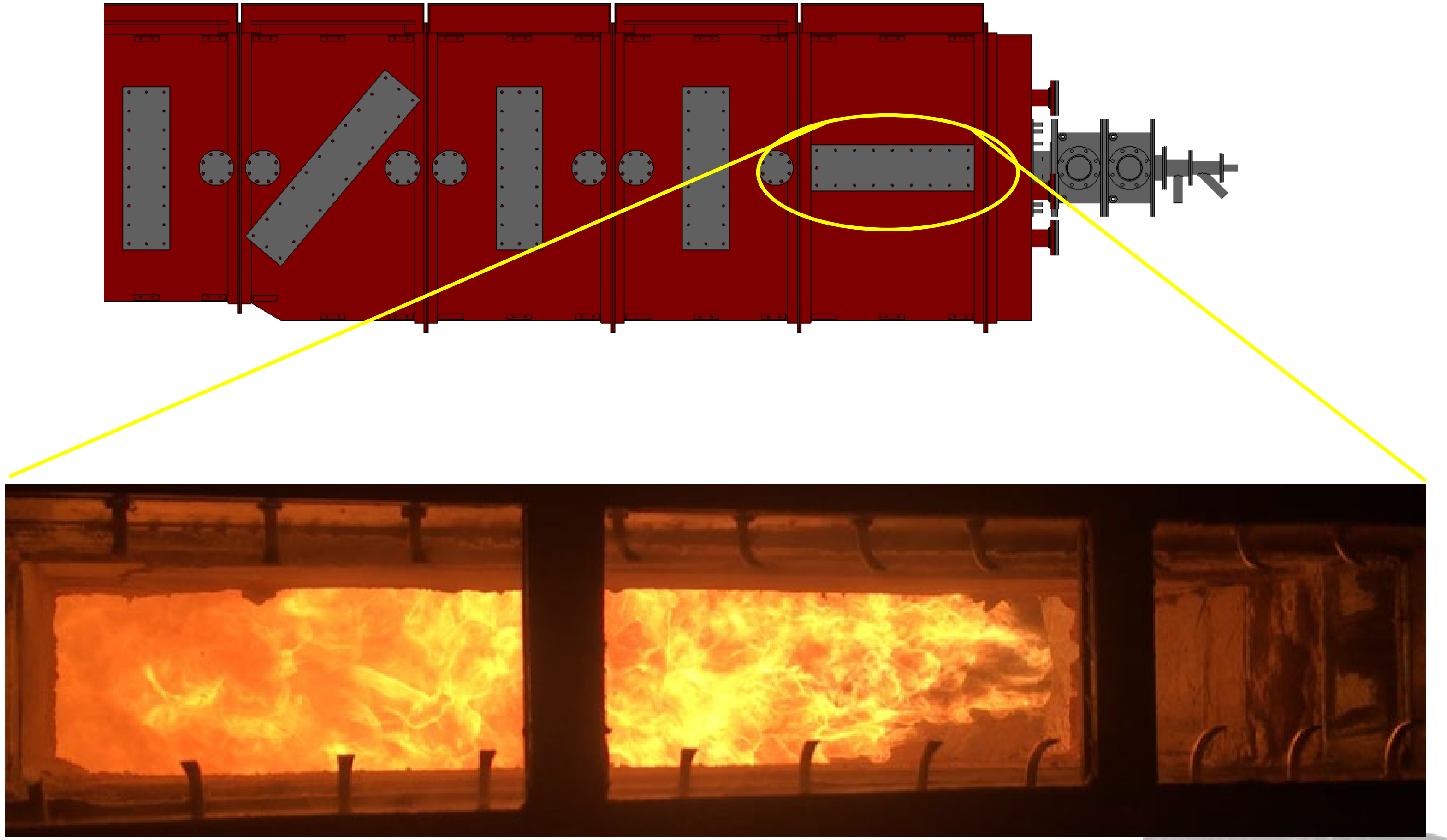

L1500: Particle and Deposit Measurements

Berner Low-pressure Impactor (BLPI)

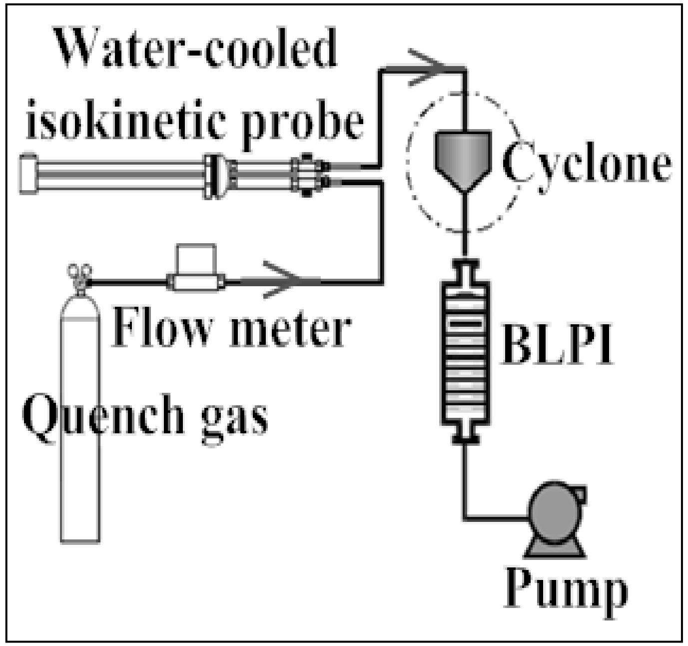

BLPI: 0.0324 – 7.33 µm
10 cutoff diameters

Collects size-segregated entrained ash samples for later gravimetric and chemical analysis

Scanning Mobility Particle Sizer (SMPS)
Aerodynamic Particle Sizer (APS)

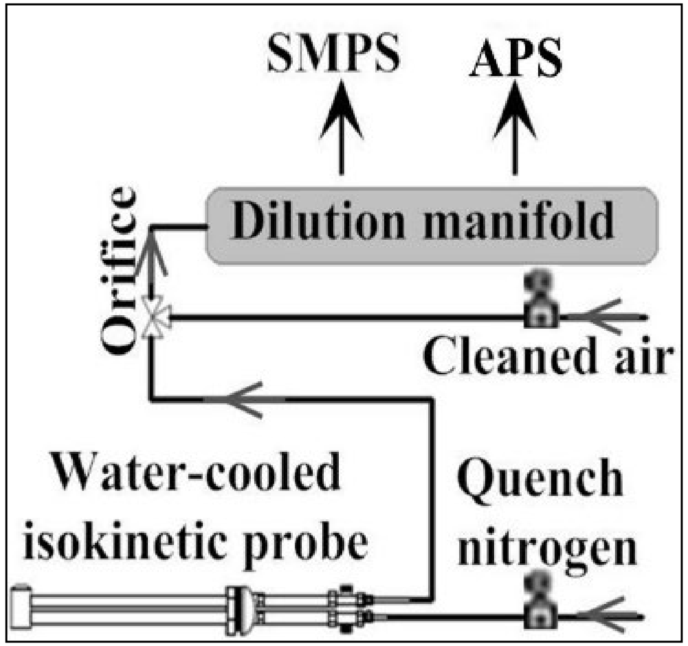

SMPS: 0.0143 – 0.6732 µm
APS: 0.532 – 20 µm

Collects real-time entrained particle size distribution data

Measuring Ash Particle Size

L1500: Particle and Deposit Measurements

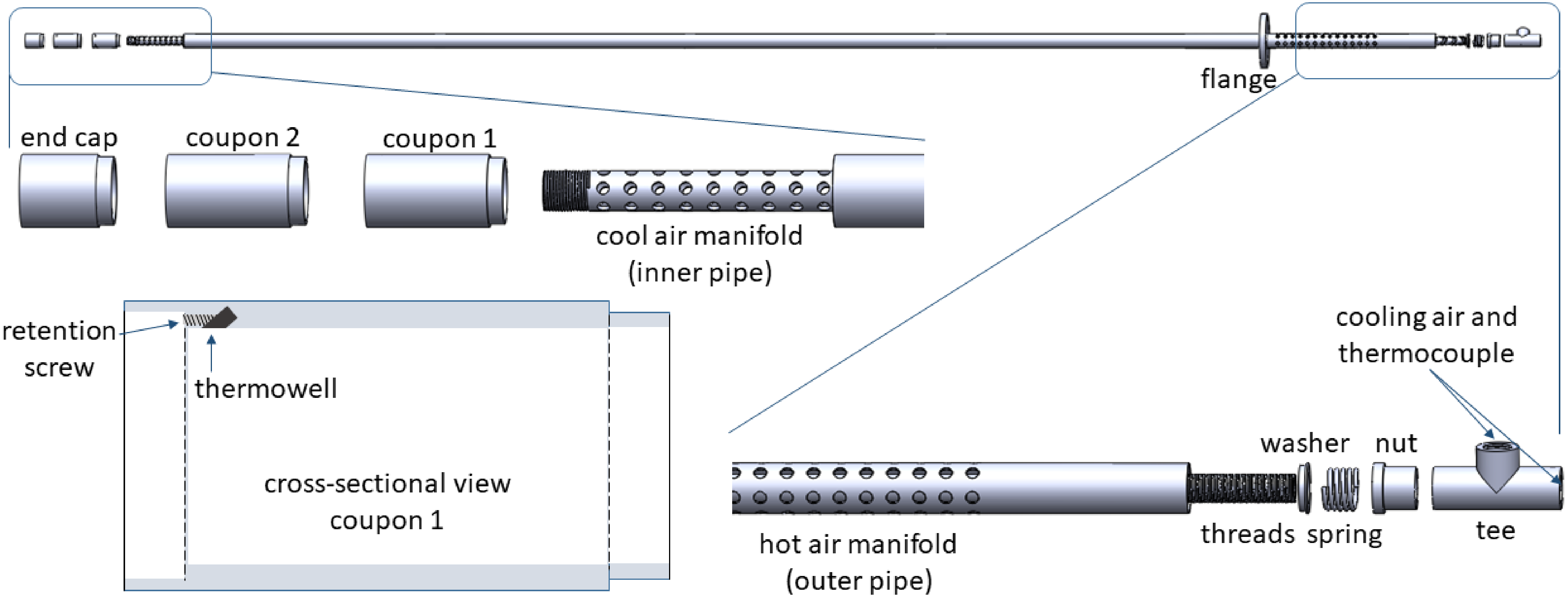

Measuring Deposition Rate

L1500: Particle and Deposit Measurements

- The probe was placed in such a way that the middle point of the two coupons was at the center of the combustor.
- The time variant deposition data was collected, but due to the low mass of the deposits, most of them were not useful in determining the rates.

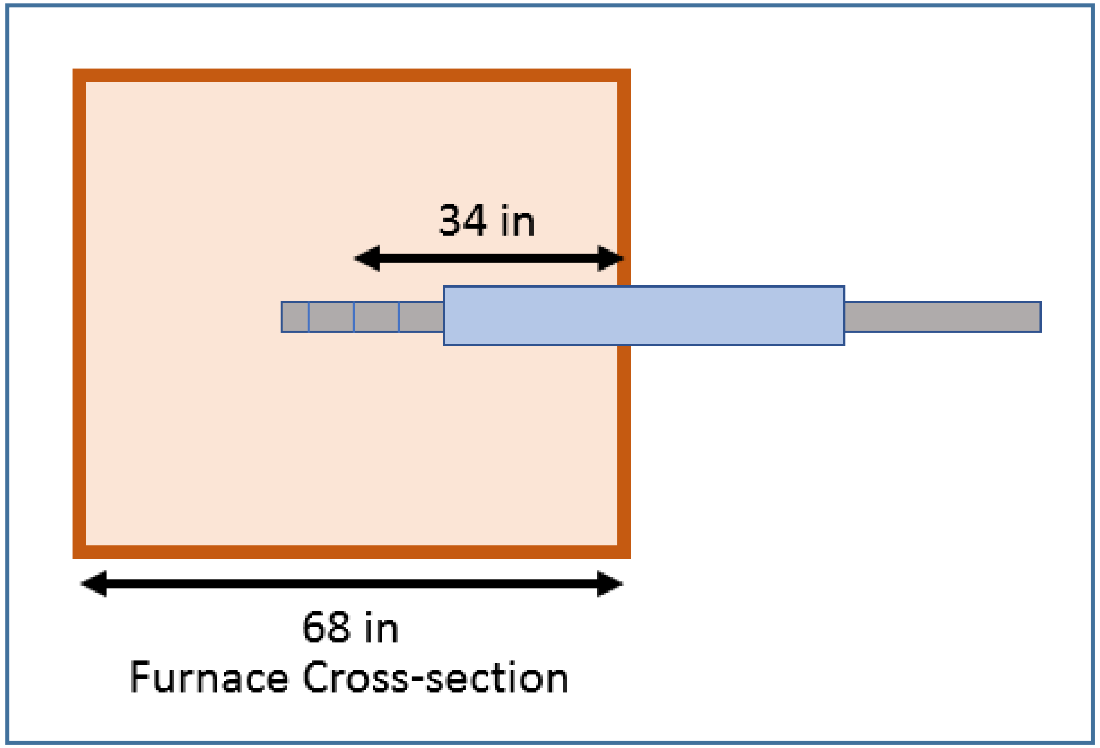

Probe Position

L1500: Fuel Analysis (Proximate)

		100% coal	75% coal	50% coal	25% coal	wood
As Rec	Moisture	3.72	2.77	4.13	3.8	3.83
	Ash	11.59	10.32	8.32	6.15	2.65
	Volatile	38.7	47.1	54.78	63.24	75.26
	Fixed C	45.98	39.82	32.77	26.81	18.25
	Sulfur	0.62	0.48	0.34	0.2	0.03
	BTU/lb	12226	11480	10581	9950	8956
Dry	Ash	12.04	10.61	8.68	6.39	2.76
	Volatile	40.2	48.44	57.14	65.74	78.26
	Fixed C	47.76	40.95	34.18	27.87	18.98
	Sulfur	0.64	0.49	0.35	0.21	0.03
	BTU/lb	12698	11807	11037	10343	9313
MAF	BTU/lb	14437	13208	12086	11049	9577

L1500: Fuel Analysis (Ultimate)

		100% coal	75% coal	50% coal	25% coal	wood
As Rec	Moisture	3.72	2.77	4.13	3.8	3.83
	C	68.1	64.61	59.62	56.92	51.73
	H	4.93	5.1	5.14	5.38	6.08
	N	1.3	1.06	0.79	0.57	0.23
	Ash	11.59	10.32	8.32	6.15	2.65
	S	0.62	0.48	0.34	0.2	0.03
	O	9.74	15.66	21.66	26.99	35.45
Dry	C	70.73	66.45	62.19	59.17	53.79
	H	5.12	5.25	5.36	5.59	6.32
	N	1.35	1.09	0.82	0.59	0.24
	Ash	12.04	10.61	8.68	6.39	2.76
	S	0.64	0.49	0.35	0.21	0.03
	O	10.11	16.11	22.6	28.06	36.86

L1500: Fuel Analysis (Ash Elemental)

	100% coal	75% coal	50% coal	25% coal	wood
Silica SiO2	52.81	50.06	46.78	43.82	35.93
Alumina, Al2O3	25.78	22.23	21.26	18.41	8.14
Titania,TiO2	1.07	1.07	0.86	0.74	0.43
Lime, CaO	7.54	8.89	10.22	12.5	24.29
Ferric Oxide, Fe2O3	4.17	4.66	6.28	6.53	11.61
Potassium Oxide, K2O	0.51	1.01	1.66	2.69	7.07
Magnesium Oxide, MgO	0.02	2.16	2.2	2.41	1.22
Sodium Oxide, Na2O	1.85	1.84	1.68	1.62	1.43
Sulfur Trioxide, SO3	5.78	7.12	7.54	7.8	4.03
Phosphorus Pentoxide,P2O5	0.25	0.38	0.41	0.63	1.28
Barium Oxide, BaO	0.13	0.13	0.13	0.13	0.16
Manganese Dioxide, MnO2	0.02	0.12	0.24	0.4	1.22
Strontium Oxide, SrO	0.16	0.15	0.14	0.13	0.1
Undetermined	-0.09	0.18	0.6	2.19	3.09

L1500: Fuel Analysis (Summary)

- The Proximate, Ultimate and Ash analysis were performed by Horizon Labs Inc., Price, Utah.
- The values obtained from the analysis followed an almost linear pattern as one goes from 100% coal to 100% wood, indicating that the mixtures of fuels were accurate
- These results were used to determine the fuel feed rate and the air feed rate during the combustion experiments.

L1500: Measured Operating Conditions

	100% coal	75% coal	50% coal	25% coal	wood	Wood (5000)
Firing rate (million BTU/hr)	3120212	2976335	2958369	3115292	3113714	3117521.34
Solid Fuel Feed (lb/hr)	255.21	259.26	279.59	313.09	347.66	348.09
Primary Air (lb/hr)	472.67	512.87	548.05	577.20	649.65	648.80
Primary Inlet Temp (°F)	85.86	92.93	105.50	105.86	123.61	116.94
Inner Secondary Air (lb/hr)	461.82	405.70	424.79	413.83	324.18	389.82
Inner Secondary Air Temp (°F)	511.95	524.48	514.92	527.56	523.85	528.96
Inner secondary Air Swirl (%)	75	75	75	75	75	75.00
Outer Secondary Air (lb/hr)	1079.0	941.82	990.09	965.39	755.18	910.27
Outer Secondary Air Temp (°F)	503.08	527.57	525.13	525.87	526.17	527.66
Outer Secondary Air Swirl (%)	75	75	75	75	75	75.00
Staging Air (lb/hr)	578.59	546.19	551.25	550.49	518.44	554.58
Staging Inlet Temp (°F)	70.75	73.12	63.82	71.79	78.01	68.78
CO2 (%)	8.024	8.245	8.412	8.406	8.36	8.01
O2 (%)	4.63	4.57	4.52	4.69	5.25	5.96
SO2 (%)	278.61	187.83	71.39	51.32	1.66	-0.94
S3Wall (F)	2418.12	2312.79	2330.27	2279.85	2226.53	2196.98
Furnace pressure (H2O)	-0.52	-0.57	-0.49	-0.43	-0.55	-0.37
Leakage (lb/hr)	389.87	413.94	225.80	408.17	767.84	652.81

This table will be updated with calculated air in-leakage (the rate that makes the combustion stoichiometery and the measured %O_2 consistent)

L1500: Measured Operating Conditions

- Wood had higher leakage value after the first 5000 points.
- The total air was lower in wood compared to the other blends.
- The air amount in first 5000 points was comparable to the total air in the other blends.
- Fuel rate in wood (first 5000 and total were consistent).
- Since air was low, Oxygen was also low.
- Furnace pressure was higher in first 5000 points which might explain the discrepancy.

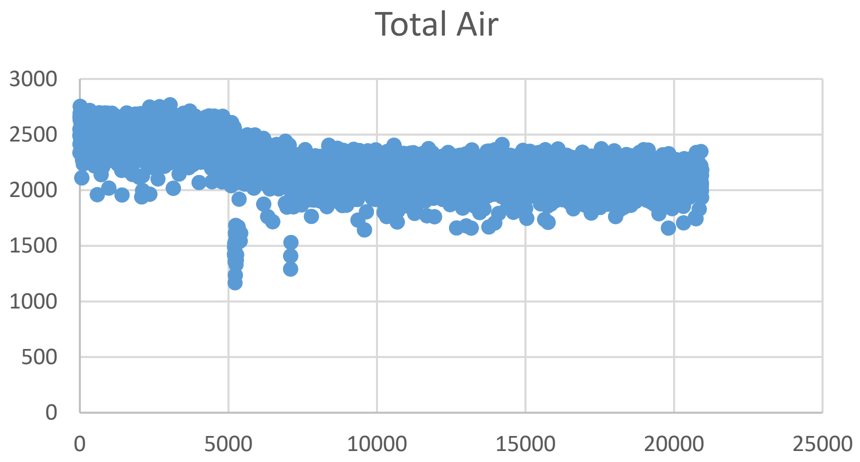

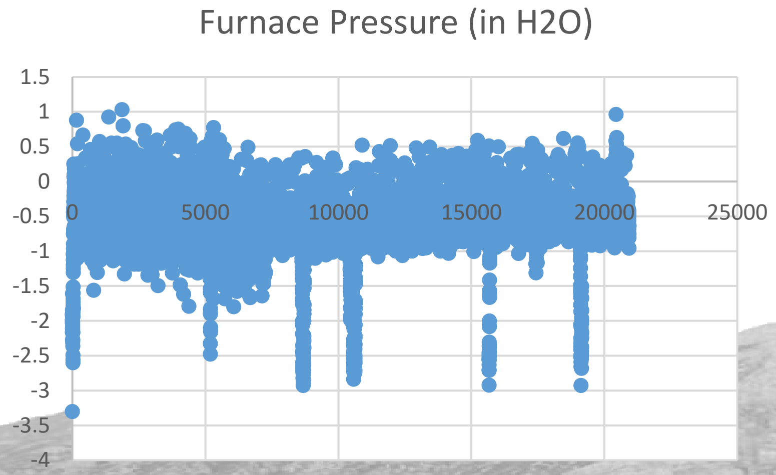

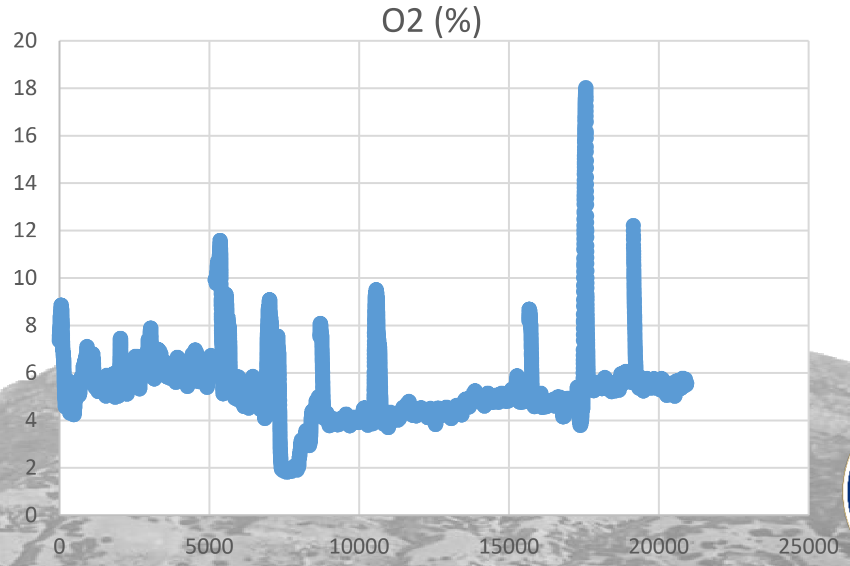

L1500: Ash Measurement Summary

Coal (100% coal)	**Coal75 (Bio25)** (75% coal, 25% biomass)	**Coal50 (Bio50)** (50% coal, 50% biomass)	**Coal25 (Bio75)** (25% coal, 75% biomass)	**Bio** (100% biomass)
Aerosol & Deposit Port 7 Port 10	Aerosol & Deposit Port 7 Port 10	Aerosol & Deposit Port 7 Port 10	Aerosol & Deposit Port 7 Port 10	Aerosol & Deposit Port 7 Port 10

L1500: Ash Deposit Pictures (90 minute)

	Port 7	Port 10
100% Coal		
75% Coal		
50% Coal		
25% Coal		
0% Coal		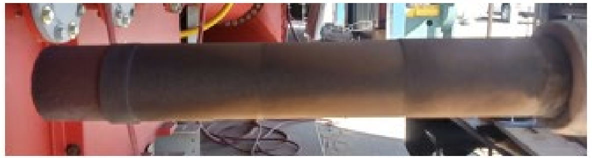

L1500: Ash Deposition in Port 7

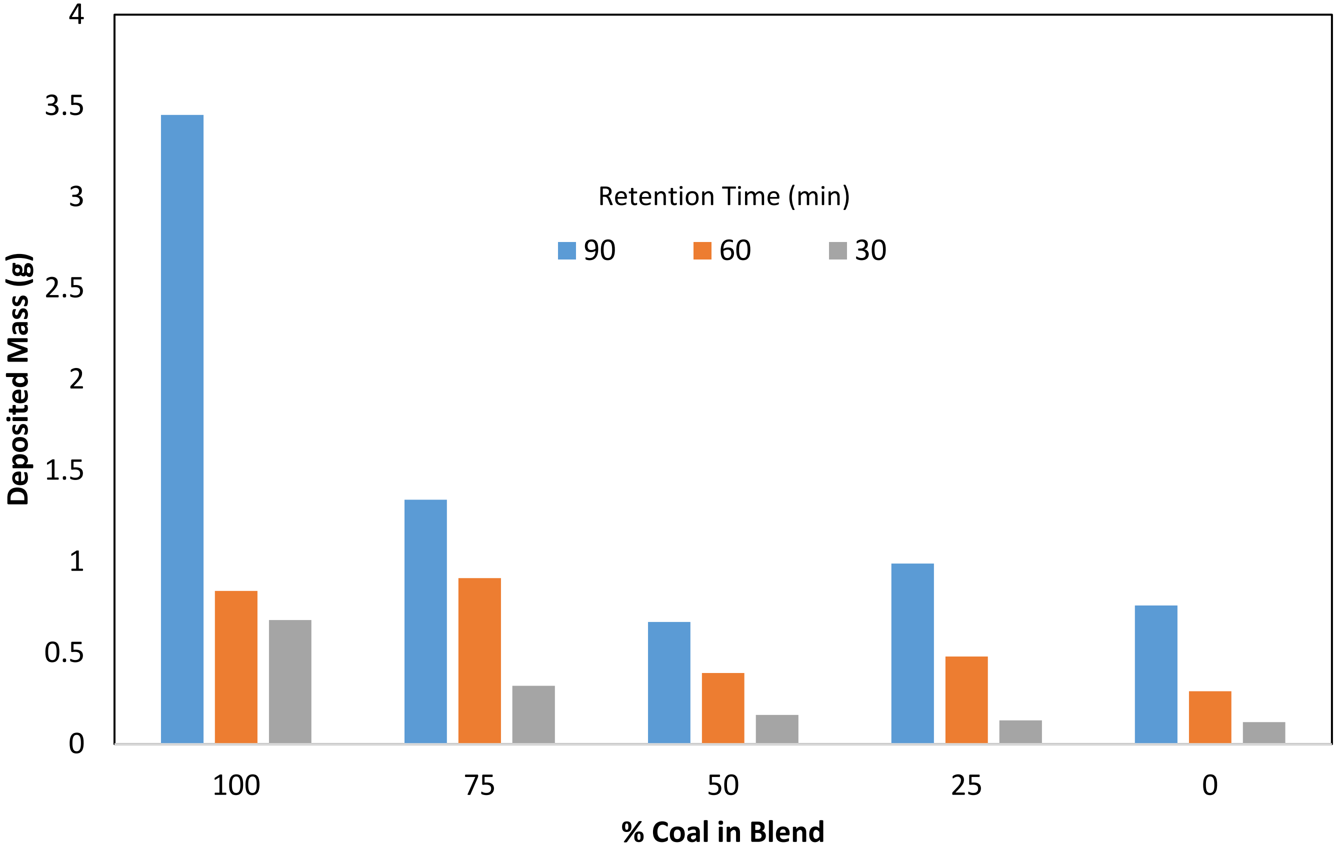

- With higher percentage of coal in the fuel blend, higher amount of deposited ash was observed in general.
- 100% Coal has around 5 times more ash than 100% wood which is consistent with the observation.

L1500: Ash Deposition in Port 10

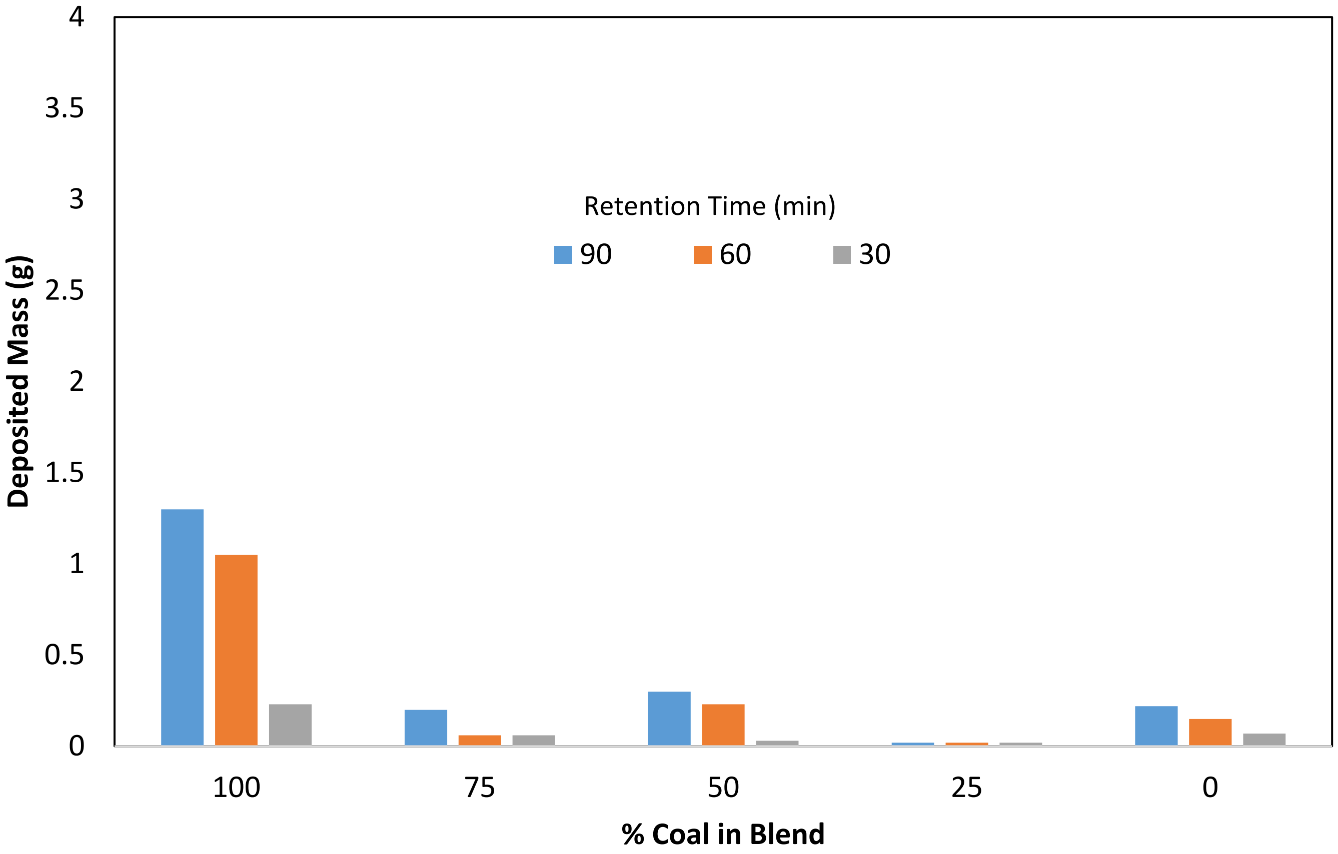

- 25% coal blend showed very low ash deposition which is difficult to explain at this point.

- 100%, 50% and 0% coal showed that the initial rate of deposition is low (<30 minutes). Most of the deposition occurs between 30 and 60 minutes and after 60 minutes, the deposition rate falls.

L1500: Ash Deposition (Observation)

- The picture represents the ash collected from 100% coal blend in port 7 for 90 minutes.
- The upper part represents the ash deposited on the upstream side of the coupons and the lower part represents the downstream side ash.

L1500: Ash Deposit Micrographs (Coal 60 min)

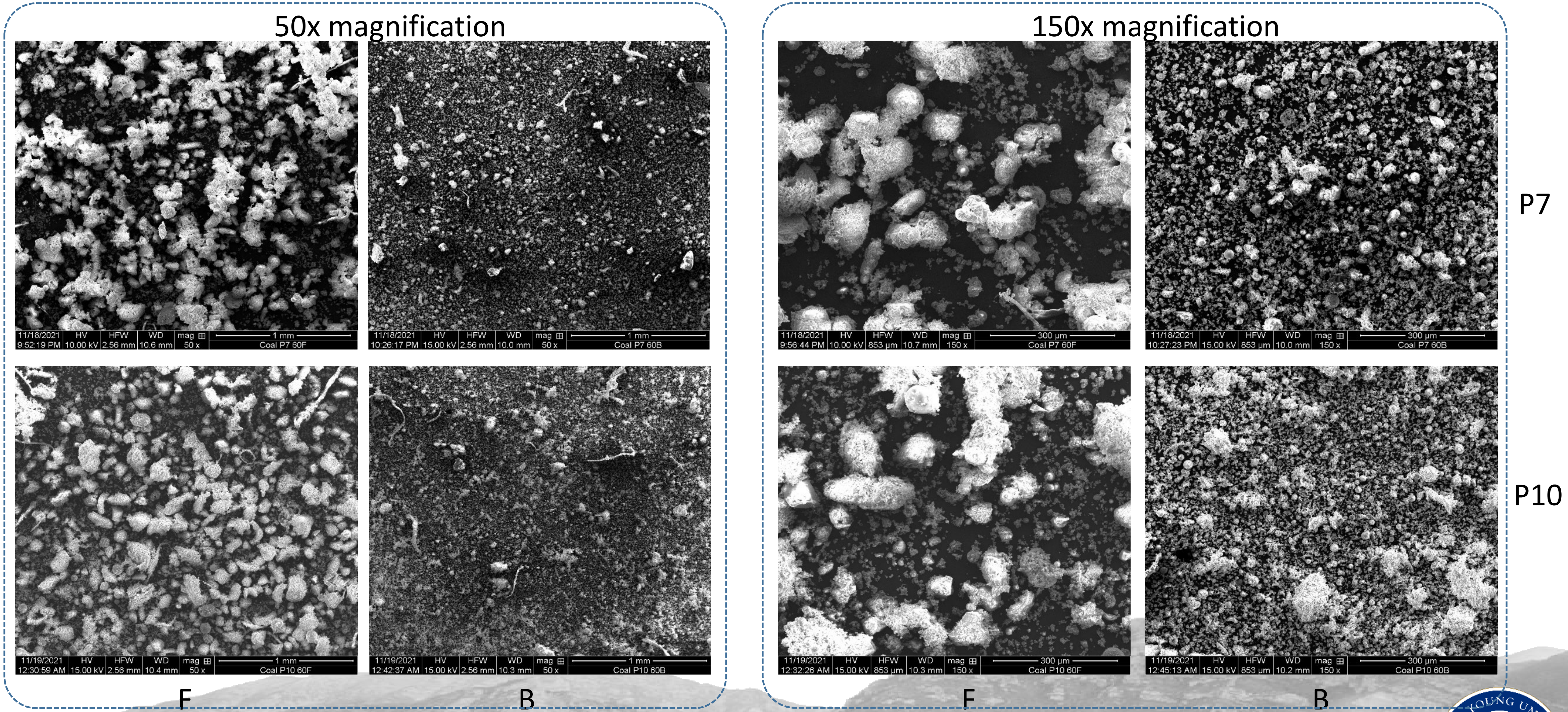

- F samples: forward deposits, upstream of flue gas on coupon surface
- B samples: backward deposits, downstream of flue gas on coupon surface

L1500: Ash Deposit Micrographs (All Fuels, 60 min, 50x)

P7

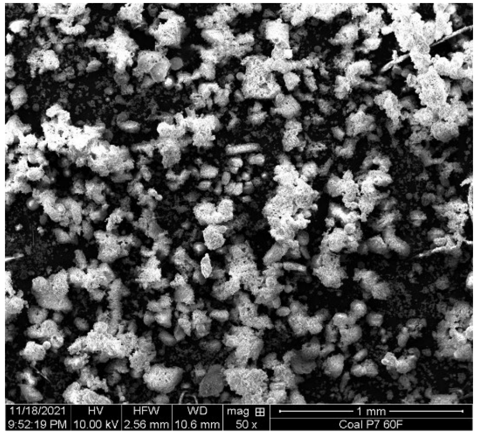

Coal (F)

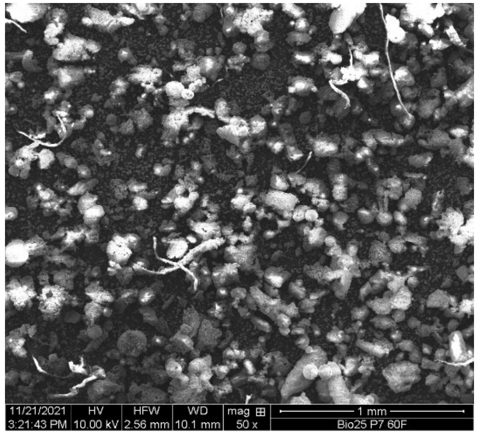

Bio25 (F)

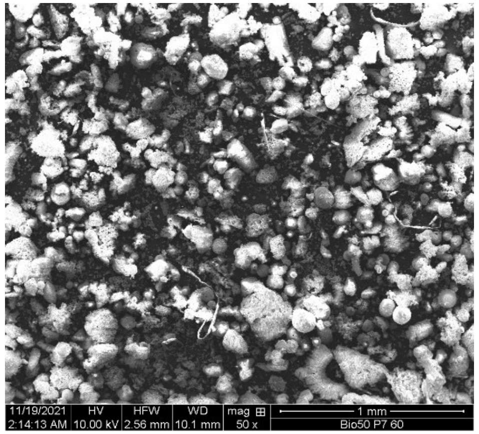

Bio50

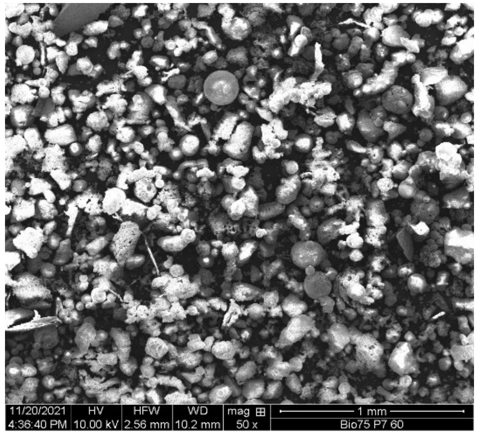

Bio75

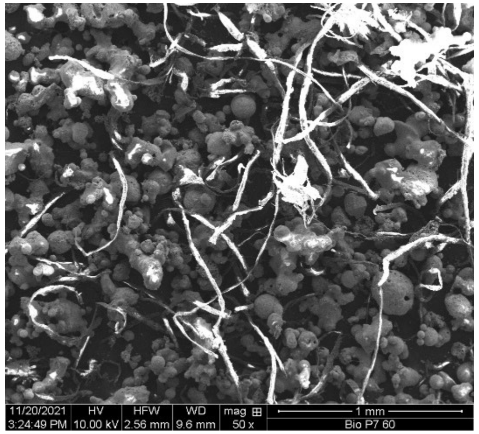

Bio

P10

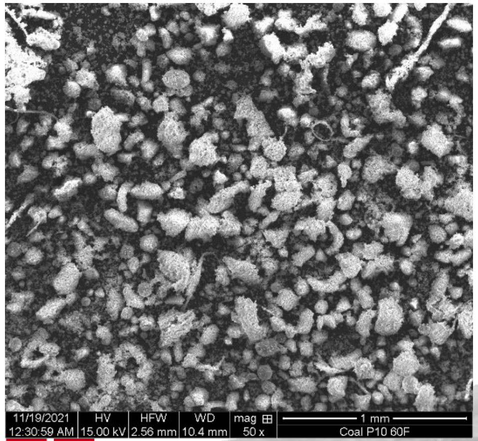

Coal (F)

Bio25

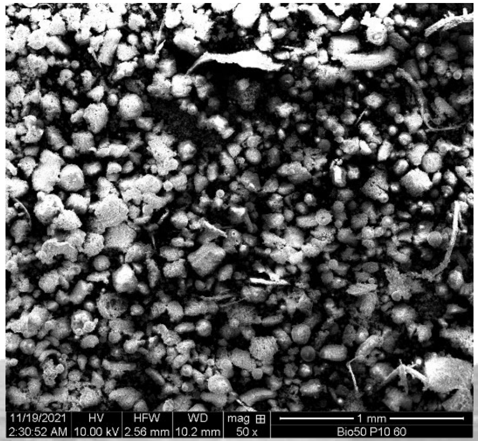

Bio50

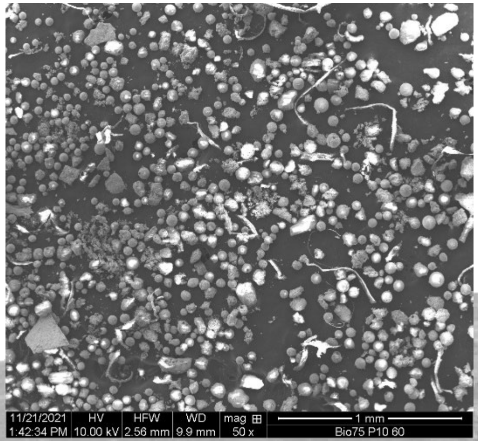

Bio75

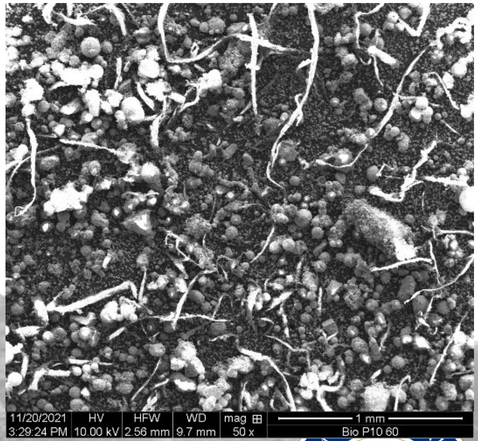

Bi

- Biomass and co-firing deposits show organic contents, millimeter long

L1500: Ash Deposit Micrographs (All Fuels, 60 min, 150x)

P7

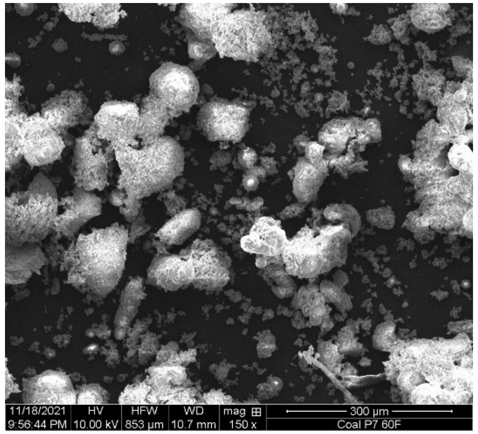

Coal (F)

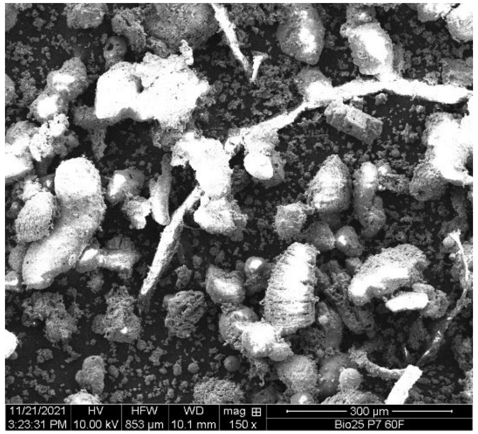

Bio25 (F)

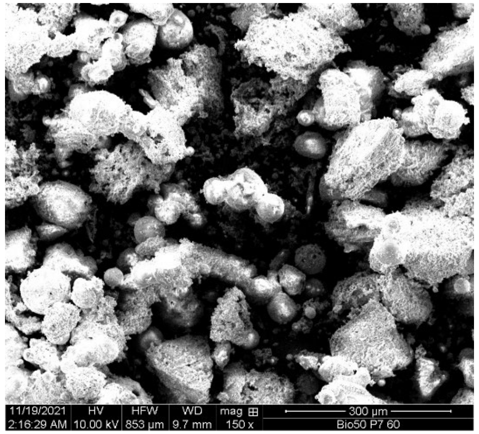

Bio50

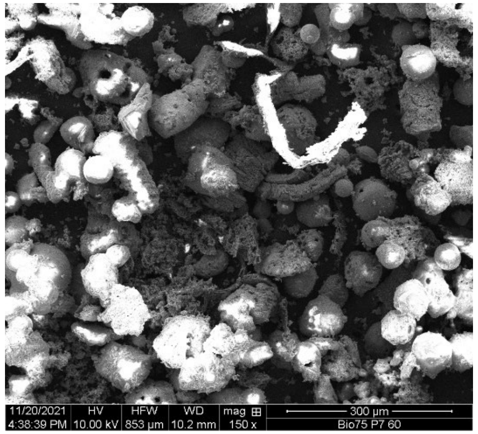

Bio75

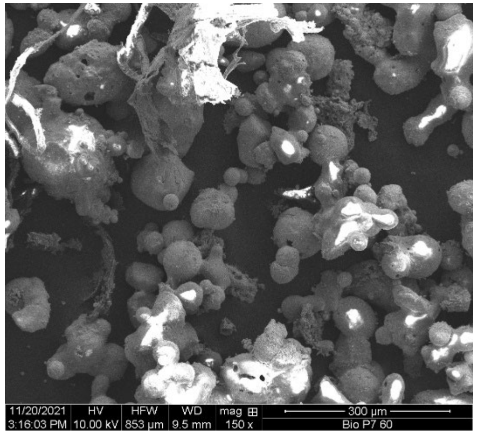

Bio

P10

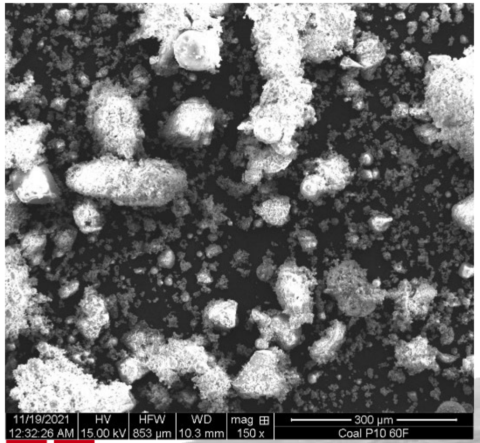

Coal (F)

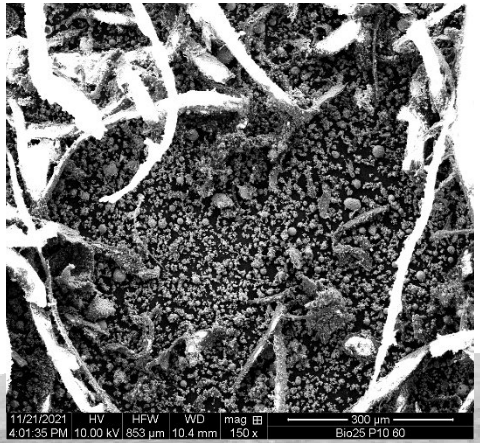

Bio25

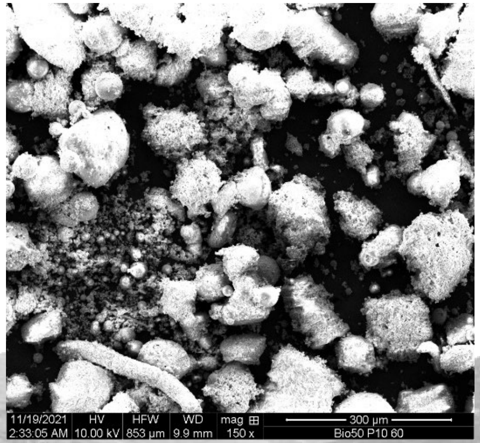

Bio50

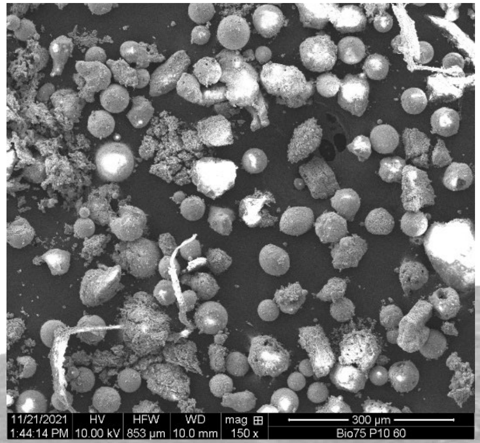

Bio75

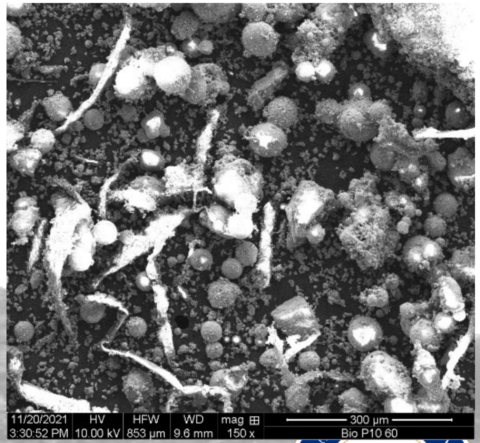

Bio

THE UNIVERSITY OF UTAH

BYU

L1500: Deposit Composition

100 % Biomass, Port 7, 30 min

	Full area	1	2	3	4	5	6	7	8	9
C	26.5	0.9	2.1				49	48.4	53.4	C K
O	42.8	50.9	50.7	46.9	45.6	35.6	48.4	48.4	37.7	O K
Na	1.6	2.5	2.5	1.8	2.9	2.6				
Mg	0.9	0.6	1.3	2.2	1.9	1.3				
Al	2.4	1.4	4.2	2.3	6.4	1.8	1.1	1.3	0.8	
Si	9.9	34.7	20.3	13.1	15.5	8.9	1.5	1.9	2.3	1.4
S				2.6	4.1	8.4				
K	5.6	6.3	7.2	5.3	13.7	22.3			2	
Ca	7.4	2.1	10	23.7	7.8	18.3			3.9	
Fe				2.1	2.1	0.8				
As			0.6							
Mo	2.9	0.6	1.1							
Tm										2.4

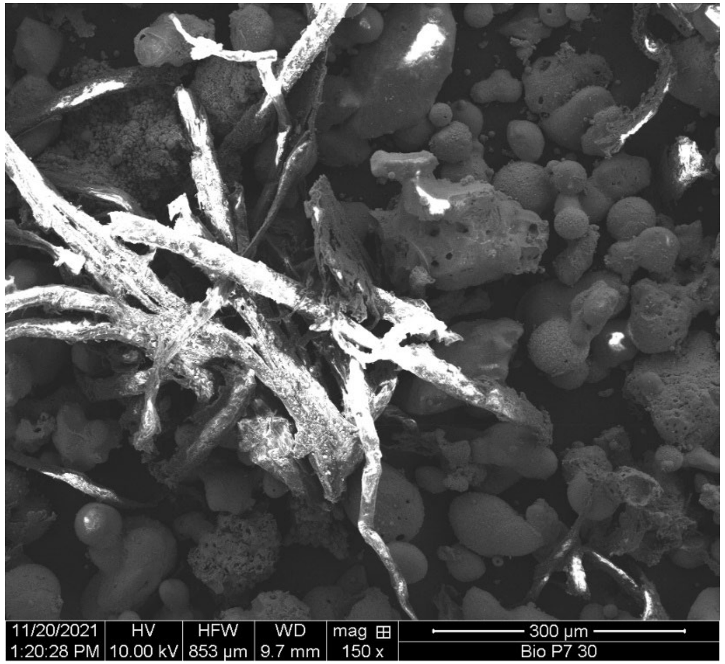

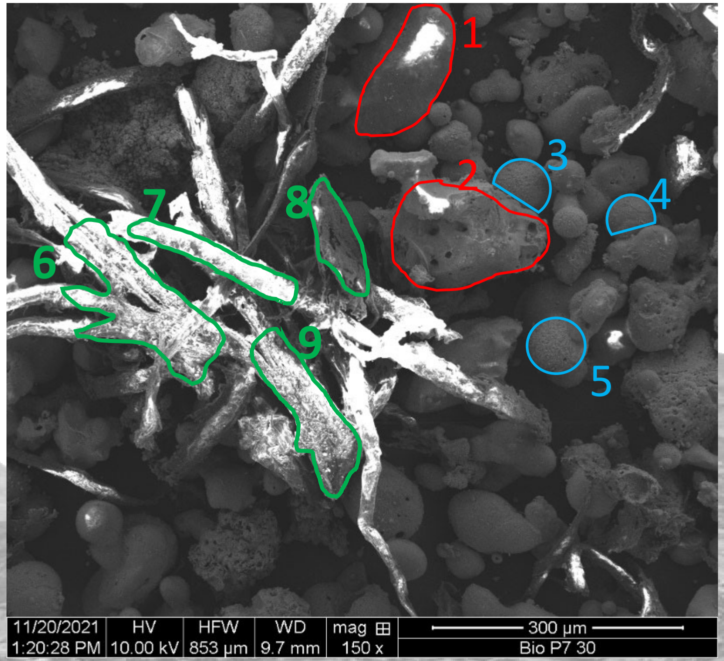

- Red 1,2: residual ash, Si, O
- Blue 3-5: vaporized ash, Si, S, K, Ca, O
- Green 6-9: organic content, C, O

L1500: Deposit Compositions (100% Coal)

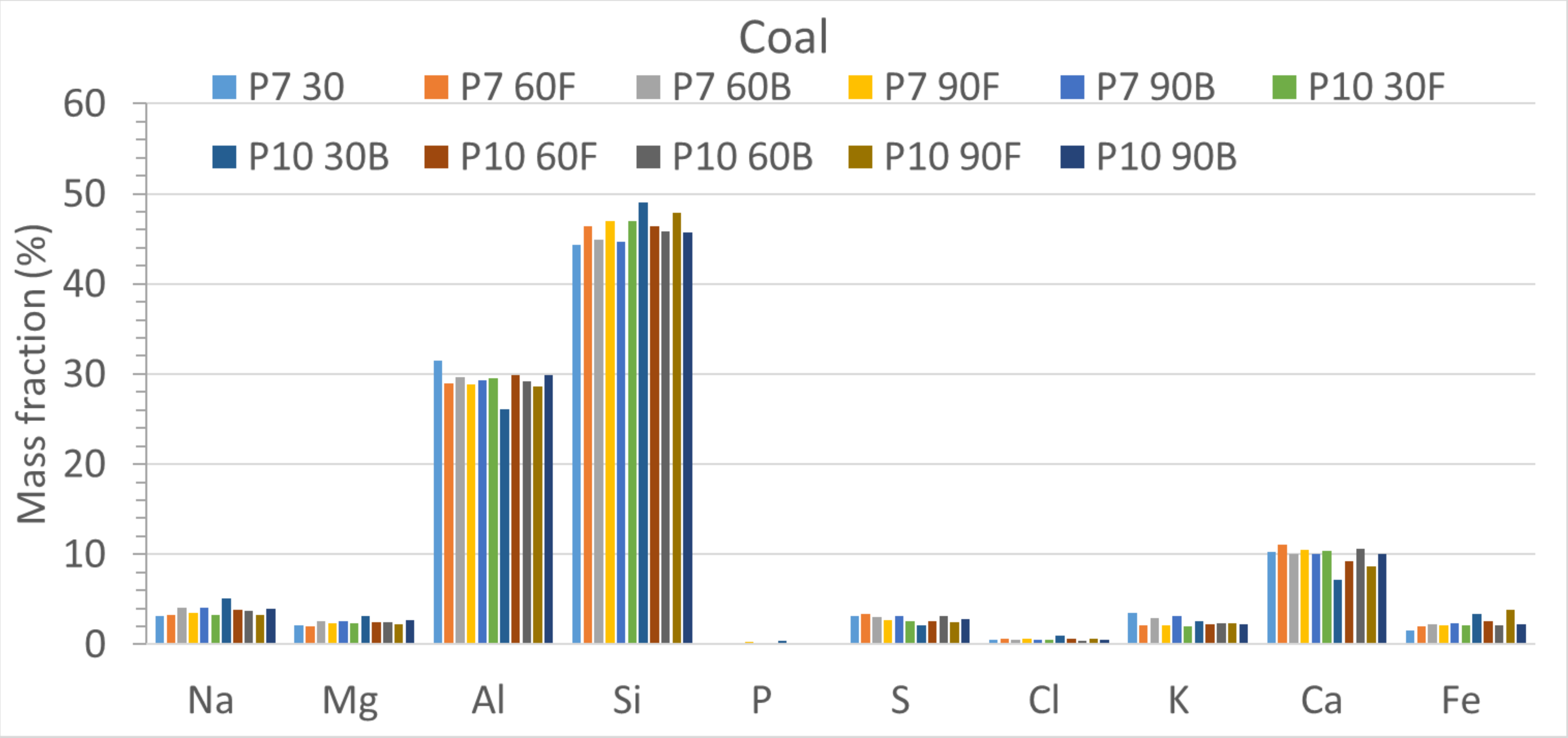

L1500: Deposit Compositions (75% Coal)

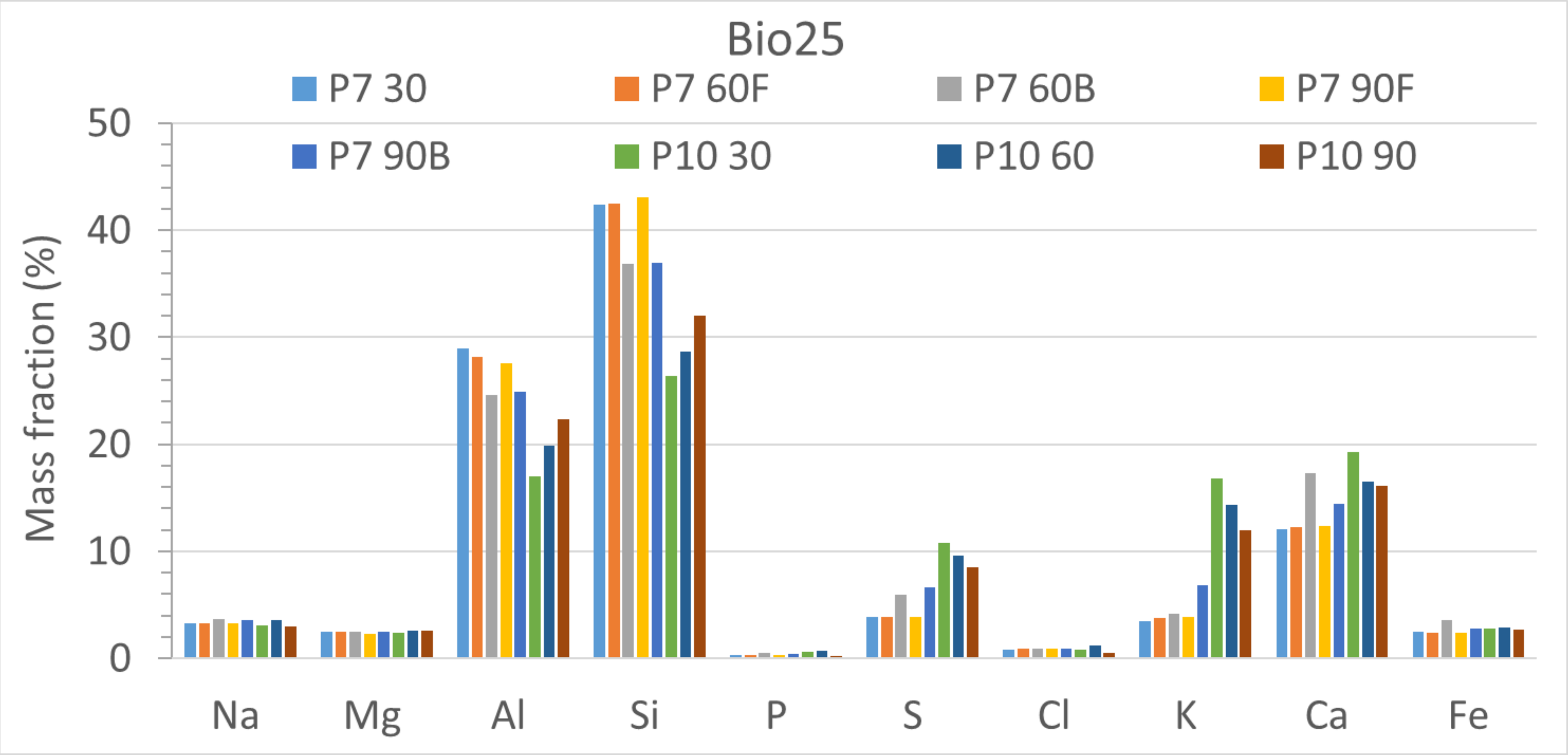

- P7 samples have more Al, Si while P10 more S, K and Ca
- P10 sample shows more small vaporized ash particles (Page 13)
- P10 compositions are time-dependent

L1500: Deposit Compositions (50% Coal)

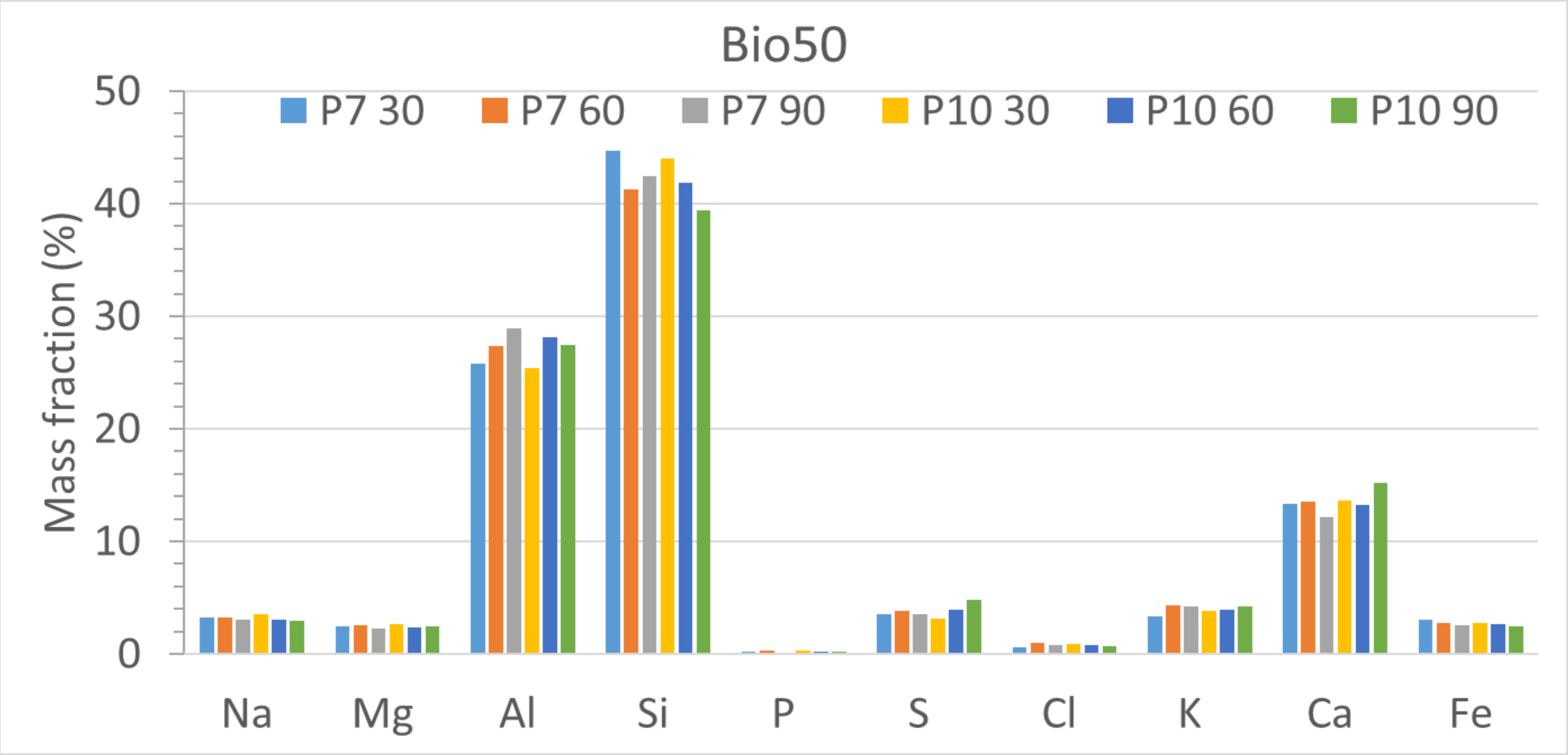

P7 and P10 samples do not show significant differences

L1500: Deposit Compositions (25% Coal)

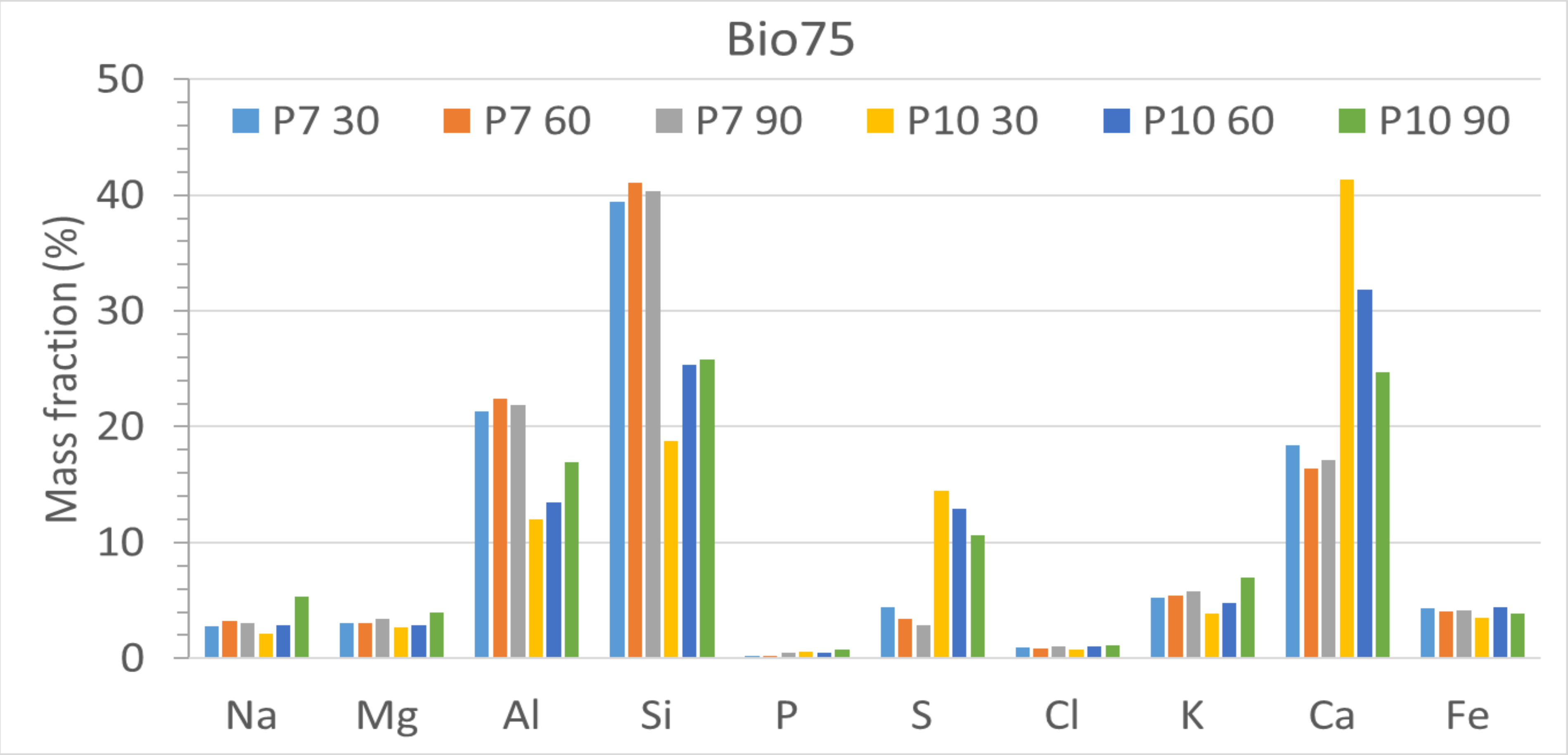

- P7 samples have more Al, Si while P10 more S, K and Ca
- P10 sample show more small vaporized ash particles (Page 13)
- P10 compositions are time-dependent

L1500: Deposit Compositions (100% Biomass)

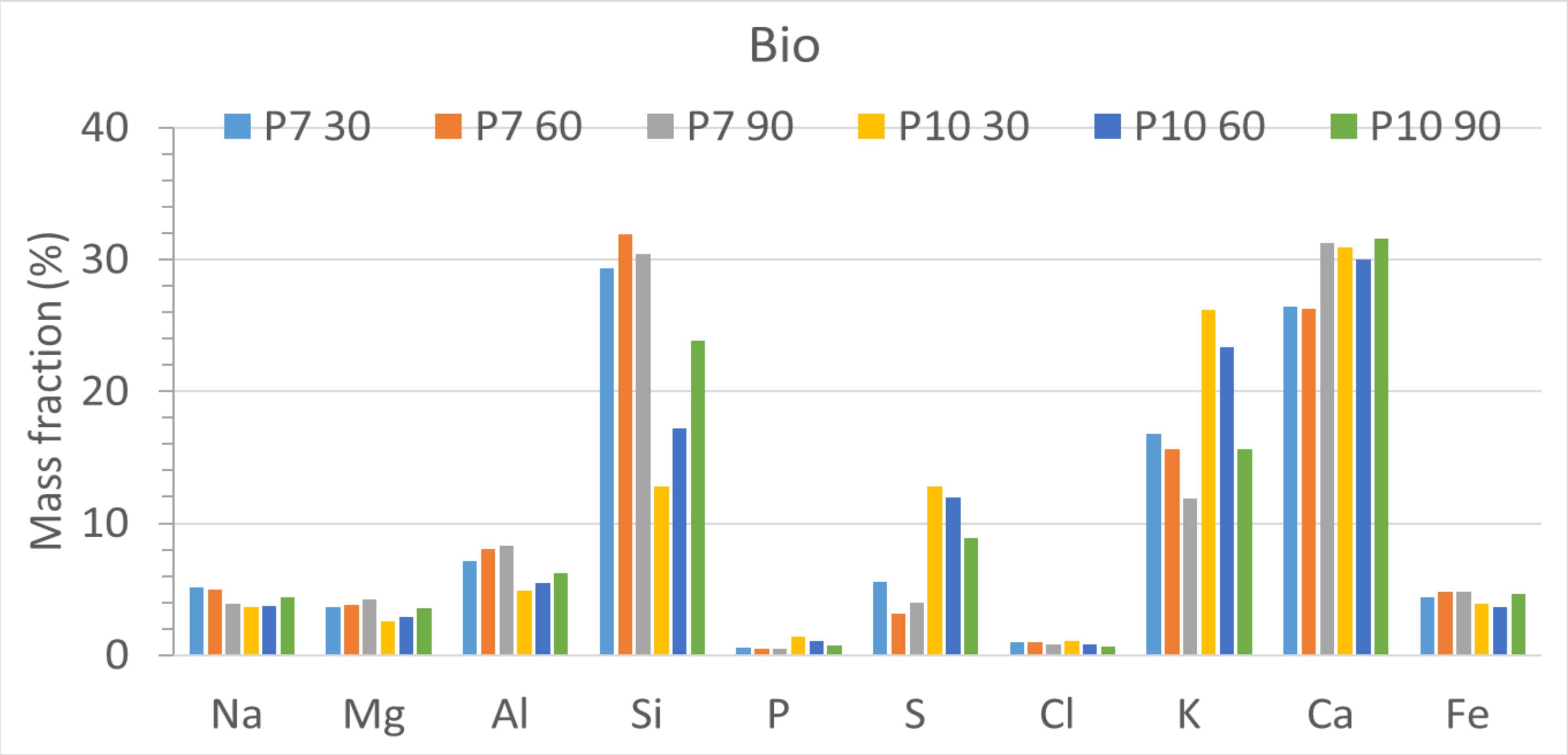

- P7 samples have more Al, Si while P10 more S, K and Ca
- P10 sample shows more small vaporized ash particles (Page 13)
- P10 compositions are time-dependent

L1500: Deposit Compositions (All Fuels, 60 min)

Port7

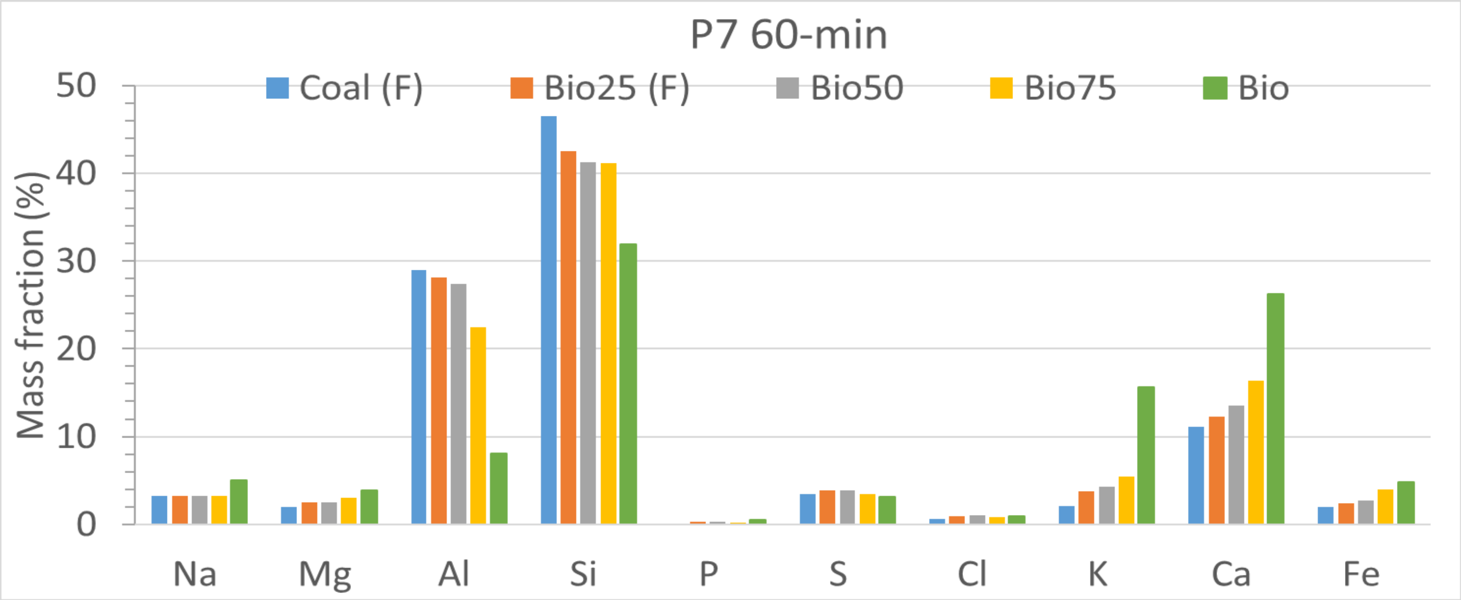

Port10

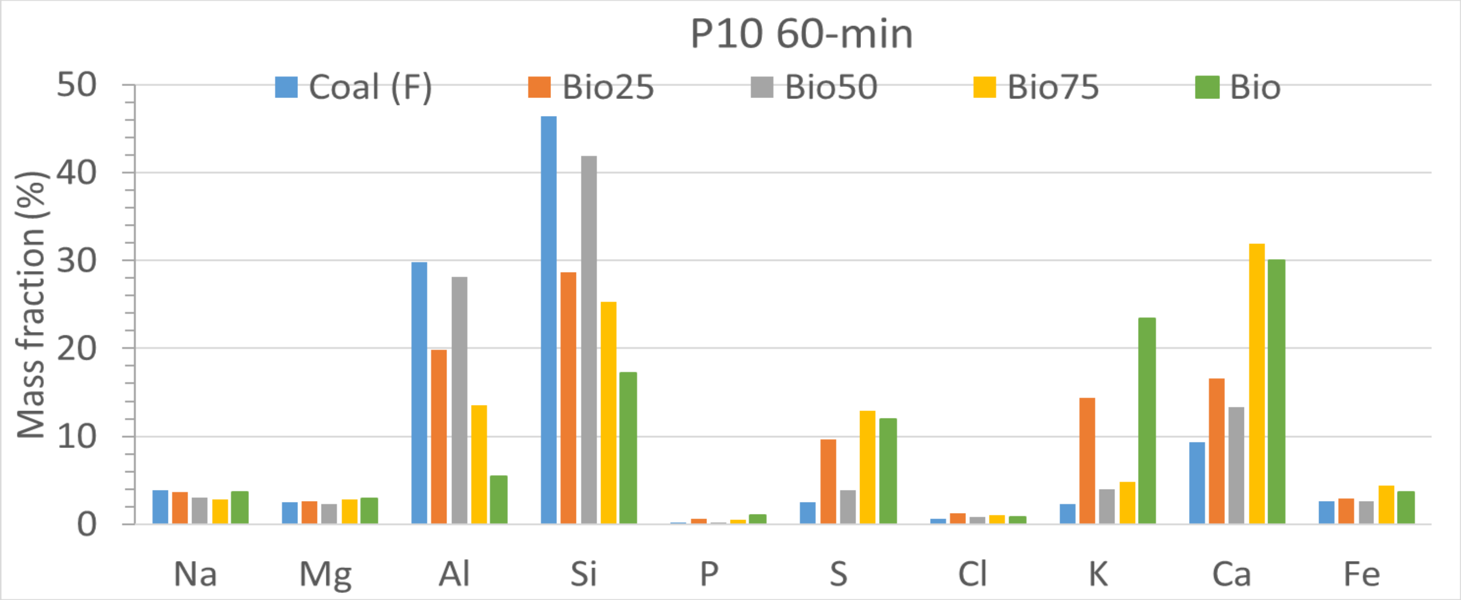

- In general, with higher biomass mixing ratio, less Al, Si and more S, K, Ca, Fe are shown in the formed ash deposits
- The Bio25 P10 sample shows high K, Ca and S contents, possibly being originated from the organically bound minerals from biomass fuel (Page 12)

Downstream vs. Upstream Ash

- Downstream ash had higher percentage of Na and K in general.
- Na and K are important contributors to condensation.
- Due to inertial impaction these alkali metal salts are diluted in the upstream ash.

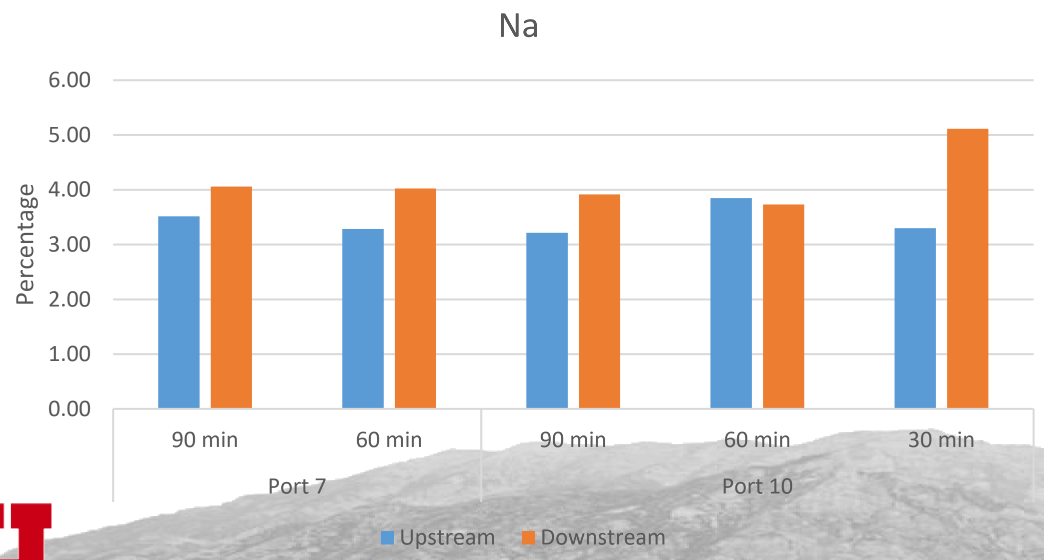

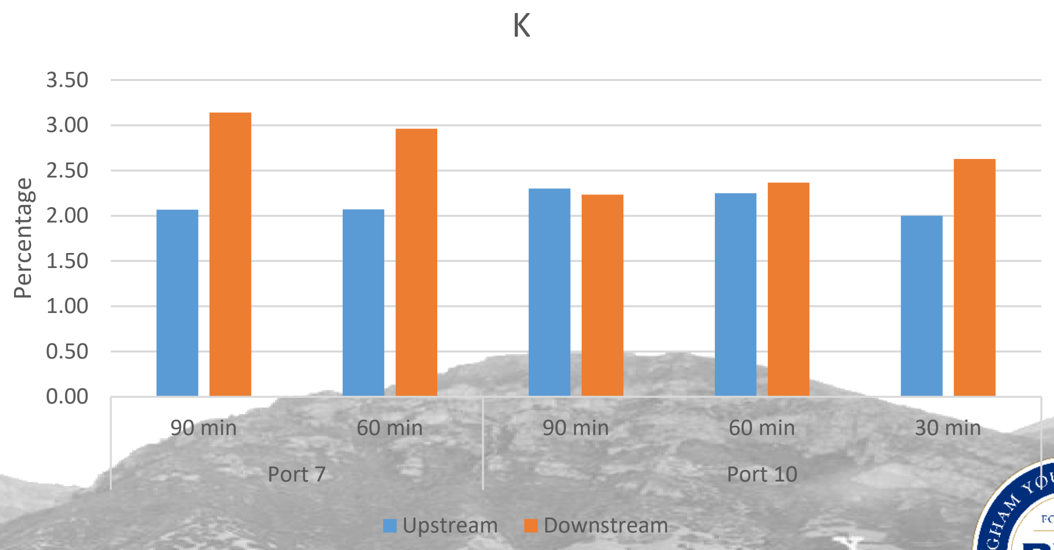

L1500: Deposit Load Cell Data (50% Coal, Port 7, 90 min)

- Data for the last 60 minutes.
- 2.5% variation in load cell data which should be at least 30 gram.
- Ash deposition on coupon is 0.67 grams.
- Data normalized for 0.67 grams. (Avg of first 500 points = 0 and last 500 points =0.67)

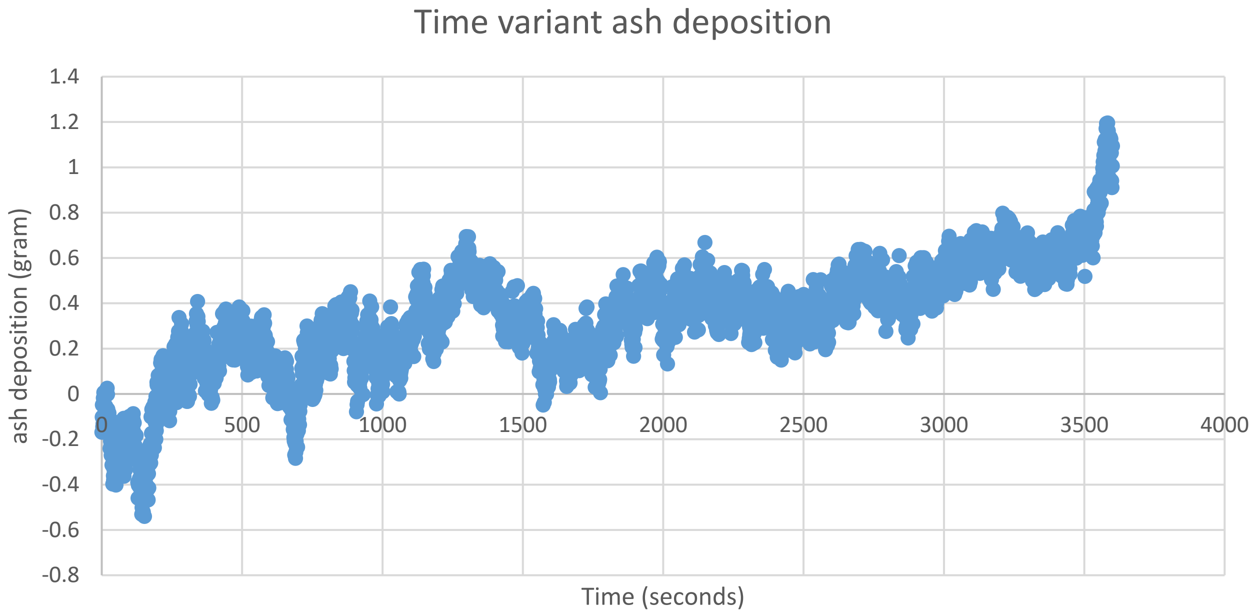

L1500: Deposit Analysis Summary

- Ash deposition amount increased with increasing percentage of coal in the fuel blend.
- Deposition on the downstream side of the coupon had much smaller particles than on the upstream side as inertial impaction is minimum on the downstream side.
- Upstream and downstream side deposited particles had very similar compositions, but upstream side had a marginally higher amount of silicon and downstream side had a marginally higher amount of potassium and sodium for 100% coal.

L1500: Ash Aerosol Analysis (Size Segregated Comp.)

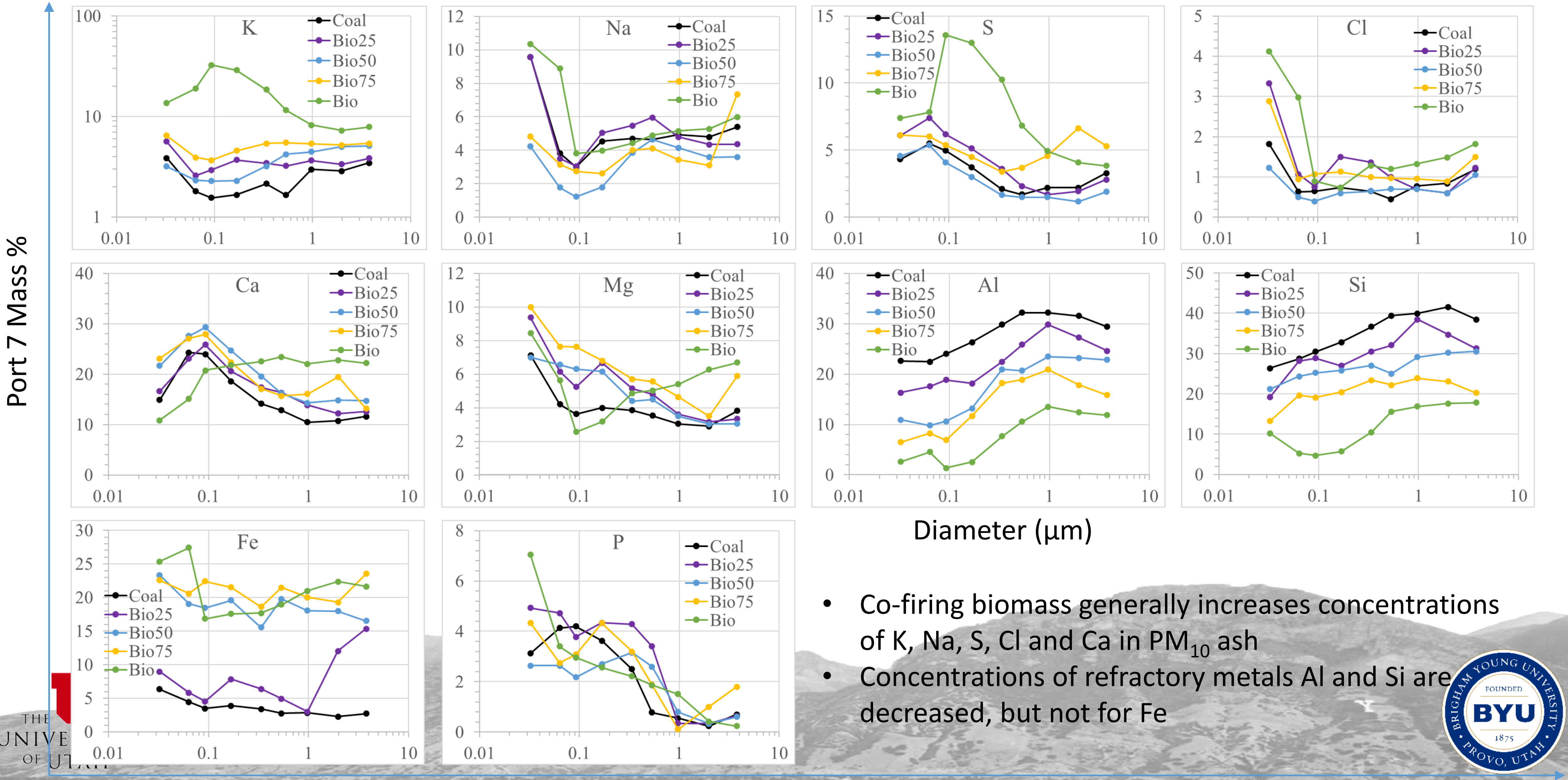

- Co-firing biomass generally increases concentrations of K, Na, S, Cl and Ca in PM_{10} ash
- Concentrations of refractory metals Al and Si are decreased, but not for Fe

L1500: Ash Aerosol Analysis (PSD, Port 7)

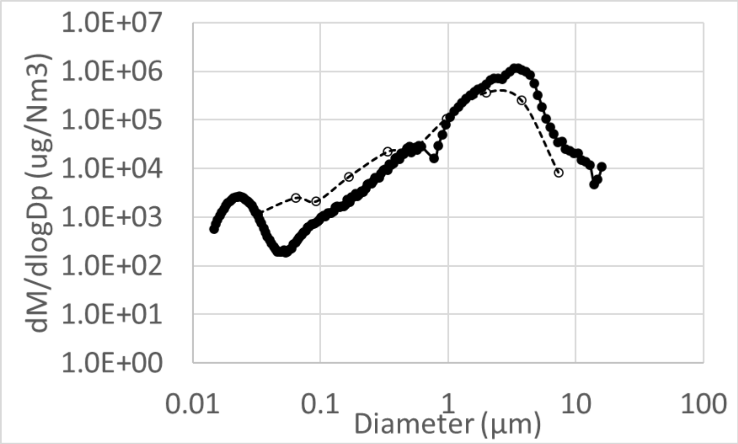

Coal

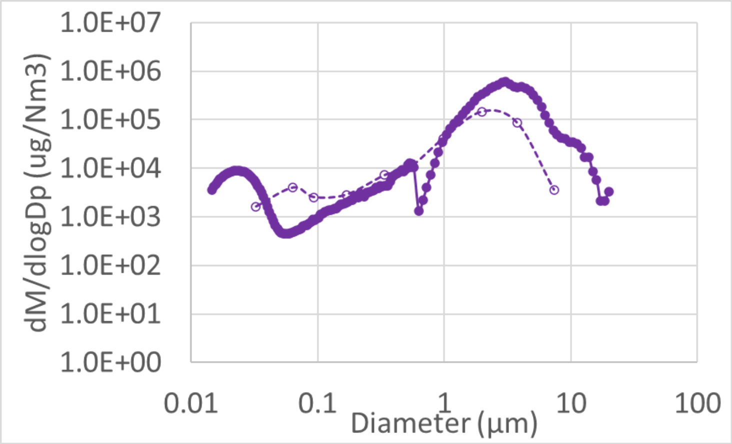

Bio25

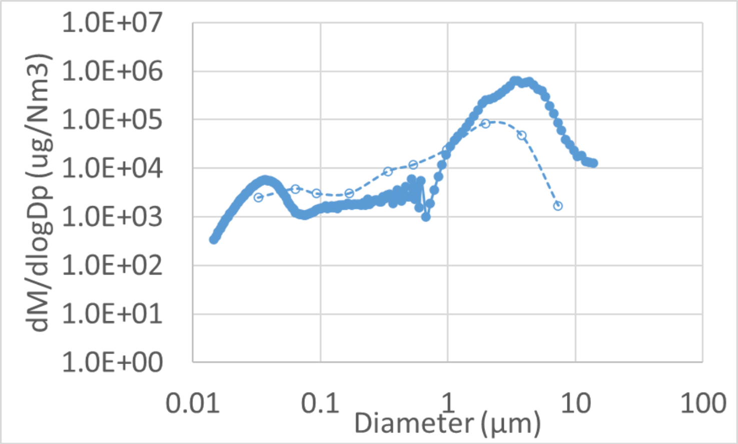

Bio50

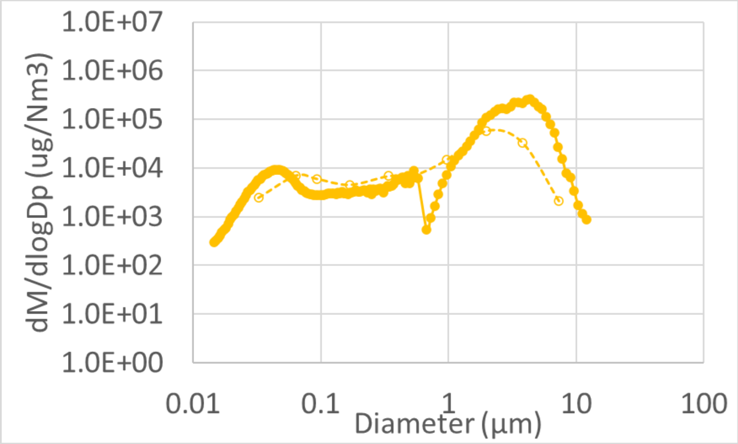

Bio75

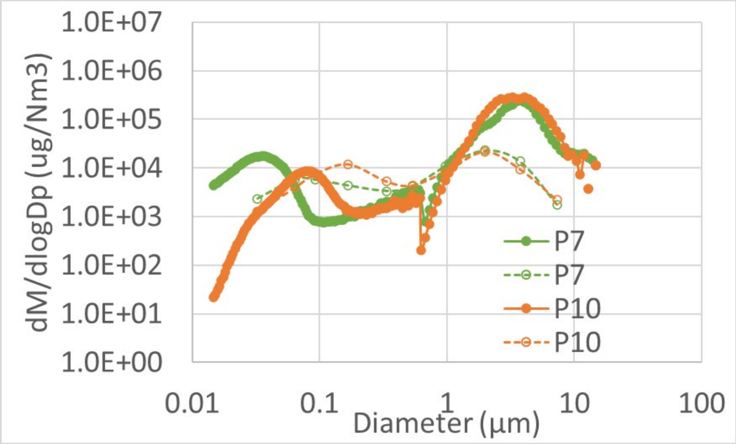

Bio

THE UNIVERSITY OF UTAH

BYU

L1500: Ash Aerosol Analysis (PSD, Port 7)

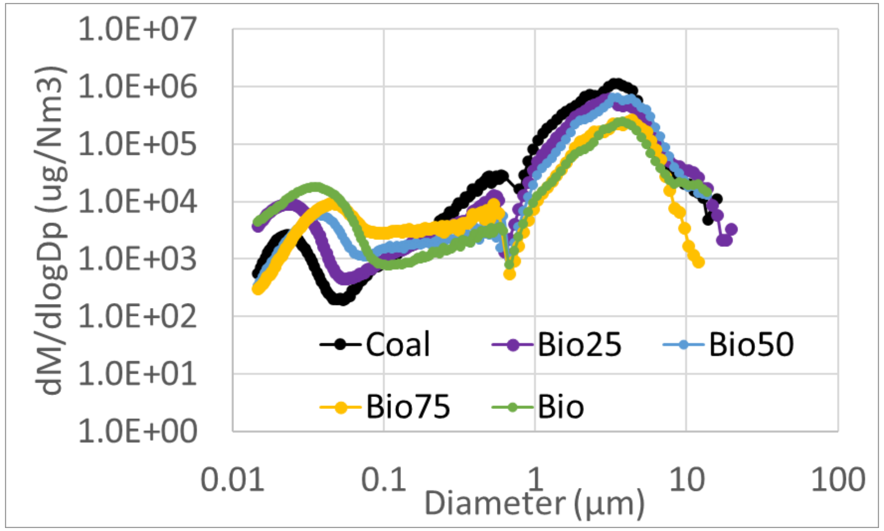

by SMPS/APS

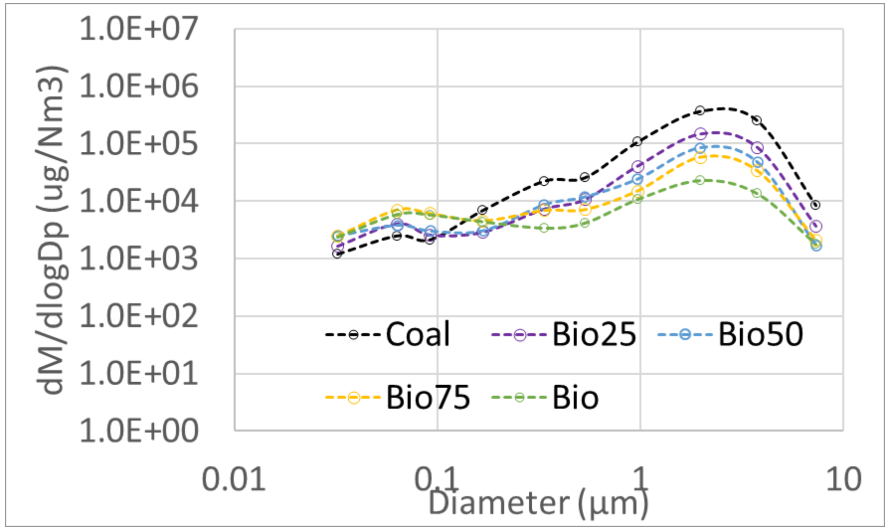

by BLPI

- Co-firing biomass changed PSDs of PM_1 particles
- PM_1 and PM_{20} concentrations in flue gas are decreased with the elevated biomass mixing ratio

L1500: Ash Aerosol Analysis (Cyclone Ash, PM 15+)

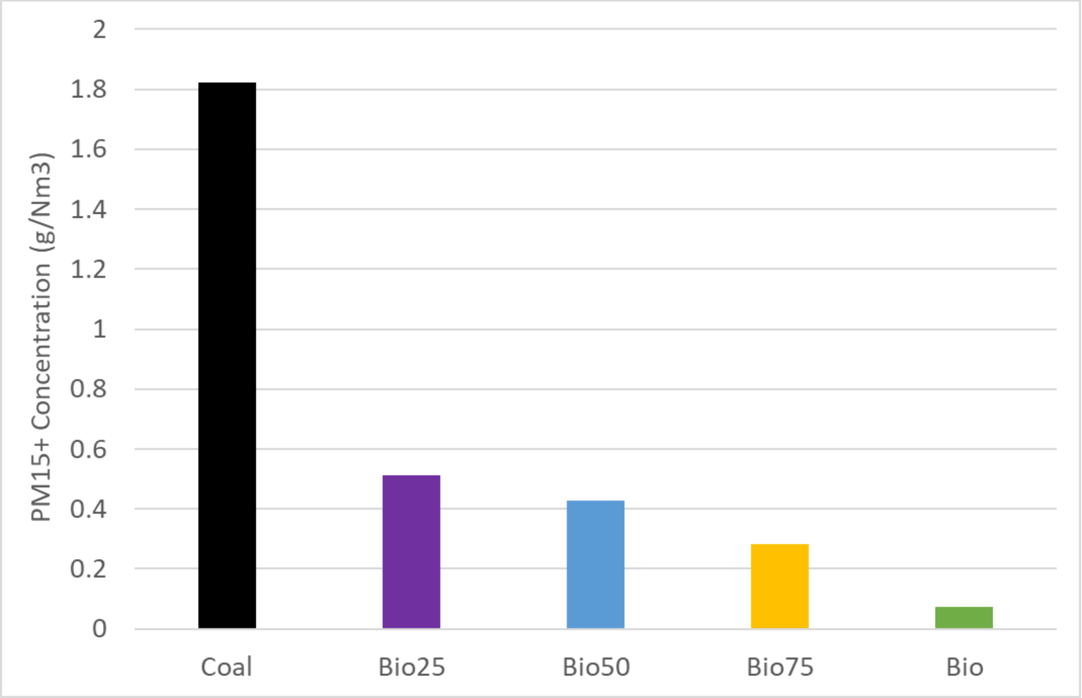

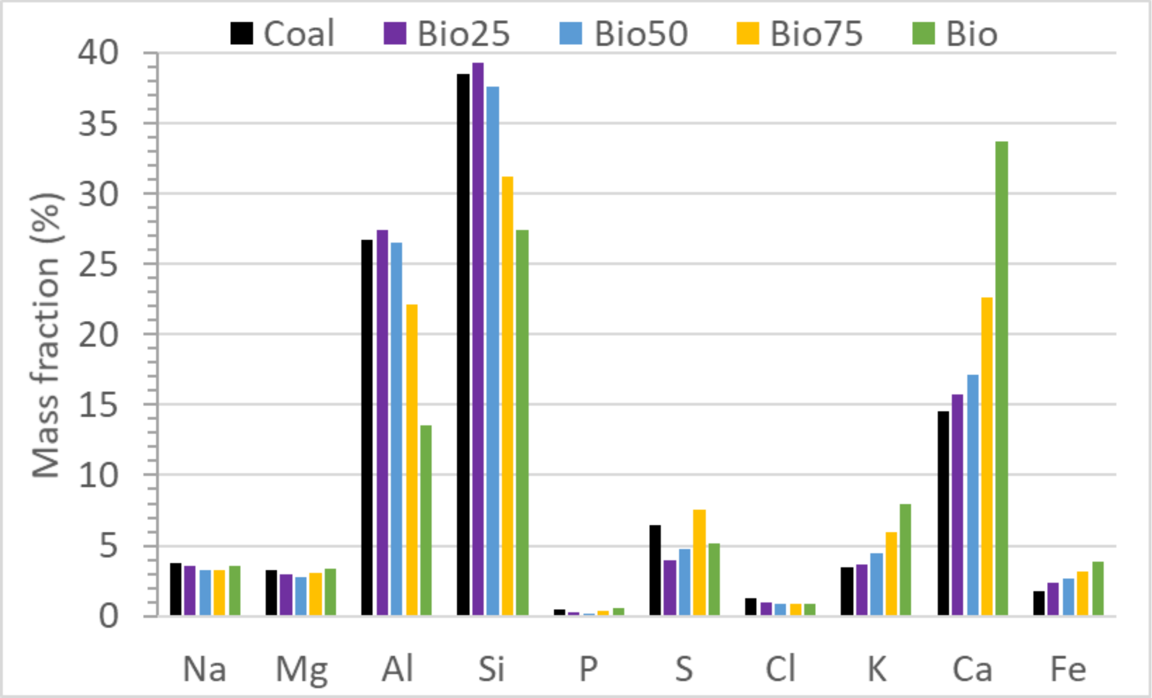

- Co-firing biomass decreases the ash concentrations in flue gas compared to coal combustion
- Similar to PM_{10}, Al and Si are decreased in PM_{15+} while K and Ca increased, as biomass mixing ratio increases

L1500: Ash Aerosol Micrographs (Cyclone PM_{15+})

Coal (F) Bio25 (F) Bio50 Bio75 Bio

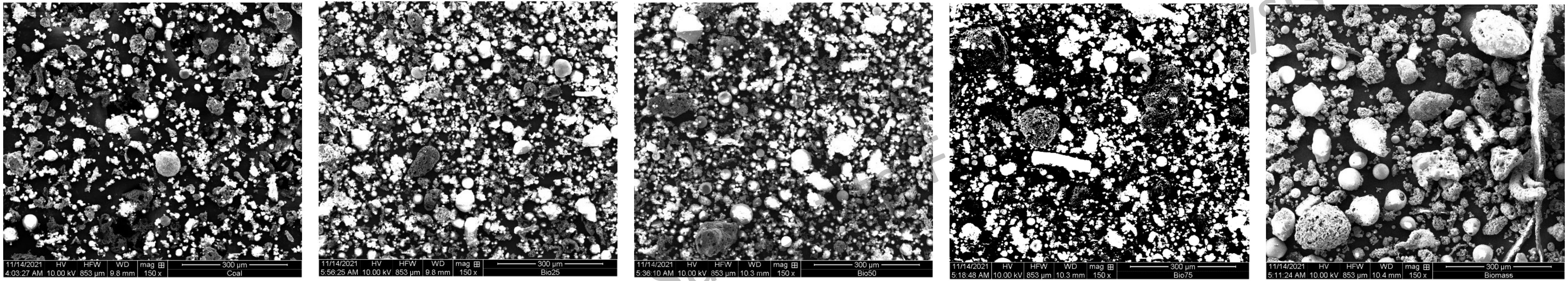

150x magnification, biomass mixing ratio ↑

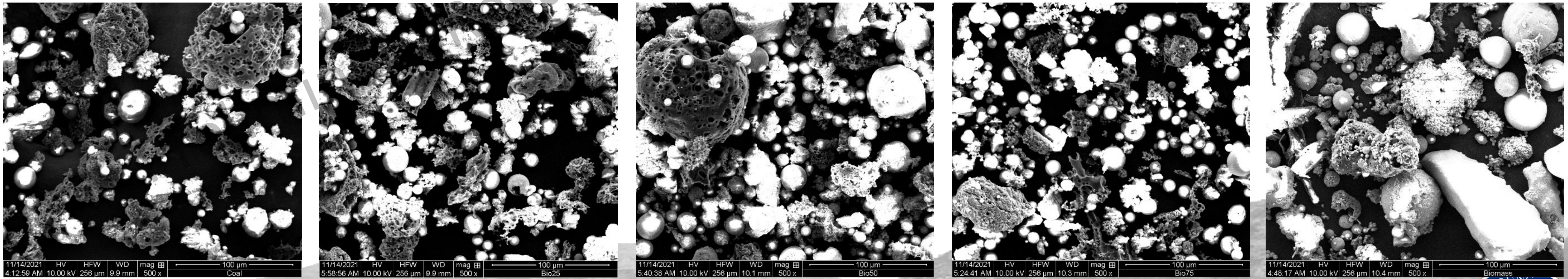

500x magnification, biomass mixing ratio ↑

THE UNIVERSITY OF UTAH

- Biomass ash aerosols contain more large particles formed in irregular shapes, compared to coal ash

L1500: Ash Aerosol Results Summary

PM$_{20}$ particle size distributions

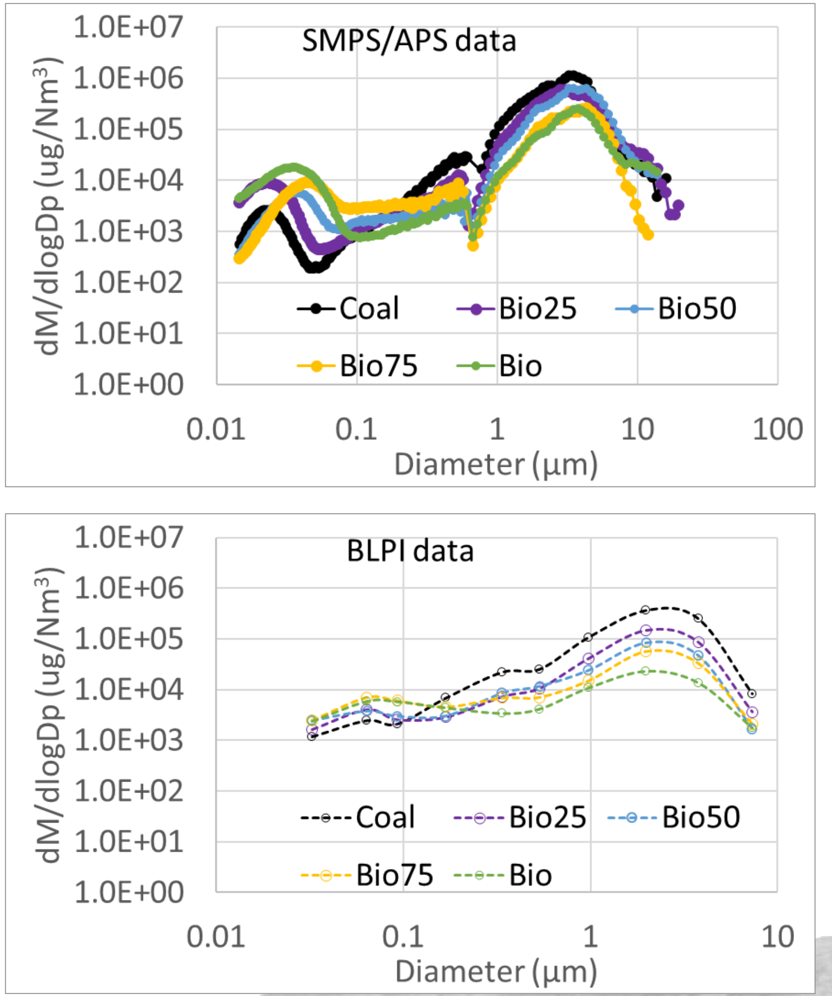

Ash aerosol size-segregated compositions

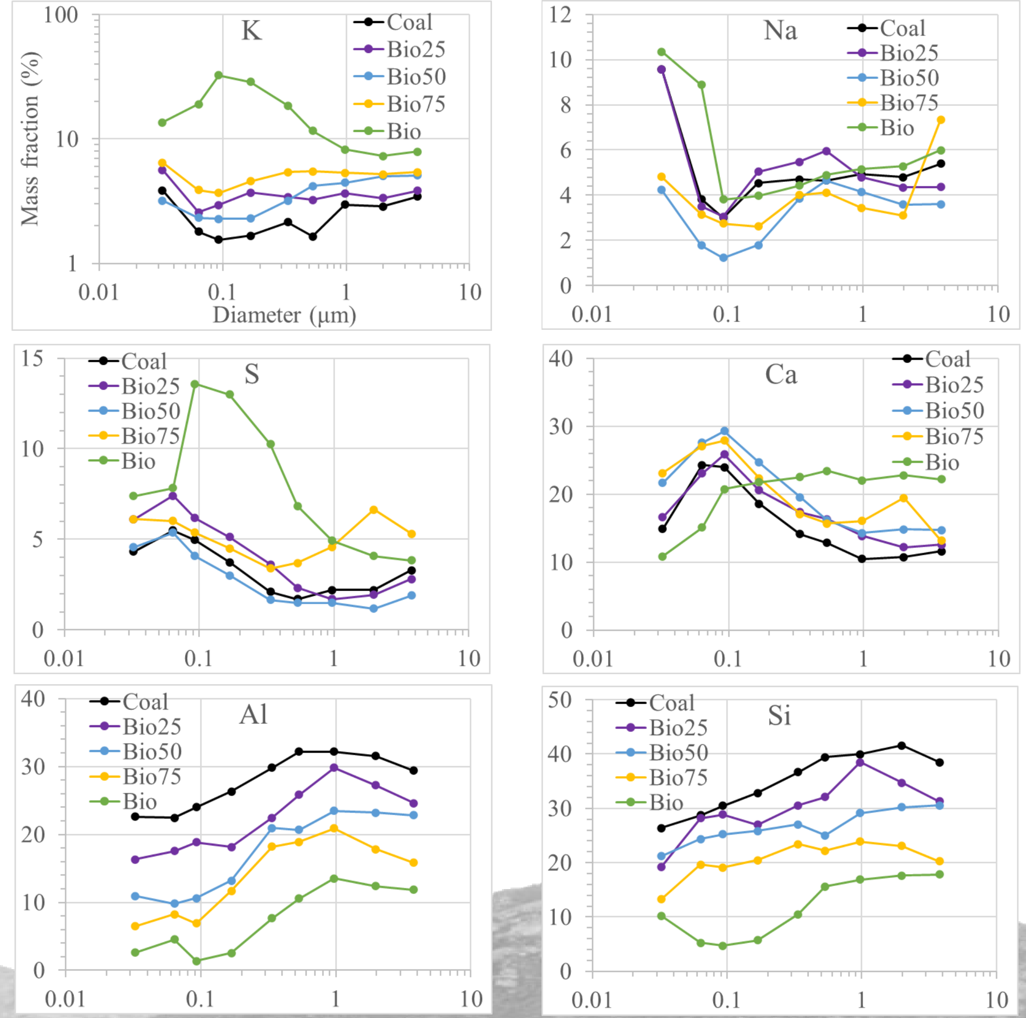

- Co-firing biomass with coal changes the sizes and compositions of PM$_1$ by changing the input ash from fuel
- Increasing biomass input decreases the PM$_1$ and PM$_{20}$ concentrations in flue gas

L1500: Ash Aerosol Results Summary

PM$_{15+}$ concentrations

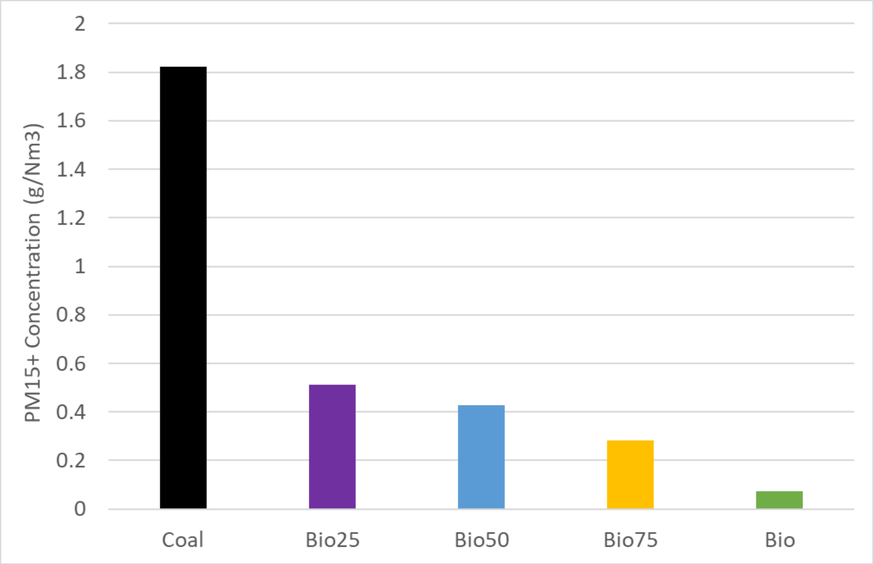

PM$_{15+}$ compositions

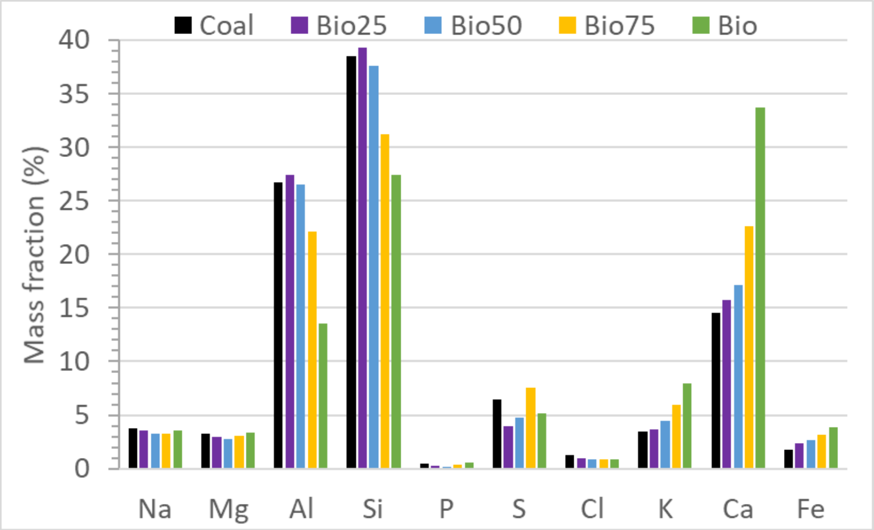

PM$_{15+}$ SEM images

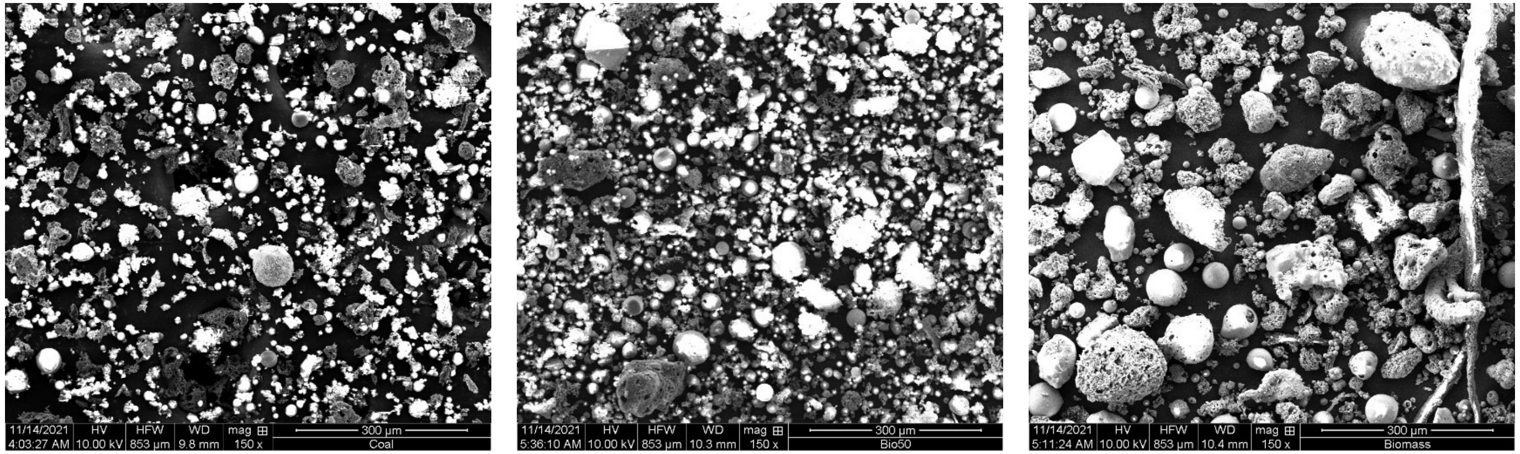

Coal Coal50 Bio

- Co-firing biomass produces less ash load in flue gas than coal combustion does
- Biomass ash aerosols contain more larger particles formed in irregular shapes compared to coal ash

L1500: NO_x Emission

- Oxygen was used as the baseline for all NOx calculations.
- The general trend was that NOx decreased with decrease in percentage of coal.
- 25% and 50% Coal were the exceptions in the general trend.
- In general, the furnace got hotter over the week. For the 50% Coal furnace wall temperature was higher than the usual trend which might explain the higher NOx.

Coal (%)	Oxygen (%)	NOx (ppmv)	Section 3 Wall Temp (F)	Day
100	4.55	131.8	2418.1	Sat
75	4.18	125.7	2312.7	Fri
50	4.06	150.3	2330.2	Tue
25	4.39	158.4	2279.8	Wed
0	4.35	102.0	2226.5	Thu

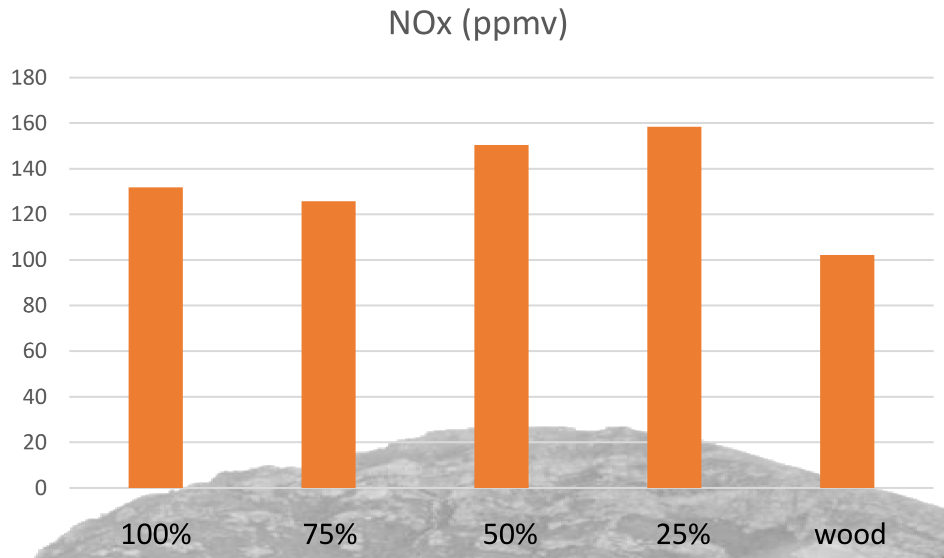

L1500: NO_x Emission

- Higher NOx cannot be explained by primary air/fuel ratio or the burner stoichiometric ratio as both were almost consistent.

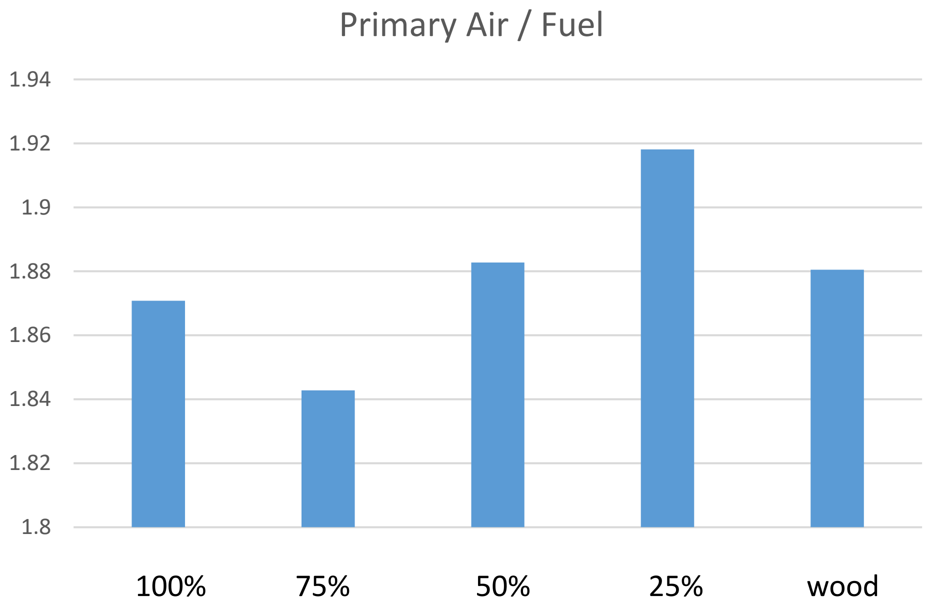

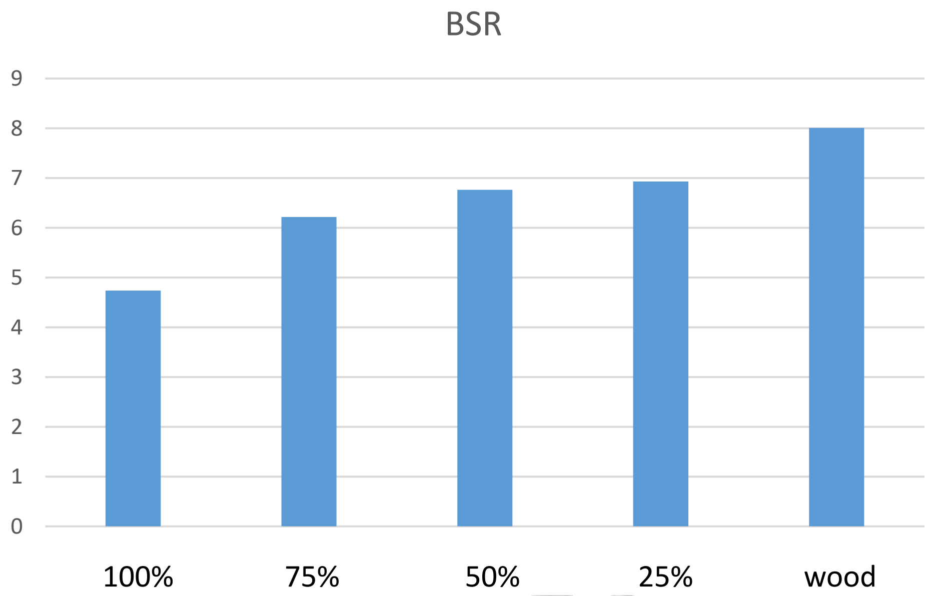

Heat Flux Measurements

Heat Flux vs. % Biomass Fired

Section 1

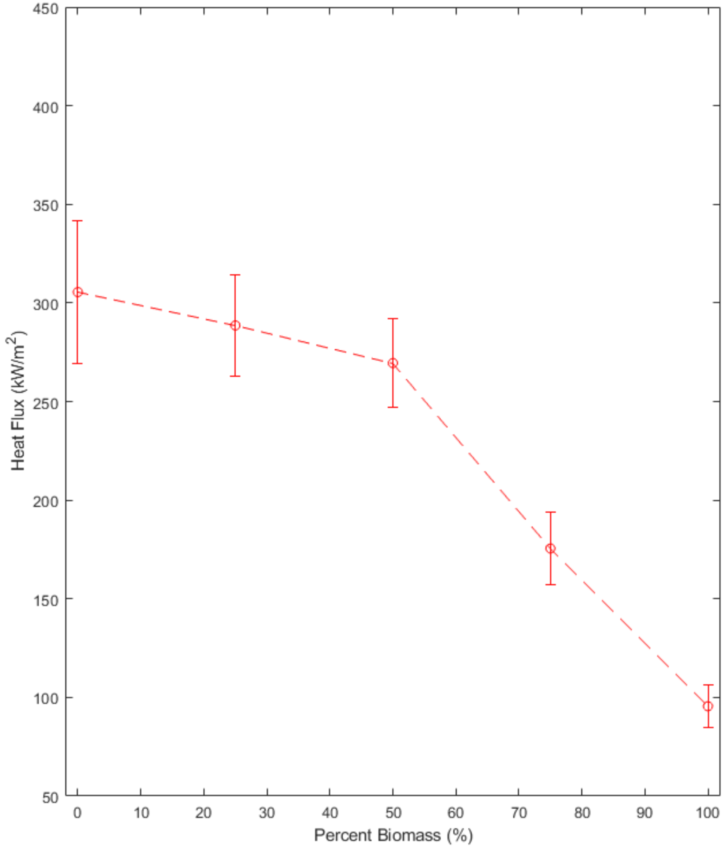

Section 2

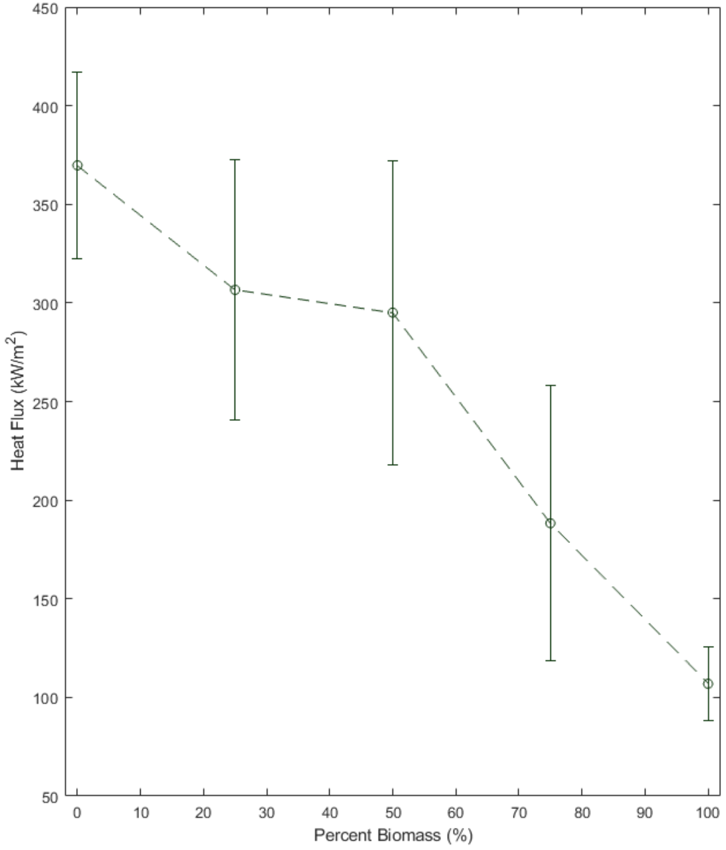

Section 3

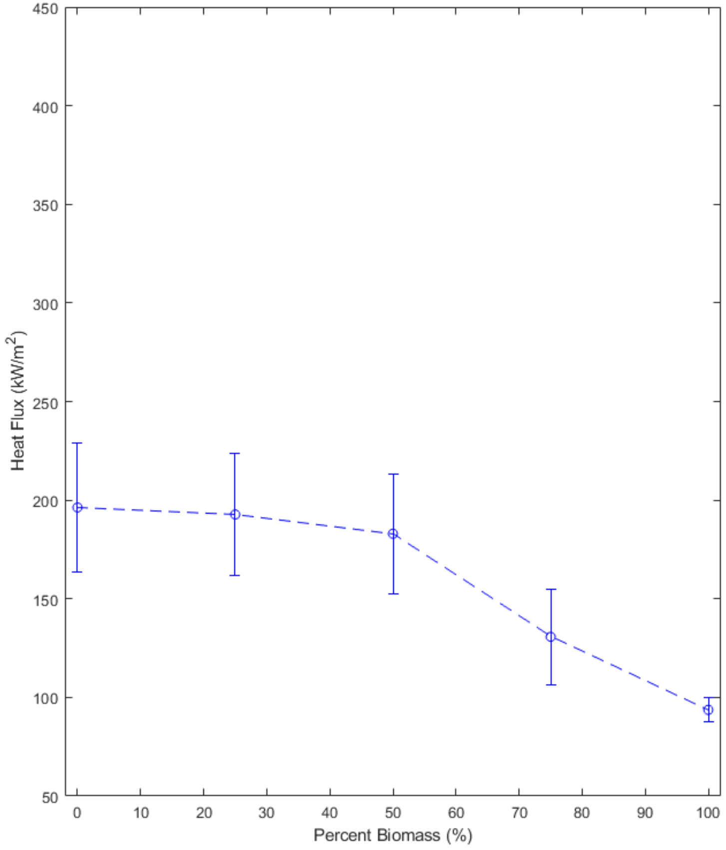

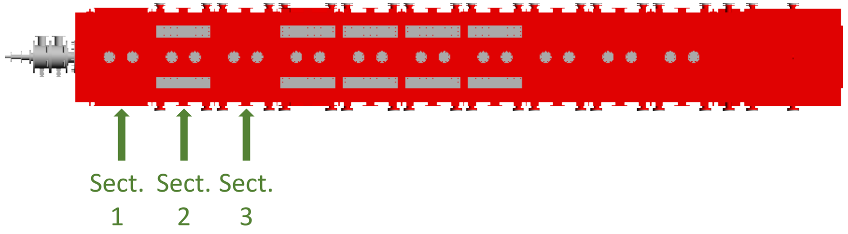

Heat Flux Measurements for Each Testing Day

Tuesday
50% Biomass

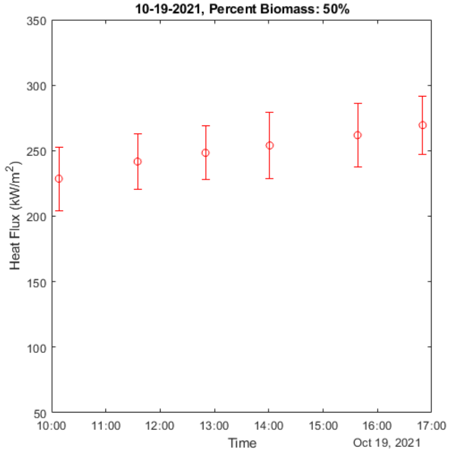

Wednesday
75% Biomass

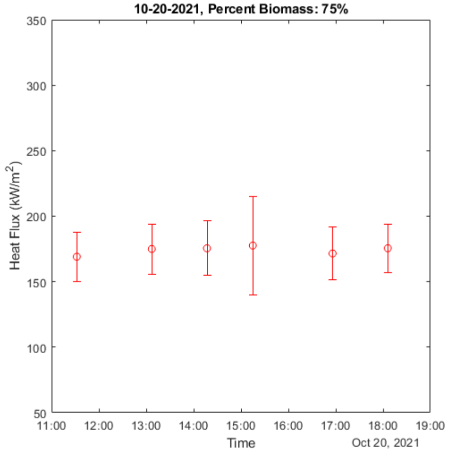

Thursday
100% Biomass

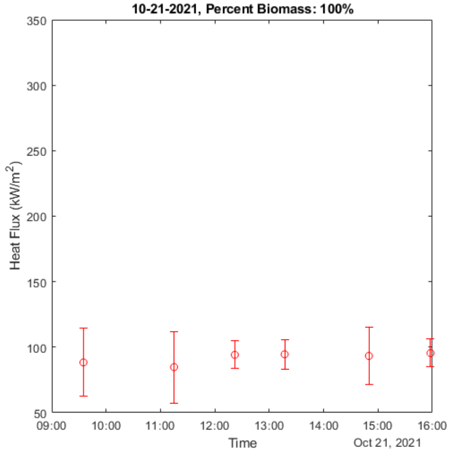

Friday
25% Biomass

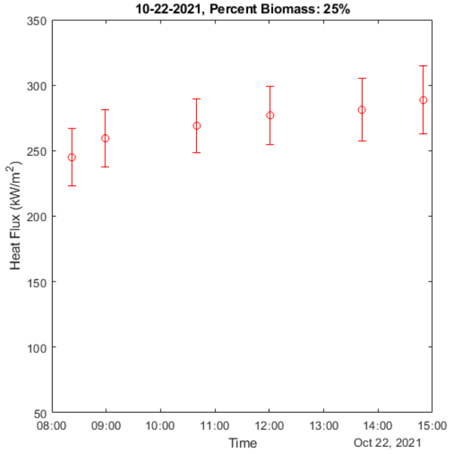

Saturday
0% Biomass

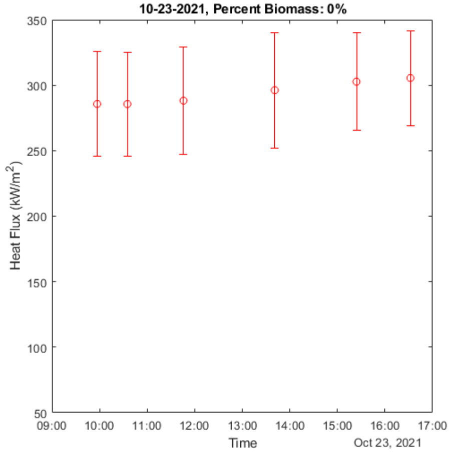

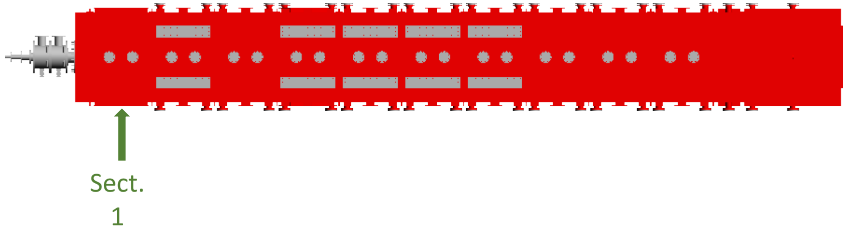

Heat Flux vs. % Biomass – Throughout the Day

Saturday
0% Biomass

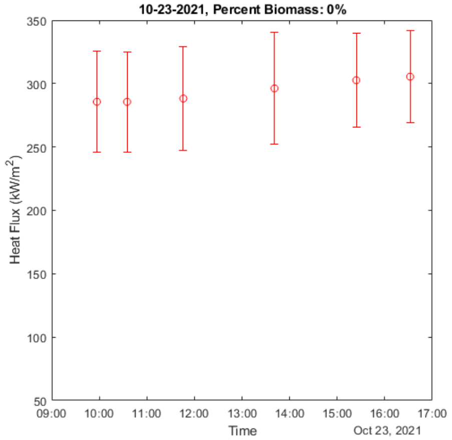

Friday
25% Biomass

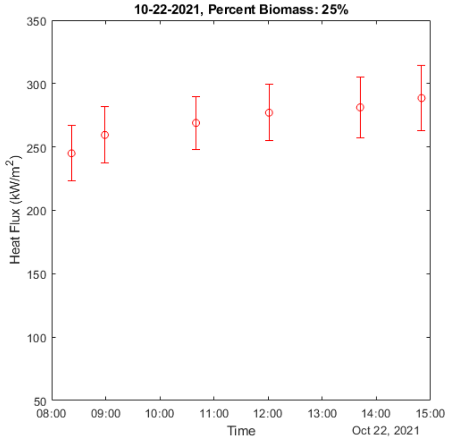

Tuesday
50% Biomass

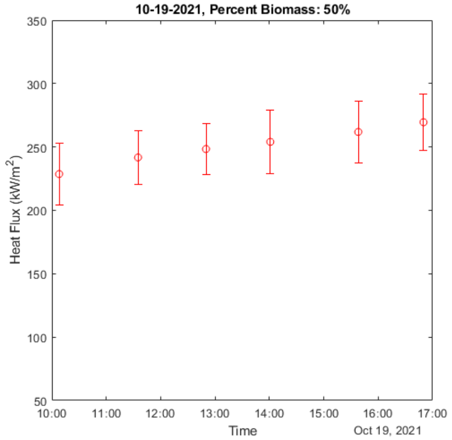

Wednesday
75% Biomass

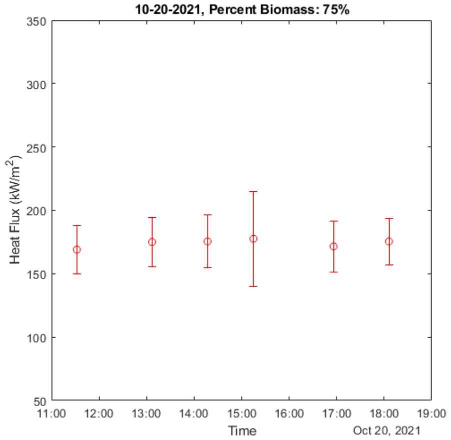

Thursday
100% Biomass

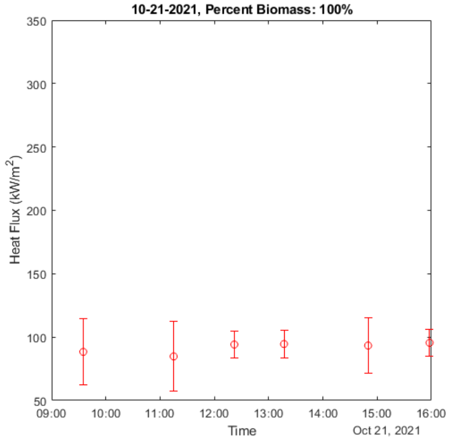

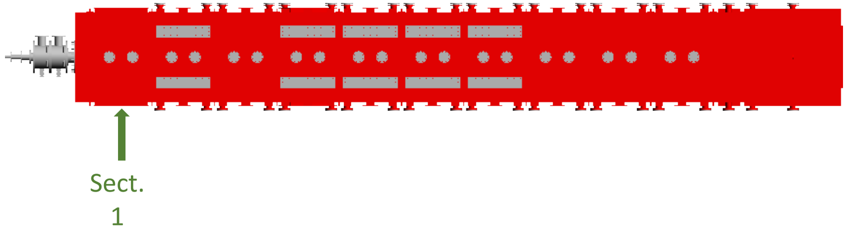

Comparison of Coal Baselines

First Testing Day (Monday)

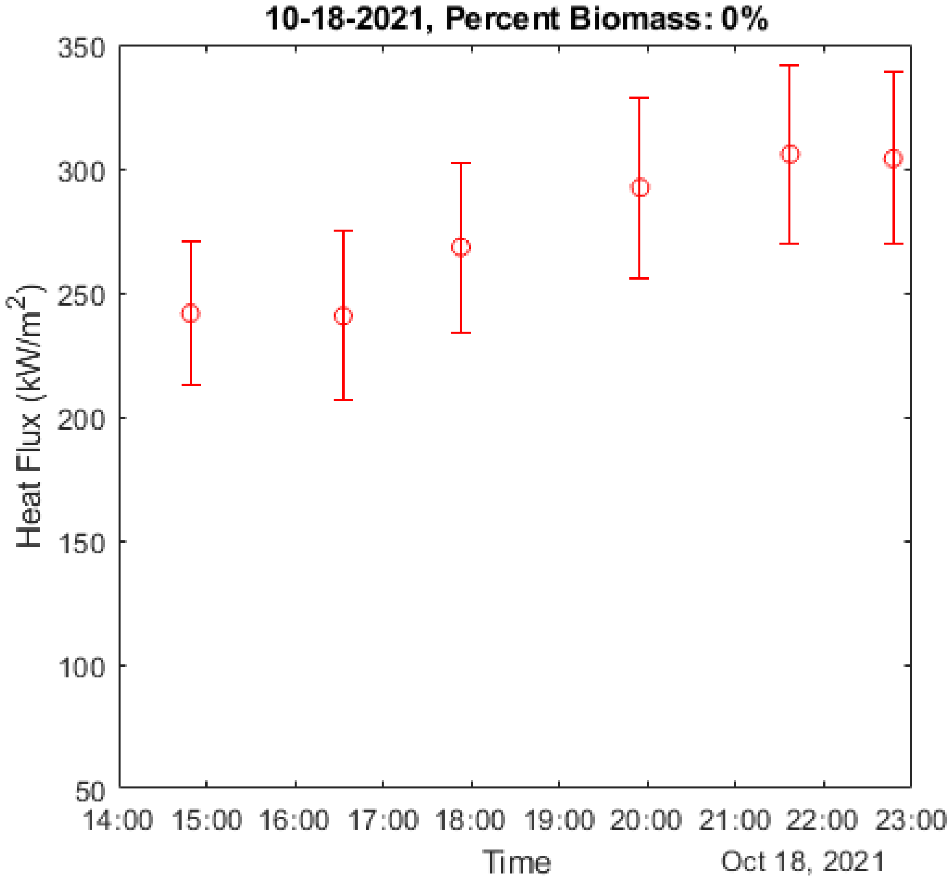

Last Testing Day (Saturday)

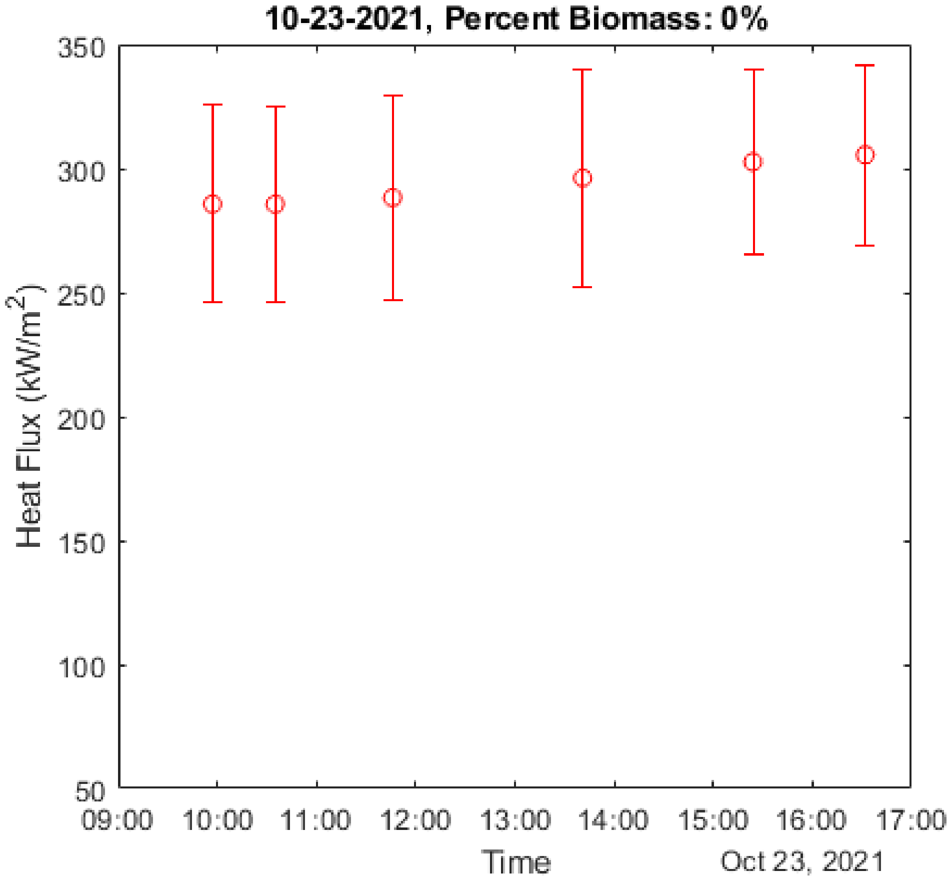

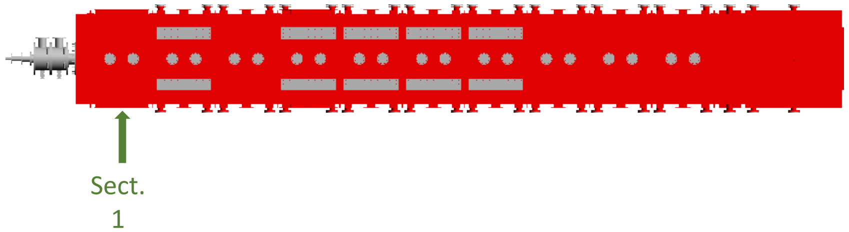

energy&fuels

pubs.acs.org/EF Article

Ash Aerosol and Deposit Formation from Combustion of Coal and Its Blend with Woody Biomass at Two Combustion Scales: Part 1—1.5 MW_{TH} Pilot-Scale Combustor Tests

Seyedhassan Fakourian, Xiaolong Li, Yueming Wang, Jost O. L. Wendt, and Andrew Fry*

Cite This: *Energy Fuels* 2022, 36, 554−564

Read Online

ACCESS | Metrics & More | Article Recommendations

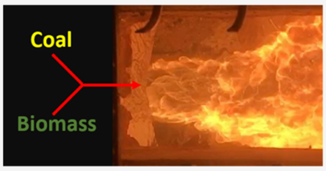

ABSTRACT: There is great interest worldwide in repurposing electric utility boilers designed to fire pulverized coal to fire, instead woody biomass or blends of woody biomass with coal. In this investigation, two prepared biomass/coal blends and the pure parent coal were fired in a 1500 kW pulverized coal combustor with a primary objective of elucidating the mineral particle behavior. The results reported here, although complete in themselves, comprise the first part of a two-part systematic study to investigate the effects of combustion scale on ash deposition rates at scales of 1500 kW (this study), and 1.2×10^6 kW (471 MW_e) using identical coal and coal/biomass fuels and similar analytical techniques. The woody biomass of interest was composed of materials collected in a Utah National Forest and was prepared using a torrefaction technique (for both combustion scales) and a separate steam explosion technique (for the 1500 kW pilot scale only, described here). Biomass samples were blended in 15 wt % biomass with a Utah bituminous coal and were pulverized along with samples of pure coal at a specification of 70 wt % passing through 200 mesh. To sample entrained and deposited mineral matter, a water-cooled extractive probe for ash aerosol and an air-cooled ash deposit probe were designed, constructed, and implemented. The probes were inserted into sample ports at gas temperatures in the range of 1200−1370 K with a deposit coupon surface temperature of 811 K, conditions representative of a utility boiler vertical reheater and of a fouling deposit mechanism. Aerosol size distributions were determined using a scanning mobility particle sizer (SMPS) and an aerodynamics particle sizer (APS), and a Berner low-pressure Impactor (BLPI) collected size-segregated aerosol samples for subsequent elemental analysis. A laser diffraction particle size analyzer (Beckman Coulter LS230) was used to determine the size distributions of ash deposit samples. Scanning electron microscopy with energy-dispersive X-ray spectroscopy (SEM/EDS) was used to determine the morphology and composition of ash deposit samples. For the pilot-scale tests reported here, the experimental results suggested little difference in mineral matter behavior between pure coal and biomass blends. The measured aerosol PSDs showed nearly identical behaviors, with modes at approximately 20 nm and 3 μm. The size-segregated aerosol particles were slightly enriched in Na, K, and Ca and deficient in Si and Al for biomass blends compared to the pure coal. The deposition rates were 60% greater in port 7 than in port 10 at 106 vs 65 g/(m^2 h). Deposit samples collected for 90 min showed essentially the same deposition rate for coal and the two biomass blends, while short deposition times (30 min) suggested higher initial deposition rates for the biomass blends. The deposit composition and morphology were nearly identical for all three fuels.

1. INTRODUCTION

The emission of carbon dioxide from coal-fired utility boilers is currently generating great interest around the world. In the western United States, many National Forests contain areas where up to 70% of trees are dead due to bark beetle infestations.[1] Many of the dead trees either deteriorate in place, leading to methane emission during decay, or burn in forest fire events, leading to uncontrolled atmospheric emission of CO_2 and particulates. Consuming woody biomass to generate power has been identified as a net zero carbon emission technology attributed to the consumption of CO_2 during the biomass growth cycle.[2] Therefore, partial replacement of coal with biomass in coal-fired utility boilers is a reasonable solution to reduce the CO_2 footprint from utility boilers and atmospheric pollution due to forest fires.[3−5]

Both the organic (combustible) and inorganic mineral matter compositions and the mechanical properties of biomass and coal can be very different, leading to potential problems in fuel handling and processing and the conversion of raw fuel to electric power in a boiler environment. The critical processing steps of coal and prepared biomass blends have been evaluated in previous studies.[4,6] Of particular interest in this study is the mineral matter behavior during combustion conditions representative of utility boiler operation. Ash deposition on

Received: October 13, 2021
Revised: December 8, 2021
Published: December 22, 2021

https://doi.org/10.1021/acs.energyfuels.1c03521
Energy Fuels 2022, 36, 554−564

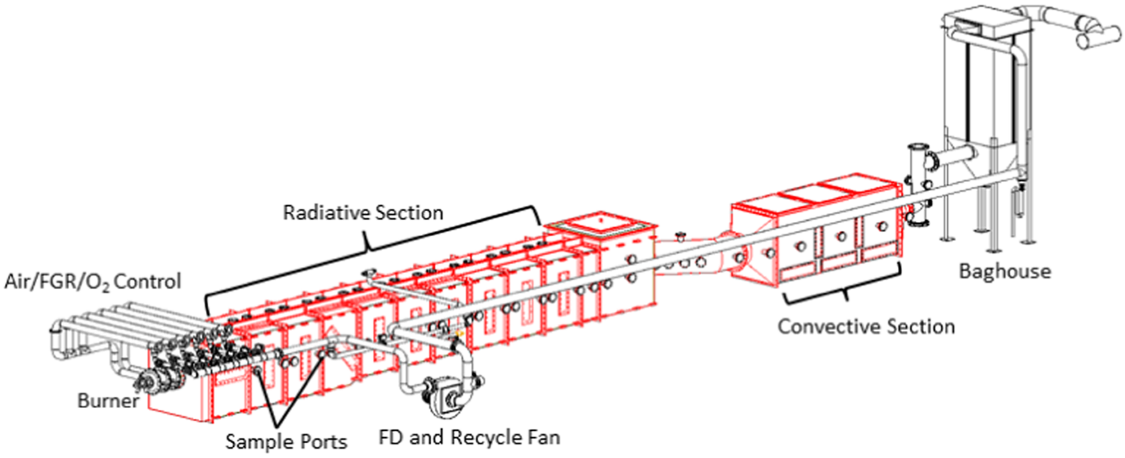

Figure 1. Schematic view of a L1500 furnace with the radiative and convective sections indicated and the burner geometry detailed.

heat exchange surfaces can induce physical phenomenon that reduce the efficiency and availability of the power system. It is expected that due to differences in the elemental content of mineral matter in coal and biomass that their cofiring may lead to changes in ash transformations and deposition.[7,8]

The elemental composition of mineral matter as a mixture of coal and biomass can have profound effects on the downstream behavior of ash. The alkali content of woody biomass fuels such as potassium (K) volatilizes during combustion and subsequently condenses in a K-rich ash deposit, lowering the melting point temperature and generating a sticky deposit layer on the heat exchange surface.[9−11] However, alkali chlorides, formed from the combustion of some biomass, may react with sulfur from coal to form alkali sulfate, which can decrease the stickiness of the impacting fly ash particles reducing ash deposit growth.[2]

Many researchers have investigated the effect of mixing mineral elemental compositions on deposit-grown characteristics while firing fuel blends. Nordgren[12] cofired straw/wood and straw/bark in a 150 kW boiler at different percentages and showed that fouling ash deposition rates of all mixtures were lower than that of pure straw combustion. This indicates that the dilution of straw ash with mineral matter from wood leads to a reduction in the deposit rate. It has been shown in a lab-scale combustor that the deposition rate while firing a blend of peat/bark increases as the fraction of bark increases in the range of 0.4−0.7 wt %.[13] Liu[14] demonstrated that the ash deposition rate decreases by increasing the ratio of bituminous coal in a blend with high-alkali coal in a 30 kW circulating fluidized bed. Qiu[15] investigated the ash deposition rate while firing a blend of coal and rice hull in a pilot furnace. Qiu observed that the ash deposit thickness increased when firing a higher concentration of rice hull in the mixture. Robinson[16] performed pilot-scale combustion tests which fired blends of three different types of coals and four types of biomass that show interactions between alkali chlorides from straw and sulfur from coal reduce the stickiness of fly ash particles. Zhang[17] cites that some researchers reported that cofiring of coal with wood wastes does not significantly change the ash deposit rate due to the low ash content of wood; however, this result may be specific to the wood composition. Ndibe[18] investigated the ash deposit characteristics of cofiring torrefied spruce and bituminous coal in a 500 kW boiler. The investigation showed that the tendency of alkali salt condensation, which results from the significant amount of potassium in such biomass, reduces while cofiring compared with the pure combustion of biomass. Cofiring low concentrations of a calcium-rich wood blended with coal has been studied by Zhou[19] in a 300 kW boiler, and it was observed that the calcium-sulfate-bonded ash deposit promotes the deposit growth. Xu[2] showed that the ash deposition resulting from cofiring wheat straw with two distinct high- and low-sulfur coals in a 25 kW down-fired combustor increased as the potassium concentration increased.

A research project was conceived involving an electric utility corporation, to determine the effects on boiler performance of burning a blend of pulverized coal and torrefied wood in a utility boiler at 1.2×10^6 kW_{TH} firing rate. This project was conducted in two phases: the first phase was pilot-scale tests that were conducted in a 1500 kW_{TH} horizontally fired test furnace to validate sampling techniques and to uncover potential problems that might occur during the second phase, which would consist of full-scale tests at a utility generation facility. Therefore, the overall project allows the effects of the combustion scale to be determined as well as those of burning blends of coal and biomass. Using the identical fuels (coal and coal/biomass blend) at both scales, the project provides a body of experimental data showing the effect of scale on heat fluxes, ash aerosol characteristics, and deposition rates. These data, only rarely found in the literature, can form the basis for the validation of simulations to predict boiler performance.

This paper describes the results of Phase 1 of this project only, and its objective is to present a detailed data set describing the pilot-scale combustion of pulverized coal and blends of pulverized coal and prepared woody biomass, which is suitable for the validation of predictive tools. To fulfill this objective, blends of Utah bituminous coal with torrefied wood or steam-exploded wood that were prepared in a previous study[4] were fired in a 1500 kW_{TH} entrained flow combustor, henceforth denoted as the L1500 combustor. Measurements were made of particle aerosol and deposition behavior, furnace heat balance, flame intensity, and combustion compositions.

2. MATERIALS AND METHODS

2.1. Overview of L1500 Combustor. The L1500 is a 1500 kW_{TH} entrained flow combustor located at the University of Utah. It was designed for NO_x emission studies during pulverized coal combustion and therefore has a realistic burner turbulent mixing scale resulting in flame behavior and fuel burnout relevant for full-scale

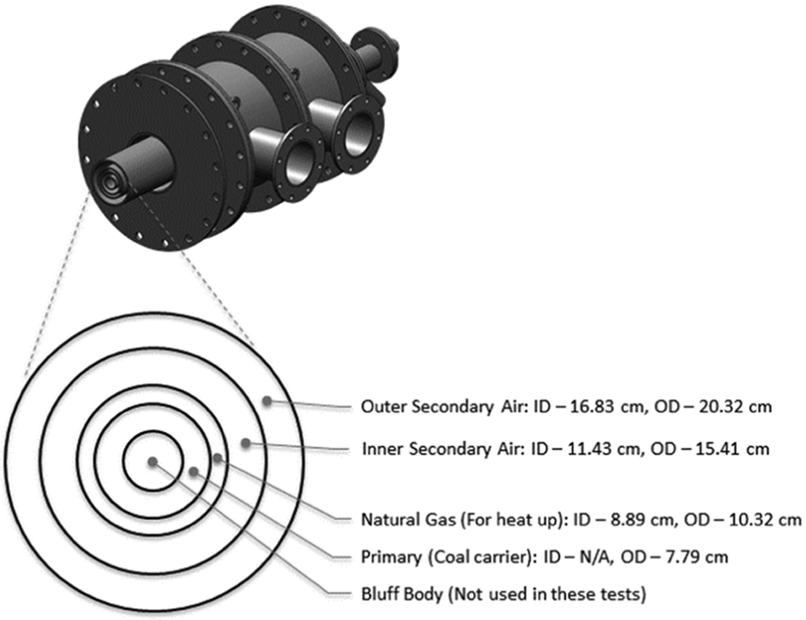

Figure 2. Schematic and dimensions of low-NO_x burner registers on the L1500.

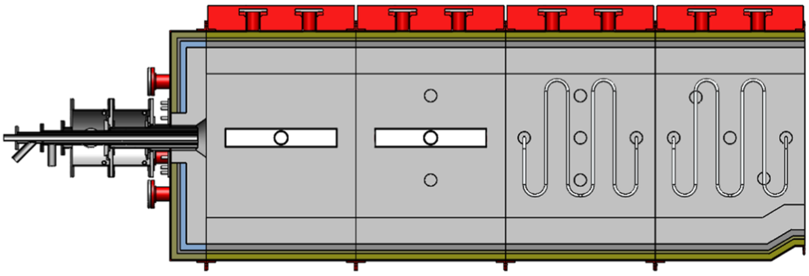

Figure 3. Cross-sectional view of the burner and first four sections of the L1500.

utility boilers. The schematic view of L1500 furnace is shown in Figure 1. The furnace includes a dual-register low-NO_x burner, a radiation section, and a connective section.

Figure 2 shows the dual-register low-NO_x burner on the L1500. It is constructed of four annular pipes and a cylindrical opening in a refractory-lined "burner plate." The innermost annulus is a bluff body and was not included in this investigation. The next larger annulus is the primary or coal-carrying pipe. The next larger annulus is for natural gas used only during heat up and overnight operation. The inner and outer secondary air registers are the outermost annulus. The dimensions of each of these flow paths are included in Figure 2. Each of the secondary registers is supplied with air through an adjustable swirl block capable of inducing a tangential component to the air velocity.

The burner is mounted on a plate cast in refractory. The exit of the annular pipe cluster terminates 6.985 cm before the face of the refractory. At the planar surface where the burner pipes terminate, the cylindrical hole through the refractory is 21.59 cm in diameter (consistent with the OD of the outer secondary air register) and then widens at a 38° angle to form a quarl, terminating at a diameter of 31.87 cm at the refractory face surface and the beginning of the radiation section. The radiation section of the furnace comprises 12 sections. The first four sections have internal dimensions of 1.0414 m wide by 1.1684 m tall and are 1.2192 m in length. Sections 5−10 have a square cross section of 1.0414 m and are 1.2192 in length. Section 11 has a square cross section of 1.0414 and is 0.6096 m in length. Section 12 has a square cross section of 1.0414 and is 1.9413 m in length, and its outlet is tapered into a 0.6604 m diameter round outlet into the transition section into the convective section. Components downstream of this point are outside the interest of this study. Each of the sections in the radiation section is lined with the layers of refractory manufactured by Harbison Walker International (HWI). The inside surface is 21.59 cm thick of Ultra-Green SR, followed by a 5.08 cm thick layer of Insboard 3000, and then two layers totaling 7.62 cm of Insboard 2600. In each of the first 11 sections, there is a sample port in the center of the section length. The centerline of the sample port in the first section is 60.960 cm from the quarl outlet, and each of the subsequent sample port centerlines is an additional 1.219 m from the previous port centerline.

A cross-sectional view of the first four sections of the L1500 is presented in Figure 3. The first two sections contain water-cooled plates on two walls installed coplanar with the inside refractory surface and centered on the sample port, which are 90.17 cm in length and 13.97 cm tall. Sections 3 and 4 contain water-cooled heat exchangers made of 1/2″ SCH 40 pipe, bent to make four full passes and two half passes up and down the furnace wall spanning a length of 91.44 cm and reaching to within 4.013 cm of the ceiling and 16.71 cm of the floor. Sections 5−11 do not have active heat exchange surfaces but do contain water-cooled liners in the center sampling port on one side of the furnace, which also removes heat. Each of these devices is equipped with flow meters on the water supply and *K* thermocouples measuring the water temperature in and out.

A sample probe removes gas from the furnace after the transition section at the inlet to the convective section detailed in Figure 1. This sample is pulled through a particle filter and then is quenched and chilled to remove moisture and is sent to a bank of analyzers whose readings are continuously recorded in the DCS system. The bank of analyzers includes Yokogawa AV8C O_2 (0−25%), California Analytical ZRH CO/CO_2 (0−2000 ppm for CO, 0−20% for CO_2),

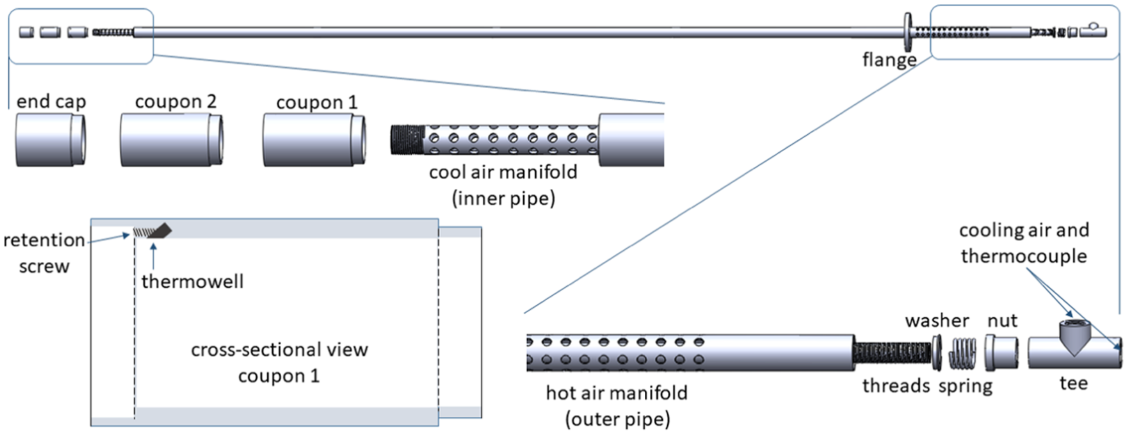

Figure 4. Air-cooled deposition probe.

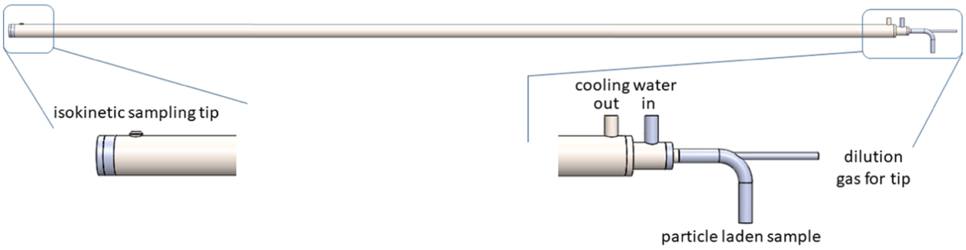

Figure 5. Water-cooled entrained ash sampling probe.

Thermo Environmental 42C NO_x (0−10 000 ppm), and California Analytical 601 SO_2 (0−5000 ppm).

2.2. Particle and Deposit Sampling. Determination of mineral matter transformations was a key component of this project. Of particular interest was the behavior of ash deposition at conditions where fouling occurs in full-scale coal-fired utility boilers in the region of the primary superheater and reheater. To fulfill this objective, probes were developed to extract the samples of entrained ash and to measure deposition rate on a surface representative of heat transfer tubing associated with the aforementioned systems.

The ash deposit probe is constructed of two stainless steel concentric pipes and is detailed in Figure 4. The inner pipe (1″ SCH 40) with an OD of 3.34 cm and an ID of 2.66 cm directs cooling air down the length of the probe and disperses it through a perforated manifold onto two deposit coupons, each 10.16 cm in length, to maintain them at the desired temperature. The coupons and the outer pipe are fabricated from 2″ SCH 80 and SCH 10 pipes, respectively, with an OD of 6.03 cm and IDs of 4.92 and 5.48 cm, respectively. After the cooling air impinges on the two coupons, it is directed back out of the combustion system using the outer pipe and ejected through a second perforated manifold. The probe was constructed at a length of approximately 5.8 m so that it could also be applied in a utility boiler in the future. A type-k thermocouple was inserted through the center of the probe with the tip embedded in a thermowell drilled into the inside surface of the first deposit coupon. The rate of cooling air flow was controlled using an actuated control valve connected to logic operating a PID control scheme to control the temperature at a given setpoint. The probe was installed on the furnace hanging from a steel frame supporting an I-beam with a beam trolley to easily insert and retract the probe without disturbing the deposit. This system is similar to the probes used in previous studies.[20]

Ash aerosol in the flue gas, which is the precursor of ash deposits, was extracted from the furnace using a water-cooled isokinetic sampling probe, which is detailed in Figure 5. This probe was constructed of four concentric stainless steel tubes. The outermost three tubes were used to direct cooling water from outside of the combustion system through the inner annulus to the probe tip and eject cooling water through the outer annulus. These three tubes had an OD of 3.81, 2.54, and 1.27 cm with wall thicknesses of 0.34, 0.21, and 0.17 cm, respectively. The particle-laden gas was removed from the combustion system through the inner cavity of these three tubes. The sample was quenched and diluted at the probe tip by injecting gas through a 0.64 cm OD, 0.38 cm ID tube. The sample from this system was further diluted and then supplied to the particle analysis equipment. This probe was similar in length to the deposit probe for later application in a full-scale utility boiler.

A real-time determination of particle size was performed using a combination of a Scanning Mobility Particle Sizer (SMPS) and an Aerodynamic Particle Sizer (APS). Alternatively, the sample could be collected in size-segregated bins using a Berner low-pressure impactor (BLPI), which are later analyzed for composition and morphology analysis through scanning electron microscopy (SEM) and energy-dispersive X-ray spectroscopy (EDS). The methods for this analysis have been well documented in other studies.[8,20,21] The SMPS/APS are installed on a two-stage dilution sampling system, in which the flue gas is diluted by nitrogen gas (N_2) with the dilution ratio about 15:1 and then diluted by filtered air in manifold with a dilution ratio about 25:1. Thus, the total dilution is about 375:1. The size range measured by SMPS is between 0.0143 and 0.6732 μm. The sample flow rate going into SMPS is 0.3 L/min, and every measurement takes about 2 min. Ten to twenty repeatable measurements are conducted and averaged for each case to ensure reliable results. The size range in APS is from 0.532 to 20 μm. The sample flow rate is 5 L/min, and one single sampling measurement takes about 20 s. For each sampling, over 100 measurements are used and an averaged result is obtained. The measurements of SMPS and APS are simultaneous, using the same sample flow. Therefore, combining PSD data from the two instruments produces a result ranging from 0.01 to 20 μm. The sample flows of SMPS/APS and BLPI are the same to save time. Therefore, it is a two-stage dilution. The size range in BLPI is between 0.0324 and 15.7 μm. The sample flow rate is 23 L/min, and every single sampling measurement takes about 30 min. It takes about 2 h for three repeatable measurements in each sampling case.

Both the deposition and the aerosol sampling probes were installed in port 7 and port 10 of the furnace, which allowed sampling at flue

Table 1. Ultimate and Proximate Analysis of Fuels from the Previous Study[6a]

	ash	C	H	N	S	O	Cl	H_2O	vol	FC	HHV (kJ/kg)
coal	12.74	63.05	4.35	1.13	0.45	11.61	0.145	6.52	38.26	42.47	25 959
torrefied	14.99	59.66	4.36	1.00	0.47	14.12	0.180	5.21	41.69	38.10	24 676
Steam X	14.16	60.57	4.49	1.06	0.48	14.16	0.178	4.89	42.32	38.63	24 746

[a] Values are % mass as received. HHV is kJ/kg as received.

Table 2. Mineral Matter Composition, % Mass, from the Previous Study[6a]

	SiO_2	Al_2O_3	TiO_2	CaO	Fe_2O_3	K_2O	MgO	Na_2O	SO_3	P_2O_5	BaO	MnO_2	SrO
coal	54.07	11.03	4.17	15.25	4.17	1.20	3.99	1.26	6.35	0.29	0.08	0.04	0.08
torrefied	55.55	10.48	0.53	15.88	4.07	1.49	4.08	1.33	5.98	0.31	0.08	0.05	0.08
Steam X	57.53	12.40	0.62	12.82	4.09	1.05	3.77	0.97	6.06	0.27	0.06	0.02	0.08

[a] Difference between sum and 100% is undetermined.

gas temperatures that are representative of the region of the boiler containing the primary superheater and the vertical reheater. These locations are 7.92 and 11.58 m from the planar face of the burner quarl exit.

2.3. Fuel Preparation and Analysis. The purpose of this study was to evaluate the combustion behavior of blends of prepared woody biomass and coal for use in unmodified coal-fired utility boilers. Raw biomass material was harvested from US Forest Service land, under their direction, near the Alta Ski Resort in Little Cottonwood Canyon, Utah. Wood from this area was chosen because of its availability and its similarity in species and composition to biomass from the Manti La-Sal National Forest. The raw material was prepared using two pretreatment processes: torrefaction and steam explosion. Torrefaction is a thermal process to make biomass more like coal so that it is easy to grind. Torrefaction removes moisture and oxygen from biomass and breaks down the fibrous hemicellulose fraction to produce a more grindable and energy-dense fuel.[22−25] The wood can be compressed into pellets before or after torrefaction to facilitate transport and reduce storage costs.[26] Its combustion is similar to coal, but its heating value is less than that of coal and the handling is more expensive. Steam explosion (Steam X) exposes the biomass to high pressures using saturated steam in a pressure vessel. Once the pressure inside the wood cells is equilibrated, the vessel pressure is suddenly released to burst the cell wall and break down the material structure.[27] After the steam explosion, the biomass is rinsed, dried, and pelletized.[28]

For the purpose of this study, each of the prepared biomass products was blended with bituminous coal mined in Utah in a 15% biomass, 85% coal by weight mixture. Large samples of these blends and the pure parent coal were milled to a 70% through 200 mesh grind using a CE 312 Raymond Bowl Mill. The observed milling behavior and resulting particle size distribution (PSD) are detailed elsewhere.[4,6]

In this paper, the pure Utah bituminous coal will be subsequently referred to as “Coal”; the coal/torrefied biomass blend will be referred to as “Torrefied” and the coal/steam-exploded blend will be referred to as “Steam X.” The ultimate and proximate analysis of these fuels are presented in Table 1, and their mineral matter compositions are presented in Table 2.

Of particular concern when firing biomass fuels is the content of sodium and potassium. Their interaction with other elements such as sulfur can contribute significantly to fouling. Table 2 shows that these biomass materials are fairly benign contributors of alkali metals. In fact, Steam X shows a notable reduction in sodium content. This observation is supported by the expected impacts of the steam exploding process. After the cell walls have been ruptured by the rapid pressure reduction, the material is rinsed, removing any sodium that resided within the solution in the cells. It is expected that blending coal with biomass should provide a lower overall ash content than pure coal because woody biomass contains less ash. The increase in ash content for the two biomass blend materials compared to the pure coal in Table 1 are surprising. This increase is likely due to the mixing process, which occurred on a concrete floor and may not have been cleaned well enough.

2.4. Experimental Section. The test plan was developed for this program to generate a data set that represents as closely as possible the operating conditions of a full-scale wall-fired pulverized coal utility boiler. The key parameters we were determined to match are consistent with low-NO_x burner operation with lower furnace staging and over fire air configuration. They are listed in Table 3.

Table 3. Target Operating Parameters Designed to Match Coal-Fired Utility Boiler Conditions, within the Capabilities of the L1500

parameter	units	value
firing rate	kW	880
primary gas/coal ratio	unitless (mass)	2.0
secondary air distribution (inner/outer)	unitless (mass)	30/70
lower furnace stoichiometric ratio	unitless	0.9
excess O_2	vol %, dry	3−4

3. RESULTS AND DISCUSSION

3.1. Actual Operating Conditions. The L1500 was operated for approximately 8 h for each of the three fuels. During this period, deposit samples were collected for 30, 60, and 90 min accumulation times in ports 7 and 10, along with the aerosol sampling. During that period, the furnace was operated at constant conditions. The sampling commenced when it was determined that the refractory walls had approached a thermal equilibrium for the given condition heat distribution. Following the experiments, the experimental conditions (including reactant flow rates, fuel compositions, and measured gas compositions) were averaged over the steady-state operating period analyzed to determine the consistency of the data and air leakage into the furnace and fuel feeding system. It should be understood that the calculated air leakage rate is the result of mass balance calculations and contains errors from all of the measured flow rates and compositions. The resulting operating conditions are summarized in Table 4.

The measured and calculated operating parameters that are relevant for aerosol and deposit sampling are summarized in Table 5. The air flow rate includes the sum of primary air, inner secondary air, outer secondary air, staging air, and air leakage. A suction pyrometer probe measures the flue gas temperature at the two sample locations.

In the following sections, whenever data are compared graphically for the three fuel conditions, the Coal data will be

Table 4. Average Measured Operating Conditions for Each Fuel

parameter	units	coal	torrefied	Steam X
firing rate	kW	922.7	873.5	881.9
fuel rate	kg/h	122.0	127.4	128.3
primary air rate	kg/h	235.4	245.7	229.8
primary air temp	K	305.8	303.2	303.3
inner secondary air rate	kg/h	198.7	191.4	197.2
inner secondary air temp	K	525.0	524.4	523.9
inner secondary air swirl	%	75	75	75
outer secondary air rate	kg/h	418.4	378.5	414.7
outer secondary air temp	K	532.6	527.5	532.4
outer secondary air swirl	%	75	75	75
air leakage (calculated)	kg/h	163.3	155.6	186.0
staging air rate	kg/h	267.4	268.2	261.7
staging air temp	K	320.7	319.5	319.2
flue gas O_2	vol %, dry	4.52	4.23	4.47
flue gas CO_2	vol %, dry	14.73	15.26	15.20

represented in gray, Torrefied data will be represented using blue, and Steam X data will be shown in orange. Comparisons of behavior due to location or other conditions will be represented by other colors.

3.2. Properties of Ash Aerosol. The aerosol PSDs measured at ports 7 and 10 are shown in Figure 6, where the ash concentrations on the left plots are based on flue gas volume at standard state, while the right plots are the total ash mass basis. The mineral compositions in fuels and combustion temperature determine the formation of submicron ash particles, which show similar PSDs in the three cases. The ultrafine mode at size < 0.1 μm is possibly formed through nucleation and condensation of vaporized inorganic species in the sampling probe.[2] Char fragmentation is the main mechanism for the supermicron mode (>1.0 μm) and is not affected by combustion temperature. The possible third mode, which is the central mode at the range of 0.1−1.0 μm, is formed through the coagulation of nuclei. The central mode is called the coagulation mode (usually around 0.3 μm). This mode for the Torrefied conditions is slightly higher than that of the other fuels. The flue gas temperature is the key parameter in vaporization and coagulation rate, which is relatively lower for the Torrefied conditions. The main processes of ash aerosol formation are described elsewhere.[30] In general, the ash aerosol sampling results suggest that cofiring prepared woody biomass with coal plays a minor role in altering the aerosol formation from the pure coal condition.

Figure 7 compares ash aerosol PSDs for the Coal condition at ports 7 and 10. These data show a reduced concentration of submicron particles in the range of 0.1−1.0 μm and increased concentration of particle sizes in the range of 1.0−5.0 μm at port 10 compared with port 7. Typically, ash particles < 5 μm follow well with the flue gas stream. However, the concentrations of fly ash particles > 10 μm, which are not measured as a component of the entrained ash, reduce along the horizontal flow path in the L1500 furnace due to low velocities and particle settling. The difference in ash aerosol concentrations at the two locations may be due to coagulation and subsequently may lead to the different growth of local ash deposition.

The compositions of ash particles sampled using the BLPI at port 7 are shown in Figure 8. The results of the BLPI analysis on samples from port 10 are similar and are not presented here. The submicron size range of ash aerosol enriched slightly with alkali species of sodium (Na) and potassium (K) for the Torrefied and Steam X cases compared to Coal conditions. This could be caused by increased vaporization of alkali species due to the introduction of woody biomass, in which potassium and other minerals are more likely to be organically bonded. The less volatile species such as Ca and Si, which contribute the most mass, have similar distributions in the three cases. Mass fraction changes of Si and Al follow each other, suggesting their common existence as alumina−silicates in fly ash. The size-segregated compositions of the three cases present slight variations; therefore, the transformation of minerals during cofiring is hardly affected by the wood content. Accordingly, the three cases with different fuels produce aerosols with similar size distributions. Higher mass fractions of calcium and sulfur are found in fine particles smaller than 0.1 um, which is likely caused by the condensation of $CaSO_4$. This is consistent with the occurrence of ultrafine mode around 0.04 μm in aerosol concentrations (see Figure 6).

3.3. Properties of Ash Deposits. The deposit sampling was performed according to plan with some small alterations due to constraints on fuel supply and the general sampling schedule. At the end of each sampling period, the deposit probe was carefully removed from the reactor using the overhead beam trolley. The deposit was photographed, and then the ash built up on temperature-controlled coupons was removed by scraping the surface clean into a sample pan. These samples were then weighed and stored for further analysis. Some selected images of the coupons after the operations are shown in Figure 9. In these images, the end cap of the deposition probe is glowing because it was not a cooled surface of the probe.

The collected ash deposit samples were weighed using a balance with 0.1 g accuracy. Ash deposition rates were determined by dividing the ash deposit mass by the total coupon surface area and the implementation time. Ash deposit masses and rates are presented in Figure 10 with port 7 data presented in the left plot and port 10 data presented in the right plot. The ash deposit rate is higher for the two blended fuels at 30 min sampling times in port 7. At this location, we

Table 5. Operating Parameters (Measured and Calculated) Relevant to the Particle Deposition Behavior

parameter	units	port	coal	torrefied	Steam X
flue gas velocity	m/s	7	1.50	1.45	1.43
		10	1.40	1.31	1.33
flue gas temperature	K	7	1363.7	1318.4	1340.9
		10	1278.2	1194.3	1254.3
coupon surface temperature	K	7 and 10	811 ± 10	811 ± 10	811 ± 10
calculated flue gas density[29]	kg/m^3	7	0.262	0.270	0.266
		10	0.279	0.299	0.285

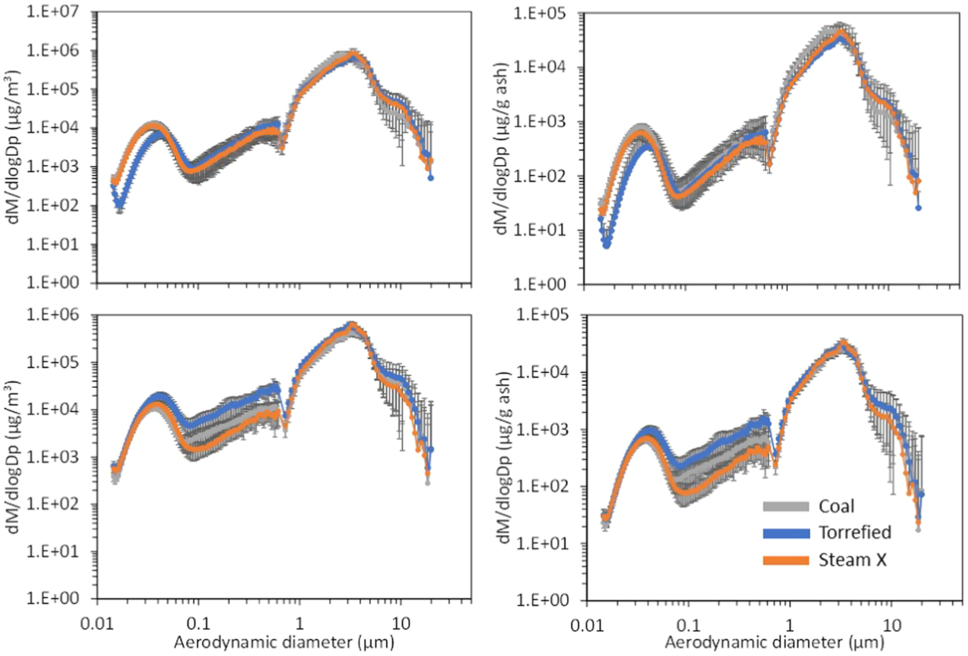

Figure 6. Comparison of ash aerosol PSDs sampled from port 7 (bottom) and port 10 (top) for the three fuel conditions.

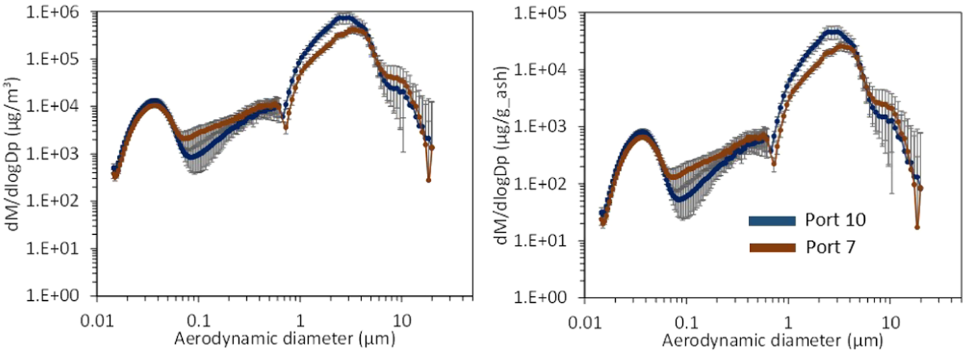

Figure 7. Comparison of ash aerosol PSD measured at port 7 and port 10 while firing coal.

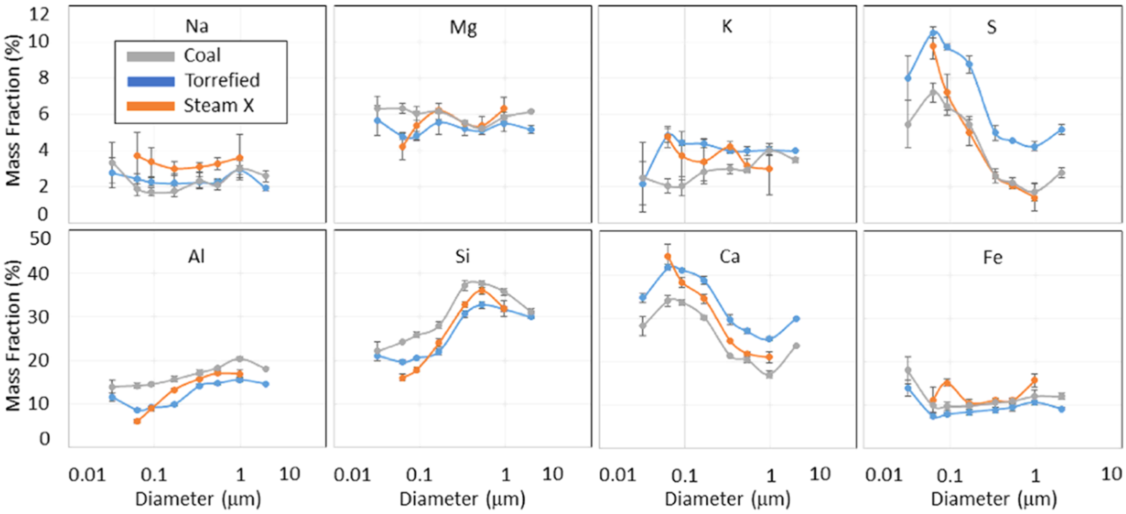

Figure 8. Size-segregated compositions of ash aerosols sampled at port 7 for each of the different fuels.

would expect higher particle concentration of particles larger than 5 μm than in port 10. The port 10 samples show that at long build-up times, there is no difference between the deposit rate of the Torrefied and Coal conditions. However, for the 30 min sample time, deposition rates may be slightly lower for blended fuels. Comparison between the deposit rates for port 7

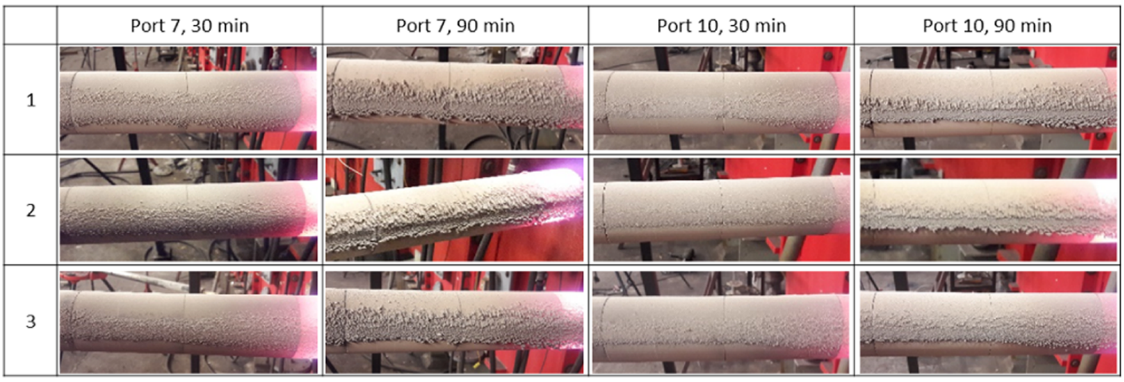

Figure 9. Images of deposit build-up on coupon surfaces for each deposit test interval and fuel. By row: (1) Coal, (2) Torrefied, and (3) Steam X. The picture on the bottom right is representative of a 68 min sample from port 10.

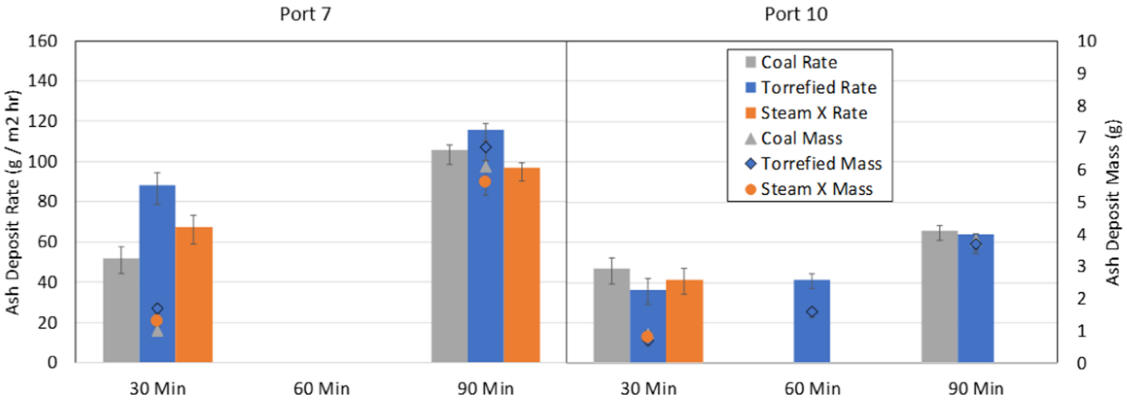

Figure 10. Mass of collected deposit and rate of deposition for the three fuel conditions in both port 7 and port 10.

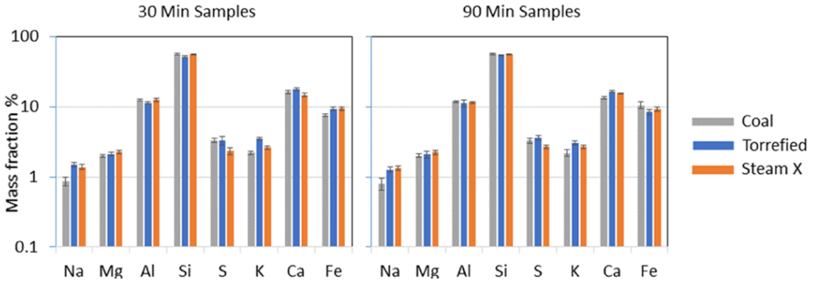

Figure 11. Ash deposit compositions for the 30 and 90 min samples taken in port 7 for all three fuel conditions.

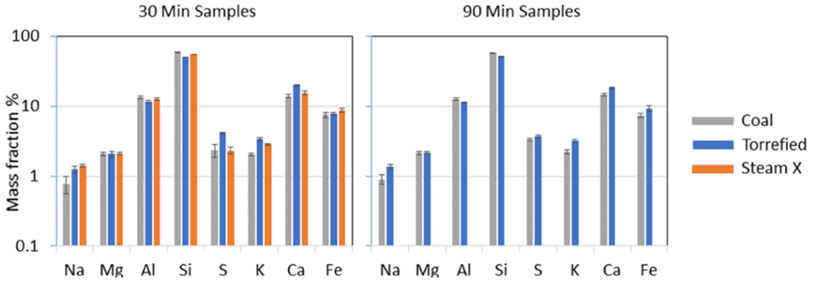

Figure 12. Ash deposit compositions for the 30 and 90 min samples taken in port 10 for all three fuel conditions.

and port 10 indicate the expected behavior, with larger rates for positions closer to the burner. Generally, it is safe to say that the deposition rates are similar while firing these blended fuels or coal.

Figure 11 shows the composition of ash deposits sampled in port 7 for 30 and 90 min retention times, and Figure 12 shows the same for port 10. Silicon (Si), aluminum (Al), calcium (Ca), and iron (Fe), which are typically found in the outer layers of ash deposits,[11] have the highest enrichments for all of the tests. The compositions of the deposits do not differ significantly as a function of fuel. The sodium content of the Coal deposits is slightly lower than for the biomass blends. The

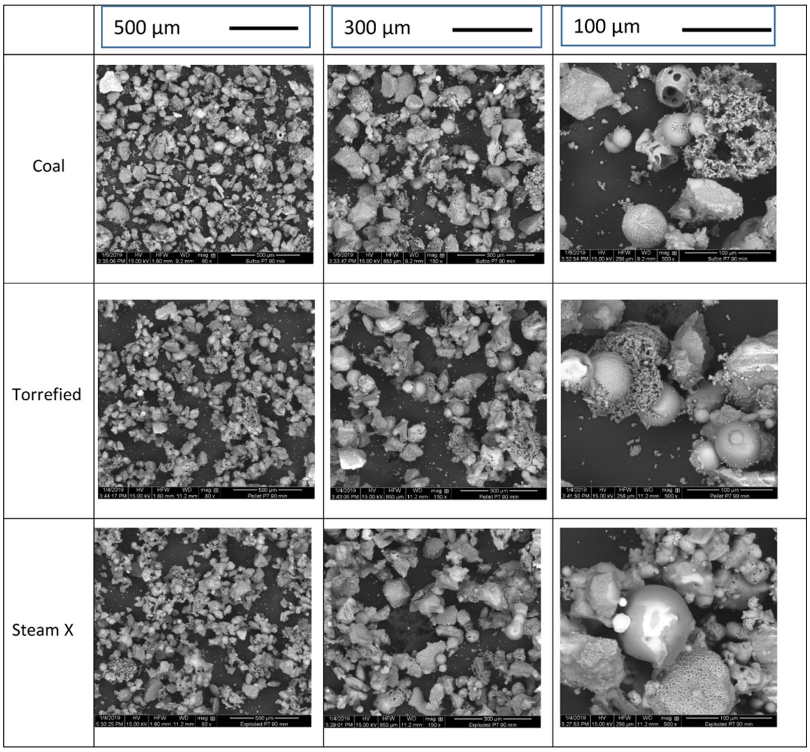

Figure 13. SEM images of ash deposit samples taken in port 7 with a deposition time of 90 min for all three conditions.

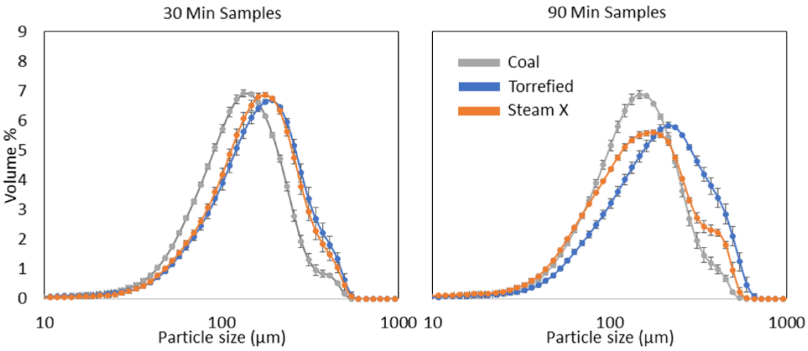

Figure 14. PSD of 30 and 90 min deposit samples collected in port 7 for all three fuel conditions.

qualitative analysis of the thermodynamic equilibrium of vapor species simulated using FactSage 7.3 suggests that the sulfur content in the condensed phase while firing the torrefied fuel should be higher than the other fuels. This observation is in agreement with the higher sulfur concentration of ash aerosol (see Figure 8) and ash deposit samples (Figure 11) for the Torrefied condition compared with the other fuels. Sulfate compounds have a higher melting temperature[31,32] and may be solid at the same temperature, where Cl compounds might be sticky. However, differences in sulfur concentration of fuels, ash aerosol, and ash deposit samples are not large. Sulfur retention efficiency, which is defined as the fraction of the total fuel sulfur that is retained in ash, is not investigated here. Yu[33] showed that the sulfur retention efficiency can increase with the molar ratio of alkali and alkaline earth metallic species to sulfur. A higher concentration of K declines the melting point temperature of ash aerosol particles and increases the melt fraction and leads to enhance ash deposit growth.[34] Variation of potassium concentration of the three fuels is not large but is highest for the torrefied fuel.

SEM images of ash deposits collected in port 7 for 90 min retention time are shown in Figure 13. They are presented in three scales of 500, 300, and 100 μm. These images show very little difference in the morphology of the deposits for the three different fuels. The ash deposits are composed of many large spherical particles. The fine particles accumulated near the surface of coarse particles may represent the nucleated alkali species, which would likely enhance the stickiness of coarse particles.[2]

The PSDs of the collected ash deposit samples were measured by a laser diffraction particle size analyzer (Beckman Coulter LS230). The results of this analysis are shown in Figure 14 for 30 and 90 min samples collected in port 7 for all three fuels. The PSD is shifted to slightly larger particles in the 90 min samples compared with the shorter sampling times. This could be a result of coagulation, as larger particles begin to be retained on the surface after a sticky layer has developed. Figure 14 also suggests that the two blended fuels result in larger particle sizes in the deposit when compared to the Coal condition. More significantly, there is a marked shift in

https://doi.org/10.1021/acs.energyfuels.1c03521
Energy Fuels 2022, 36, 554−564

deposited particle size for the blended fuels at the long retention times in the particle sizes between 300 and 400 μm. It is also interesting that there is little difference in the Coal PSDs for short and long retention times, indicating a difference in behavior between the Coal and the biomass blends.

4. CONCLUSIONS

A 1500 kW_{TH} pulverized coal combustor was used to elucidate the differences in mineral matter transformations and deposition between pure coal and blends of coal with torrefied wood and steam-exploded wood. This study was the first phase of a two-phase project in which the second phase involved similar tests on a full-scale 1.2×10^6 kW_{TH} boiler operated by a utility. The blends were prepared at an 85 mass % composition of Utah bituminous coal and fired using combustion conditions relevant for a full-scale coal-fired utility boiler. Detailed measurements of particle size distribution, composition, and morphology were performed for both the entrained ash aerosol and deposits. The rate of deposition was also determined at two locations in the furnace for the pure coal and the two blends. Overall, these data provided confidence that blends of prepared woody biomass can be fired in an unmodified boiler without significant impacts on ash behavior.

Ash aerosol measurements showed that the particle size distributions were nearly the same for the three fuels tested. However, there was a deviation where the torrefied blend showed an increase in concentration in the 0.1−1 μm size range. Analysis of pure coal samples showed that aerosol at longer furnace residence times the PSD shifted from fine particles 0.1−1 μm to larger particles in the 1−5 μm range. This is likely due to the coagulation of aerosol particles. Composition measurements of the collected aerosol indicated that the blended fuels displayed slightly higher concentrations of alkali metals in the submicron range, possibly due to increased vaporization of organically bound metals. Calcium concentrations were also higher for the blended fuels. However, transformations are only slightly impacted by the wood blending.

Deposition measurements showed that the rates were higher at the location closer to the burner, likely due to the saltation of large particles in low-velocity flue gas, resulting in lower overall particle concentrations in ports further from the burner. The deposit rates were higher (30−70%) for the biomass blends at locations closer to the burner and at short collection times, but nearly the same for all fuels at long collection times. At locations further from the burner and at short collection times, the deposit rates were slightly lower (11−22%) for the biomass blends, but there was no difference at long collection times. The composition of the deposits did not vary significantly as a function of fuel. The deposits were slightly enriched in sodium for the biomass blend tests. SEM imaging of the deposit materials showed essentially no difference in morphology due to the biomass blending. Particle size distributions of deposits indicated that there was a measurable change toward larger particles in the 300−400 μm range when firing biomass blends for all retention times. The shift toward larger particles was greater for longer collection times. However, the coal PSD remained constant for long retention times.

These preparatory pilot-scale tests suggested that the full-scale boiler tests in the field could proceed without undue concern of an upset caused by unsustainable ash deposition rates. These tests also allowed techniques allowing ash sampling and determination of ash deposition rates to be perfected for use in the Phase 2 full-scale boiler tests that followed.

AUTHOR INFORMATION

Corresponding Author

Andrew Fry − *Department of Chemical Engineering, Brigham Young University, Provo, Utah 84602, United States;* orcid.org/0000-0002-4172-9266; Email: afry@byu.edu

Authors

Seyedhassan Fakourian − *Department of Chemical Engineering, Brigham Young University, Provo, Utah 84602, United States*

Xiaolong Li − *Department of Chemical Engineering and Institute for Clean and Secure Energy (ICSE), University of Utah, Salt Lake City, Utah 84112, United States*

Yueming Wang − *Department of Chemical Engineering and Institute for Clean and Secure Energy (ICSE), University of Utah, Salt Lake City, Utah 84112, United States;* orcid.org/0000-0002-2059-4315

Jost O. L. Wendt − *Department of Chemical Engineering and Institute for Clean and Secure Energy (ICSE), University of Utah, Salt Lake City, Utah 84112, United States;* orcid.org/0000-0002-0104-0763

Complete contact information is available at: https://pubs.acs.org/10.1021/acs.energyfuels.1c03521

Notes

The authors declare no competing financial interest.

ACKNOWLEDGMENTS

The authors would like to acknowledge Jinze Dai for his kindly assistance.

REFERENCES

(1) Robbins, J. Bark Beetles Kill Millions of Acres of Trees in West, 2008. https://www.nytimes.com/2008/11/18/science/18trees.html (accessed Sept 01, 2020).

(2) Xu, X. G.; et al. Effect of Co-firing Straw with Two Coals on the Ash Deposition Behavior in a Down-Fired Pulverized Coal Combustor. *Energy Fuels* **2010**, *24*, 241−249.

(3) Stroh, A.; et al. 3-D numerical simulation for co-firing of torrefied biomass in a pulverized-fired 1 MWth combustion chamber. *Energy* **2015**, *85*, 105−116.

(4) Fakourian, S.; Fry, A.; Jasperson, T. Analysis of particle behavior inside the classifier of a Raymond Bowl Mill while co-milling woody biomass with coal. *Fuel Process. Technol.* **2018**, *182*, 95−103.

(5) Shah, M.; et al. Near zero emissions oxy-combustion CO2 purification technology. *Energy Procedia* **2011**, *4*, 988−995.

(6) Dobó, Z. A.; Fry, A. Investigation of co-milling Utah bituminous coal with prepared woody biomass materials in a Raymond Bowl Mill. *Fuel* **2018**, *222*, 343−349.

(7) Jenkins, B. M.; et al. Combustion properties of biomass. *Fuel Process. Technol.* **1998**, *54*, 17−46.

(8) Wang, Y. et al. Ash Aerosol and Ash Deposit Formation During High Temperature OXY-Combustion of Various Solid Fuels. In *Department of Chemical Engineering*; The University of Utah, 2019.

(9) Baxter, L. L.; et al. The behavior of inorganic material in biomass-fired power boilers: field and laboratory experiences. *Fuel Process. Technol.* **1998**, *54*, 47−78.

(10) Hansen, S. B.; Frandsen, F. J.; Jensen, P. A. Model for Deposition Build-up in Biomass Boilers. In *Department of Chemical and Biochemical Engineering*; Technical University of Denmark, 2015; p 228.

(11) Deng, L.; Jin, X.; Long, J.; Che, D. Ash deposition behaviors during combustion of raw and water washed biomass fuels. *J. Energy Inst.* **2019**, *92*, 959−970.

(12) Nordgren, D.; et al. Ash transformations in pulverised fuel co-combustion of straw and woody biomass. *Fuel Process. Technol.* **2013**, *105*, 52−58.

(13) Theis, M.; et al. Fouling tendency of ash resulting from burning mixtures of biofuels. Part 2: Deposit chemistry. *Fuel* **2006**, *85*, 1992−2001.

(14) Liu, Y.; et al. Ash deposition behavior in co-combusting high-alkali coal and bituminous coal in a circulating fluidized bed. *Appl. Therm. Eng.* **2019**, *149*, 520−527.

(15) Qiu, K.; et al. Experimental investigation of ash deposits characteristics of co-combustion of coal and rice hull using a digital image technique. *Appl. Ther. Eng.* **2014**, *70*, 77−89.

(16) Robinson, A. L.; Junker, H.; Baxter, L. L. Pilot-Scale Investigation of the Influence of Coal-Biomass Cofiring on Ash Deposition. *Energy Fuels* **2002**, *16*, 343−355.

(17) Zhang, D. Ash Fouling, Deposition and Slagging in Ultra-Supercritical Coal Power Plants. In *Ultra-Supercritical Coal Power Plants*; Woodhead Publishing Limited, 2013.

(18) Ndibe, C.; et al. Emissions reduction and deposits characteristics during cofiring of high shares of torrefied biomass in a 500 kW pulverized coal furnace. *Fuel* **2015**, *156*, 177−189.

(19) Zhou, H.; et al. Ash deposition behavior under coal and wood co-firing conditions in a 300 kW downfired furnace. *J. Energy Inst.* **2018**, *91*, 743−755.

(20) Zhan, Z.; et al. Novel Temperature-Controlled Ash Deposition Probe System and Its Application to Oxy-coal Combustion with 50% Inlet O2. *Energy Fuels* **2014**, *28*, 146−154.

(21) Zhan, Z. H.; et al. Ash aerosol formation from oxy-coal combustion and its relation to ash deposit chemistry. *Proc. Combus. Inst.* **2015**, *35*, 2373−2380.

(22) http://www.omafra.gov.on.ca/english/engineer/facts/11-035.htm#3 (accessed April 06, 2019).

(23) van der Stelt, M. J. C.; et al. Biomass upgrading by torrefaction for the production of biofuels: A review. *Biomass Bioenergy* **2011**, *35*, 3748−3762.

(24) Lepisto, C. Is there a renewable energy secret in your cup of coffee?. 2014, http://www.treehugger.com/renewable-energy/there-renewable-energy-secret-your-cup-coffee.html (accessed April 06, 2019).

(25) Bridgeman, T. G.; et al. Torrefaction of reed canary grass, wheat straw and willow to enhance solid fuel qualities and combustion properties. *Fuel* **2008**, *87*, 844−856.

(26) Stelte, W.; et al. Pelletizing properties of torrefied spruce. *Biomass Bioenergy* **2011**, *35*, 4690−4698.

(27) Kataria, R. et al. *Bench Scale Steam Explosion Pretreatment of Acid Impregnated Elephant Grass Biomass and Its Impacts on Biomass Composition, Structure and Hydrolysis*; Industrial Crops and Products, 2016.

(28) Biswas, A. K. *Thermochemical Behavior of Pretreated Biomass*; KTH Royal Institute of Technology, 2012.

(29) Hansen, S. B.; et al. Mechanistic Model for Ash Deposit Formation in Biomass Suspension Firing. Part 1: Model Verification by Use of Entrained Flow Reactor Experiments. *Energy Fuels* **2017**, *31*, 2771−2789.

(30) Xu, M.; et al. Coal combustion-generated aerosols: Formation and properties. *Proc. Combust. Inst.* **2011**, *33*, 1681−1697.

(31) Robinson, A. L.; Junker, H.; Buckley, S. G.; Sclippa, G.; Baxter, L. L. In *Interactions between Coal and Biomass When Cofiring*, Twenty-Seventh Symposium (International) on Combustion, 1998.

(32) Mwabe, P.O.; Wendt, J. O. L. In *Mechansims Governing Trace Sodium Capture by Kaolinite in a Downflow Combustor*, Twenty-Sixth Symposium (International) on Combustion, 1996.

(33) Yu, D.; et al. Ash and deposit formation from oxy-coal combustion in a 100 kW test furnace. *Int. J. Greenhouse Gas Control* **2011**, *5*, S159−S167.

(34) Cai, Y.; et al. Modeling of ash formation and deposition processes in coal and biomass fired boilers: A comprehensive review. *Appl. Energy* **2018**, *230*, 1447−1544.

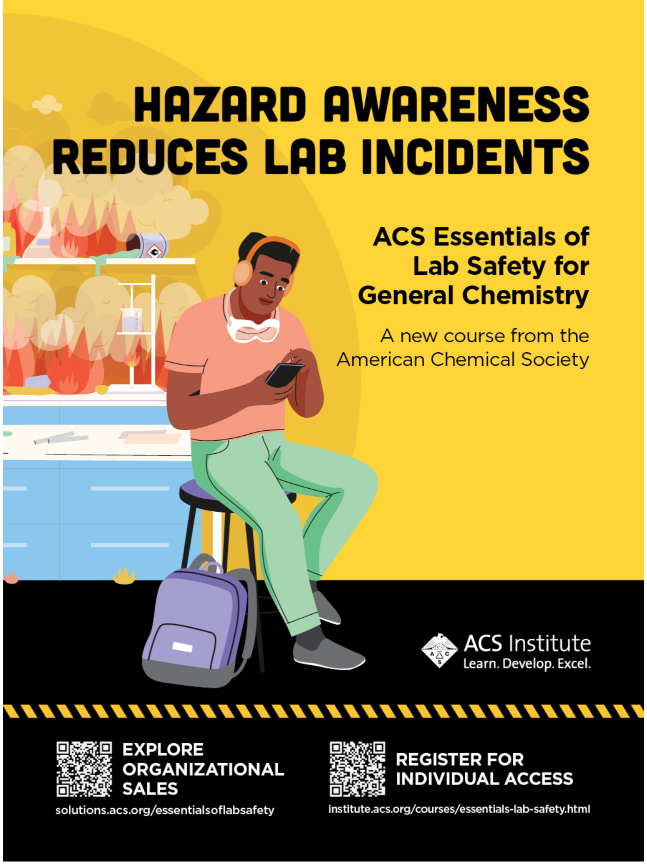

https://doi.org/10.1021/acs.energyfuels.1c03521

Technical Assistance in Support of Biomass Co-firing Demonstration

Pilot-scale Combustion Testing, November 2018

Andrew Fry, Seyedhassan Fakourian
Brigham Young University, Department of Chemical Engineering

Eric Eddings, Jost Wendt, Yueming Wang, Xiaolong Li, Marc Backman, Teri Draper, Kaitlyn Scheib, Stan Harding
University of Utah, Institute for Clean and Secure Energy

Klas Andersson, Thomas Allgurén, Adrian Gunnarsson, Dan
Chalmers University,

PacifiCorp Presentation, February 20, 2019

Presentation Road Map

- Configuration of Hunter, Unit 3
- Description of pilot-scale furnace and measurement equipment
  - Measuring heat removal through cooling surfaces
  - Measuring wall temperature and refractory heat flux
  - Measuring radiative heat flux
  - Deposition measurement
- Experimental conditions & results
  - Heat balance
  - Gas temperatures & radiative heat flux
  - Gas species
  - Entrained ash
  - Deposition
- Summary & conclusions

Testing Purpose

Objective: To produce data sets describing the expected performance of Hunter, Unit 3 while co-firing both torrified and steam exploded woody biomass with Utah Sufco coal using University of Utah's 1.5 MW pilot-scale combustor (L1500).

Quantities of Greatest Interest:

- Flame Stability
- Furnace heat distribution
- Particle deposition at fouling temperatures

In order to achieve this objective it is necessary to understand how the firing system in Hunter, Unit 3 is operated and configure the L1500 to mimic that system.

Configuration of Hunter, Unit 3

Hunter, Unit 3 - Boiler Layout

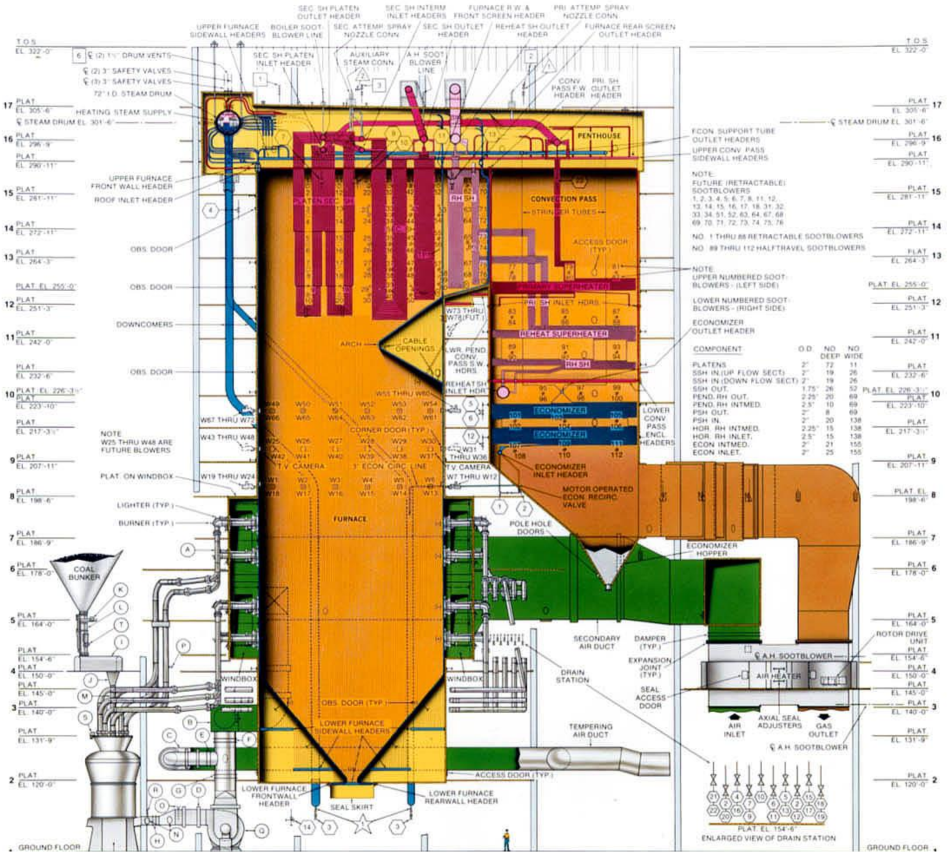

NOTE:
FUTURE (RETRACTABLE) SOOTBLOWERS
1, 2, 3, 4, 5, 6, 7, 8, 11, 12,
13, 14, 15, 16, 17, 18, 31, 32,
33, 34, 51, 52, 63, 64, 67, 68,
69, 70, 71, 72, 73, 74, 75, 76

NO. 1 THRU 88 RETRACTABLE SOOTBLOWERS

NO. 89 THRU 112 HALFTRAVEL SOOTBLOWERS

NOTE:
UPPER NUMBERED SOOT-BLOWERS - (LEFT SIDE)

LOWER NUMBERED SOOT-BLOWERS - (RIGHT SIDE)

COMPONENT	O.D.	NO. DEEP	NO. WIDE
PLATENS	2"	72	11
SSH IN (UP FLOW SECT.)	2"	19	26
SSH IN (DOWN FLOW SECT.)	2"	19	26
SSH OUT.	1.75"	26	52
PEND. RH OUT.	2.25"	20	69
PEND. RH INTMED.	2.5"	10	69
PSH OUT.	2"	8	69
PSH IN.	2"	20	138
HOR. RH INTMED.	2.25"	15	138
HOR. RH INLET.	2.5"	15	138
ECON. INTMED.	2"	21	155
ECON. INLET.	2"	25	155

Hunter, Unit 3 - Boiler Geometry

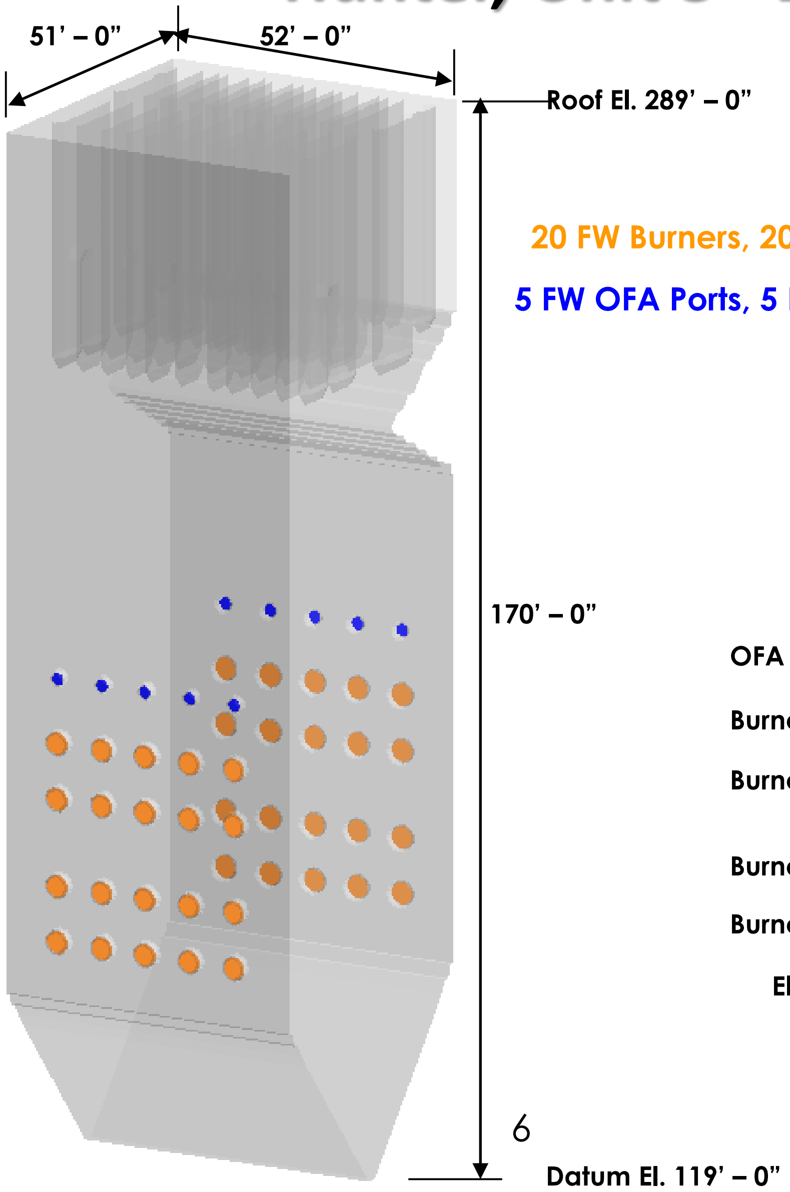

20 FW Burners, 20 RW Burners

5 FW OFA Ports, 5 RW OFA Ports

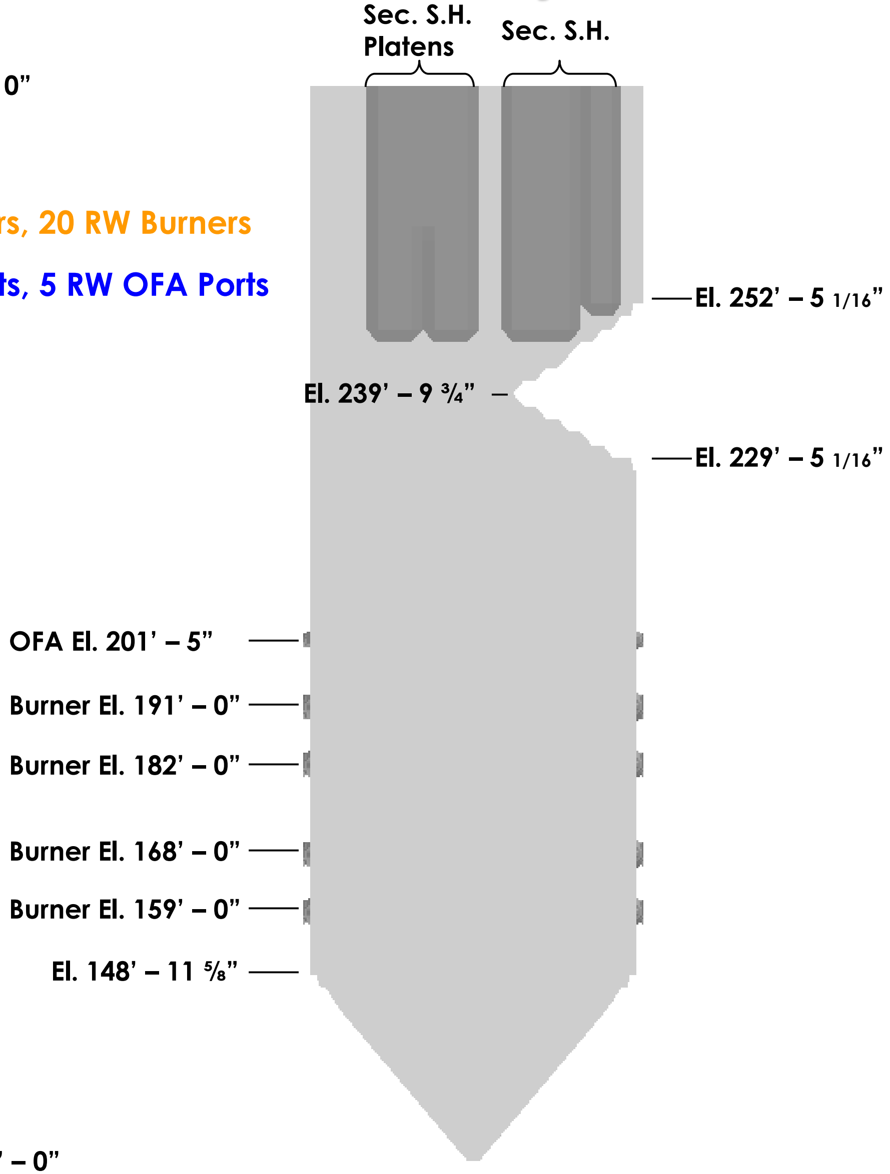

Hunter, Unit 3 - Burner Geometry

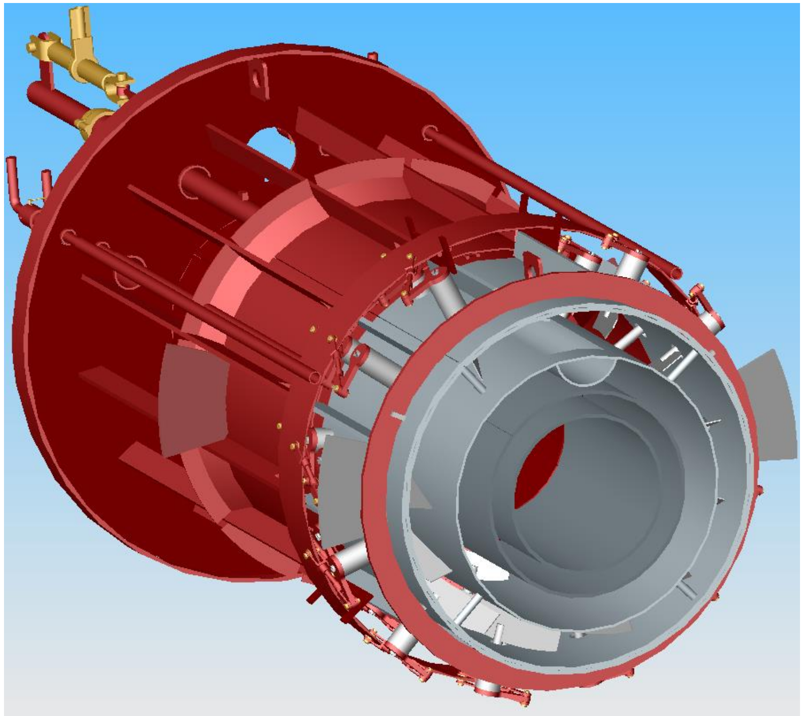

End View

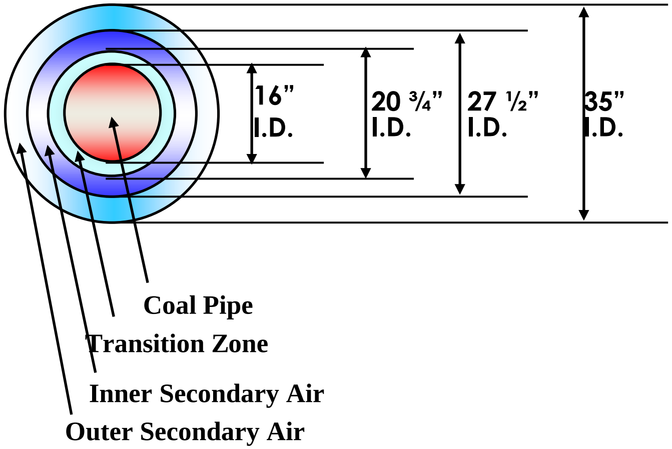

Side View

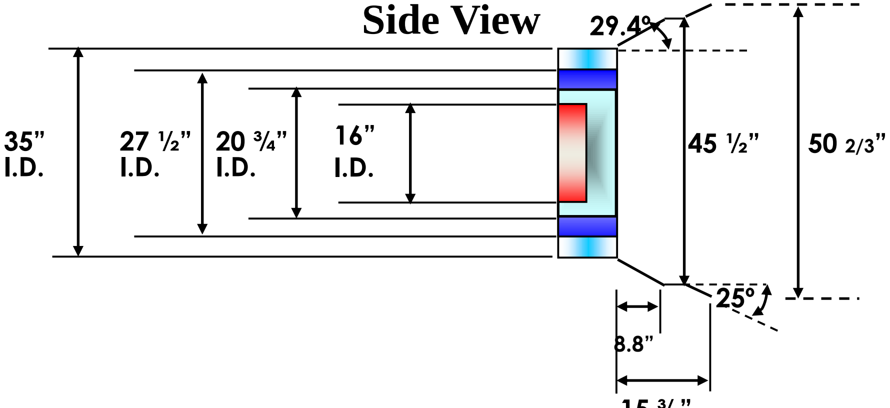

Hunter, Unit 3 - Baseline Operating Conditions

From 2010 Performance Testing

Furnace Operational Data	**Baseline**
Firing Rate (MBtu/h)	**4528**
Stoichiometric Ratio	**1.182**
Lower Furnace Stoichiometric Ratio	**0.900**
Coal Flow Rate (klb/h)	**399.1**
Total Combustion Air/O_2 Flow (klb/h)	**4052.0**
Theoretical Excess O_2, (%, wet)	**3.03%**
Burner Zone Air/O_2 Flow (klb/h)	**3085.1**
OFA Flow Air/O_2 (klb/h)	**966.9**
Burner Operational Data (per burner)	
Coal Flow Rate (klb/h)	**9.98**
Primary Air/O_2 Flow (klb/h)	**19.66**
Primary Gas/Coal	**1.97**
Primary Air Temperature (ºF)	**150**
Secondary Air/O_2 Flow (klb/h)	**57.47**
Transition Air Flow (klb/h)	**4.60**
Inner Secondary Air Flow (klb/h)	**15.86**
Outer Secondary Air Flow (klb/h)	**37.01**
Secondary Air Temperature (ºF)	**528**
OFA Port Operational Data (per port)	
Air/O_2 Flow (klb/h)	**96.7**
Core Zone Air/O_2 Flow (klb/h)	**58.0**
Core Zone Velocity (ft/s)	**256.4**
Outer Zone Air/O_2 Flow (klb/h)	**38.7**
Outer Zone Velocity (ft/s)	**114.5**
Temperature (ºF)	**528**

Lower Furnace is Staged

Primary gas/coal mass ratio

Neglecting the Transition Air, the secondary air distribution is 30/70 mass % Inner/Outer

Description of Pilot-scale Furnace and Measurement Equipment

5.0 MBtu/hr Pilot-Scale Furnace (L1500)

Unique L1500 Capabilities:

- Realistic Burner Turbulent Mixing Scale
- Realistic Radiative Conditions
- Realistic Time – Temperature Profile

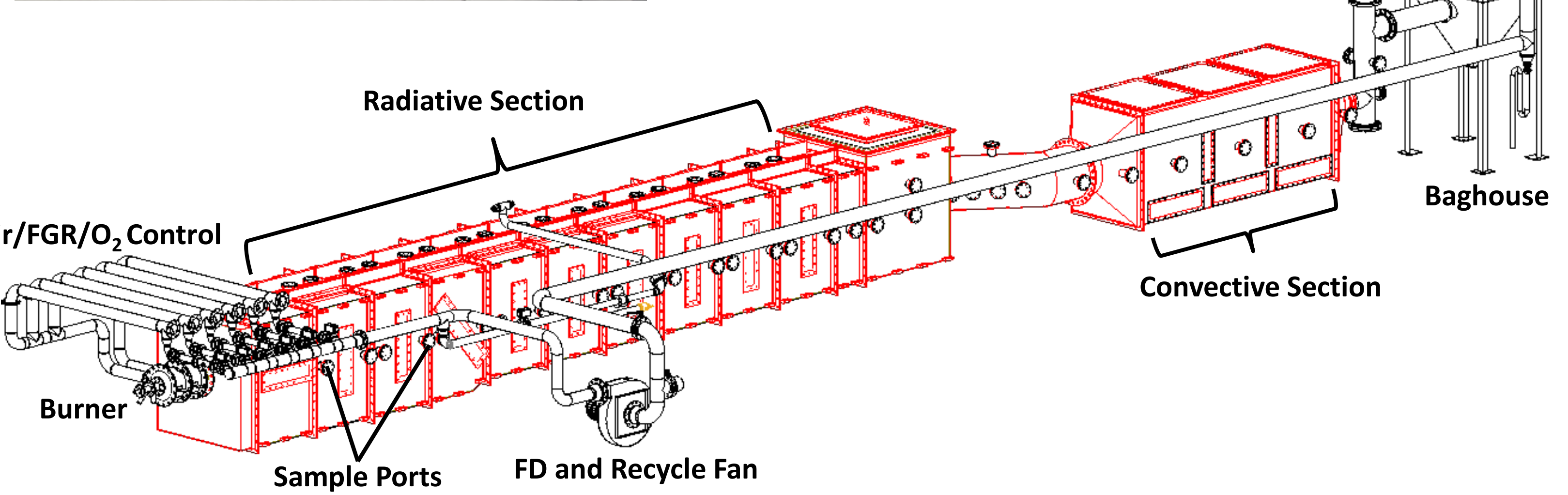

Dual Register Low-NO_x Burner (LNB)

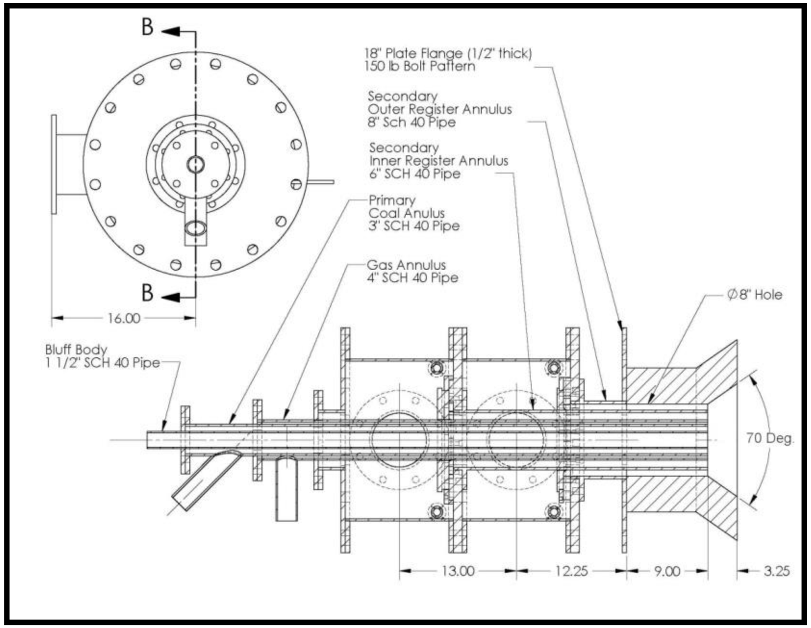

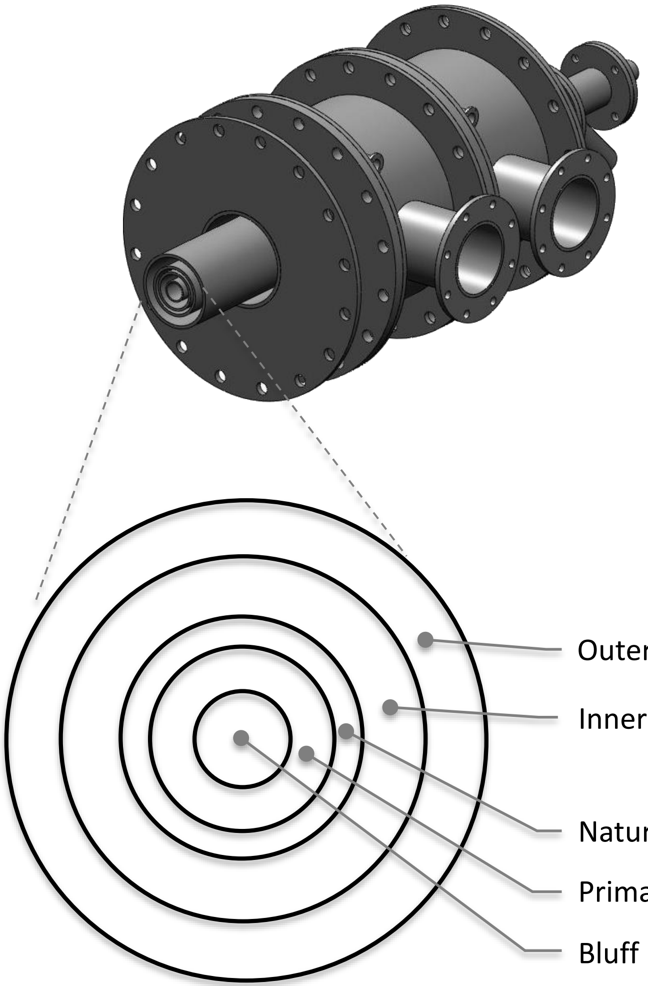

Outer Secondary Air or O_2/FGR Mixture [OD – 8.0”, ID – 6.56”]

Inner Secondary Air or O_2/FGR Mixture [OD – 6.06, ID – 4.5”]

Natural Gas (For heat up) [OD – 4.06”, ID – 3.88”]

Primary (Coal carrier) [OD – 3.5”]

Bluff Body (Not used in these tests)

L1500 Heat Balance

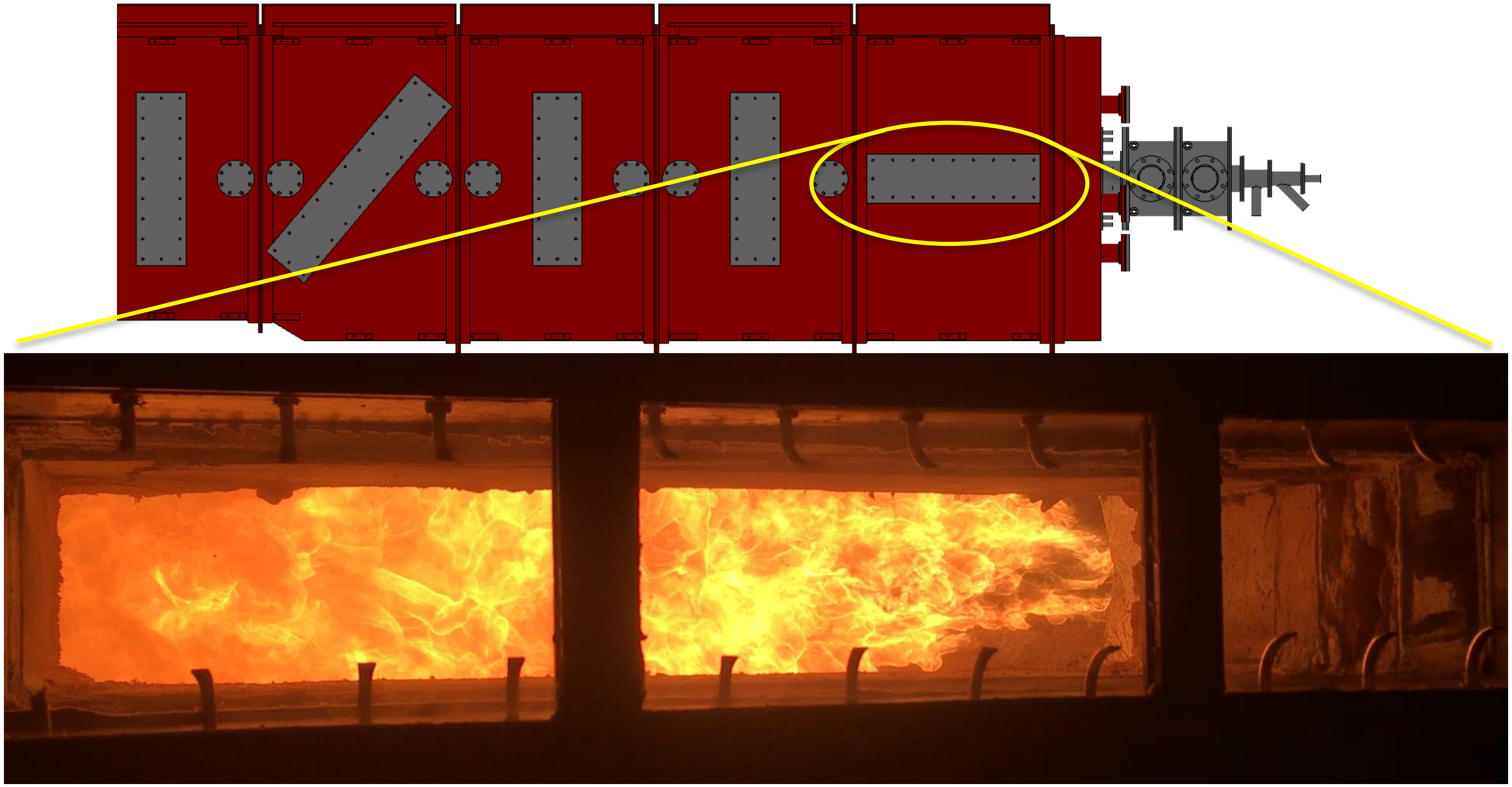

* Air-fired flame at the end of the high temperature oxygen test

L1500 Furnace Configuration (Measurements)

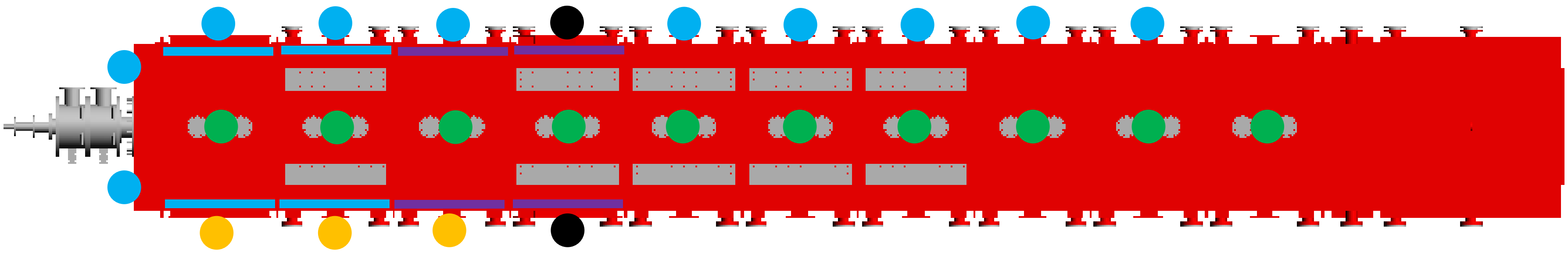

🟢 Locations where B-thermocouple assembly is cast in refractory (2 thermocouples, multi-depth)
Heat Flux, Inside Refractory Surface Temperature

⚫ Locations where water cooled Over-fired Air Port (OFA) is installed
Upgraded for determination of heat removal

🔵 Locations where cooled sample ports are installed (2 ½” ID access, water cooled, thermocouples & flow meter)
Total Heat Removal, Location for: Soot Blowing, Gas sampling, Solid Sampling, FTIR Gas Temperature Measurement

🟡 Locations where narrow beam radiometers are installed
Total Incident Radiation

▬ Locations where cooling panels are installed (water cooled, thermocouples & flow meter, multi-depth thermocouples)
Total Heat Removal, Heat Flux, Surface Temperature, Deposition

▬ Locations where cooling coils are installed (water cooled, thermocouples & flow meter)
Total Heat Removal, Surface Temperature

L1500 Particle and Deposit Measurements

Performed alternately in south ports of sections 7 and 10

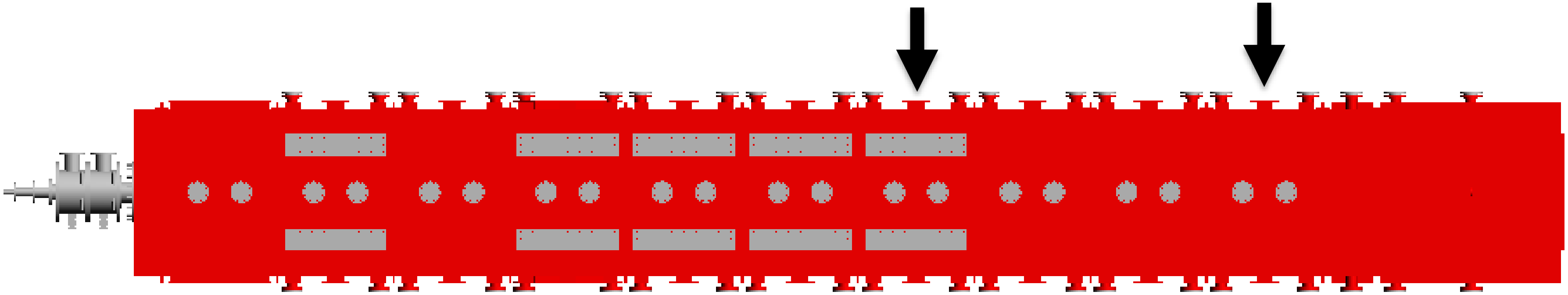

Entrained Particle Size Distribution – Using the methodology developed for OFC (SMPS & APS & BLPI)
Utilizing the new particle sampling probe designed for Hunter 3

Deposition (Fouling) – Using the same methodology developed for OFC testing
Utilizing the new probe developed for Hunter 3 testing

L1500 Additional Measurements

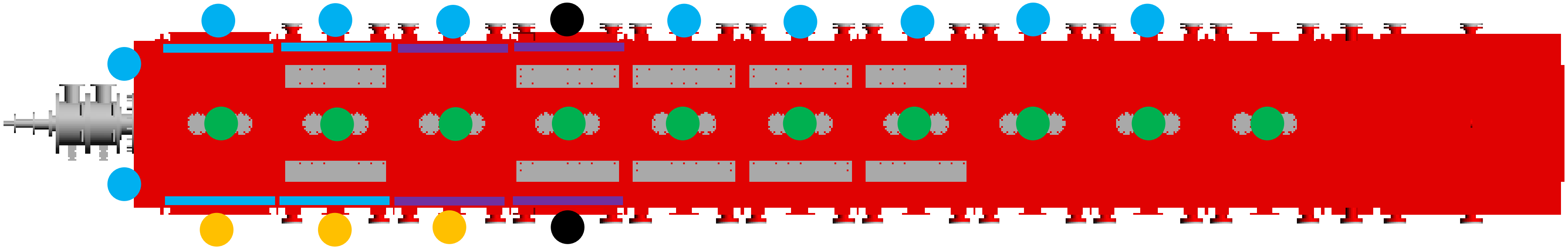

Suction Pyrometer Probe for HVT Measurements. Performed in the first 3 sections

Radiative intensity profiling probe. Performed in the first 3 sections

Gas composition sampling for trace species by FTIR. Performed in Sections 1,2,3 and 7.

Measuring Heat Removal Through Cooling Surfaces

Cooling Coils and Panels

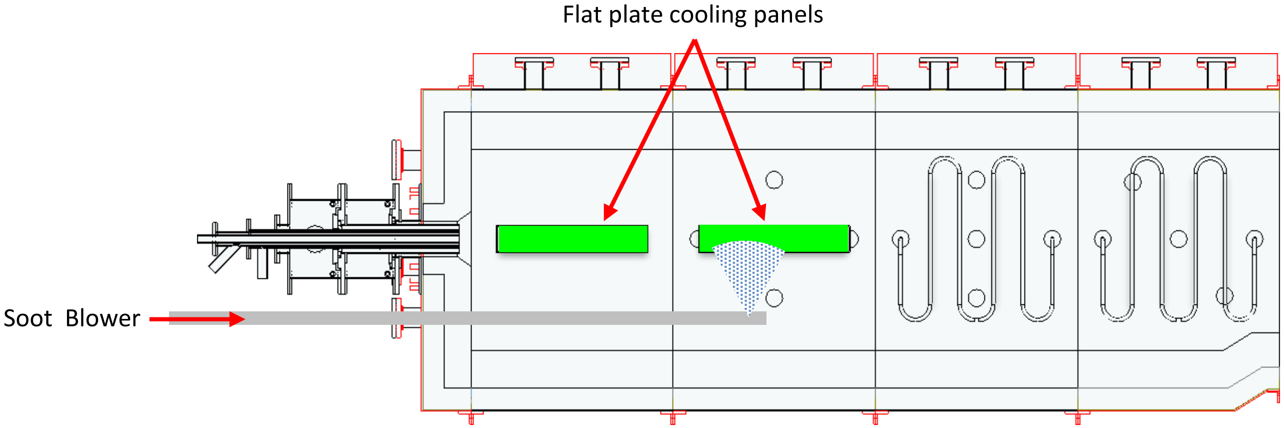

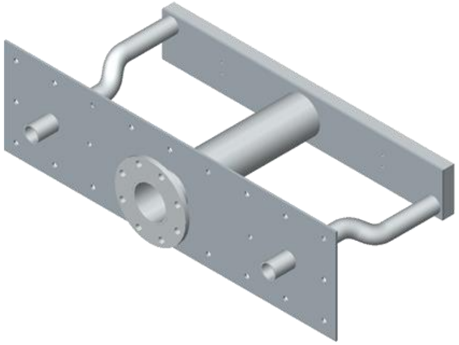

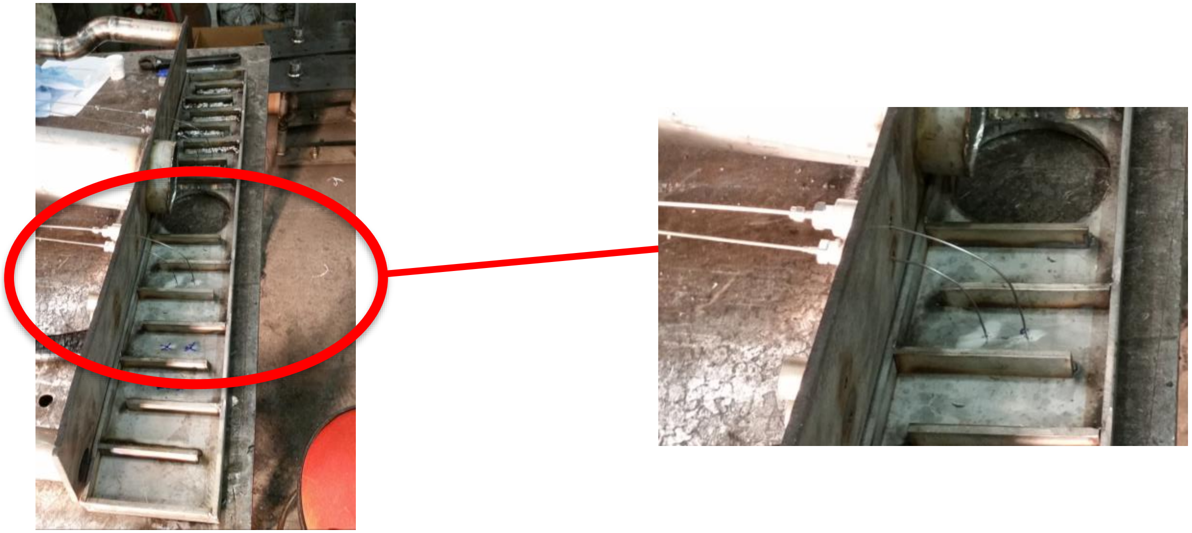

Multiple depth thermocouples placed in the hot-side plate for heat flux measurements

2 thermocouple sets / heat exchanger

8 total heat flux measurements

Cooling Coils and Panels

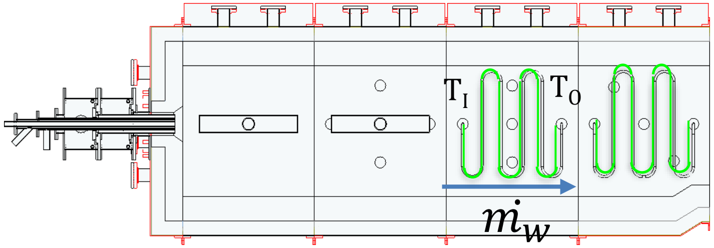

- Cooling surfaces are necessary to provide steady state temperature profile
- Heat removal is determined by measuring the mass flow of water and the temperature of the water in and out

$$Q = \dot{m}_w \cdot c_p(T_O - T_I)$$

- Measurement is very sensitive to particle deposition

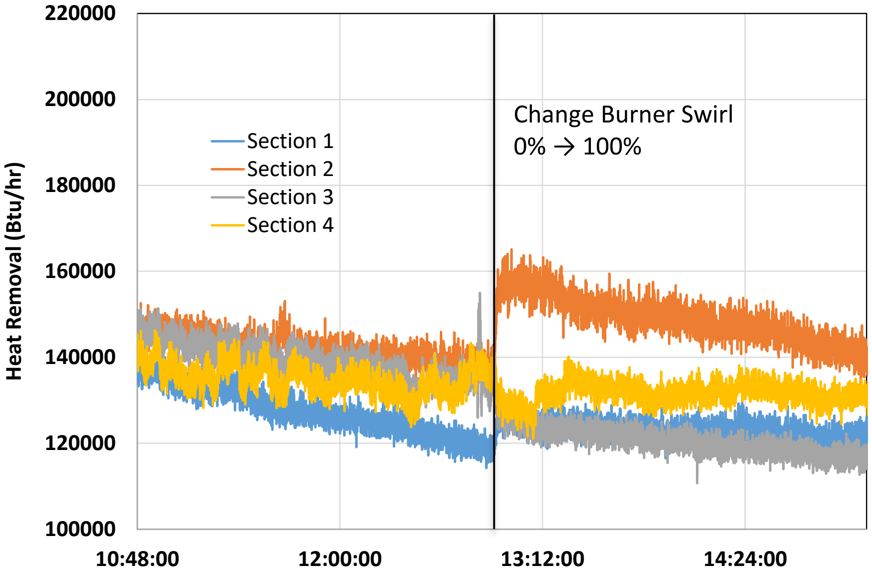

Cooling Coils and Panels

Cooling panel cross section

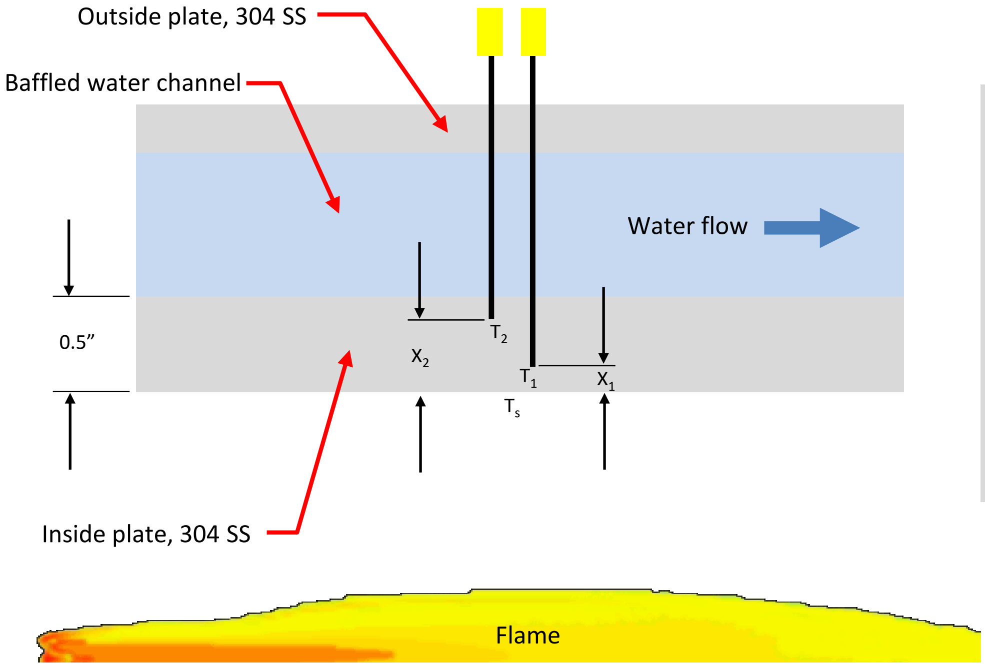

Outside plate, 304 SS

Baffled water channel

Water flow

0.5”

X_2

T_2

T_1

X_1

T_s

Inside plate, 304 SS

Flame

Thermocouple cross section

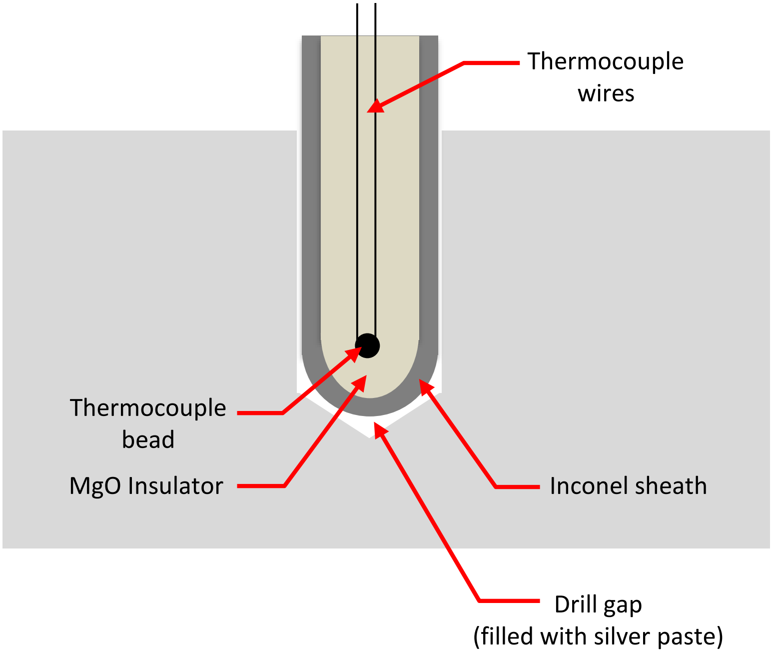

Thermocouple wires

Thermocouple bead

MgO Insulator

Inconel sheath

Drill gap
(filled with silver paste)

Measuring Wall Temperatures and Wall Refractory Heat Flux

Wall Thermocouples

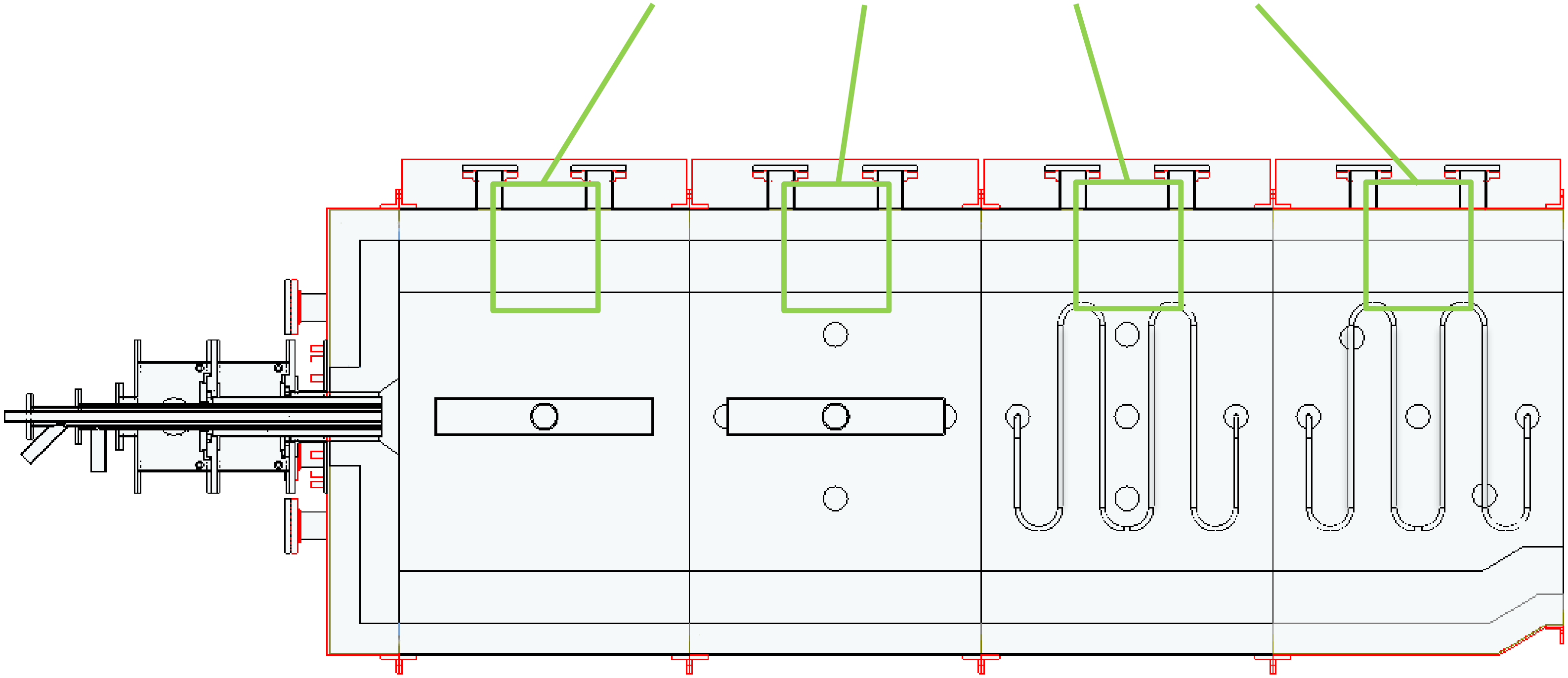

Installed in the center of the top wall of each section

Permanently installed indicator of temperature profile
(continuous data)

Wall Thermocouple Device

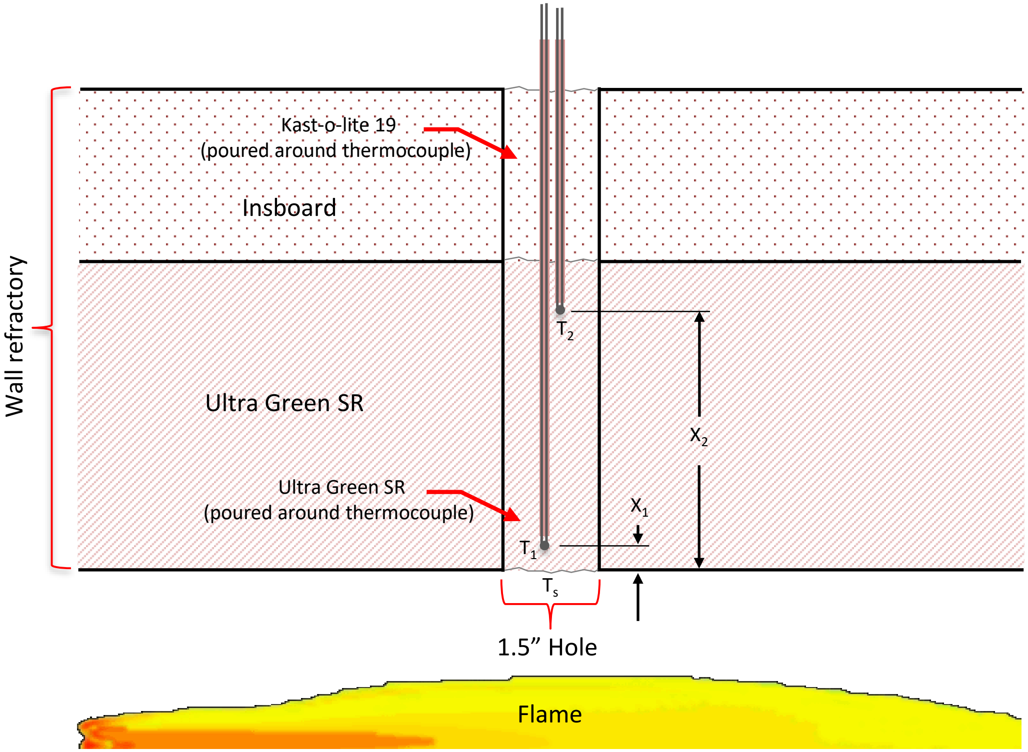

Advantages:

- Environment closely approximates the natural furnace wall
- Simple mathematical description of temperature profile
- Both surface temperature and heat flux can be acquired

Disadvantages:

- Expensive
- Difficult to install

Measuring Radiative Heat Flux

Radiometer Configuration

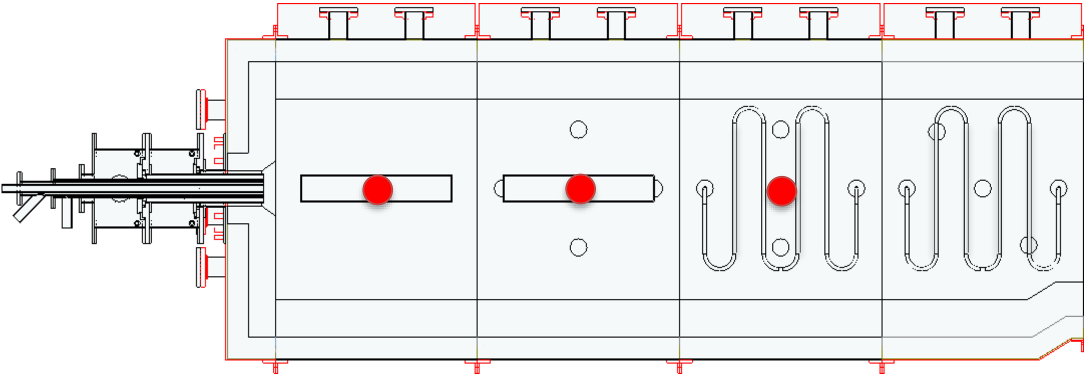

- Installed on the center port in the first three sections of the furnace
- Open 4” cavity (optically dark) on the opposite side of the furnace
  - Minimize the wall effects and measure only flame properties

Deposition Measurement

Deposition Measurement

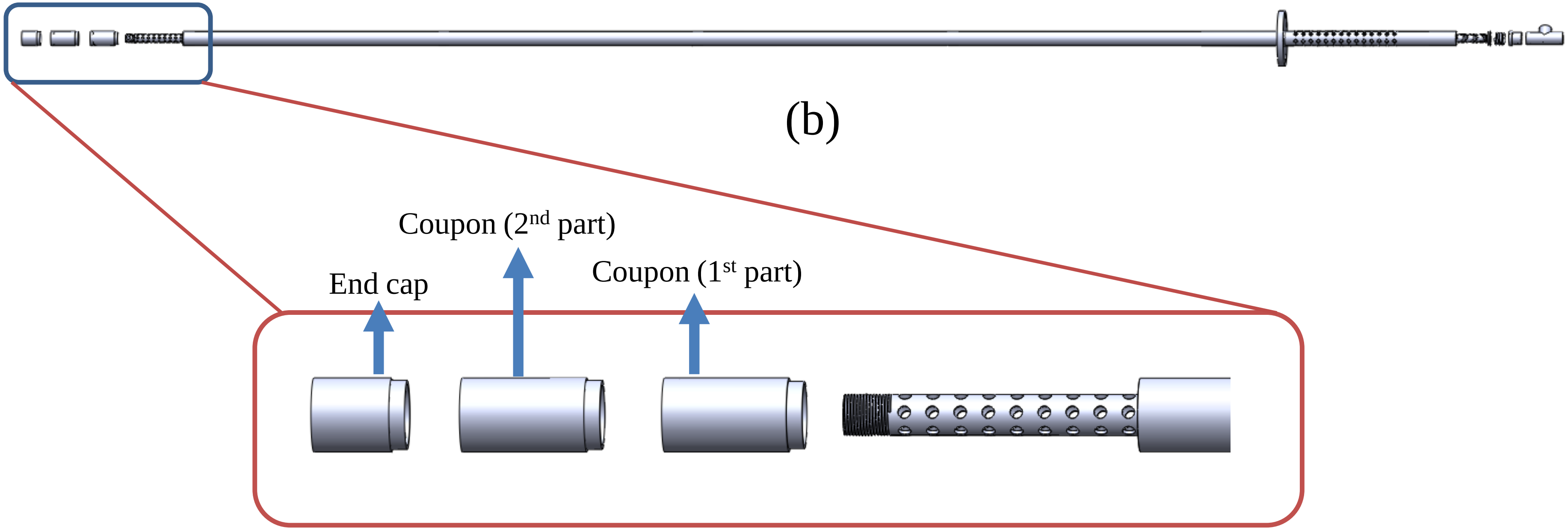

Coupon includes two parts to facilitate inserting the sensor of thermocouple into the first part of coupon. The internal surface of first part of coupon has a hole to keep the sensor of thermocouple.

Deposition Measurement

Experimental Conditions and Results

L1500 Experiment Conditions

Measured Fuel Compositions

	Sufco	Blend – Steam Xploded	Blend – Torrefied @ 325°C
C	63.14	60.68	59.77
H	4.36	4.50	4.37
N	1.13	1.06	1.00
S	0.45	0.48	0.47
O	11.63	14.19	14.15
Ash	12.76	14.19	15.02
H2O	6.53	4.90	5.22
HHV (Btu/lb)	11168	10616	10646

* all values in mass % unless otherwise specified

Blend - 85% Sufco Coal / 15% Biomass

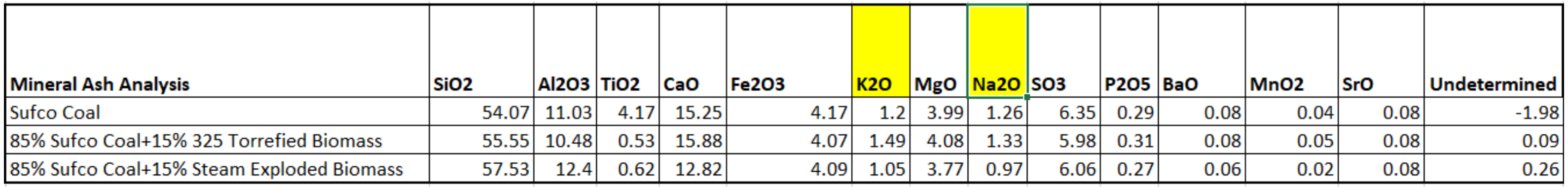

Mineral Ash Analysis	SiO2	Al2O3	TiO2	CaO	Fe2O3	K2O	MgO	Na2O	SO3	P2O5	BaO	MnO2	SrO	Undetermined
Sufco Coal	54.07	11.03	4.17	15.25	4.17	1.2	3.99	1.26	6.35	0.29	0.08	0.04	0.08	-1.98
85% Sufco Coal+15% 325 Torrefied Biomass	55.55	10.48	0.53	15.88	4.07	1.49	4.08	1.33	5.98	0.31	0.08	0.05	0.08	0.09
85% Sufco Coal+15% Steam Exploded Biomass	57.53	12.4	0.62	12.82	4.09	1.05	3.77	0.97	6.06	0.27	0.06	0.02	0.08	0.26

L1500 Actual Operating Conditions

Value	Units	Sufco	Blend – Steam Exploded	Blend – Torrefied @ 325°C
Coal rate (inst)	lb/hr	280.95	282.86	282.11
Primary Air	lb/hr	541.65	506.55	505.95
Inner Secondary Air	lb/hr	421.90	434.64	434.64
Outer Secondary Air	lb/hr	834.47	914.35	913.78
Staging Air	lb/hr	591.22	576.89	574.94
Air Leakage	lb/hr	343.00	380.00	485.00
Primary temp	F	86.08	86.34	86.56
Inner Secondary Temp	F	484.22	483.31	483.23
Outer Secondary Temp	F	489.78	498.57	498.75
Staging Temp	F	115.44	114.85	114.68
Exhaust Temp	F	317.10	357.56	359.95
Trans Temp NO	F	1459.99	1524.56	1525.47
Trans Temp SO	F	1455.44	1520.05	1521.86
Cooling Tower Inlet Temp	F	67.91	78.40	78.18
Cooling Tower Outlet Temp	F	64.66	74.81	75.14
Ambient Press	in Hg	26.05	25.91	25.90
Furnace Press	in H2O	0.22	-0.08	-0.03
FG moisture	% Vol	5.82	6.12	6.16
FG - O2	% Vol	4.23	4.47	4.54
FG - CO2	% Vol	15.26	15.20	15.11

Heat Balance

L1500 Heat Balance

Torrefied Wood (325 °C)/Coal Blend

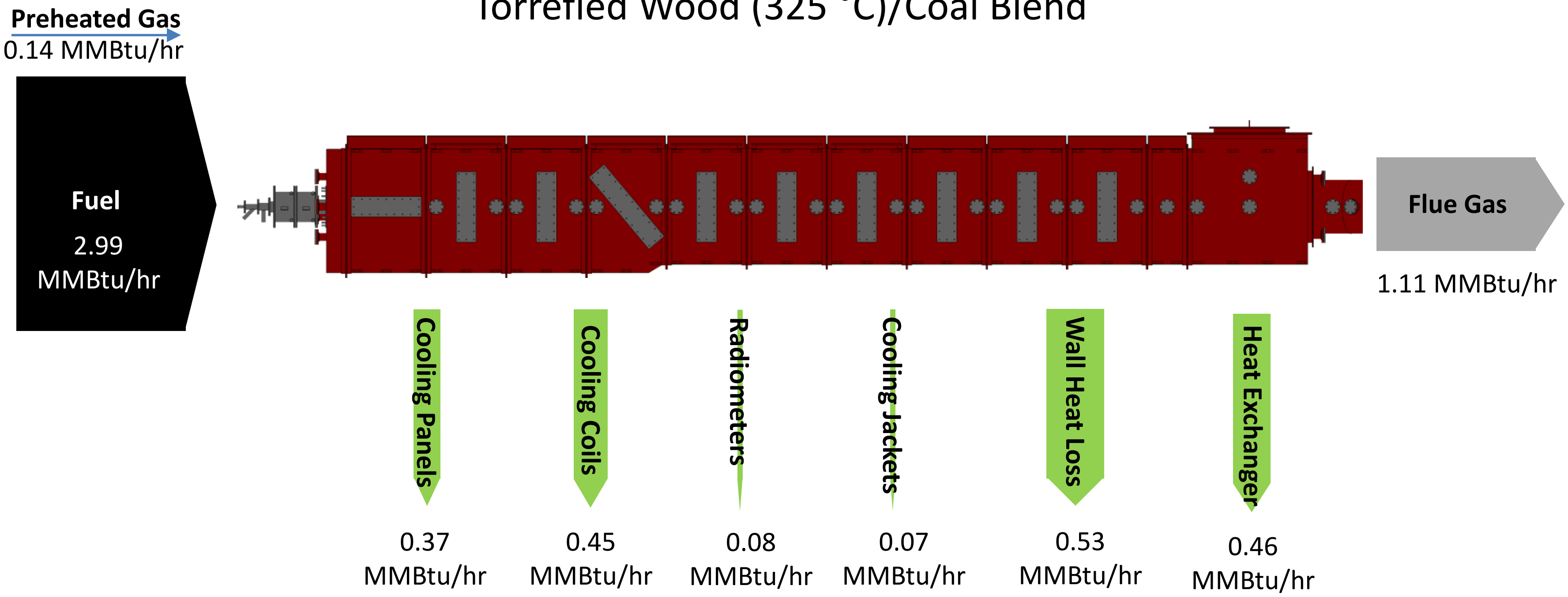

Preheated Gas
0.14 MMBtu/hr

Fuel
2.99
MMBtu/hr

Flue Gas
1.11 MMBtu/hr

Cooling Panels
0.37
MMBtu/hr

Cooling Coils
0.45
MMBtu/hr

Radiometers
0.08
MMBtu/hr

Cooling Jackets
0.07
MMBtu/hr

Wall Heat Loss
0.53
MMBtu/hr

Heat Exchanger
0.46
MMBtu/hr

Heat Loss From Furnace
2.02 MMBtu/hr

2.8 % Difference

Measured Heat Removal
1.96 MMBtu/hr

L1500 Heat Balance

Steam Exploded Wood / Coal Blend

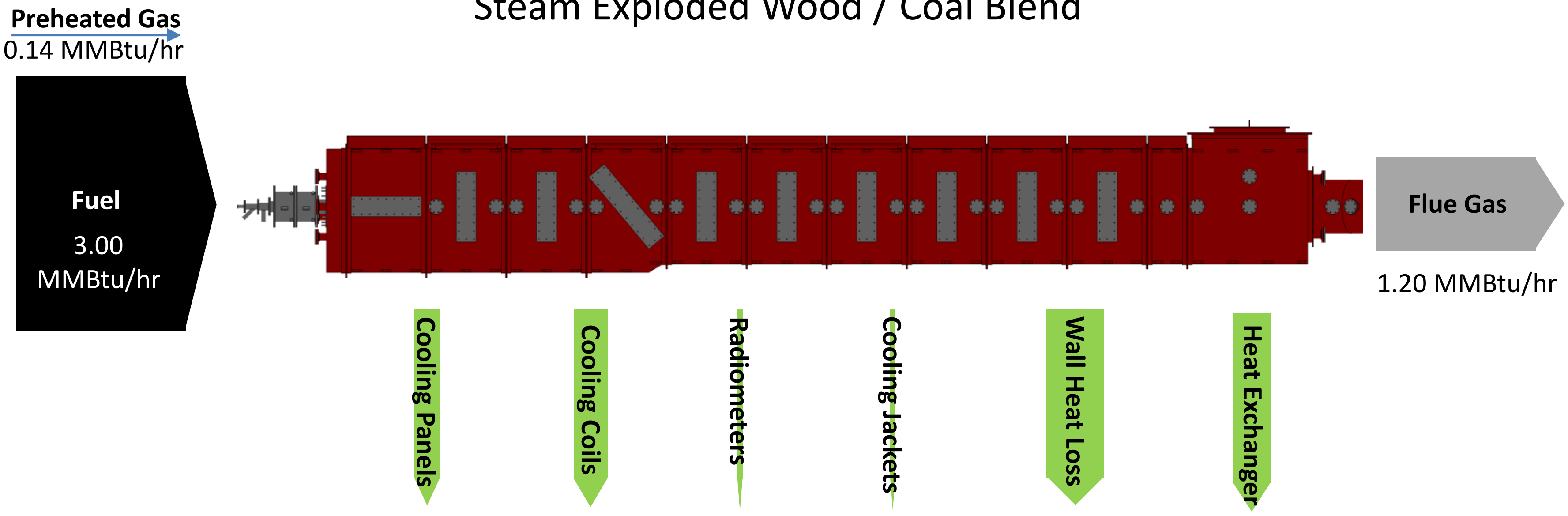

Preheated Gas
0.14 MMBtu/hr

Fuel
3.00 MMBtu/hr

Flue Gas
1.20 MMBtu/hr

Cooling Panels
0.33 MMBtu/hr

Cooling Coils
0.41 MMBtu/hr

Radiometers
0.05 MMBtu/hr

Cooling Jackets
0.06 MMBtu/hr

Wall Heat Loss
0.69 MMBtu/hr

Heat Exchanger
0.44 MMBtu/hr

Heat Loss From Furnace

1.95 MMBtu/hr

↔

1.4 % Difference

Measured Heat Removal

1.97 MMBtu/hr

L1500 Heat Balance

Sufco Coal

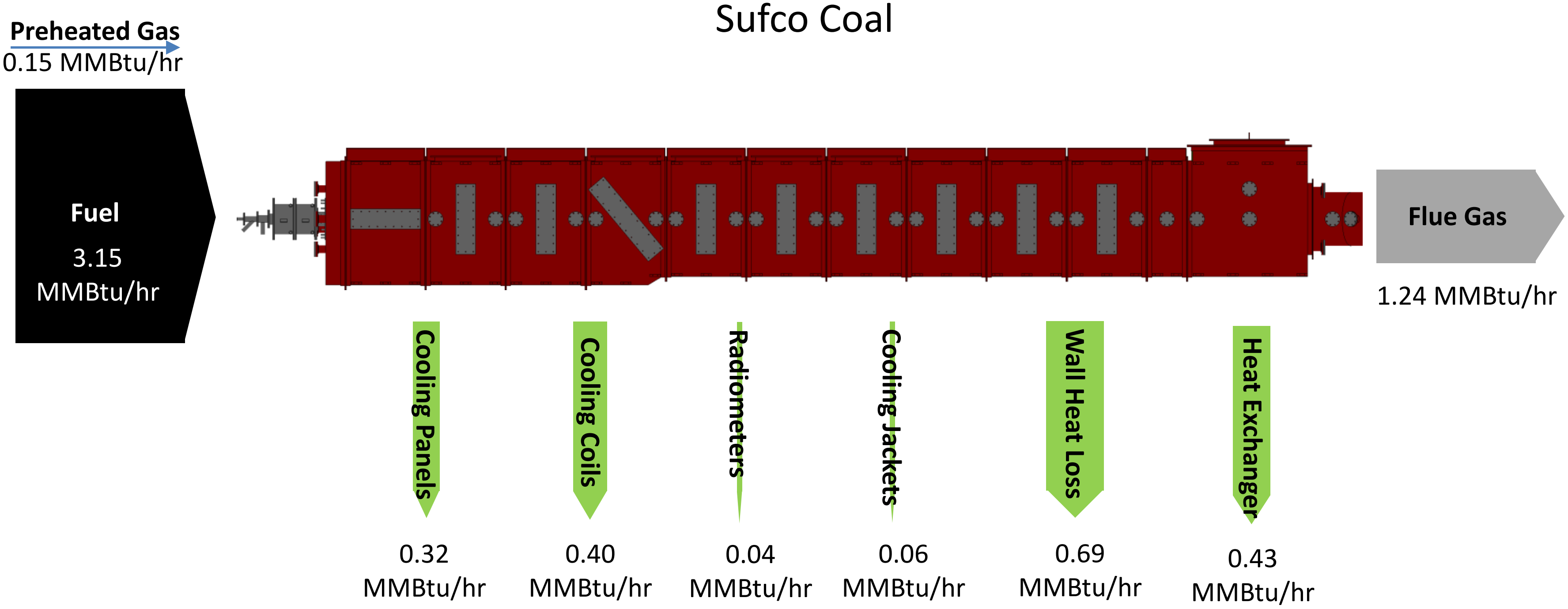

Preheated Gas
0.15 MMBtu/hr

Fuel
3.15 MMBtu/hr

Flue Gas
1.24 MMBtu/hr

Cooling Panels
0.32 MMBtu/hr

Cooling Coils
0.40 MMBtu/hr

Radiometers
0.04 MMBtu/hr

Cooling Jackets
0.06 MMBtu/hr

Wall Heat Loss
0.69 MMBtu/hr

Heat Exchanger
0.43 MMBtu/hr

Heat Loss From Furnace
2.06 MMBtu/hr

5.3 % Difference

Measured Heat Removal
1.95 MMBtu/hr

Heat Removal Through Panels and Coils

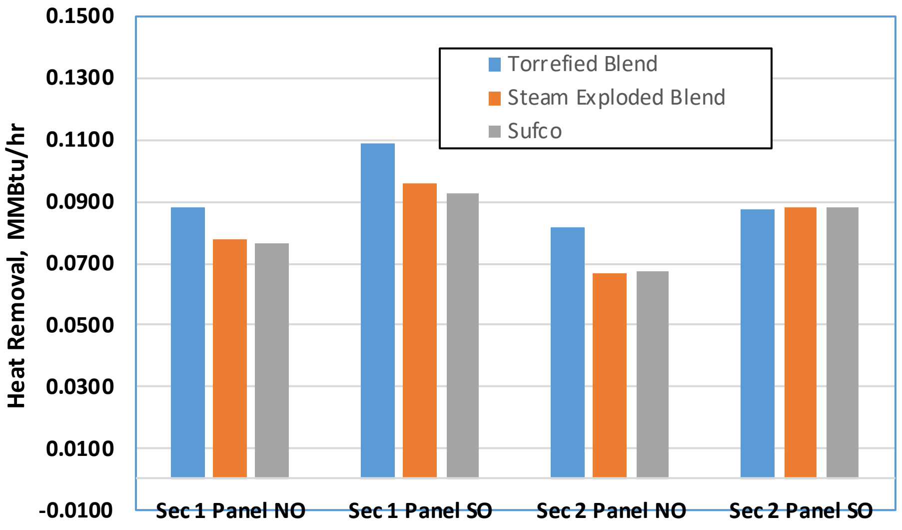

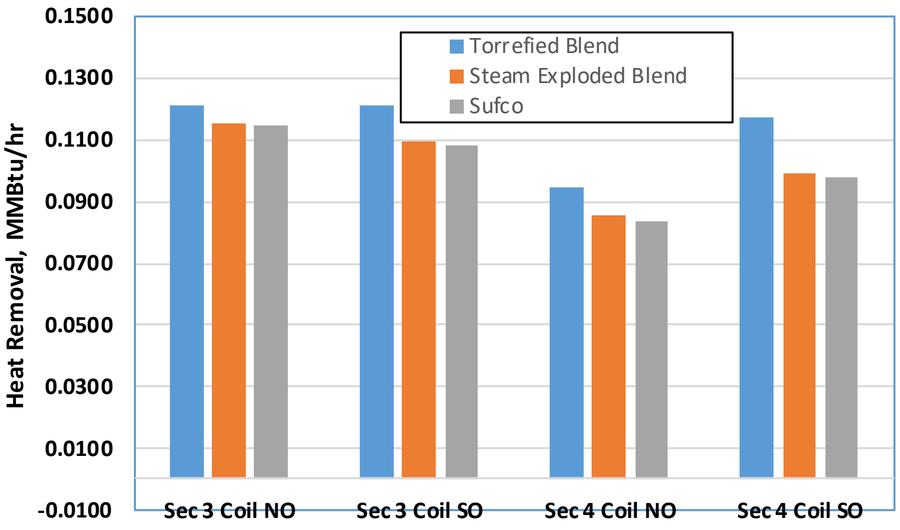

Gas Temperature and Radiative Heat Flux

Gas Temperature (Chalmers)

Sufco Temp Map

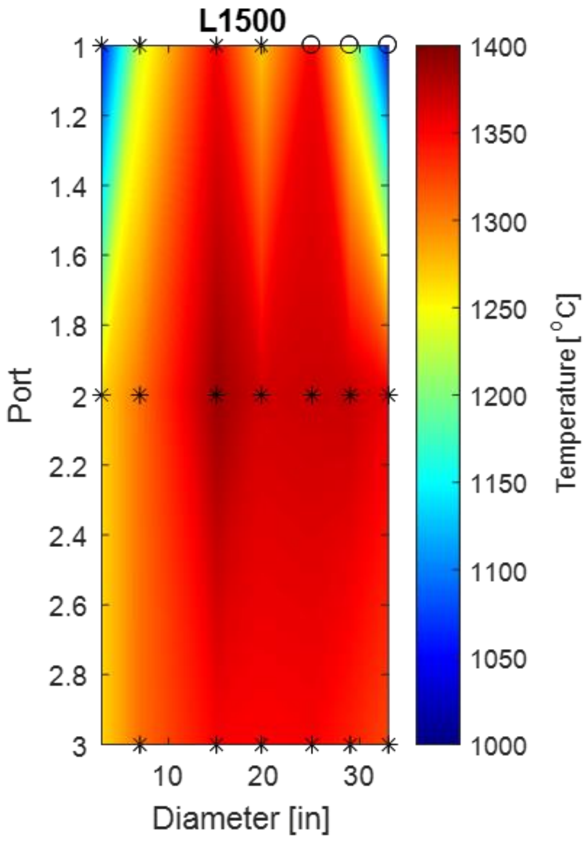

Port 1

Port 2

Port 3

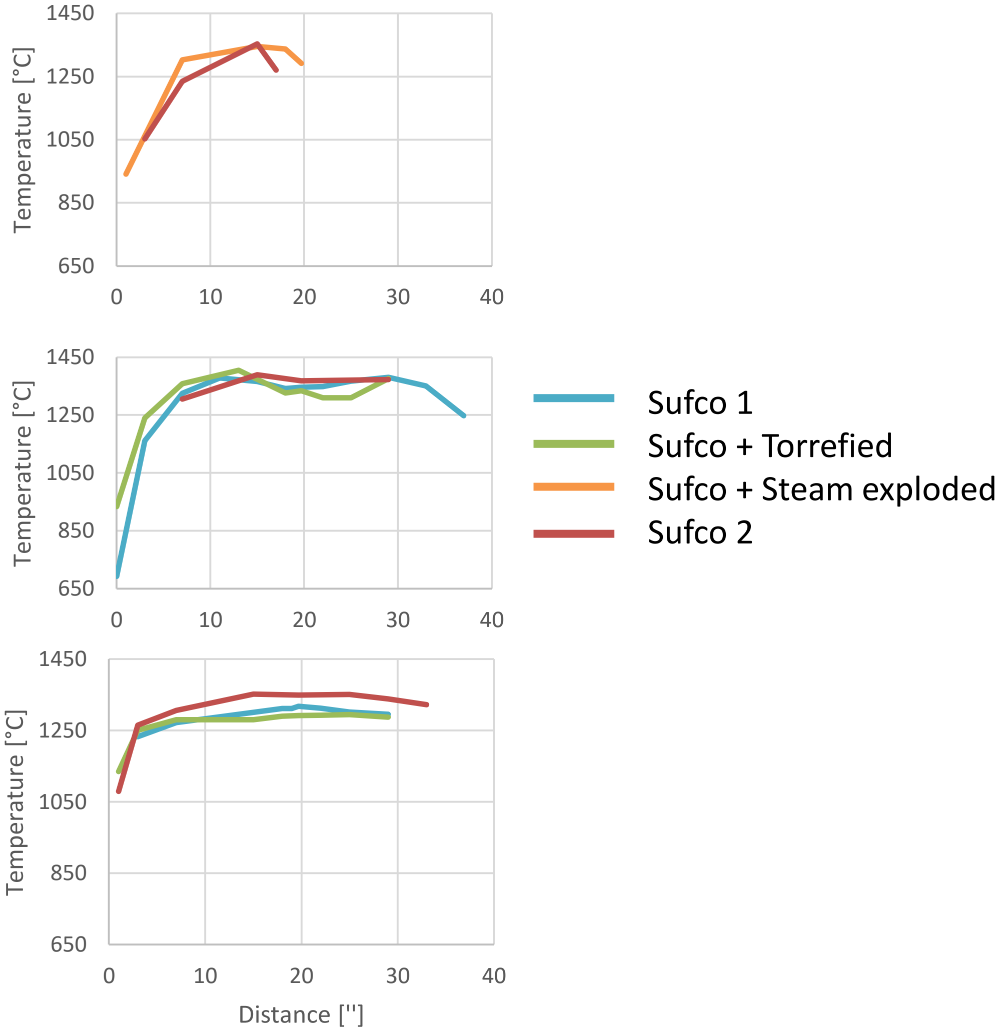

Radiative Heat Flux

Chalmers

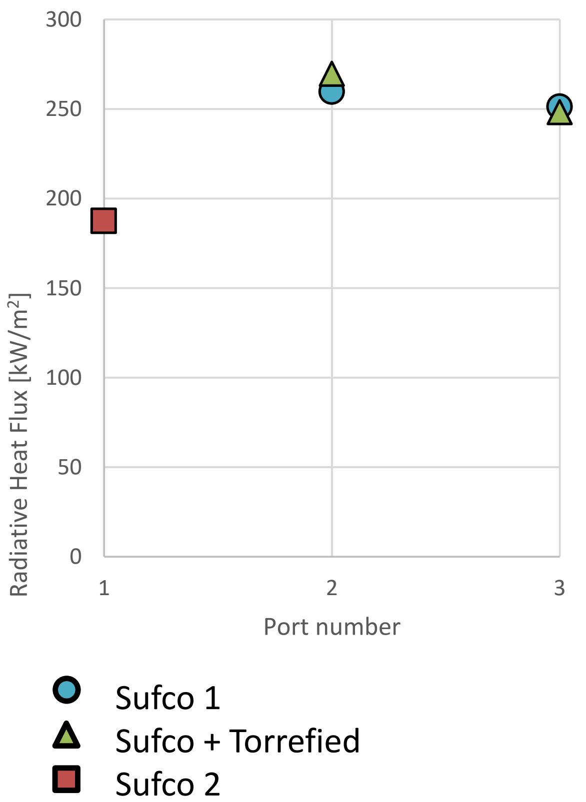

University of Utah

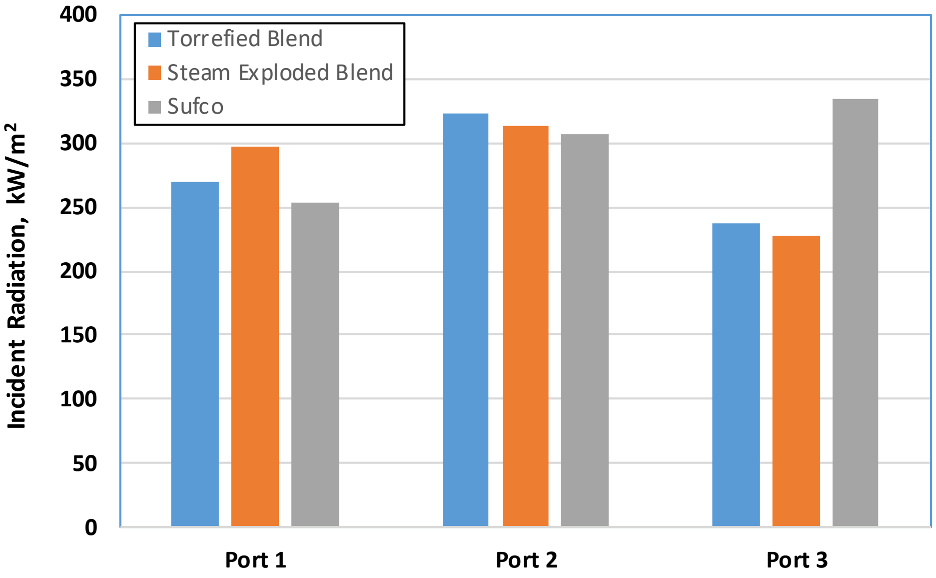

Radiative Intensity (Chalmers)

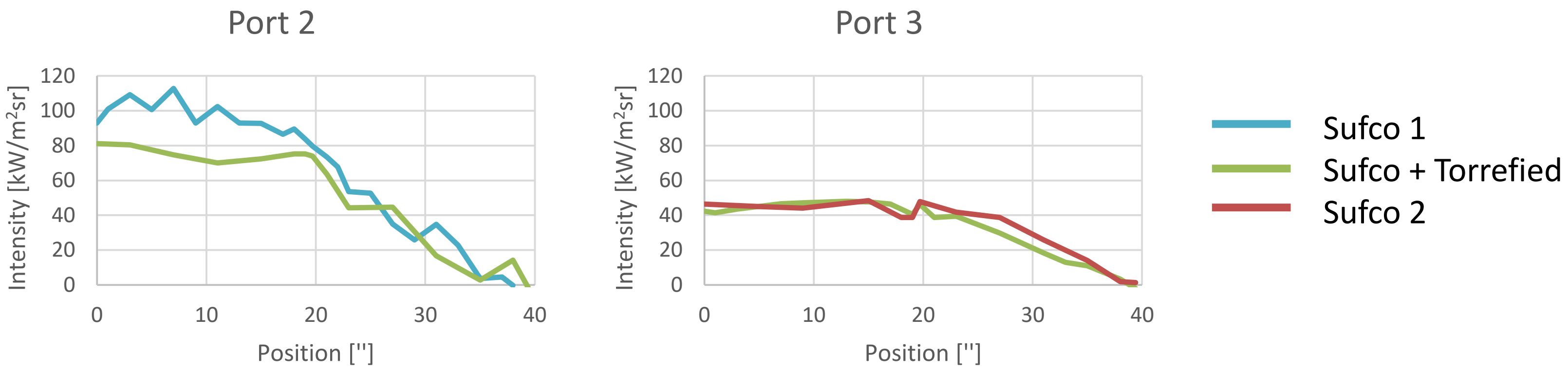

The measured radiative intensities are rather similar for the two cases studied at Port 2

The measured radiative intensities are very similar for the two cases studied at Port 3

Gas Species

Gas Species

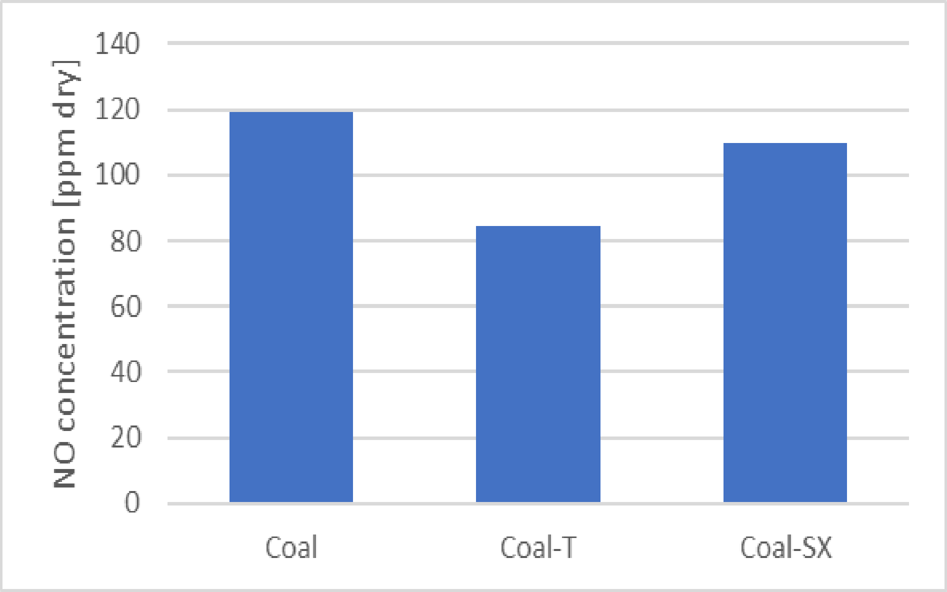
NO concentration [ppm dry]
140
120
100
80
60
40
20
0
Coal
Coal-T
Coal-SX

Gas Species

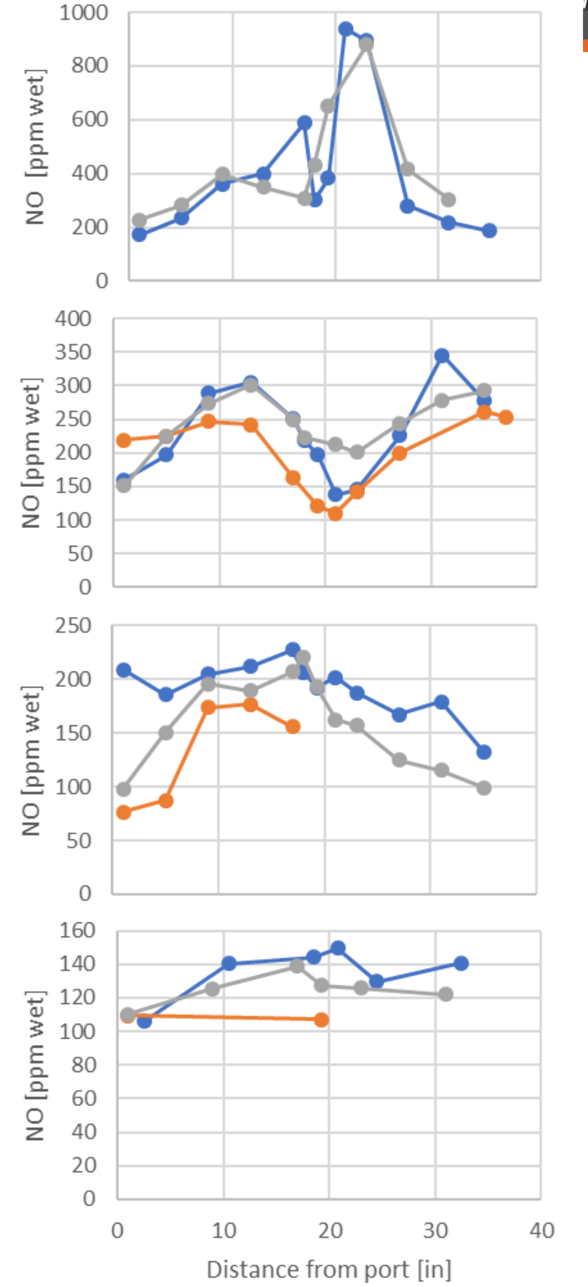

Port 1

Port 2

Coal Coal-T Coal-SX

Port 3

Port 7

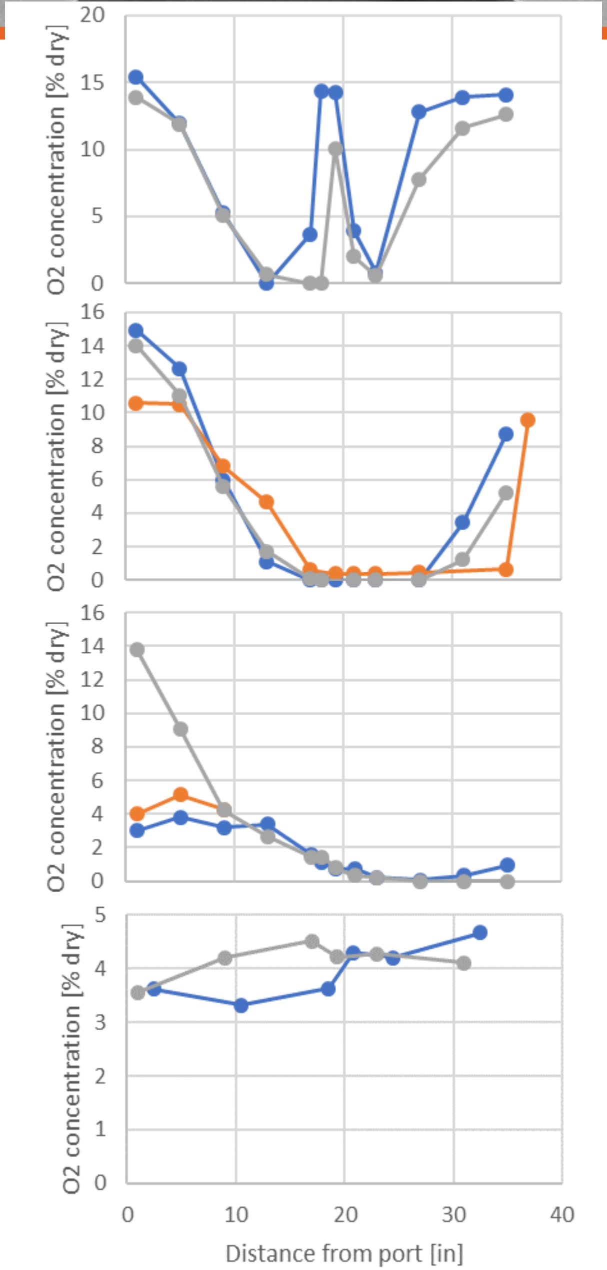

Gas Species

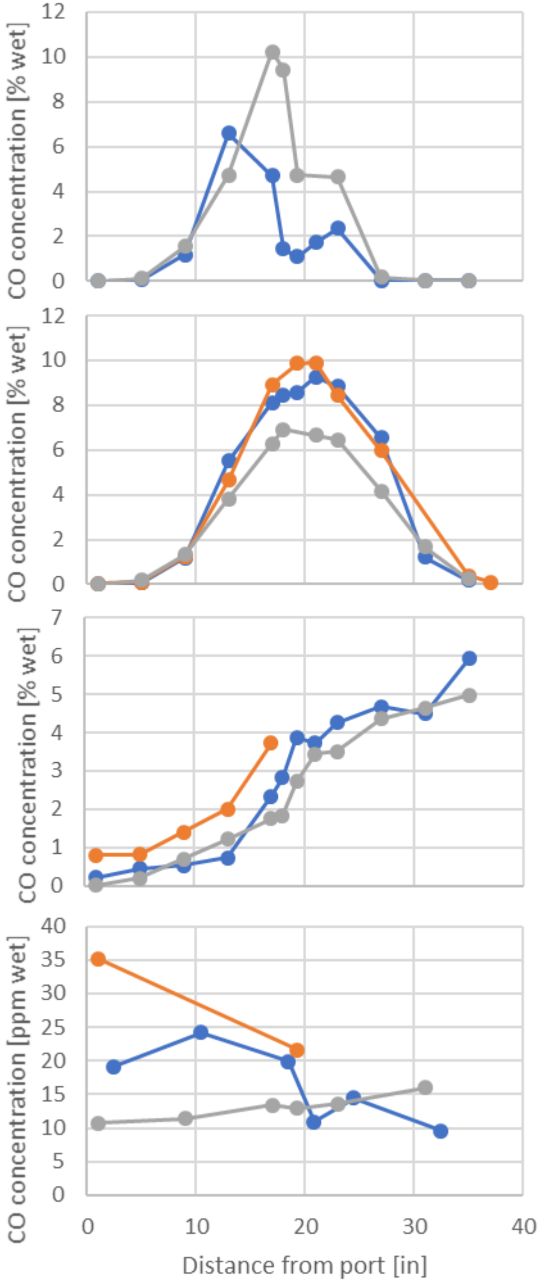

Port 1

Port 2

Coal　Coal-T　Coal-SX

Port 3

Port 7

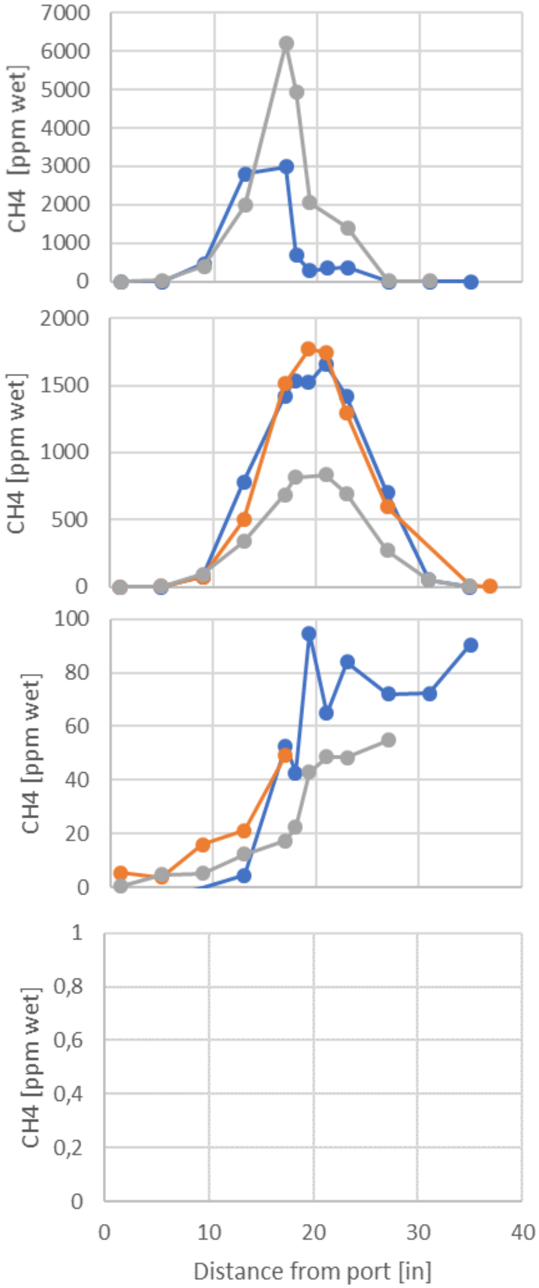

Gas Species

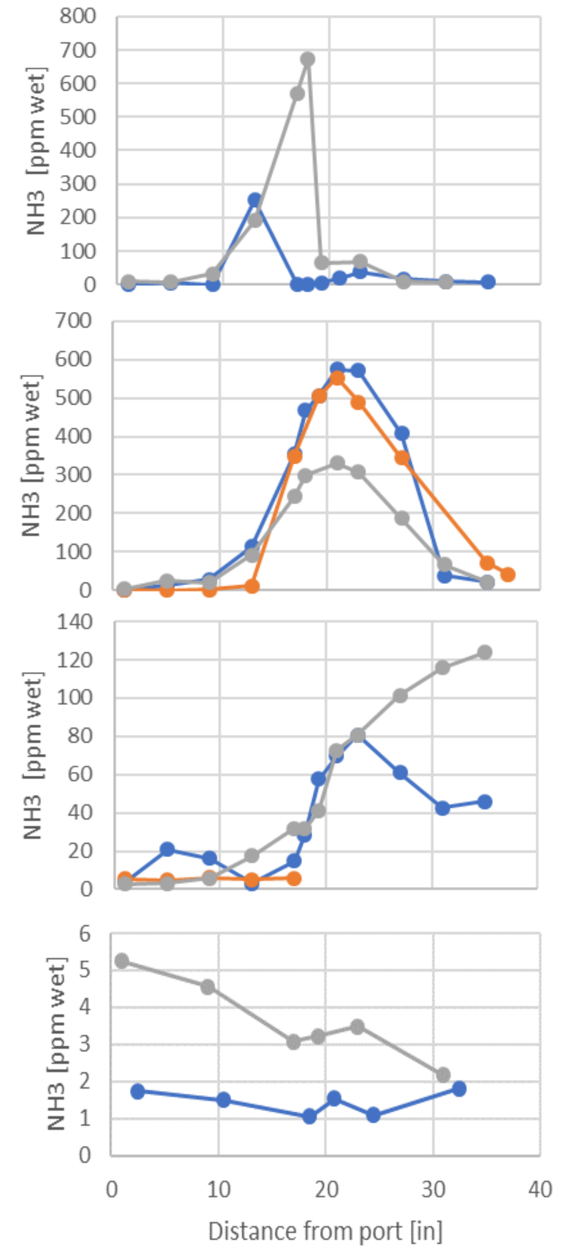

Port 1

Port 2

Port 3

Port 7

Coal Coal-T Coal-SX

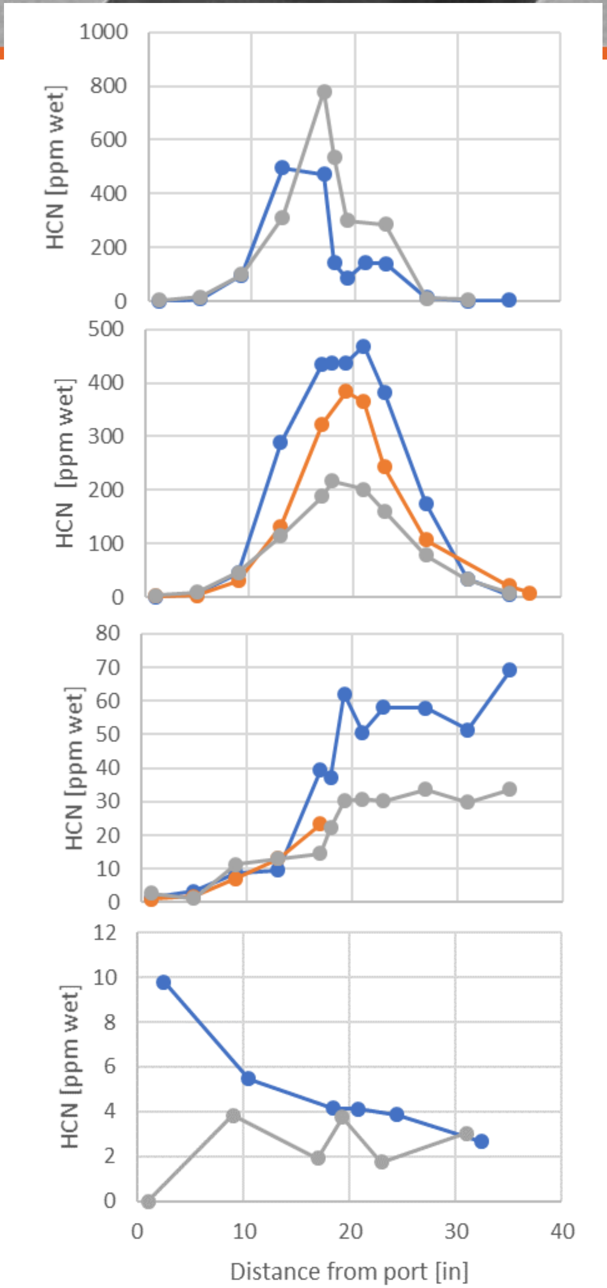

Entrained Ash

Entrained Ash PSD (Port 7)

Sufco and Torrefied Blend

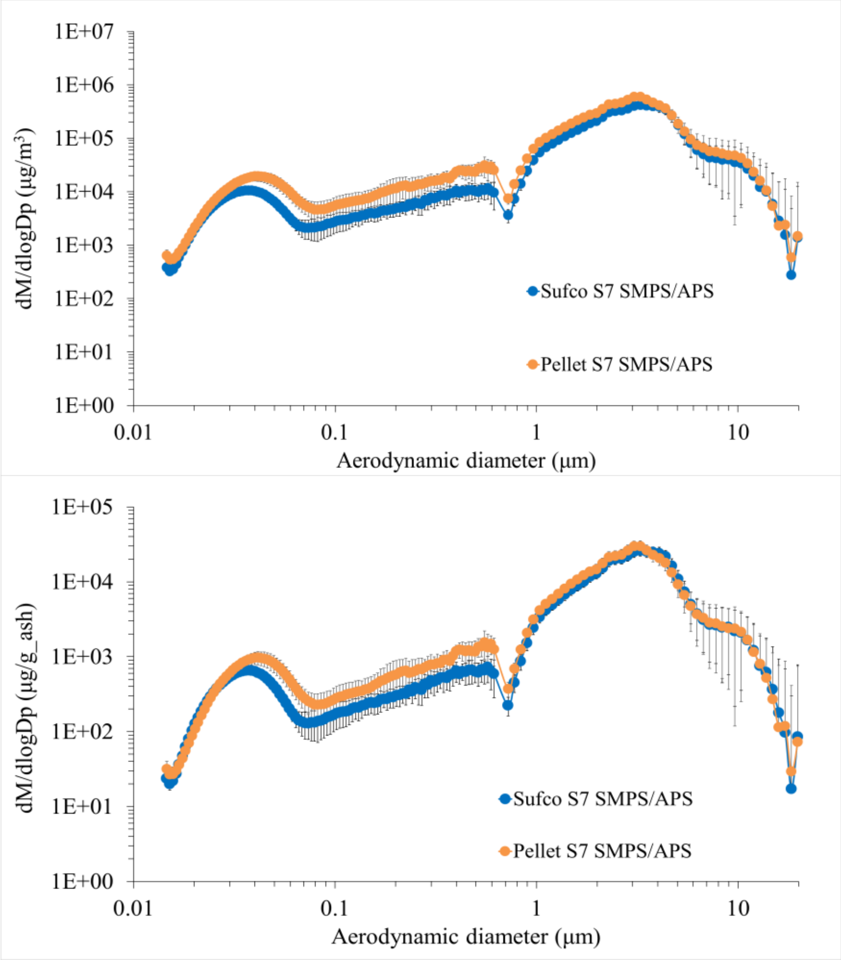

Sufco and Steam Exploded Blend

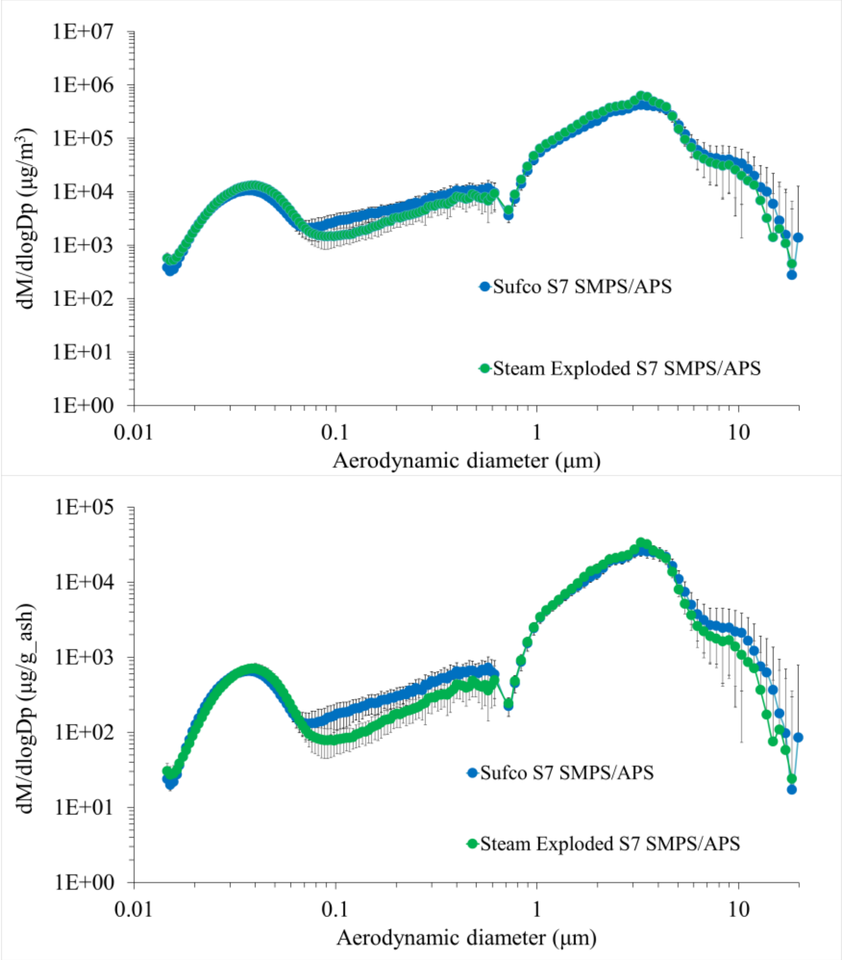

Entrained Ash PSD (Port 10)

Sufco and Torrefied Blend

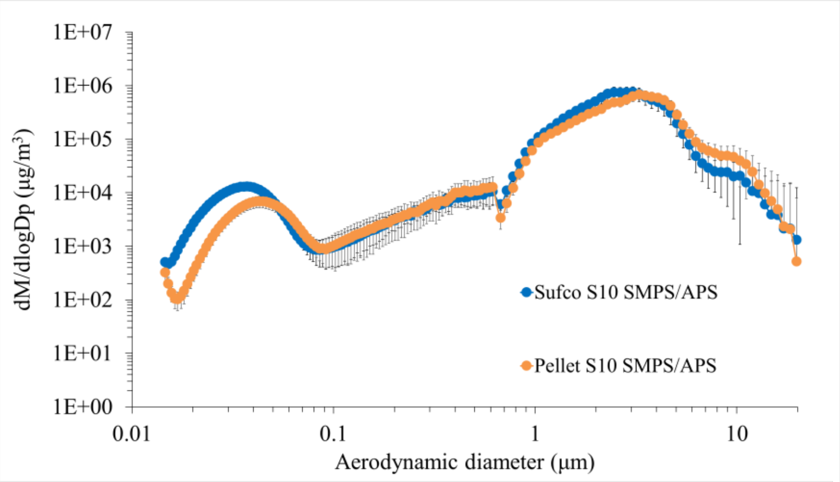

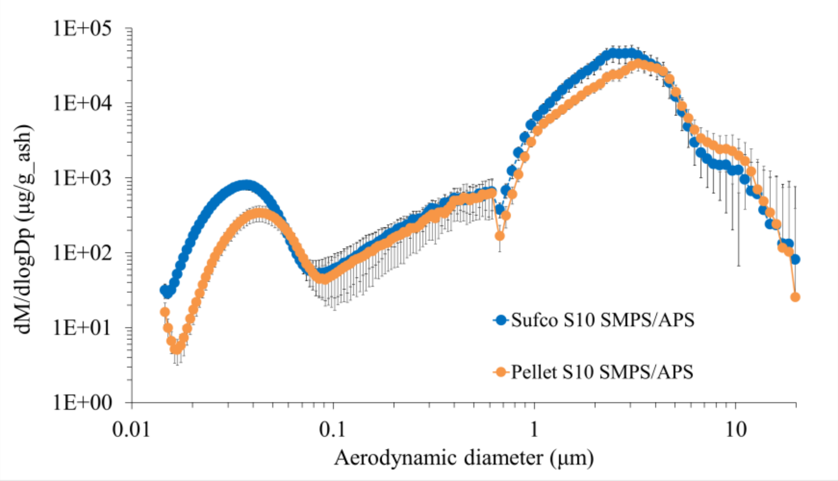

Sufco and Steam Exploded Blend

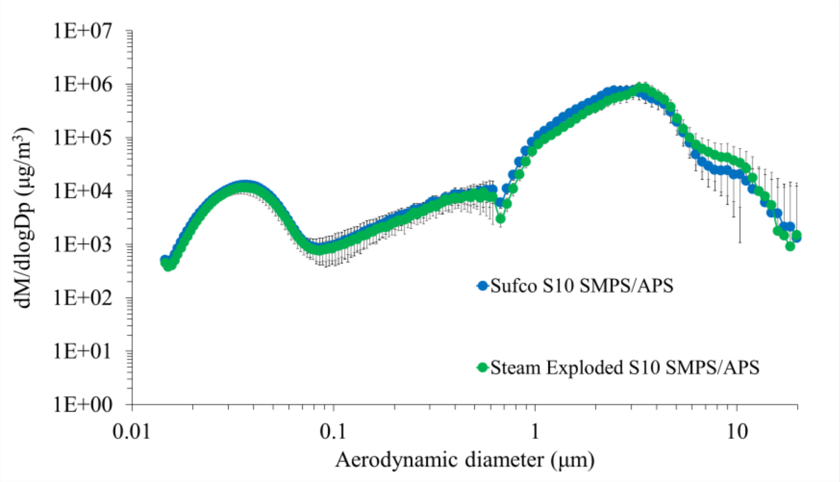

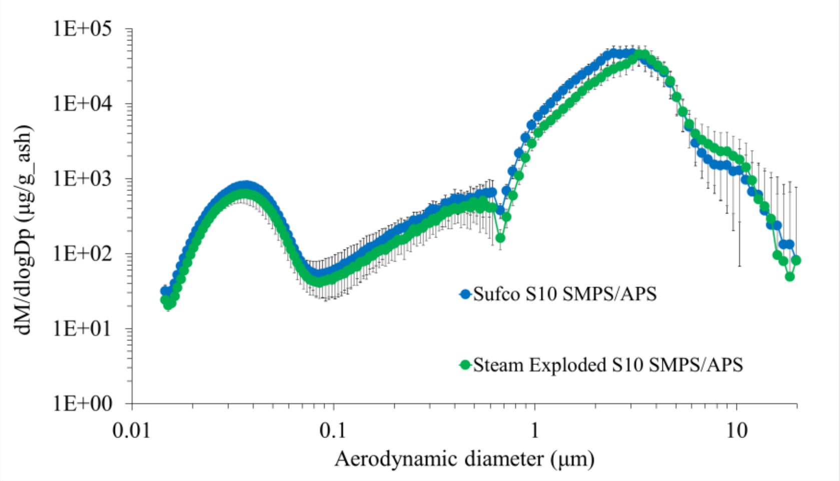

Entrained Ash Composition (Port 7)

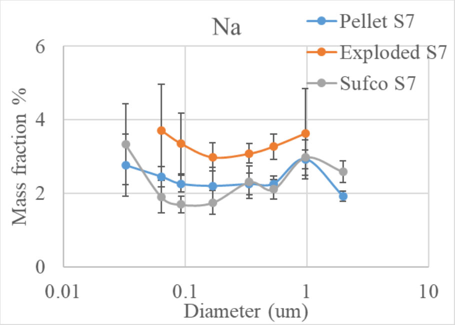

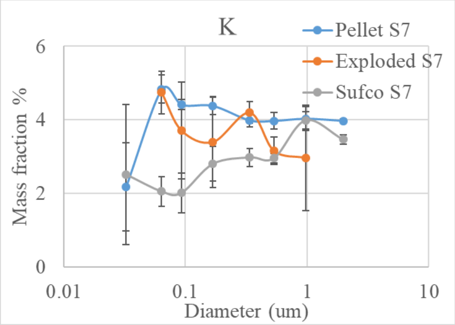

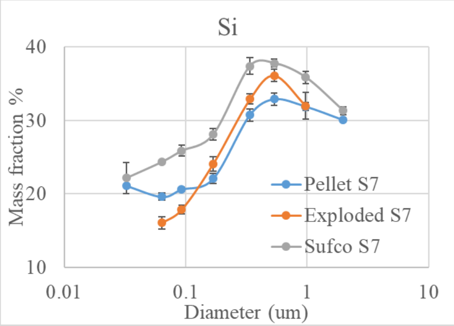

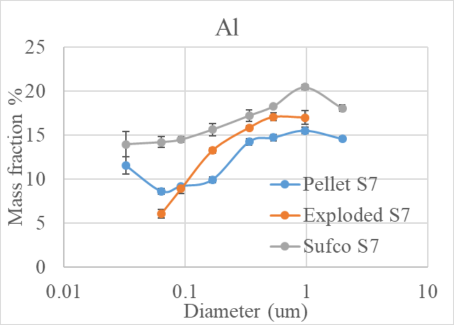

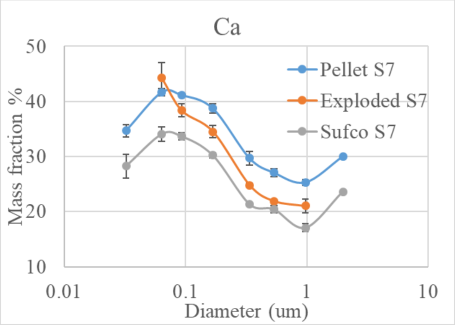

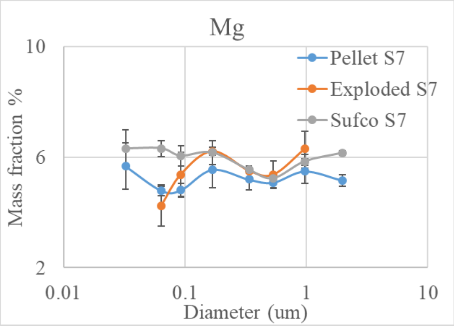

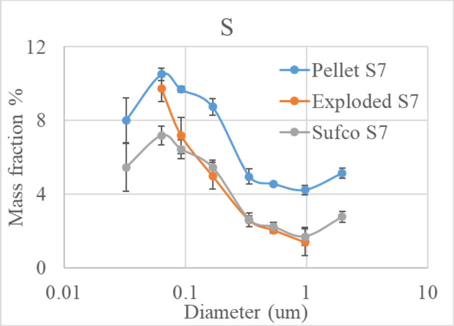

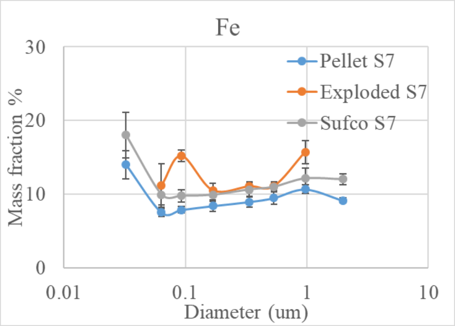

Entrained Ash Composition (Port 10)

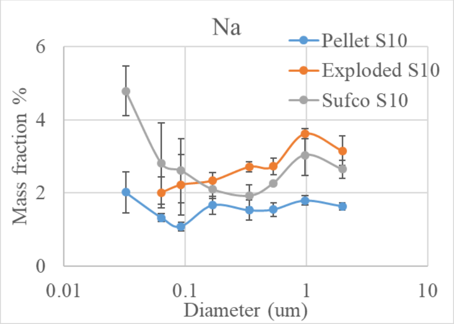

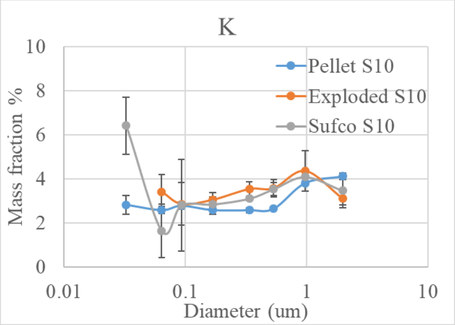

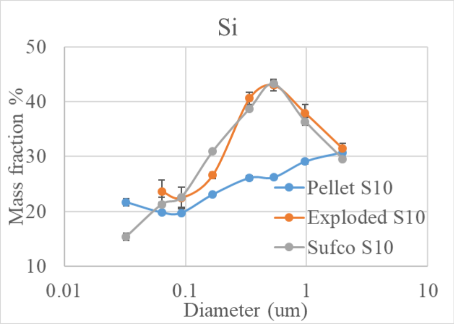

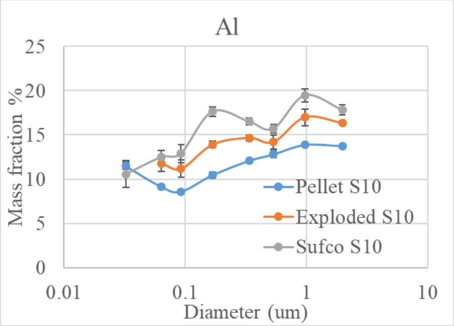

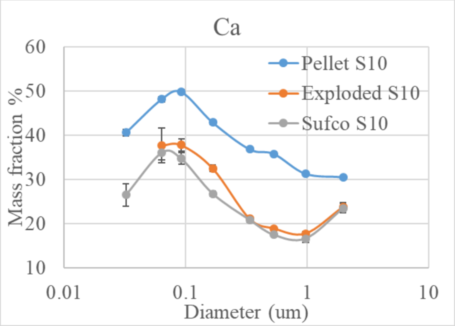

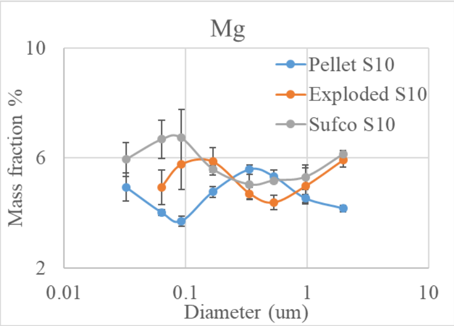

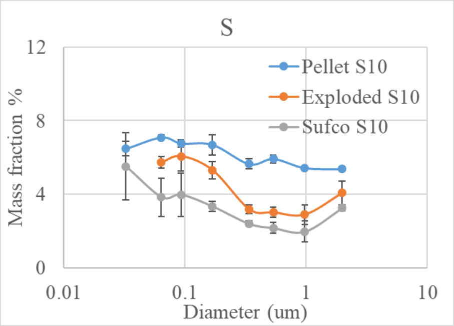

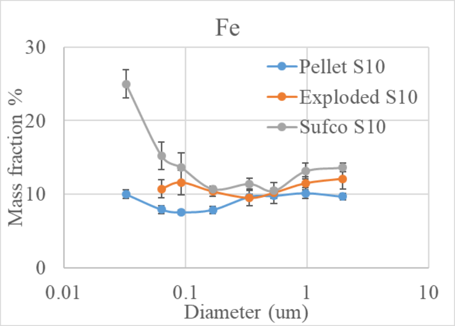

Deposition

Deposition Images

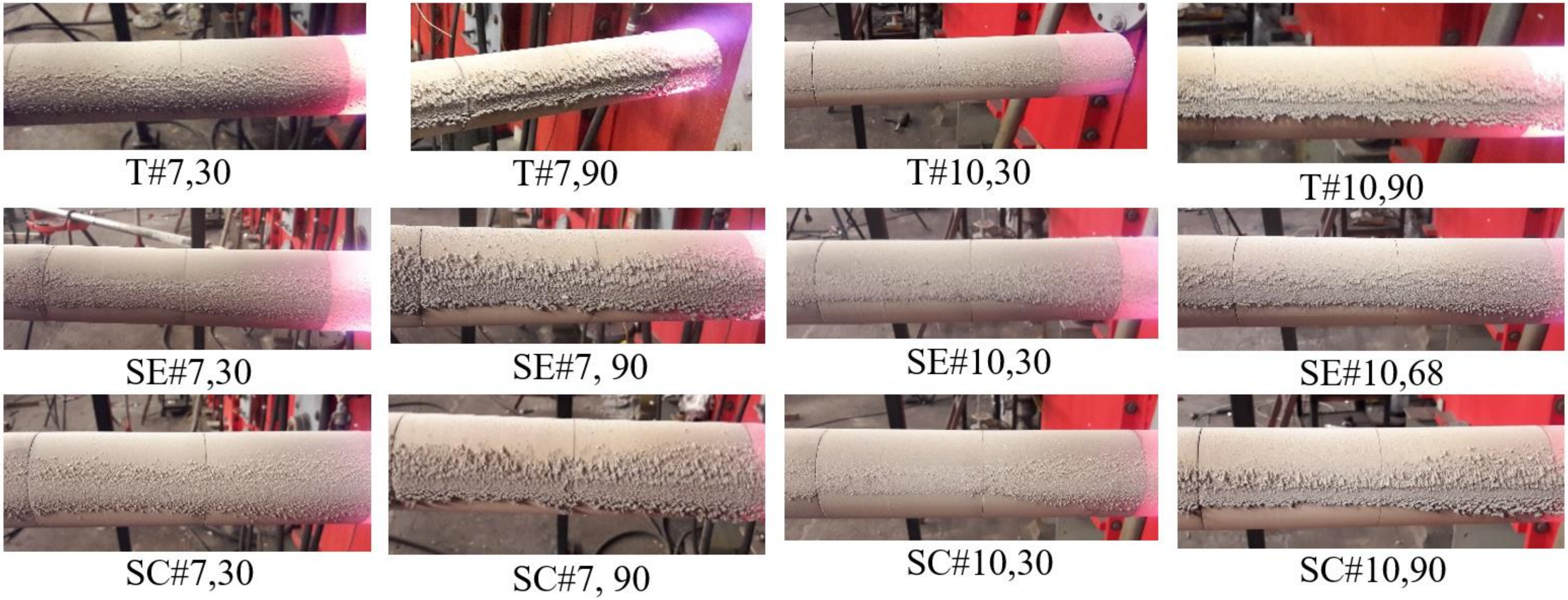

T#7,30 T#7,90 T#10,30 T#10,90

SE#7,30 SE#7, 90 SE#10,30 SE#10,68

SC#7,30 SC#7, 90 SC#10,30 SC#10,90

Images of ash collected on the coupon surface: (Fuel type# Port number, Time operation).
T: torrefied blend, SE: Steam Exploded blend, SC: Sufco Coal

Deposition Rate (Port 7)

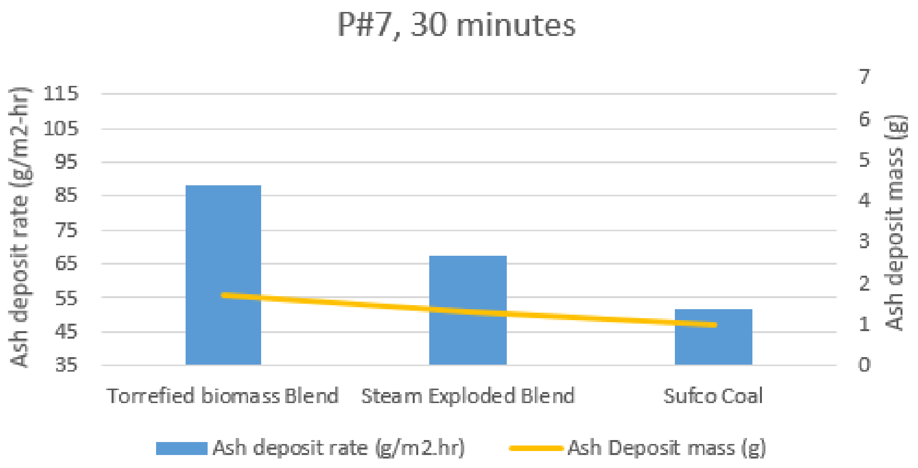
P#7, 30 minutes

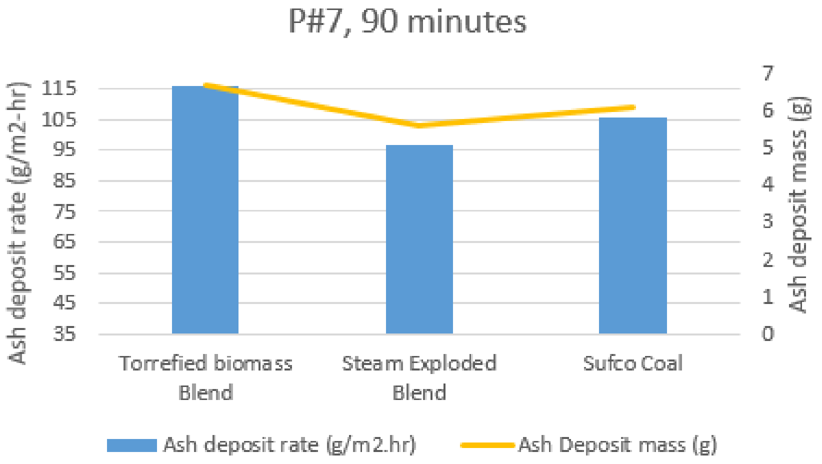
P#7, 90 minutes

Deposition Rate (Port 10)

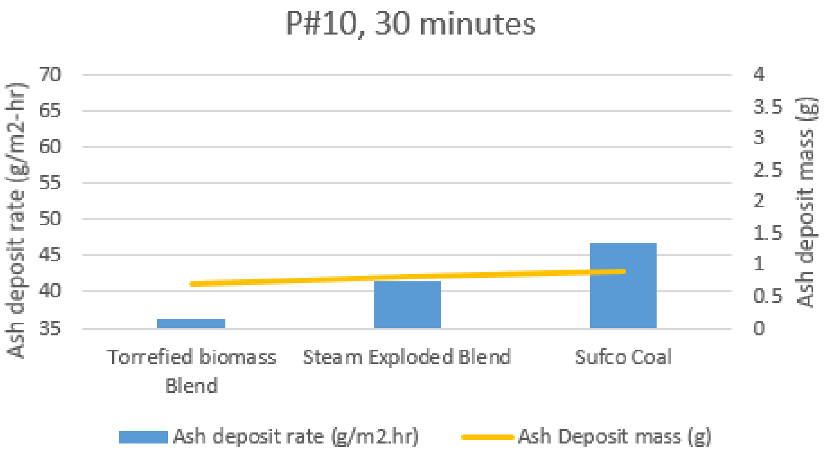

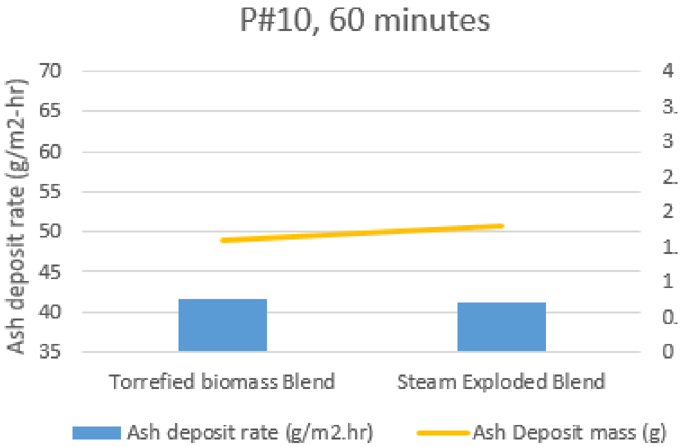

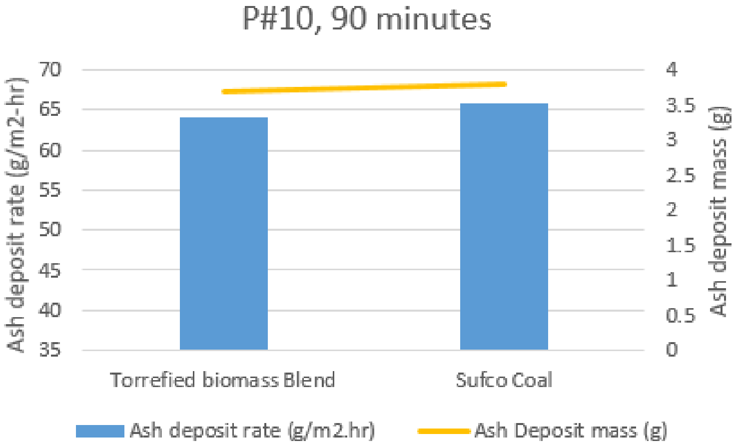

Deposit Analysis (CCSEM with EDS)

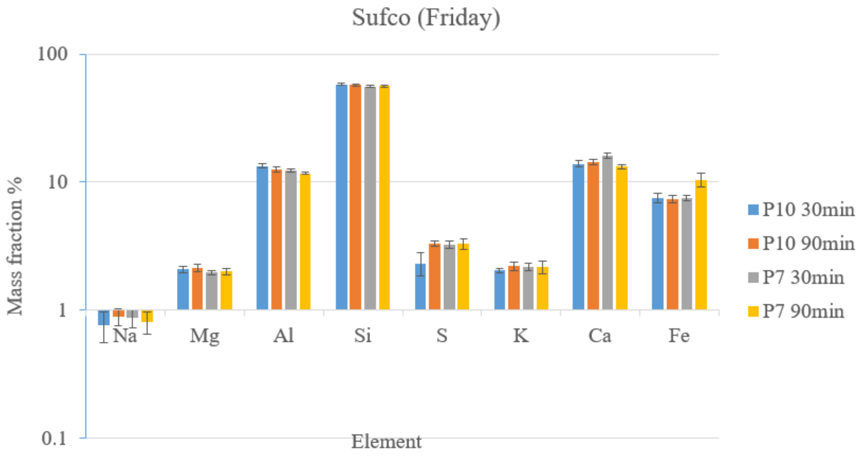

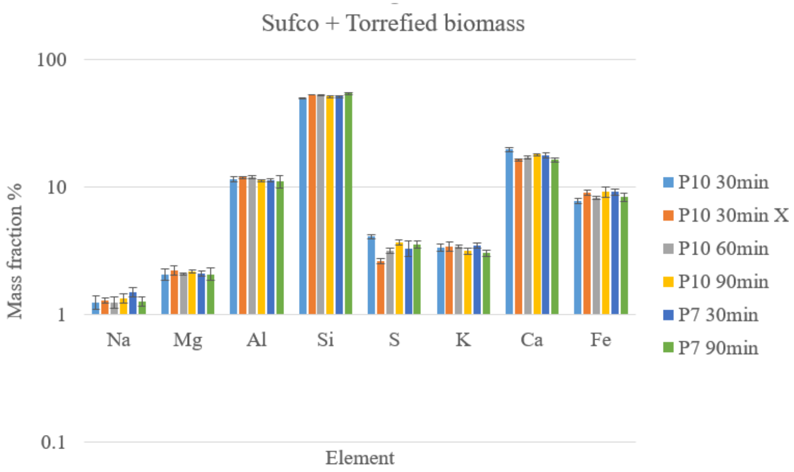

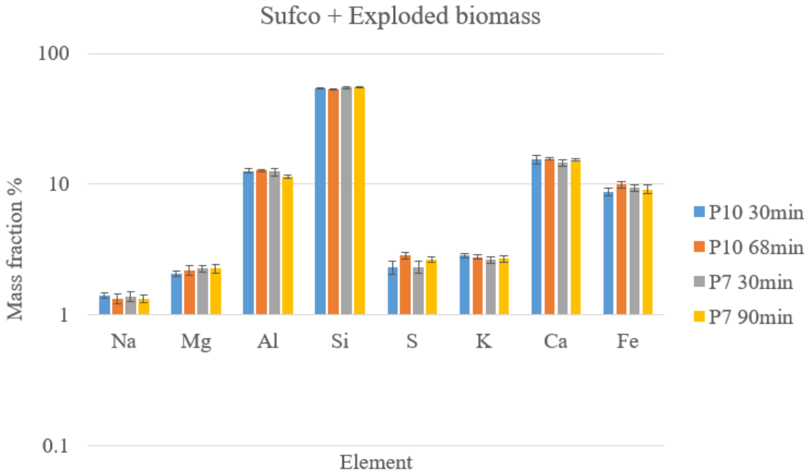

Deposit Analysis (SEM)

Port 7, 90 Min

Sufco

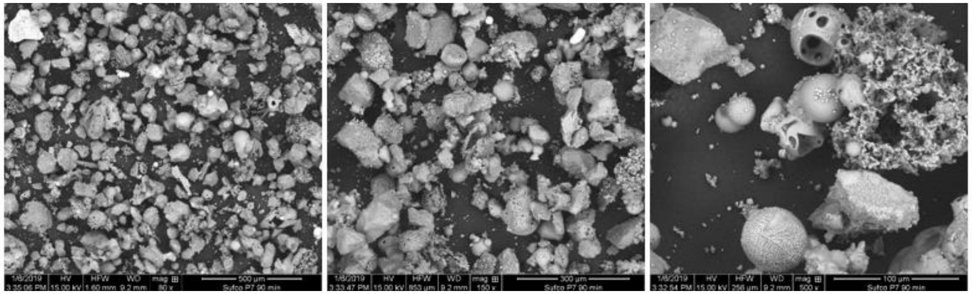

Blend – Steam Exploded

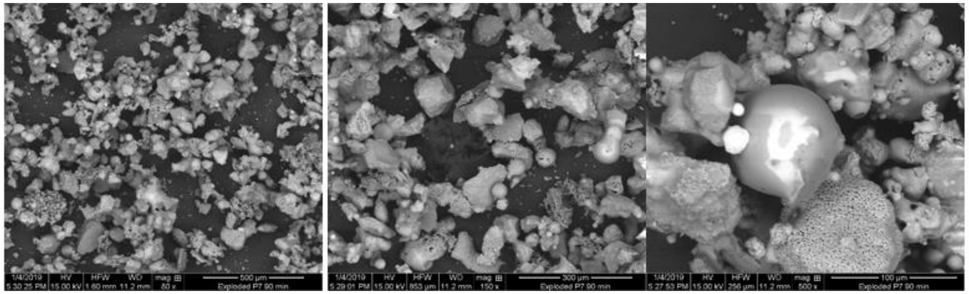

Blend – Torrefied @ 325°C

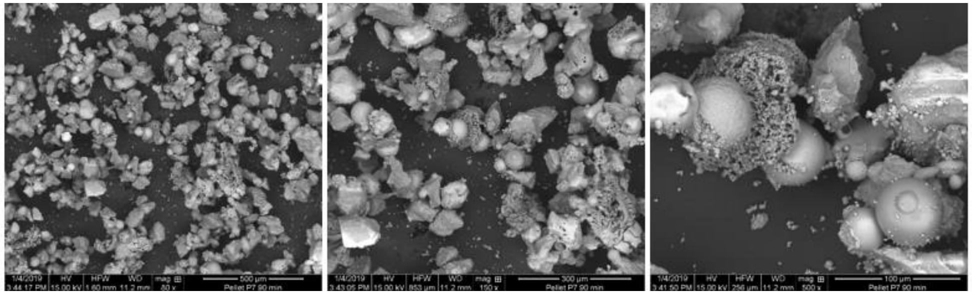

Summary & Conclusions

- Heat Balance
  - Heat Balance on the furnace closed with errors 1.4 – 5.3%
  - Torrefied blend showed slightly higher heat transfer in first four sections of the furnace
  - Behavior is substantially the same for all three fuels
- Gas Temperature and Radiative Heat Flux
  - Substantially the same temperature, radiative intensity and heat flux behavior for all three fuels

Summary & Conclusions

- Entrained Ash
  - Very little effect of the biomass on the small particle size distribution
  - Composition data shows only a dilution effect of the biomass
- Deposition
  - Biomass blends showed similar, or slightly higher deposition rates in port 7 compared with coal
  - Biomass blends showed lower deposition rates in port 10 compared with coal
  - Composition and PSD of deposits were substantially the same for all fuels

Summary & Conclusions

- Gas Species
  - NO_x concentrations where similar, or lower, for the two biomass blends compared with the Sufco coal conditions.
  - Steam exploded biomass showed higher concentrations of CO, CH_4, NH_3 and HCN in the near burner region
  - At port 7 the species concentrations were substantially the same
- Overall
  - Small, or even negligible, effects are expected when burning 15% biomass blends at Hunter 3

Questions

Ash aerosol characteristics from combustion of coal / woody biomass blends at Laboratory, Pilot and Industrial scales

Xiaolong Li[1], Yueming Wang[1,*], Seyedhassan Fakourian[2], Andrew Fry[2], Jost O.L. Wendt[1]

[1]Department of Chemical Engineering, University of Utah, USA

[2]Department of Chemical Engineering, Brigham Young University, USA

[*]Current affiliation: Key Laboratory of Energy Thermal Conversion and Control, Southeast University, P.R. China

Research background

Forest restoration project on Wasatch Plateau

The Manti-La Sal National Forest plans to log 30,000 acres of dead spruce as part of an effort to restore an ailing ecosystem that has been hammered by bark beetles, drought and the historic elimination of wildfire that has allowed subalpine fir to proliferate at the expense of aspen.

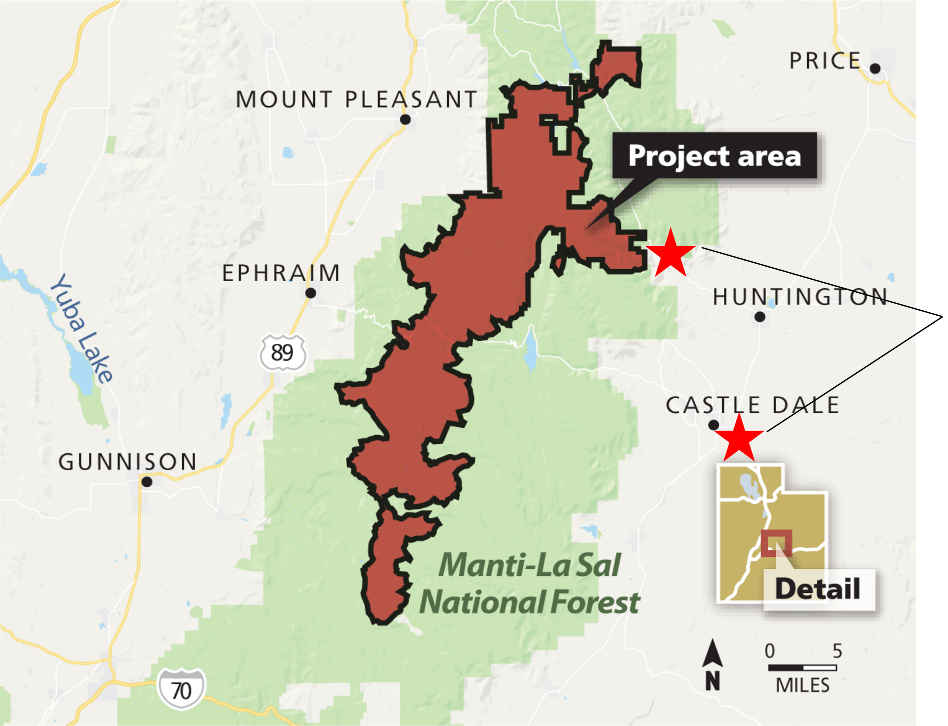

Source: U.S. Forest Service **GRAPHIC BY CHRISTOPHER CHERRINGTON** | *The Salt Lake Tribune*

Coal-fired
power plants

Woody biomass as a supplementary fuel to coal

- Abundantly and locally available
- Renewable
- Carbon-neutral

Wood torrefication

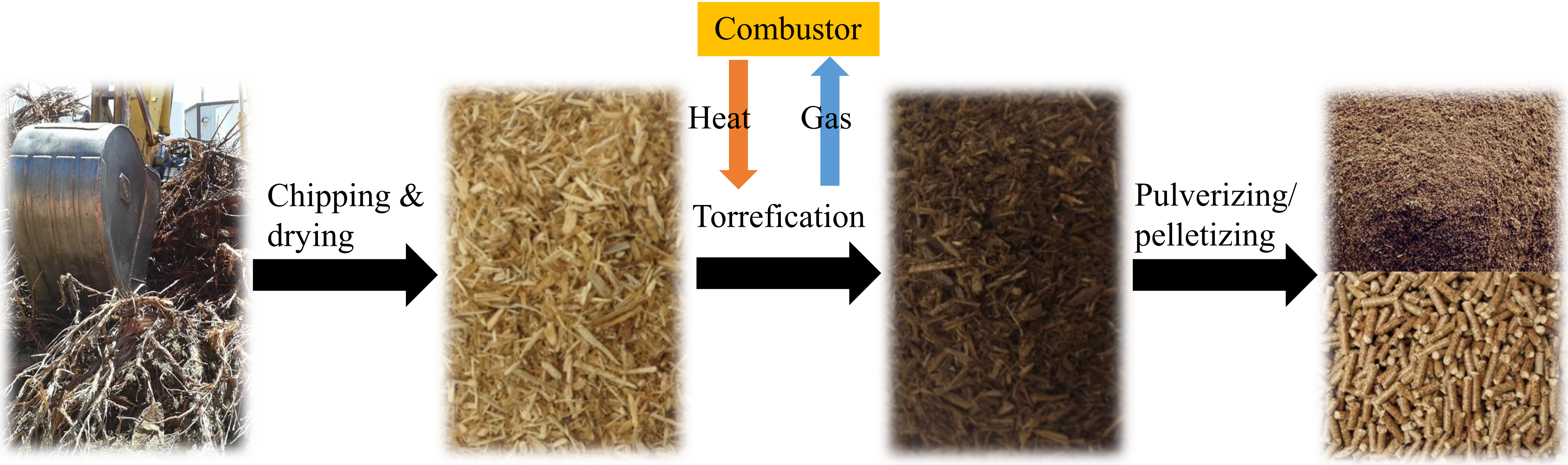

Combustor

Heat

Gas

Chipping & drying

Torrefication

Pulverizing/ pelletizing

Woody debris

- Low energy density
- High moisture
- Hygroscopic
- Poor grindability

Wood chip

Torrefied wood

- Higher energy density
- Low moisture
- Hydrophobic
- Better grindability

Powder/pellet

Images: Amaron Energy

Research objectives

- Sample ash aerosols and measure particle concentrations in three combustors operated at 27/52 kW_{TH}, 1 MW_{TH} and 1250 MW_{TH}
- Study fly ash formation in coal combustion and co-firing with woody biomass
- Investigate the effect from combustor scale on ash aerosol characteristics
- Provide information for ash deposition study

Oxy-fuel Combustor (OFC) at 27 and 52kW$_{TH}$

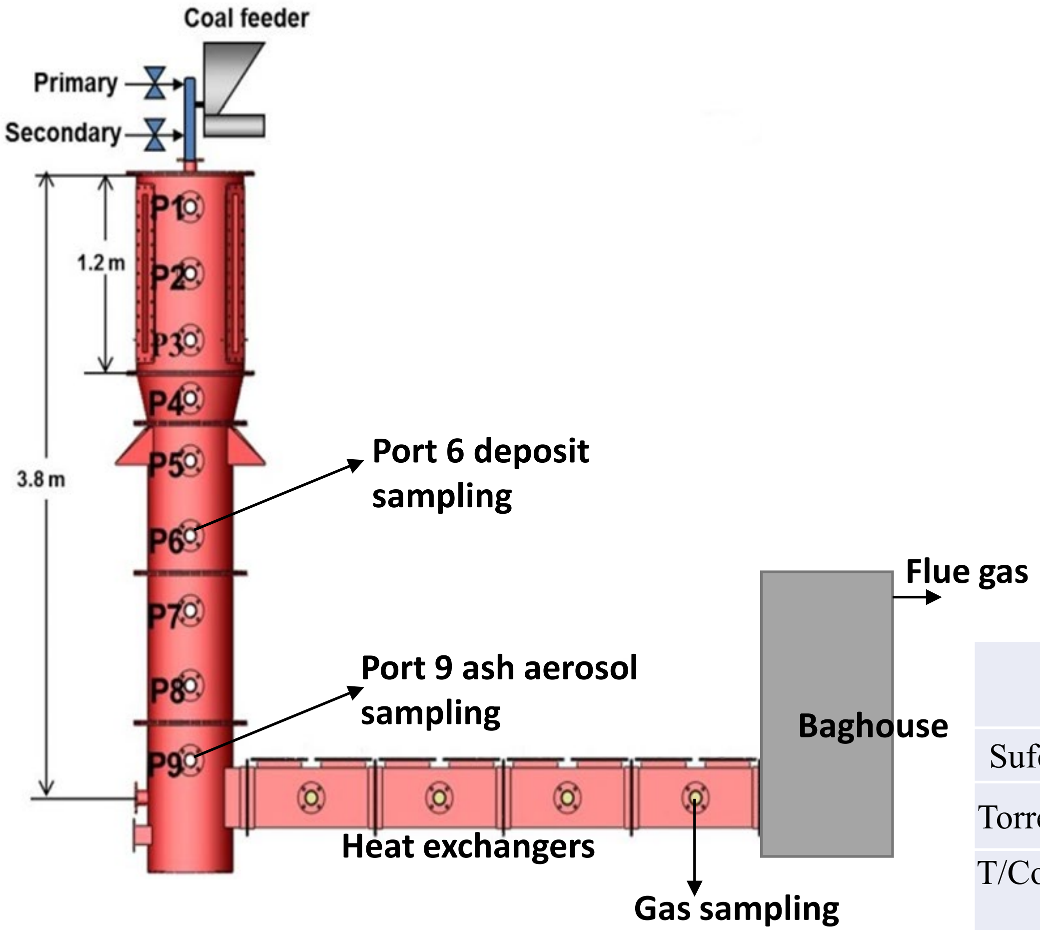

- 100 kW$_{TH}$ (rated) lab scale
- Down-fired, self-sustained no external heating
- Air- and Oxy-fuel combustion
- Vertical radiation zone: 0.9 ft ID and 12.5 ft high

Fuel	ASH (%)	C (%)	H (%)	N (%)	S (%)	O (%)	H2O (%)	V (%)	FC (%)	HHV (kJ/kg)
Sufco coal (Coal)	13.96	62.41	4.52	1.1	0.46	11.04	6.52	37.36	42.16	27319
Torrefied wood (T)	0.19	51.75	5.29	0.14	0.02	36.29	6.32	74.2	19.29	21534
T/Coal 50/50 blend (T Blend)	7.08	57.08	4.91	0.62	0.24	23.67	6.42	55.78	30.73	24427

Fuel	Al2O3	CaO	Fe2O3	MgO	MnO	P2O5	K2O	SiO2	Na2O	SO3	TiO2
Sufco coal (Coal)	12.09	11.9	3.62	3.94	0.03	0.25	1.13	62.48	0.81	1.83	0.68
Torrefied wood (T)	2.67	51.72	8.28	10.39	4.73	4.16	4.61	6.82	1.6	5.03	0
T/Coal 50/50 blend (T Blend)	11.95	12.33	3.7	4.04	0.1	0.29	1.32	61.71	0.83	1.84	0.67

Multi-fuel Combustor (L1500) at 1 MW_{TH}

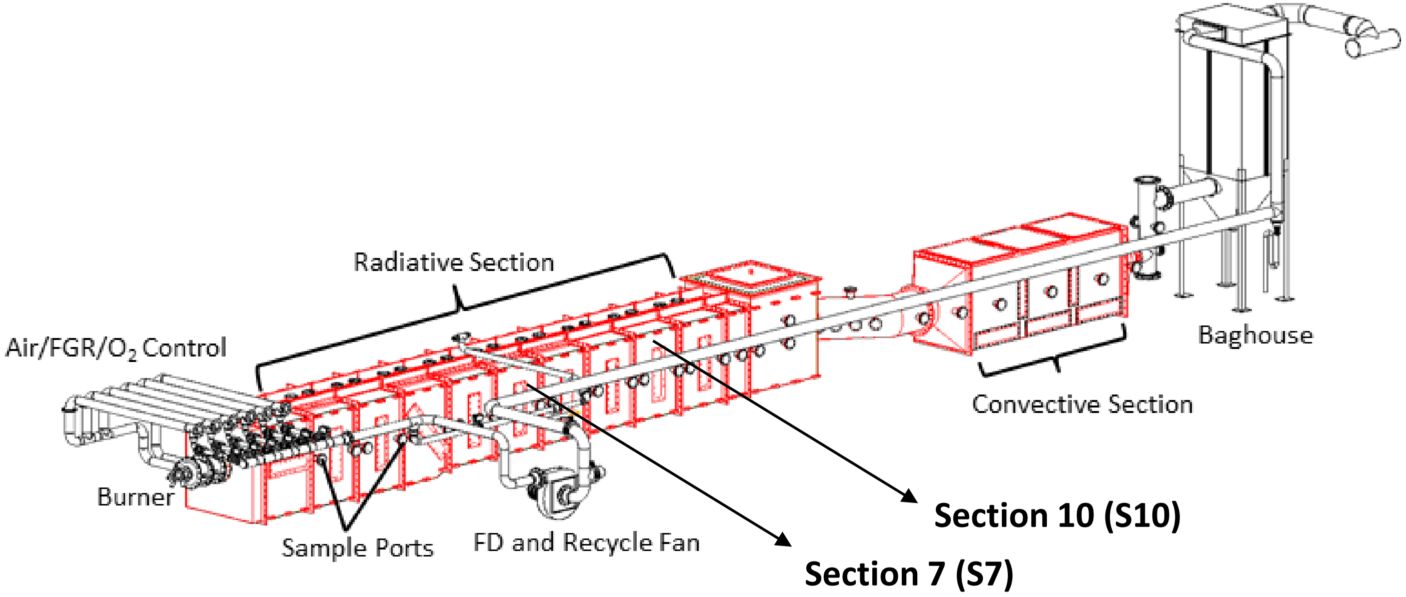

- 1500 kW_{TH} (rated) pilot scale
- Horizontal fired
- Radiative section: inside 3.5 ft x 3.5 ft square and 46 ft long

Fuel	ASH (%)	C (%)	H (%)	N (%)	S (%)	O (%)	H2O (%)	V (%)	FC (%)	HHV (kJ/kg)
Sufco coal (Coal)	12.74	63.05	4.35	1.13	0.45	11.61	6.52	38.26	42.47	25959
T wood/Coal 15/85 blend (T Blend)	14.99	59.66	4.36	1.00	0.47	14.12	5.21	41.69	38.10	24676
Steam exploded/Coal 15/85 blend (SX Blend)	14.16	60.57	4.49	1.06	0.48	14.16	4.89	42.32	38.63	24746

Fuel	Al2O3	CaO	Fe2O3	MgO	MnO	P2O5	K2O	SiO2	Na2O	SO3	TiO2
Sufco coal (Coal)	11.03	15.25	4.17	3.99	0.04	0.29	1.20	54.07	1.26	6.35	4.17
Torrefied wood 15/85 blend (T Blend)	10.48	15.88	4.07	4.08	0.05	0.31	1.49	55.55	1.33	5.98	0.53
Steam exploded 15/85 blend (SX Blend)	12.40	12.82	4.09	3.77	0.02	0.27	1.05	57.53	0.97	6.06	0.62

Hunter Unit 3 at 1250 MW_{TH}

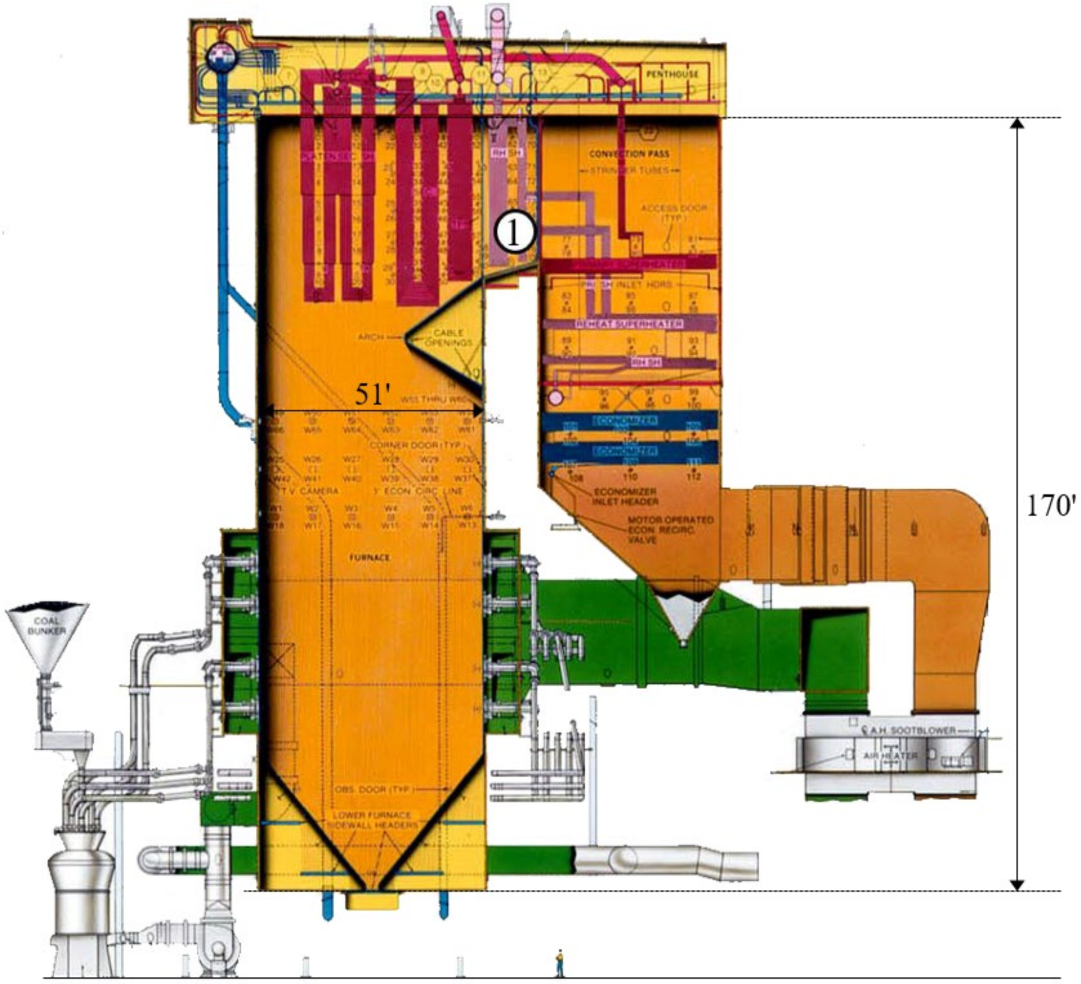

- 1300 MW_{TH} 500 MW_{E} full load
- Radiative section: inside 51 ft x 51 ft square and 170 ft high

Fuel	ASH (%)	C (%)	H (%)	N (%)	S (%)	O (%)	H2O (%)	V (%)	FC (%)	HHV (kJ/kg)
Sufco coal (Coal)	11.5	63.8	4.5	1.3	0.6	9.5	8.8	36	43.7	26409
T/Coal 15/85 blend (T)	10.5	60.1	4.5	1	0.4	12.3	11.4	39.4	38.7	24300

Fuel	Al2O3	CaO	Fe2O3	MgO	MnO2	P2O5	K2O	SiO2	Na2O	SO3	TiO2
Sufco coal (Coal)	14.9	8.5	4.3	3.8	0.04	0.4	1.1	56.0	2.2	8.8	0.7
Torrefied wood (T)	14.1	10.1	3.8	4.2	0.04	0.4	1.4	56.7	2.4	6.2	0.7

Combustion at three scales

	OFC				L1500			Hunter	
Fuel type	Coal	Coal	T	T Blend	Coal	T Blend	SX Blend	Coal	T Blend
Mixing ratio (wt. wood/coal)	-	-	-	50:50	-	15/85	15/85	-	15/85
Firing rate	27kW	52kW	27kW	27kW	923kW	874kW	882kW	1232MW	1250MW
Fuel feed rate (kg/hr)	3.5	6.8	4.5	4.0	122	127	128	168,000	184,000
Ash concentration in flue gas (g/Nm^3)	17.5	17.0	0.28	10.12	16.2	20.1	18.7	14.5	15.8

Ash aerosol sampling

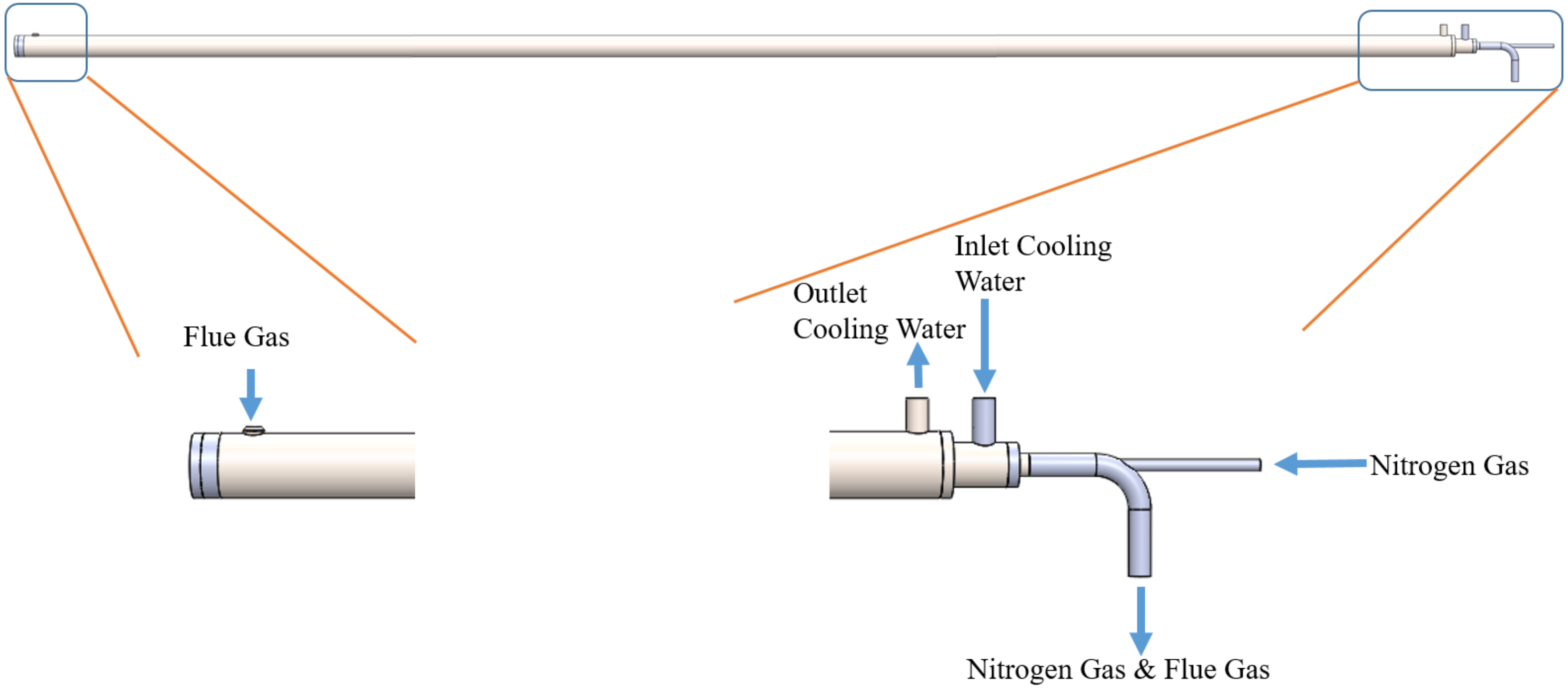

Scanning Mobility Particle Sizer (SMPS): 0.0143-0.6732 µm
Aerodynamic Particle Sizer (APS): 0.532-20 µm

Berner Low Pressure Impactor (BLPI): 0.0324-15.7 µm

PM0.6 and PM1 formation

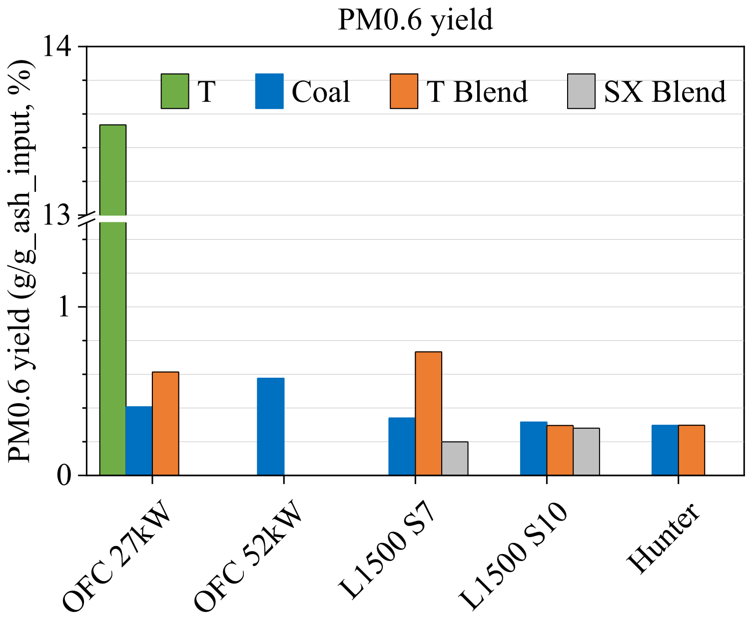

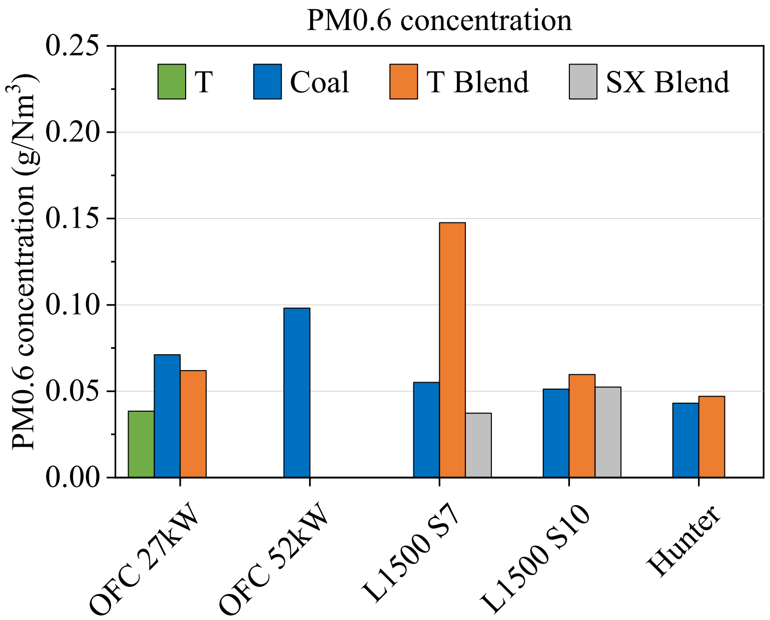

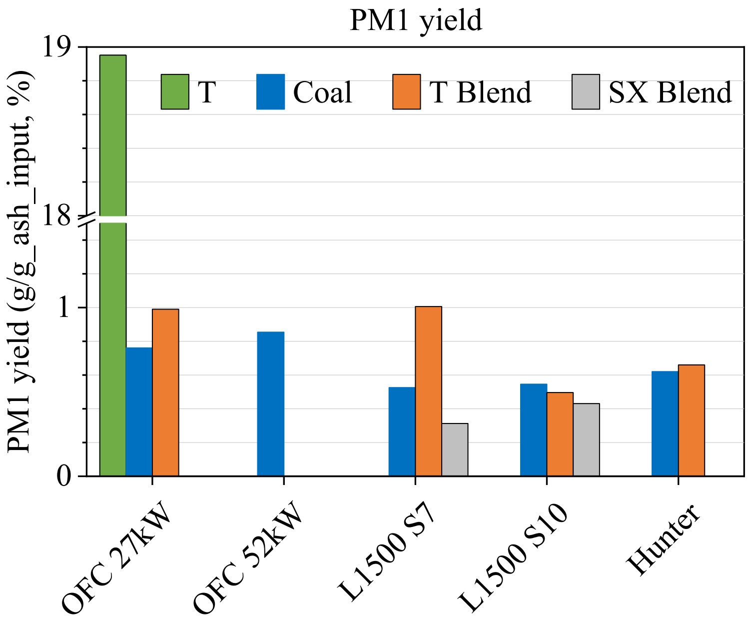

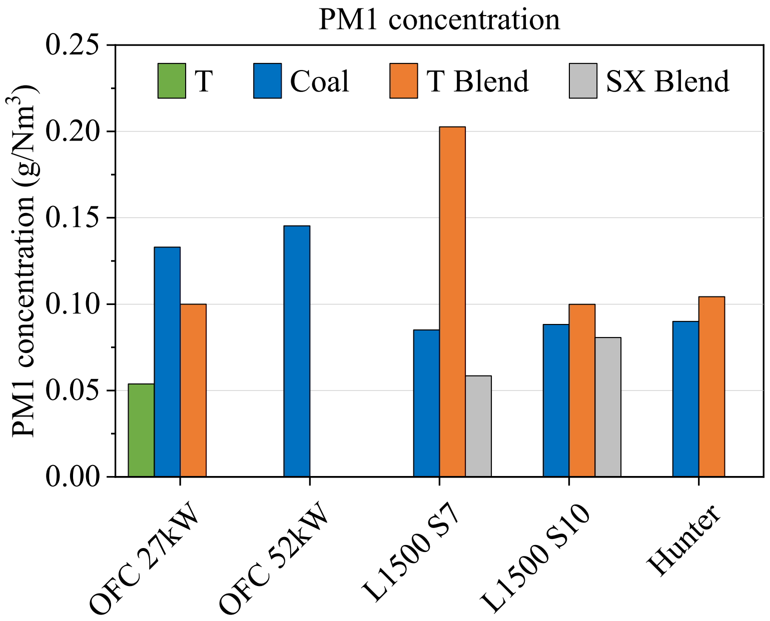

Ash aerosol particle size distributions of Coal combustion

by SMPS/APS:

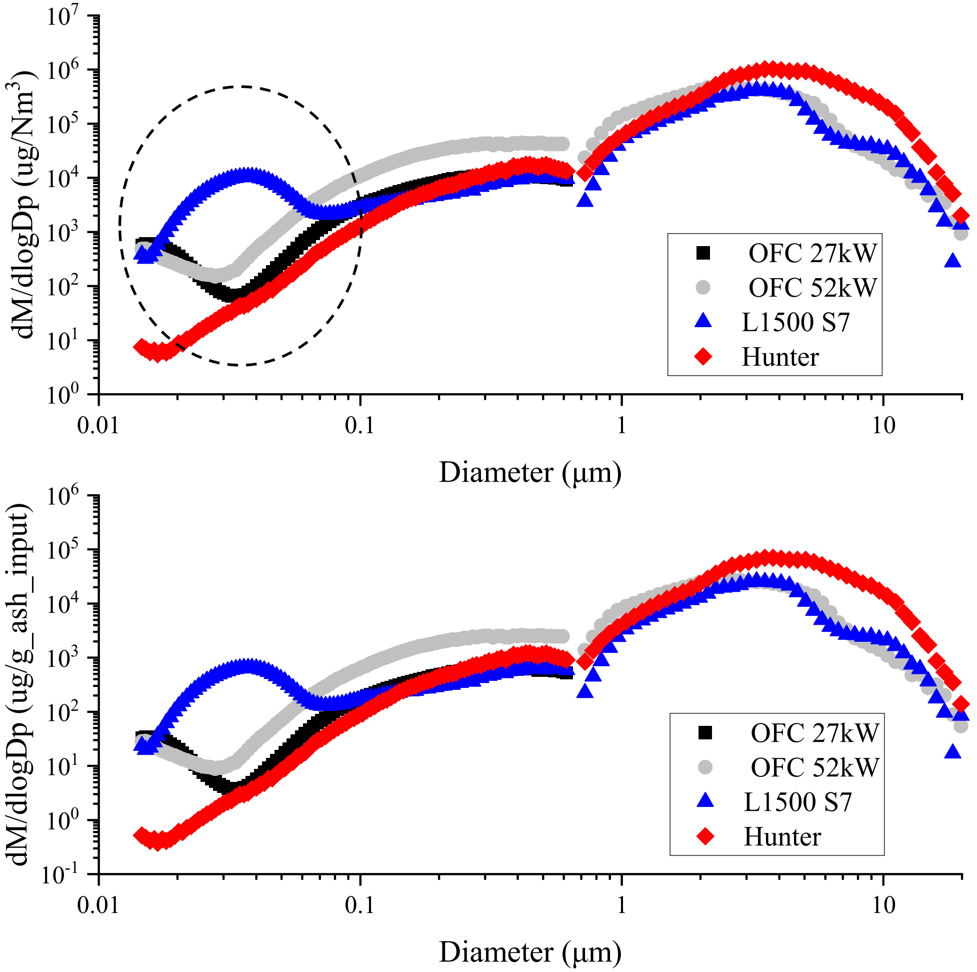

by BLPI:

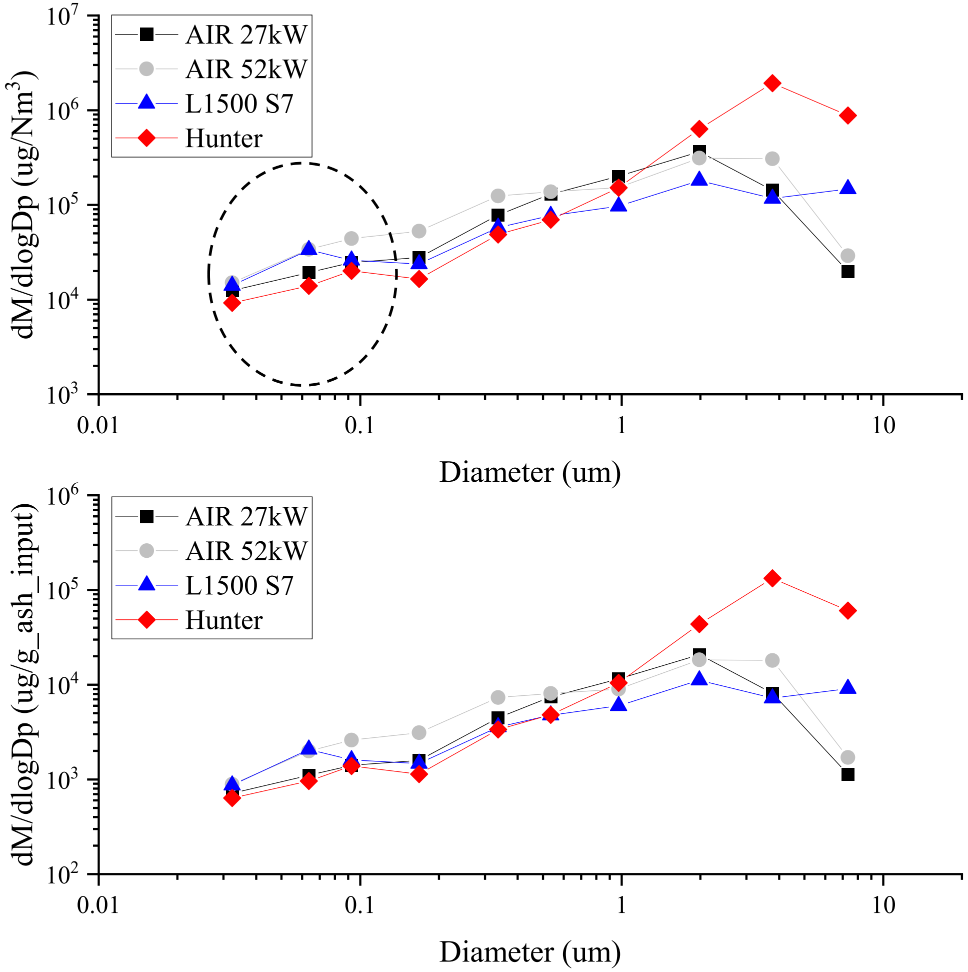

Ash aerosol compositions of Coal combustion

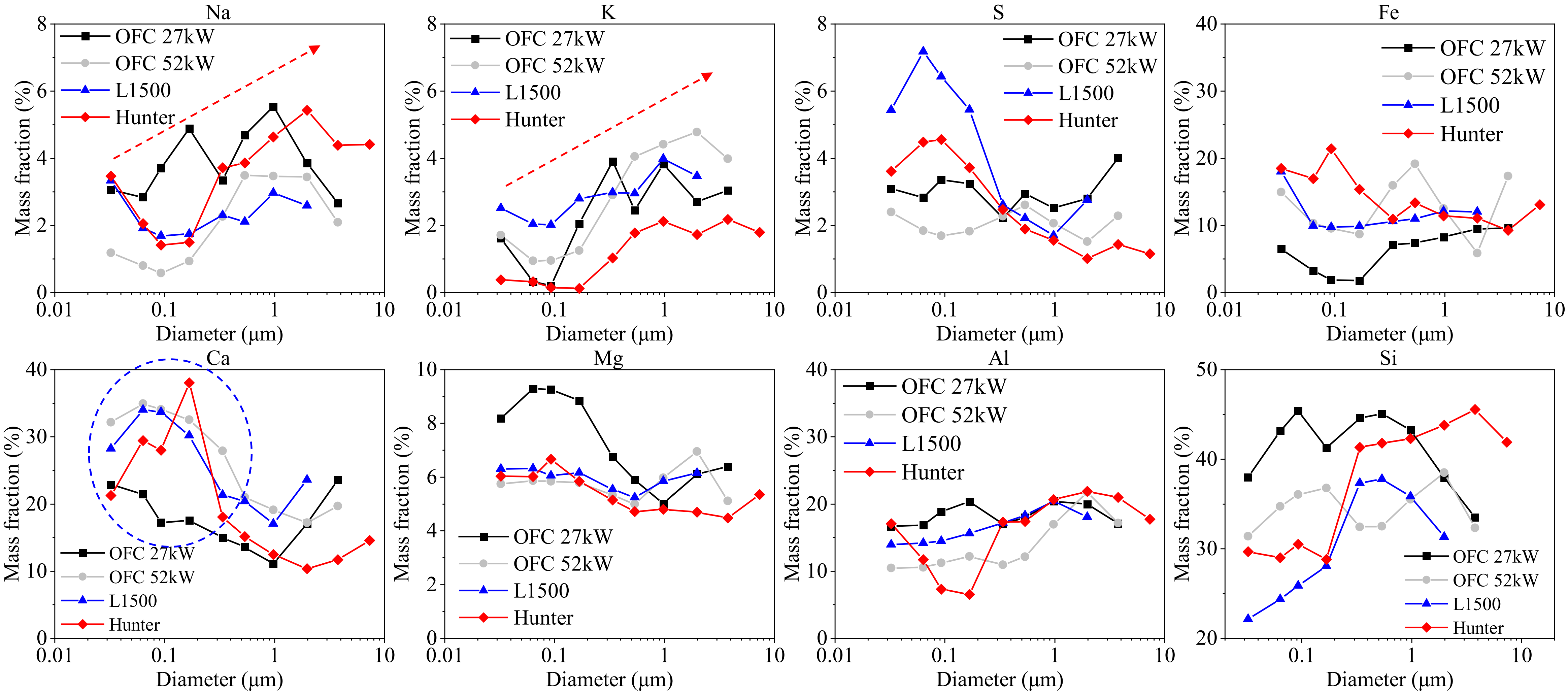

Ash aerosol particle size distributions in L1500 and Hunter

Mass concentrations:

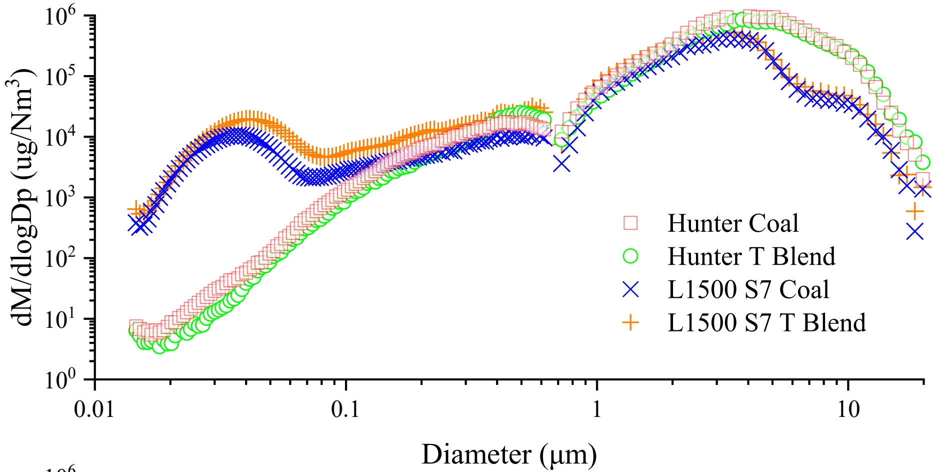

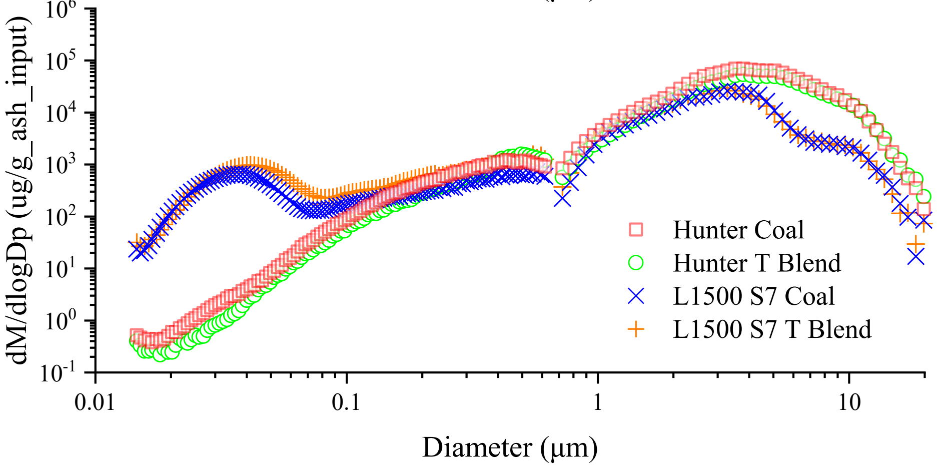

Number concentrations:

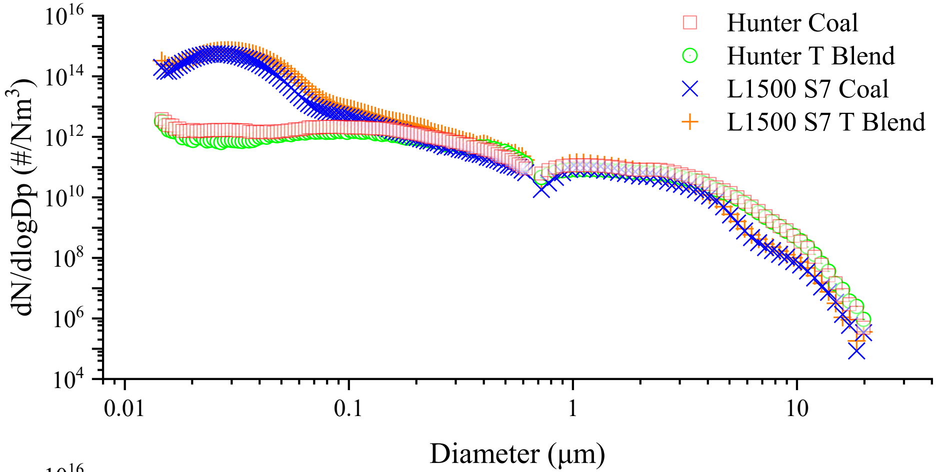

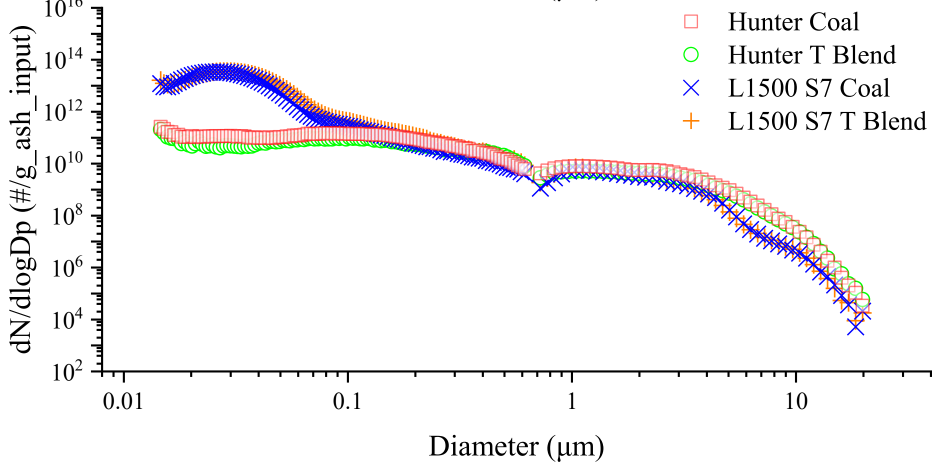

Ash aerosol compositions in L1500 and Hunter

L1500 results:

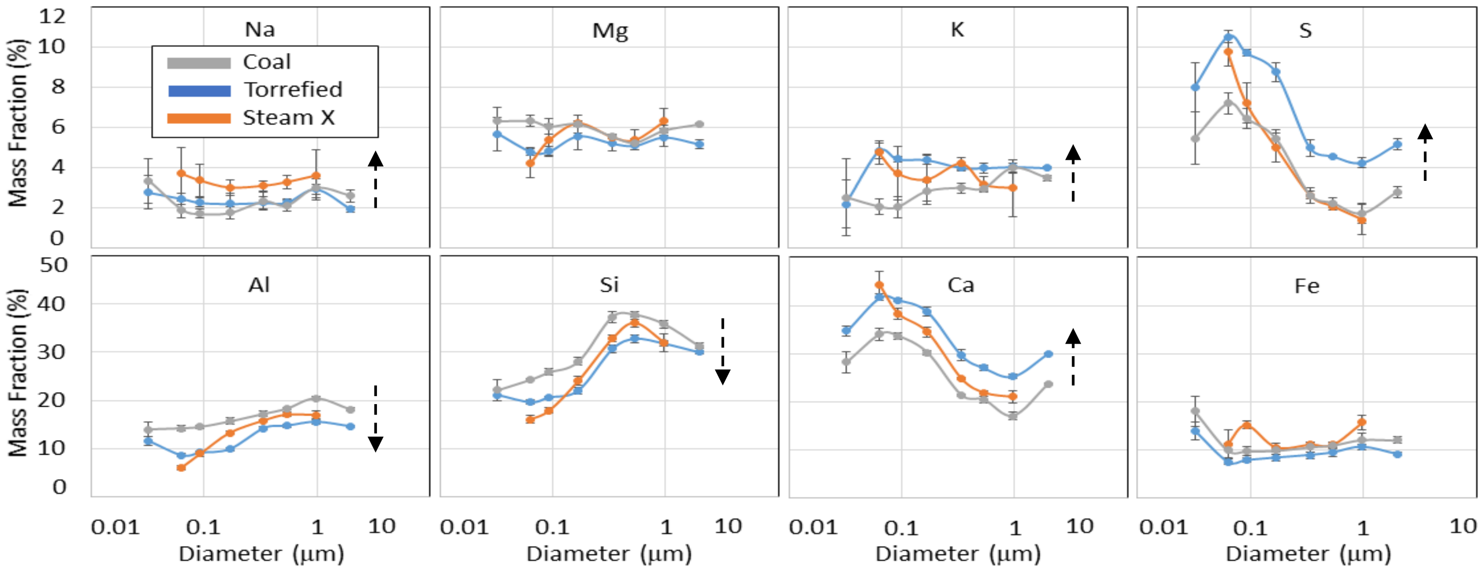

Hunter results:

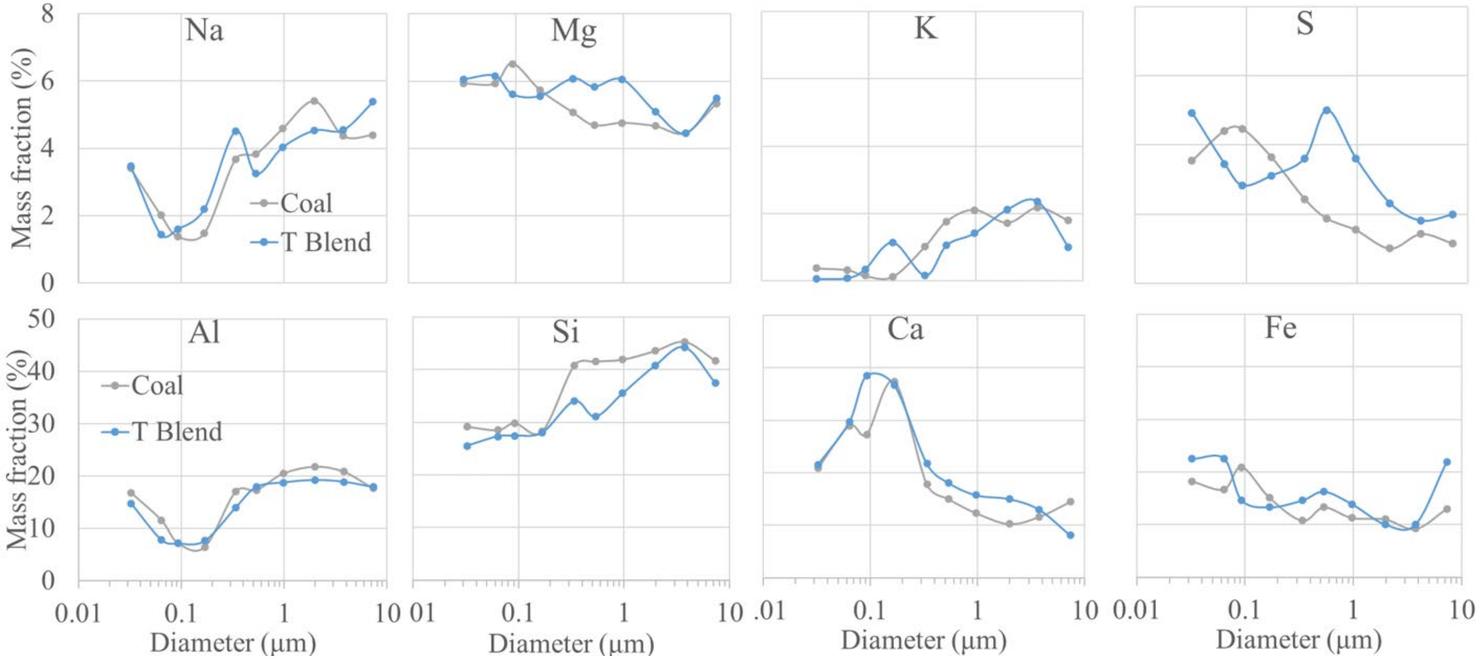

Conclusions

- Torrefied wood has much higher sub-micron ash yield through vaporization than coal does, but the particle concentration is low
- The pilot and full scale combustors have more similar sub-micron ash yields and concentrations in coal and woody biomass blend combustion
- The full scale utility boiler produces monomodal particle size distributions with alkali metals being enriched in the larger size range, suggesting fully coagulation and reaction of fly ash particles
- The more alkali contents brought in by the wood minerals are scavenged from sub-micron ash by larger particles when co-firing with coal on the full scale
- Co-firing torrefied wood with coal at 15/85 mixing ratio on the full scale boiler does not show significant changes from coal combustion in terms of size distributions and compositions of ash aerosols

Acknowledgement

PACIFICORP

Mr. Jack Mitchell

Mr. David A. Wagner

Dr. Eric G. Eddings

End
Thank you!

Cyclone ash

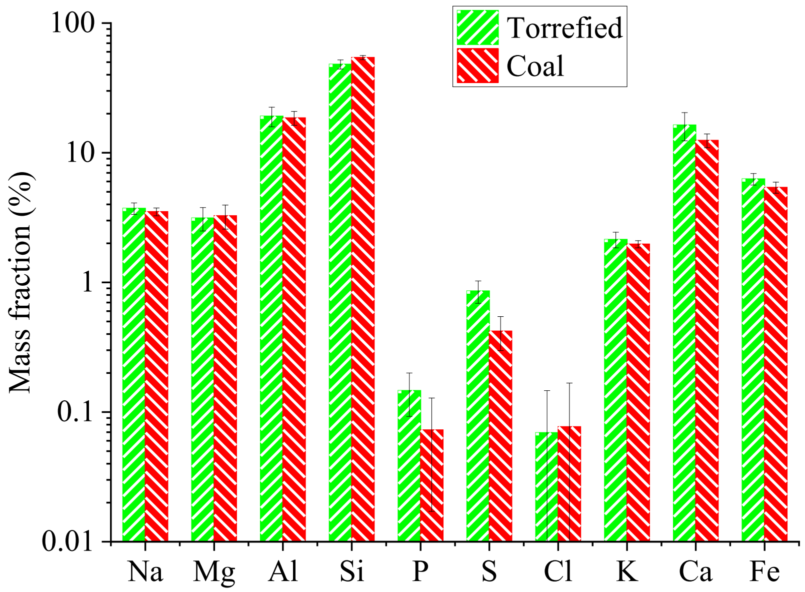

Compositions of ash aerosols (above 15.7 µm) collected in the cyclone and analyzed by EDS

Mineral Matter Deposition Behavior while Firing a Woody Biomass/Coal Blend at Lab, Pilot and Industrial Scales

Andrew Fry, Seyedhassan Fakourian
Department of Chemical Engineering, Brigham Young University

Xiaolong Li, Jost Wendt
Department of Chemical Engineering, University of Utah

Presentation Overview

- Project objective
- Overview of combustors (3 Scales) and fuel
- Deposition measurement hardware
- Comparison of sample conditions
- Comparison of deposition rate
- Comparison of deposit morphology
- Summary

Project Objective

To measure and compare the rate of ash deposition from combustion of pure coal and biomass/coal blends at three scales (27 kW, 1 MW_{TH} and 471 MW_{E})

1) Determine the impact of coal/biomass blends on deposition
2) Prove the efficacy of pilot scale testing to determine deposition behavior
3) Provide data sets for model validation

27 kW$_{TH}$ – Oxy Fuel Combustor (OFC)

Dimensions

- Burner Zone Dimensions – 4.1 m tall x 0.5 & 0.27 m ID
- Convective Zone Dimensions – 3.7 m x 0.15m Square

Typical Operating Conditions

Firing Rate	27	kW
Coal Feed Rate	7.6	lb/hr
Air Feed Rate	74	lb/hr

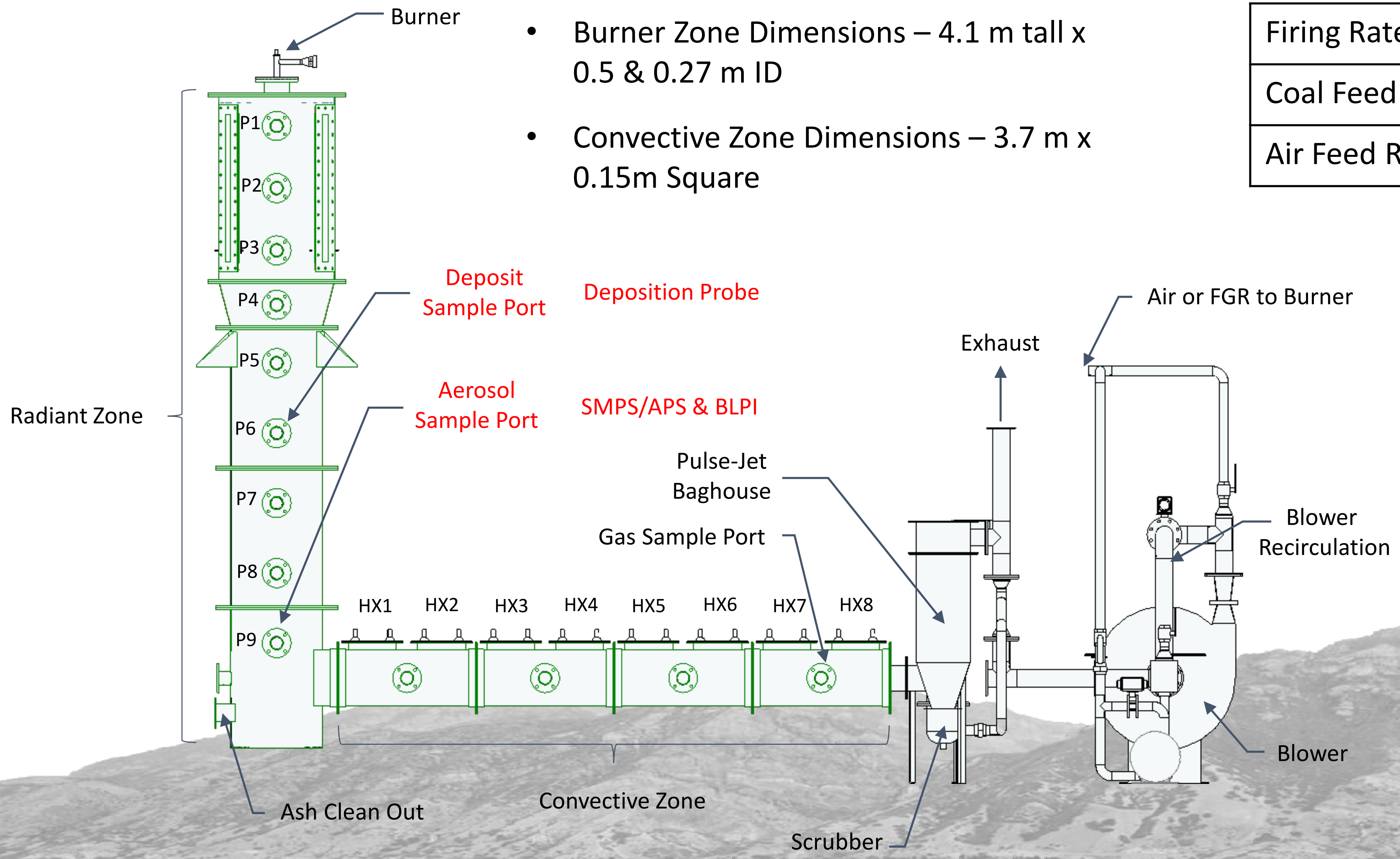

Burner

Radiant Zone

Deposit Sample Port

Deposition Probe

Aerosol Sample Port

SMPS/APS & BLPI

Pulse-Jet Baghouse

Gas Sample Port

Exhaust

Air or FGR to Burner

Blower Recirculation

Blower

Ash Clean Out

Convective Zone

Scrubber

27 kW$_{TH}$ – Fuel Analysis

Ultimate Fuel Analysis

	Coal	T	T Blend
C	62.41	51.57	57.08
H	4.52	5.29	4.91
N	1.1	0.14	0.62
S	0.46	0.02	0.24
O	11.04	36.29	23.67
Ash	13.96	0.19	7.08
H2O	6.52	6.32	6.42
HHV (Btu/lb)	11753	9264	10509

Blend is 50% biomass by mass

Ash Elemental Fuel Analysis

Fuel	Al2O3	CaO	Fe2O3	MgO	MnO	P2O5	K2O	SiO2	Na2O	SO3	TiO2
Coal	12.09	11.9	3.62	3.94	0.03	0.25	1.13	62.48	0.81	1.83	0.68
T	2.67	51.72	8.28	10.39	4.73	4.16	4.61	6.82	1.6	5.03	0
T Blend	11.95	12.33	3.7	4.04	0.1	0.29	1.32	61.71	0.83	1.84	0.67

1 MW_{TH} – Multi-fuel Combustor (L1500)

Dimensions

- Radiative Zone Inside Dimensions 14.1m long x 1.0 m square

Typical Operating Conditions

Firing Rate	1.0	MW_{TH}
Coal Feed Rate	302	lb/hr
Air Feed Rate	620	lb/hr

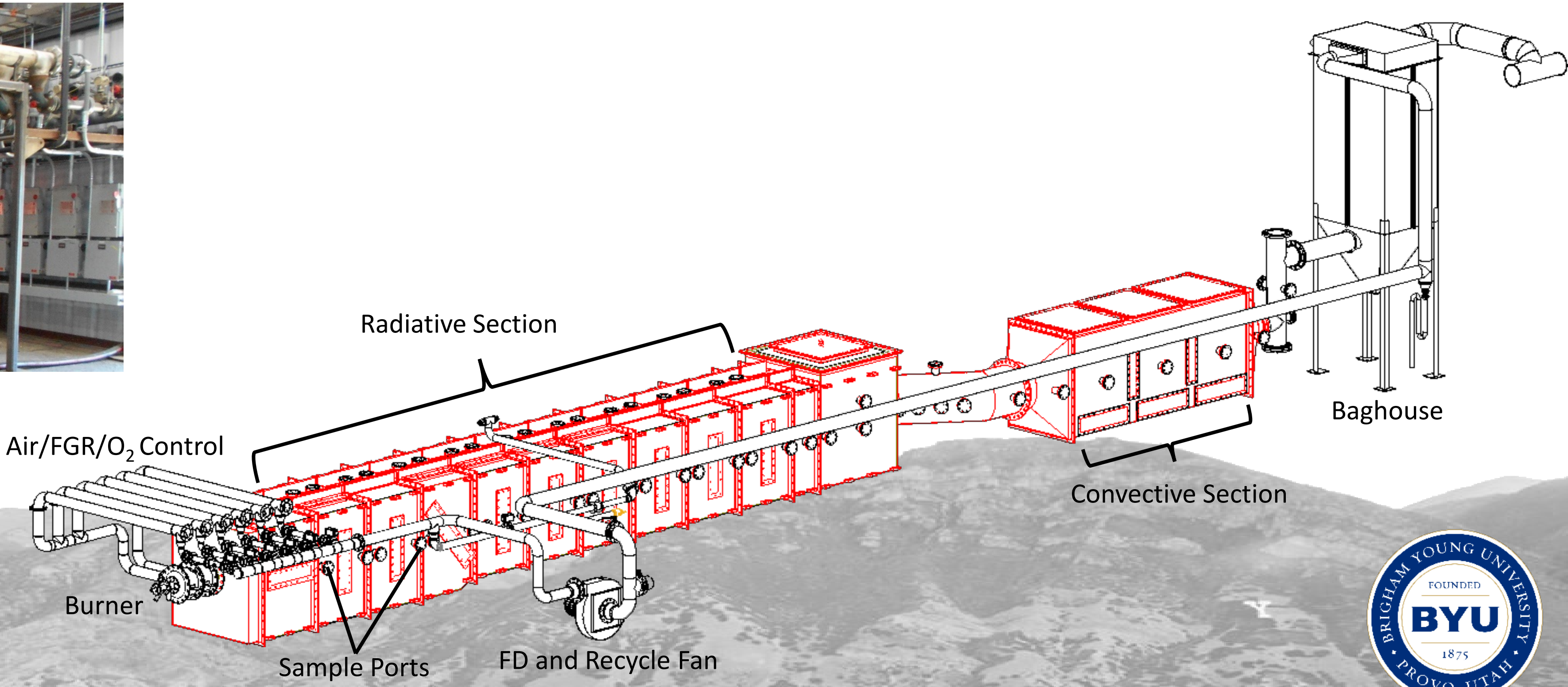

1 MW$_{TH}$ – Fuel Analysis

Ultimate Fuel Analysis

	Coal	T Blend	SX Blend
C	63.14	59.77	60.68
H	4.36	4.37	4.5
N	1.13	1	1.06
S	0.45	0.47	0.48
O	11.63	14.15	14.19
Ash	12.76	15.02	14.19
H2O	6.53	5.22	4.9
HHV (Btu/lb)	11168	10646	10616

Blend is 15% biomass by mass

Ash Elemental Fuel Analysis

Fuel	Al2O3	CaO	Fe2O3	MgO	MnO	P2O5	K2O	SiO2	Na2O	SO3	TiO2
Coal	11.03	15.25	4.17	3.99	0.04	0.29	1.2	54.07	1.26	6.35	4.17
T Blend	10.48	15.88	4.07	4.08	0.05	0.31	1.49	55.55	1.33	5.98	0.53
SX Blend	12.42	12.82	4.09	3.77	0.02	0.27	1.05	57.53	0.97	6.06	0.62

471 MW_E – Hunter, Unit 3

Dimensions

- Radiative Zone Dimensions ~ 52m tall x 15.5 m almost square cross section

Typical Operating Conditions

Firing Rate	1327	MW_{TH}
Coal Feed Rate	399	kpph
Air Feed Rate	4052	kpph

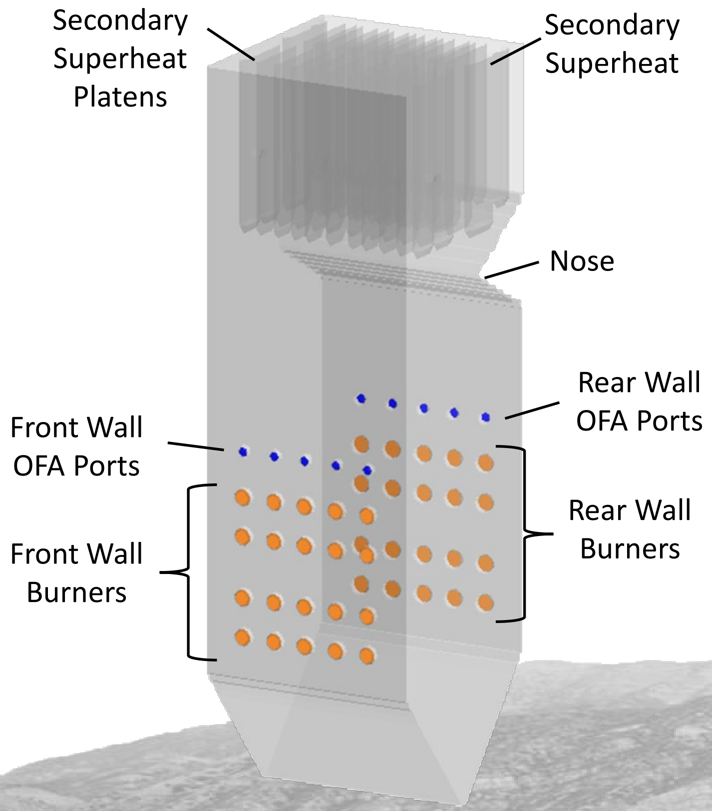

*This figure generated by REI for PacifiCorp's Hunter, Unit 3 under cooperative agreement DE-NT0005288

471 MW$_E$ – Fuel Analysis

Ultimate Fuel Analysis

	Coal	T	T Blend
C	63.34	47.74	60.06
H	4.43	5.2	4.42
N	1.23	0.23	1.06
S	0.48	0.02	0.41
O	10.44	35.55	12.91
Ash	11.64	0.85	11.48
H2O	8.45	10.4	9.67
HHV (Btu/lb)	11093	8219	10582

Blend is 15% biomass by mass

Ash Elemental Fuel Analysis

Fuel	Al2O3	CaO	Fe2O3	MgO	MnO	P2O5	K2O	SiO2	Na2O	SO3	TiO2
Coal	14.88	8.48	4.32	3.83	0.04	0.38	1.12	56.03	2.16	8.76	0.72
T Blend	14.08	10.48	4.01	4.88	0.04	0.33	1.3	56.61	2.17	6.74	0.67
SX Blend											

Deposit Probe

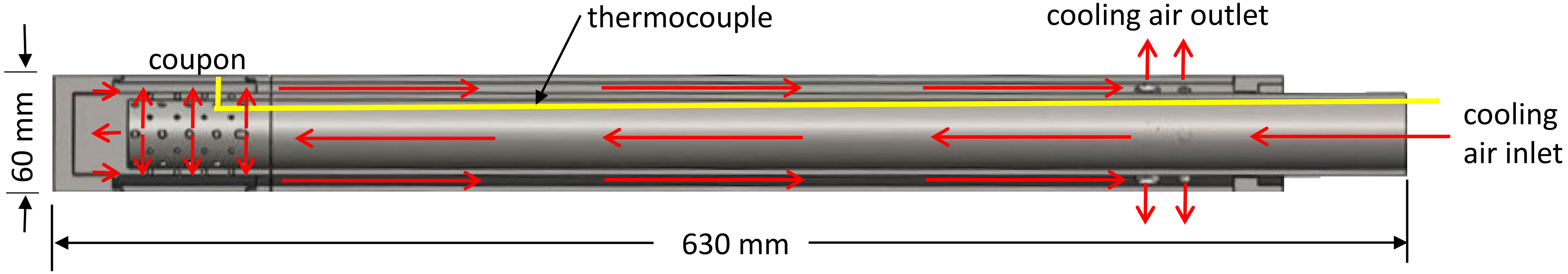

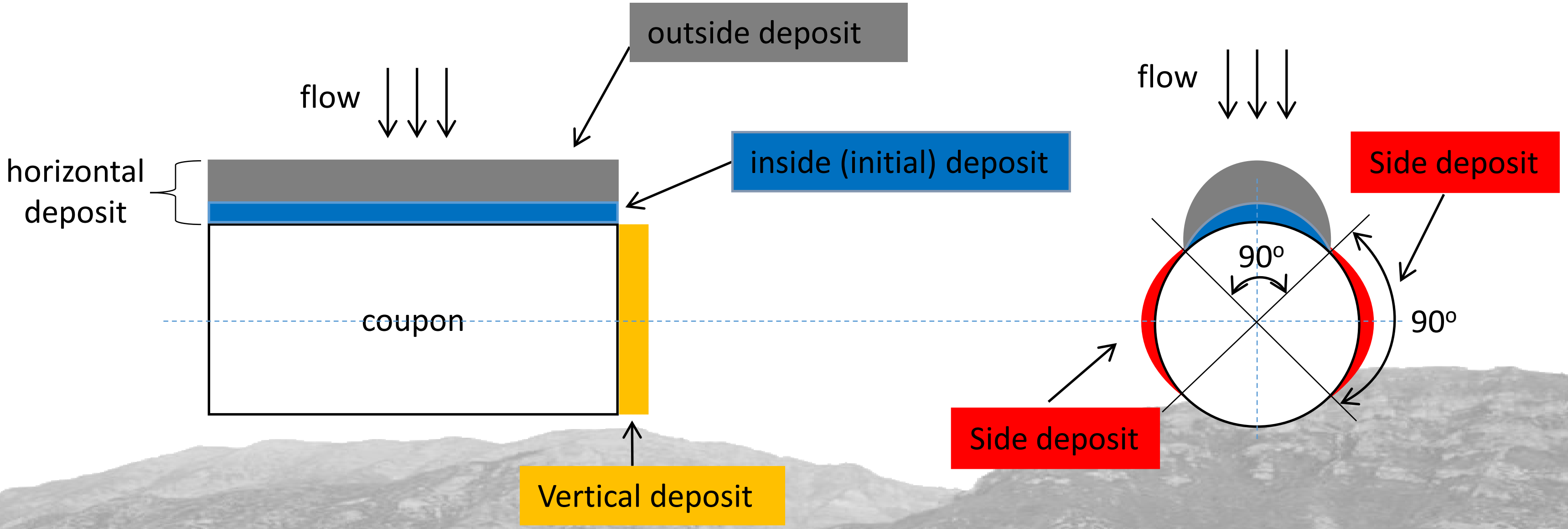

Deposit Probe

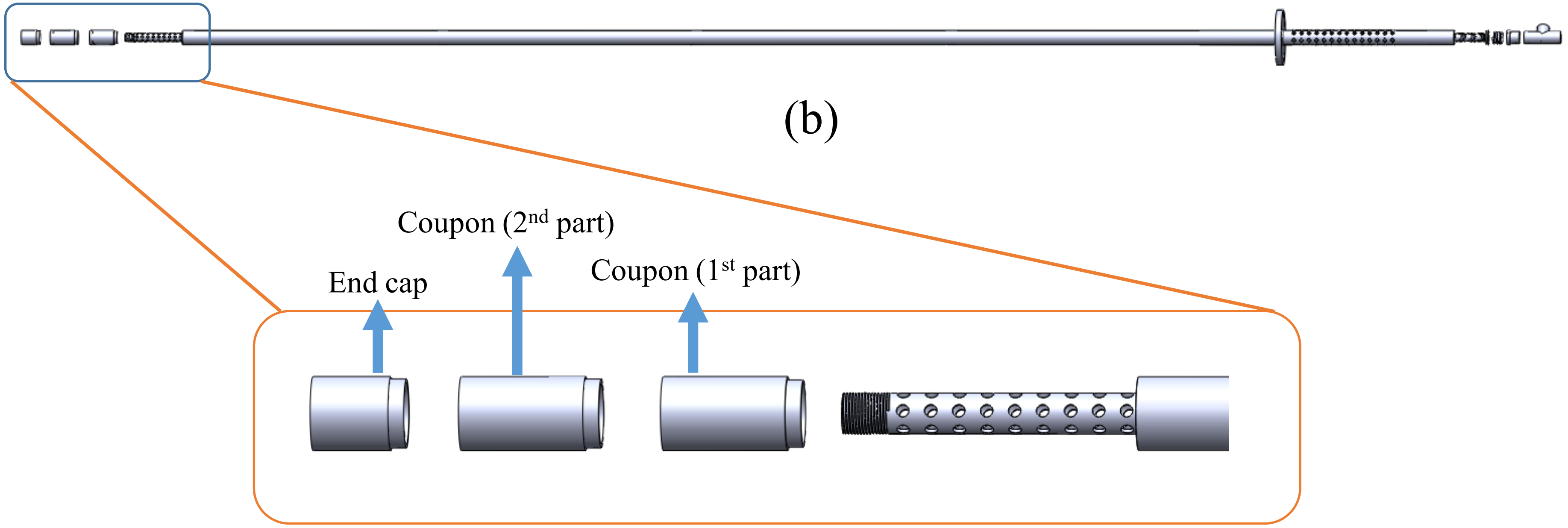

Coupon includes two parts to facilitate inserting the sensor of thermocouple into the first part of coupon. The internal surface of first part of coupon has a hole to keep the sensor of thermocouple.

Deposit Probe – L1500 & Hunter, Unit 3

Sample Locations

27 kW_{TH}

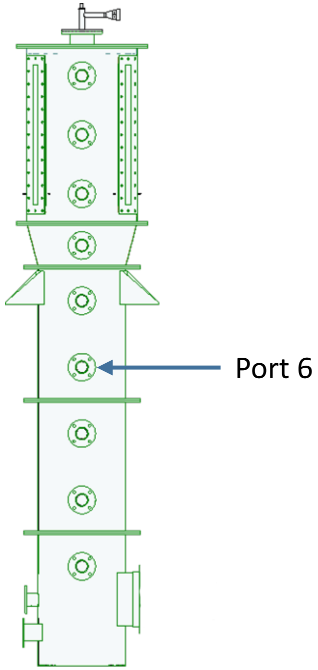

1 MW_{TH}

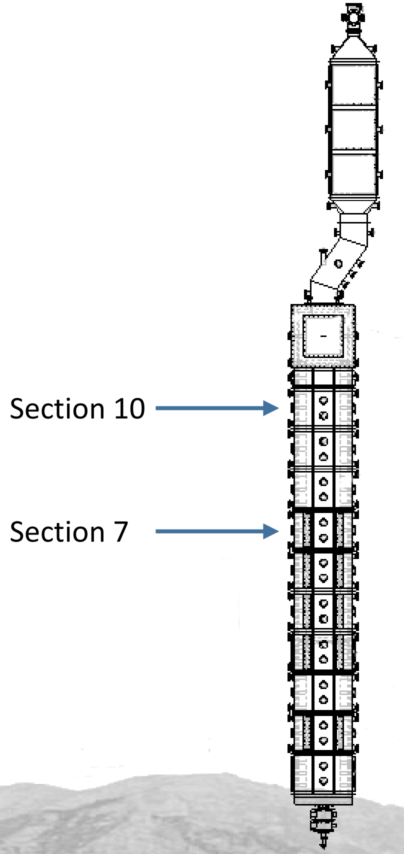

471 MW_{E}

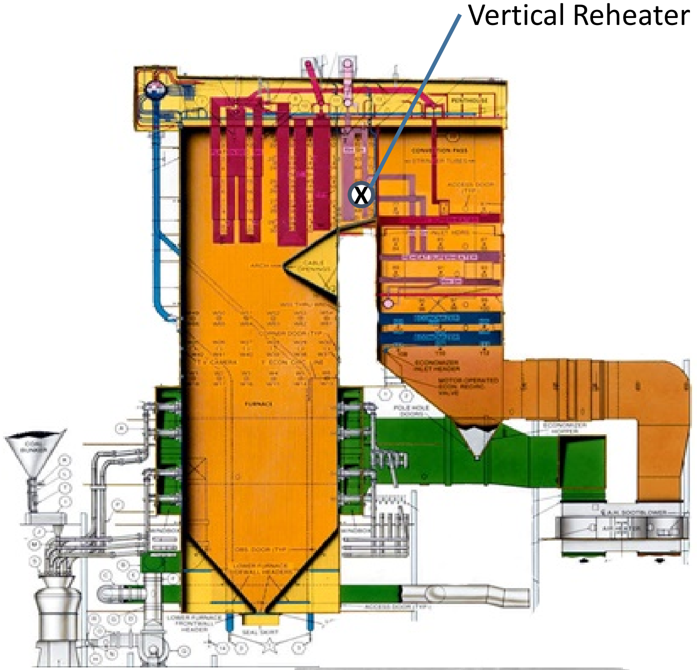

Comparison of Conditions

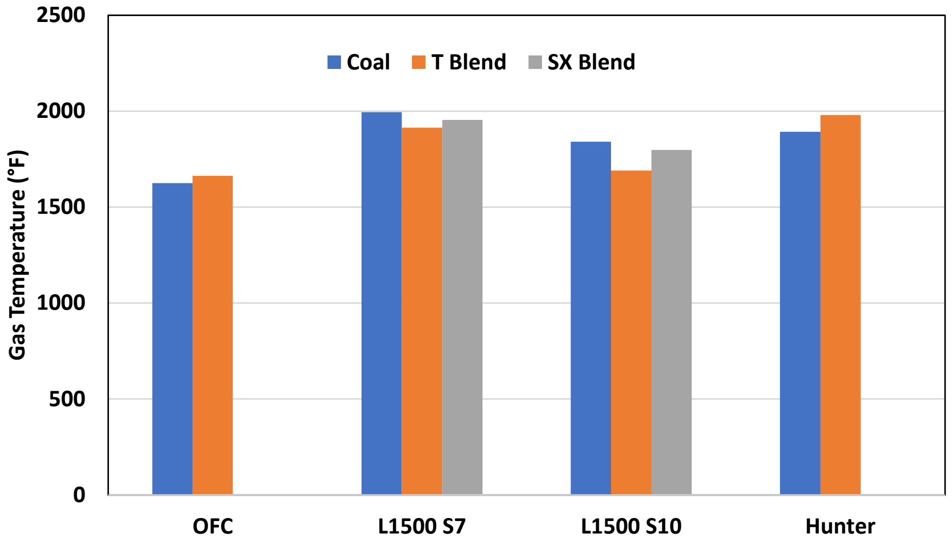

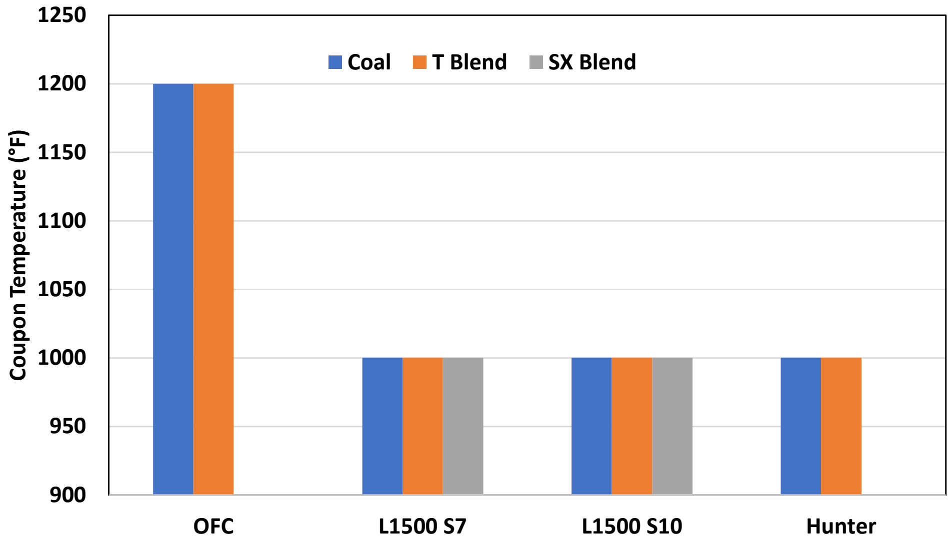

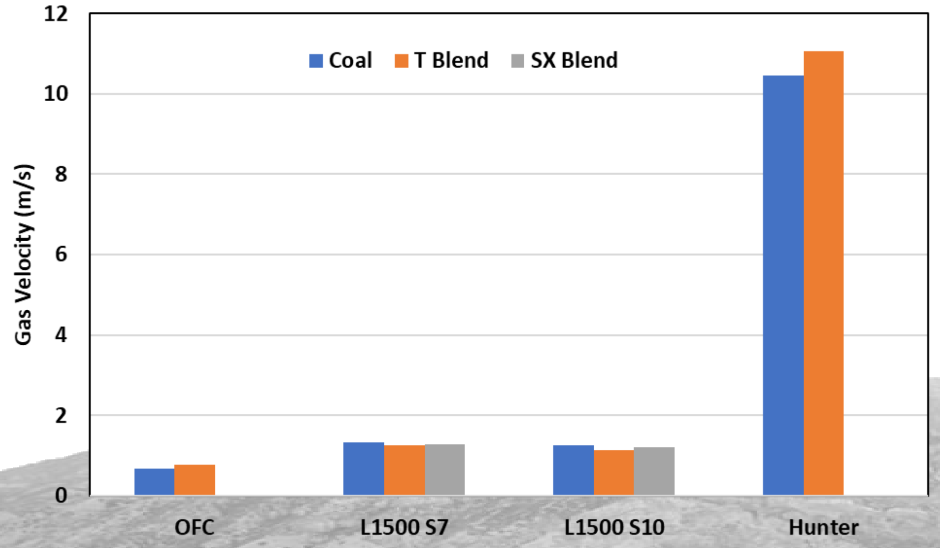

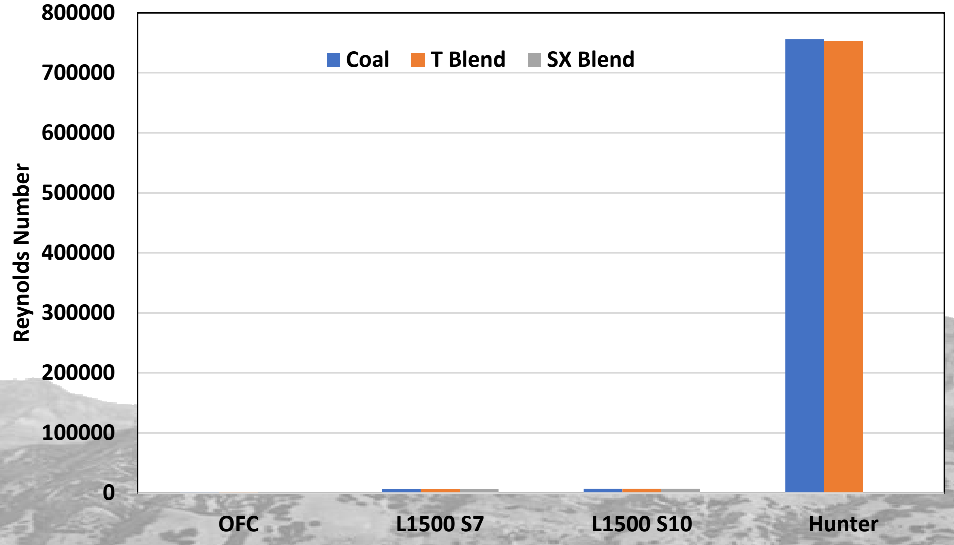

Comparison Images – L1500

	Port 7, 30 min	Port 7, 90 min	Port 10, 30 min	Port 10, 90 min
Coal				
T Blend				
SX Blend				

Comparison Images – Hunter, Unit 3

	30 min	60 min	90 min
Coal		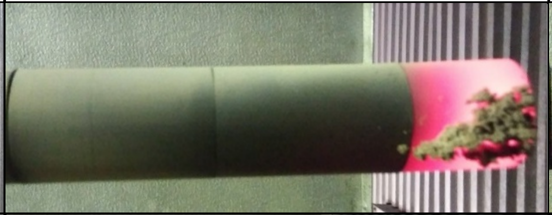	
T Blend	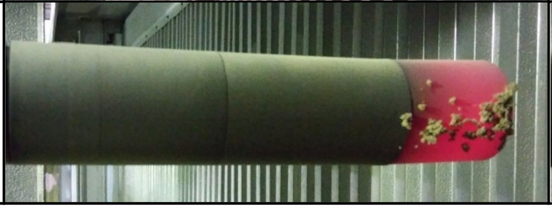		

Deposition Results

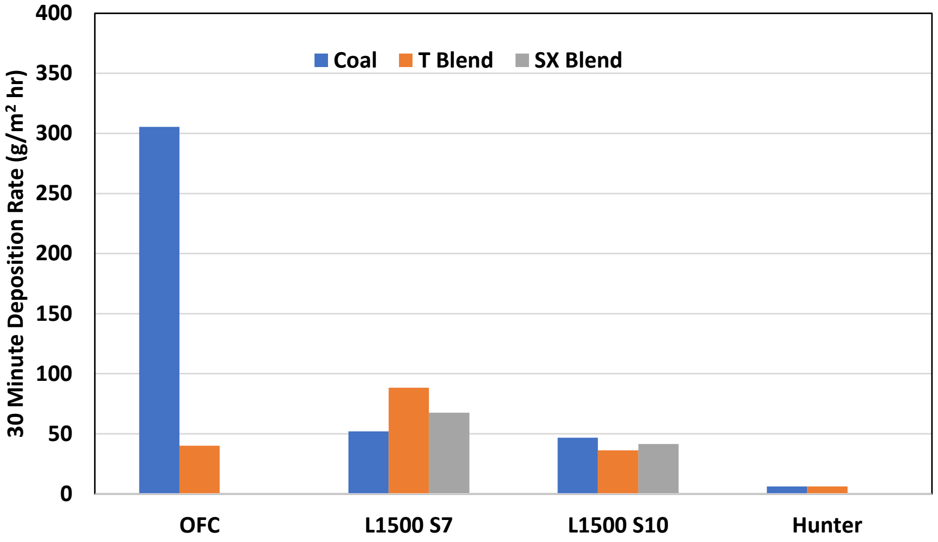

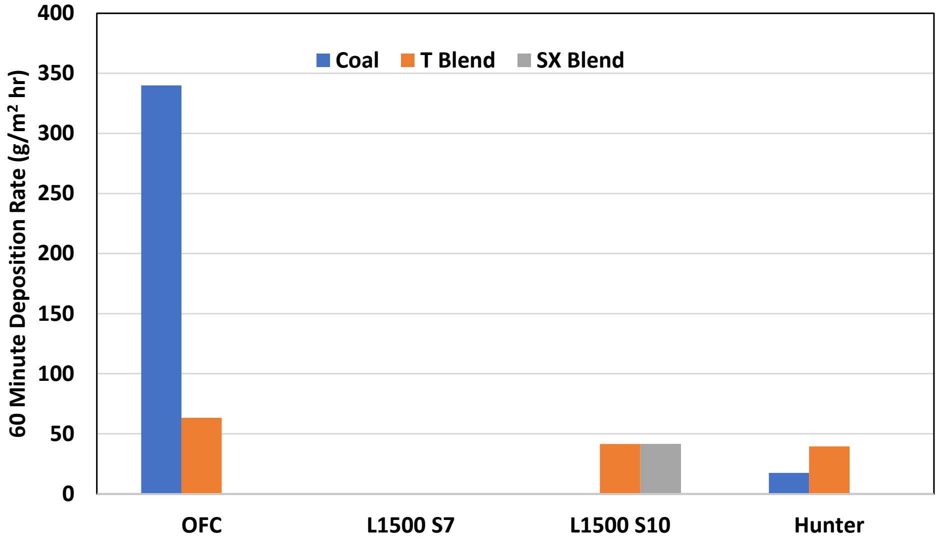

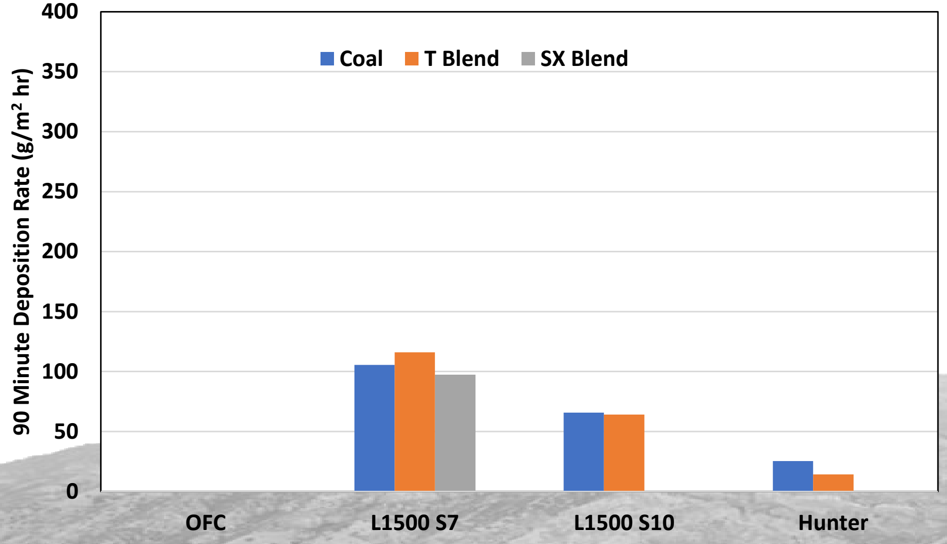

Deposit Composition

OFC 60 minute, outside; L1500 90 minute S7 and S10; Hunter 90 minute

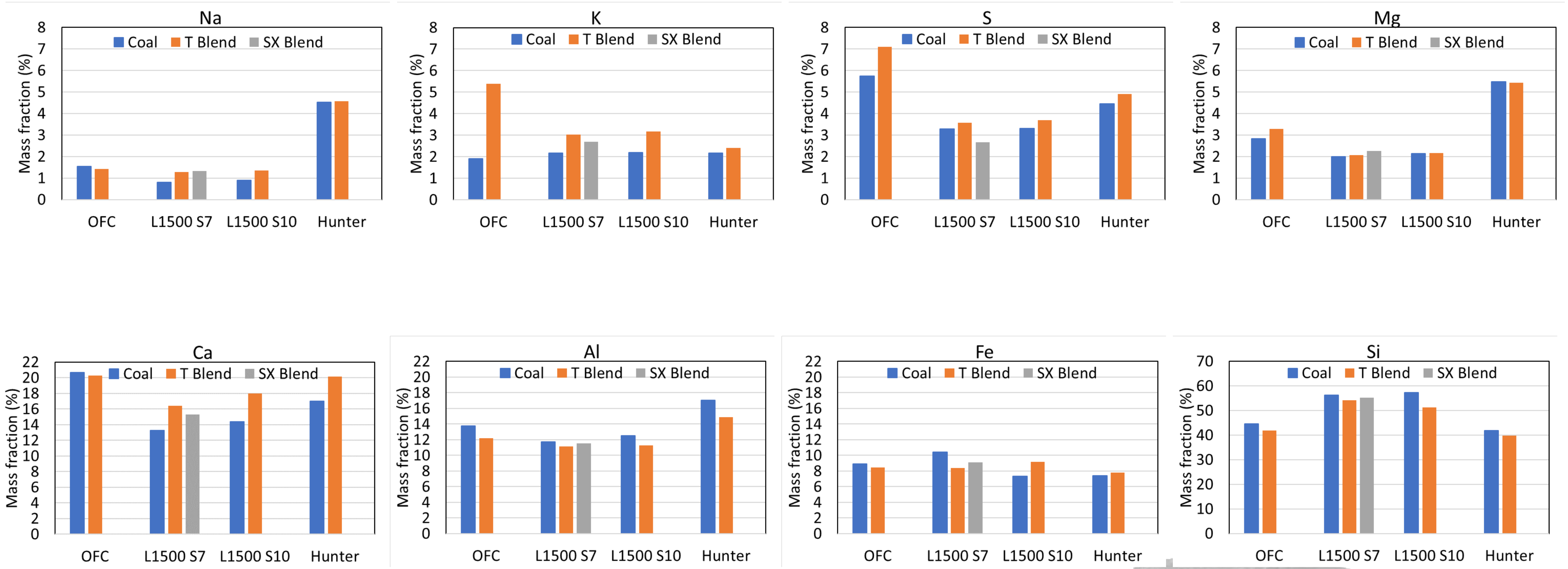

Deposit SEM – OFC

60 min sample time

500 µm

300 µm

Coal

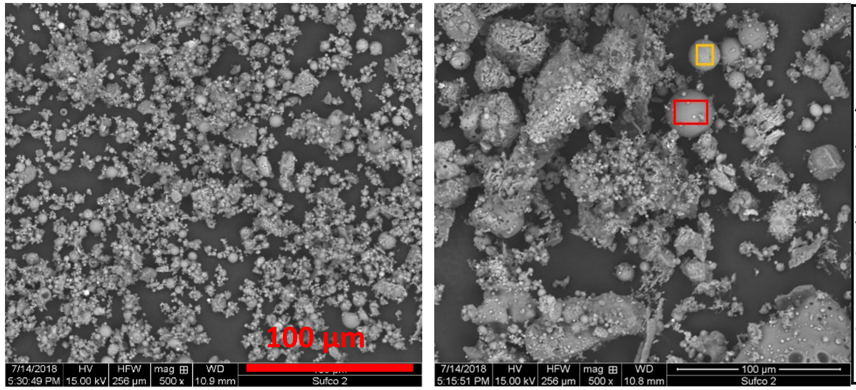

Na	0.6	0.4	
Mg	10.6	16.1	
Al	10.0	1.6	
Si	39.5	3.1	
P	0.1	0.1	
S	3.8	7.3	←
Cl	0.0	0.0	
K	2.0	0.2	←
Ca	26.2	44.4	
Fe	7.2	26.8	

T Blend

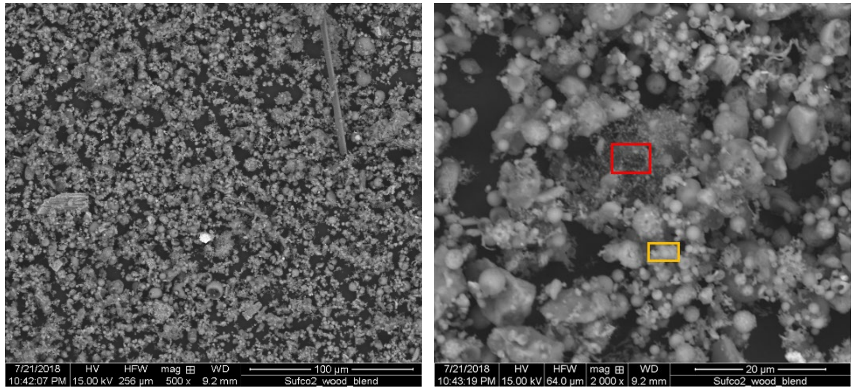

Na	1.3	3.4	
Mg	6.4	4.5	
Al	8.1	19.9	
Si	32.3	28.3	
P	0.0	0.3	
S	15.2	10.1	←
Cl	0.5	0.0	
K	3.2	8.0	←
Ca	20.5	16.2	
Fe	12.5	9.3	

increased K and S when blending with biomass

Deposit SEM – L1500

Section 7, 90 min sample time

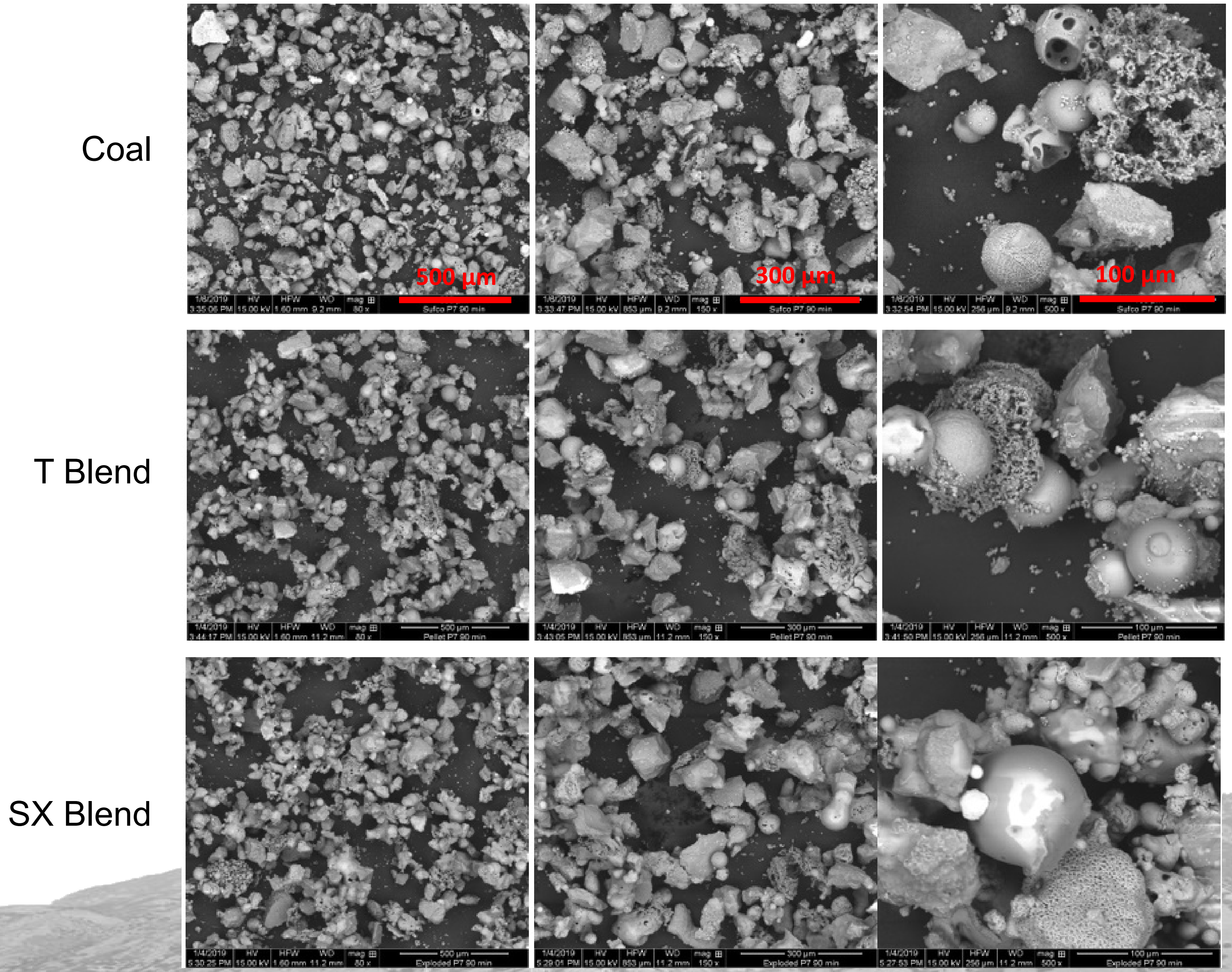

Deposit SEM – Hunter, Unit 3

60 min sample time

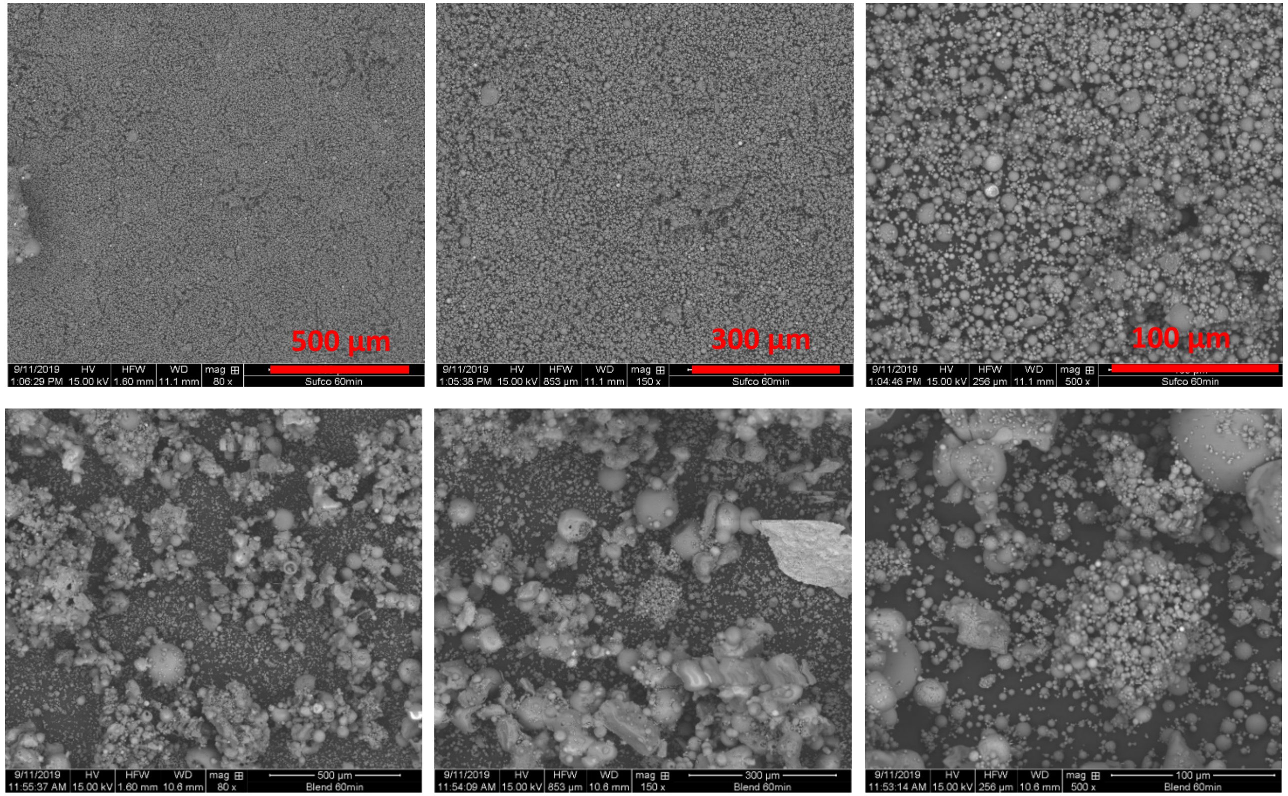

Coal

T Blend

Deposit SEM – Hunter, Unit 3

90 min sample time

Coal

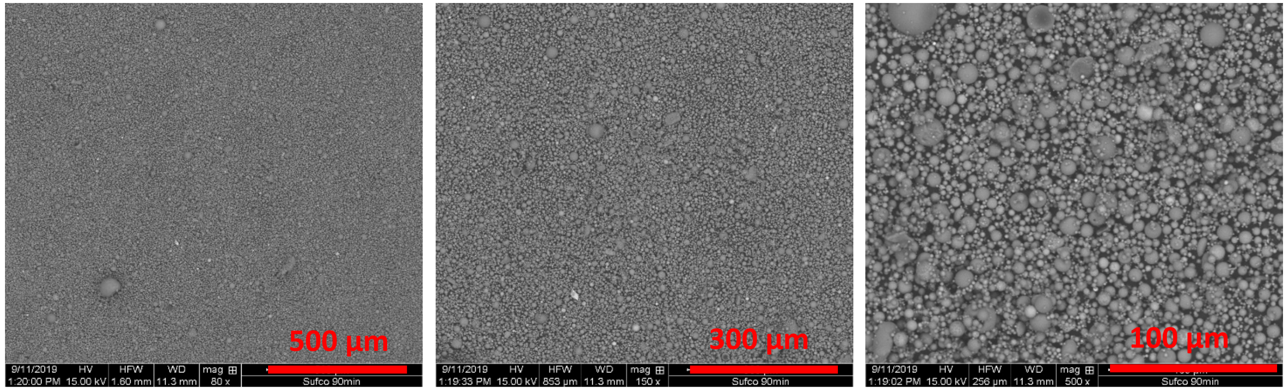

T Blend

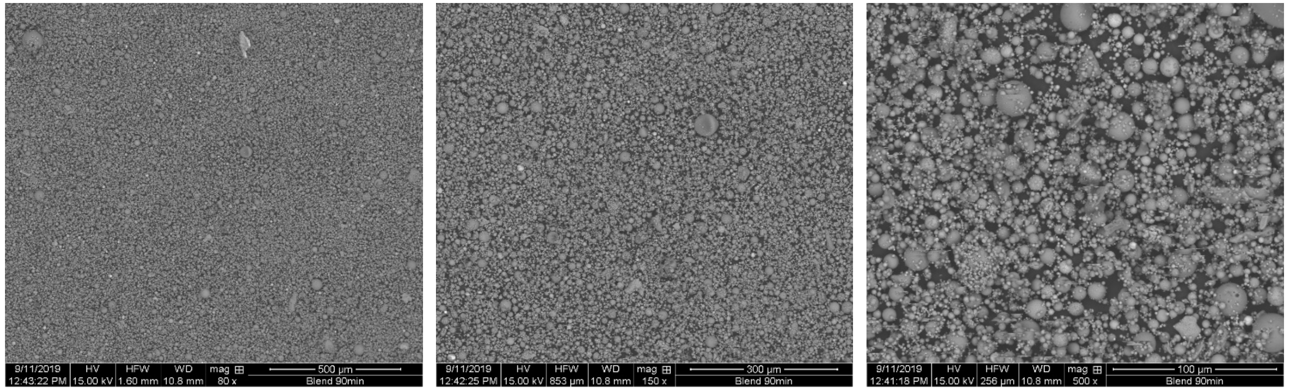

Summary

- Deposition Experiments have been performed to determine the impact of blending biomass with coal and experimental scale (27 kW$_{\mathrm{TH}}$, 1 MW$_{\mathrm{TH}}$, 471 MW$_{\mathrm{E}}$) on ash deposition
- Utah bituminous coal and a blend of prepared woody biomass (torrefied and steam exploded) and coal was fired at each scale and deposits were collected.
  - 15% biomass (by mass) blend at 1 MW$_{\mathrm{TH}}$ and 500 MW$_{\mathrm{E}}$
  - 50% biomass (by mass) blend at 27 kW$_{\mathrm{TH}}$
- Deposition rate was determined using a temperature controlled probe
- Deposition rate was generally smaller for the biomass blends commensurate with the lower ash content of the biomass
  - Consistent across all scales, with the exception of 1 MW$_{\mathrm{TH}}$ in port 7
- Large “chunk” deposits appeared at the 471 MW$_{\mathrm{E}}$ scale which accumulated at high rates in random locations
- Some deposit sample derived from the blended fuel were enriched in potassium and sulfur
- Size of particles in the 1 MW$_{\mathrm{TH}}$ deposits are larger than at 471 MW$_{\mathrm{E}}$ scale

Acknowledgements

The authors gratefully acknowledge financial support provided by PacifiCorp/Rocky Mountain Power and the State of Utah through the Utah Sustainable Transportation and Energy Plan (STEP).

Questions

NO_X Formation during Co-combustion of Coal and Biomass in a 480MWe Power Plant

Thomas Allgurén[1], Klas Andersson[1], Andrew Fry[2], Eric G. Eddings[3]

[1] Department of Space Earth & Environment, Chalmers University of Technology, Sweden

[2] Department of Chemical Engineering, Brigham Young University, Provo, Utah

[3] Department of Chemical Engineering, University of Utah, Salt Lake City, Utah

Impact on NOx during co-firing

- Biomass vs coal
  - Nitrogen content
  - Release conditions related to fuel
  - Release conditions related to combustion
  - Fate of fuel-nitrogen

Method

Experiments – L1500

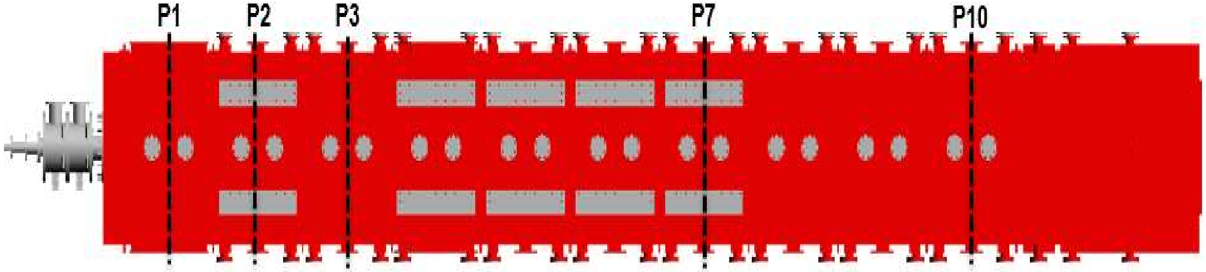

G = gas composition data is available, T = temperature data is available.

	Coal	Coal-T	Coal-SX
Port 1	G/T	-	G/T
Port 2	G/T	G/T	G
Port 3	G/T	G*/T	G/T
Port 7	G/T**	G*/T**	G/T**
Port 10	T**	T**	T**
Flue gas	G	G	G

Method

Fuels

Fuel composition is presented in % based on mass.

Fuel or Case	Mixture	C	H	N	S	O	Ash	H_2O
Sufco	-	61.48	4.47	0.91	0.58	12.21	16.20	4.15
Torrefied	-	54.98	5.16	0.59	0.00	29.60	7.44	2.24
Steam exploded	-	59.59	5.50	0.59	0.00	28.04	3.52	2.76
Coal	Sufco	61.48	4.47	0.91	0.58	12.21	16.20	4.15
Coal-T	Sufco/Torrefied – 85/15	60.51	5.01	0.86	0.49	14.82	14.88	3.86
Coal-SX	Sufco/Steam exploded - 85/15	61.20	5.07	0.86	0.49	14.58	14.29	3.94

Method

Experiments – Hunter unit 3

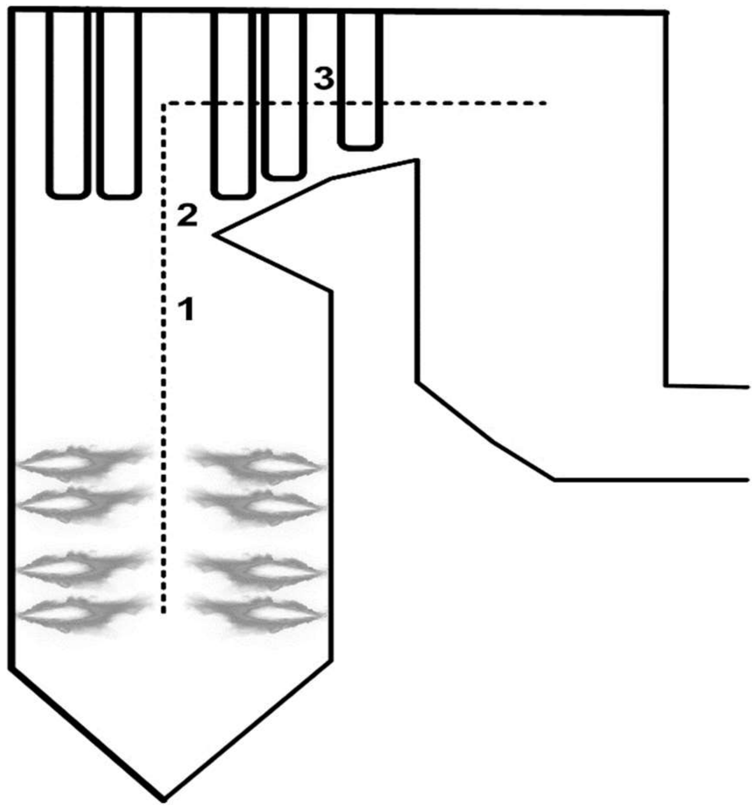

Results

NO stack gas concentration, pilot & full-scale

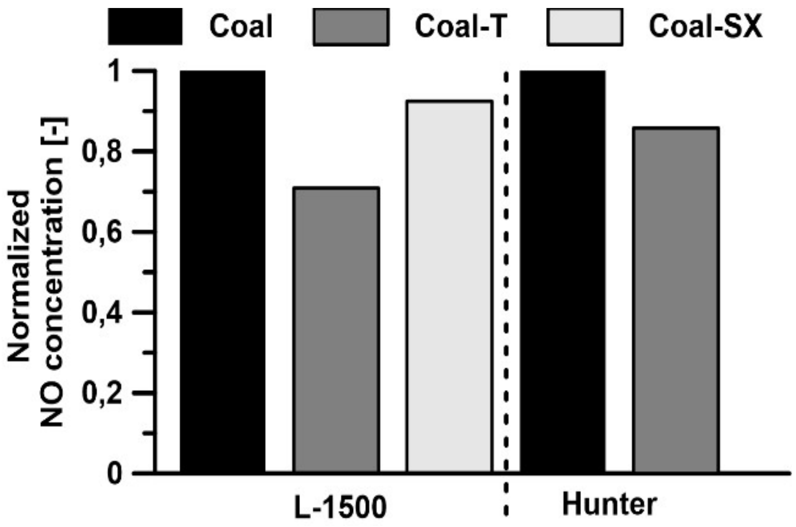

Results

Temperature conditions, pilot scale

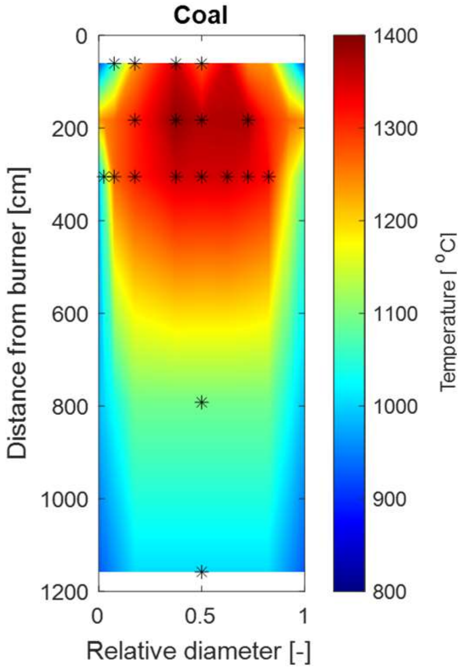

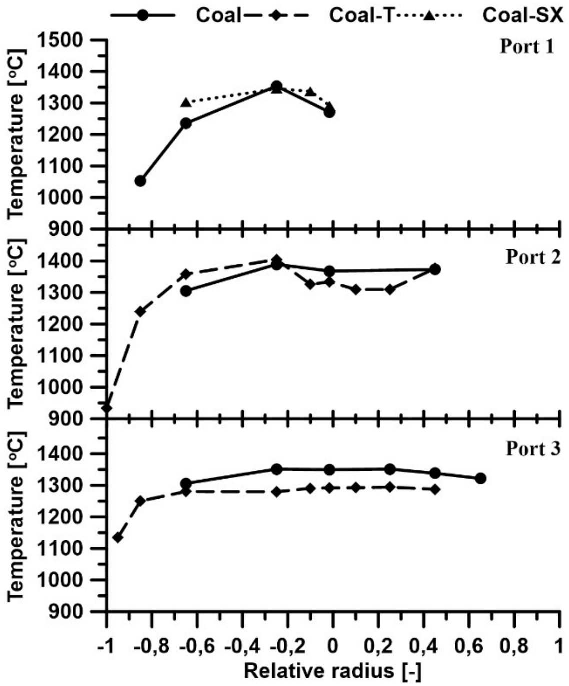

Results

Oxygen and CO concentrations, pilot scale

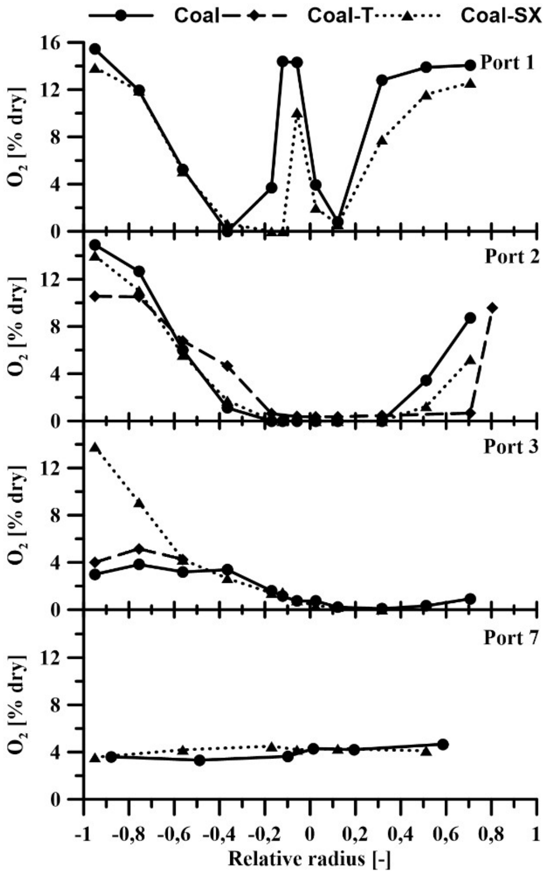

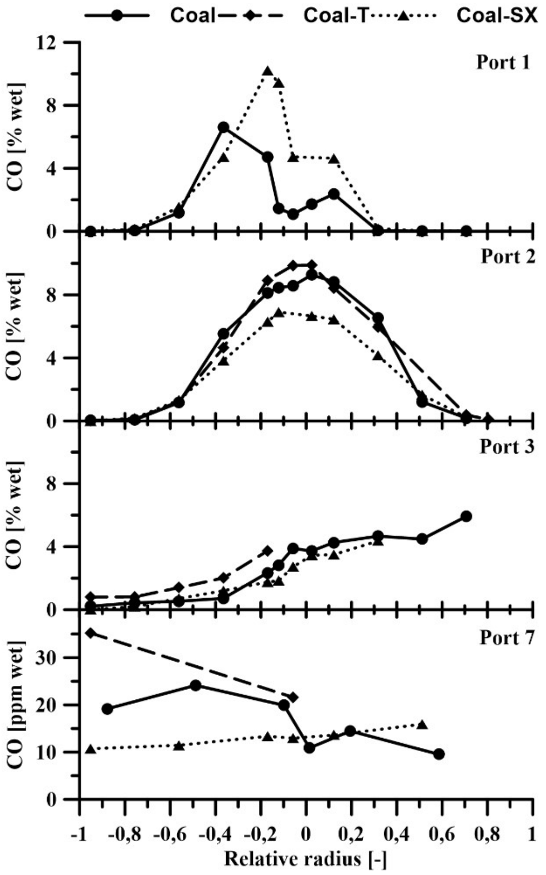

Results

Oxygen concentration, pilot & full-scale

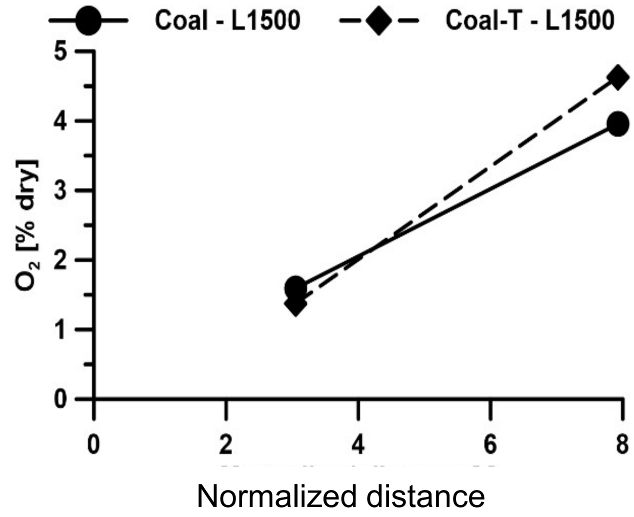

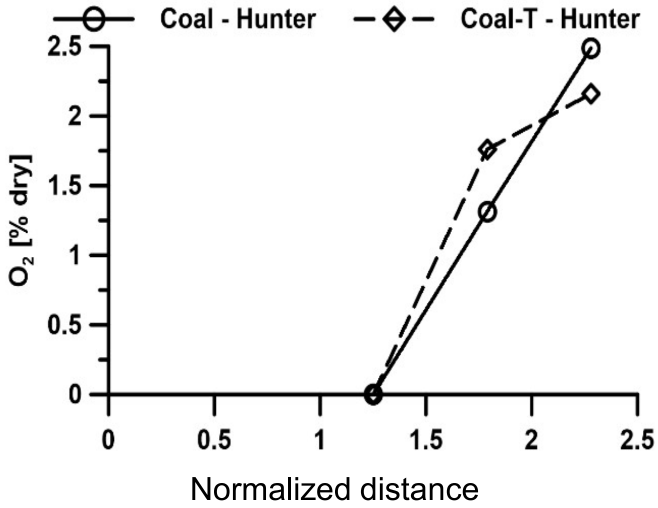

Results

CO concentration, pilot & full-scale

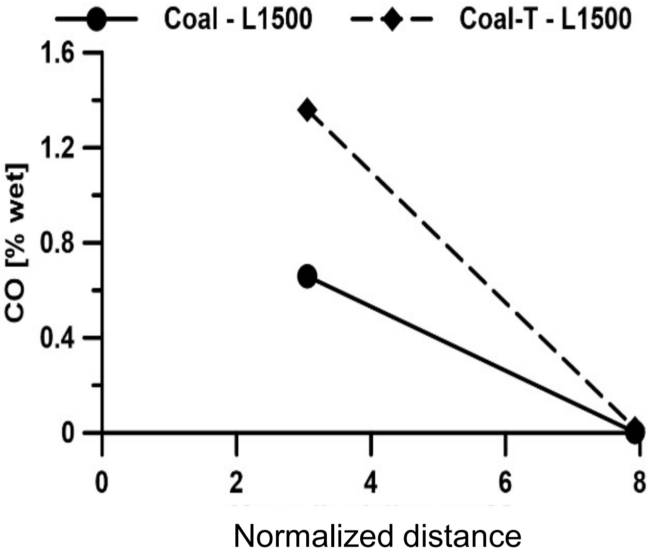

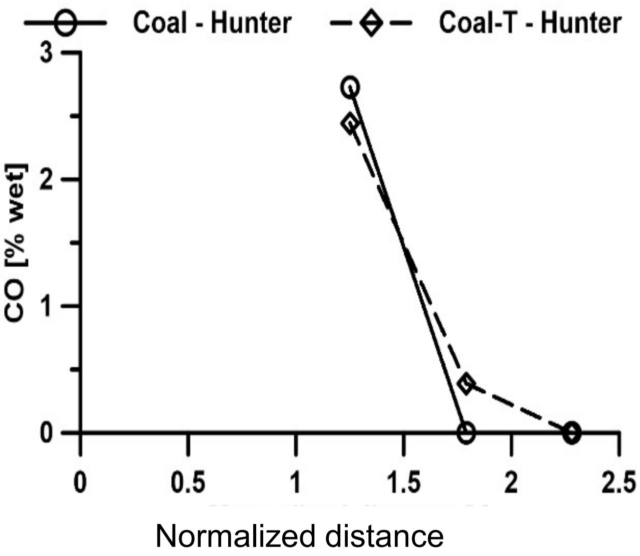

Results

HCN concentration, pilot & full-scale

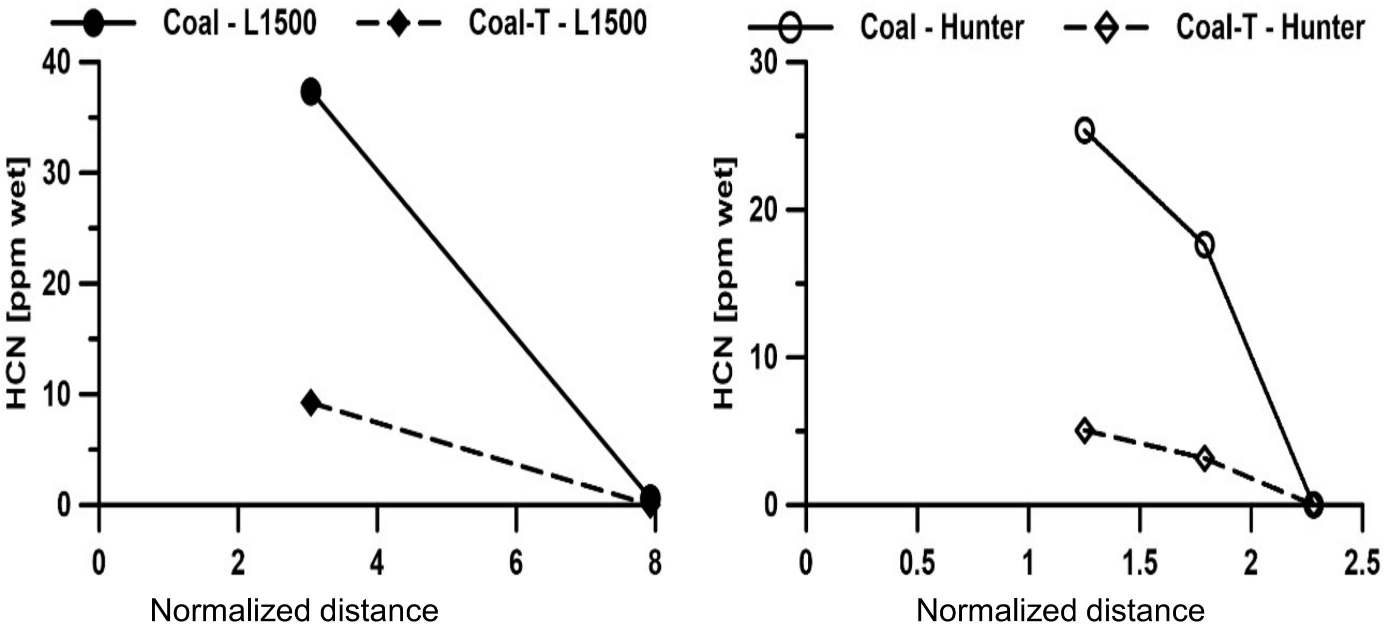

Results

NH3 concentration, pilot & full-scale

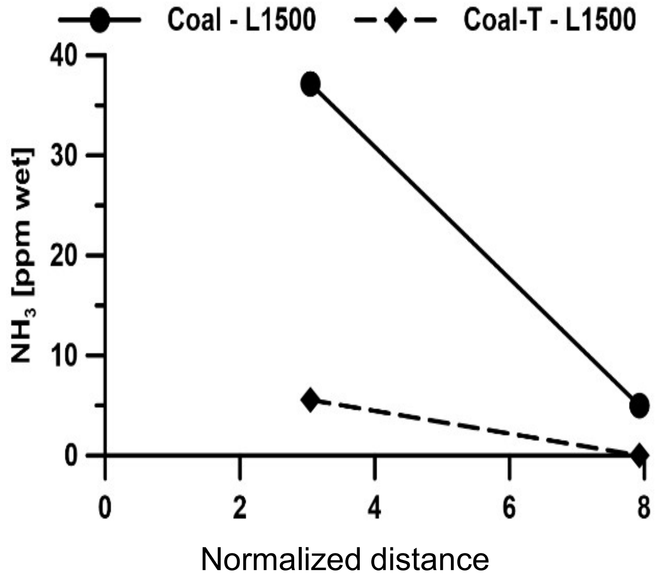

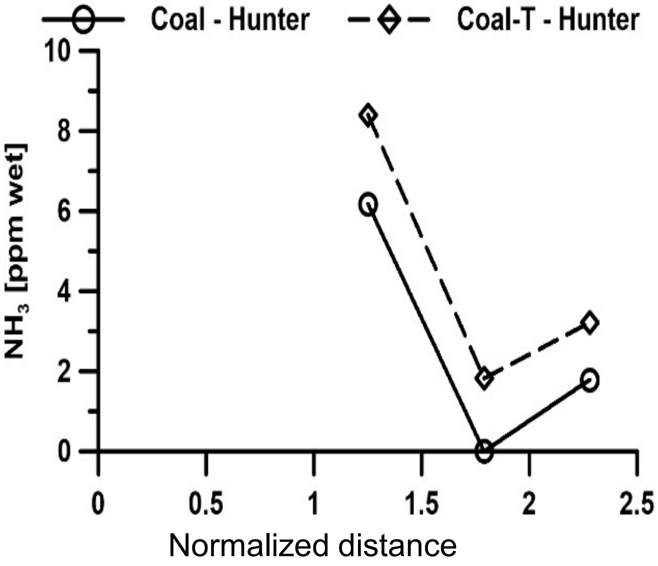

Conclusions

Torrefied and steam exploded biomass co-combusted with Utah Sufco coal

Replacing 15% of the Sufco coal with steam exploded or torrefied biomasses resulted in a reduction in NO concentration in the flue gas of 8% and 30% respectively in L1500.

Combustion conditions remained similar in pilot -scale

Plausible effects: PSD, release patterns and N-fate

Hunter, 15% NOx reduction with torrefied biomass

NO formation during co-combustion of coal with two thermally treated biomasses

Thomas Allgurén
thomas.allguren@chalmers.se

Co-authors:
Rikard Edland[1], Klas Andersson[1], Andrew Fry[2], Eric G. Eddings[3], Fredrik Normann[1]

[1] Department of Space Earth & Environment, division of Energy Technology, Chalmers University of Technology, Göteborg, Sweden
[2] Department of Chemical Engineering, Brigham Young University, Provo, Utah
[3] Department of Chemical Engineering, University of Utah, Salt Lake City, Utah

BYU
BRIGHAM YOUNG
UNIVERSITY

CHALMERS
UNIVERSITY OF TECHNOLOGY

THE
UNIVERSITY
OF UTAH

Background

Wiled fires in Utah 2018

- 490 000acres burned
- $110 million of fire fighting costs
- Bad air quality

Background

Background

A combination of reasons

- Drought
- Large areas of dead trees
- Human activates

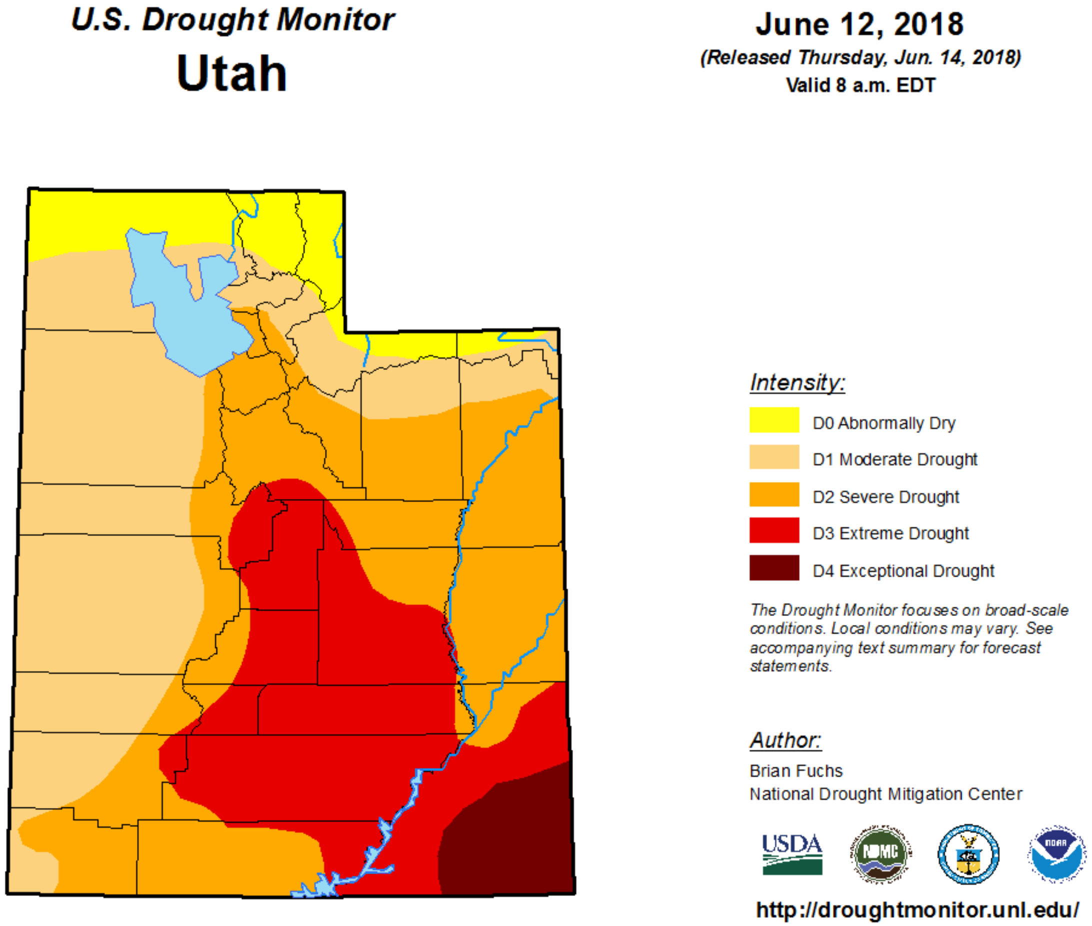

Aim

Over all

- Collect dead wood for co-combustion with coal in power plants.

Specific in this work

- How is the combustion chemistry effected by replacing 15% of coal with pre treated woody biomass?
  - Focusing on the nitrogen chemistry
- What is the reason for any eventual difference?

Experiments

Fuel or Case	Mixture	C	H	N	S	O	Ash	H_2O
Sufco	-	61.48	4.47	0.91	0.58	12.21	13.20	4.15
Torrefied	-	54.98	5.16	0.59	0.00	29.60	7.44	2.24
Steam exploded	-	59.59	5.50	0.59	0.00	28.04	3.52	2.76
Coal	Sufco	61.48	4.47	0.91	0.58	12.21	13.20	4.15
Coal-T	Sufco/Torrefied – 85/15	60.51	5.01	0.86	0.49	18.25	14.88	3.86
Coal-SX	Sufco/Steam exploded - 85/15	61.20	5.07	0.86	0.49	18.09	14.29	3.94

- Utah Sufco coal
- Torrefaction at 325° C
- Steam explosion at 20 bar
- 1 MW
- 3 vol% dry of O_2 in flue gas

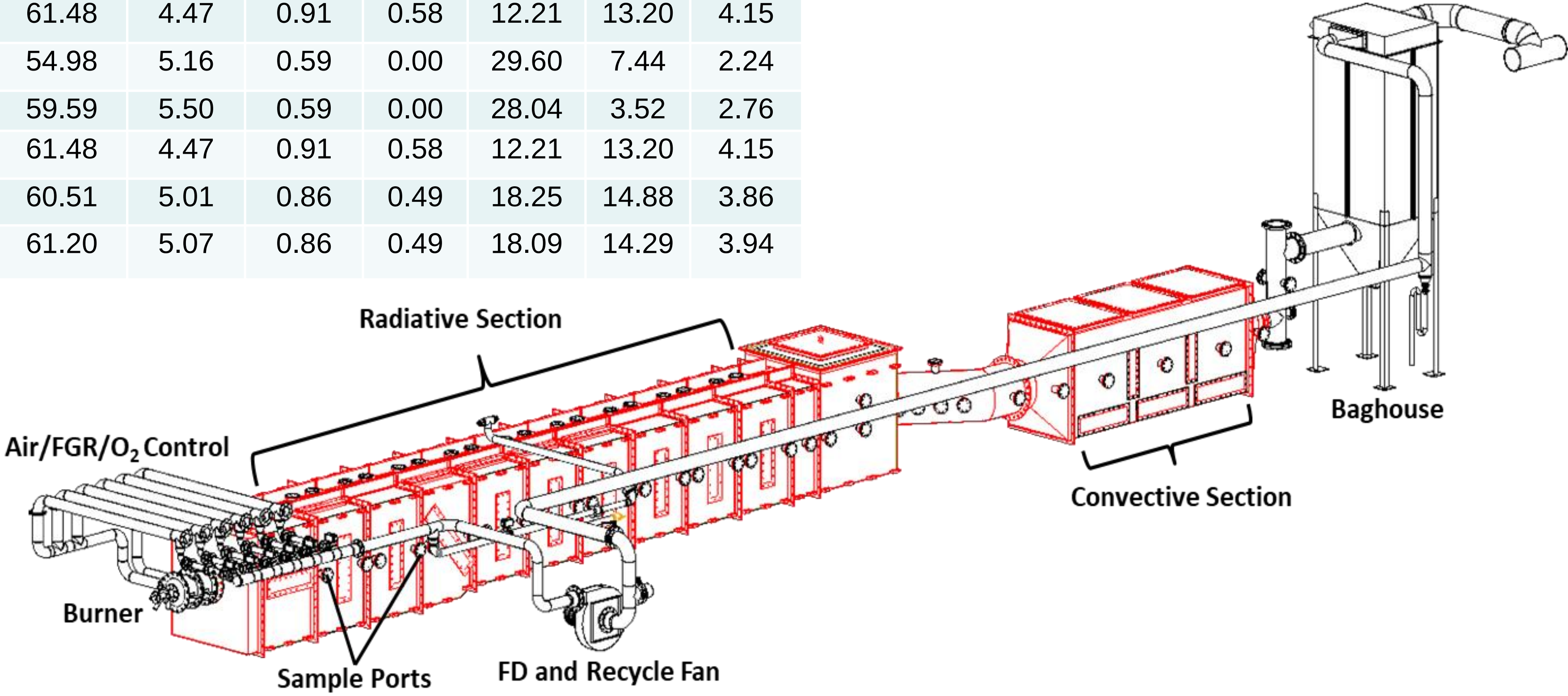

Experiments

- Gas compositions
  - Paramagnetic (O_2)
  - FTIR (e.g NO, NO_2, N_2O, HCN, NH_3, CO, CO_2, H_2O)
- Temperature
  - Suction pyrometer

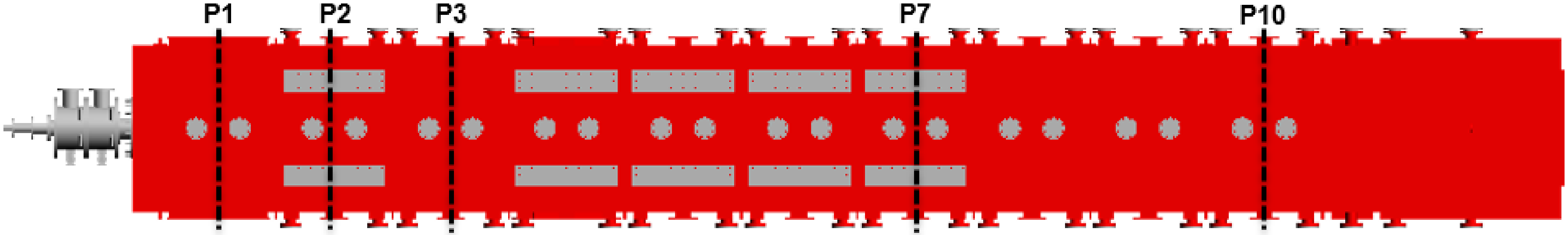

Results

- Similar temperature profiles for all cases
- Clear differences in flue gas NO concentration
  - Why?

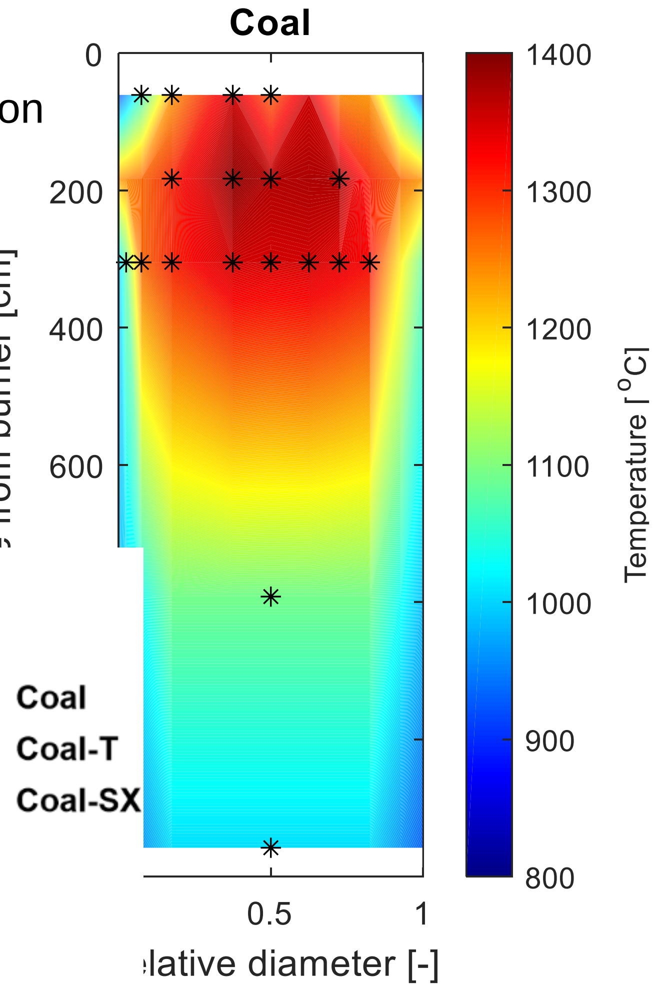

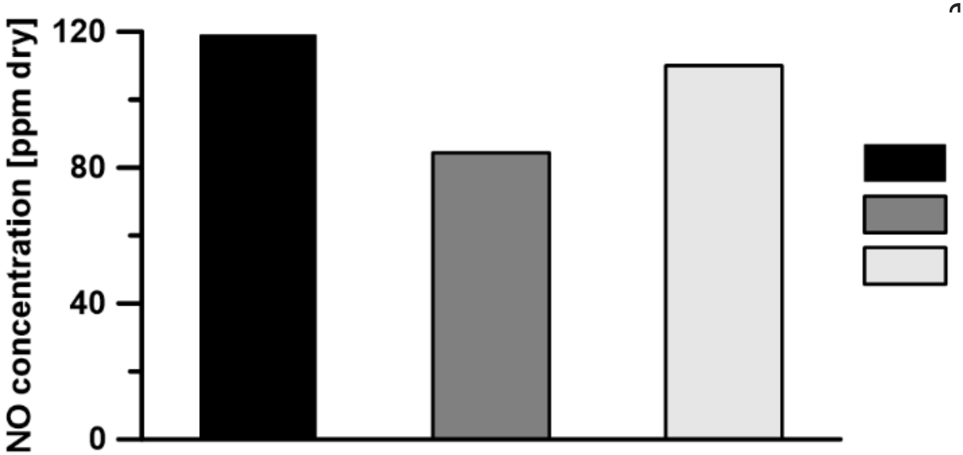

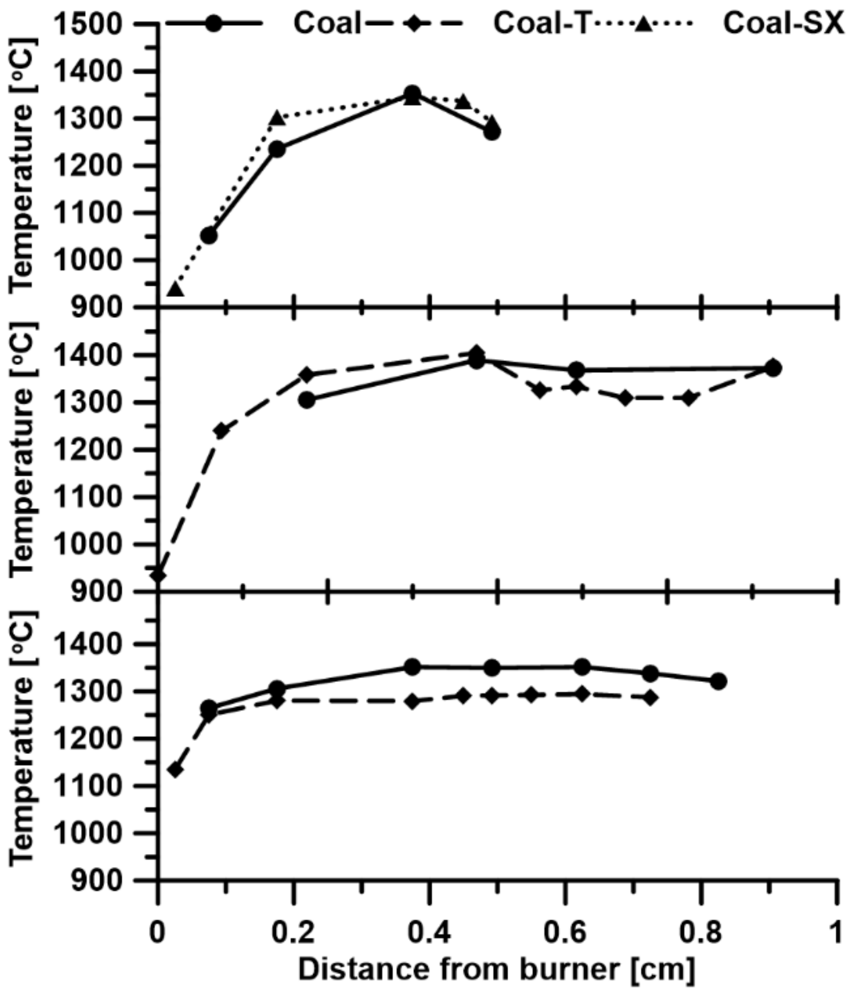

Results

- O2 and CO concentration profiles in port 1, 2, 3 and 7.
- Coal-SX slightly different in port 2 and for CO also in port 3.
- Similar trend seen for CH_4 and other small HC-species.

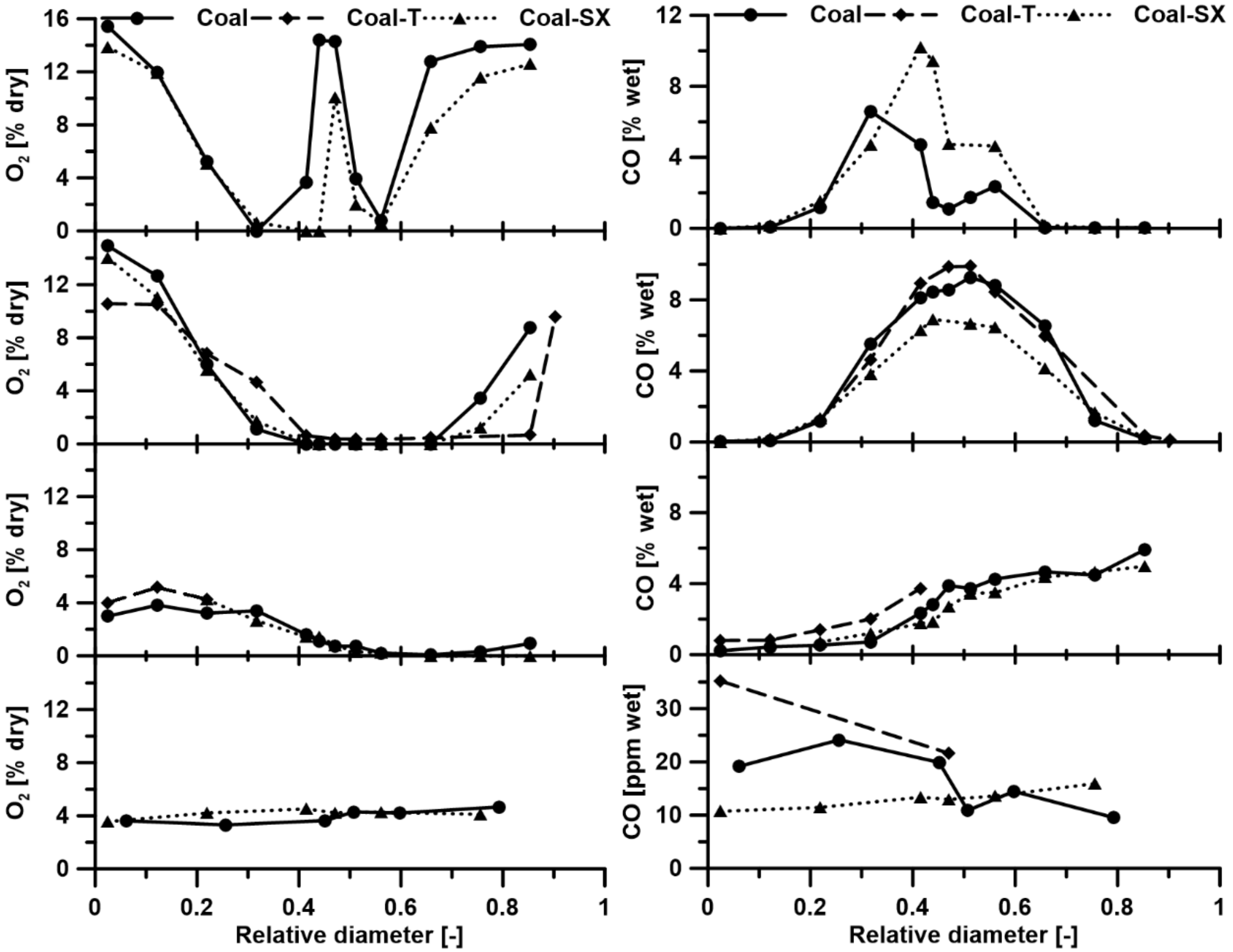

Simulations

- Software – Chemkin
- Model – Plug Flow Reactor
  - Fixed temperature profile
  - Oxidizer and fuel injection profiles
- Combined reaction mechanisms
  - CO/H, N subsets + C1-C3 oxidation subsets

	Coal$_M$	Coal-T$_M$	Coal-SX$_M$
HCN	0,0121	0,0117	0,0115
H_2S	0,0034	0,0029	0,0029
CH_4	0,2018	0,2110	0,2109
CO	0,7398	0,7337	0,7336
H_2O	0,0429	0,0407	0,0411

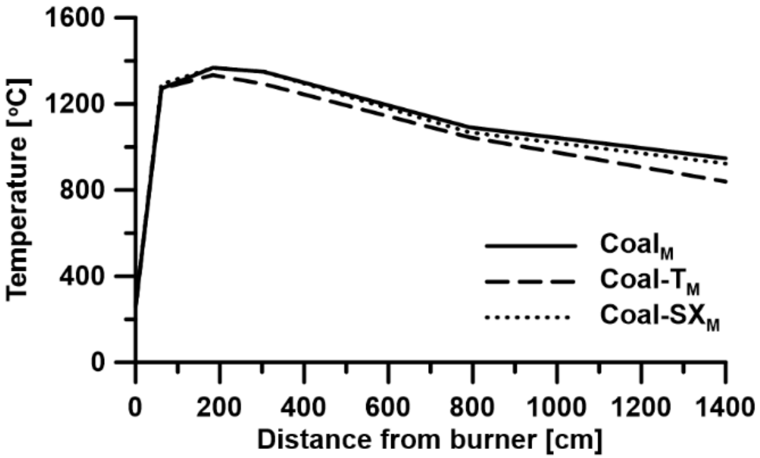

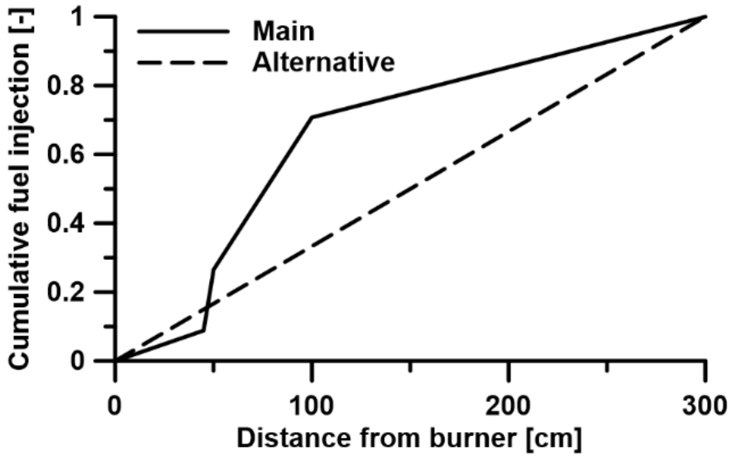

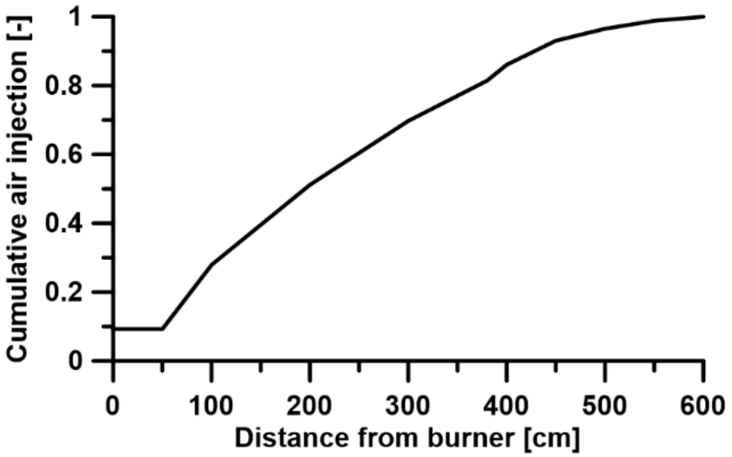

Simulations

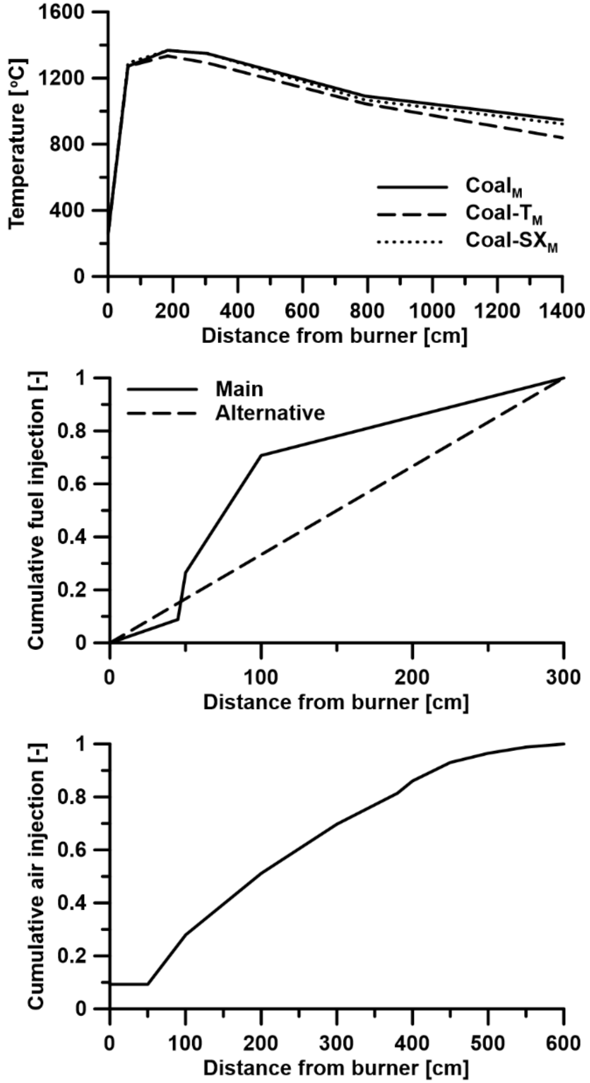

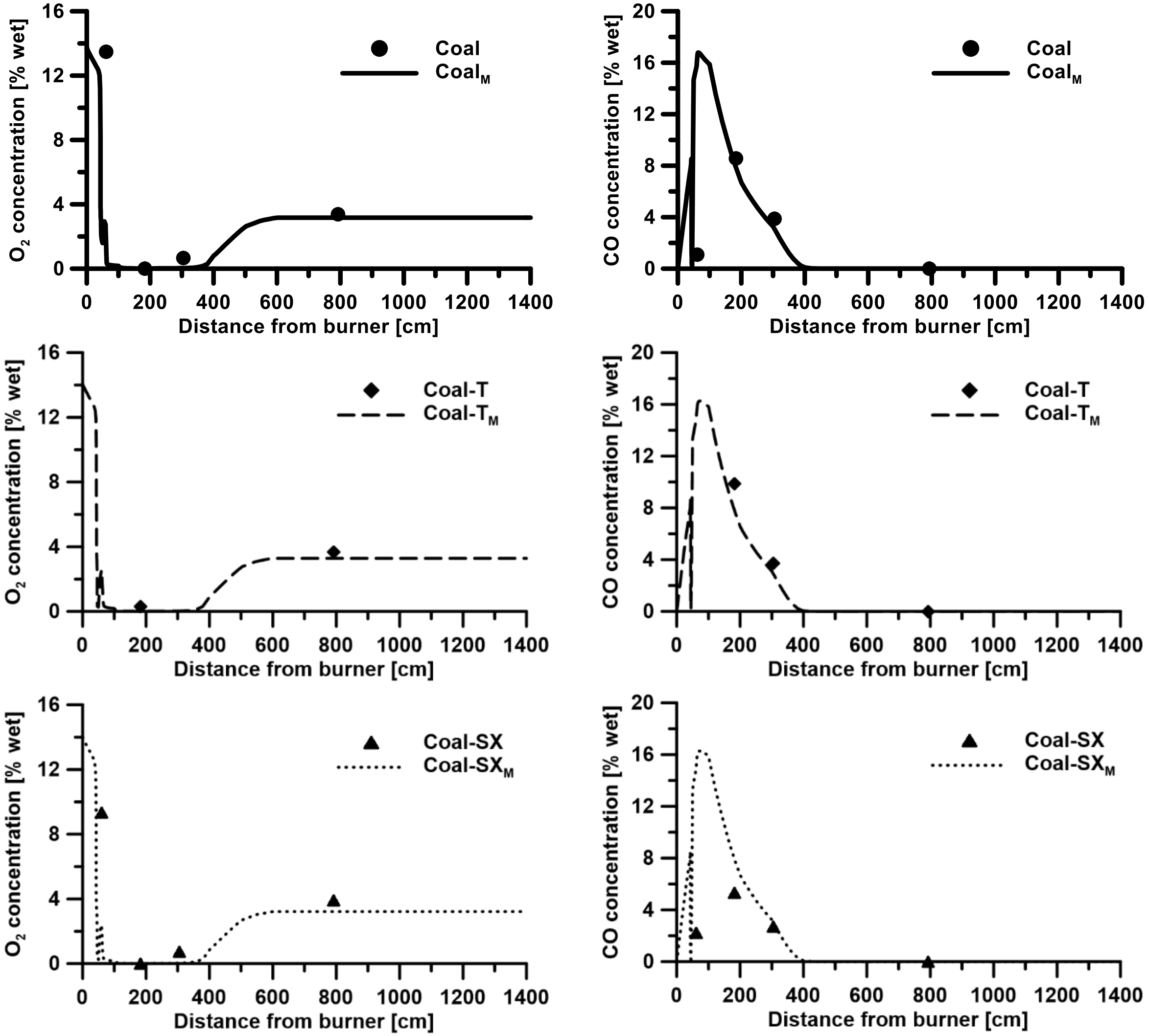

Results

- Normalized concentration with respect to outlet NO in the Coal case.
- Good agreement also with respect to NO concentration
- The lower NO in Coal-T case is better captured than in Coal-SX

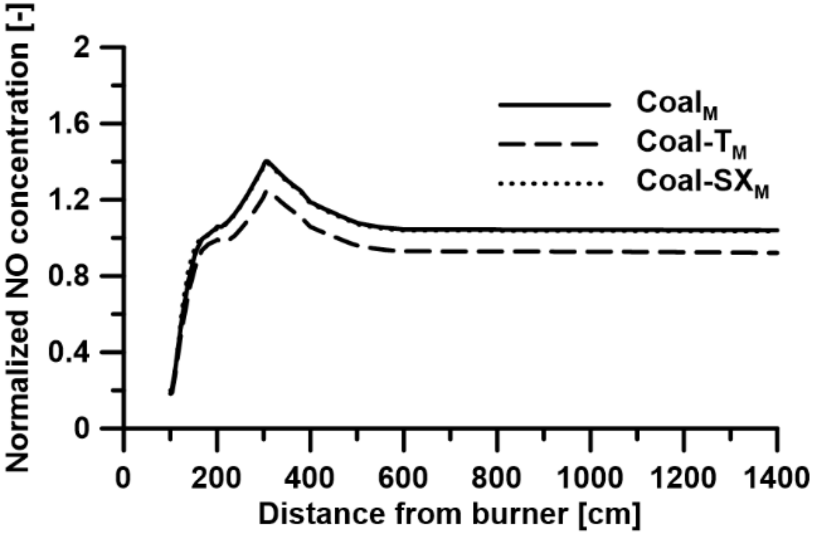

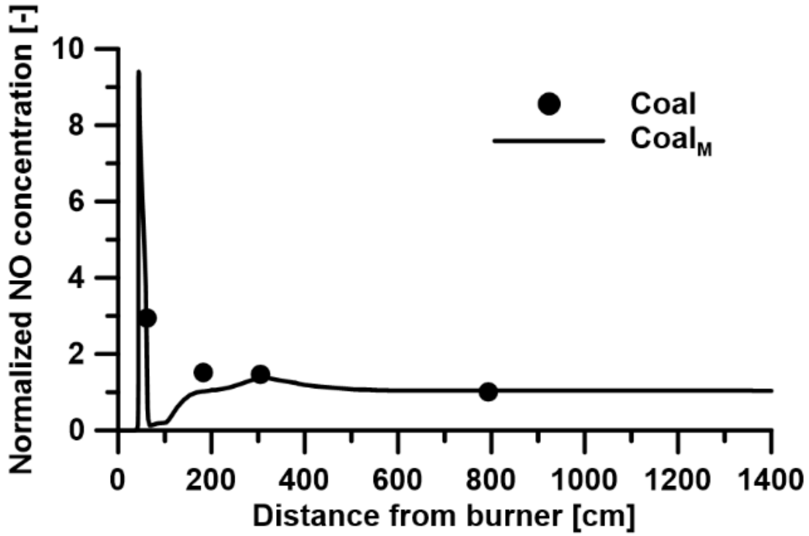

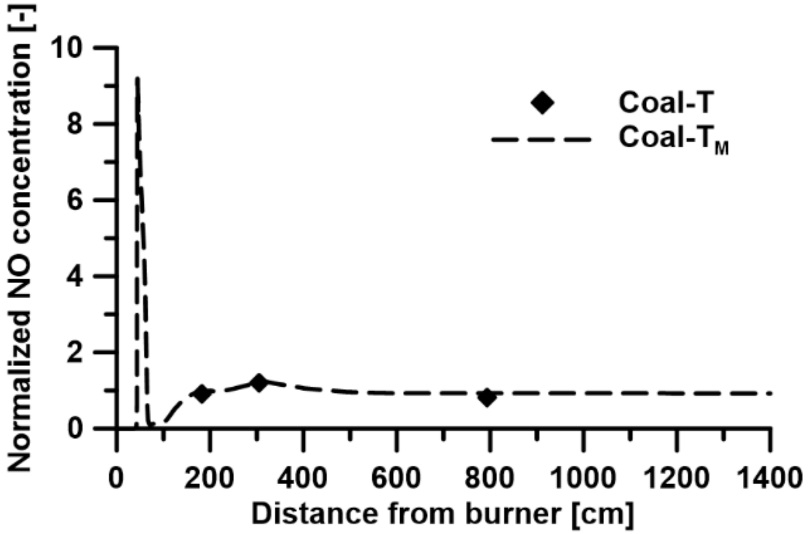

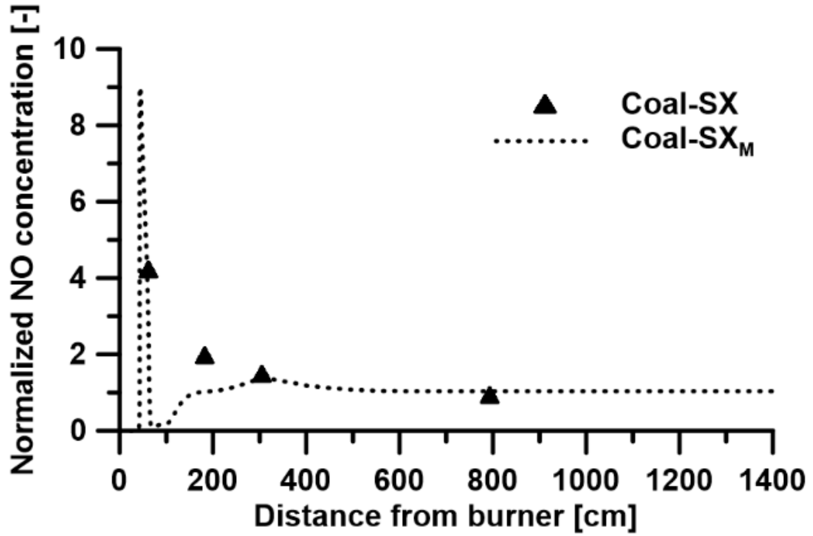

Results

- Suggested difference in volatile matter including N-vol.
- Same N-content in booth biomasses.
- No lager difference in NH_3 and HCN according to simulations.

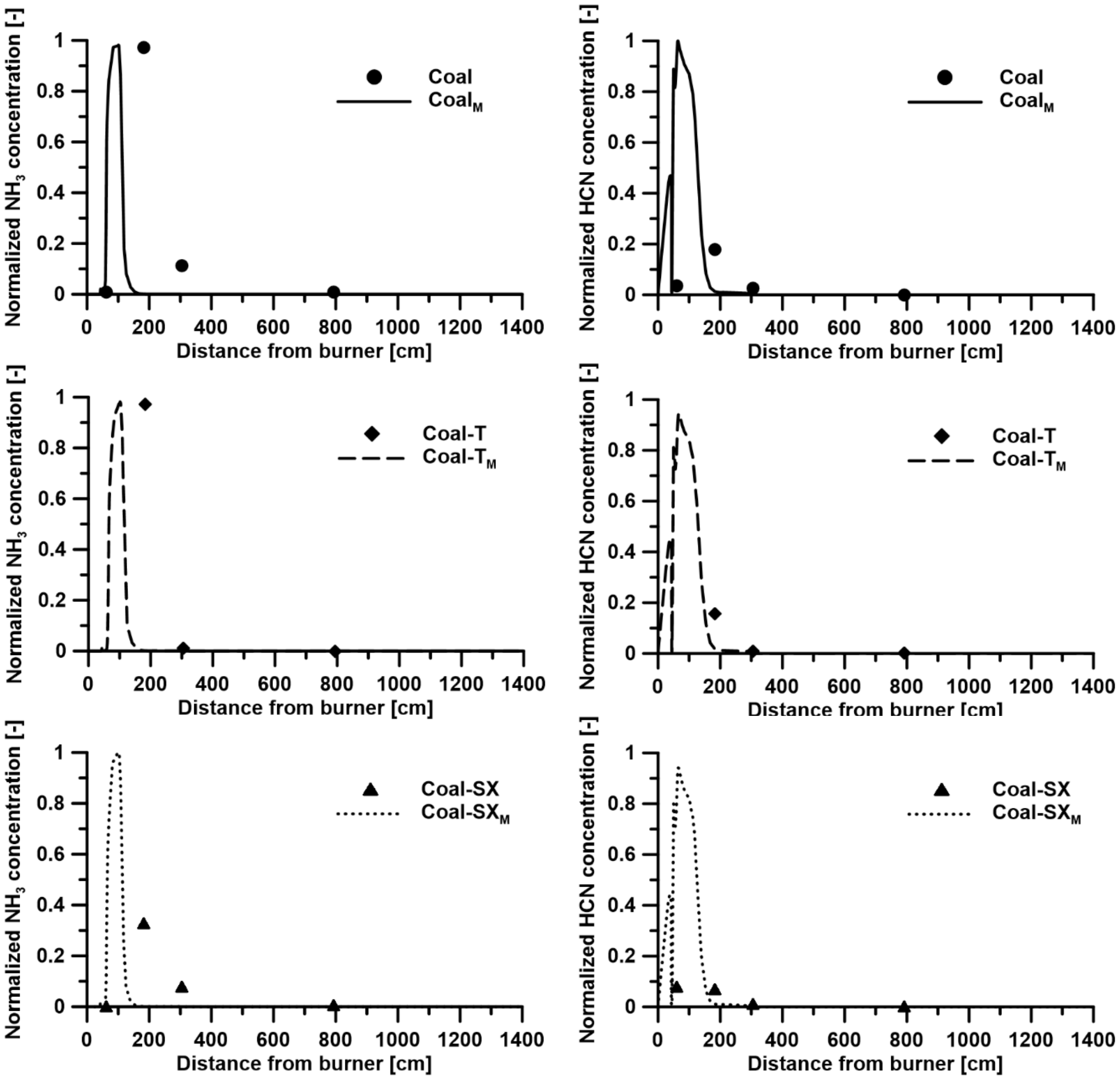

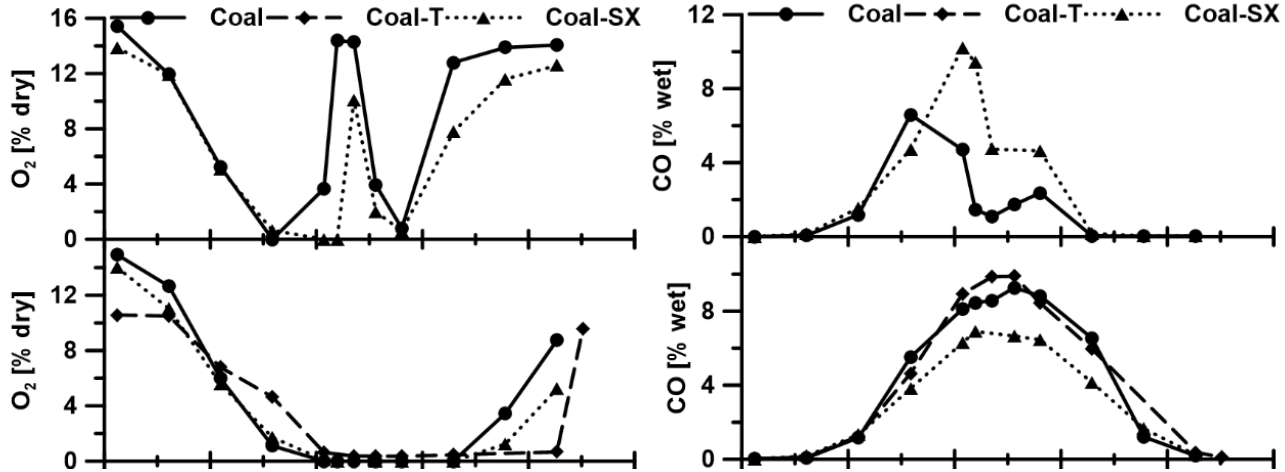

Results

- Injection of N-species separated from main fuel.
- Only minor difference between 100% HCN and 100% NH_3.
- The release of N-vol in relation to overall combustion is important for the formation of NO.

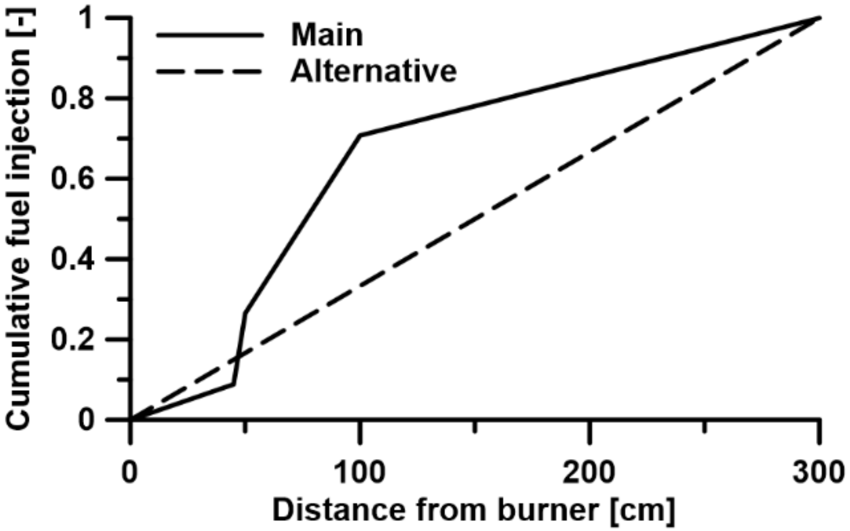

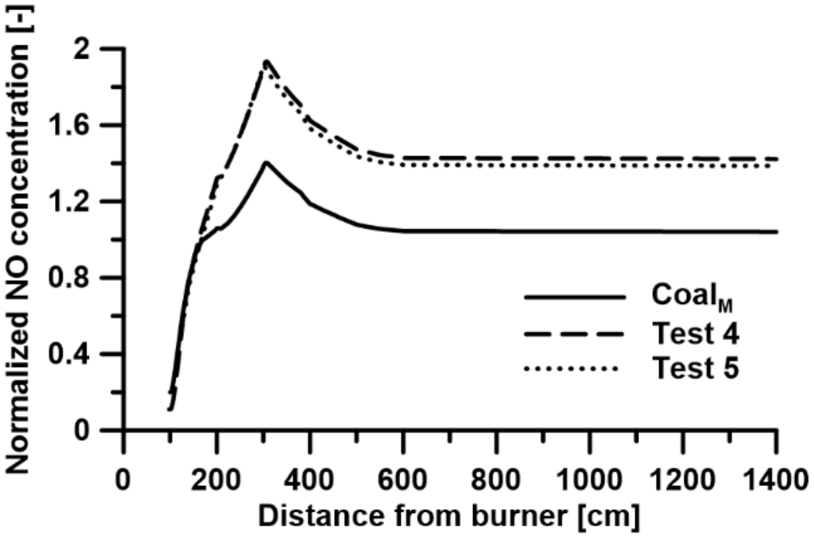

Conclusions

- Lower NO concentration during co-combustion.
- Good agreement between experiments and simulations.
- When and at what conditions the volatile nitrogen species are released plays a key role in the formation of NO.

NO formation during co-combustion of coal with two thermally treated biomasses

Thomas Allgurén

thomas.allguren@chalmers.se

Co-authors:

Rikard Edland[1], Klas Andersson[1], Andrew Fry[2], Eric G. Eddings[3], Fredrik Normann[1]

[1] Department of Space Earth & Environment, division of Energy Technology, Chalmers University of Technology, Göteborg, Sweden
[2] Department of Chemical Engineering, Brigham Young University, Provo, Utah
[3] Department of Chemical Engineering, University of Utah, Salt Lake City, Utah

BYU
BRIGHAM YOUNG
UNIVERSITY

CHALMERS
UNIVERSITY OF TECHNOLOGY

THE
UNIVERSITY
OF UTAH

energy&fuels

pubs.acs.org/EF Article

Ash Aerosol and Deposit Formation from Combustion of Coal and Its Blend with Woody Biomass at Two Combustion Scales: Part 2—Tests on a 471 MWe Full-Scale Boiler

Xiaolong Li,* Seyedhassan Fakourian, Boden Moyer, Jost O. L. Wendt, and Andrew Fry*

Cite This: *Energy Fuels* 2022, 36, 565−574 Read Online

ACCESS | Metrics & More | Article Recommendations

ABSTRACT: Dead trees killed by bark beetles are abundantly available in western US forests. To reduce wildfire risks, it is proposed to collect and use this low-value biomass as a supplementary fuel in existing coal-fired power plants. Burning biomass-based fuel is considered to be carbon neutral and results in a lowering of net carbon dioxide emissions when it replaces fuels such as coal in the generation of electricity. However, potential impacts to boiler performance when co-firing wood with coal may be caused by changes in ash deposition on heat transfer surfaces. This paper presents results from the second phase of a two-phase project in which the effects of combustion scale on ash deposition from combustion of identical coals and coal/biomass blends were investigated in a 1.5 $\mathrm{MW_{th}}$ pilot-scale furnace (part 1) and a 471 $\mathrm{MW_e}$ operating full-scale boiler (this work). Results presented in this paper, however, can stand by themselves, with a focus on practical effects of biomass addition to coal fired in a full scale unit. The coal/biomass co-fired blend consisted of 15% of torrefied wood made from local dead spruce and 85% of pulverized bituminous coal. Of interest are the effects of addition of woody biomass feedstock to pulverized coal on the ash aerosol and ash deposition. Fly ash and ash deposits were alternatively sampled by an iso-kinetic sampling probe and a surface temperature-controlled deposition probe, respectively, which were inserted to the same boiler penetration in the vertical reheat tube bundles. Measurements include real-time particle size distributions and ash deposition rates during both coal combustion and co-firing cases. The size-segregated (0.0324−15.7 μm) particles and time-differentiated deposits were analyzed in terms of composition and microscopic morphology. Results show no significant changes in ash transformation when switching from coal combustion to co-firing with torrefied wood. The results of this full-scale demonstration are further compared with those obtained in the pilot-scale furnace (part 1) to investigate the scale effect on ash aerosol formation and deposition in coal and co-firing biomass combustion.

1. INTRODUCTION

The Intergovernmental Panel on Climate Change has concluded that the utilization of fossil fuels is a primary contributor to climate change.[1] Biomass is a relatively plentiful, renewable, and carbon-neutral supplemental fuel. Co-firing of pulverized coal with overstocked dead wood in coal-fired power plants was proposed to reduce CO_2 emissions[2] and to lower the risk of forest wildfires.[3,4] However, this may potentially affect ash formation and deposition in the boiler due to the physical and chemical differences between the coal and biomass properties.[5−7] The ash content of woody biomass is generally lower than that of coal, but biomass contains higher percentages of alkali and alkaline earth elements on ash basis.[8,9] Potassium and sodium are the most common alkali metals in biomass and coal, respectively, and these play important roles in ash deposition because of their devolatilization.[10,11] The volatile alkalis tend to react with released chlorine to form aerosols and deposits, which impede heat transfer and can also cause high-temperature corrosion (HTC) on metal surfaces.[12−14] The severity of this process varies among solid fuels for different mineral compositions and alkali−Cl−S chemistry in combustion. In this work, the raw woody biomass collected from Utah forest was pre-treated by torrefaction, a process to improve energy density, grindability, and hydrophobic behavior of the raw wood,[15] pelletized, and then co-fired with pulverized Utah coal in a local plant. Focus is given on the effects from the wood minerals upon mechanisms of ash formation and fouling deposition.

Ash deposition on the heat exchanger surfaces is one of the most concerning operational problems in power plants. Mineral vapors and ash aerosols can deposit on cooled surfaces through the mechanisms of condensation,[16] thermophoresis,[17] inertial impaction,[18] eddy impaction,[17] and chemical reaction.[19] Deposition related to biomass combustion has been widely studied in recent years. Luan et al.[20] burned straw/sawdust with a bituminous coal and found that the biomass introduction greatly reduces the ash sintering

Received: October 13, 2021
Revised: December 9, 2021
Published: December 22, 2021

temperature, which leads to higher deposition tendency. Wang et al.[21] compared ash deposits generated during combustion of two rice husk resources different in fuel particle size and chemical analysis. These differences are shown to have great influences on rebound probability and composition of the impacting particles, which determine their fouling behavior. Teixeira et al.[22] studied co-firing bituminous coals with herbaceous, fruity, and woody biomass. They found the wood to be the least inclined to cause deposition problems due to the lack of sulfur and chlorine contents and furthermore, the ash sintering in the other biomass combustion can be alleviated through co-firing. Deposition in coal-biomass combustion has also been investigated under oxy-fuel conditions (O_2/CO_2) other than air firing. Some work showed a similar deposition behavior under both oxidation conditions but higher fouling tendency on the blend fuel than on the coal.[23] Others, however, suggest increased deposition propensity in oxy-combustion and lower tendency on the blend fuel.[24] These are all valuable research on ash deposition in biomass combustion conducted on lab- or pilot-scale combustors such as drop tubes or fluidized beds. One novelty of this work lies in demonstrating the effects of biomass co-firing on fly ash properties and deposition on a full-scale utility boiler.

The objective of this work is to improve the understanding of ash aerosol and fouling deposit formation in co-firing torrefied woody biomass with pulverized coal in an existing full-scale coal-fired boiler. The boiler of interest was Rocky Mountain Power's Hunter Unit 3, which is a 471 MW_E wall-fired unit, which fires Utah bituminous coal. To meet this objective, an ash deposition probe, which was first successfully tested in part 1 of this study on the 1.5 MW_{th} horizontal combustion furnace, described in a parallel work part 1, was modified to perform in the full-scale boiler. A baseline coal combustion test was also conducted for comparison to the co-firing case, and as noted before, the coal and coal/biomass blend were identical to those burned previously in the 1.5 MW_{th} pilot-scale furnace.

This work is a part of a joint project which includes the following measurements and tasks:

1. deposit and entrained ash aerosol sampling (Brigham Young University and the University of Utah);
2. radiation intensity measurements (University of Utah and Chalmers University);
3. FTIR gas analysis (Chalmers University); and
4. continuous gas analysis (PacifiCorp and Brigham Young University).

Only item 1 above is dealt with in this paper. Subsequent publications will describe results from items 2 to 4, which are mentioned here only for the sake of completeness.

2. MATERIALS AND METHODS

2.1. Overview of the Hunter-3 Boiler. A schematic view of the full-scale boiler, Hunter Unit 3, with the dimensions is shown in Figure 1. There are 20 burners in four rows and five over-fire-air (OFA) ports in one row on each of the front and back walls arranged in an opposed-wall or boxer firing pattern. Fouling, which is the ash deposit in the convection zone, is mostly formed near the secondary super heater and makes significant problems for the boiler performance. The entrained ash and deposit were sampled at the same location of the vertical reheat tube bundles, labeled as location 1 in Figure 1. Then, 90% full capacity load was targeted for operation during this project.

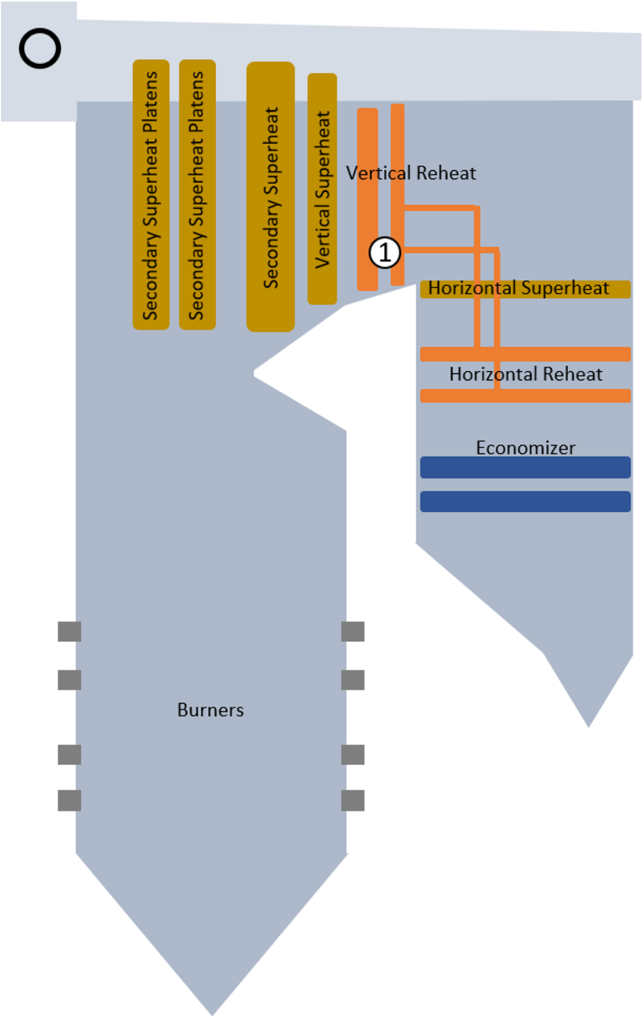

Figure 1. Layout of the Hunter Unit-3 boiler; location 1 is the sampling port for ash deposit and aerosol sample collection.

2.2. Fly Ash Particle and Deposit Sampling. Ash deposit formation on heat exchanger surfaces of a boiler leads to deficient heat transfer and increased maintenance costs. Therefore, determination of mineral matter transformations of fly ash aerosol and ash deposit is essential in this project. To fulfill this objective, probes have been developed to extract samples of entrained ash and to measure the deposition rate on a temperature-controlled surface at the penetration location in the middle of vertical reheater tubes, as shown in Figure 1.

As shown in Figure 2, the ash aerosol probe is the same one that was used in the 1.5 MW_{th} furnace test, which is described in the part 1 paper of this series in this journal. The probe is water-cooled and adopts a two-stage dilution method. The first stage dilution, using nitrogen, occurs at the gas-entering tip on the probe, with the sample velocity matching the flue gas flow in the duct ensuring iso-kinetic sampling. The second dilution is realized post-probe with clean compressed air to reduce the concentration of the aerosol sample to a proper level for instrument measurements. TSI particle sizers employing electrical mobility (SMPS) and laser scattering (APS) were used to obtain the real-time particle size distributions (PSDs) within 0.0324−20 μm. The size-segregated ash samples were collected by a 10-stage gravimetric impactor (BLPI). Prior to the impactor, a cyclone cup was used to separate and sample the bulk fly ash, with a particle diameter larger than 15.7 μm.

The ash deposition probe is also detailed in the parallel part 1 paper of this journal. After a specific holding time, the probe was taken out of the furnace and fouling ash deposits were carefully collected from the coupon surfaces, which faced the flue gas flow. The

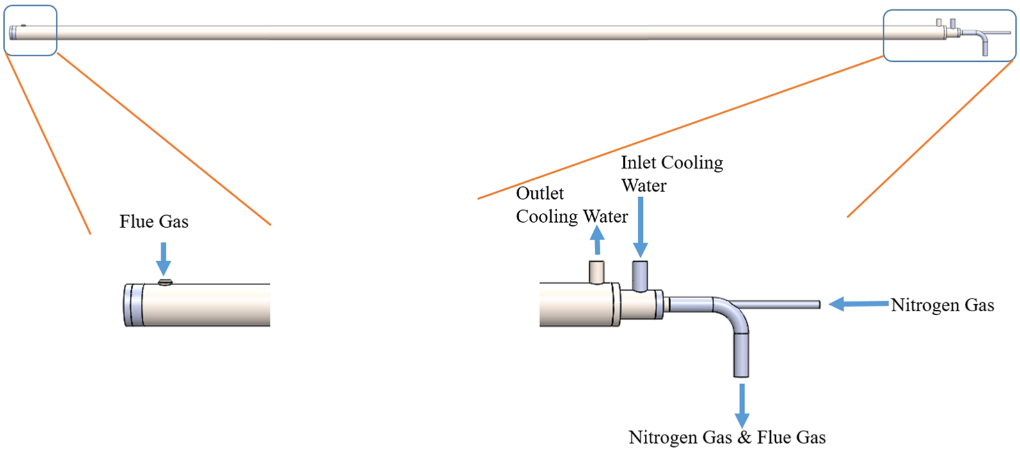

Figure 2. Configuration of the ash aerosol sampling probe.

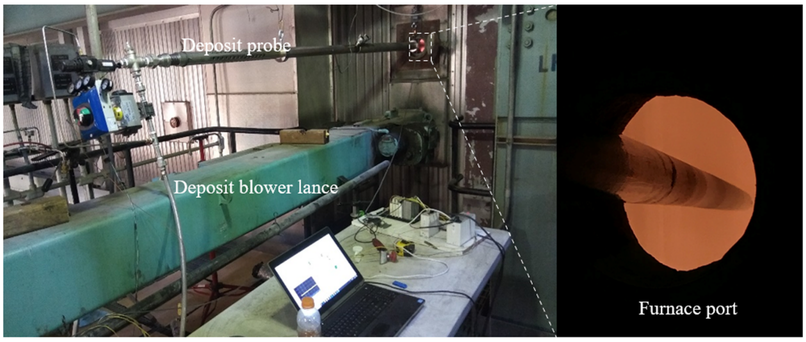

Figure 3. Ash deposit sampling probe installed on the furnace at location 1.

Table 1. Ultimate and Proximate Analysis of Fuels, % Mass as Received

fuel	ash	C	H	N	S	O	H_2O	Vol.	FC	HHV (kJ/kg)
Torrefied #1	11.5	60.1	4.4	1.1	0.4	12.9	9.7	38.9	40	24,614
Torrefied #2	10.5	60.1	4.5	1	0.4	12.3	11.4	39.4	38.7	24,300
Coal	11.5	63.8	4.5	1.3	0.6	9.5	8.8	36	43.7	26,409

Table 2. Mineral Matter Compositions of Torrefied and Coal, % Mass

fuel	SiO_2	Al_2O_3	TiO_2	CaO	Fe_2O_3	K_2O	MgO	Na_2O	SO_3	P_2O_5	BaO	MnO_2	SrO
Torrefied #1	56.6	14.1	0.7	10.5	4	1.3	4.9	2.2	6.7	0.3	0.2	0.04	0.1
Torrefied #2	56.7	14.1	0.7	10.1	3.8	1.4	4.2	2.4	6.2	0.4	0.2	0.04	0.1
Coal	56	14.9	0.7	8.5	4.3	1.1	3.8	2.2	8.8	0.4	0.1	0.04	0.1

surface temperature was controlled at 811 K using compressed air with feedback from the imbedded thermocouples.

The ash aerosol and deposit sampling probes were inserted alternately into the flue gas through the same opening port. They were mounted on an I-beam trolley, which facilitated easy insertion and removal from the boiler without collision to the furnace wall. Figure 3 is a photo taken during the ash deposit sampling.

2.3. Fuel Preparation and Analysis. Raw woody biomass collected near ALTA Ski Resort in the Wasatch−Cache National Forest, which was easily available and similar in composition to biomass of Manti La-Sal National Forest nearer the Hunter Power Station, was harvested by Amaron, a Salt Lake City company who torrefies biomass, to prepare 724 tons of pelletized torrefied wood. In this work, the torrefied biomass was blended with coal (a bituminous coal from a Utah mine) at a weight ratio of 15% biomass and 85% coal.

In this paper, the pure bituminous coal testing will be subsequently referred to as "Coal", and the coal/torrefied wood blend fuel testing will be referred to as "Torrefied", in the same manner as that of the part 1 work. Samples of the as-fired fuels were collected from the Redler conveyor (upstream of the coal silos) during the tests. These samples represent discrete snapshots of the fuel across the entire duration of testing. It took around 8 h for the fuels at the top level of silos to arrive at the mills to be pulverized and fed to the burners. The ultimate and proximate analysis of two Torrefied samples and one Coal sample are presented in Table 1, and their mineral matter compositions are presented in Table 2.

Table 2 shows that the 15/85 wt % wood/coal blend, Torrefied, has a similar mineral composition to that of Coal. Percentages of calcium, magnesium, and potassium of Torrefied are slightly higher than those of Coal. Since the woody biomass contains less ash content than the coal does, the Torrefied co-firing is expected to produce less ash.

2.4. Experimental Conditions. The test plan was developed for Hunter Unit 3 to operate at 90% of the full load. The targeted operating conditions of the Torrefied (co-firing torrefied wood with coal) and Coal (baseline) tests are presented in Table 3.

Table 3. Target Operating Parameters Designed of Hunter Unit 3

Parameter	Units	Value
firing rate	MW_{th}	1194
primary gas/coal ratio	unitless (mass)	1.97
secondary air distribution (inner/outer)	unitless (mass)	30/70
lower furnace stoichiometric ratio	unitless	0.9
excess O_2	vol %, dry	3−4

The Hunter Unit 3 operated for approximately 24 h for each fuel. After the steady state conditions in the furnace have been reached, ash deposit and aerosol sampling were conducted. The soot blowers near the sampling location were turned off during the sampling but on during the intervals. The orders of sampling during Torrefied and Coal tests are presented in Table 4. Some of the operating parameters, including reactant flow rates and measured gas compositions, were averaged during the 90 min deposit sampling of Torrefied and Coal and are summarized in Table 5.

Table 4. Sampling Order during Torrefied and Coal Tests

fuel	sampling order
Torrefied	soot blowers on
	30 min deposit
	60 min deposit
	soot blowers on
	SMPS APS aerosol
	BLPI aerosol
	soot blowers on
	90 min deposit
Coal	soot blowers on
	30 min deposit
	60 min deposit
	soot blowers on
	SMPS APS aerosol
	BLPI aerosol
	soot blowers on
	90 min deposit

Table 5. Averaged Measured Operating Conditions during Each Fuel Test

Parameter	units	Torrefied	Coal
firing rate	MW_{th}	1250	1232
fuel rate	kg/h × 10^3	184	168
primary air rate	kg/h × 10^3	401	395
primary air temp	K	481	451
secondary air rate	kg/h × 10^3	235	235
secondary air temp	K	543	543
secondary air swirl[a]	%	75	75
OFA flow rate	kg/h × 10^3	536	528
OFA temperature	K	543	543
flue gas O_2	vol %, Dry	3.3	3.3

[a] Estimated value.

The measured and calculated operating parameters that are relevant to the ash aerosol and deposit sampling are summarized in Table 6. A suction pyrometer probe was used to measure the flue gas temperature at the sampling location.

3. RESULTS OF THE FULL-SCALE TESTING

3.1. Fly Ash Aerosols.

Figure 4 shows the comparison of PSDs between the Coal and Torrefied tests. The results on the left are particle mass concentrations based on the flue gas standard volume, while those on the right are based on input ash mass, which accounts for the gas volume change between the two tests. Although the particle sizers and the impactor produced inconsistent concentrations for particles smaller than 0.1 μm, no significant variation was found between Coal and Torrefied when using the same analyzing method for the whole size range. Coal combustion produced a slightly higher ash mass concentration in flue gas than blend co-firing does because the input ash is lower in the blend than in the coal. This suggests that co-firing torrefied wood with bituminous coal in the current facility does not affect the general aerosol size distribution and slightly reduces the concentration of fly ash particles (PM_{20}) compared to coal combustion.

Table 6. Operating Parameters Relevant to the Particle Deposition Behavior

parameter	units	Torrefied	Coal
particle density (laboratory analysis)	kg/m^3	232.2	233.9
measured flue gas temperature[a]	K	1355	1307
coupon surface temperature	K	811 ± 10	811 ± 10
calculated flue gas density[25]	kg/m^3	0.263	0.273

[a] The temperature was measured after the 60 min sampling of ash deposits.

For fine particles, PM_1, no apparent mode is measured by the SMPS in either test. The gravimetric measurements from the BLPI impactor, however, show a gentle nucleation mode in both tests, near a particle diameter of 0.1 μm. In general, the mass concentration of the sub-micron particles accumulates as the size increases as a result of coagulation of the condensed ash species. Minerals from the wood usually consist of high contents of elements such as K and Ca. However, such vaporizing species from the torrefied wood do not pose an effect on changing PM_1 formation during co-firing at the current fuel mixing ratio and with this woody fuel source composition. This will be discussed later with the size-segregated compositions of PM_1. The distinct mode found around 4 μm in both tests is formed by the super-micron particles released through char fragmentation and mineral coalescence. The result based on the input ash mass suggests that this mechanism is unchanged when switching from coal combustion to co-firing.

The size-segregated particulate compositions analyzed by energy-dispersive X-ray (EDS) are shown in Figure 5. Overall, all the elements have similar mass distributions for Coal and Torrefied. Torrefied wood contains more magnesium and calcium than the original ash analysis, which is mainly distributed as organically bound ions in the biomass carbon material. These metals are released to form vaporized ash followed by condensation during volatilization and char burnout. This ash formation mechanism of the volatile species produces ultra-fine particles composed of Na and Ca species as well as sub-micron coagulation ash consisting of K, Mg, and S compounds. Chlorine contents in both Coal and Torrefied are relatively low and comparable in amount, with some Cl being enriched in Torrefied as vaporized potassium chlorides roughly at 0.2 μm size. The less volatile species, such as silicon and aluminum, retain higher concentrations in the coarse particles, formed by char fragmentation and mineral coalescence, than in the vaporizing PM_1 fume. In Figure 5, Si and Al are shown to be the major contents of the fly ash, which contribute to the super-micron PSD mode composed of aluminosilicates.

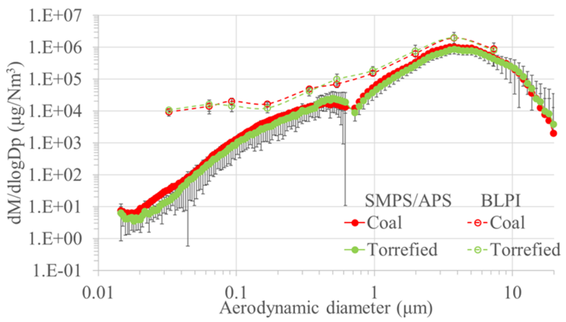

Figure 4. PSDs of ash aerosols in baseline and co-firing cases.

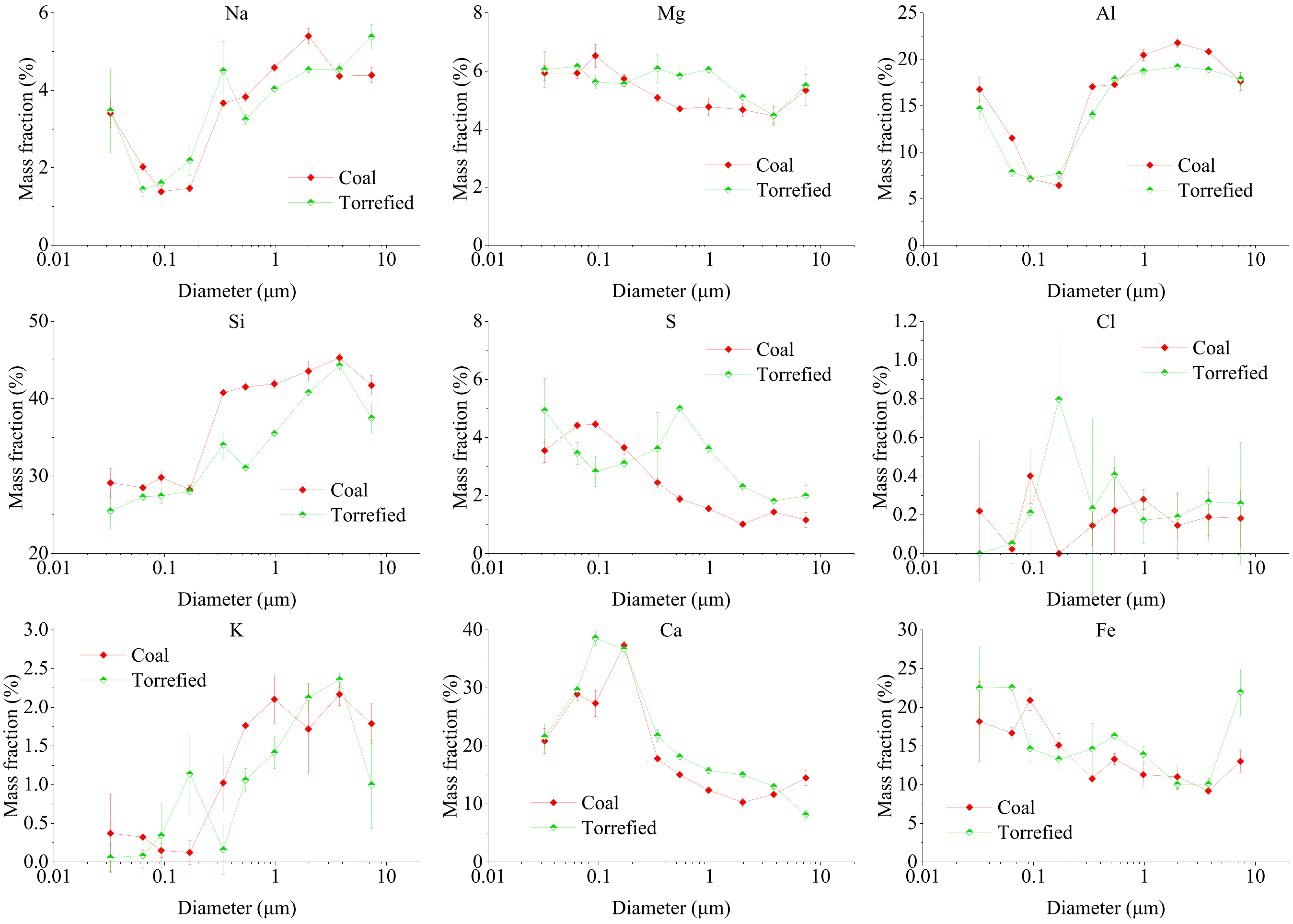

Figure 5. Size-segregated compositions of ash aerosols (PM_{10}) in the two tests collected by BLPI and analyzed by EDS.

Despite the fact that torrefied wood contains much less Si in raw ash than coal does, the Torrefied fuel sample collected during the test shows even slightly higher Si in ash content (Table 2). However, a decrease in silicon partitioning is found in Torrefied PM_{10} as shown in Figure 5. In general, the differences of mineral transformation between the coal combustion and co-firing did not yield significant variations on the size distributions of the fly ash particles discussed above.

A cyclone cup with the cut-off size at 15.7 μm collected the bulk fly ash aerosols prior to the low-pressure impactor. Compositions of the cyclone ash in the two tests are compared in log scale in Figure 6. It shows that the elemental mass fractions of the fly ash particles in Torrefied and Coal are almost identical. The chlorine concentration in the solid phase is not significantly changed between the two tests. Specifically, Torrefied chlorine is slightly higher in the PM_{10} (Figure 5) but slightly lower in the larger particles, $PM_{15.7+}$ (Figure 6), compared to the Coal test. Phosphorus and sulfur concentrations in the bulk ash in Torrefied are higher than in Coal, even though they are low in both tests. This could lead to an increase in the melting point of the deposit ash concerning the chlorine species and a decrease in the probability of impacting particles to stick on the heat exchanger surface and the coupon surface of the deposition probe.

3.2. Ash Fouling Deposition.

Ash deposit samples were collected on the probe coupons, of which the surface temperature was controlled at 811 K by internal cooling air, with holding times of 30, 60, and 90 min in both coal

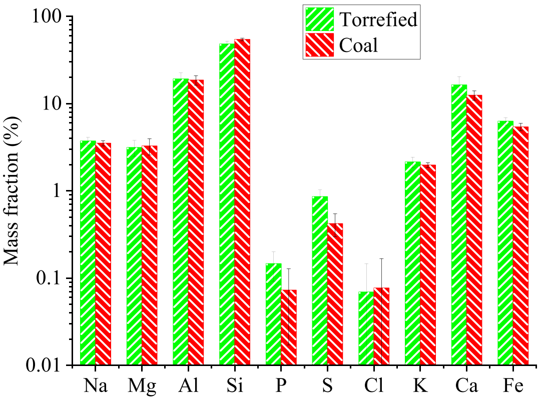

Figure 6. Compositions of ash aerosols (above 15.7 μm) collected in the cyclone and analyzed by EDS.

combustion and co-firing tests. Figure 7 shows the images of the collected ash deposits on the probe as it was removed from the furnace. The end cap, unlike the coupons, was not cooled and therefore is glowing. It was observed that there were two kinds of particles collected on the probe, both fine particle deposition and chunks. The chunk ash on the end cap suggests that it may have originated from the upstream heat exchanger surfaces or furnace walls as shedding deposits or was formed by other deposition mechanism taking place on the high-temperature uncooled surface. It is important to note that there was a significant carryover of this deposit from the probe tip onto the coupon in the Torrefied 60 min sampling. This made the deposit sample consist of a normal powdery part and an additional chunk part.

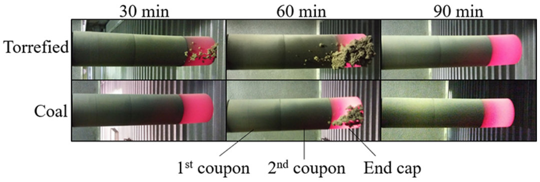

Figure 7. Images of deposits sampled on the probe tip as they were removed from the furnace. The chunk deposits under the 30 and 60 min torrefied conditions and the 60 min coal condition were collected on the upstream side of the probe.

Figure 8 reports the total weights and the averaged growth rates of the ash deposits collected during the specific holding time from the coupon surfaces, which do not include the end cap ash but include the part of the chunk ash that spreads to the coupon, if there was any. The samples were carefully scrapped off and then weighed using a balance of 0.01 g accuracy. Due to the significant ambient air convection outside the furnace and air leakage toward it, air entrained a small portion of the scrapped ash deposit from the coupon surface during scrapping. The error of the collected deposit weights due to this inevitable loss is estimated not to exceed 10% of the total deposit that sticks to the coupon in both tests. The deposition rate was calculated as the total deposit mass on the coupon per the coupon surface area per holding time and, thus, is considered as the overall rate.

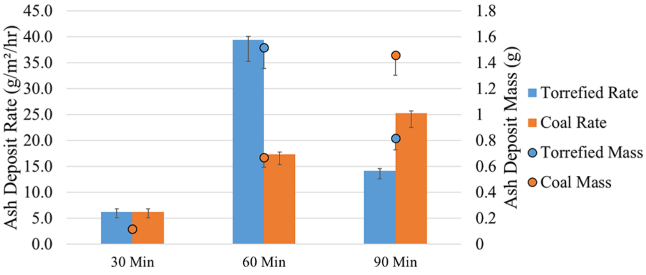

Figure 8. Ash deposition rates and deposit weights for different probe holding times (the g Torrefied 60 min data also includes some of the chunk ash that is not present in the other samples).

The outstanding deposit weight of the Torrefied 60 min is around twice that of the Coal due to the carryover part of the chunk ash on the coupon surface and inclusion in the sample. Shedding from upstream heat exchanger surfaces is one explanation for the formation of the chunk ash; however, there may be other possible mechanism causing the deposition on the high temperature cap. For the 30 min holding time, the ash deposit weights are almost the same during Coal and Torrefied tests, therefore the two overall deposition rates are similar. The observed lower deposition rate for the torrefied conditions compared to the coal condition for the 90 min holding time is likely due to the lower ash content of the blended fuel.

It should be noted in Figure 8 that the ash deposition rates are generally increased as the probe holding time is extended in both Coal and Torrefied tests. This may suggest that the deposition sticking efficiency was increasing over 90 min. However, this needs further validation since the deposition data are limited due to the impractical testing repetition on a combustor at full scale.

Compositions of ash deposit samples are presented in Figure 9. Results of the 30 and 90min conditions only show minor changes from the coal combustion to co-firing with torrefied biomass, although Al and Si are generally lower, while Ca is higher in concentration in the Torrefied test than in the Coal test.

The ash deposit sample of the 60 min holding time is divided into two parts, the normal powder part and the additional chunk part on the coupon surface, which were separated using a screen. Figure 9 shows that these two deposits have a similar mineral composition, both having higher silicon and lower calcium contents than all the other samples, suggesting that the chunk and powder deposits originate from the same source particles.

The deposit morphologies are presented in Figure 10, which shows SEM images of the ash deposit samples from the 30, 60, and 90 min holding times at the same magnification of 150×. It is clear that the powder portion of the 60 min Torrefied deposit contains large ash particles with diameters at approximately hundreds of micrometers. These also comprise the main component of the chunk portion. It is likely that portions of the chunk deposit were included with the powder portion during the screen separation. The 30 min Torrefied deposit also has some large particles even though only a small carryover chunk piece was collected on the coupon (Figure 7). The other deposit samples mainly consist of super-micron spherical particles aggregated with micron-sized fine particles. The fine particles on the surface of the larger particles may represent the condensed alkali vapor species following nucleation.[26]

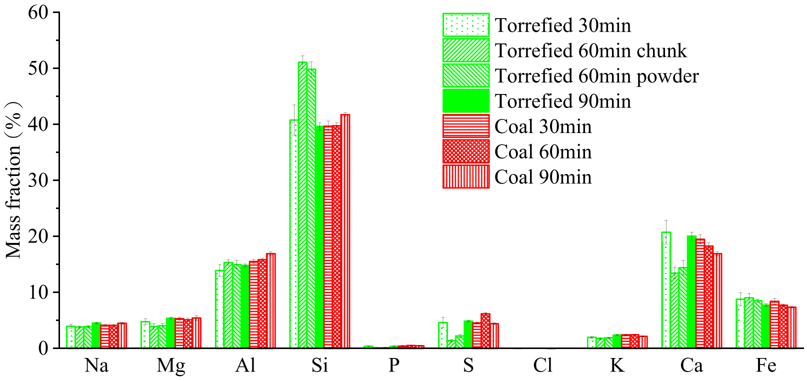

Figure 9. Deposit compositions (determined by EDS) from samples with different holding times (from left to right: Torrefied, 30, 60, and 90 min; Coal, 30, 60, 90 min).

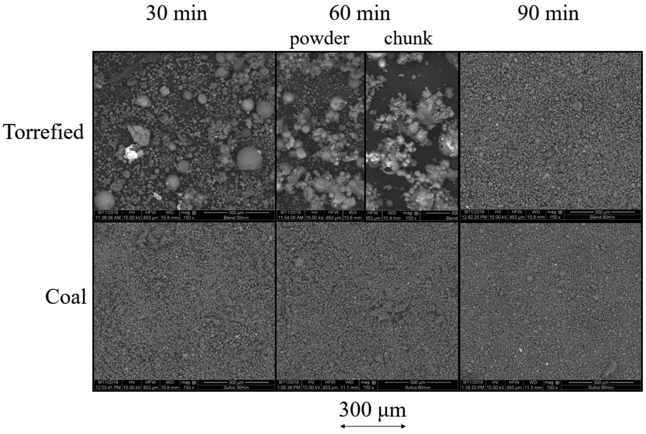

Figure 10. SEM images of 30, 60, and 90 min deposits (top: Torrefied; bottom: Coal).

4. COMPARISON WITH THE 1.5 MW_{TH} PILOT-SCALE FURNACE DATA

4.1. Ash Aerosol Comparison. The same fuels, Coal and Torrefied, were also burned at a similar stoichiometry on a 1.5 MW_{th} pilot-scale horizontal furnace, L1500, the results of which are reported in part 1. Figure 11 shows the PSDs measured in the 471 MW_e Hunter boiler and the 1.5 MW_{th} L1500 (port 7, closer to the burner) for both the Coal and Torrefied tests. The utility boiler yielded monomodal particle size distributions within a 0.01−20 μm diameter range during coal combustion and co-firing with 15% torrefied wood. The fragmentation mode is found at a diameter of ~4 μm. This suggests that the fine fly ash particles have fully coagulated, reacted, and been consumed in the flue gas before reaching the superheaters where samples were collected. The pilot-scale L1500, in addition to the fragmentation modes, also produced distinct ultra-fine modes smaller than 0.1 μm. This is probably due to vaporized metal that has been sampled with the flue gas and its subsequent nucleation at the sampling probe entrance. Comparison with the full-scale data below 0.1 μm suggests that in contrast to this, metal vapors in the full scale are scavenged, prior to sampling, possibly by condensation on abundant cooled surfaces at this scale.

As shown by the PSDs on input ash basis in Figure 11, it is found that the utility boiler yielded less PM_1 by burning the blend Torrefied fuel than the Coal, while the pilot-scale furnace displays the opposite effect. The result at smaller scale does not show any difference on the super-micron fly ash between the Torrefied and Coal tests. The super-micron PSDs, PM_{1-20}, in the utility boiler measured for both tests have higher mass concentrations than those in the pilot-scale furnace. The lower particle concentrations in the pilot scale are likely due to lower average gas velocities in the pilot scale and its horizontal orientation resulting in particle deposition on the furnace floor prior to the sample location.

In both the pilot-scale furnace and the utility boiler, co-firing torrefied wood produces higher calcium and sulfur concentrations but lower aluminum and silicon concentrations in ash aerosols than coal combustion. However, co-firing in the utility boiler does not increase the alkali contents in the ash aerosols as it does in the pilot-scale furnace. Although the enrichment of calcium in the ultra-fine particles during co-firing is found in both combustors, sodium, potassium, and sulfur are all partitioned into the coarser size range within PM_{10} formed in the utility boiler. This is a result of the reaction, coagulation, and heterogeneous condensation at longer residence times. The co-firing PM_{10} in the pilot-scale furnace, however, shows increased Na, K, and S contents in all sizes compared to coal combustion.

4.2. Ash Deposition Rates at Two Scales. In both the 471 MWe Hunter Unit 3 and 1.5 MW_{th} L1500, the ash deposition rates are increased when the probe holding time is extended from 30 to 90 min for both the Coal and Torrefied tests. The deposition rates in the Hunter boiler only accounts for 10% of those in the pilot-scale L1500 during the first 30 min and 20% for 90 min, respectively. Such a difference can be clearly observed by the deposits accumulated on the probe surface after 90 min as shown in Figure 12.

The utility boiler produces ash aerosols with comparable mass concentrations to those in the pilot-scale furnace. However, the local ash deposition rates in the utility boiler are much lower. Figure 13 shows the micrographs of ash deposits collected from the deposition probe surface in the two combustors with the same magnification ratio. Burning Coal and Torrefied fuels in the utility boiler yielded much smaller spherical ash particles compared to the tests in the pilot-scale furnace. This suggests that the chars in the utility boiler experienced more intense fragmentation during oxidation and the resulting mineral coalescence was suppressed, leading to the overall smaller ash particle size. This accounts for the higher fragmentation mode found in the PSDs of the utility boiler fly ash PM_{20} (Figure 11). Another fact that should not be ignored is that the gas flow near the sampling location in the utility boiler is turbulent and complicated, which could cause

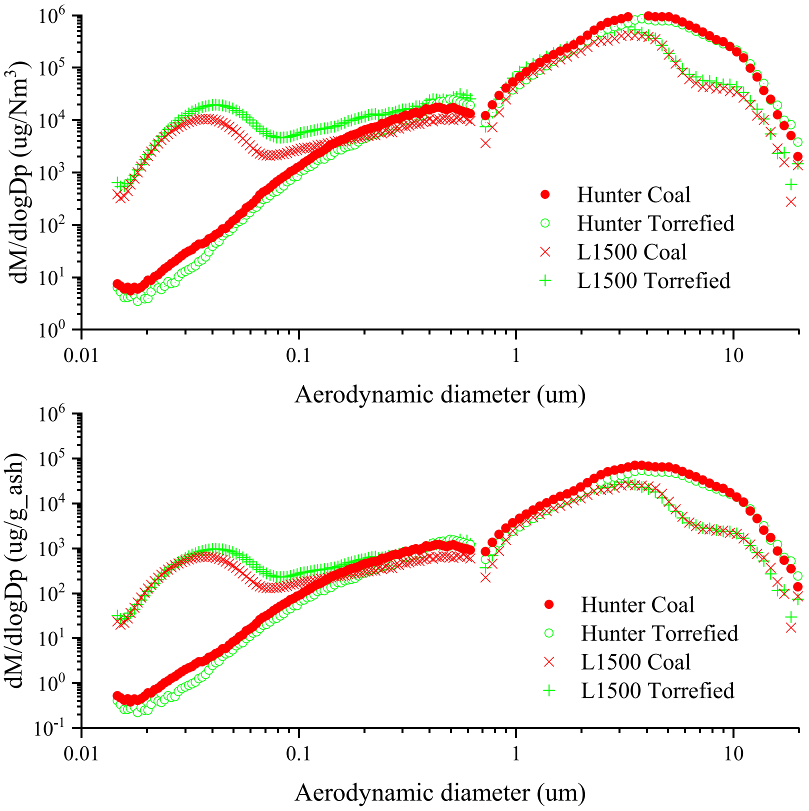

Figure 11. Comparison of the entrained ash PSD between the 1200 MW_{th} utility boiler and the pilot-scale 1.5 MW_{th} combustor.

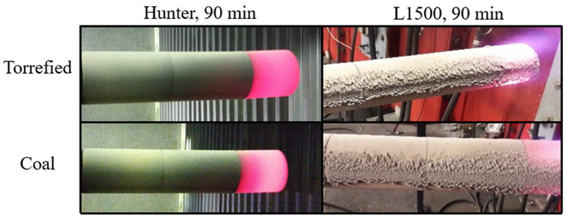

Figure 12. Deposit build-up on the probe surface after 90 min in Hunter and L1500.

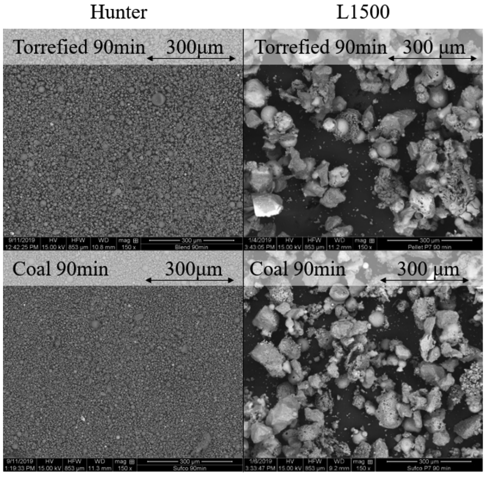

Figure 13. SEM images of the deposits sampled after 90 min in Hunter and L1500 combustors.

more arbitrary particle impactions and entrained gas around the deposit surface. The higher possibilities of particle bounce-off and deposit shedding thus reduced the deposition rate in the utility boiler compared to the pilot-scale furnace.

Figure 14 compares the ash deposit compositions between Hunter and L1500. The utility boiler deposits contain more Na, Mg, Al, S, and Ca but much less Si than the pilot-scale furnace deposits. Some of this variation could be due to differences in parent coal composition between the full-scale tests and the pilot-scale tests reported in part 1.

Regarding the fuel effect on ash deposition, co-firing in the utility boiler reduces the ash deposition rate compared to coal combustion. However, this was not true in the pilot-scale furnace at least for the sampling location closer to the burner. No significant difference was found in deposit compositions between Coal and Torrefied in the utility boiler, but higher alkali contents appear in the Torrefied deposits from the pilot-scale furnace. This is consistent with the increased Na, K, and S in the Torrefied PM_1 in L1500. The alkali enrichment in fly ash during co-firing in L1500 will contribute to the increased ash deposition rate compared to coal combustion.

5. CONCLUSIONS

Ash aerosols and deposits were sampled in a 471 MW_E utility boiler, Hunter Unit 3, during pulverized bituminous coal combustion and co-firing with torrefied wood (85/15 wt % coal/biomass). Results from the two tests with different fuels are compared. The ash aerosols were characterized in both particle size distributions and size-segregated compositions. Furthermore, the deposition data not only includes information on deposit composition but also the gravimetrically measured ash deposition rates, which are rarely found for utility boilers. In general, no significant change is found in the fly ash aerosol size and composition as well as the ash deposit

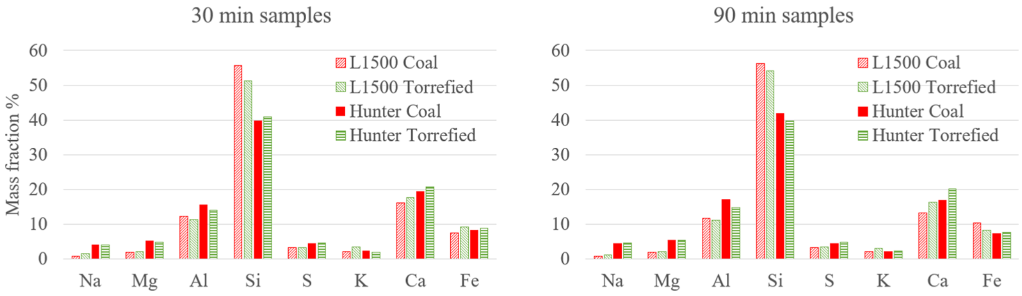

Figure 14. Comparison of ash deposit compositions collected in the utility boiler (Hunter) and the pilot-scale furnace (L1500).

composition when switching from coal combustion to co-firing biomass. The same fuels, Coal and Torrefied, were also burned in a 1.5 MW_{th} pilot-scale horizontal furnace, L1500. The ash aerosol and deposit results in coal combustion and co-firing are compared between the utility boiler and the pilot-scale furnace. The major conclusions include the following:

1) The fly ash particle size distributions remain largely unchanged from coal combustion to co-firing with torrefied wood, with the latter one slightly decreasing the aerosol mass concentrations. The monomodal PSDs indicate full particulate growth in the utility boiler.
2) Insignificant differences are shown by compositions of the impactor and bulk ash aerosols between Coal and Torrefied tests. Sulfur in Torrefied flue gas is scrubbed by fly ash particles to a larger extent compared to the Coal test, but the alkali concentrations of ash aerosols are the same during both tests in the utility boiler.
3) The overall ash deposition rates are increased as the probe holding time is extended from 30 to 90 min. The deposition rate in Torrefied is the same as in Coal for 30 min but is reduced to almost the half of that in Coal for 90 min. Decreased aluminum and silicon compounds and increased calcium species within the deposits alleviate fouling deposition during co-firing in the utility boiler.
4) Compared to the pilot-scale furnace, combustion in the utility boiler did not yield the ultra-fine modes in ash aerosol PSDs, suggesting more complete fly ash developments prior to the sampling in the full-scale combustor. The utility boiler also produced higher mass concentrations of the fragmentation particles in PM_{20} than the pilot-scale furnace.
5) The two combustors both produced more Ca and S and less Al and Si in ash aerosols during the Torrefied test than the Coal test. However, co-firing in the utility boiler did not increase the partitioning of alkali, Na and K, into PM_{10} as it did in the pilot-scale furnace.
6) Ash deposition rates in the utility boiler are much lower than in the pilot-scale furnace, supported by the greatly reduced deposit particle size, possibly as a result of the more intense char fragmentation and decreased mineral coalescence. The complicated aerodynamic conditions in the utility boiler could also make large particles rebound and shed from the deposit surface. Flue gas velocities are much higher in the full-scale with much higher turbulence intensity.
7) Co-firing torrefied wood with coal produces opposite effects on the ash deposition rate in the two combustors: the Torrefied deposition rate is lower than the Coal deposition rate in the utility boiler, while it is higher in the pilot-scale furnace. The smaller scale combustor burning Torrefied blend fuel yielded increased alkali species in ash aerosols and deposits compared to burning Coal, and this could increase the particle bounce-off possibility in co-firing in the pilot-scale furnace.

AUTHOR INFORMATION

Corresponding Authors

Xiaolong Li − *Department of Chemical Engineering and Institute for Clean and Secure Energy (ICSE), University of Utah, Salt Lake City, Utah 84112, United States;*
Email: Xiaolongli922@gmail.com

Andrew Fry − *Department of Chemical Engineering, Brigham Young University, 84602 Provo, Utah, United States;*
orcid.org/0000-0002-4172-9266; Email: afry@byu.edu

Authors

Seyedhassan Fakourian − *Department of Chemical Engineering, Brigham Young University, 84602 Provo, Utah, United States*

Boden Moyer − *Department of Chemical Engineering, Brigham Young University, 84602 Provo, Utah, United States*

Jost O. L. Wendt − *Department of Chemical Engineering and Institute for Clean and Secure Energy (ICSE), University of Utah, Salt Lake City, Utah 84112, United States;*
orcid.org/0000-0002-0104-0763

Complete contact information is available at:
https://pubs.acs.org/10.1021/acs.energyfuels.1c03522

Notes

The authors declare no competing financial interest.

ACKNOWLEDGMENTS

The authors would like to acknowledge PacifiCorp for the financial support to this work. Help from Dr. Eric Eddings, Mr. Jack Mitchell, and Spencer Flindt are appreciated. We also give great thanks to the staff at Hunter Power Plant for their generous help during the tests, including (alphabetized by first name) Alex Crawford, Bruce Wilson, Cameron Hansen, Carson Grimm, Doug Farley, Glen Keller, Jamie Phillips, Jared Erickson, Jeff Westergard, Jordan Sitterud, Levi Ferguson, Mindy Jackson, Nick Larsen, Pete McElprang, Rhyker Allred, and Troy Anderson.

REFERENCES

(1) IPCC *Climate Change 2013: The Physical Science Basis. Contribution of Working Group I to the Fifth Assessment Report of the Intergovernmental Panel on Climate Change*; Stocker, T. F.; Qin, D.;

Plattner, G.-K.; Tignor, M.; Allen, S. K.; Boschung, J.; Nauels, A.; Xia, Y.; Bex, V.; Midgley, P.M. eds.. Cambridge University Press: Cambridge, United Kingdom and New York, NY, USA, 1535, 2013.

(2) Basu, P.; Butler, J.; Leon, M. A. Biomass co-firing options on the emission reduction and electricity generation costs in coal-fired power plants. *Renewable Energy* **2011**, *36*, 282−288.

(3) Perlack, R.D.; Eaton, L.M.; Turhollow, A.F., Jr; Langholtz, M. H.; Brandt, C. C.; Downing, M. E.; Graham, R. L.; Wright, L. L.; Kavkewitz, J. M.; Shamey, A. M.; Nelson, R. G. *U.S. Billion-Ton Update: Biomass Supply for a Bioenergy and Bioproducts Industry*; 2011.

(4) Neary, D. G.; Zieroth, E. J. Forest bioenergy system to reduce the hazard of wildfires: White Mountains, Arizona. *Biomass Bioenergy* **2007**, *31*, 638−645.

(5) Baxter, L. L. Ash deposition during biomass and coal combustion - A mechanistic approach. *Biomass Bioenergy* **1993**, *4*, 85−102.

(6) Heinzel, T.; Siegle, V.; Spliethoff, H.; Hein, K. R. G. Investigation of slagging in pulverized fuel co-combustion of biomass and coal at a pilot-scale test facility. *Fuel Process. Technol.* **1998**, *54*, 109−125.

(7) Bryers, R. W. Fireside Slagging, Fouling, and High-Temperature Corrosion of Heat-Transfer Surface Due to Impurities in Steam-Raising Fuels. *Prog. Energy Combust. Sci.* **1996**, *22*, 29−120.

(8) Vassilev, S. V.; et al. An overview of the chemical composition of biomass. *Fuel* **2010**, *89*, 913−933.

(9) Doshi, V.; et al. Development of a modeling approach to predict ash formation during co-firing of coal and biomass. *Fuel Process. Technol.* **2009**, *90*, 1148−1156.

(10) Jones, J. M.; et al. An investigation of the thermal and catalytic behaviour of potassium in biomass combustion. *Proceedings of the Combustion Institute* **2007**, *31*, 1955−1963.

(11) Baxter, L. L.; et al. The behavior of inorganic material in biomass-fired power boilers: field and laboratory experiences. *Fuel Process. Technol.* **1998**, *54*, 47−78.

(12) Glarborg, P. Hidden interactions—Trace species governing combustion and emissions. *Proceedings of the Combustion Institute* **2007**, *31*, 77−98.

(13) Ekvall, T.; et al. K−Cl−S chemistry in air and oxy-combustion atmospheres. *Proceedings of the Combustion Institute* **2017**, *36*, 4011−4018.

(14) Uusitalo, M. A.; Vuoristo, P. M. J.; Mäntylä, T. A. High temperature corrosion of coatings and boiler steels below chlorine-containing salt deposits. *Corros. Sci.* **2004**, *46*, 1311−1331.

(15) van der Stelt, M. J. C.; Gerhauser, H.; Kiel, J. H. A.; Ptasinski, K. J. Biomass upgrading by torrefaction for the production of biofuels: A review. *Biomass Bioenergy* **2011**, *35*, 3748−3762.

(16) Helble, J.; Neville, M.; Sarofim, A. F. Sarofim, Aggregate formation from vaporized ash during pulverized coal combustion. *Symp. (Int.) Combust.* **1988**, *21*, 411−417.

(17) Baxter, L.L., *Ash Deposit Formation and Deposit Properties: A Comprehensive Summary of Research Conducted at Sandia's Combustion Research Facility*; 2000, Sandia Report.

(18) Srinivasachar, S.; Helble, J. J.; Boni, A. A. An experimental study of the inertial deposition of ash under coal combustion conditions. *Symp. (Int.) Combust.* **1991**, *23*, 1305−1312.

(19) Glarborg, P.; Marshall, P. Mechanism and modeling of the formation of gaseous alkali sulfates. *Combust. Flame* **2005**, *141*, 22−39.

(20) Luan, C.; You, C.; Zhang, D. Composition and sintering characteristics of ashes from co-firing of coal and biomass in a laboratory-scale drop tube furnace. *Energy* **2014**, *69*, 562−570.

(21) Wang, Y.; et al. Comparison Study of Ash Partitioning and Deposition Behavior between Two Rice Husk Fuels under a 100 kW Combustor. *Energy Fuels* **2019**, *33*, 11968−11975.

(22) Teixeira, P.; et al. Evaluation of slagging and fouling tendency during biomass co-firing with coal in a fluidized bed. *Biomass Bioenergy* **2012**, *39*, 192−203.

(23) Jurado, N.; et al. Effect of co-firing coal and biomass blends on the gaseous environments and ash deposition during pilot-scale oxy-combustion trials. *Fuel* **2017**, *197*, 145−158.

(24) Fryda, L.; et al. Study on ash deposition under oxyfuel combustion of coal/biomass blends. *Fuel* **2010**, *89*, 1889−1902.

(25) Hansen, S. B.; Jensen, P. A.; Frandsen, F. J.; Sander, B.; Glarborg, P. Mechanistic Model for Ash Deposit Formation in Biomass Suspension Firing. Part 1: Model Verification by Use of Entrained Flow Reactor Experiments. *Energy Fuels* **2017**, *31*, 2771−2789.

(26) Xu, X. G.; et al. Effect of Co-firing Straw with Two Coals on the Ash Deposition Behavior in a Down-Fired Pulverized Coal Combustor†. *Energy Fuels* **2010**, *24*, 241−249.

Firing of Torrefied Biomass in PacifiCorp’s Hunter, Unit 3

Andrew Fry, Seyedhassan Fakourian
Brigham Young University

Eric Eddings, Jost Wendt, Stan Harding, Teri Draper, Xiaolong Li,
Alex Prlina
University of Utah

Klas Andersson, Thomas Allgurén, Dan Gall, Adrian Gunnarsson
Chalmers University

Configuration of Hunter, Unit 3

Hunter, Unit 3 – Boiler Layout

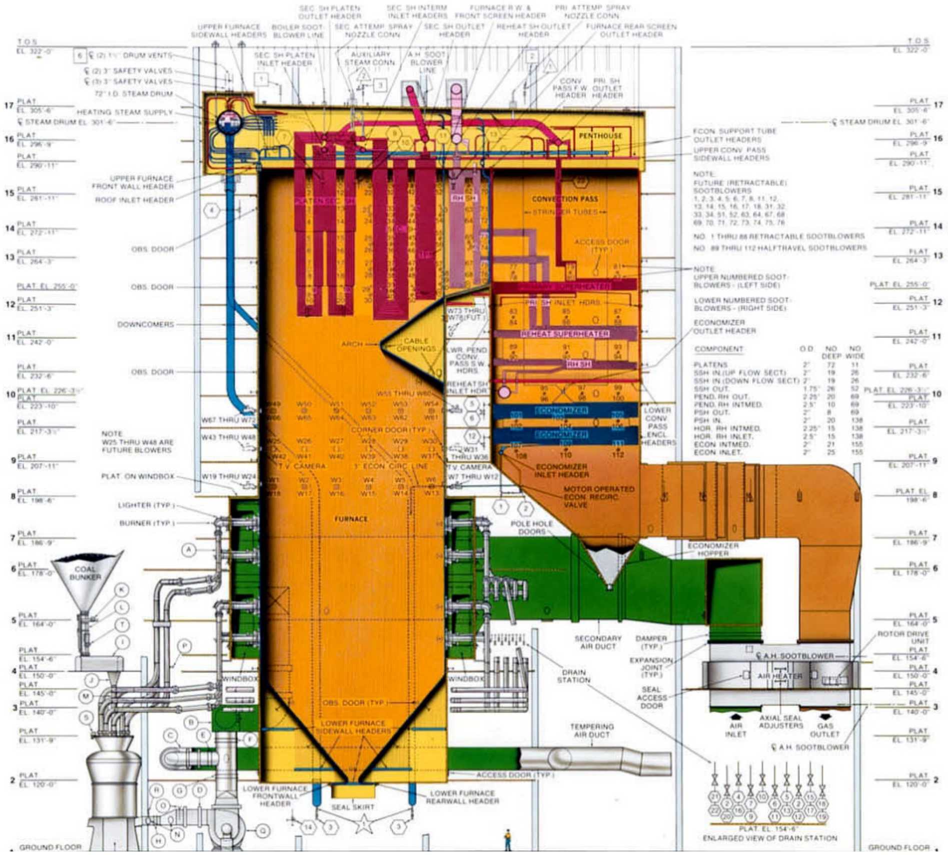

NOTE
W25 THRU W48 ARE FUTURE BLOWERS

NOTE
FUTURE (RETRACTABLE) SOOTBLOWERS
1, 2, 3, 4, 5, 6, 7, 8, 11, 12,
13, 14, 15, 16, 17, 18, 31, 32,
33, 34, 51, 52, 63, 64, 67, 68
69, 70, 71, 72, 73, 74, 75, 76

NO. 1 THRU 88 RETRACTABLE SOOTBLOWERS

NO. 89 THRU 112 HALFTRAVEL SOOTBLOWERS

NOTE
UPPER NUMBERED SOOT-BLOWERS - (LEFT SIDE)

LOWER NUMBERED SOOT-BLOWERS - (RIGHT SIDE)

COMPONENT	O.D.	NO DEEP	NO WIDE
PLATENS	2"	72	11
SSH IN.(UP FLOW SECT)	2"	19	26
SSH IN (DOWN FLOW SECT)	2"	19	26
SSH OUT.	1.75"	26	52
PEND. RH OUT.	2.25"	20	69
PEND. RH INTMED.	2.5"	10	69
PSH OUT.	2"	8	69
PSH IN.	2"	20	138
HOR. RH INTMED.	2.25"	15	138
HOR. RH INLET.	2.5"	15	138
ECON INTMED.	2"	21	155
ECON INLET.	2"	25	155

Hunter, Unit 3 – Boiler Geometry

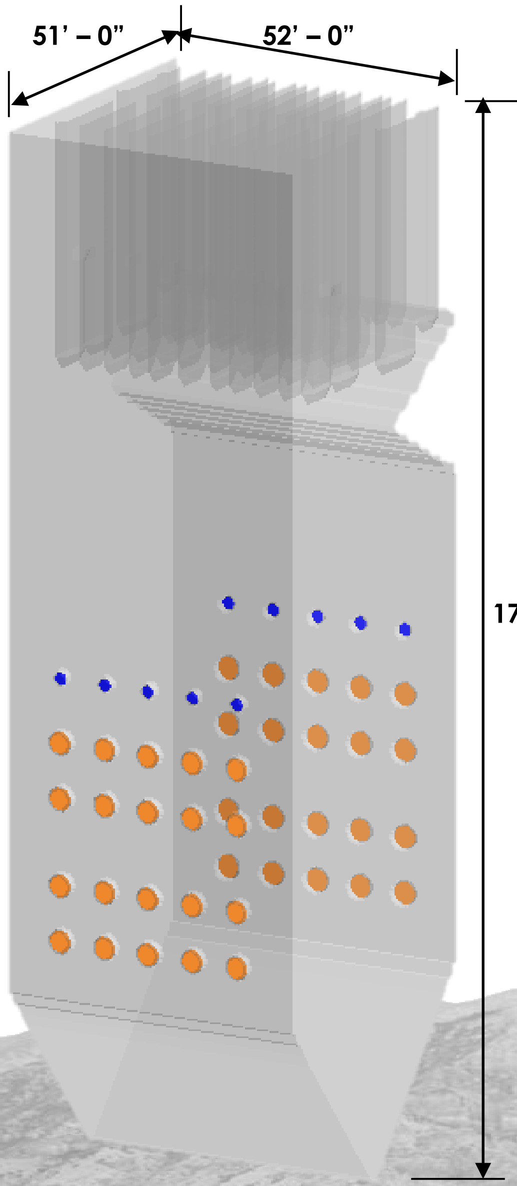

51' – 0"

52' – 0"

Roof El. 289' – 0"

170' – 0"

Datum El. 119' – 0"

20 FW Burners, 20 RW Burners

5 FW OFA Ports, 5 RW OFA Ports

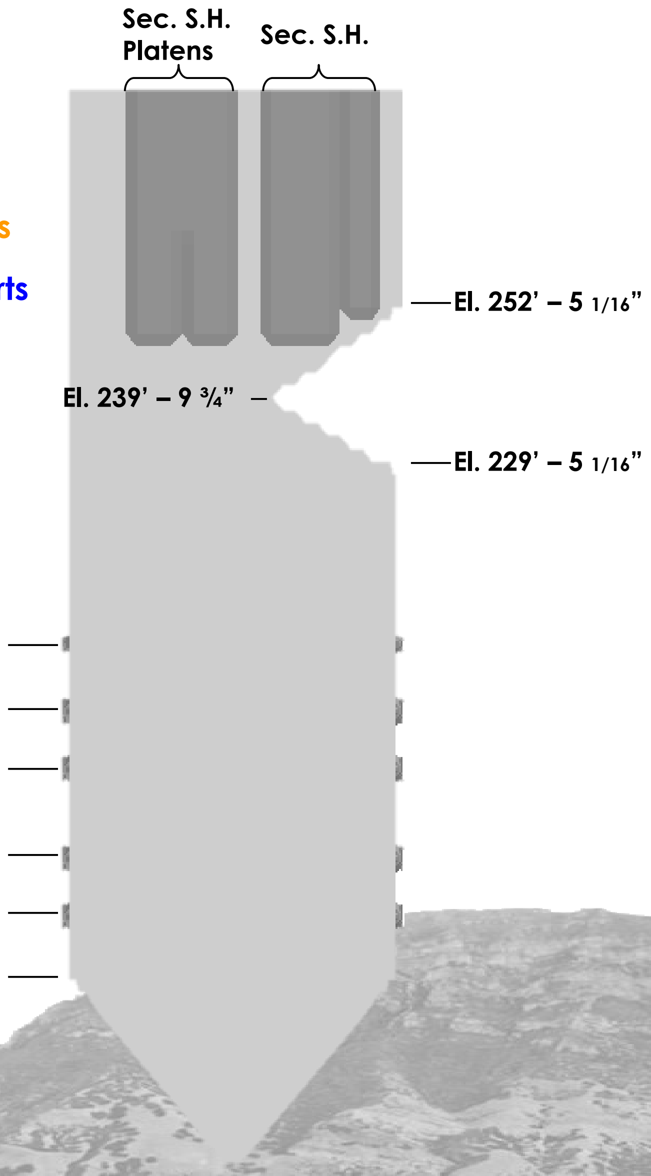

Sec. S.H. Platens

Sec. S.H.

El. 252' – 5 1/16"

El. 239' – 9 ¾"

El. 229' – 5 1/16"

OFA El. 201' – 5"

Burner El. 191' – 0"

Burner El. 182' – 0"

Burner El. 168' – 0"

Burner El. 159' – 0"

El. 148' – 11 ⅝"

Hunter, Unit 3 – Burner Geometry

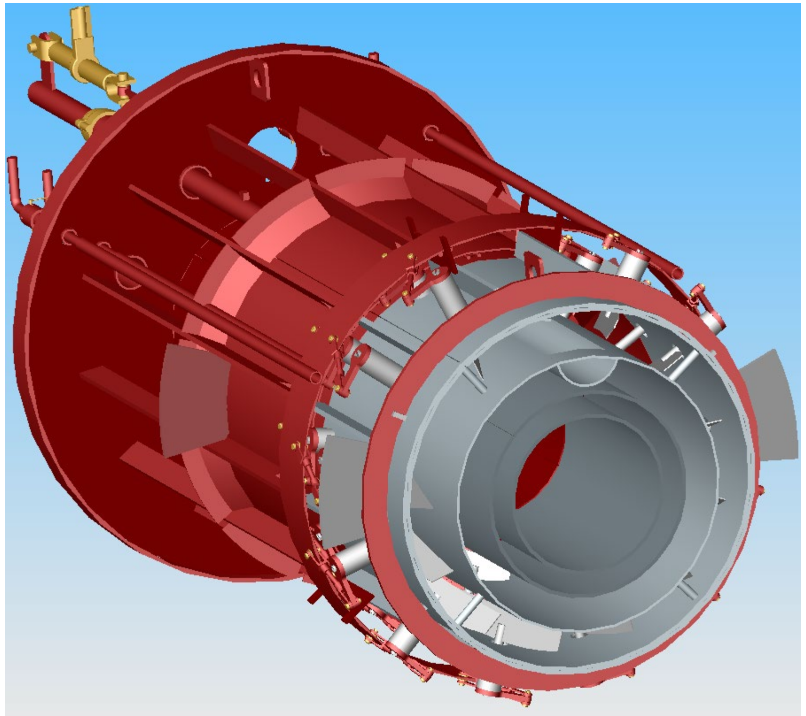

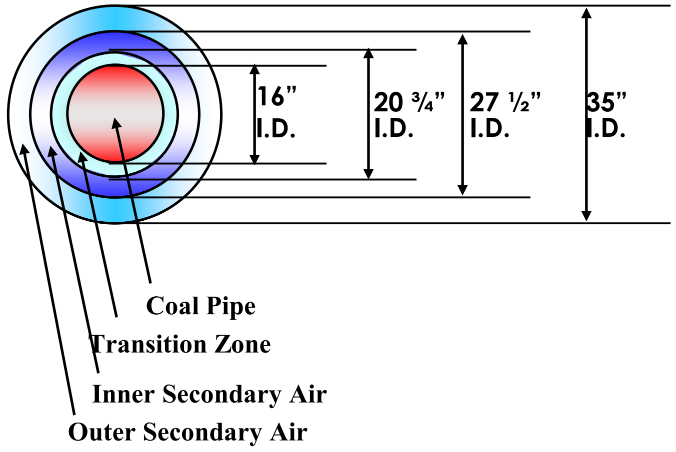

End View

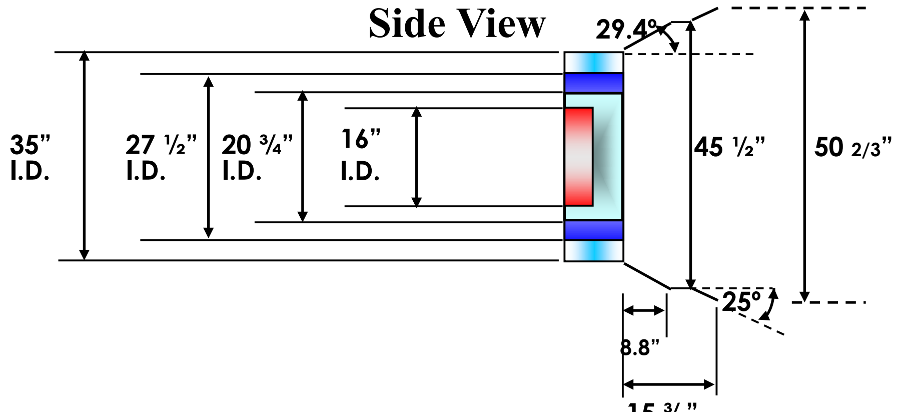

Side View

Hunter, Unit 3 – Baseline Operating Conditions

From 2010 Performance Testing

Furnace Operational Data	**Baseline**
Firing Rate (MBtu/h)	**4528**
Stoichiometric Ratio	**1.182**
Lower Furnace Stoichiometric Ratio	**0.900**
Coal Flow Rate (klb/h)	**399.1**
Total Combustion Air/O_2 Flow (klb/h)	**4052.0**
Theoretical Excess O_2, (%, wet)	**3.03%**
Burner Zone Air/O_2 Flow (klb/h)	**3085.1**
OFA Flow Air/O_2 (klb/h)	**966.9**
Burner Operational Data (per burner)	
Coal Flow Rate (klb/h)	**9.98**
Primary Air/O_2 Flow (klb/h)	**19.66**
Primary Gas/Coal	**1.97**
Primary Air Temperature (ºF)	**150**
Secondary Air/O_2 Flow (klb/h)	**57.47**
Transition Air Flow (klb/h)	**4.60**
Inner Secondary Air Flow (klb/h)	**15.86**
Outer Secondary Air Flow (klb/h)	**37.01**
Secondary Air Temperature (ºF)	**528**
OFA Port Operational Data (per port)	
Air/O_2 Flow (klb/h)	**96.7**
Core Zone Air/O_2 Flow (klb/h)	**58.0**
Core Zone Velocity (ft/s)	**256.4**
Outer Zone Air/O_2 Flow (klb/h)	**38.7**
Outer Zone Velocity (ft/s)	**114.5**
Temperature (ºF)	**528**

Lower Furnace is Staged

Primary gas/coal mass ratio

Neglecting the Transition Air, the secondary air distribution is 30/70 mass % Inner/Outer

Executed Test Parameters and Schedule

- Operate at 90% Full Load
- Assumed Full Load 1327 MW_{th} (Based on 2011 Project Baseline Conditions)
- 1194 MW_{th} (Expected Condition)
- Operate at “typical” burner and staging conditions
- Amaron delivered 724 tons of pelletized torrefied biomass
- Planed to test for a 24 hour period at approximately a 15% blend
- Brief fuel blend test was performed on 08/21/19 at the coal yard. This material was immediately fed to Unit 3 silos.
- Testing of the biomass blend was performed from 08/22/19 20:10 to 08/23/19 06:43
- Baseline testing was performed from 08/23/19 14:53 to 08/24/19 02:31

Measurement Locations

Port #	Description
1	Center of the reheater
2	Front of the reheater
3	Middle of the nose
4	Front of the boiler, above the nose
5	Above the over-fire air
6	Top Burner elevation
7	Bottom burner elevation
8	Economizer outlet

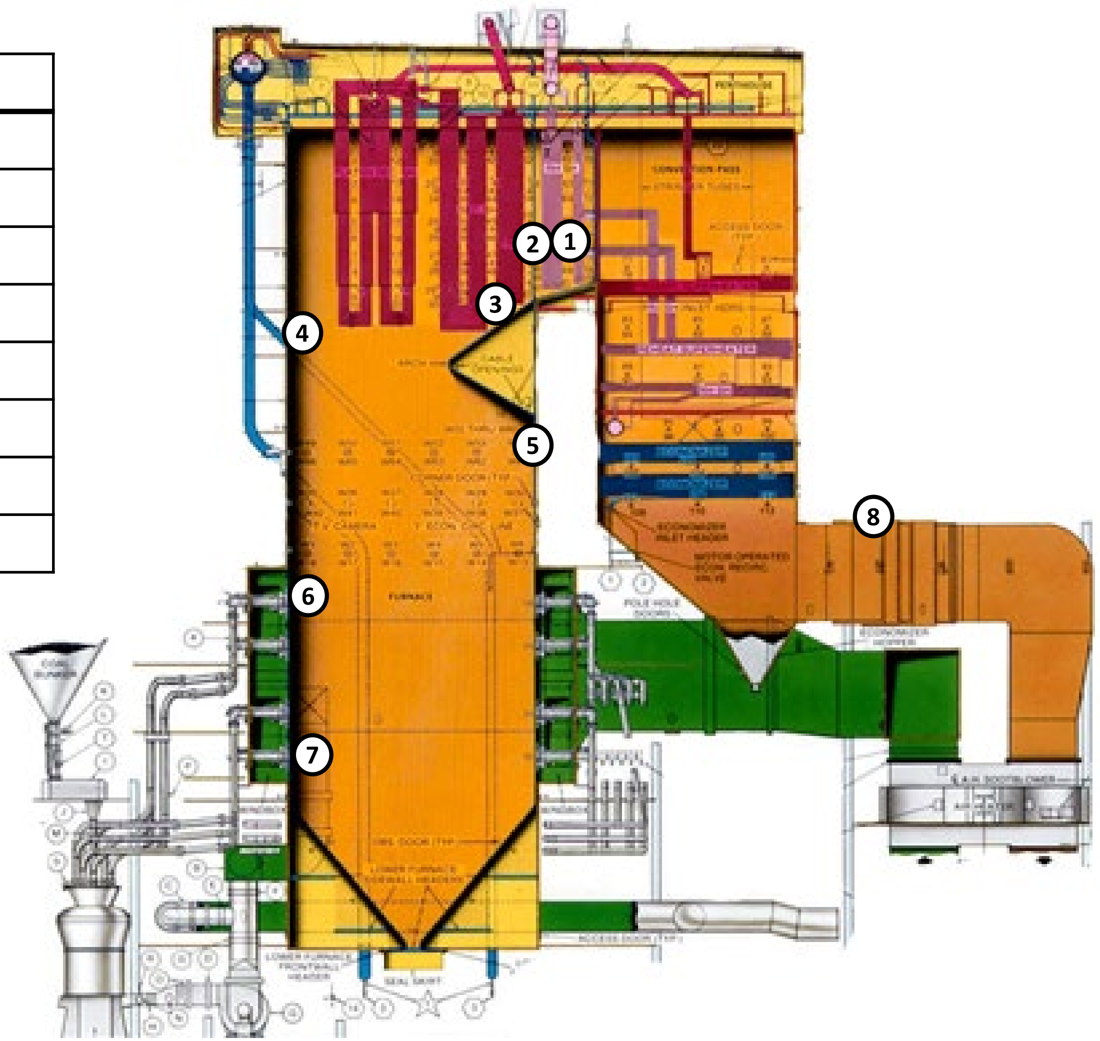

Pictures and dimensions of sample ports can be downloaded at:

https://byu.box.com/s/aaangzzm6367idwp4k5m13wzeroq40ue

Measurements

- Deposit and entrained ash sampling
- Fuel and ash sampling
- Radiation intensity and incident radiative heat flux(radiometers)
- FTIR gas analysis
- Gas temperatures using suction pyrometery and/or shielded thermocouple
- Continuous gas analysis
- Evaluation of PI Data

Analysis of Fuel Blending and Boiler Injection Periods

Determination of Fuel Blend (Coal Yard Data)

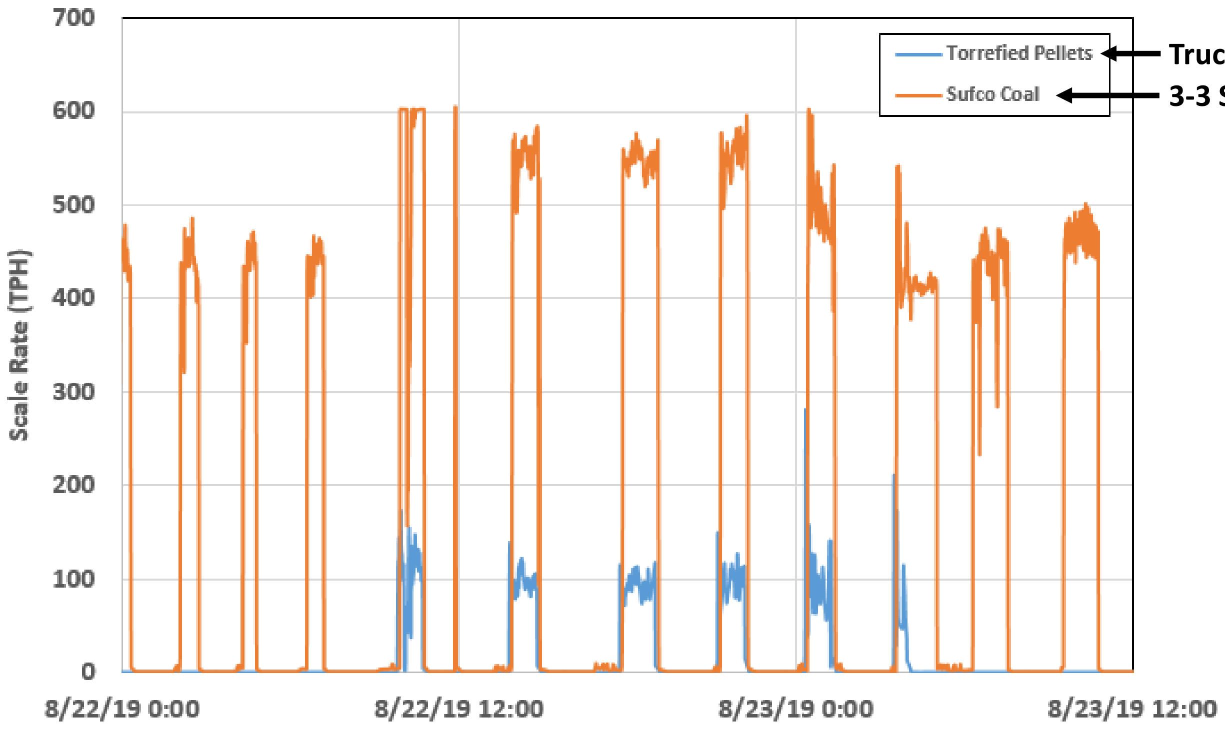

Truck Scale

3-3 Scale

Fuel Blend Times (Coal Yard)

Date	Start Time	End Time
8-21-19*	00:44	01:26
8-22-19	09:49	10:53
8-22-19	13:84	14:57
8-22-19	17:44	19:10
8-22-19	21:14	22:14
8-23-19	00:21	01:27
8-23-19	03:30	04:08

* Test blending period, not plotted

- Fuel blending was performed by controlling the relative rate of belts feeding torrefied pellets and biomass, based on belt scale readings
- Total biomass delivered to Hunter – 724 Tons
- Total biomass fed on Truck Scale – 577 Tons (Integrated Scale Reading)
- Blend based on biomass delivered – 19.6%
- Blend based on scale readings – 15.0%

Difference assumed from losses and scale calibration

Nice work coal yard

Determination of Fuel Blend (Based on Fuel Analysis)

			Redler Fuel Samples			
	Sufco	Torrefied Pellets	08/22/19 20:16	08/23/19 02:00	08/23/19 22:59	08/24/19 18:15
C	63.34	47.74	60.06	60.06	63.83	61.63
H	4.43	5.20	4.42	4.45	4.47	4.36
N	1.23	0.23	1.06	0.97	1.25	1.18
S	0.48	0.02	0.41	0.35	0.63	0.49
O	10.44	35.55	12.91	12.25	9.53	9.77
Ash	11.64	0.85	11.48	10.53	11.52	15.71
Moist	8.45	10.40	9.67	11.39	8.76	6.85
HHV (Btu/lb)	11093	8219	10582	10447	11354	10693
			↑ 17.8%	↑ 22.5%	↑ 0.0%	

← **Plant obviously went back to low quality coal.**

- Torrefied pellets were analyzed prior to demonstration
- Sufco coal analysis was provided by Hunter, representative of the week
- Fuel blend can be estimated by minimization of sum squared error

Estimation of Time When Fuel Blend Arrived at Mills

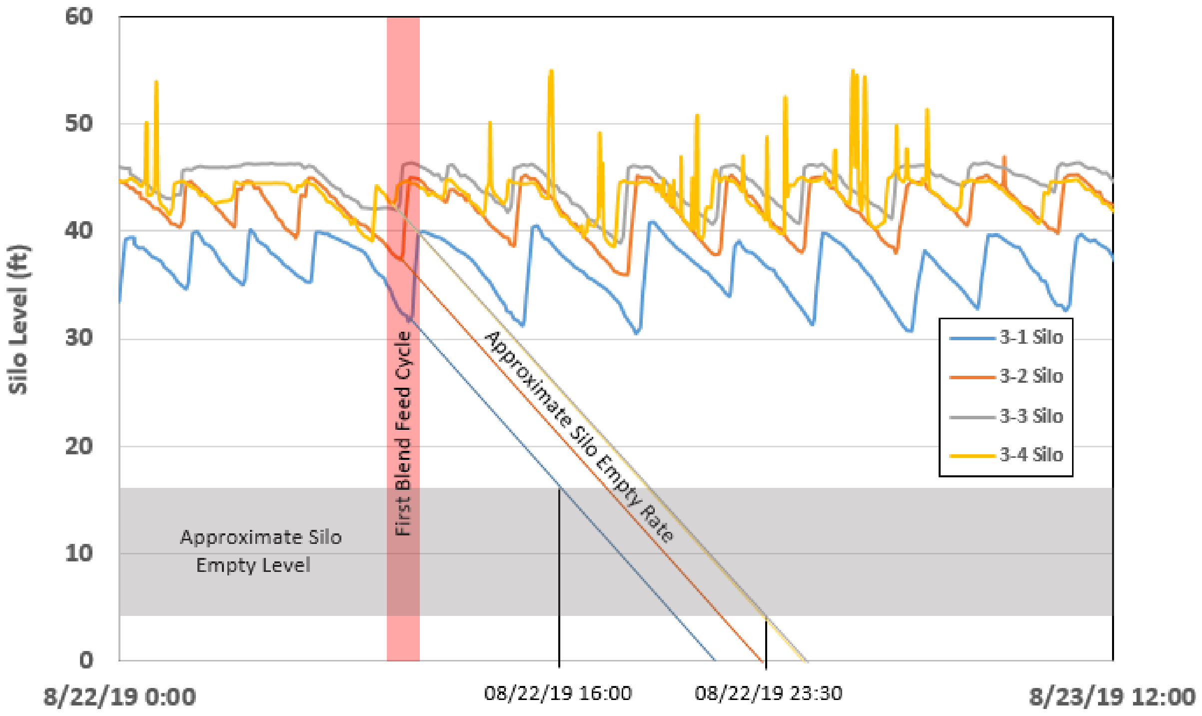

- Silo fill profile and empty rate used to approximate of time blended fuel arrived at the mills
- Empty mills register at 4 – 16 foot silo level
- Early estimate of blended fuel reaching mills/boiler: 16:00 on 08/22/19
- Late estimate of blended fuel reaching mills/boiler: 23:30 on 08/22/19

Estimation of Time When Fuel Blend Arrived at Mills

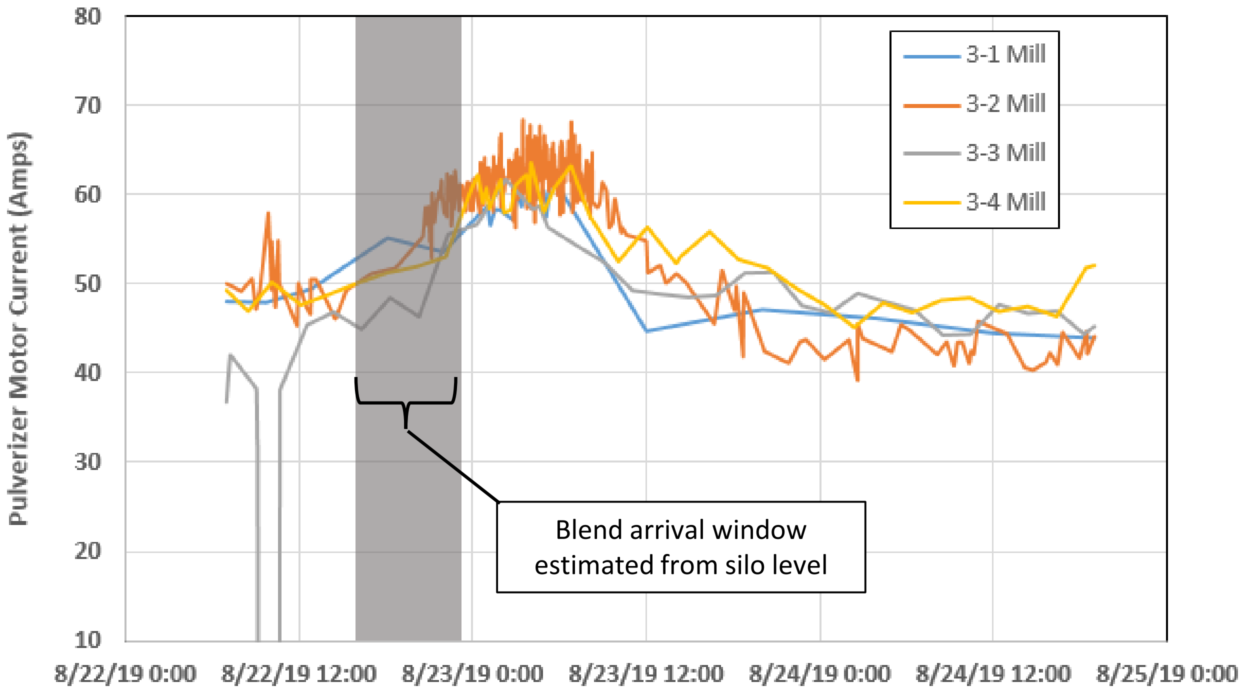

Blend arrival window estimated from silo level

- Mill behavior should corroborate blended fuel arrival time

Estimate of When Fuel Blend Finished at Mills

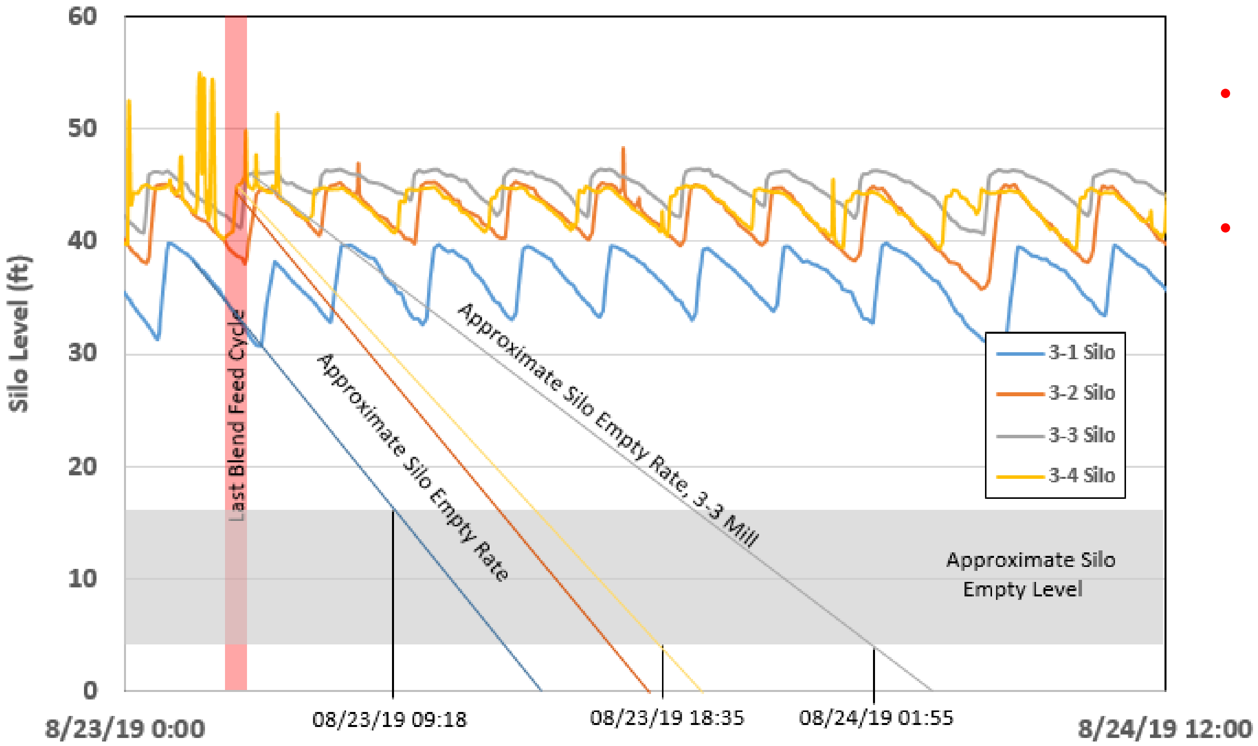

- Mill 3-3 appeared to behave differently after blend test
- Blend may have lingered in mill 3-3 until as late as 01:55 on 08/24/19

- Silo fill profile and empty rate used to approximate of time blended fuel arrived at the mills
- Empty mills register at 4 – 16 foot silo level
- Early estimate of blended fuel finishing at mills/boiler: 09:18 on 08/23/19
- Late estimate of blended fuel finishing at mills/boiler: 18:35 on 08/23/19

Comparison of Sampling Times with Biomass Combustion

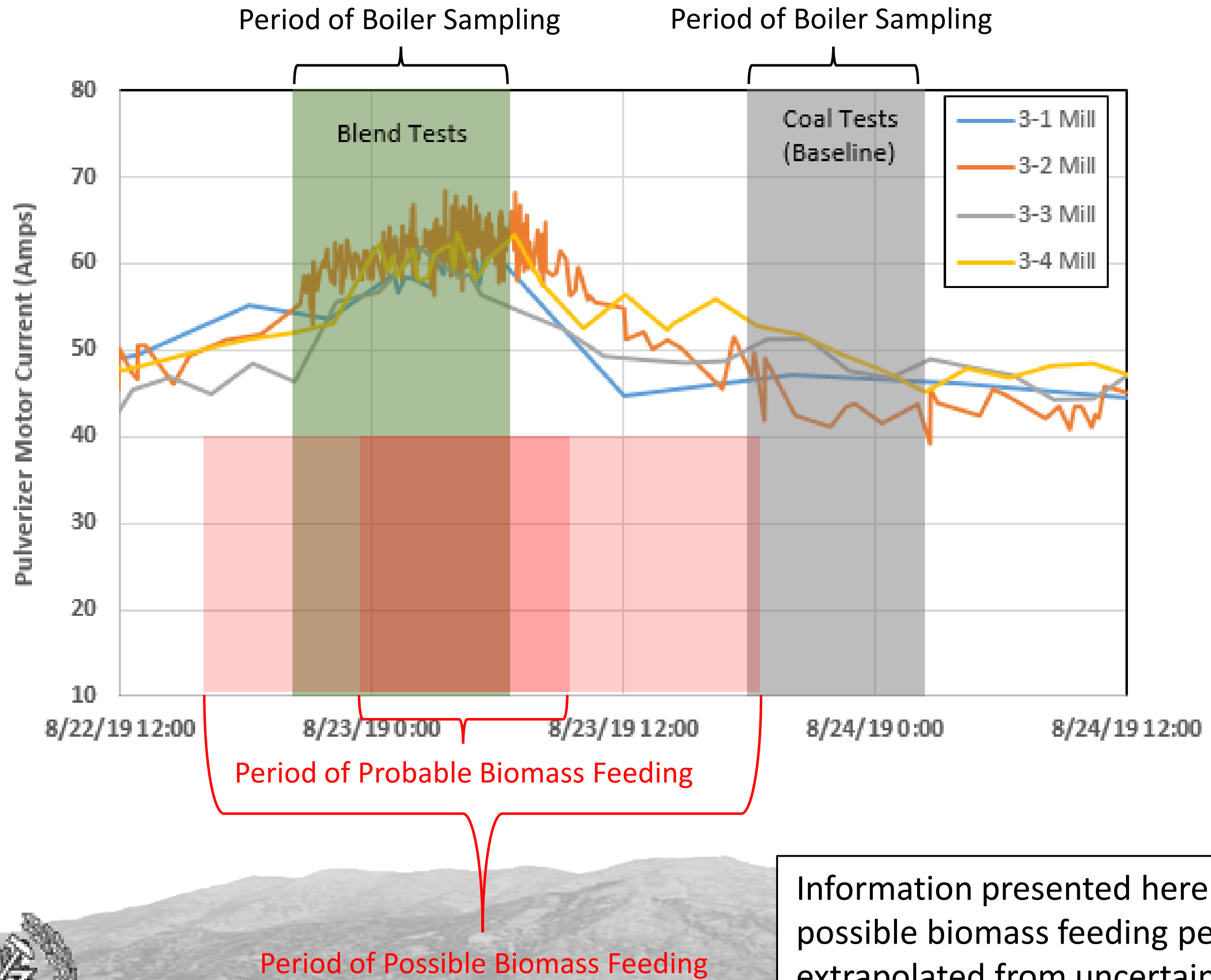

Information presented here for probable and possible biomass feeding periods are extrapolated from uncertain silo level meters.

Boiler Behavior (Information from Plant PI Data)

Load

- There was no change in load between blend and pure coal operation

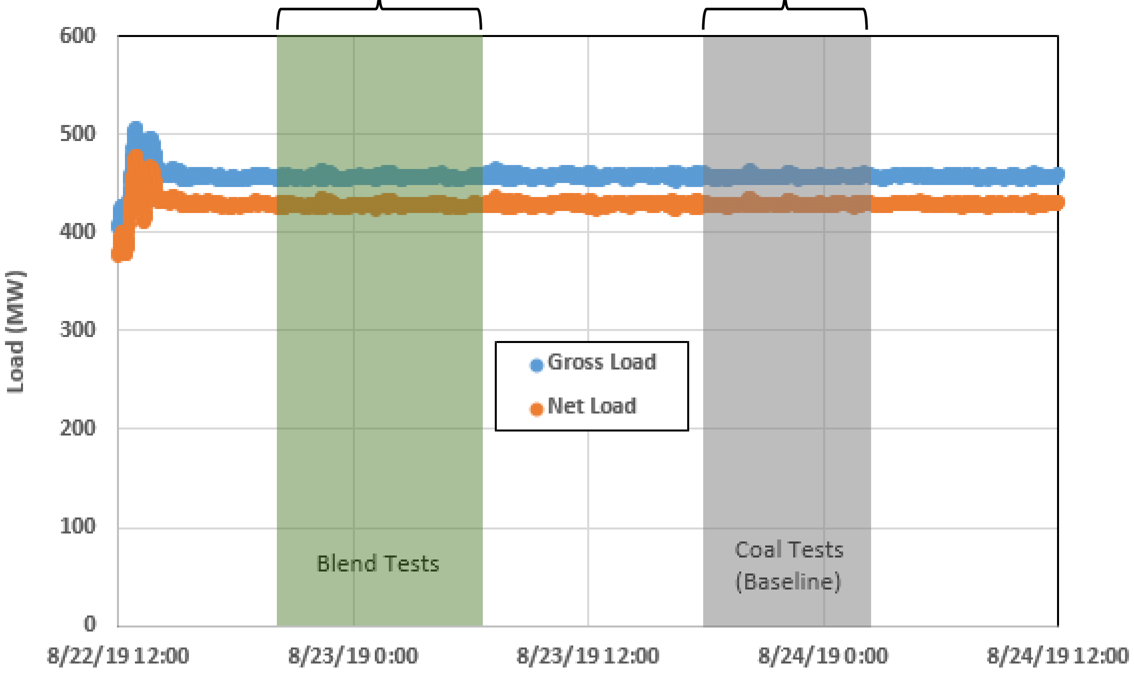

Gross – 456.7 MW
Net – 428.1 MW

Gross – 457.2 MW
Net – 428.9 MW

Gross Load – 99.9% of coal condition
Net Load – 99.8% of coal condition

Turbine Throttle Pressure

- There was no change in turbine throttle pressure between blend and pure coal operation

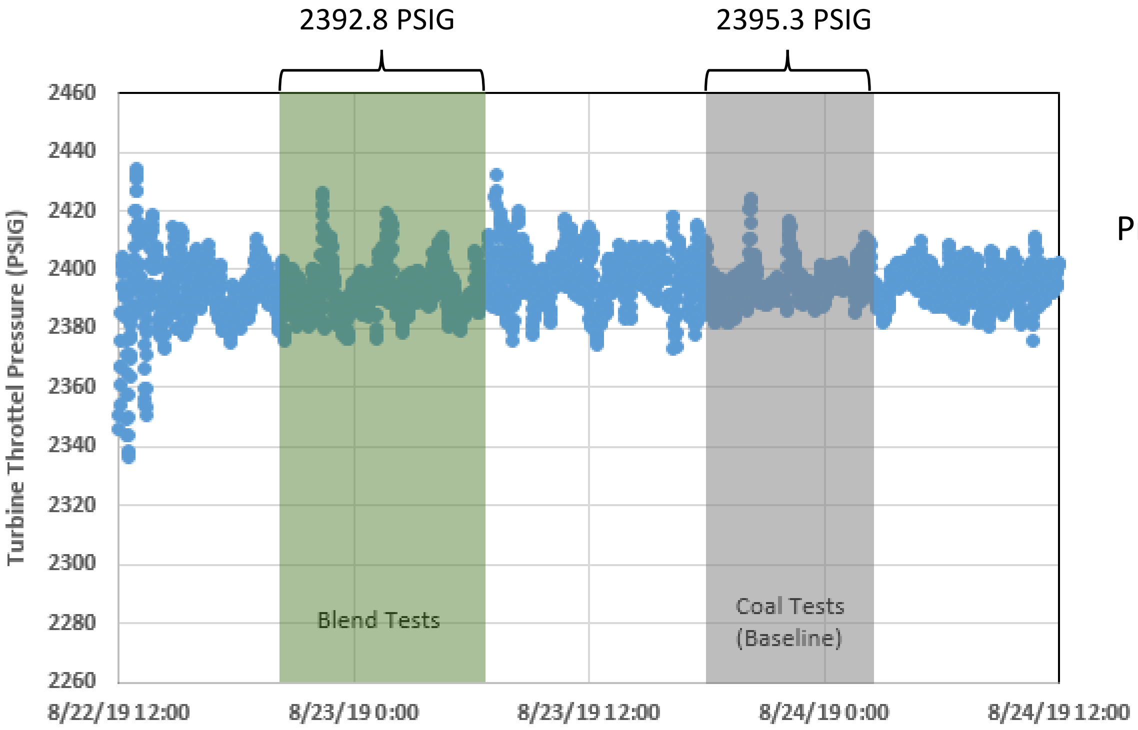

Pressure – 99.9% of coal condition

Boiler O_2

- Boiler O_2 was maintained at essentially the same value for each of the tests

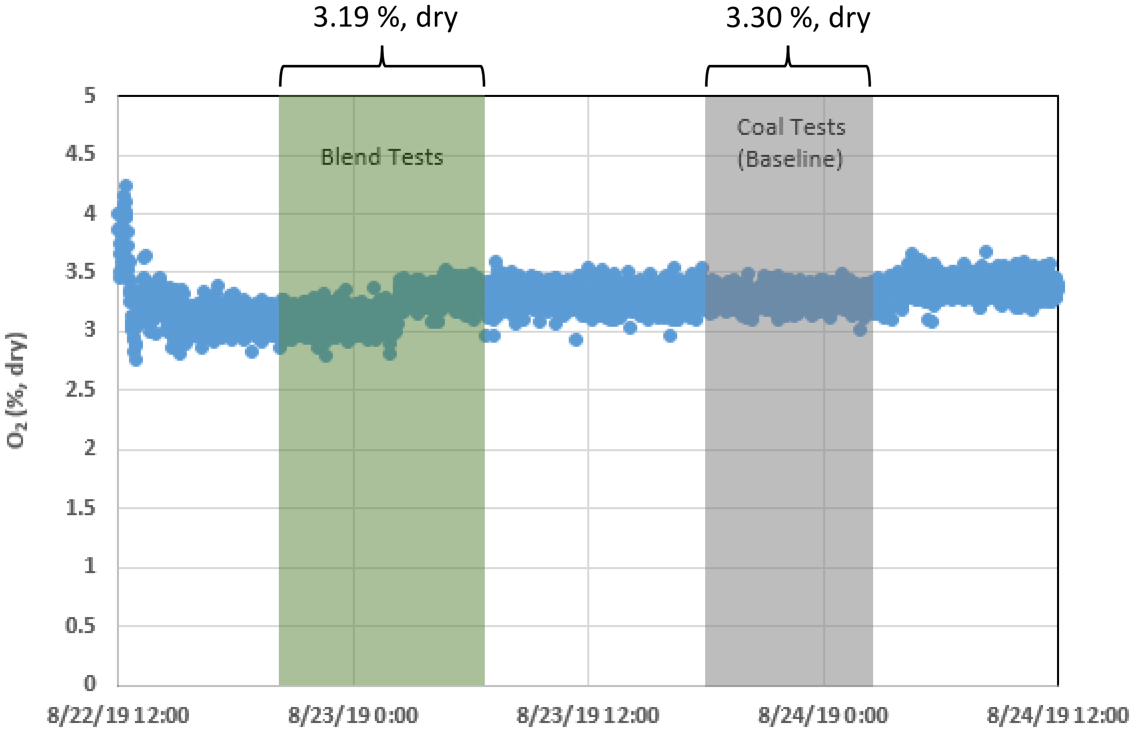

O_2 – 96.7% of coal condition

Coal Flow

- Fuel feed rate was about 6.6% higher during the biomass blend test
- Calculated necessary increase based on measured heating value of blend and coal was 6.6%

3-1 – 100.5 kpph
3-2 – 100.5 kpph
3-3 – 100.5 kpph
3-4 – 100.5 kpph

3-1 – 94.3 kpph
3-2 – 94.3 kpph
3-3 – 94.3 kpph
3-4 – 94.2 kpph

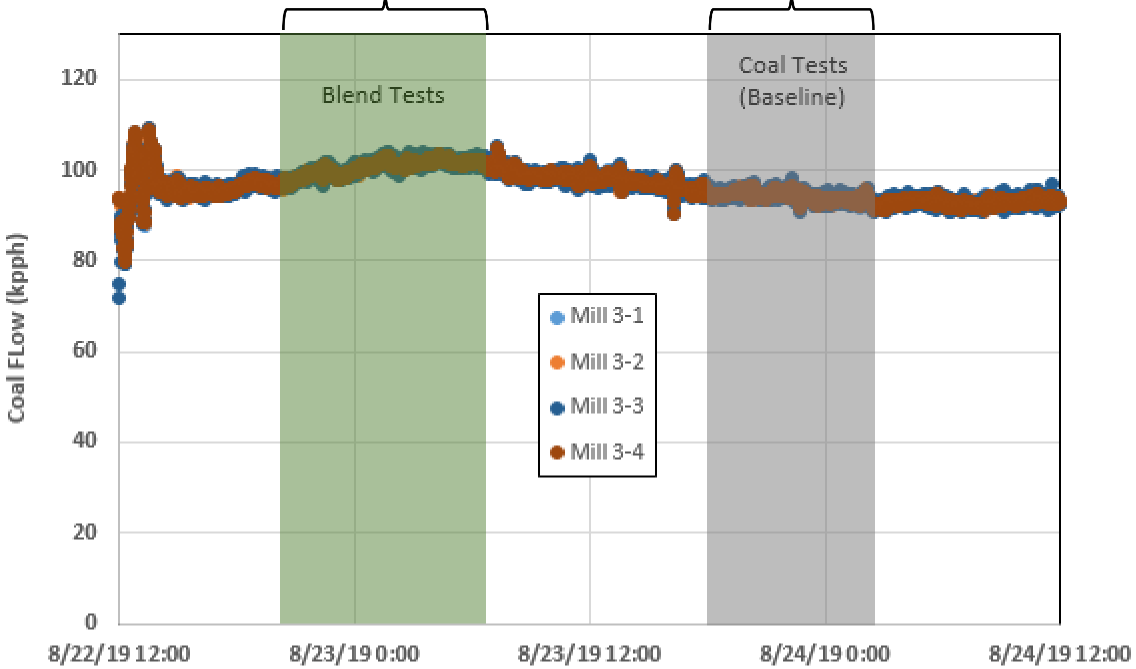

Mill 3-1 – 106.6% of coal condition
Mill 3-2 – 106.6% of coal condition
Mill 3-3 – 106.6% of coal condition
Mill 3-4 – 106.7% of coal condition

Flue Gas Pressure Drop

- Flue gas pressure drop through the economizer was the same for both fuel conditions
- Pressure drop through the superheater was slightly lower for the biomass blend case

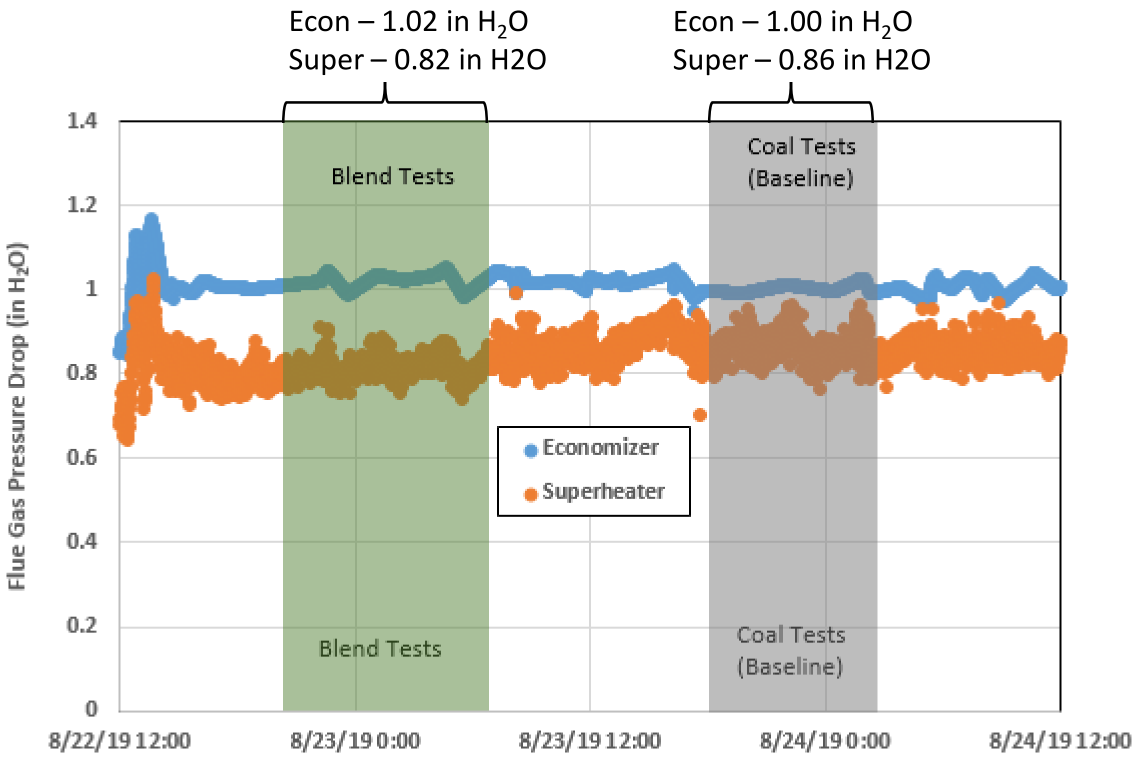

Econ – 101.7% of coal condition
Super – 94.6% of coal condition

Boiler NOx

- NO_x was reduced to 88.6% of the pure coal condition while firing the biomass blend

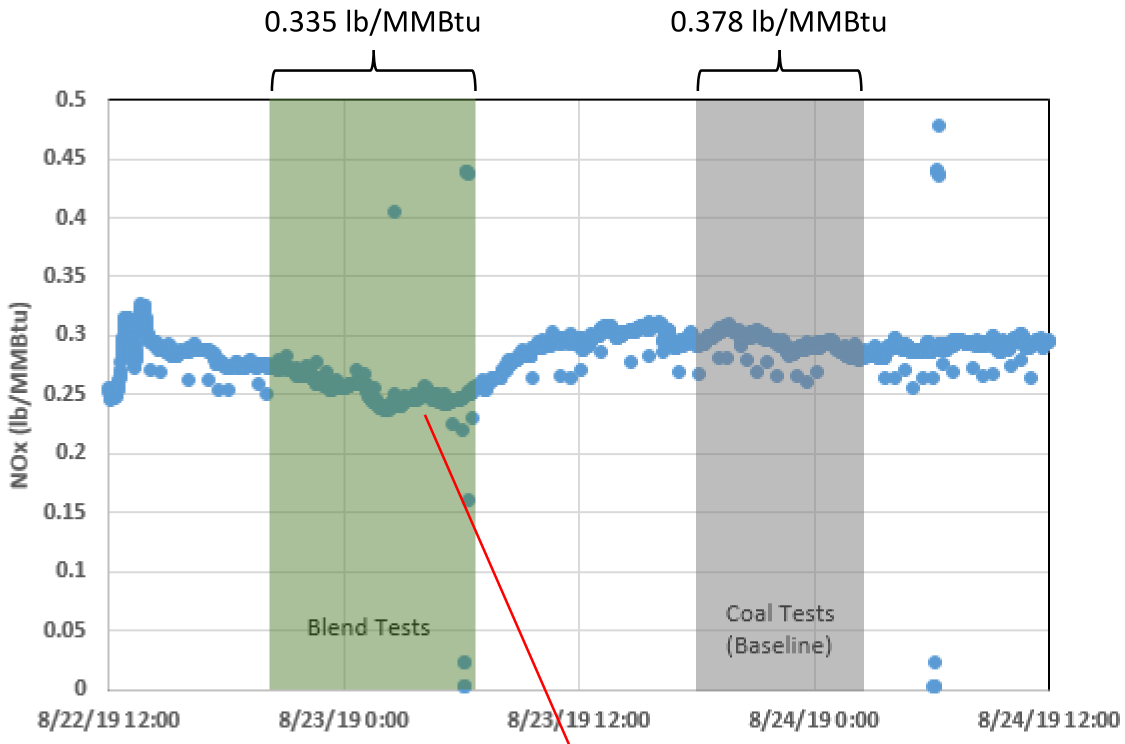

NOx – 88.6% of coal condition

More like 65% of coal condition

Boiler SO_2

- SO_2 was reduced to 71.9% of the pure coal condition while firing the biomass blend

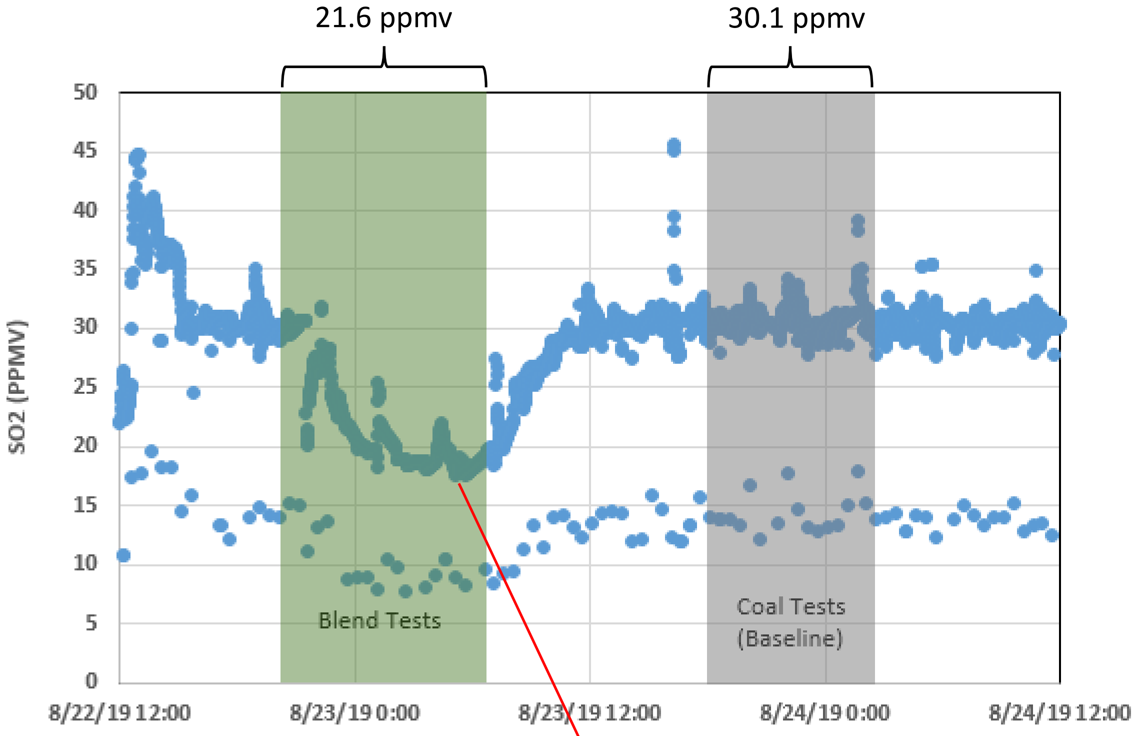

SO_2 – 71.9% of coal condition

More like 62% of coal condition

Boiler CO

- CO was increased by four times while firing the biomass blend compared to the pure coal condition

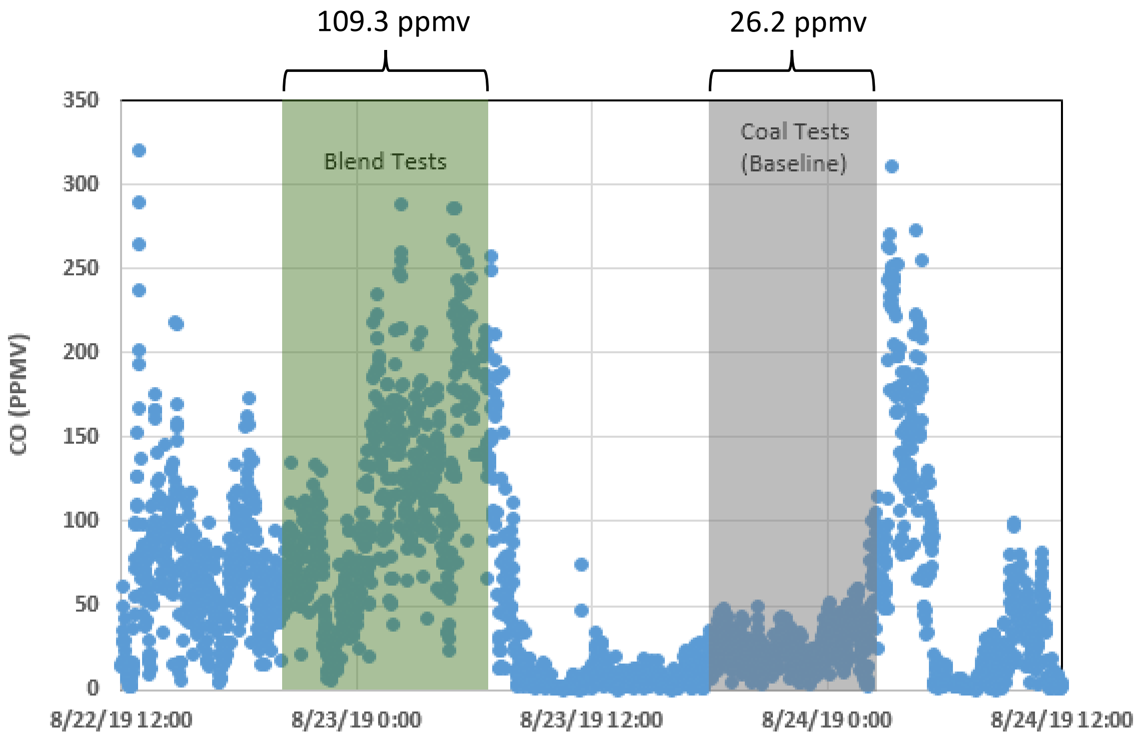

CO – 417% of coal condition

Mill Behavior (Information from Plant PI Data)

Primary Air Fan Motor Current

- Primary air fan power requirements were essentially unchanged

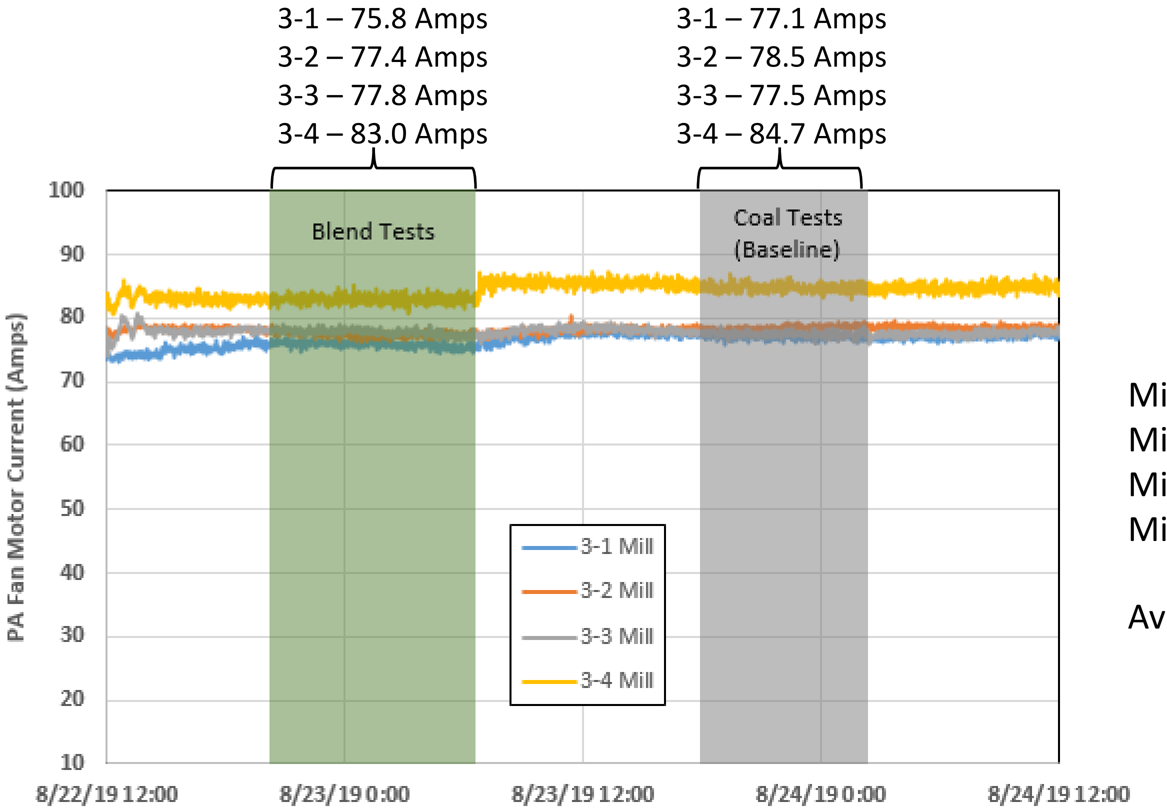
3-1 – 75.8 Amps
3-2 – 77.4 Amps
3-3 – 77.8 Amps
3-4 – 83.0 Amps

3-1 – 77.1 Amps
3-2 – 78.5 Amps
3-3 – 77.5 Amps
3-4 – 84.7 Amps

Mill 3-1 – 98.4% of coal condition
Mill 3-2 – 98.6% of coal condition
Mill 3-3 – 100.4% of coal condition
Mill 3-4 – 97.9% of coal condition

Ave – 98.8% of coal condition

Pulverizer Outlet Temperature

- Mill outlet temperatures were essentially unchanged, with the exception of the 3-2 mill which was lower for the blend processing condition

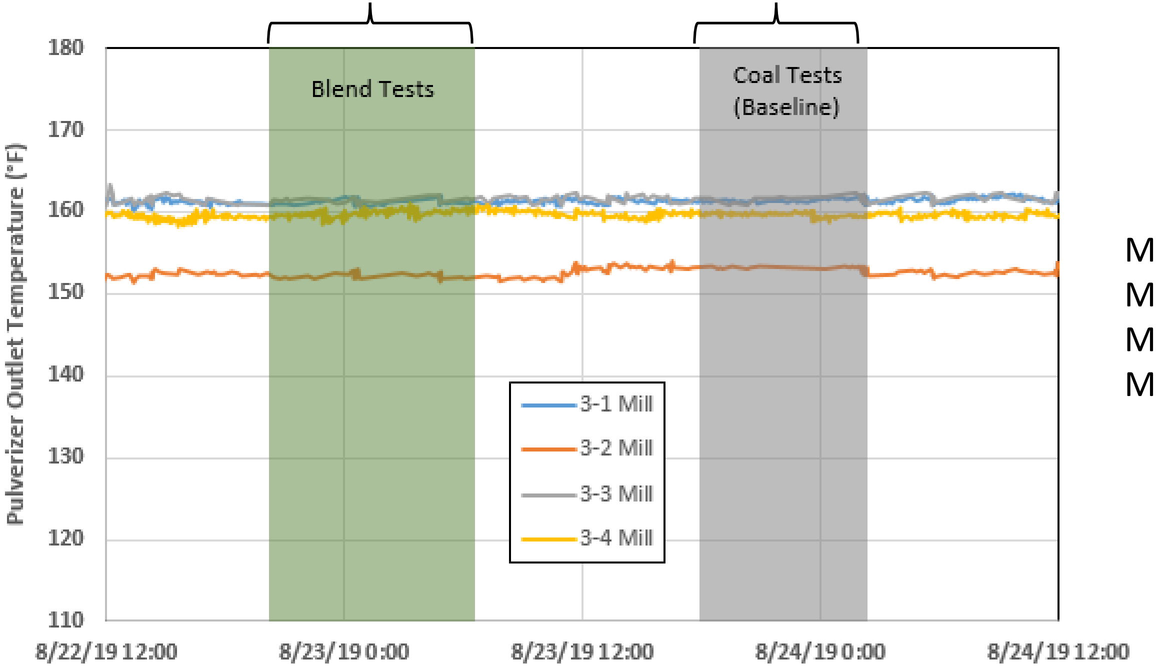

3-1 – 161.2 °F
3-2 – 152.1 °F
3-3 – 161.5 °F
3-4 – 159.8 °F

3-1 – 161.2 °F
3-2 – 152.1 °F
3-3 – 161.5 °F
3-4 – 159.8 °F

Mill 3-1 – 99.9% of coal condition
Mill 3-2 – 90.9% of coal condition
Mill 3-3 – 99.9% of coal condition
Mill 3-4 – 100.1% of coal condition

Pulverizer Motor Current

- Pulverizer motor current increased for all four mills while process the biomass blend
- Increase in current was especially pronounced for the 3-2 mill (at 40%) along with the fluctuations in current for that mill

3-1 – 57.6 Amps
3-2 – 60.9 Amps
3-3 – 56.4 Amps
3-4 – 58.4 Amps

3-1 – 46.7 Amps
3-2 – 43.4 Amps
3-3 – 49.1 Amps
3-4 – 49.6 Amps

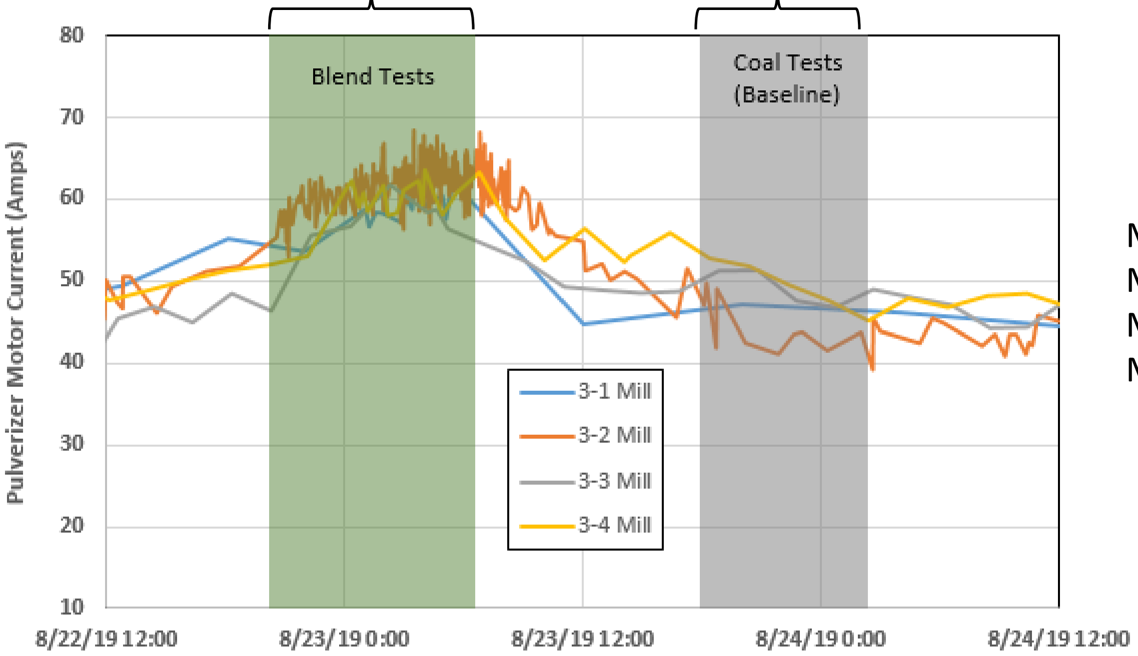

Mill 3-1 – 123.2% of coal condition
Mill 3-2 – 140.5% of coal condition
Mill 3-3 – 114.8% of coal condition
Mill 3-4 – 117.7% of coal condition

Pulverizer Particle Size Distribution (PSD)

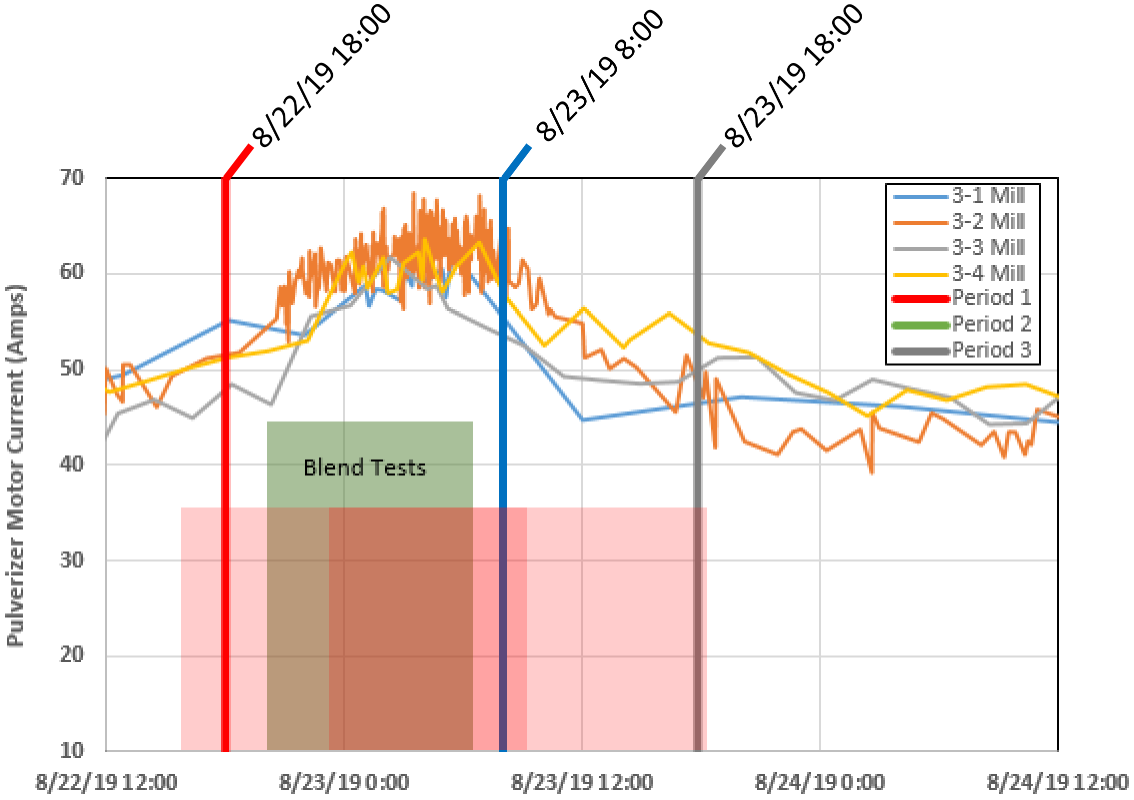

Coal Pipe Sampling Times

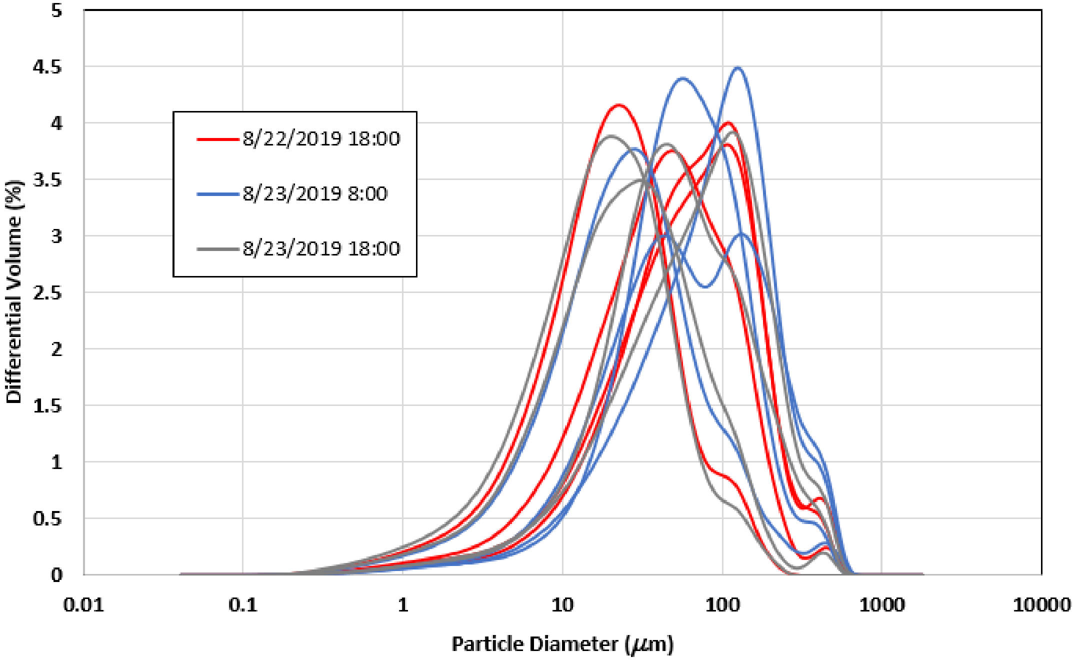

Pulverized Coal (PSD)

- Coal PSD represented by various colors:
  - Red – Mostly Coal
  - Blue – Biomass Blend
  - Grey – Mostly Coal

- There seems to be little correlation with sampling time (coal vs. biomass)

Pulverizer Particle Size Distribution (PSD)

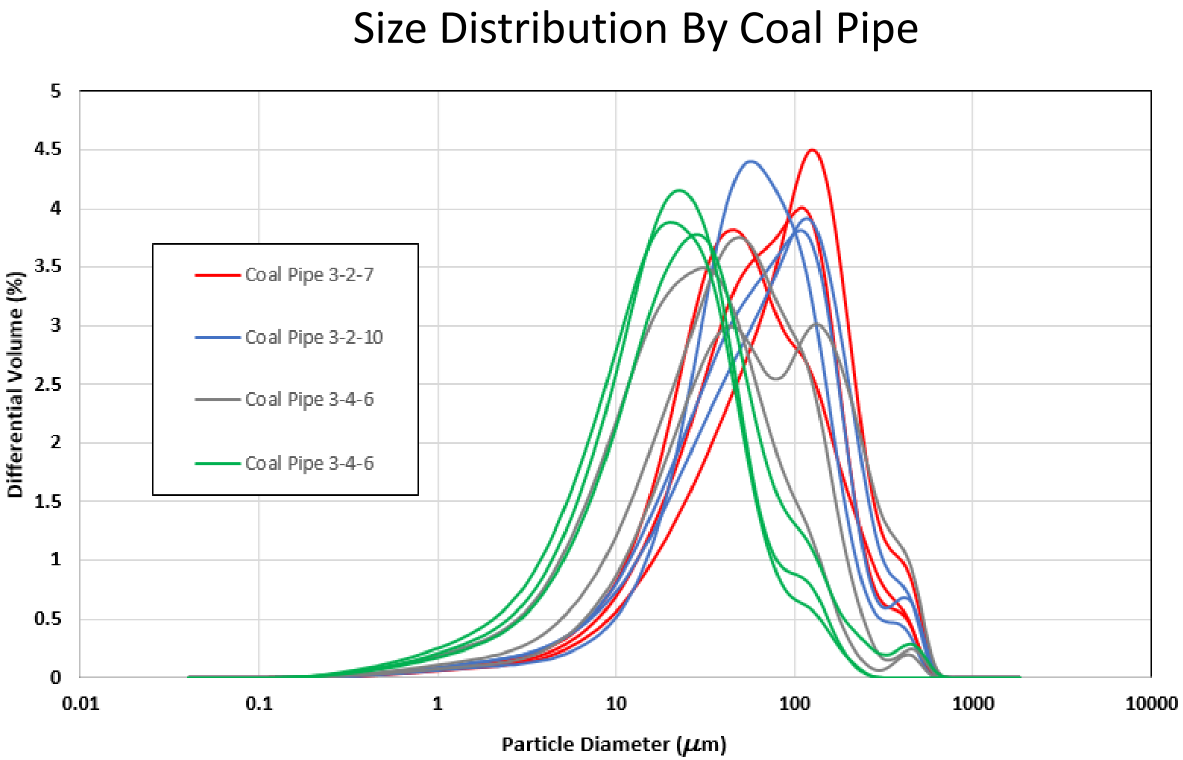

- It appears that the particle size distribution is correlated more with coal pipe than sample time
- Probably due to geometry of outlet in the classifier

Pulverizer Particle Size Distribution (PSD)

- Red – Mostly Coal
- Blue – Biomass Blend
- Grey – Mostly Coal

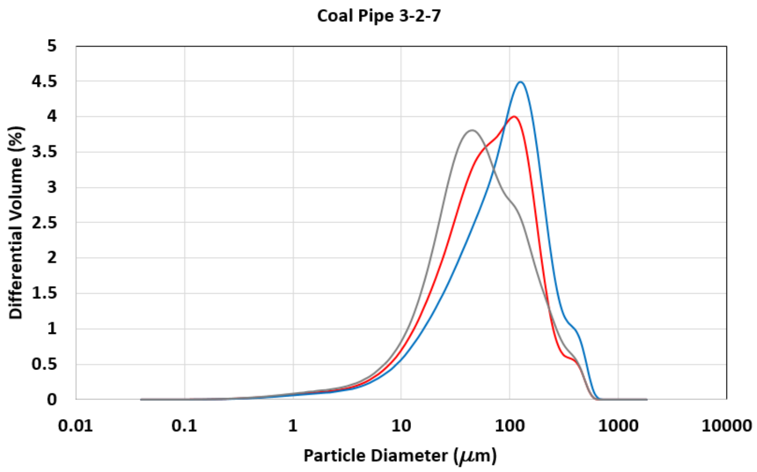
Coal Pipe 3-2-7

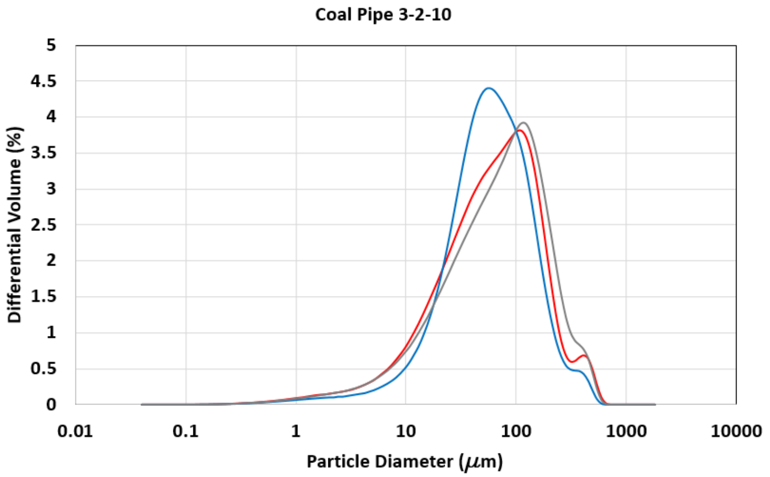
Coal Pipe 3-2-10

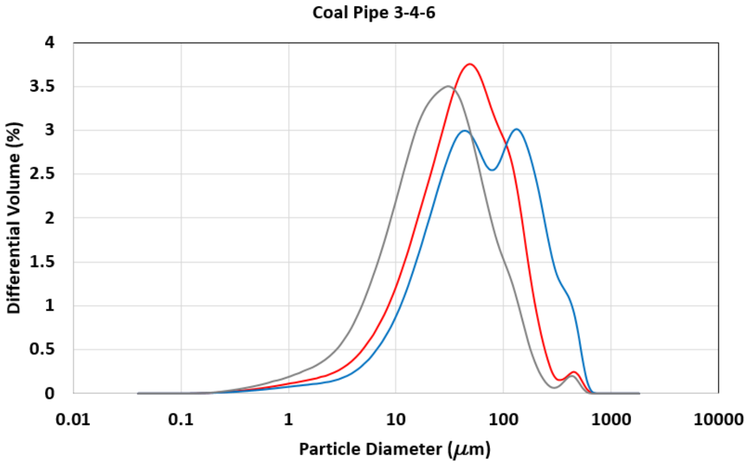
Coal Pipe 3-4-6

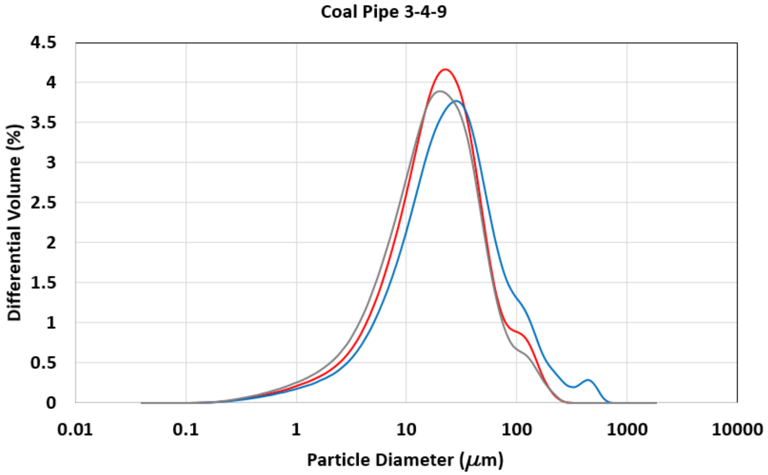
Coal Pipe 3-4-9

- Generally, the biomass blend results in shifting the PSD to larger sizes

Pulverizer Pyrites

The flow increased and composition changed of pyrites from **mill 3-4** during the blend test

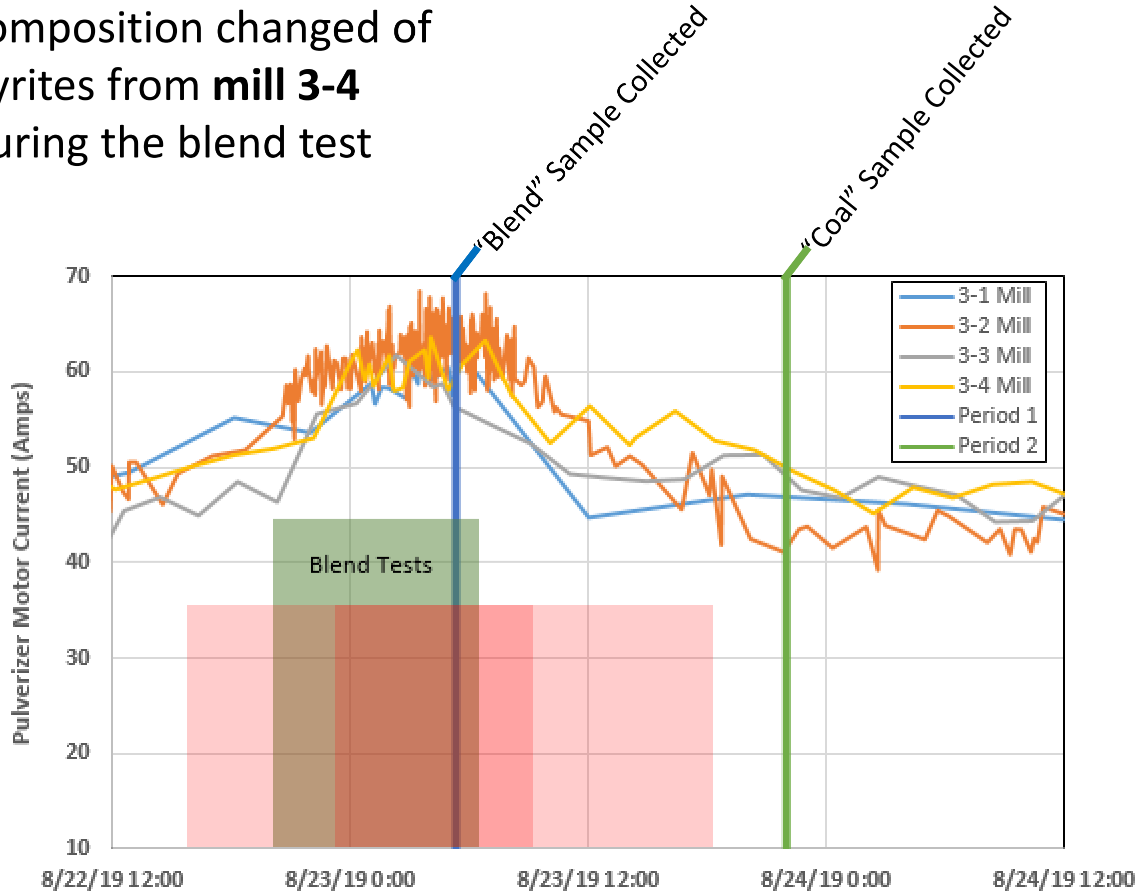

"Blend" Sample

"Coal" Sample

- Each sample was split into constituents and the mass of each was determined
- It was determined by plant operators that the mass flow of pyrites significantly increased during the blend test

Pulverizer Pyrites


1
Unburned coal


2
Dark gray rocks


3
Gray rocks


4
Wood pellets

"Blend" Sample

Sample	Mass %
1	33.3
2	35.4
3	28.2
4	3.1


1
Unburned coal


2
Dark gray rocks


3
Gray rocks


4
Light-color rocks

"Coal" Sample

Sample	Mass %
1	10.3
2	23.0
3	55.9
4	10.8

Gas Composition Measurements

Gas Composition Measurements Methodology

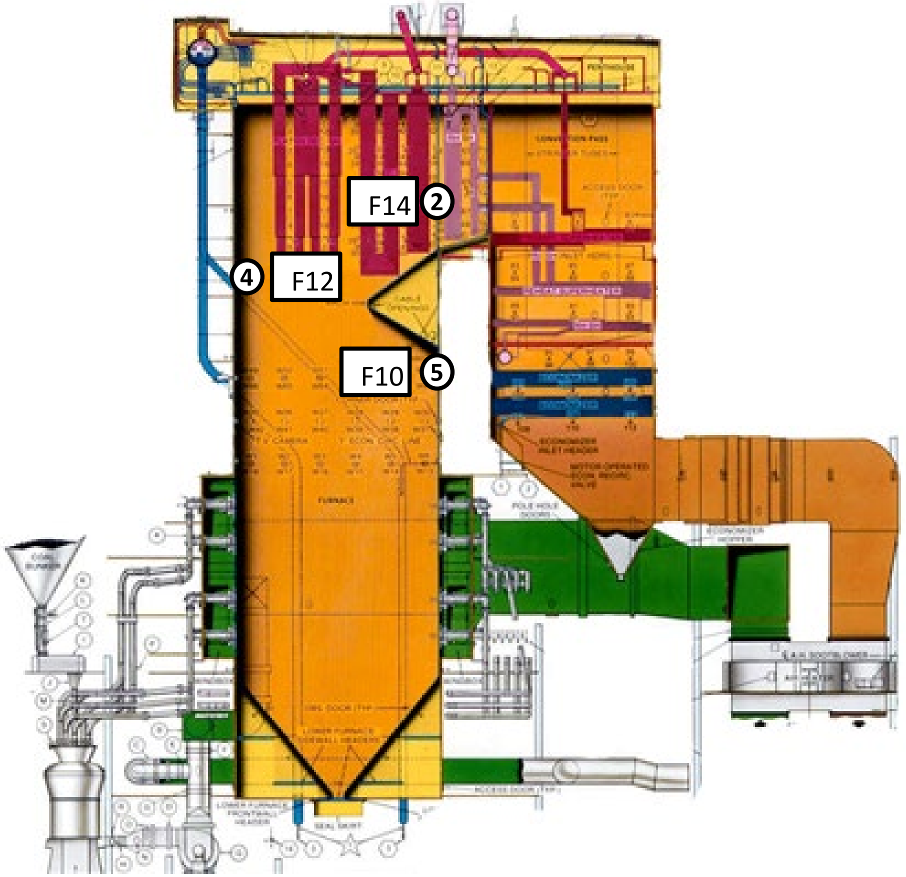

- Measured on floor 10, 12 and 14 (Port 5, 4, and 2 respectively).
- Three positions (depths) in each port.
- Gas samples taken using a temperature controlled probe.
- Analyzed using a FTIR and paramagnetic analyzer.

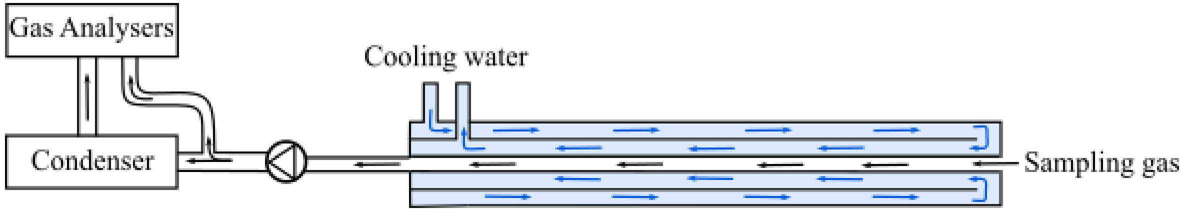

Gas Composition Measurements (O_2 & CO)

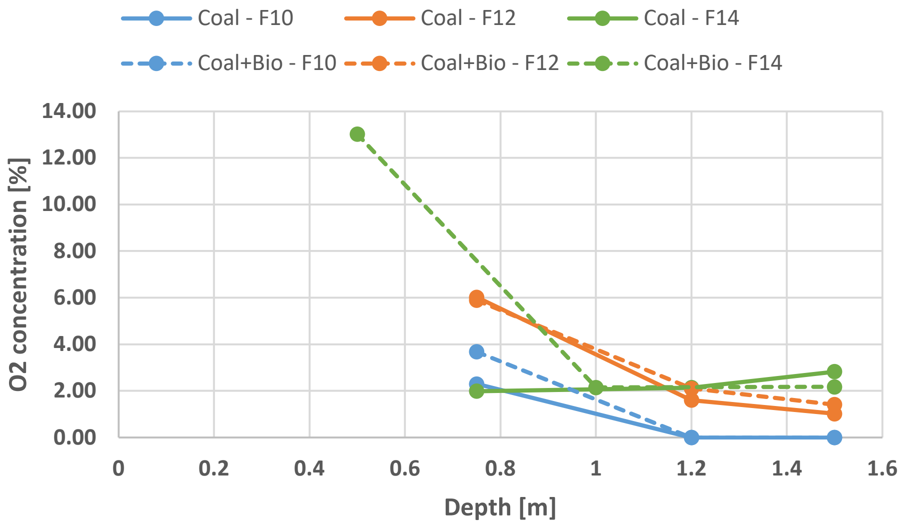

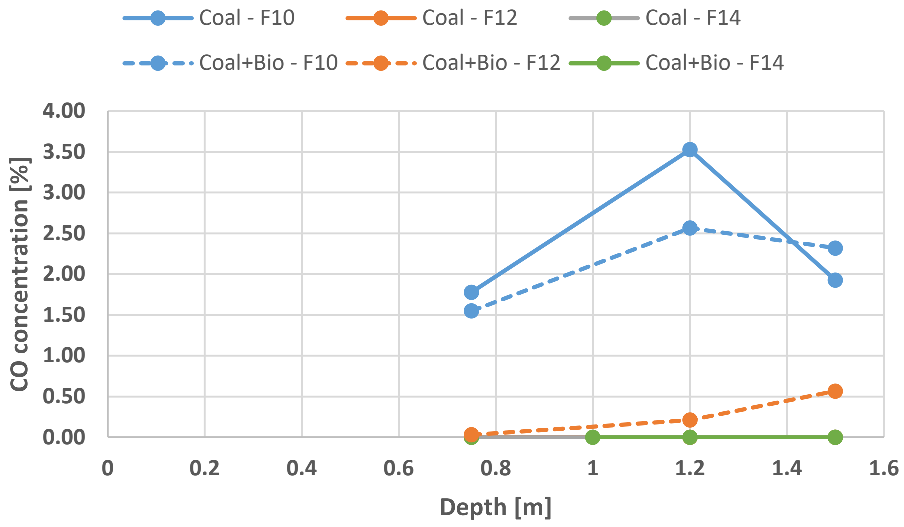

- Risk of air dilution from the port opening if to close to the wall.
- Some variations depending on the sampling depth

Gas Composition Measurements (O_2 & CO)

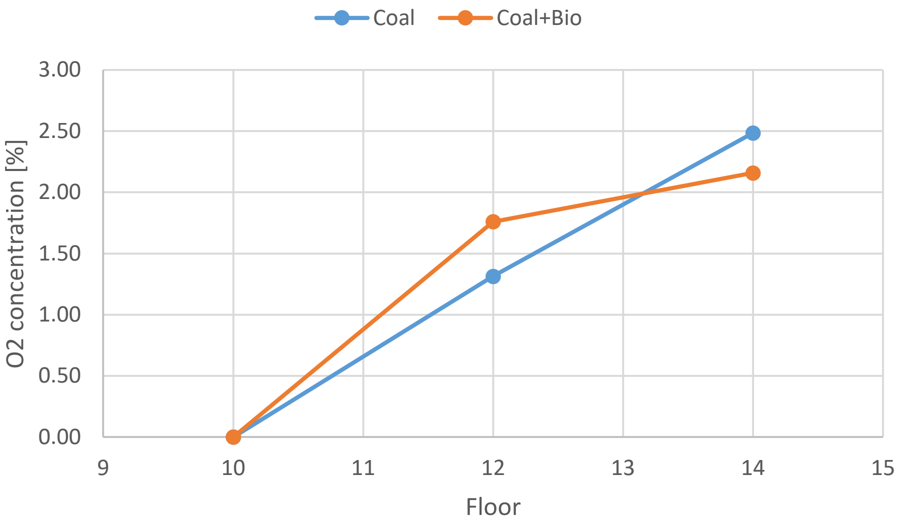

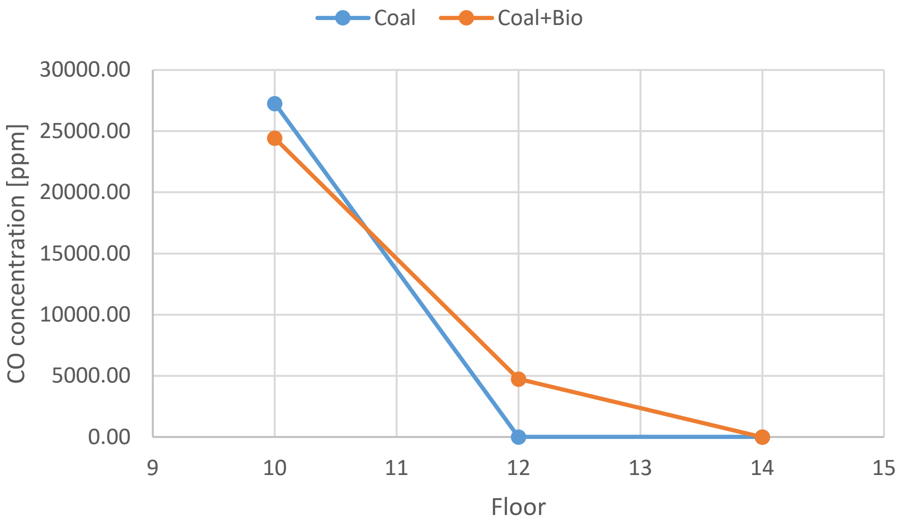

- Average values of the inner most positions in each port.
- Some combustion still at floor 12 in both cases.
- Slight change in the combustion due to the addition of biomass
- PI Data suggested that CO is 4x higher for the biomass combustion condition.
  - CO production and consumption is highly sensitive to fuel-air mixing and therefore is dependent on where it is measured

Gas Composition Measurements (NO_x)

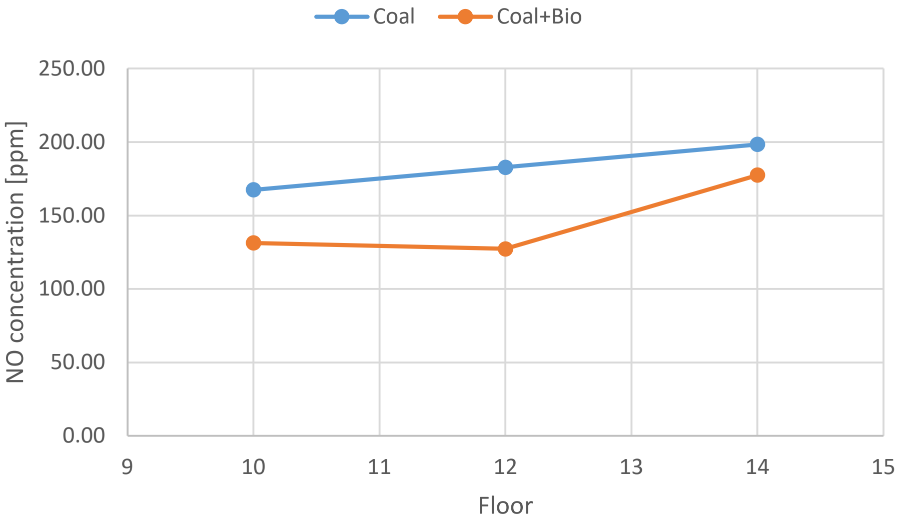

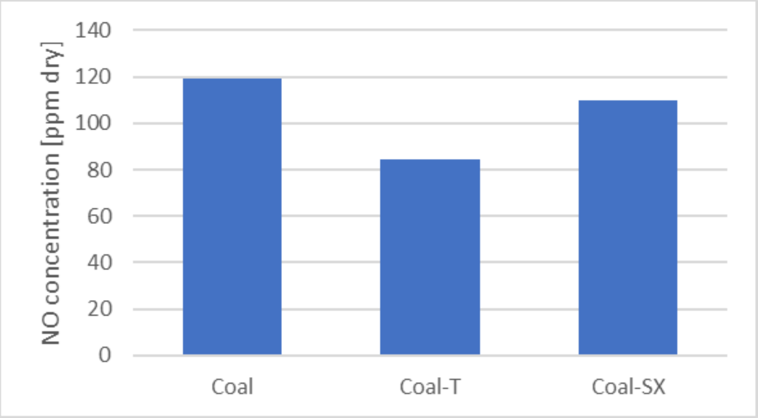

Result from the L1500 campaign

- NO_x concentration is 89.5% of the baseline condition while firing biomass at floor 14.
  - This measurement is consistent with plant measurements in PI data (88.6%).
- Not as high as the difference found during the L1500 test but still higher than what could be allocated to the 6% lower n-content in the fuel during co-combustion.

Gas Composition Measurements (SO_2 & HCl)

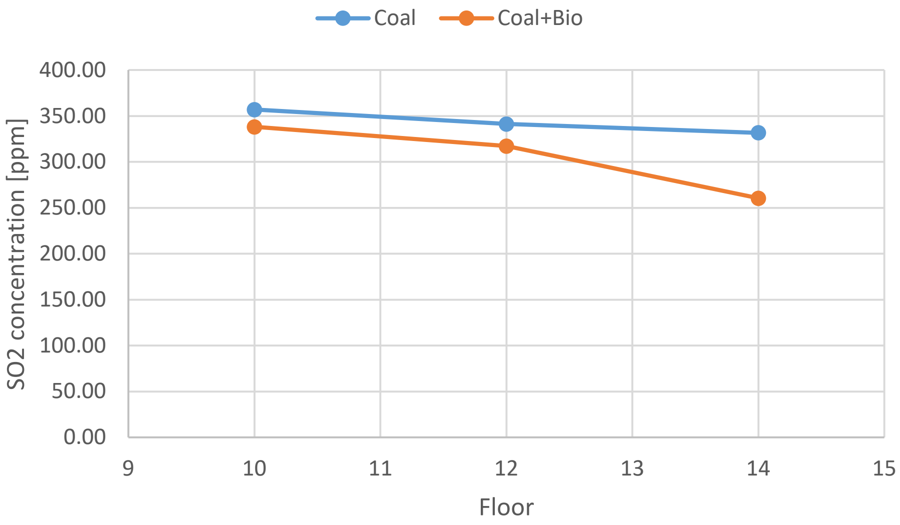

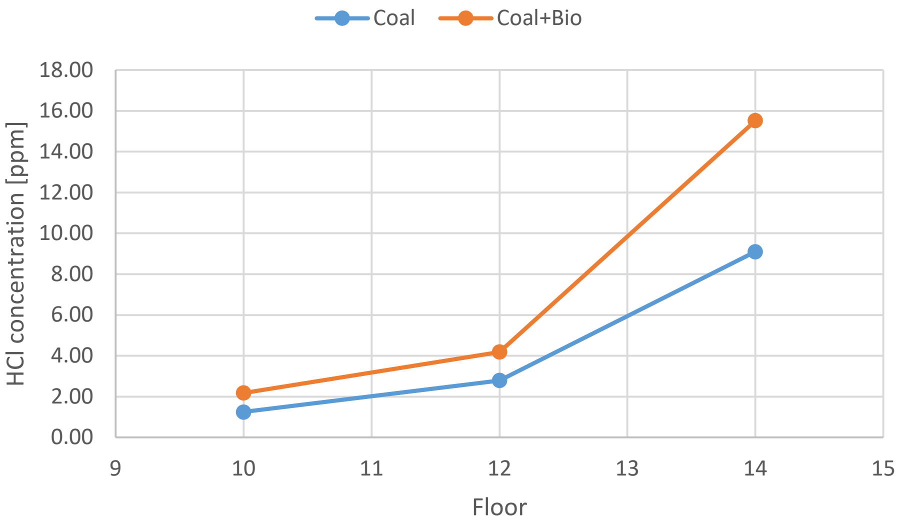

- SO_2 concentration was found to be 78.5% of the baseline concentration while combusting the biomass blend at floor 14.
    - PI data suggested it was 71.9% of the concentration
- Decrease in SO_2 concentration going from floor 10 to 14 in both cases.
    - This could be due to mixing, but adsorption on deposits is also possible
- HCl concentration was found to be 170% of the baseline concentration.
- A larger difference between the cases found at floor 14 compared to floor 10 and 12 for both SO_2 and HCl.

Gas Composition Measurements (Soot Blowing)

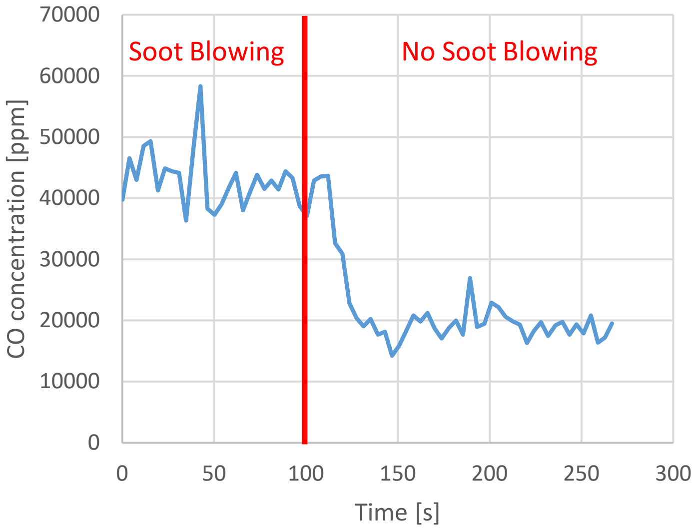

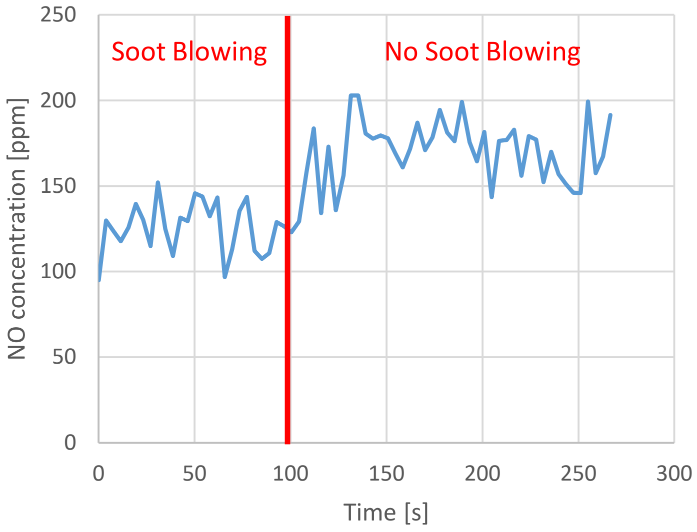

- Continuous measurement started at floor 10 (1.5m from wall) with one of the soot blowers active.
- Soot blowing stopped after 100s.
- CO and NO are affected by the soot blower but not the SO_2 concentration.

Entrained Ash Sampling

Particle Sampling Methodology

Berner Low-pressure Impactor (BLPI)

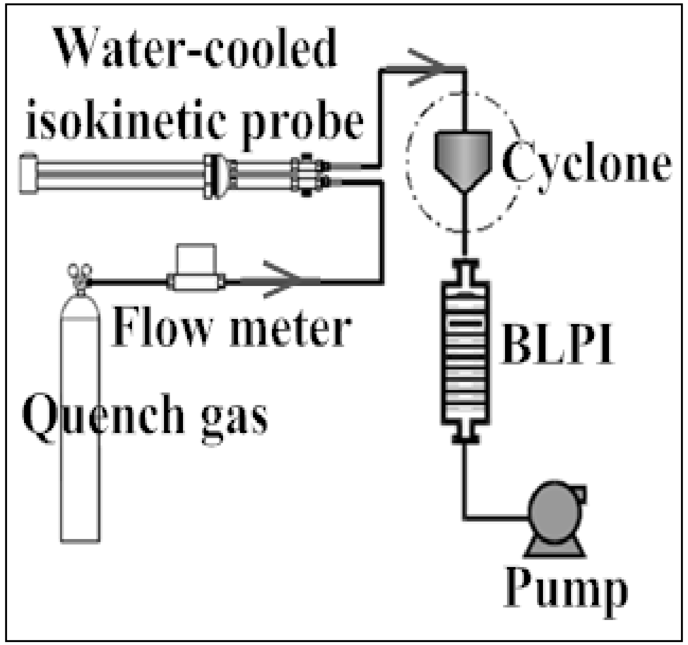

BLPI: 0.0324 – 7.33 µm
10 cutoff diameters

Collects size-segregated entrained ash samples for later gravimetric and chemical analysis

Scanning Mobility Particle Sizer (SMPS)
Aerodynamic Particle Sizer (APS)

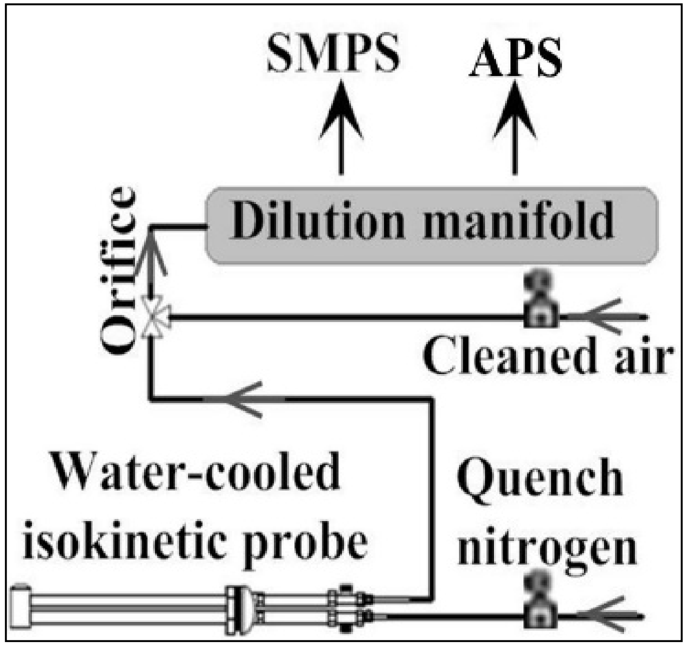

SMPS: 0.0143 – 0.6732 µm
APS: 0.532 – 20 µm

Collects real-time entrained particle size distribution data

Particle Sampling Methodology

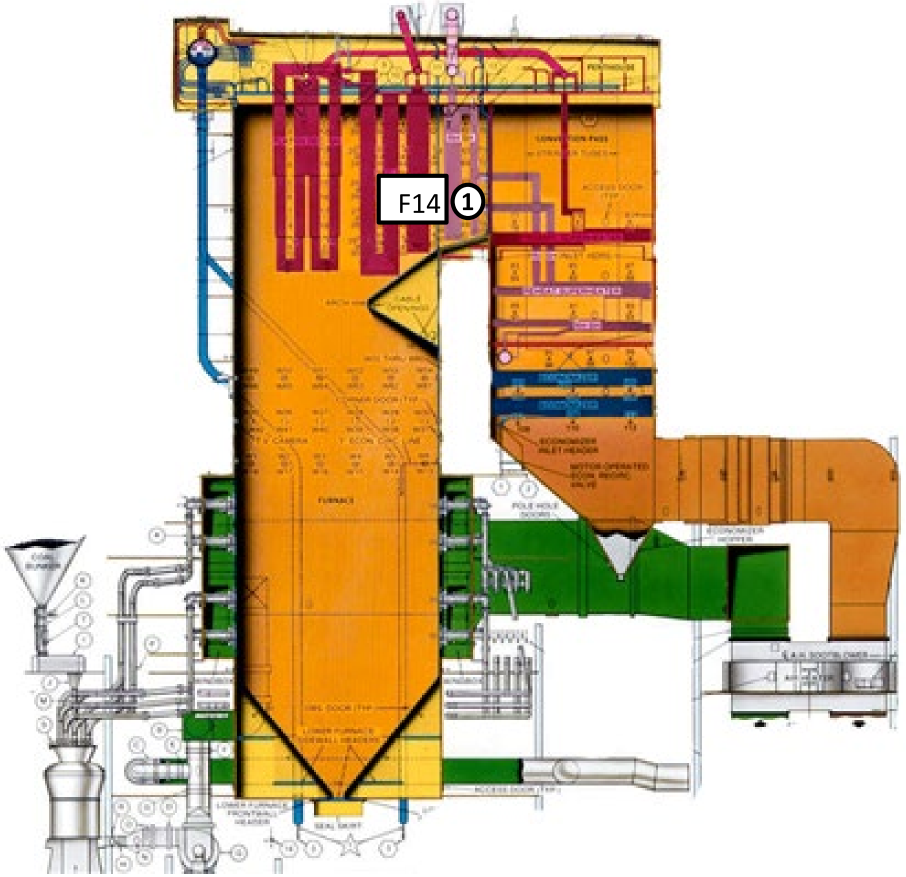

Ash aerosol particle size distributions (Sufco vs. Blend)

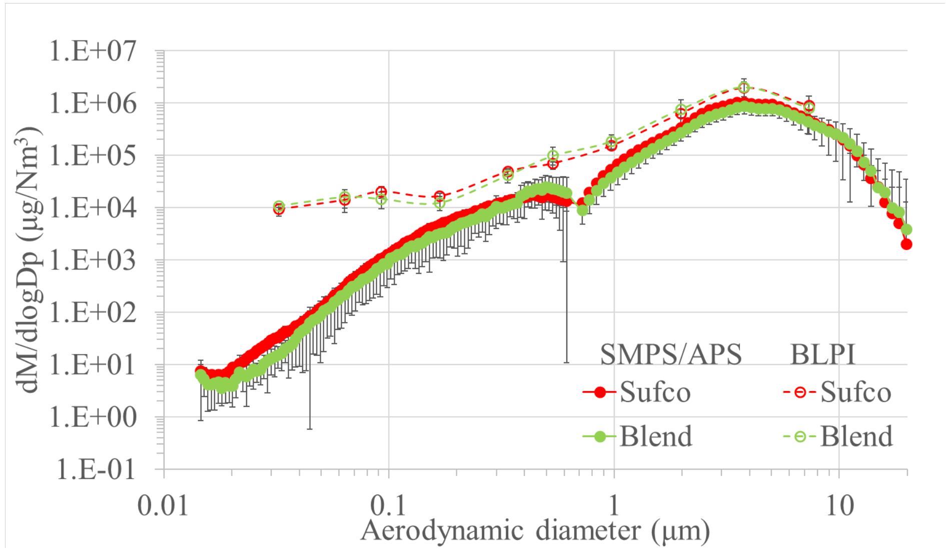

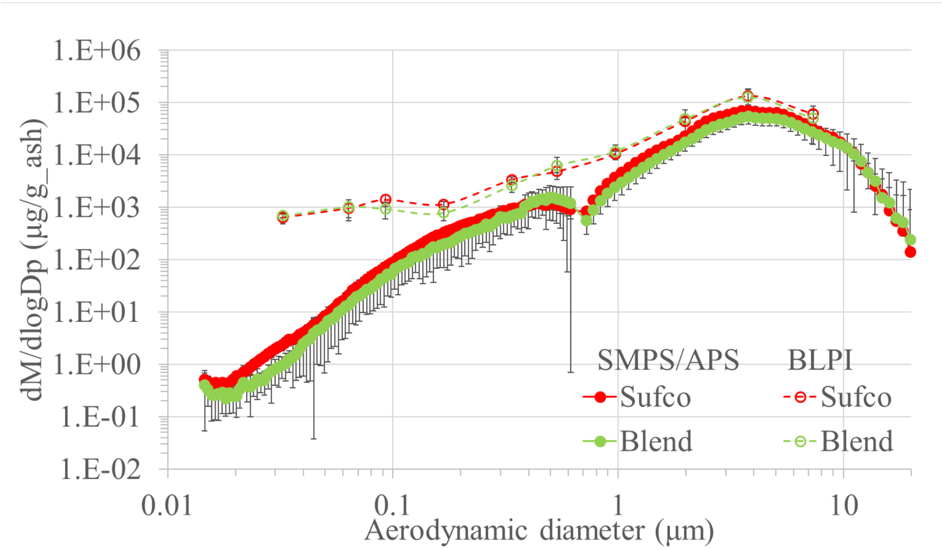

- Aerosol PSDs show little change between two cases
- Co-firing case has slightly lower concentration of PM_{10}.

Ash aerosol particle size distributions

(Soot-blow vs. Non-soot-blow; Sufco combustion)

Mass Concentrations

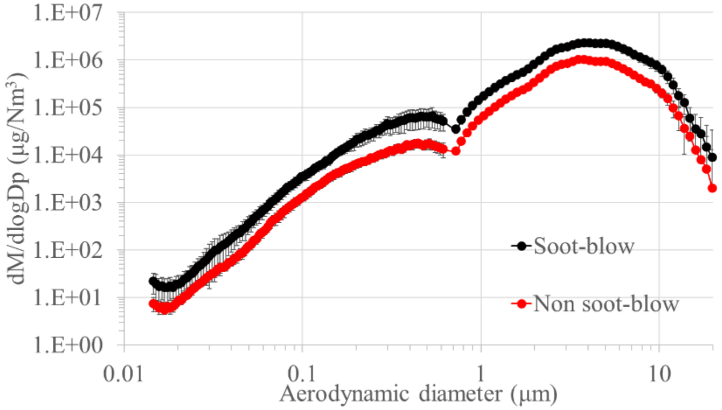

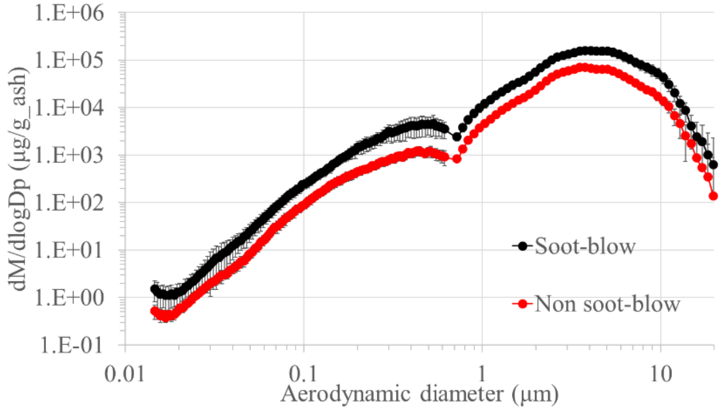

Number Concentrations

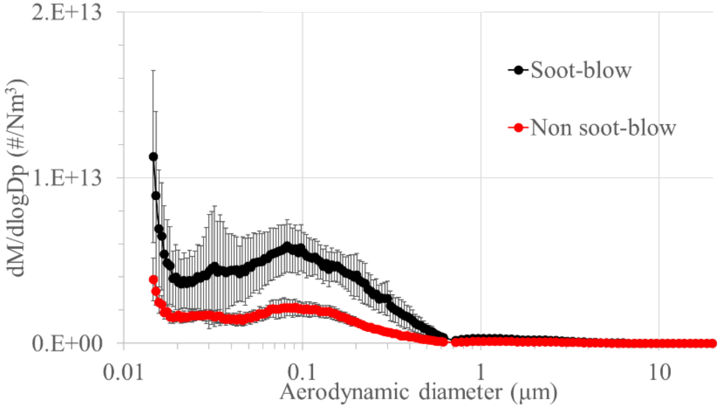

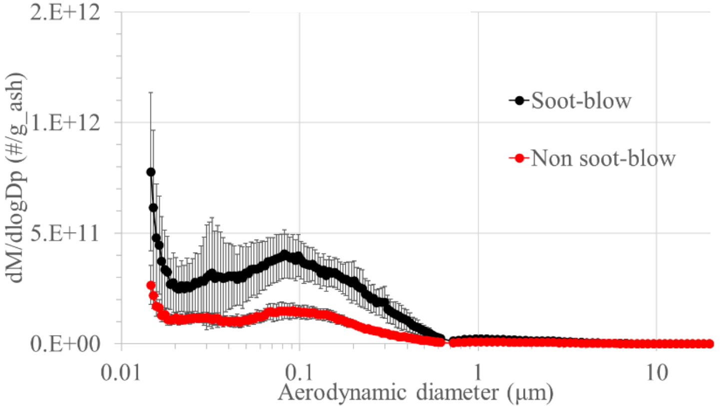

- Particle concentration in flue gas is increased during soot blow operation.
- More PM_1 particles are entrained in flue gas by soot blow.

Particle size segregated compositions (Sufco vs. Blend)

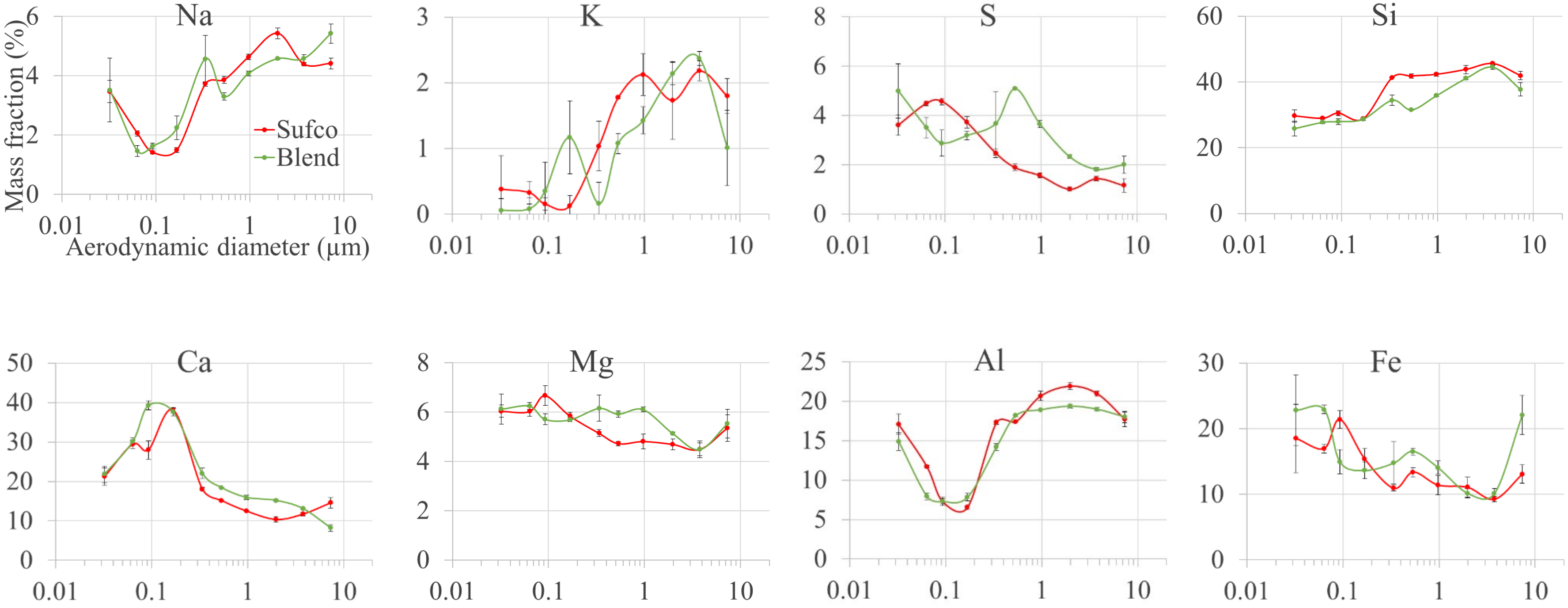

- No significant change in the compositions of PM_{10} between the coal combustion and co-firing.
- Sulfur is the most affected element, which is increased in PM_{10} and decreased in gas phase (Slide 35) when co-firing.

Particle size segregated compositions

(Soot-blow vs. Non-soot-blow; Sufco combustion)

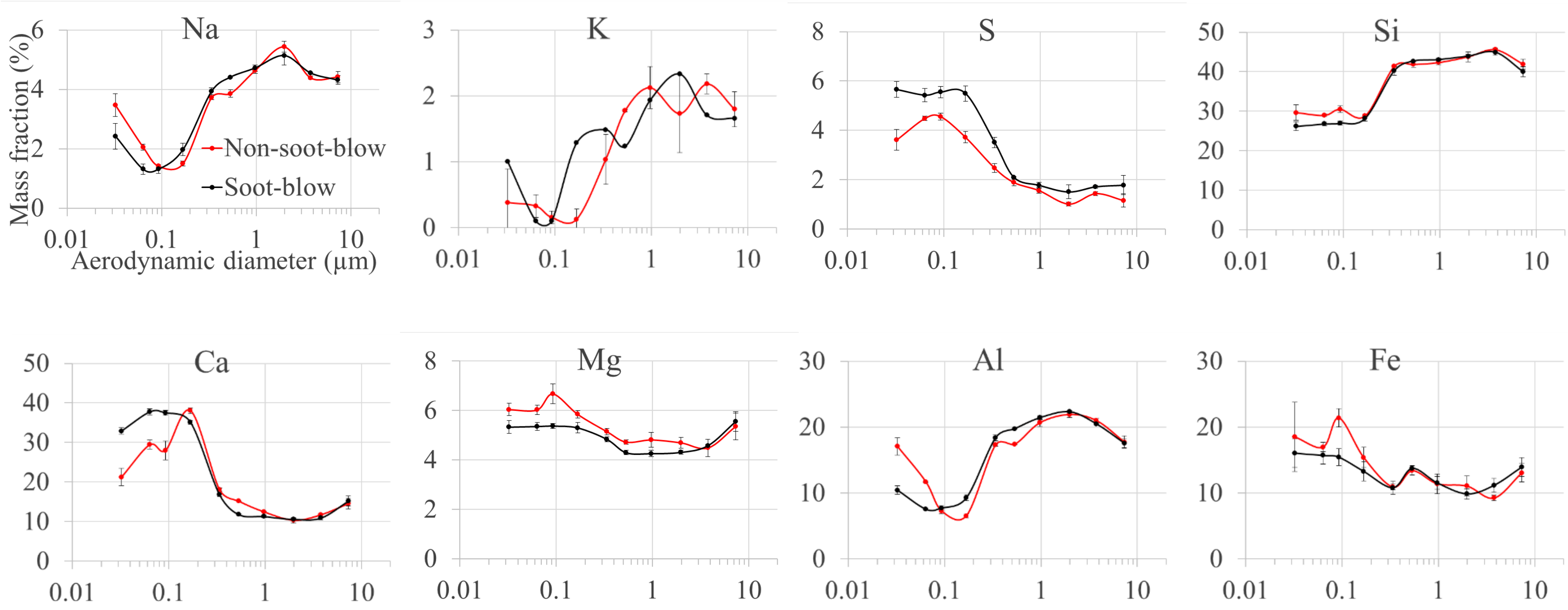

- PM$_{10}$ blown down from steam tube deposits have similar compositions of those in flue gas.
- Higher sulfur contents during soot blow suggests enriched sulfates in ash deposits.

Compositions of cyclone ash (Sufco vs. Blend)

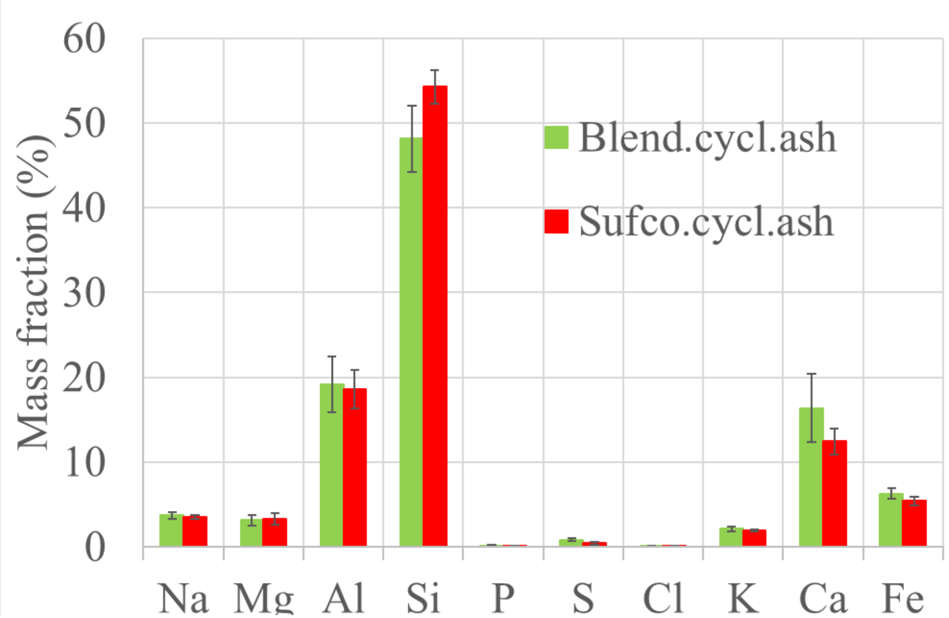

- Cyclone ash (particles > 10 µm) compositions are similar in two cases.
- Ash compositions reflect the raw ash analysis of the coal and torrefied wood (lower Si and higher Ca in wood).

SEM images of cyclone ash

Coal

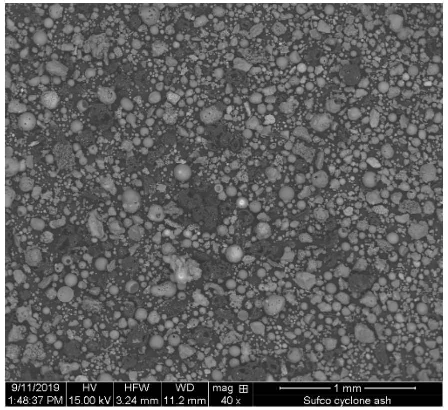

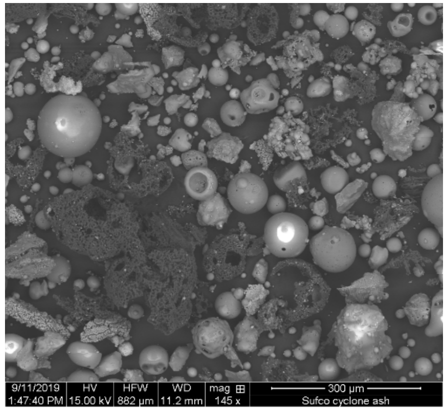

Blend

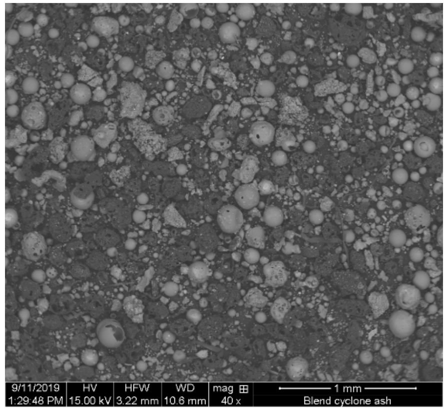

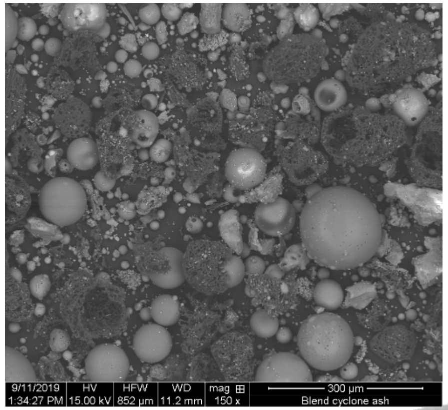

- Cyclone ash (particles > 10 µm) does not change much difference between two cases.
- More chars in blend case?

Deposited Ash Sampling

Deposit Sampling Methodology

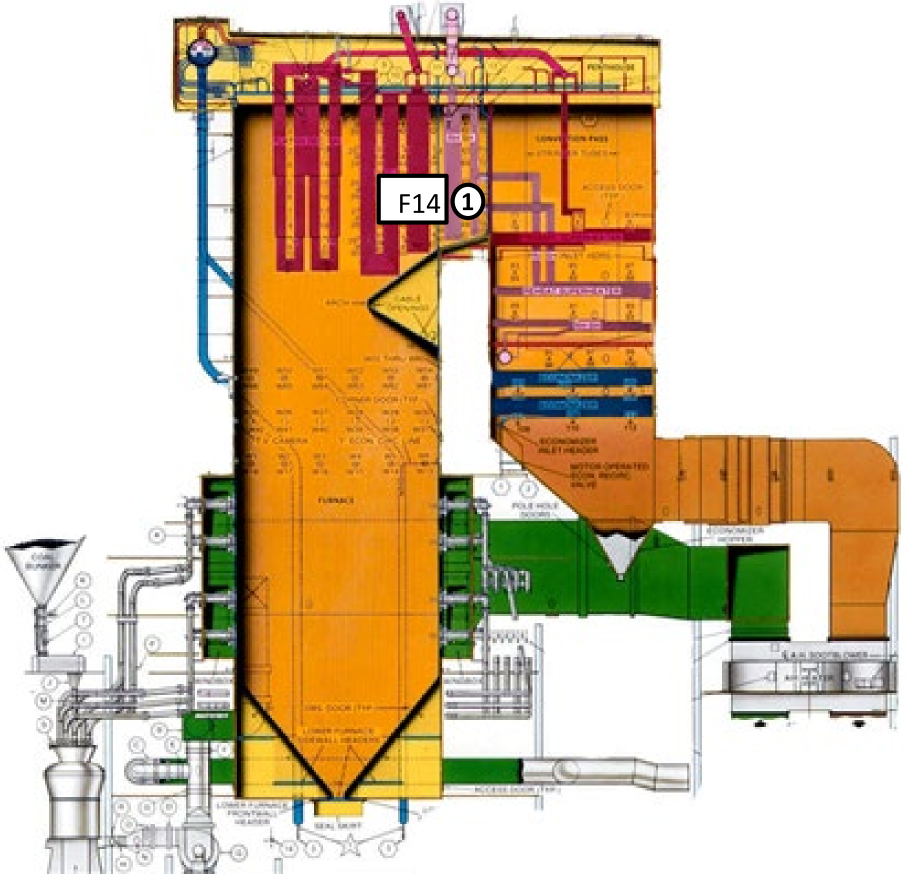

Ash Deposit Samples were collected for 30, 60 and 90 minutes during biomass blend combustion and pure coal combustion

Deposition Measurement

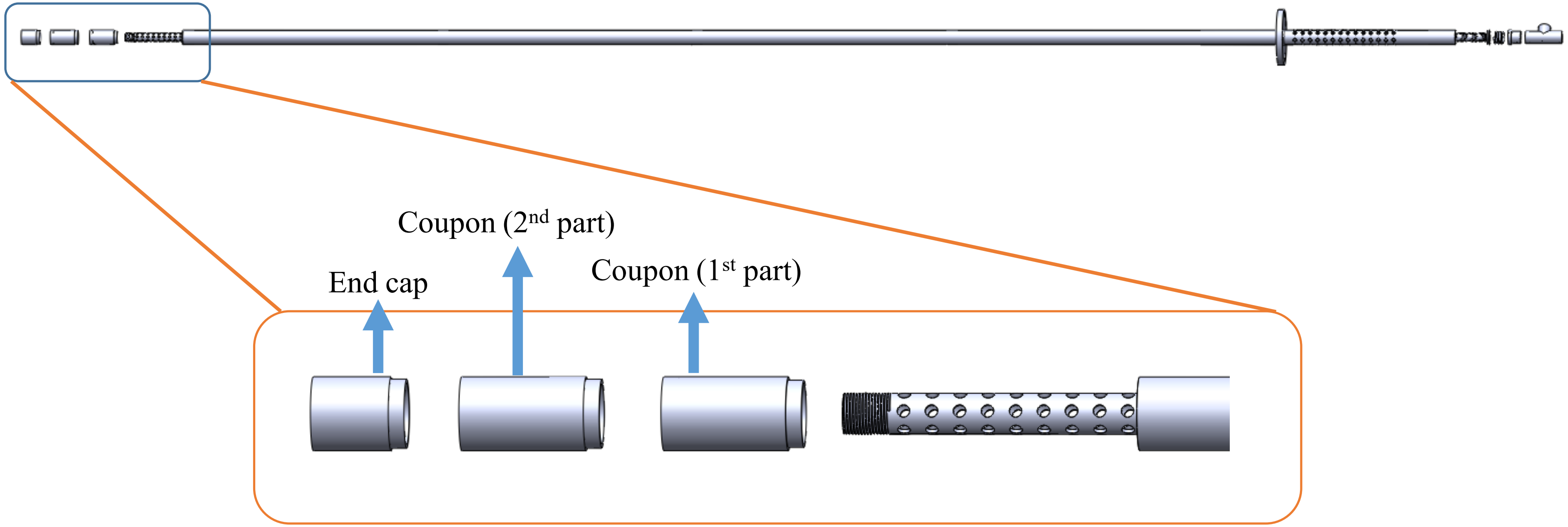

Coupon (2nd part)

End cap

Coupon (1st part)

Coupon includes two parts to facilitate inserting the sensor of thermocouple into the first part of coupon. The internal surface of first part of coupon has a hole to keep the sensor of thermocouple.

Deposition Rates

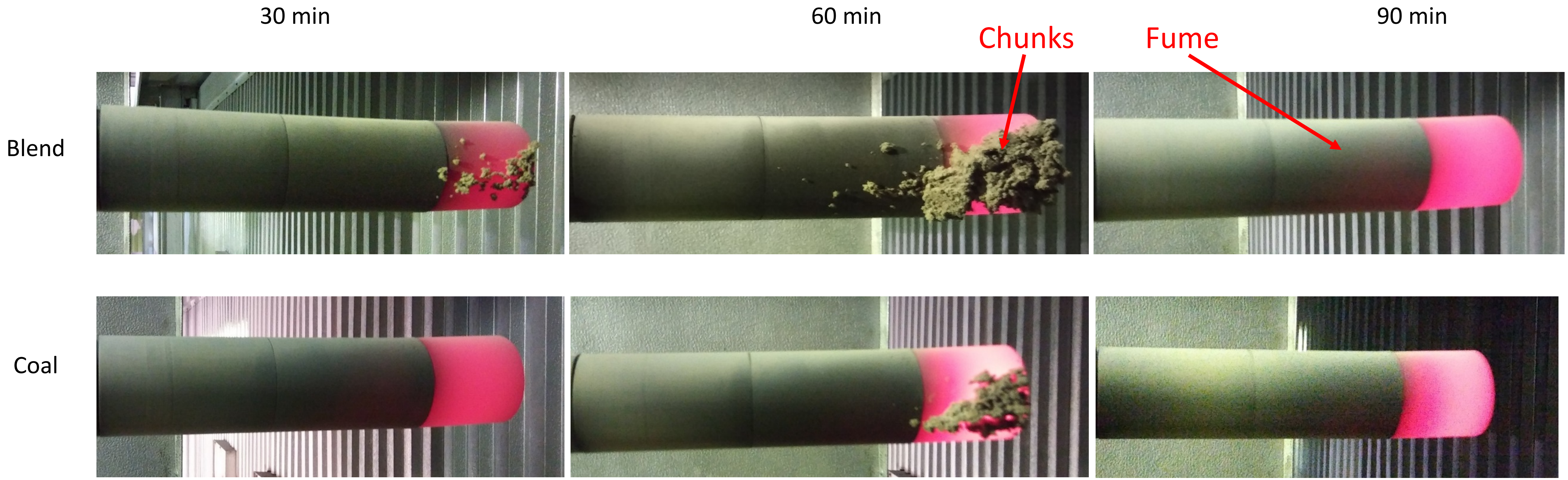

- Deposits were made up of two kinds of accumulation
    - Fume & Chunks (These were not observed in the L1500)
- Collected deposit included everything that was attached to coupon 1 & 2 including both fume and chunks (they were too difficult to separate)
- 60 minute blend sample was the only condition where chunks accumulated on the coupon

Deposition Rates

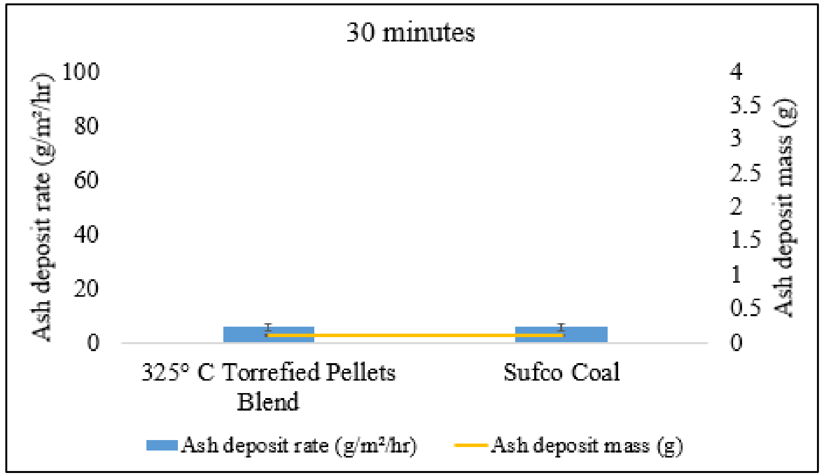

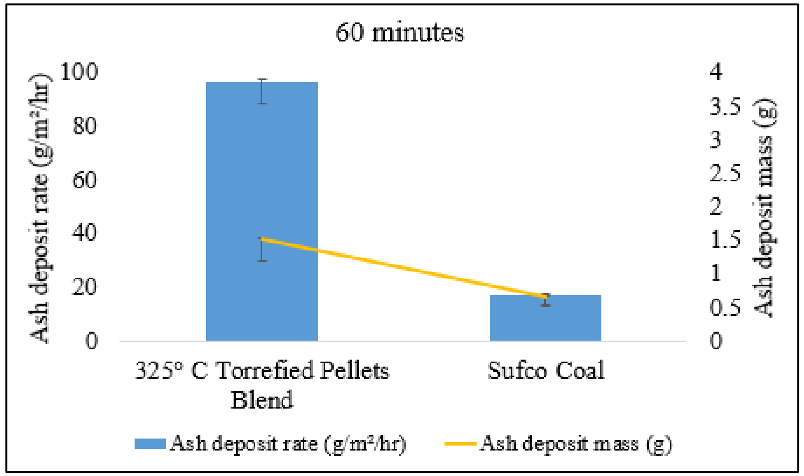

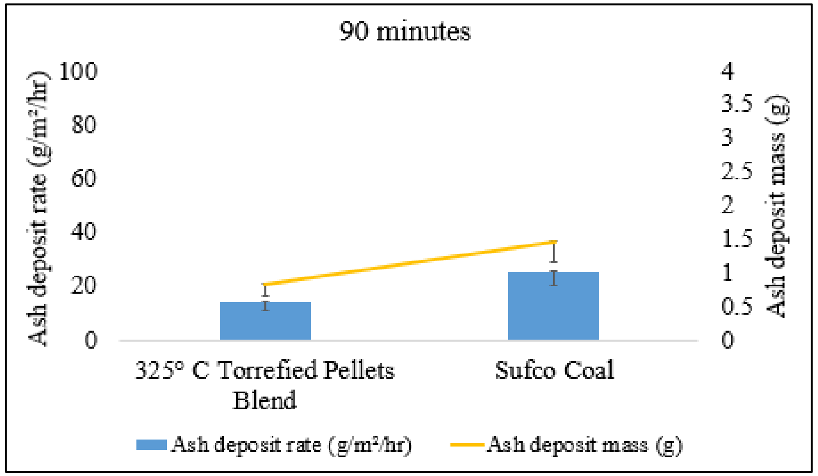

- Deposit rate behavior was similar to the L1500 testing.
  - Deposition rate was 56% of the baseline condition while firing biomass blend (90 minute sample time)
  - L1500 was approximately 91% of the baseline condition (90 min)

Compositions of ash deposits

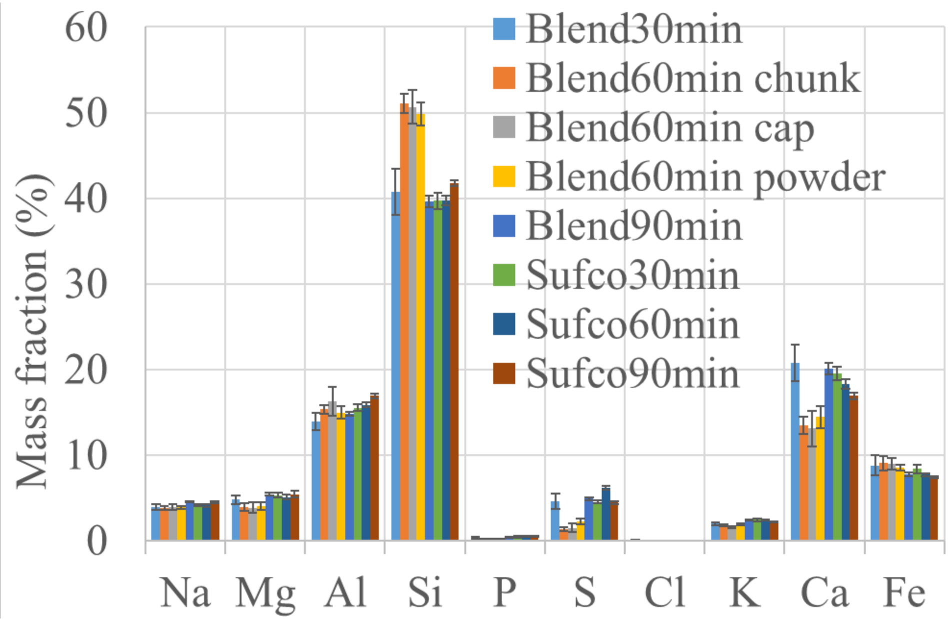

- The three types of deposits in 60-minute blend case show higher Si and lower Ca and S.
- Deposits in other cases (coal and blend) have similar compositions.

SEM images of ash deposits

Sufco 60 min

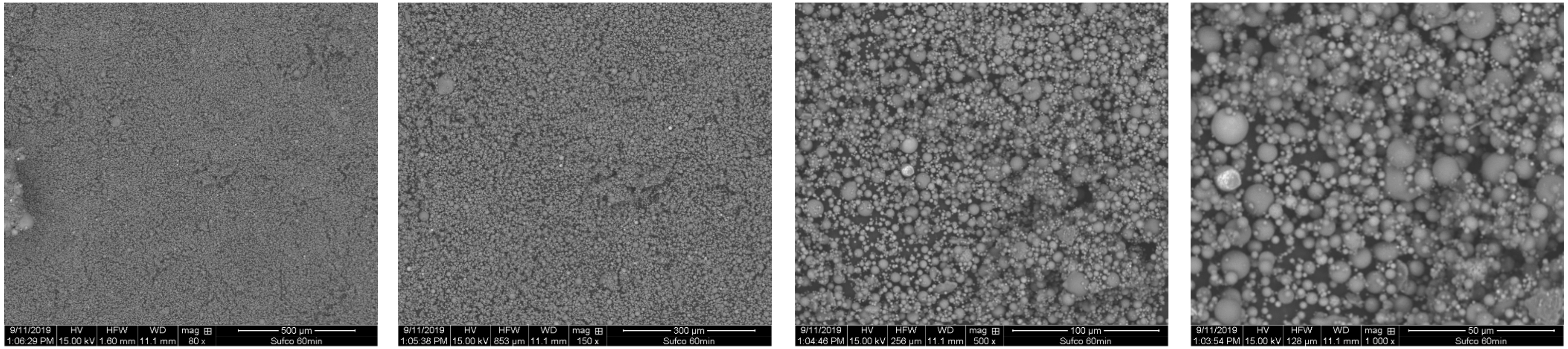

Increasing Magnification →

Sufco 30 min

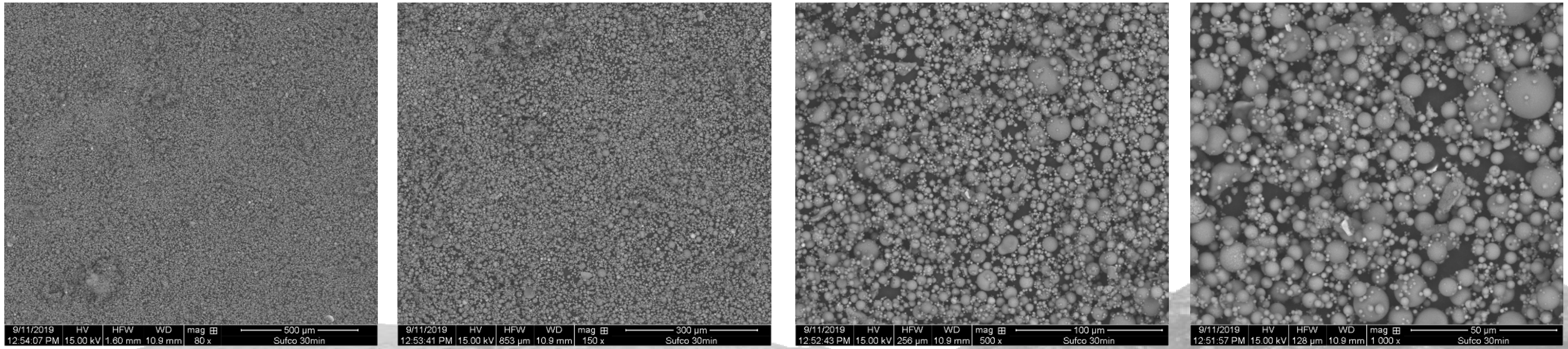

THE UNIVERSITY OF UTAH

SEM images of ash deposits

Blend 30 min

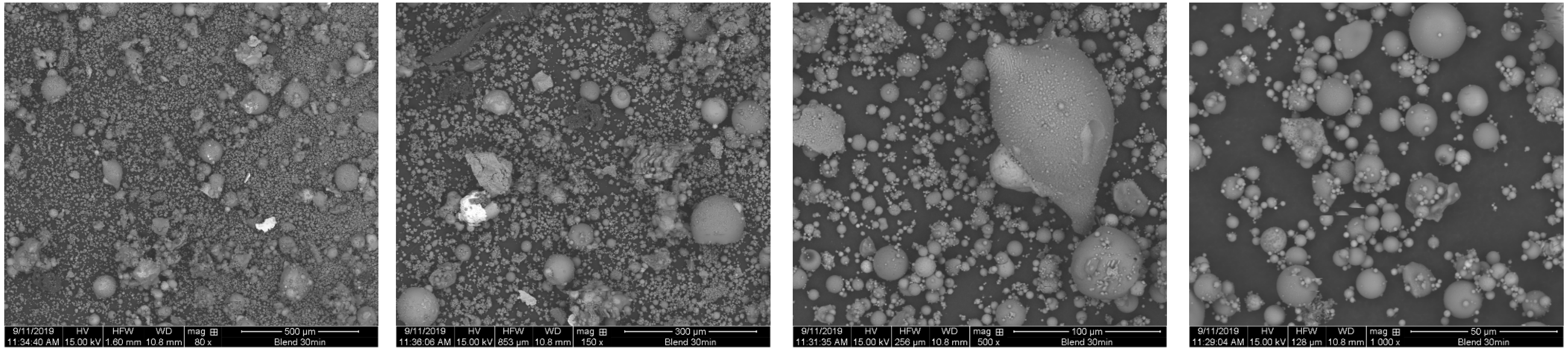

Increasing Magnification →

Blend 60 min (powder)

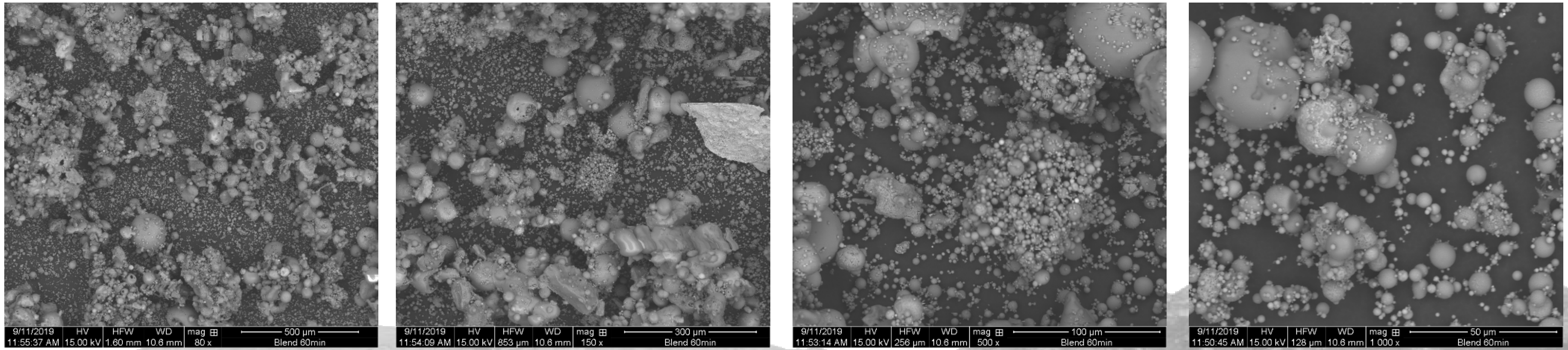

THE UNIVERSITY OF UTAH

BYU

SEM images of ash deposits

Blend 60 min (chunk)

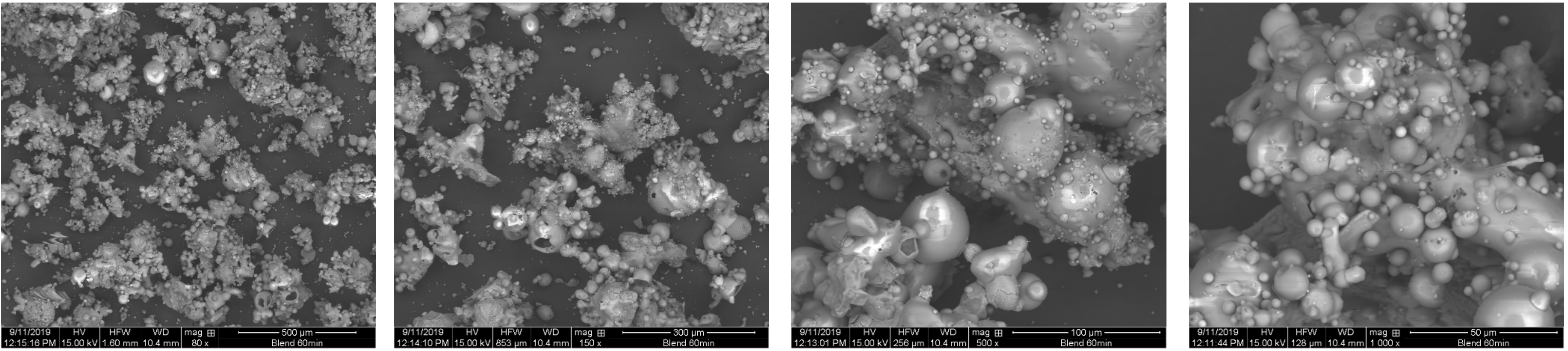

Increasing Magnification →

Blend 60 min (cap)

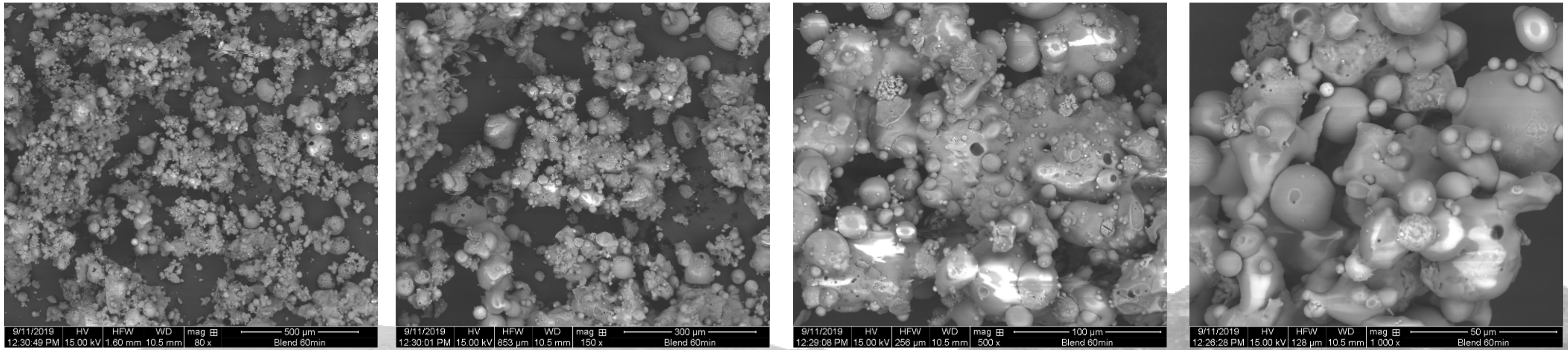

SEM images of ash deposits

Blend 90 min

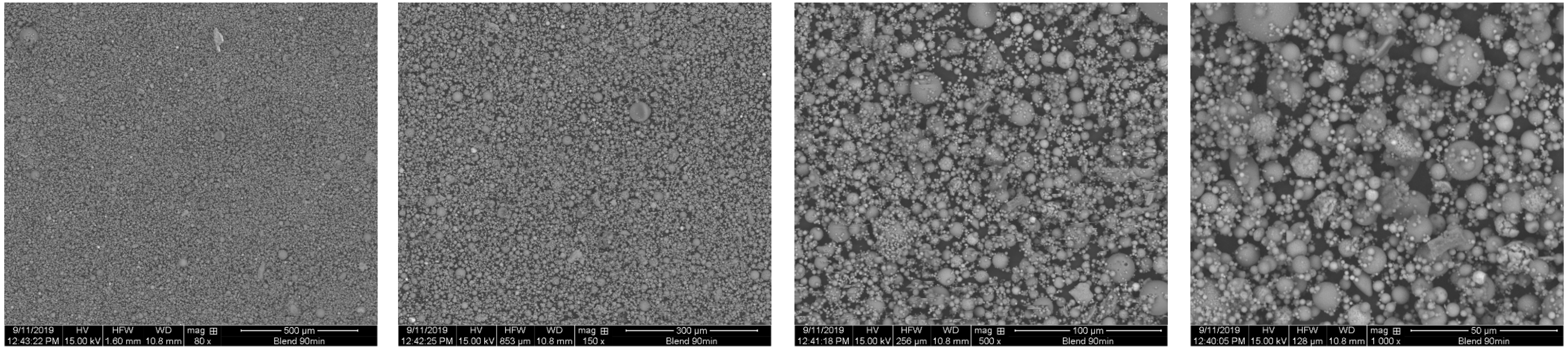

Increasing Magnification →

Sufco 90 min

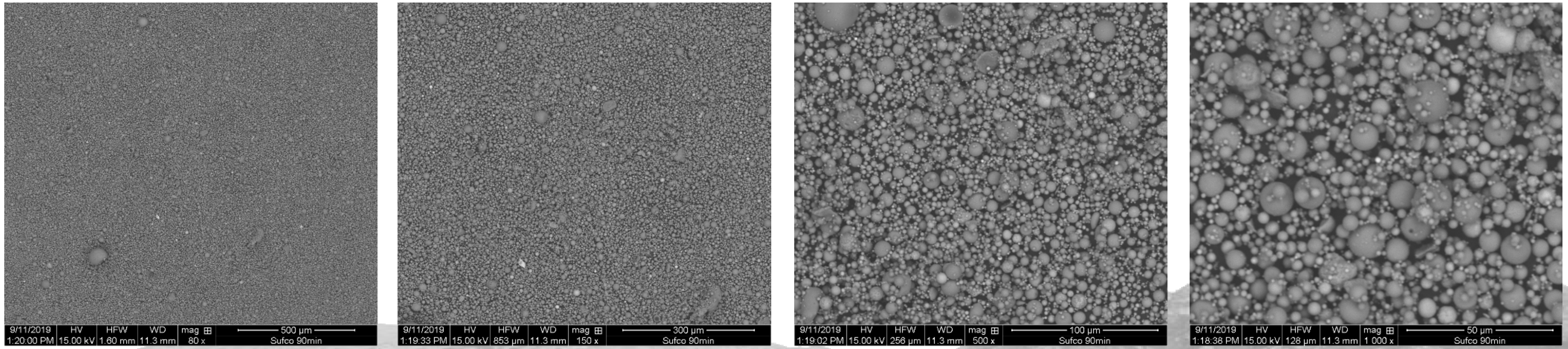

Baghouse Ash Sampling

Compositions of baghouse fly ash

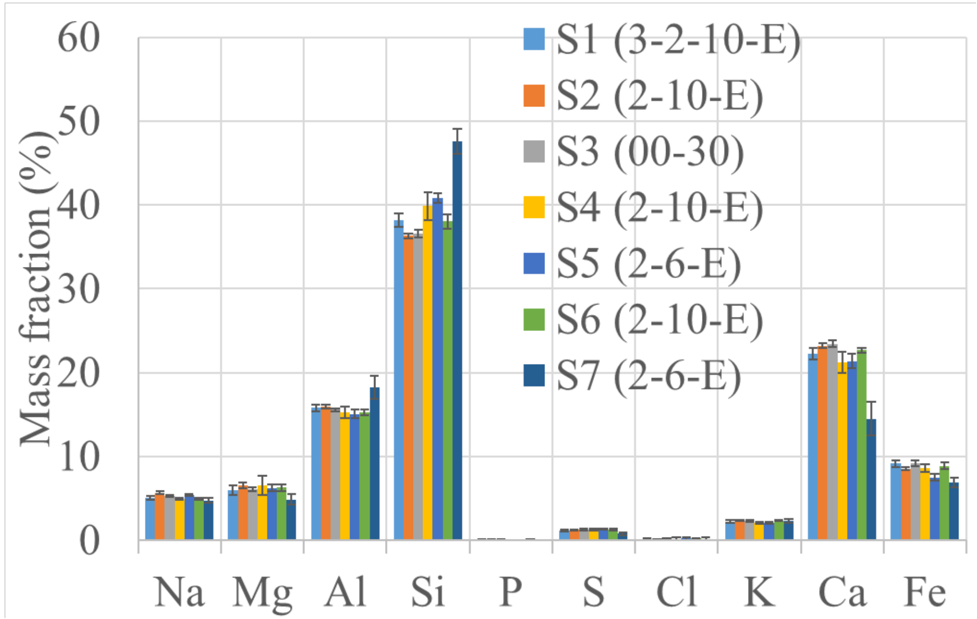

SEM images of baghouse fly ash

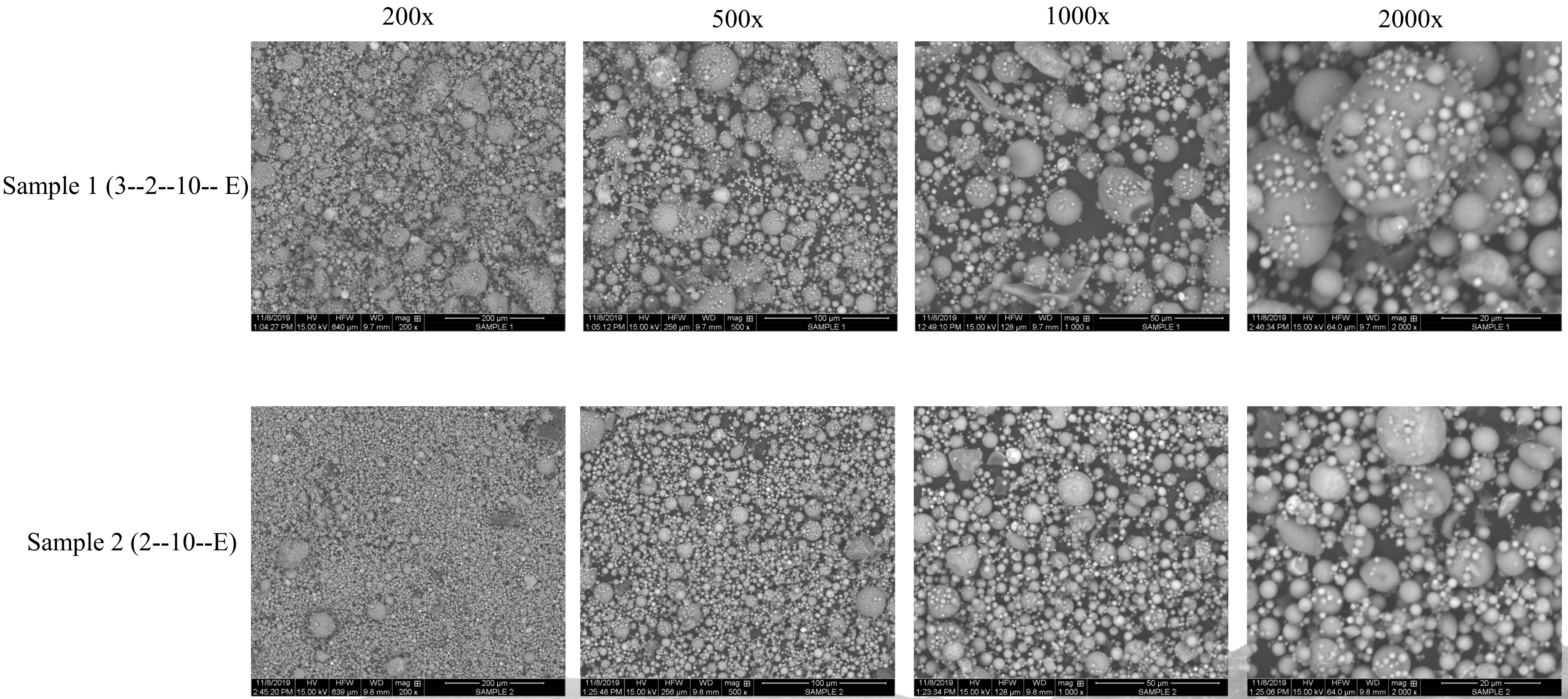

SEM images of baghouse fly ash

200x
500x
1000x
2000x

Sample 3 (00--30)

Sample 4 (2--10--E)

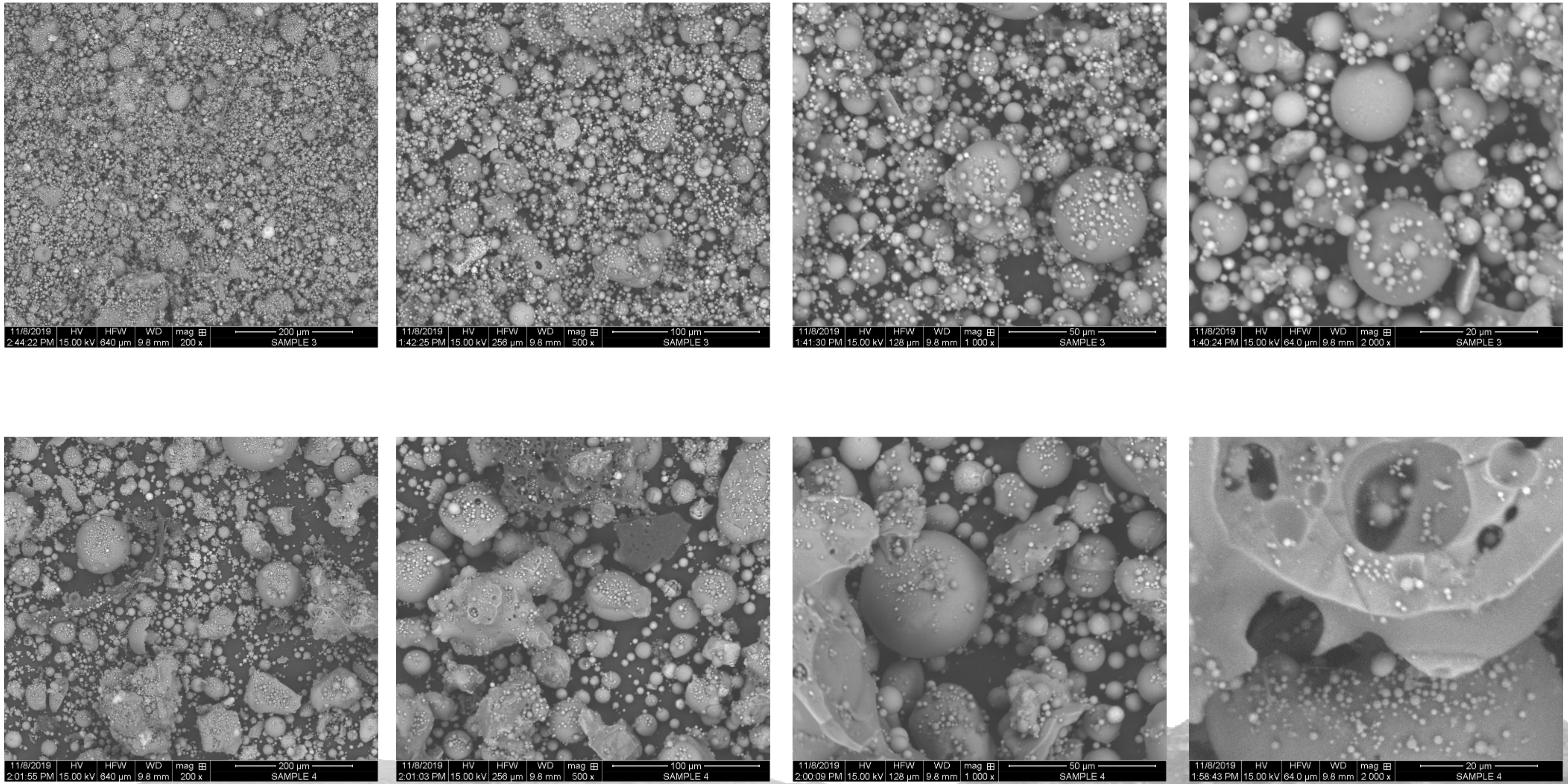

SEM images of baghouse fly ash

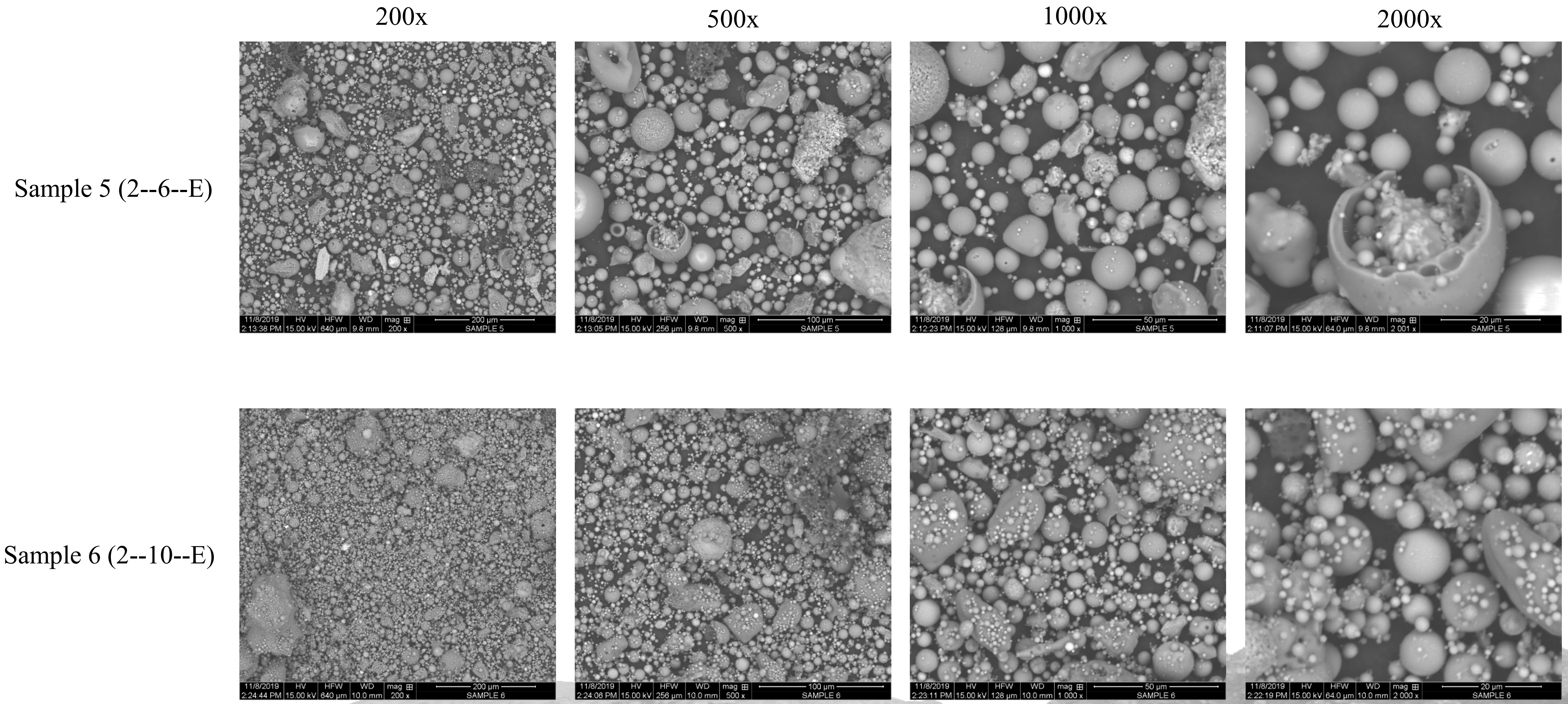

SEM images of baghouse fly ash

Sample 7 (2--6--E)

200x

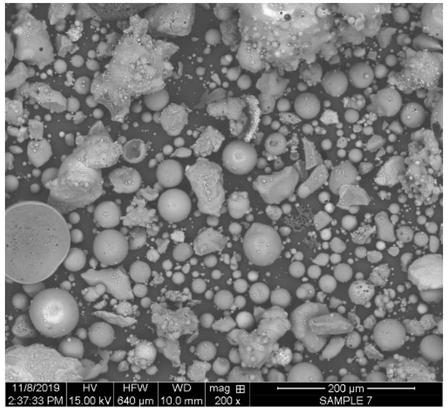

500x

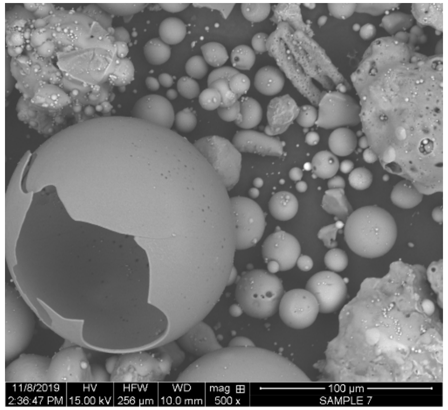

1000x

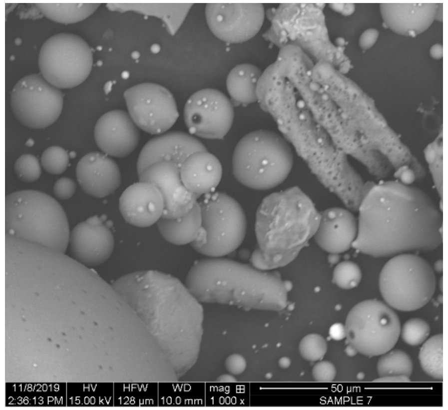

2000x

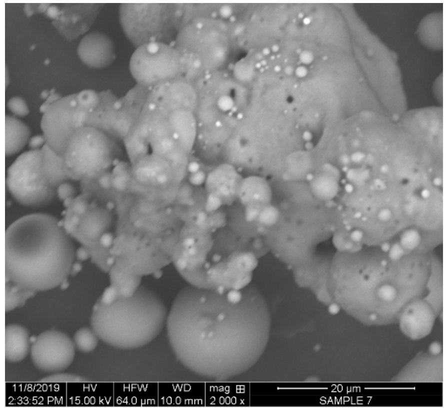

Radiation and Temperature Measurements

Radiation and Temperature Measurement Methodology

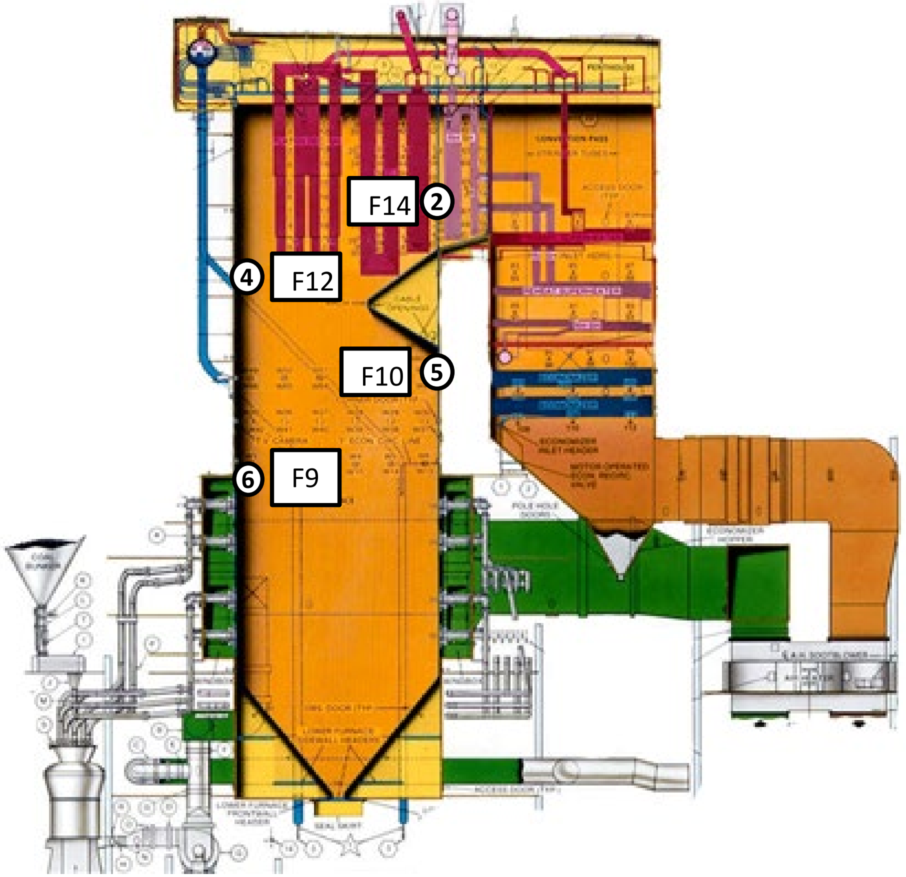

- Measured on floor 9, 10, 12 and 14 (Port 6, 5, 4, and 2 respectively).
- Temperatures were measured using either a suction pyrometer or shielded thermocouple
- Radiation Intensity was measured using two different narrow angle radiometers
- Radiation flux was measured using a hemispherical radiometer

Temperature Measurements

- Thermocouple (suction pyrometer without ceramic or suction)
- A few positions at each of the floors 10, 12 and 14
  - Approximate steps of 0.5 m (~20”) from the wall (0.5 – 1.5 m)

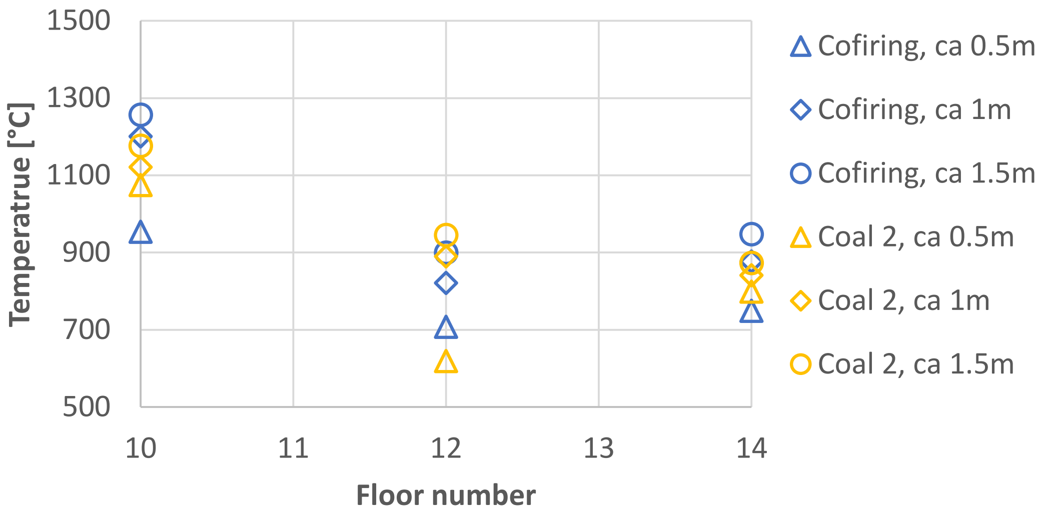

→ Coal and cofiring temperatures are similar
→ Highest measured temperatures at floor 10
→ In general: similar temperatures at floors 12 and 14

Radiative Heat Flux Measurements

(Method 1)

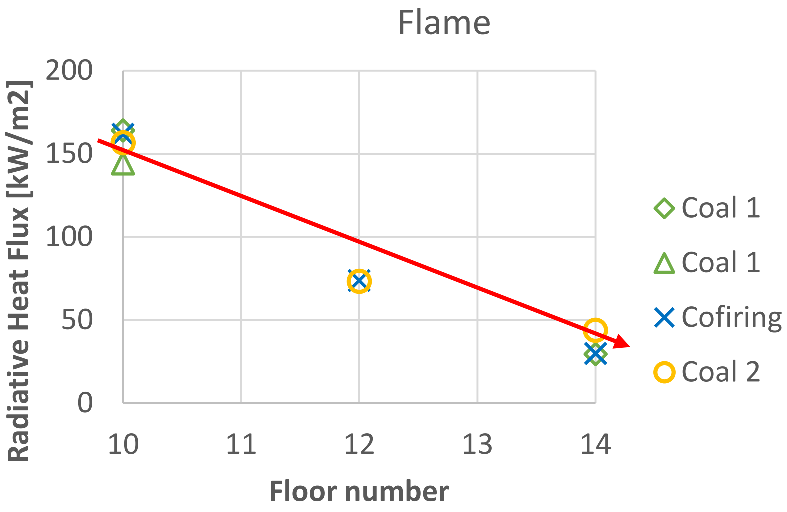

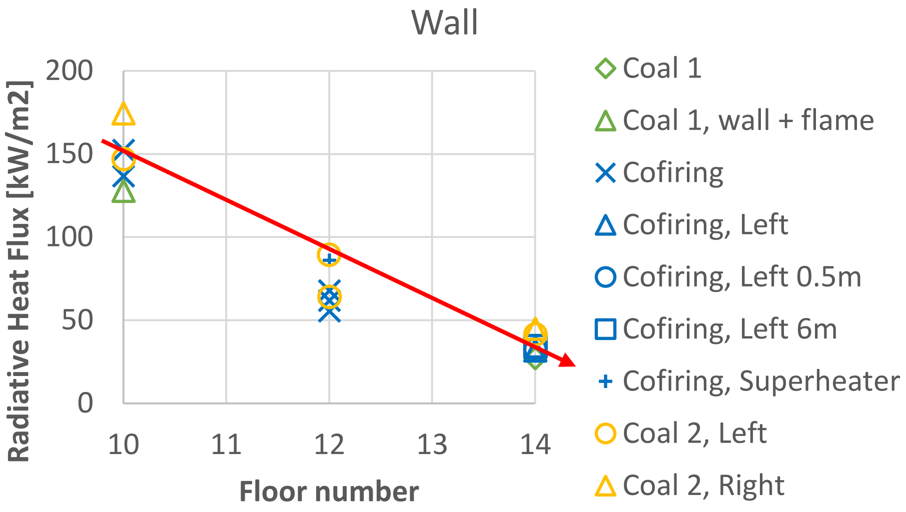

→ Flux values decreases with increased floor number

→ Similar levels for coal and cofiring cases

- Ellipsoidal radiometer
- Probe was positioned at the inner wall at floors 10, 12 and 14
- The probe was directed towards:
  - flame or wall
  - the left and right, towards the wall aiming at certain approximate distances
  - the superheater

Radiative Heat Flux Measurements

(Method 2)

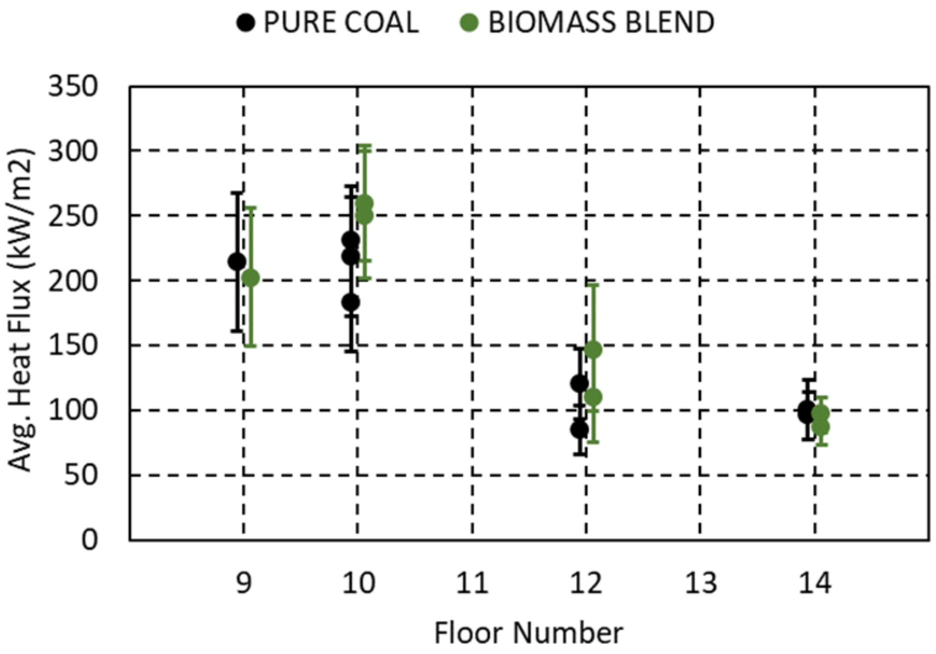

- Narrow angle radiometer
- The probe was directed towards:
  - Flame or hot gasses

Radiative Intensity Measurement

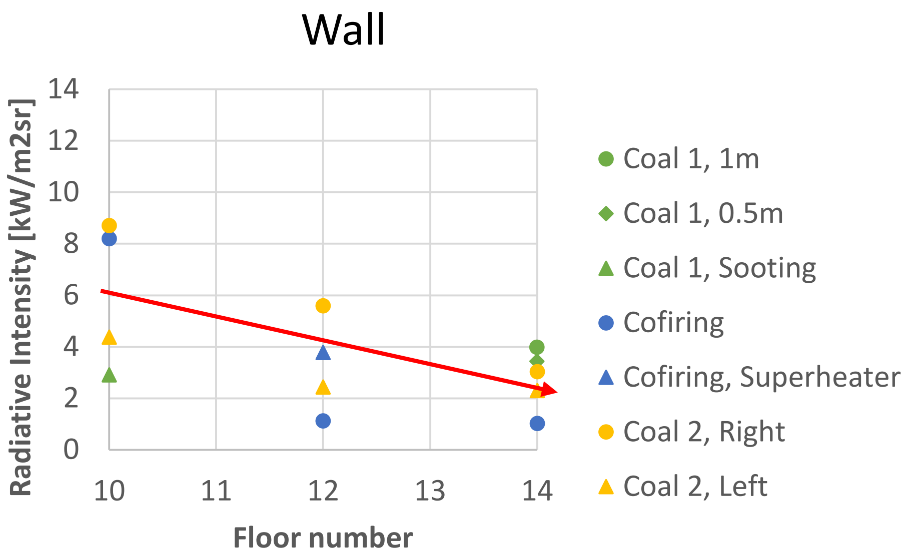

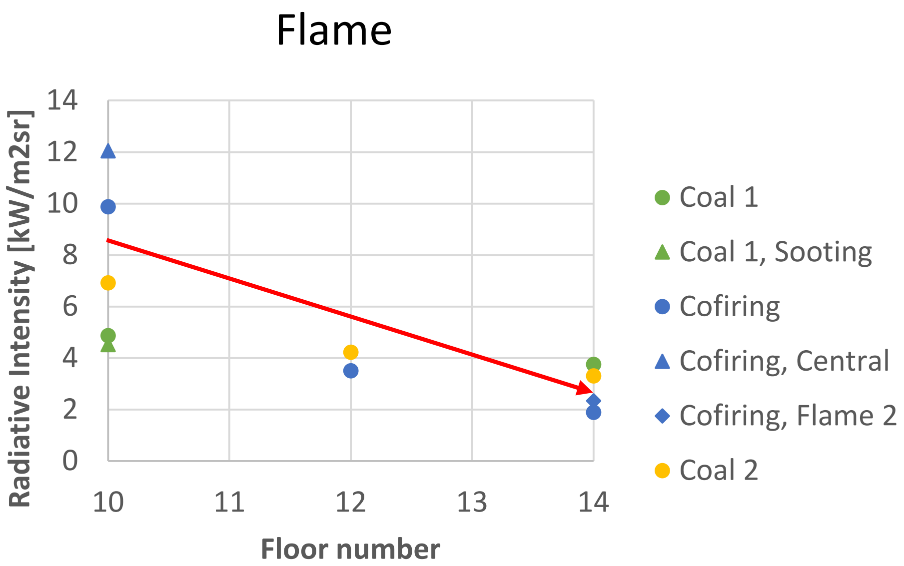

- Narrow angle radiometer
- The probe was directed towards:
  - flame or wall
  - the left and right, towards the wall aiming at certain approximate distances
  - the superheater

Steam Gen Expert Modeling

Steam Gen Expert Model (Process Model)

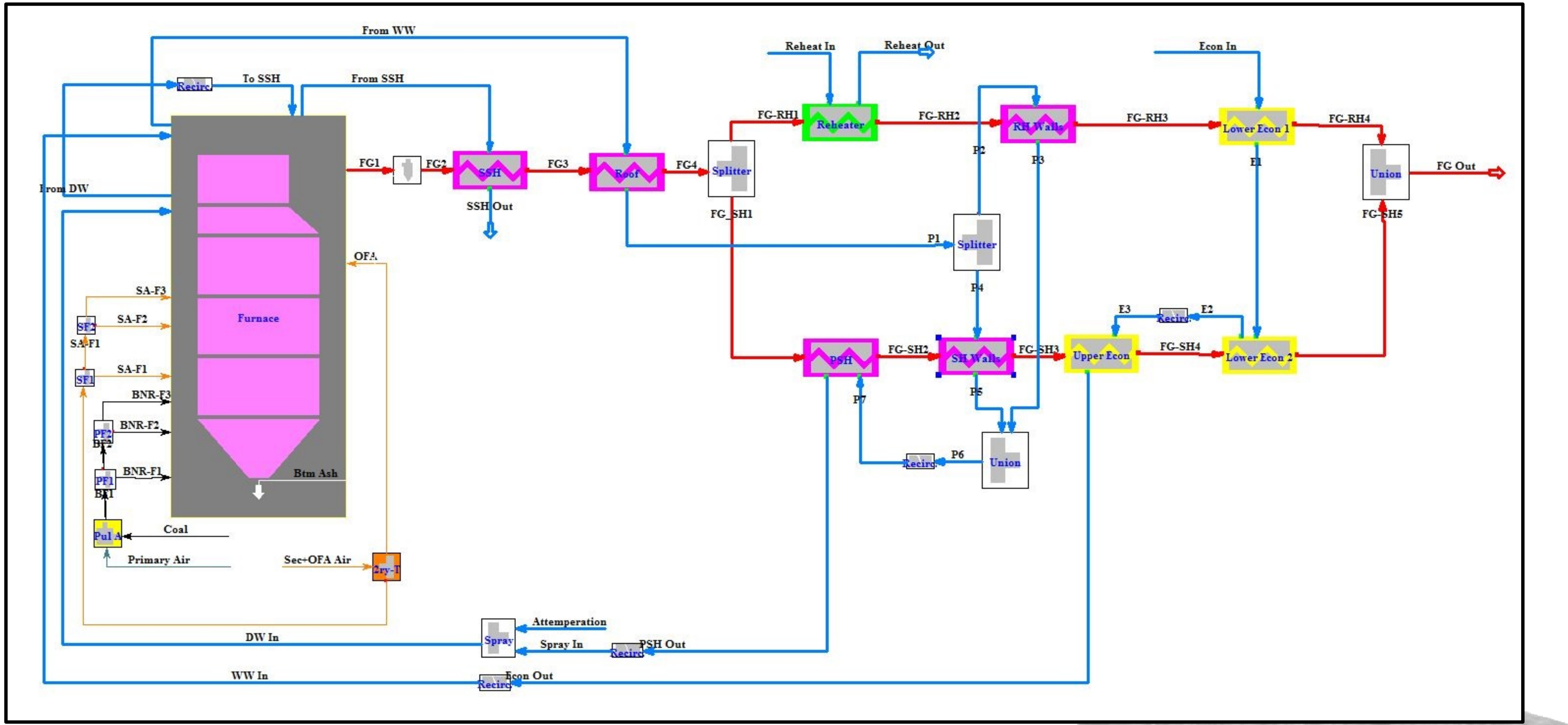

Steam Gen Expert Model (Process Model)

These simulations are ongoing. Results will contain:

- A comparison of fouling factors on the outside of heat exchange tubes for the blend test and the coal test
    - Expected result – little difference

- A prediction of gas temperatures at our various sampling locations which is consistent with all operating parameters

- An understanding of the consistency of the PI data set from a combustion perspective

What is next?

Experiment and Process Scale-up

- We have now performed testing at 3 scales
  - Conclusions from each scale of testing are the same
- We have CFD models of each of these devices built
  - Should we exercise the models for the conditions tested?

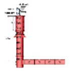

OFC, pilot-scale 27 kW, 50% / 50%

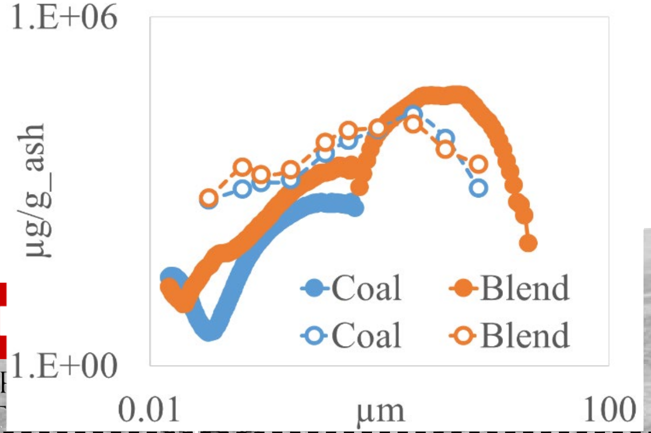

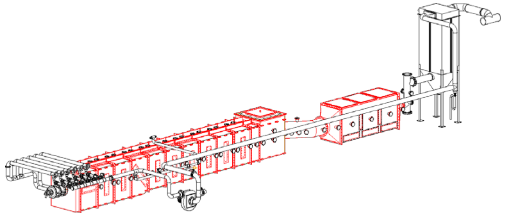

L1500, pilot-scale
1025 kW, 85%coal / 15%wood

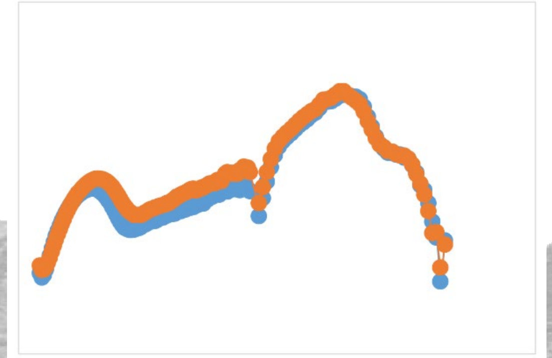

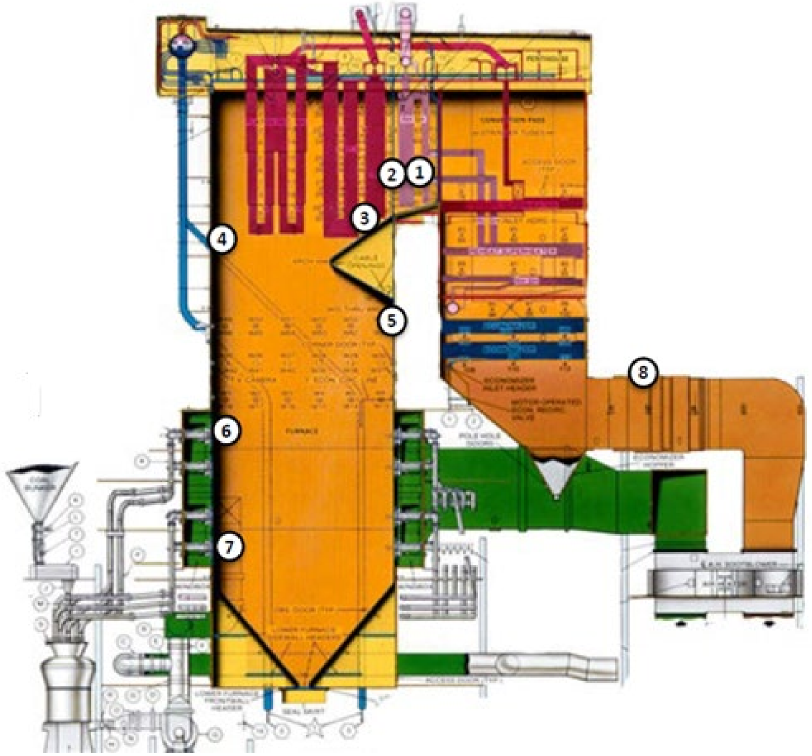

Real plant, industrial scale
1.2×10^6 kW, 85%coal / 15%wood

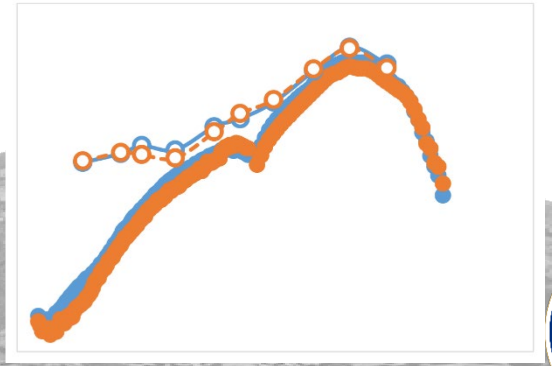

Steam exploded pellet testing Summer 2020?

Summary and Conclusions

Summary & Conclusions

- Fuel Blending and delivery
  - Based on scale readings, coal yard hit exactly 15% blend
    - Truck scale only accounted for 577 tons of the 724 tons of torrefied pellets delivered
  - Assuming all 724 tons were fed in the same time period we blended at 19.6% biomass in coal
  - Analysis of fuel samples collected from redler suggest between 17.8 and 22.5% biomass in coal
  - We were likely operating closer to 20% biomass in coal blend
  - There was some uncertainty concerning when the biomass blend arrived at all of the mills at the desired concentration
    - Most certain period of biomass feeding was 08-22-19 23:30 to 08-23-19 09:18
    - This period coincided with our measurements

Summary & Conclusions

- General Unit Behavior
  - There was essentially no change in boiler load, excess O_2, turbine throttle pressure or flue gas pressure drop
  - There was a 6.6% increase in fuel flow (exactly as expected)
  - NO_x concentration during the entire blend test was 88.6% of the baseline condition, but was 65% during the last 4 hours of the blend test
  - SO_2 concentration during the entire blend test was 71.9% of the baseline condition, but was 62% during the last 4 hours of the blend test
  - CO concentrations were 4 times higher during the blend test

Summary & Conclusions

- Mill Behavior
  - There was no change in PA fan current and mill outlet temperature
  - There was a 15 – 40% increase in mill current during the blend test
  - Pulverizer PSD is more impacted by classifier pipe outlet geometry than by fuel blend
  - Blended fuel generally pushed the PSD to larger sizes
  - Pyrite flow increased (especially in 3-4 mill) and the proportion of coal and biomass also increased

Summary & Conclusions

- Gas Composition Measurements
  - FTIR CO and O_2 concentrations were similar for the blended fuel and pure coal
    - This result for CO is different than PI data suggest
  - NO concentrations during blend combustion were 89.5% of the coal condition
  - SO_2 concentrations decreased as gas moved through the boiler
    - This was especially pronounced during the blend condition
    - This behavior suggests SO_2 is being adsorbed by the particles
  - Soot blowing increased CO and decreased NO

Summary & Conclusions

- Entrained Particle Behavior
  - PSD was essentially the same for the biomass blend and for coal
  - Soot blowing increased the particle concentrations and shifted to more particles in the sub-micron region
    - Suggesting deposits are dominated by sub-micron particles
  - Particle compositions remained essentially the same for the blended fuel
    - Sulfur concentration increased in particles

Summary & Conclusions

- Deposit Behavior
  - Deposited “Chunks” obscured the results of this test (this behavior was not observed in the L1500 tests)
  - Deposition rate was 56% of baseline for the 90 minute sample time
  - Sulfur concentration is lower in the deposited particles
    - This suggests that the SO_2 adsorption is occurring on the surface of entrained particles
  - There was no observable impact to the particle morphology
  - There was little impact to the baghouse ash composition and morphology

Summary & Conclusions

- Radiation and Temperature Measurements
  - For the gas temperature measurements there is a greater spread in repeated measurements than the difference between the blend and coal conditions
  - Radiative heat flux measurements also show a greater spread in replicate measurements than the difference between blend and coal conditions
  - Narrow angle radiometer measurements were higher for the blend condition in port 5 (below the nose) than the coal condition
    - All other measurements were similar

Summary & Conclusions

- We feel like this was a very successful test
- Thank you to all plant personnel who participated
- Special thanks to the Utility Workers who helped us clean up afterwords
  - By the end, we were just DONE

Discussion

Demonstration of Torrefied Woody Biomass and Coal Co-firing at PacifiCorp's Hunter, Unit 3 (Plant Impacts)

Andrew Fry
Department of Chemical Engineering, Brigham Young University

Laren Huntsman
Rocky Mountain Power

Project Contributors

ROCKY MOUNTAIN POWER
A DIVISION OF PACIFICORP

Ken Clark
Bruce Wilson
Troy Anderson
Cameron Hansen
Alex Crawford
Doug Farley
Jamie Phillips
Rhyker Allred
Nick Larsen
Pete McElprang
Levi Ferguson
Jordan Sitterud
Glen Keller
Carson Grimm
Jared Erickson
Mindy Jackson
Jeff Westergard

CHALMERS
UNIVERSITY OF TECHNOLOGY

Klas Andersson
Thomas Allgurén
Dan Gall
Adrian Gunnarsson

THE UNIVERSITY OF UTAH

Eric Eddings
Jost Wendt
Xiaolong Li
Teri Snow Draper
Alex Prlina
Jack Mitchell

BYU

Seyedhassan Fakourian
Spencer Flindt

Presentation Overview

- Project objective
- Overview of Hunter, Unit 3 and fuel
- List of Measurements Performed
- Presentation of PI Data Baseline/Co-firing
- Presentation of Mill Data Baseline/Co-firing
- Summary

Project Objective

To demonstrate that prepared woody biomass could be burned with coal in Unit 3 of Rocky Mountain Power's Hunter Plant with no modifications to plant equipment and with minimum impact on operating conditions

- Biomass for this project was harvested in American Fork Canyon in Utah
- Approximately 700 tons of biomass pellets were prepared by torrefaction in a rotary kiln at 325°C and delivered to the plant
- Demonstration testing at Hunter occurred in August of 2019
- Biomass co-firing occurred for a period of approximately 24 hours

Hunter, Unit 3

- Rocky Mountain Power – Hunter Plant Unit No. 3 – 471 MW_e
  - Located near Castle Dale, UT
  - 471 MW_E – firing pulverized Utah bituminous coal
  - Wet lime scrubber, cloth filter baghouse

Hunter, Unit 3 – Measurement Locations

Port #	Description
1	Center of the reheater
2	Front of the reheater
3	Middle of the nose
4	Front of the boiler, above the nose
5	Above the over-fire air
6	Top Burner elevation
7	Bottom burner elevation
8	Economizer outlet

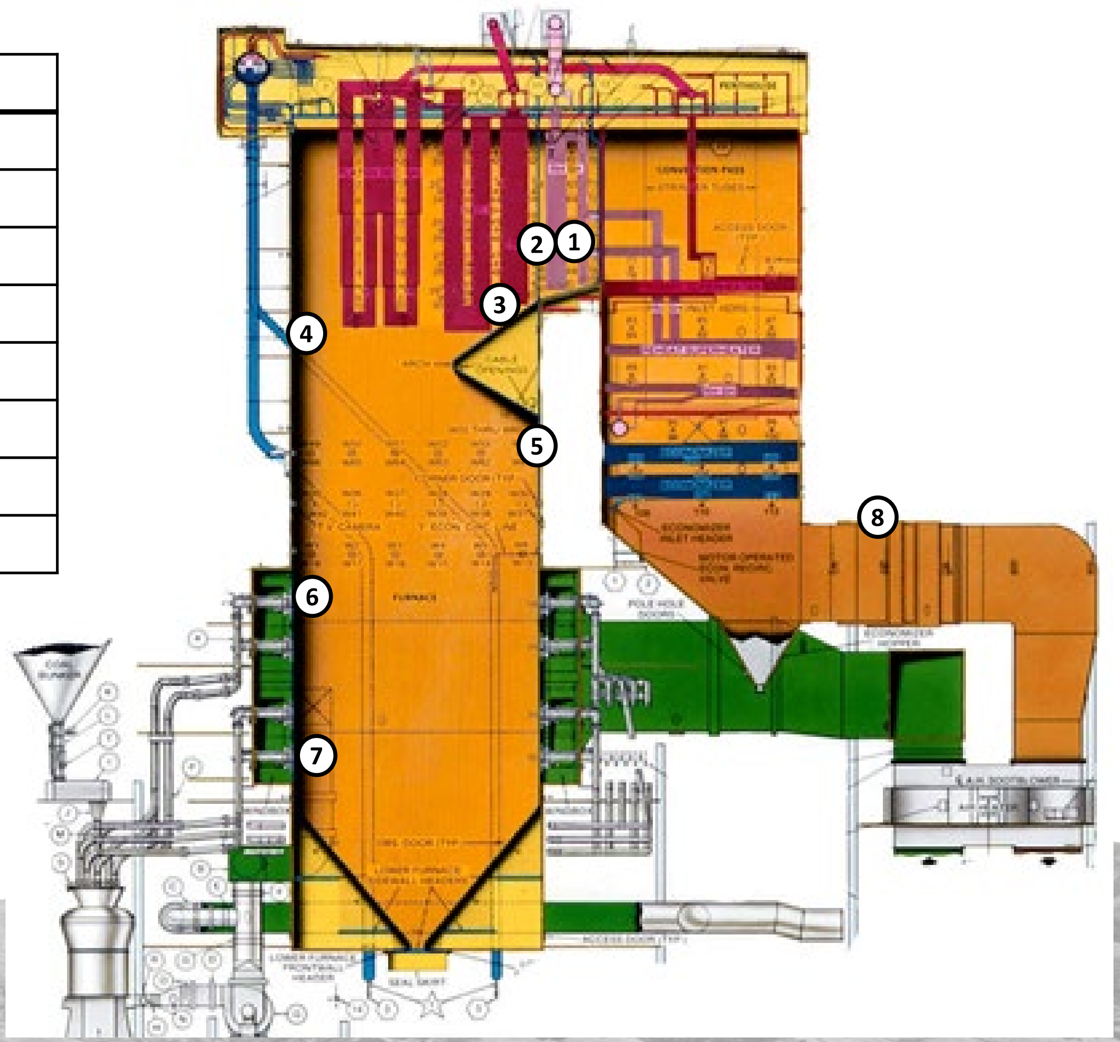

* Plant representation from Babcock & Wilcox – Steam, Its Generation and Use

Hunter, Unit 3 – Fuel Conditions

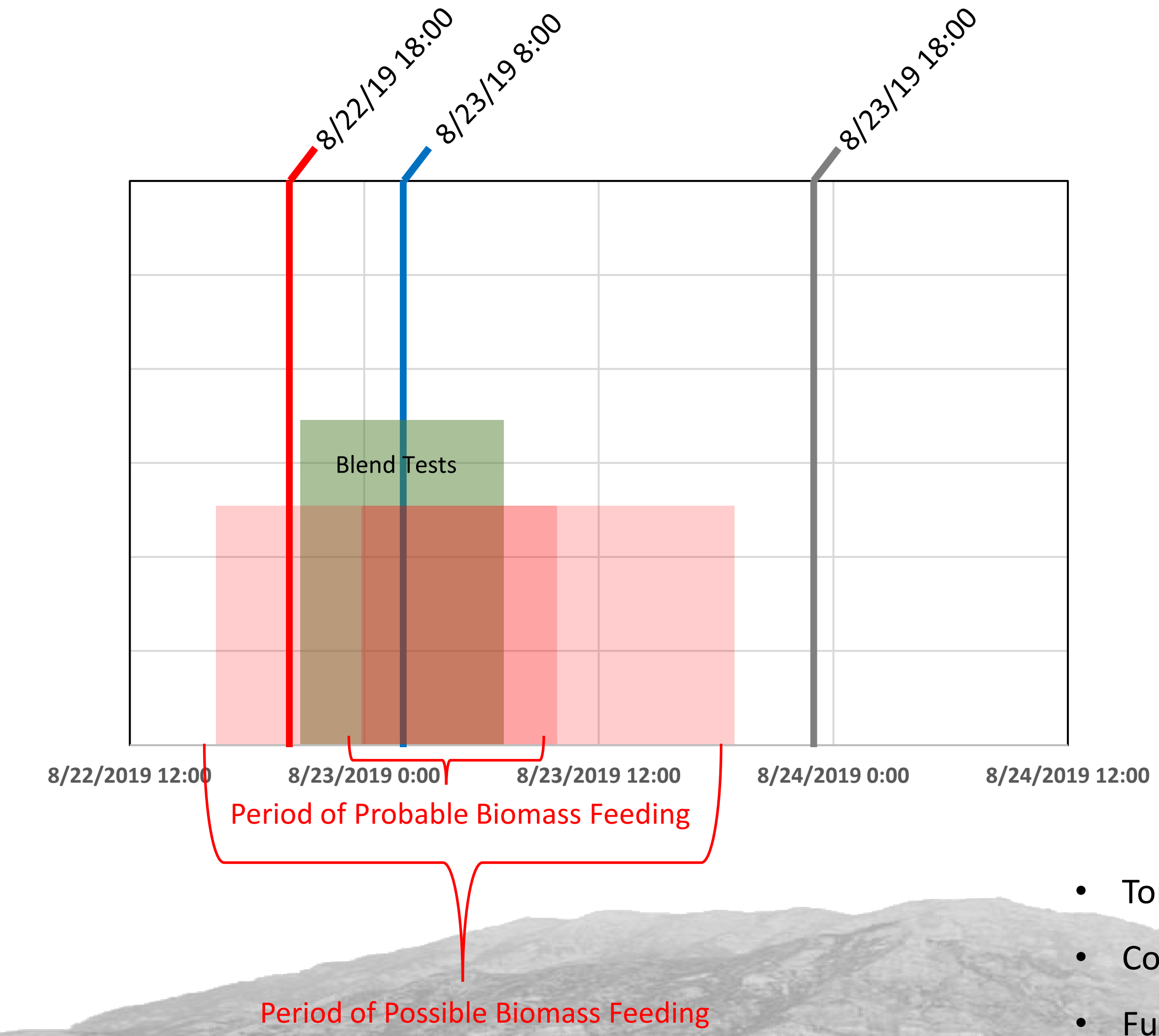

	Coal	Torrefied Pellets	08/22/19 20:16	08/23/19 02:00	08/23/19 22:59
C	63.34	47.74	60.06	60.06	63.83
H	4.43	5.20	4.42	4.45	4.47
N	1.23	0.23	1.06	0.97	1.25
S	0.48	0.02	0.41	0.35	0.63
O	10.44	35.55	12.91	12.25	9.53
Ash	11.64	0.85	11.48	10.53	11.52
Moist	8.45	10.40	9.67	11.39	8.76
HHV (Btu/lb)	11093	8219	10582	10447	11354

17.8% 22.5% 0.0%

- Torrefied pellets were analyzed prior to demonstration
- Coal analysis was provided by Hunter, representative of the week
- Fuel blend can be estimated by minimization of sum squared error

Hunter, Unit 3 - Measurements

- Deposit and entrained ash sampling
- Fuel and ash sampling
- Radiation intensity and incident radiative heat flux(radiometers)
- FTIR gas analysis
- Gas temperatures using suction pyrometery and/or shielded thermocouple
- Continuous gas analysis
- Evaluation of PI Data

Plant Load

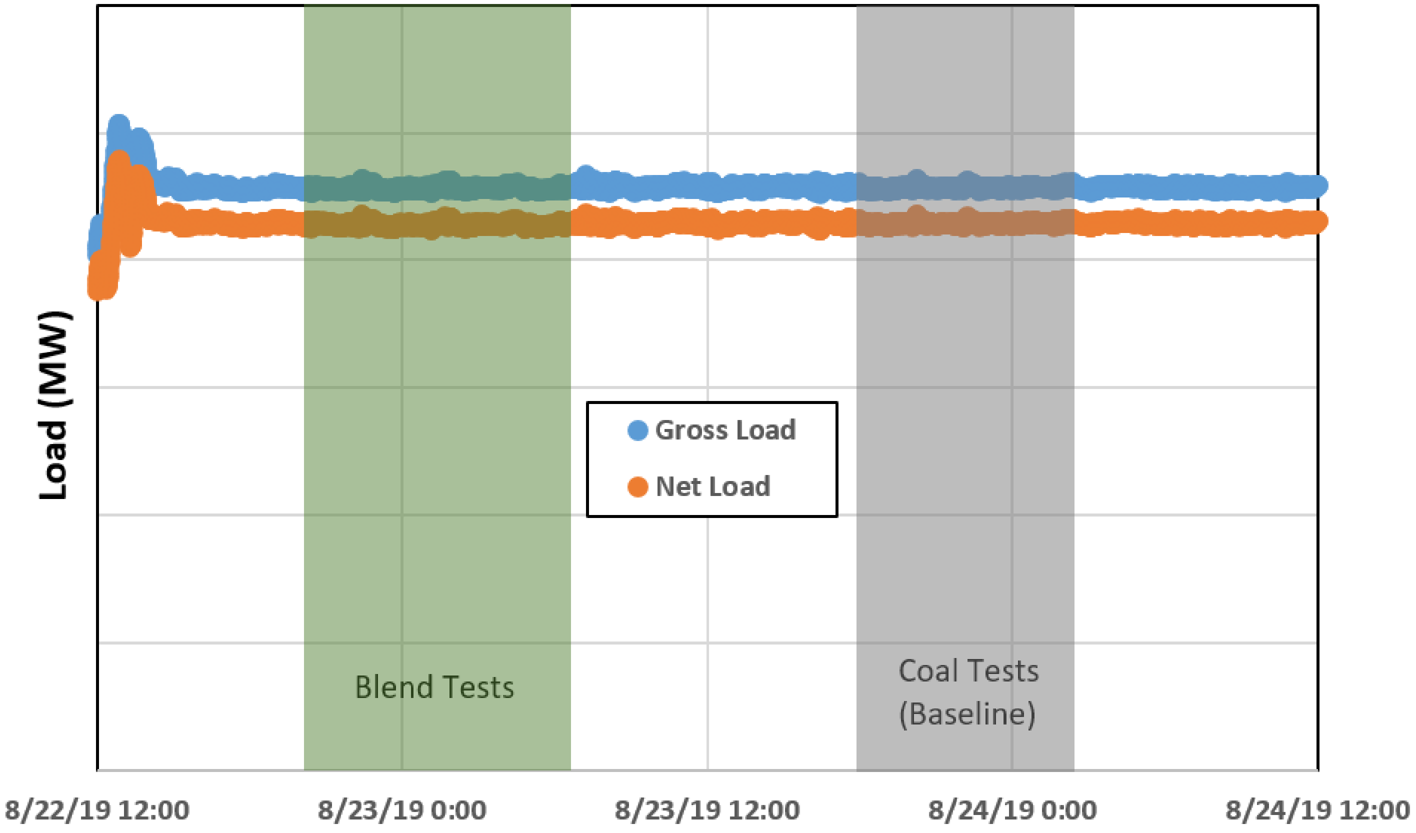

Gross Load – 99.9% of coal condition
Net Load – 99.8% of coal condition

- There was no change in load between blend and pure coal operation

Coal Flow

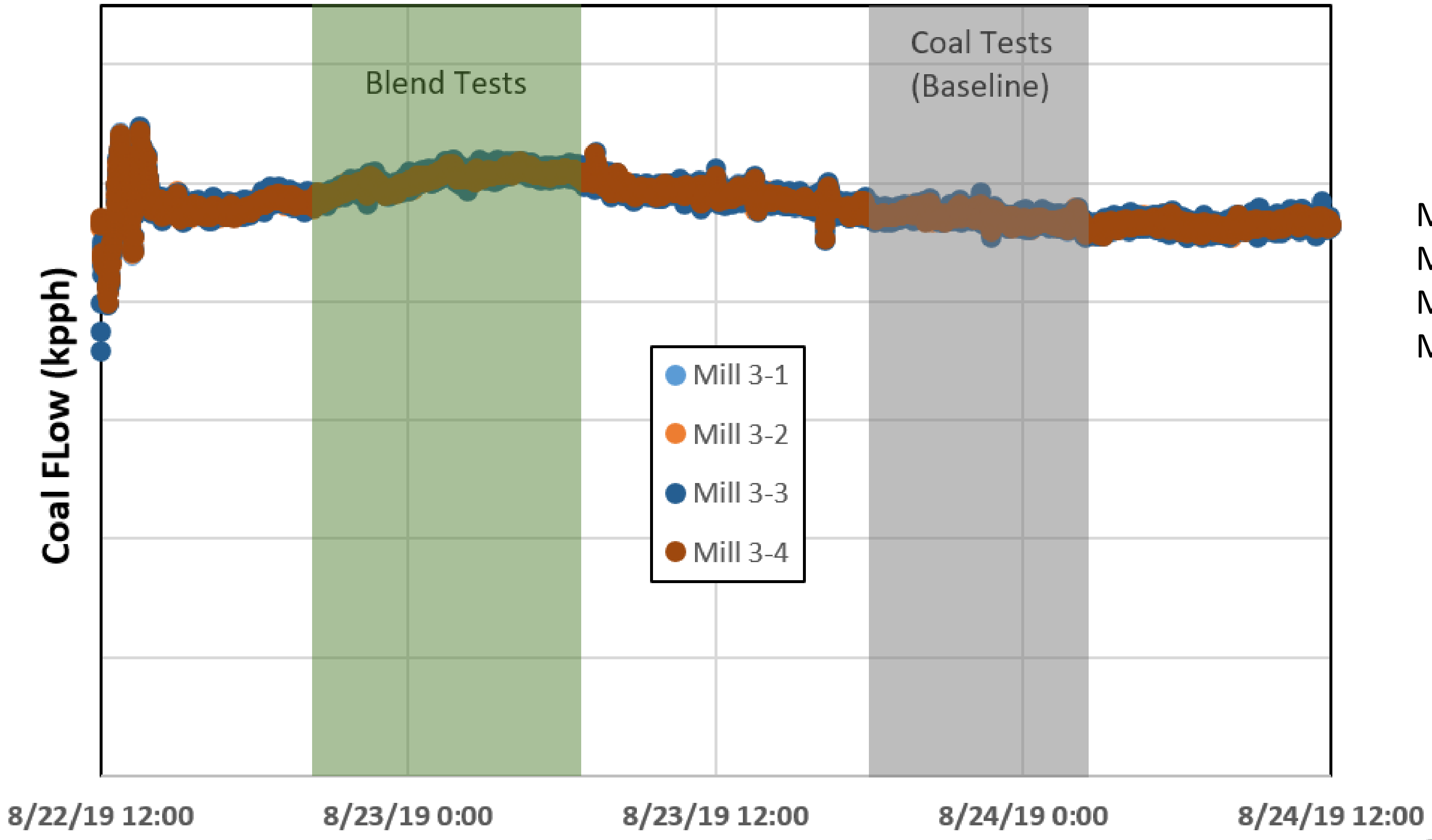

Mill 3-1 – 106.6% of coal condition
Mill 3-2 – 106.6% of coal condition
Mill 3-3 – 106.6% of coal condition
Mill 3-4 – 106.7% of coal condition

- Fuel feed rate was about 6.6% higher during the biomass blend test
- Calculated necessary increase based on measured heating value of blend and coal was 6.6%

Turbine Throttle Pressure

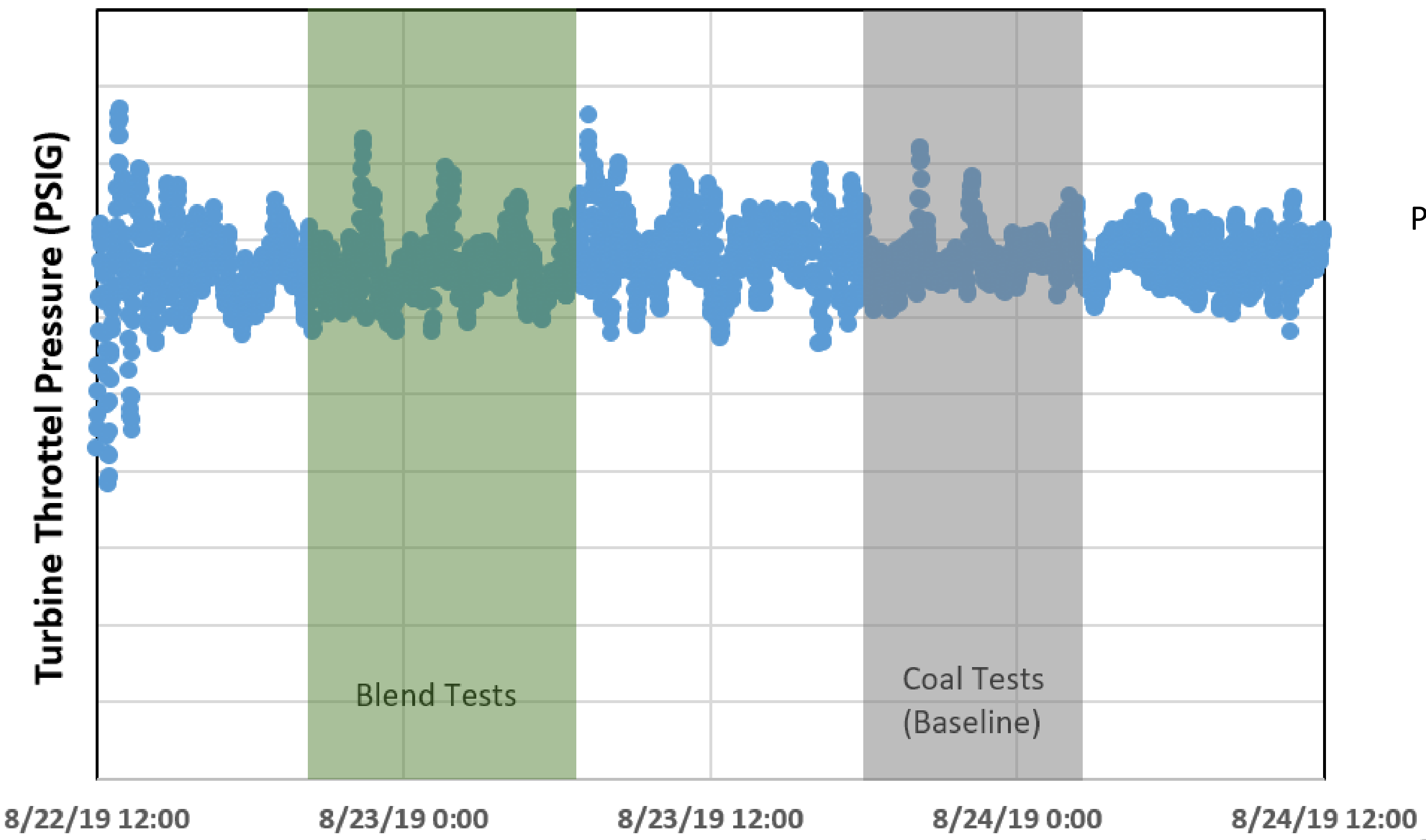

Pressure – 99.9% of coal condition

- There was no change in turbine throttle pressure between blend and pure coal operation

Stack O_2 Measurement

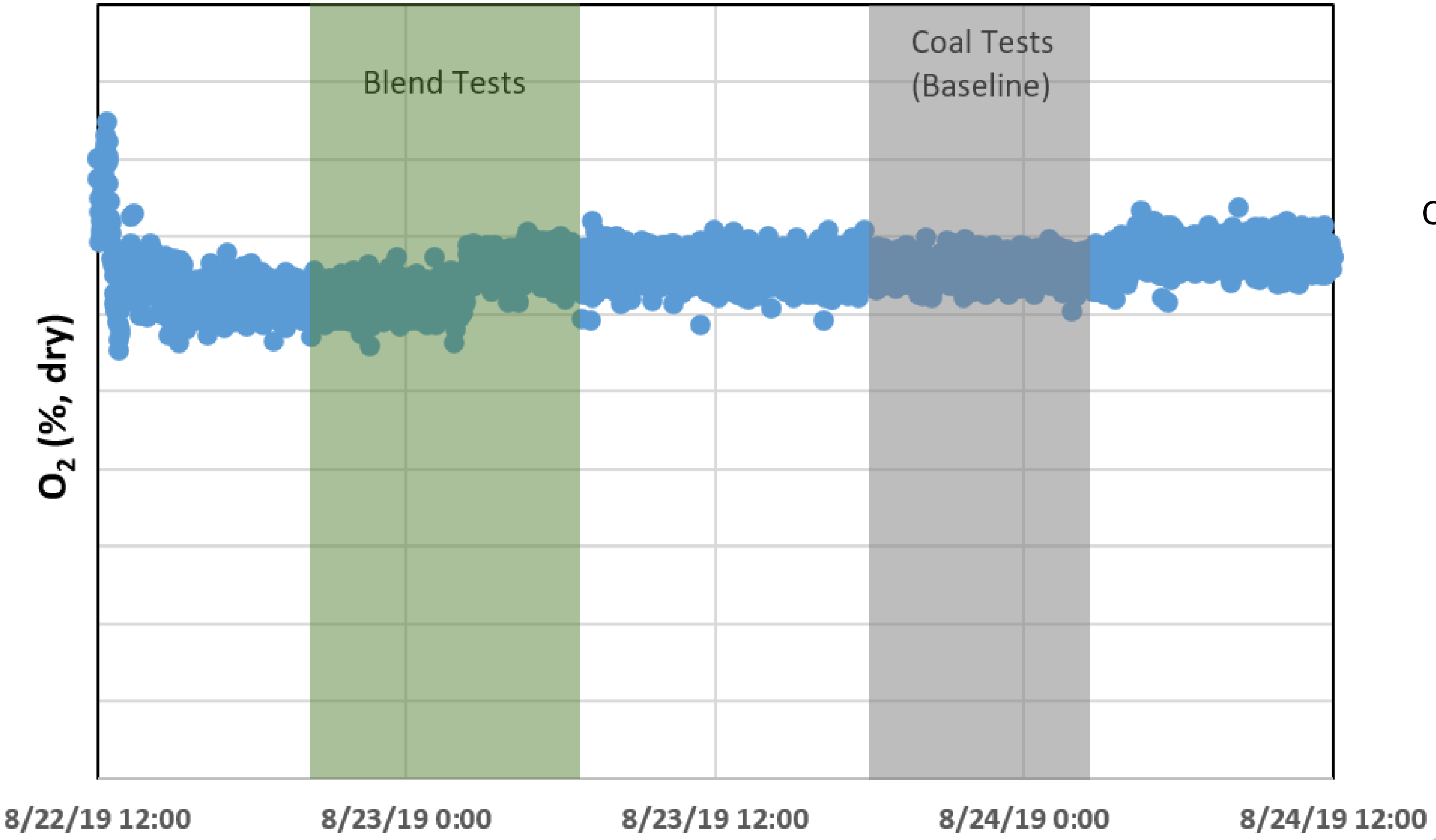

O_2 – 96.7% of coal condition

- Boiler O_2 was maintained at essentially the same value for each of the tests

Stack NO_x Measurement

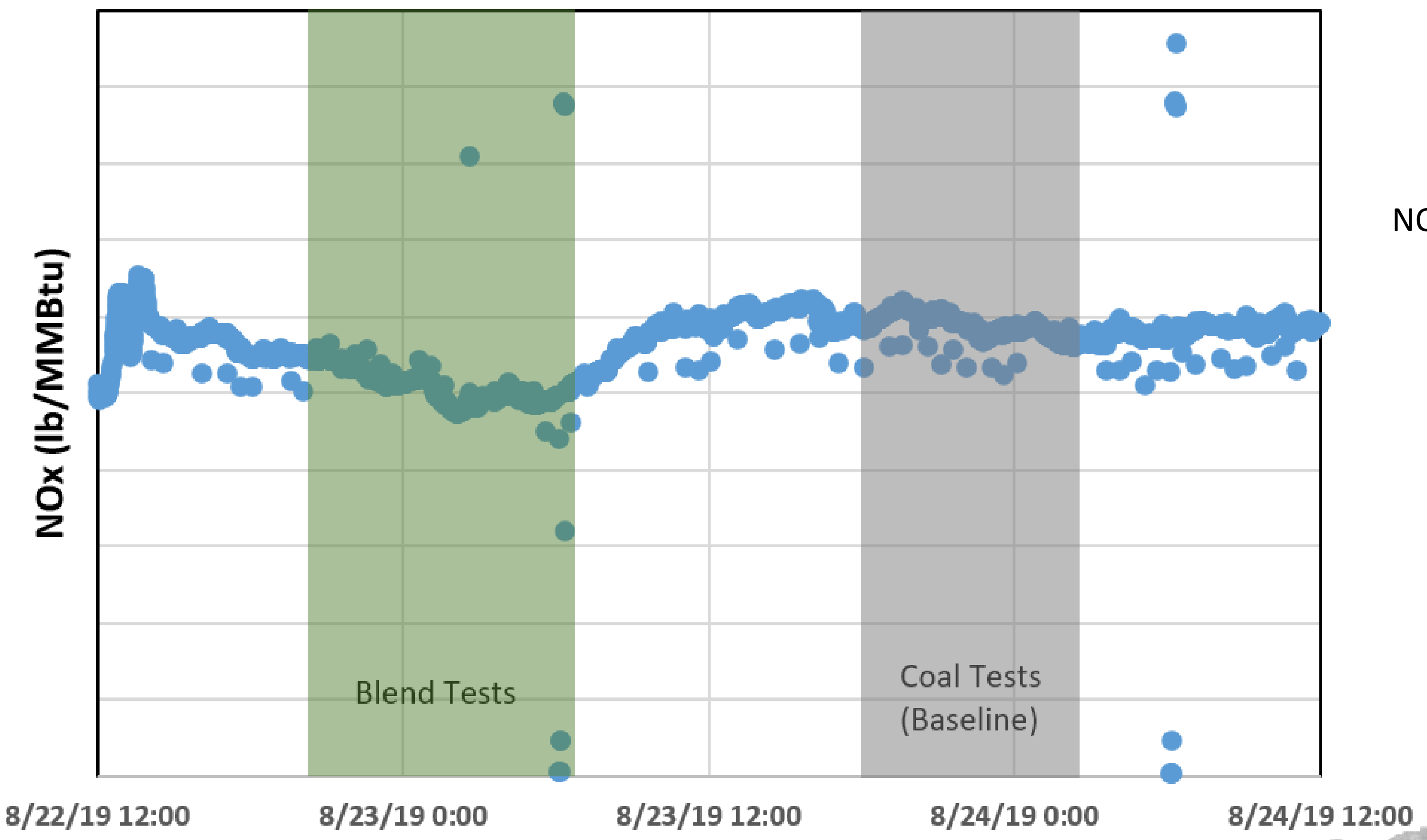

NOx – 88.6% of coal condition

- NO_x was reduced to 88.6% of the pure coal condition while firing the biomass blend

Stack SO_2 Measurement

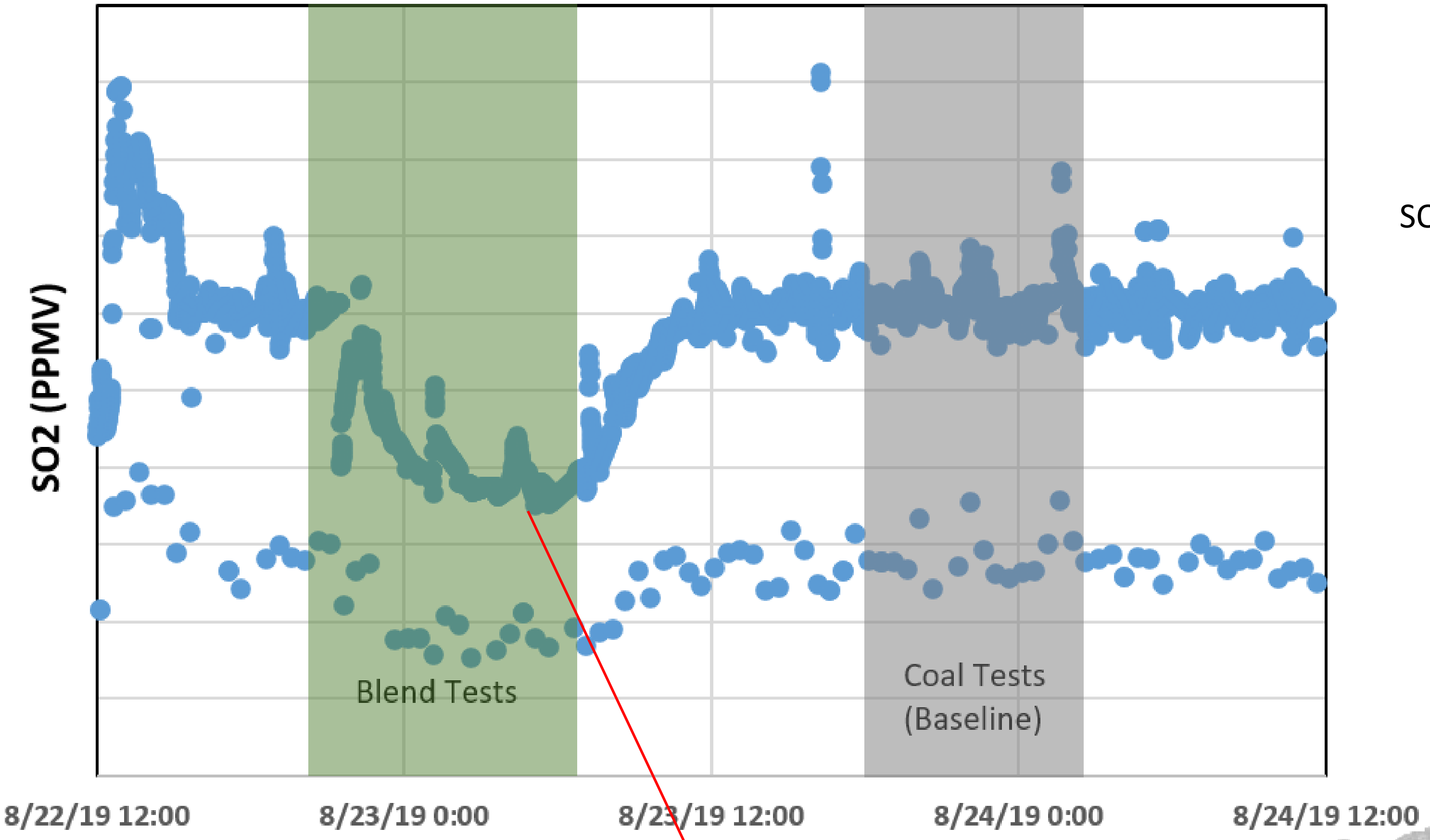

SO_2 – 71.9% of coal condition

More like 62% of coal condition

- SO_2 was reduced to 71.9% of the pure coal condition while firing the biomass blend

Flue Gas dP

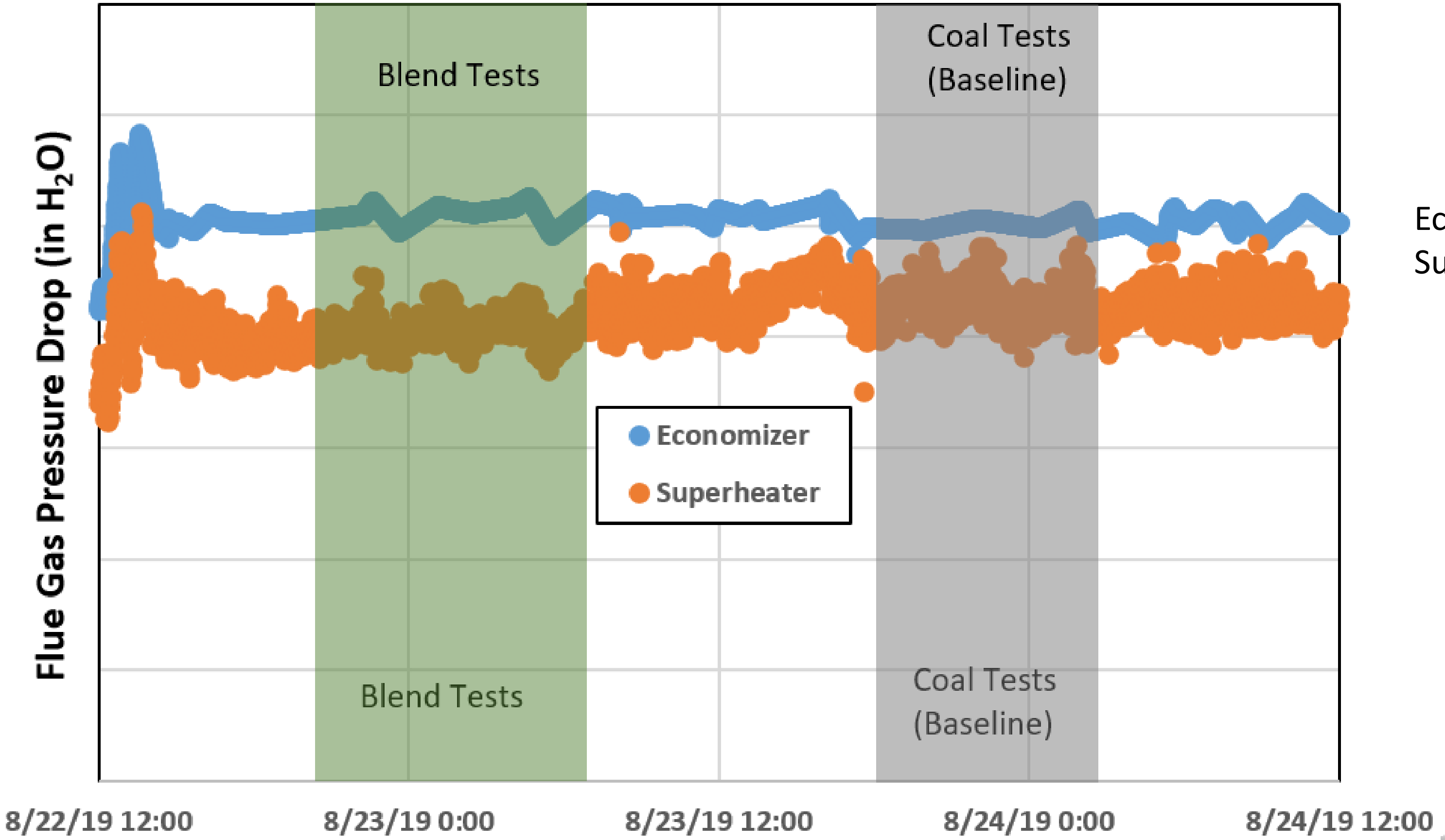

Econ – 101.7% of coal condition
Super – 94.6% of coal condition

- Flue gas pressure drop through the economizer was the same for both fuel conditions
- Pressure drop through the superheater was slightly lower for the biomass blend case

Pulverizer Motor Current

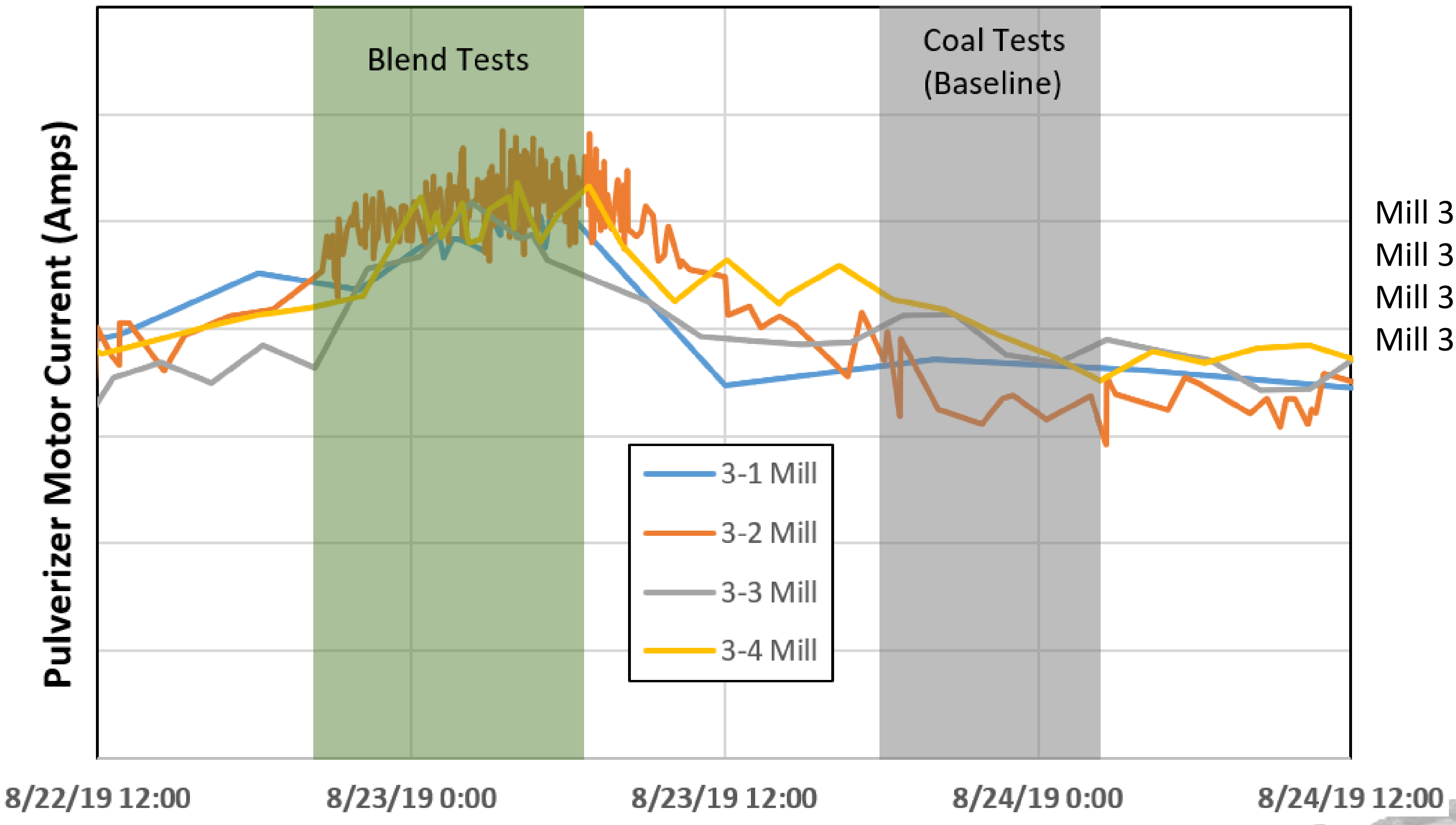

Mill 3-1 – 123.2% of coal condition
Mill 3-2 – 140.5% of coal condition
Mill 3-3 – 114.8% of coal condition
Mill 3-4 – 117.7% of coal condition

- Pulverizer motor current increased for all four mills while process the biomass blend
- Increase in current was especially pronounced for the 3-2 mill (at 40%) along with the fluctuations in current for that mill

Primary Air Fan Current

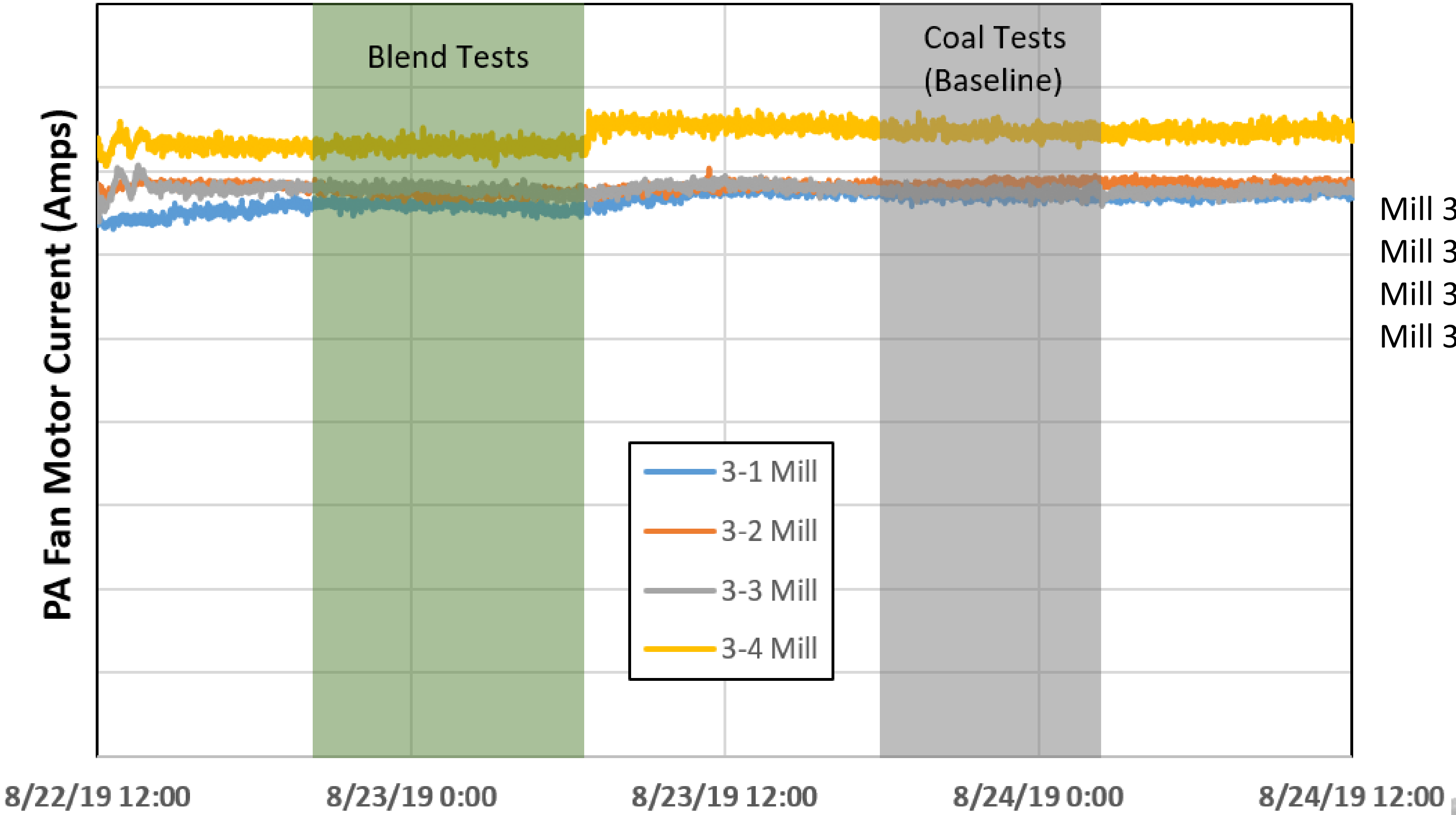

Mill 3-1 – 98.4% of coal condition
Mill 3-2 – 98.6% of coal condition
Mill 3-3 – 100.4% of coal condition
Mill 3-4 – 97.9% of coal condition

- Primary air fan power requirements were essentially unchanged

Pulverizer Outlet Temperature

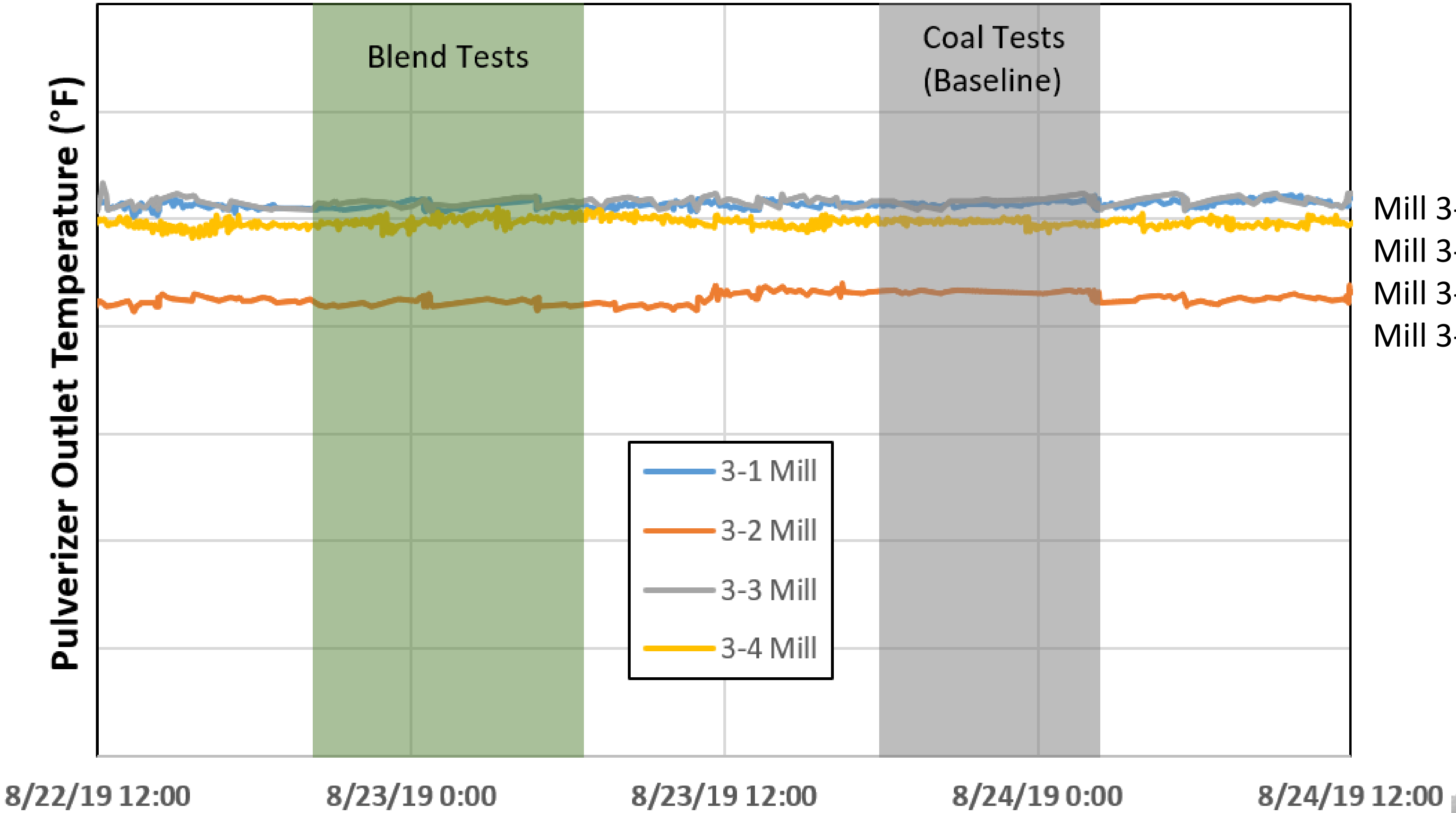

Mill 3-1 – 99.9% of coal condition
Mill 3-2 – 90.9% of coal condition
Mill 3-3 – 99.9% of coal condition
Mill 3-4 – 100.1% of coal condition

- Mill outlet temperatures were essentially unchanged, with the exception of the 3-2 mill which was lower for the blend processing condition

Pulverizer Particle Size Distribution (PSD)

- Coal PSD represented by various colors:
  - Red – Mostly Coal
  - Blue – Biomass Blend
  - Grey – Mostly Coal

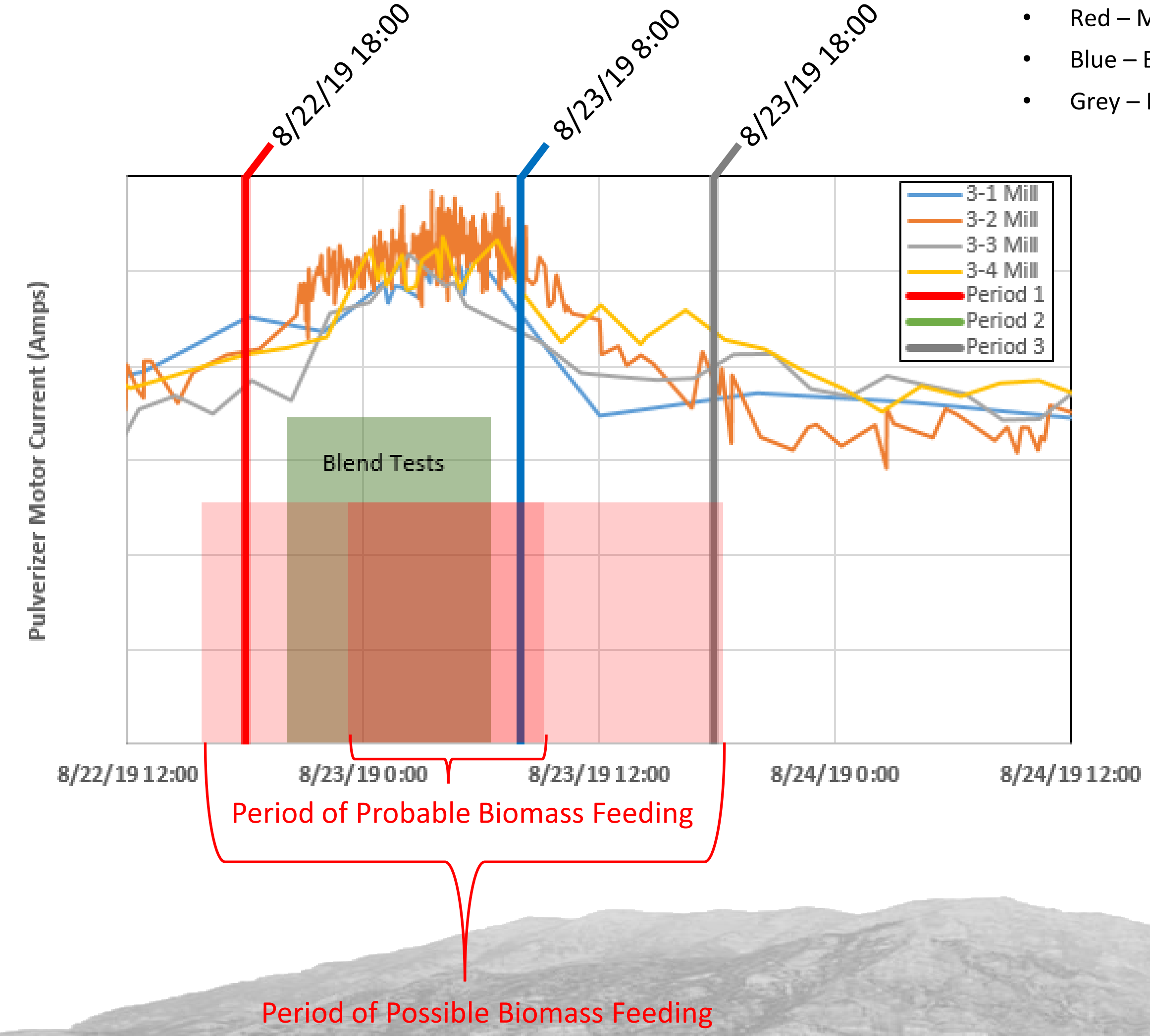

Period of Probable Biomass Feeding

Period of Possible Biomass Feeding

Pulverized Coal (PSD)

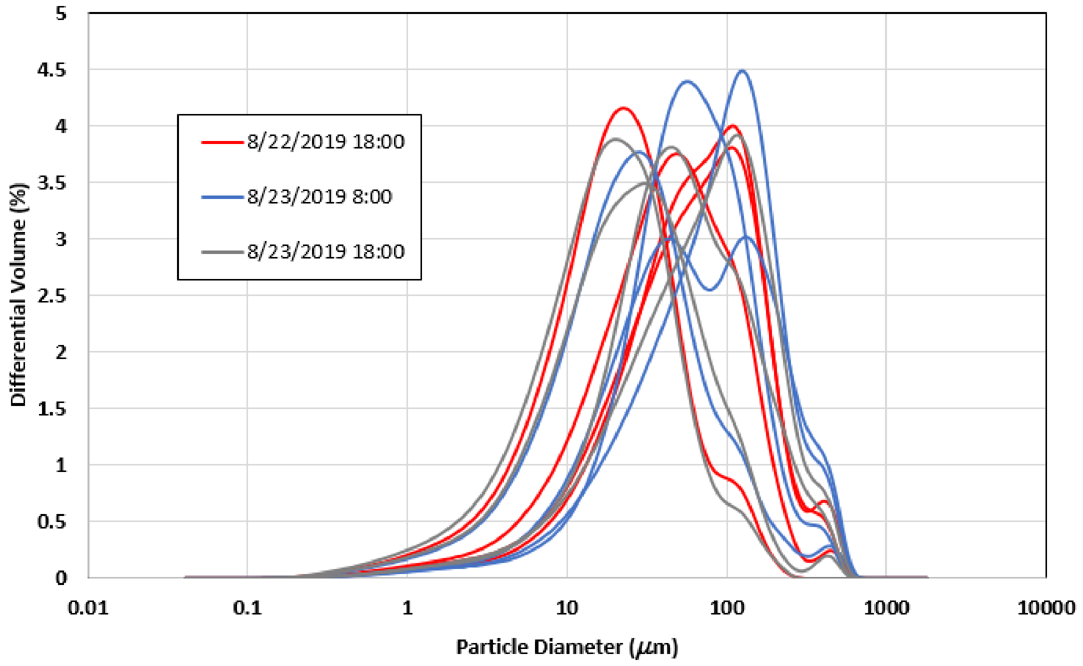

- There seems to be little correlation with sampling time (coal vs. biomass)

Pulverizer Particle Size Distribution (PSD)

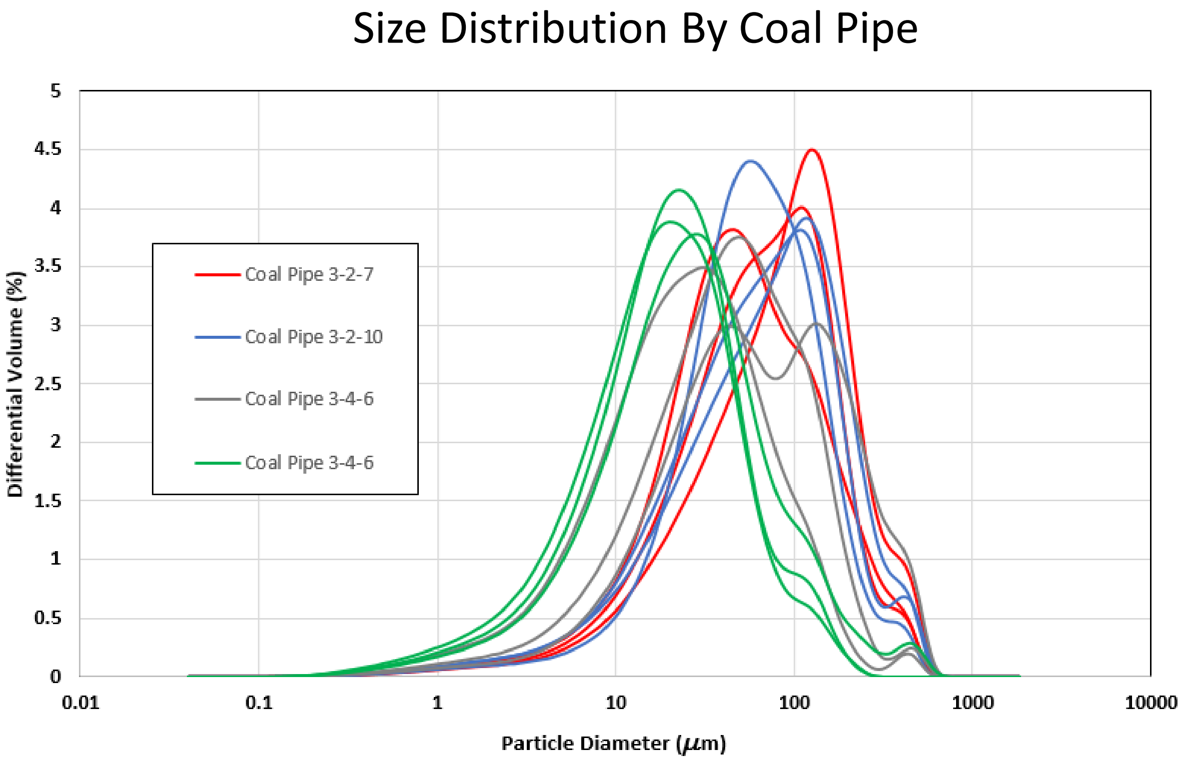

- It appears that the particle size distribution is correlated more with coal pipe than sample time
- Probably due to geometry of outlet in the classifier

Pulverizer Particle Size Distribution (PSD)

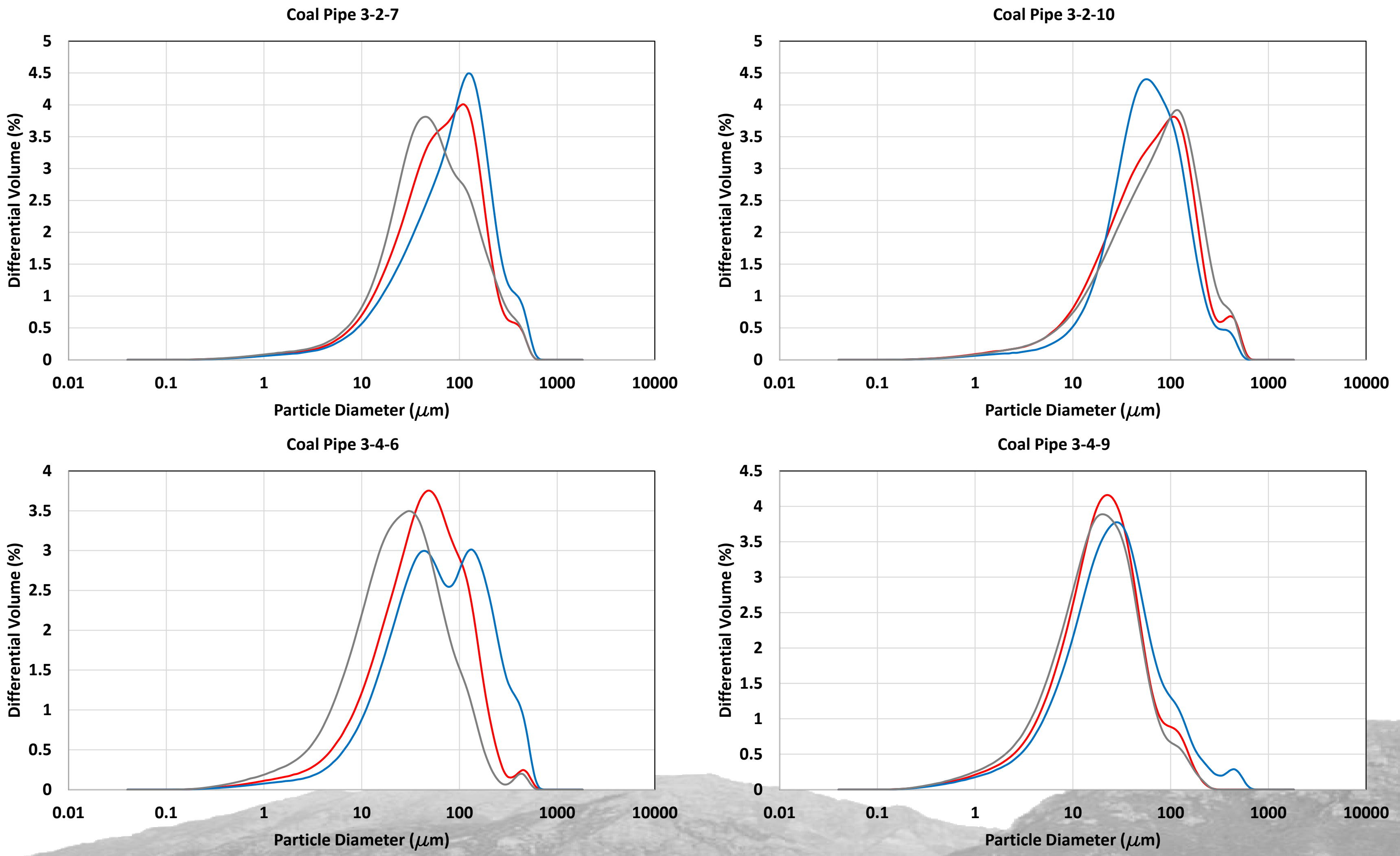

Red – Mostly Coal

Blue – Biomass Blend

Grey – Mostly Coal

- Generally, the biomass blend results in shifting the PSD to larger sizes

Summary

- A demonstration of co-firing torrefied woody biomass with coal was performed at Rocky Mountain Power's Hunter, Unit 3
- Torrefied biomass was blended with coal at approximately 15% by mass for a period of 24 hours.
- Plant PI data were evaluated to determine the impact of cofiring
  - Plant generation was held constant throughout blend and baseline testing
  - NO_x emission was 88.6% of the baseline during blend firing
  - SO_2 emission was 71.9% of the baseline during blend firing
- Pulverizers were negatively impacted
  - Mill motor current increased by 15 - 41%
  - Rate of pyrite rejection increased
  - Particle size distribution was nearly the same and differed differently for each mill

Acknowledgements

The authors gratefully acknowledge financial support provided by PacifiCorp/Rocky Mountain Power and the State of Utah through the Utah Sustainable Transportation and Energy Plan (STEP).

Questions

A Comparison of Industrial-Scale (471 MWe) Radiometer Heat Flux Measurements Between Pulverized-Coal and 85% Coal/15% Biomass Co-firing Combustion

Department of Chemical Engineering, University of Utah, USA:
Teri Draper, Alex Prlina, Terry Ring, and Eric Eddings*

Department of Space, Earth and Environment, Chalmers University of Technology, SWEDEN:
Adrian Gunnarsson, Thomas Allgurén, Dan Gall, and Klas Andersson

Department of Chemical Engineering, Brigham Young University, USA:
Stan Harding and Andrew Fry

Objective

- Examine the effect of biomass co-firing on the heat flux profile in an industrial boiler
- Pulverized-coal boilers are carefully designed for a certain heat flux profile
  - Sharp changes in heat flux are NOT desirable
  - Switch to biomass co-firing could impact heat transfer in flame directly or indirectly through changes in deposit formation

Hunter powerplant located in Castle Dale, Utah.

Hunter Power Plant Campaign (Aug 2019)

- Hunter Power Plant, Castle Dale, Utah, Unit 3 (471 MW_e)
- Radiation data taken at three heights
  - Floor 10, 8.9 m (29.2 ft) above burners
  - Floor 12, 16.3 m (53.5 ft) above burners
  - Floor 14, 22.6 m (74.1 ft) above burners
- Three radiometers:
  - 2 narrow-angle radiometers (NARs)
  - 1 ellipsoidal radiometer (ER)
- Data were taken at two different fuel conditions:
  - 100% Utah-sourced coal
  - 85% Utah-sourced coal/15% torrefied biomass (by weight)

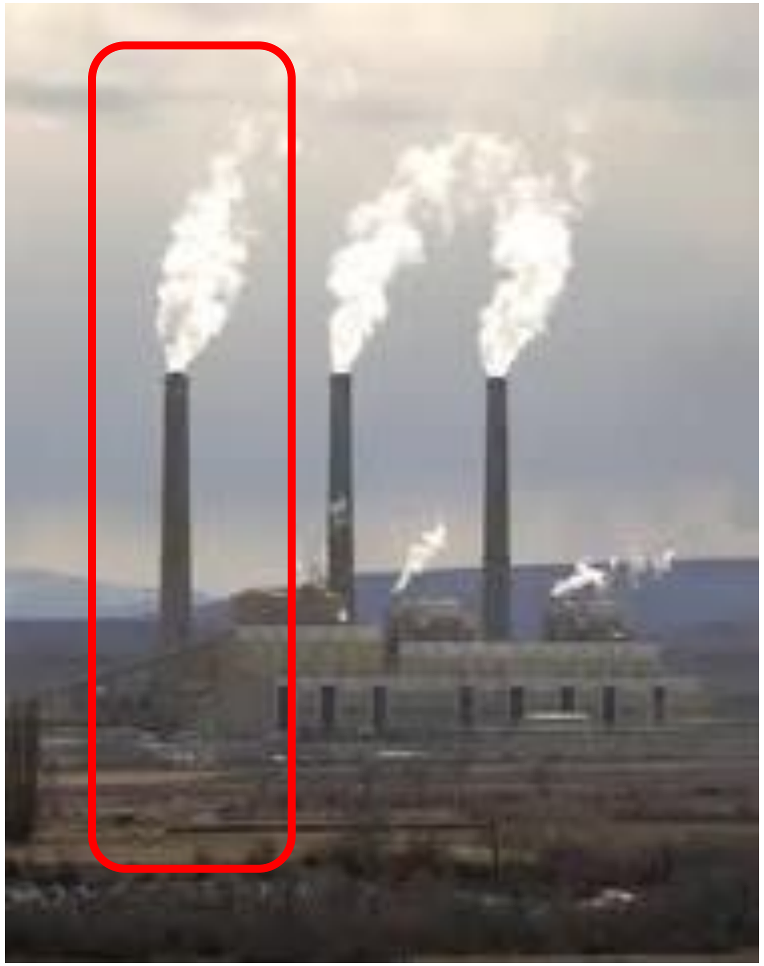

Hunter powerplant, Unit 3 circled.

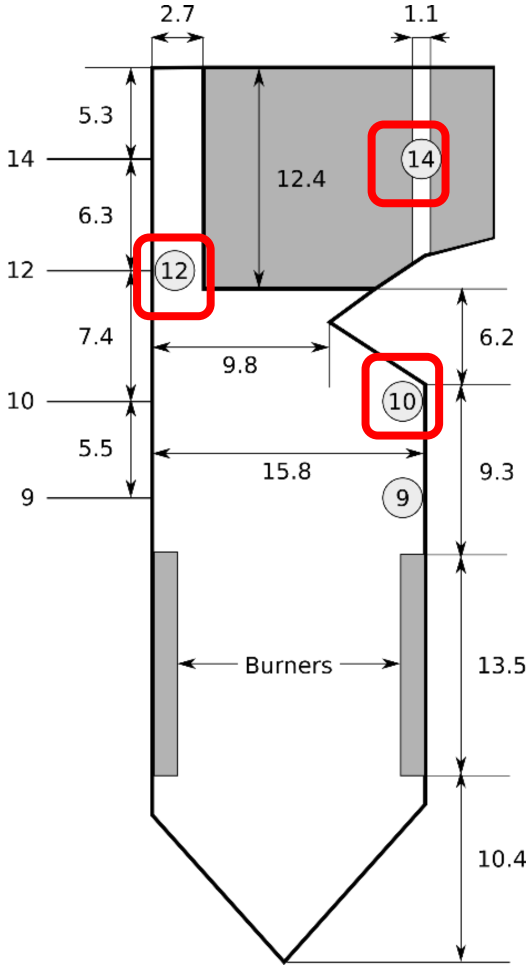

Boiler schematic, measurement ports circled.

CARBON CAPTURE MULTIDISCIPLINARY SIMULATION CENTER

Instruments: Narrow-angle Radiometers (NARs)

- Two NARs used to take data
  - University of Utah (UofU)
  - Chalmers University of Technology (CTH)
- Very similar instruments
- Both have:
  - Thermopile detector that outputs voltage proportional to incident intensity
  - Long view tubes result in a very narrow field of view (FOV)
  - View tubes manufactured to prevent reflections and keep narrow FOV
  - Measures: narrow-angle intensity (kW/m^2-sr)

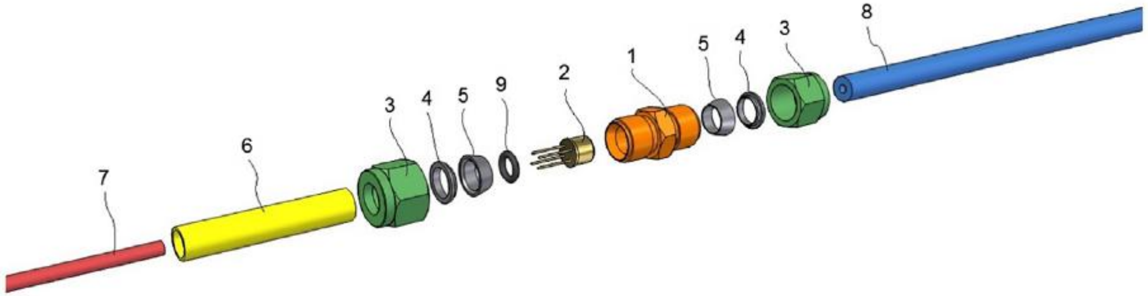

Exploded view of University of Utah’s narrow-angle radiometer (UofU NAR).

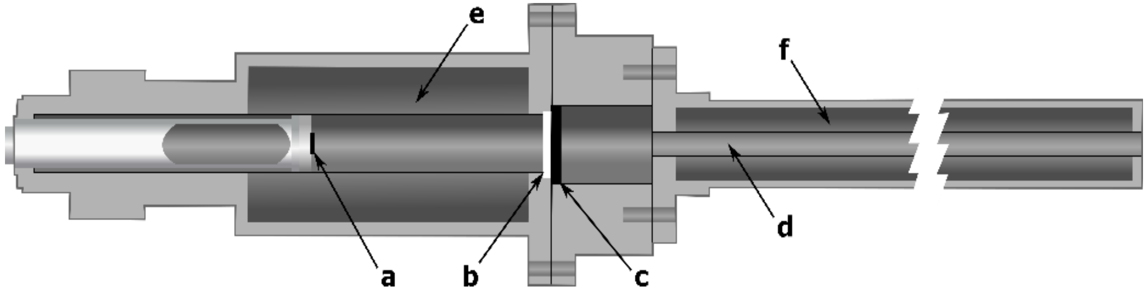

Cross-section view of Chalmers University narrow-angle radiometer (CTH NAR).

Instruments: Ellipsoidal Radiometer (ER)

- Instrument from Chalmers University (CTH)
- Thermopile detector that outputs voltage proportional to incident radiation
- Gold plated inner cavity and lens to focus incoming radiation from all directions onto a detector
  - Large FOV
- Measures: total heat flux (kW/m²)

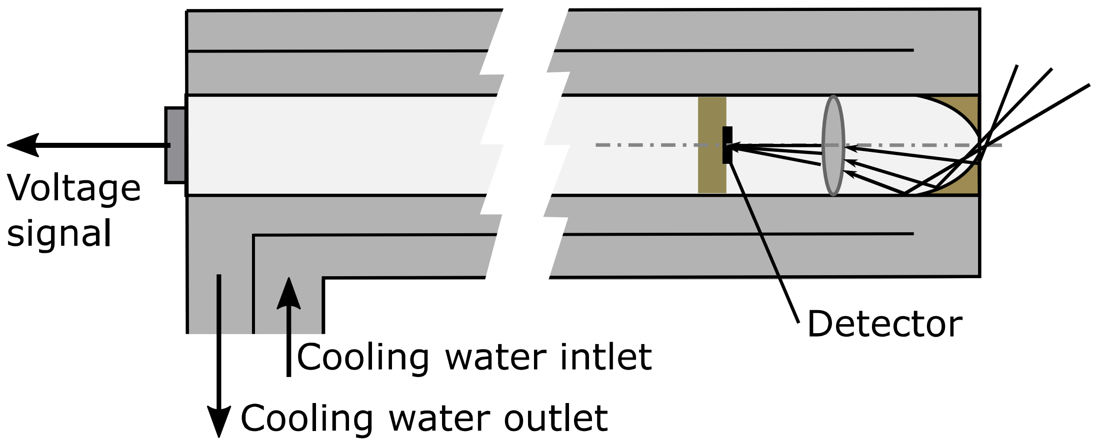

Cross section schematic of CTH ER.

Taking data in an industrial setting…

- Difficult conditions
  - Shaky
  - Difficult to repeat alignment each time
  - Each port had different access issues
  - Cooling water but no refrigeration unit
  - Had to travel multiple stories with all equipment and set up for each data point and instrument
  - Loud/hard to communicate
  - High ambient temperatures (average: 130 °F, peak: 143 °F)

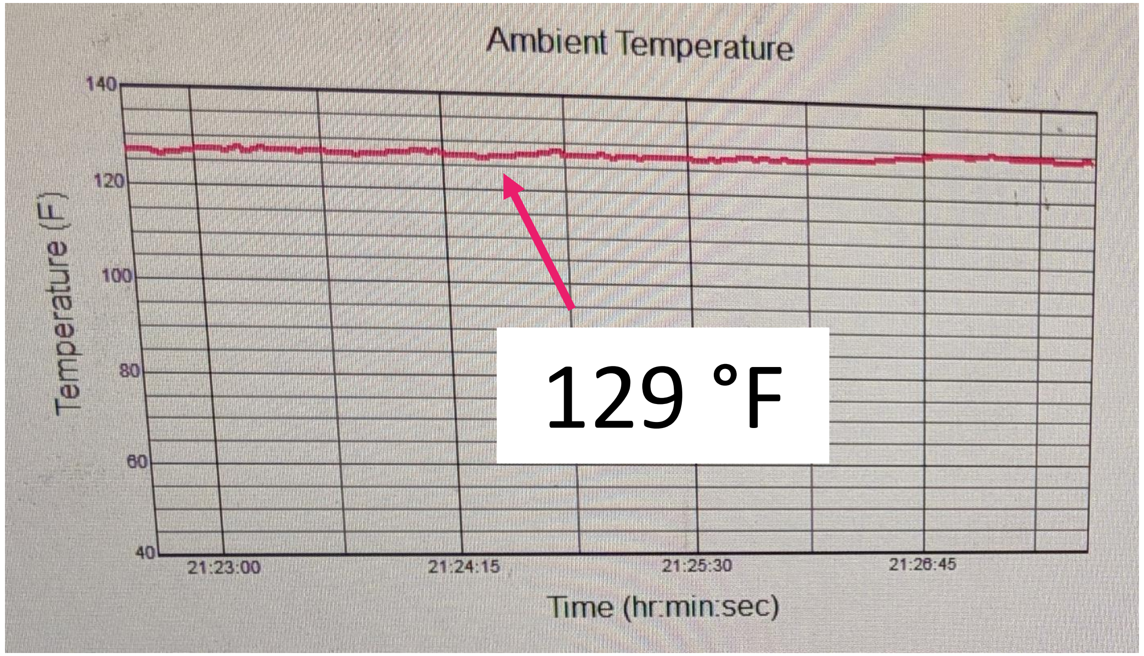

Cell phone image of opto readout of ambient temperature while taking data.

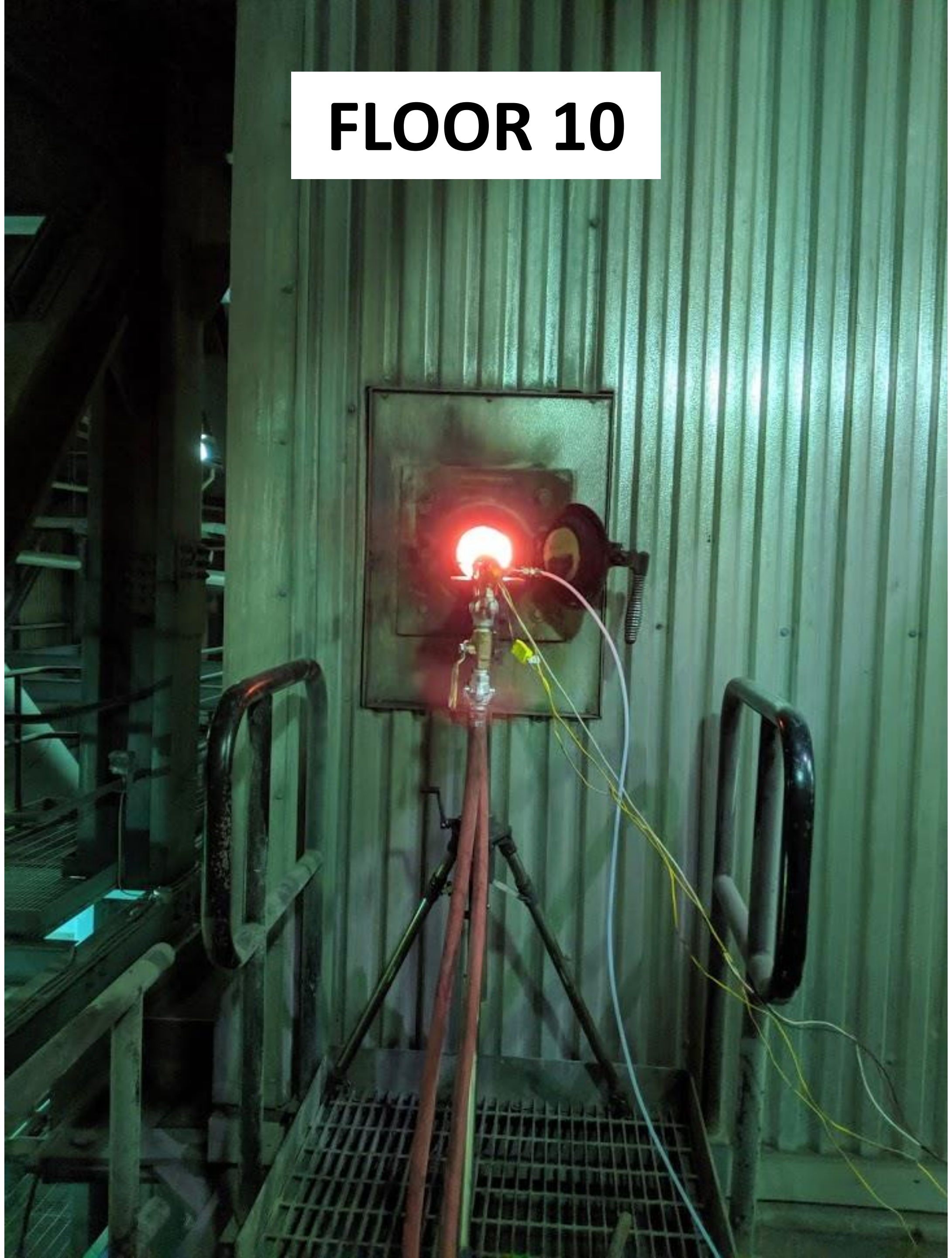
FLOOR 10

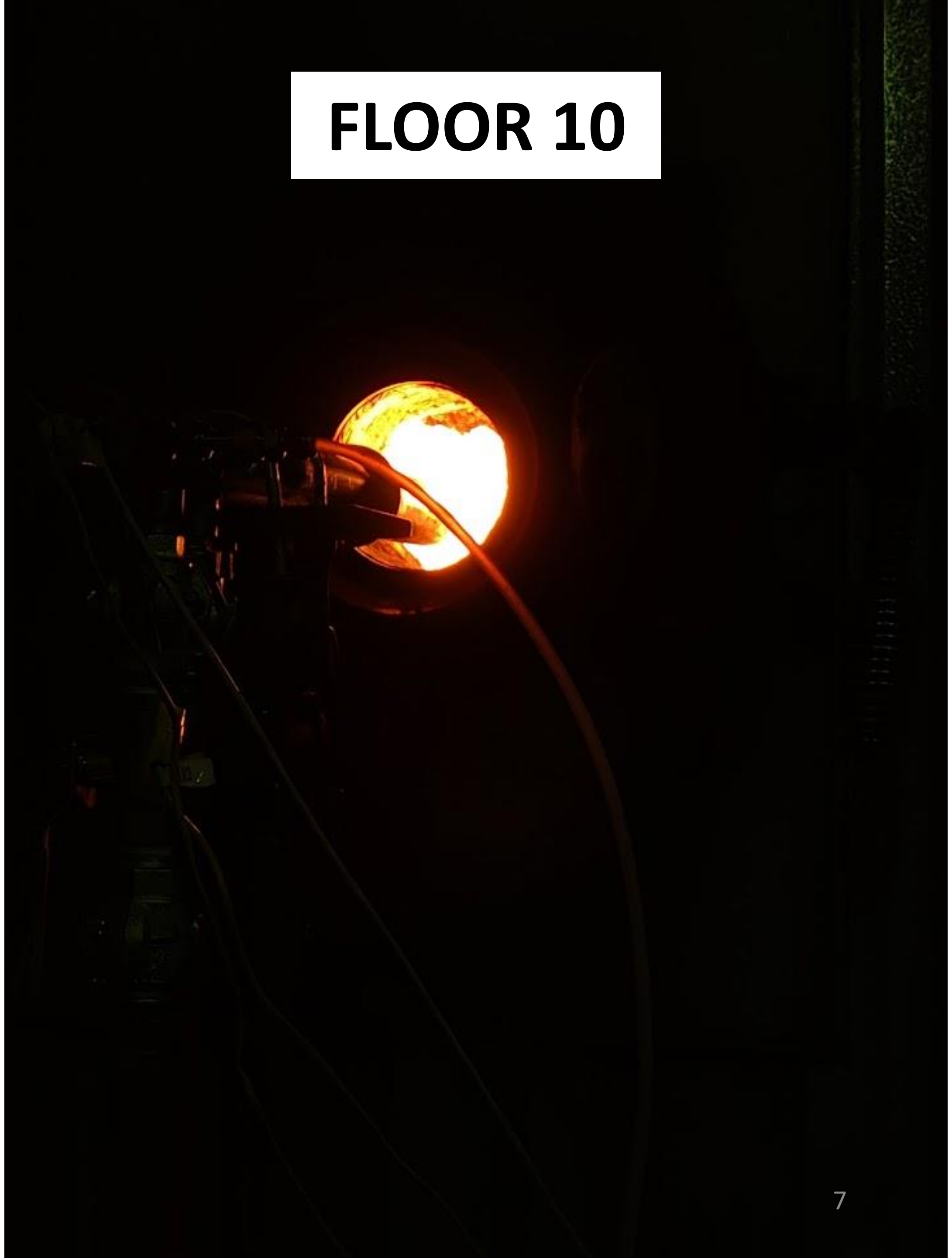
FLOOR 10

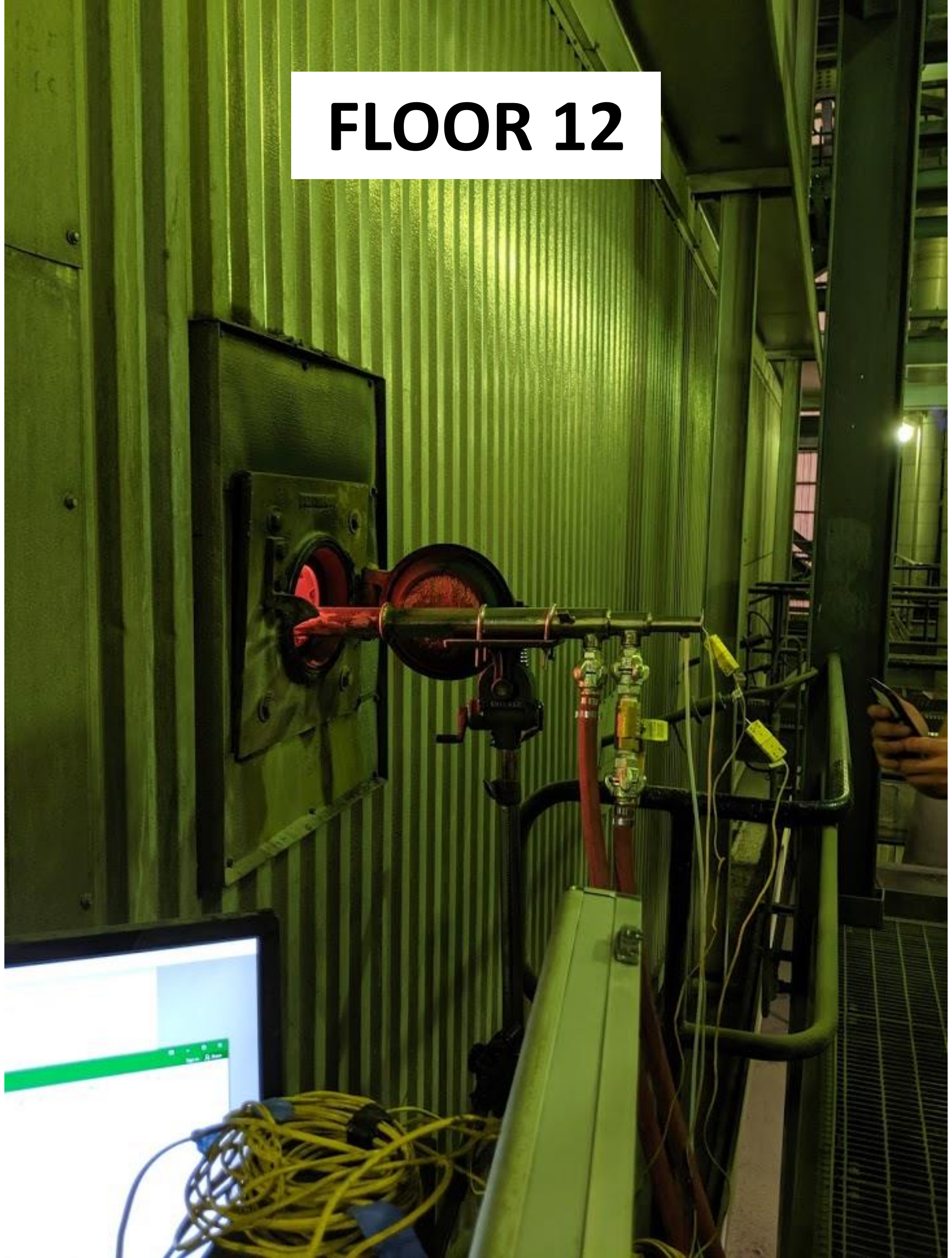

FLOOR 12

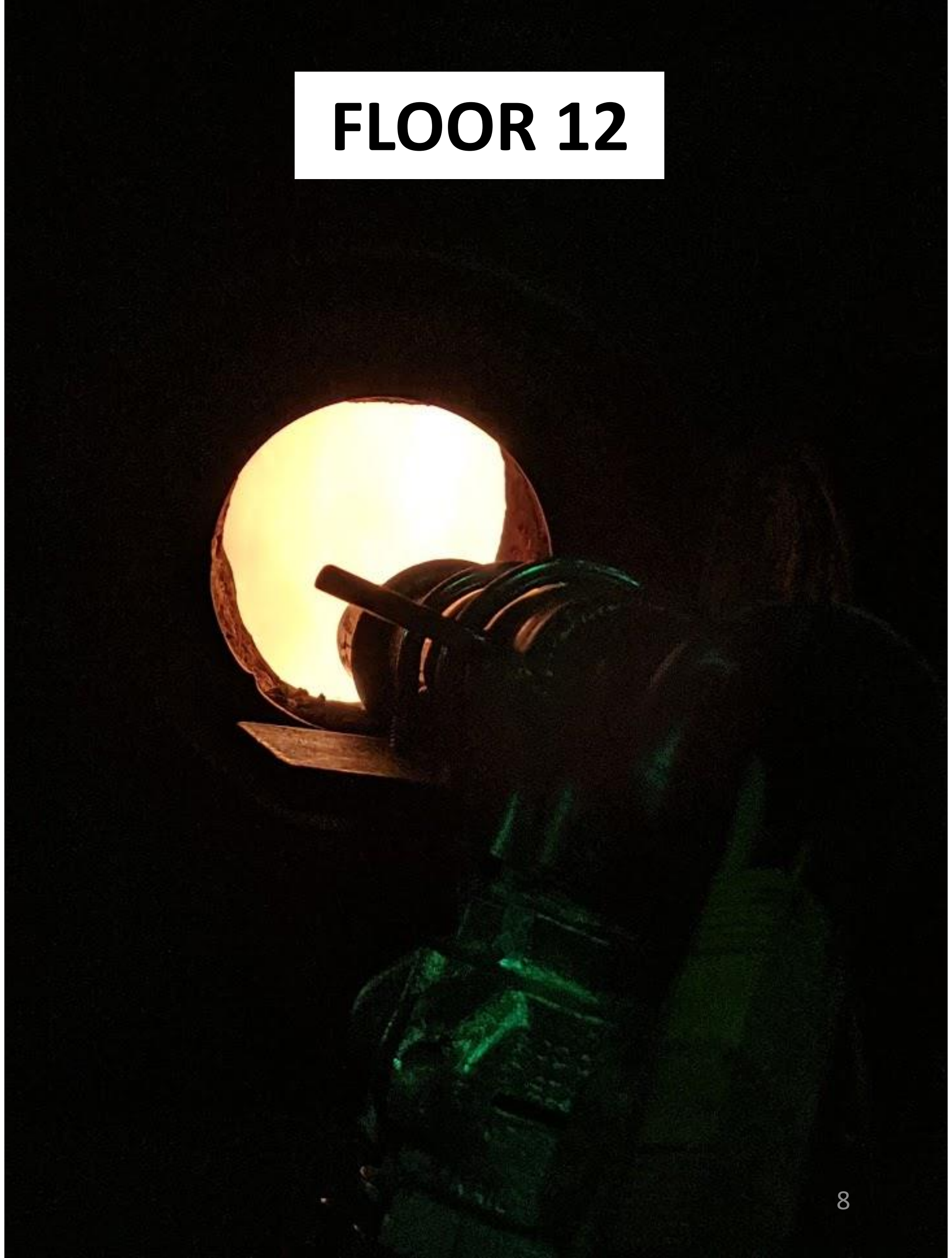

FLOOR 12

FLOOR 14

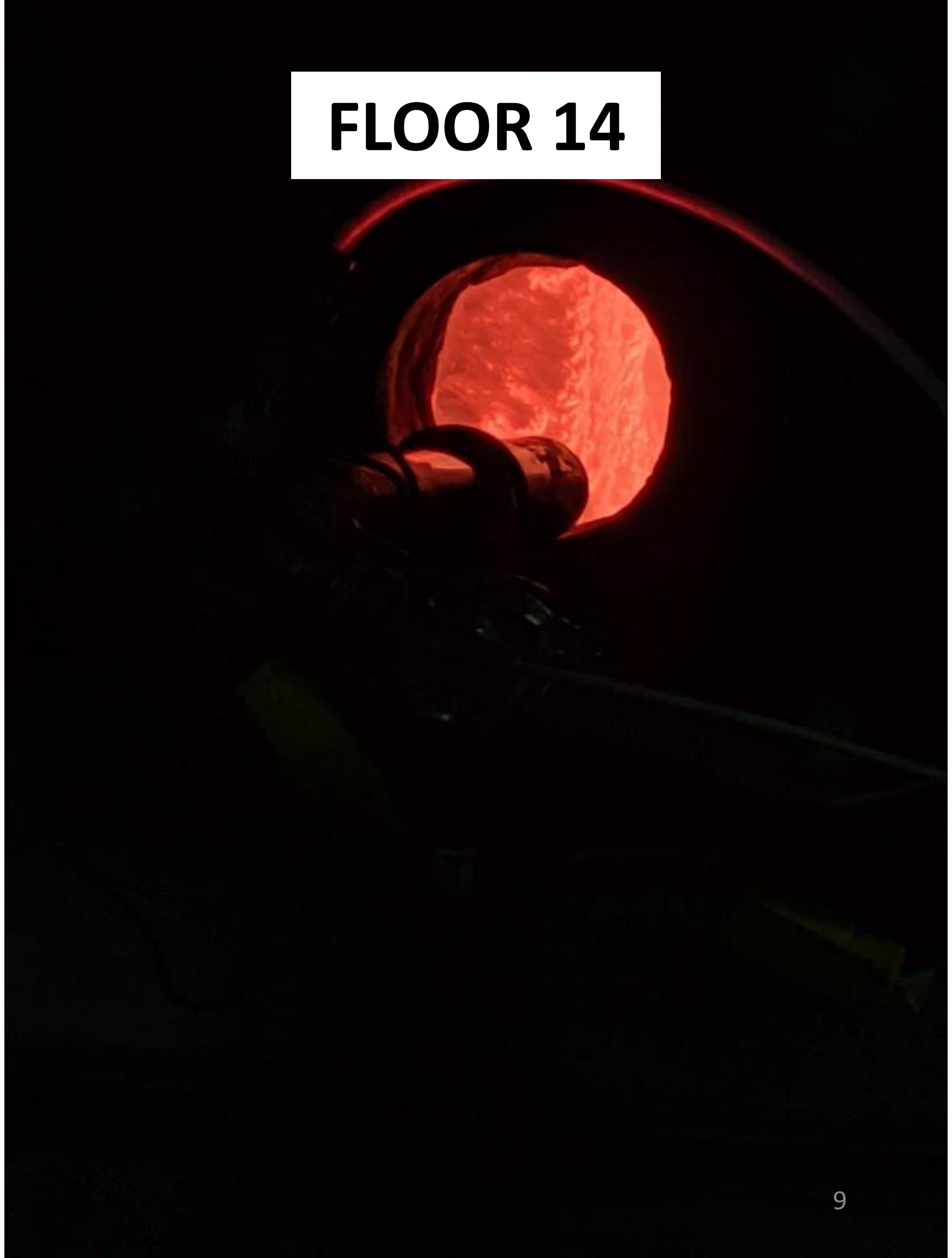

FLOOR 14

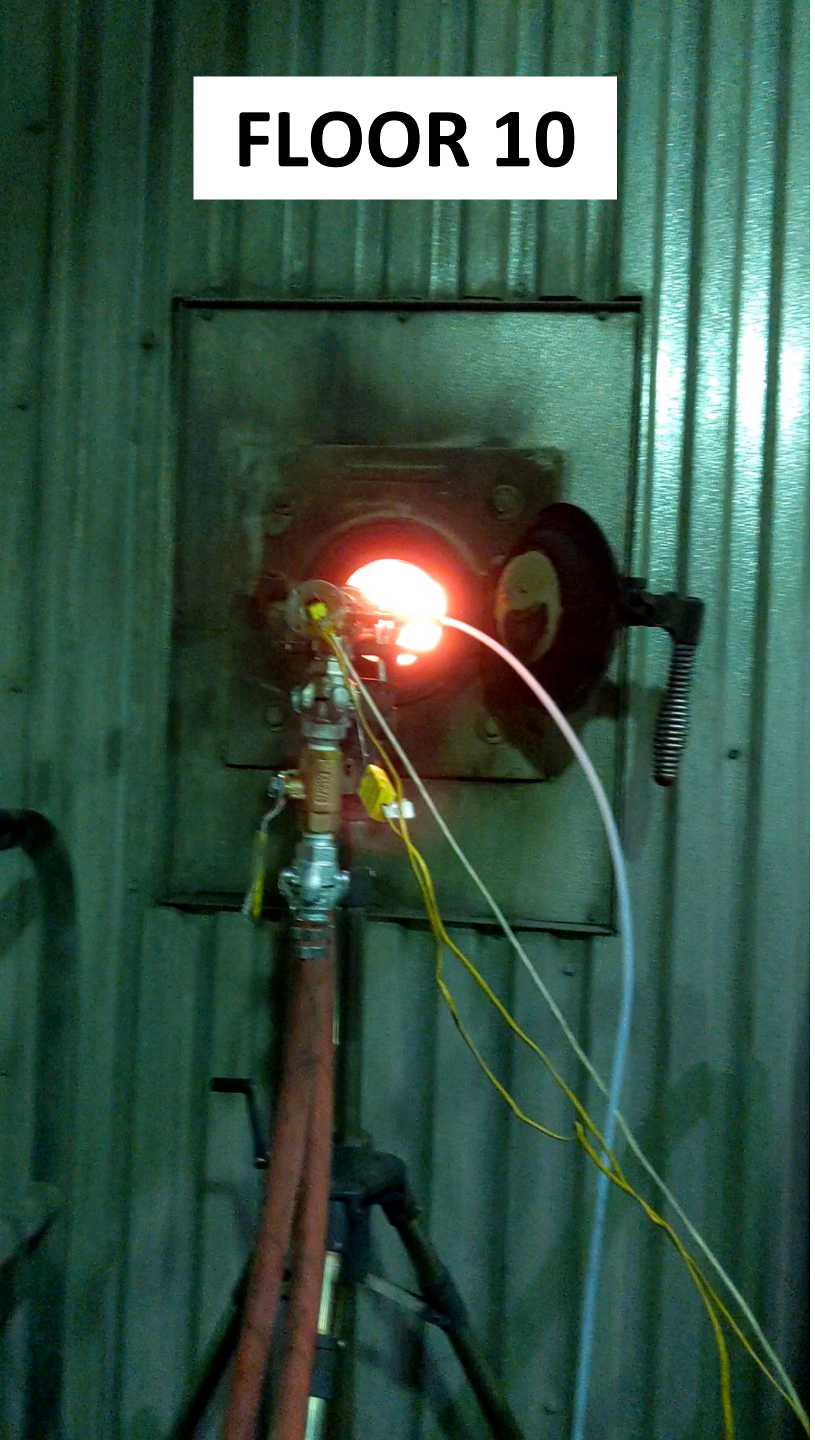

FLOOR 10

FLOOR 12

FLOOR 14

UofU Narrow-Angle Radiometer (UofU NAR)

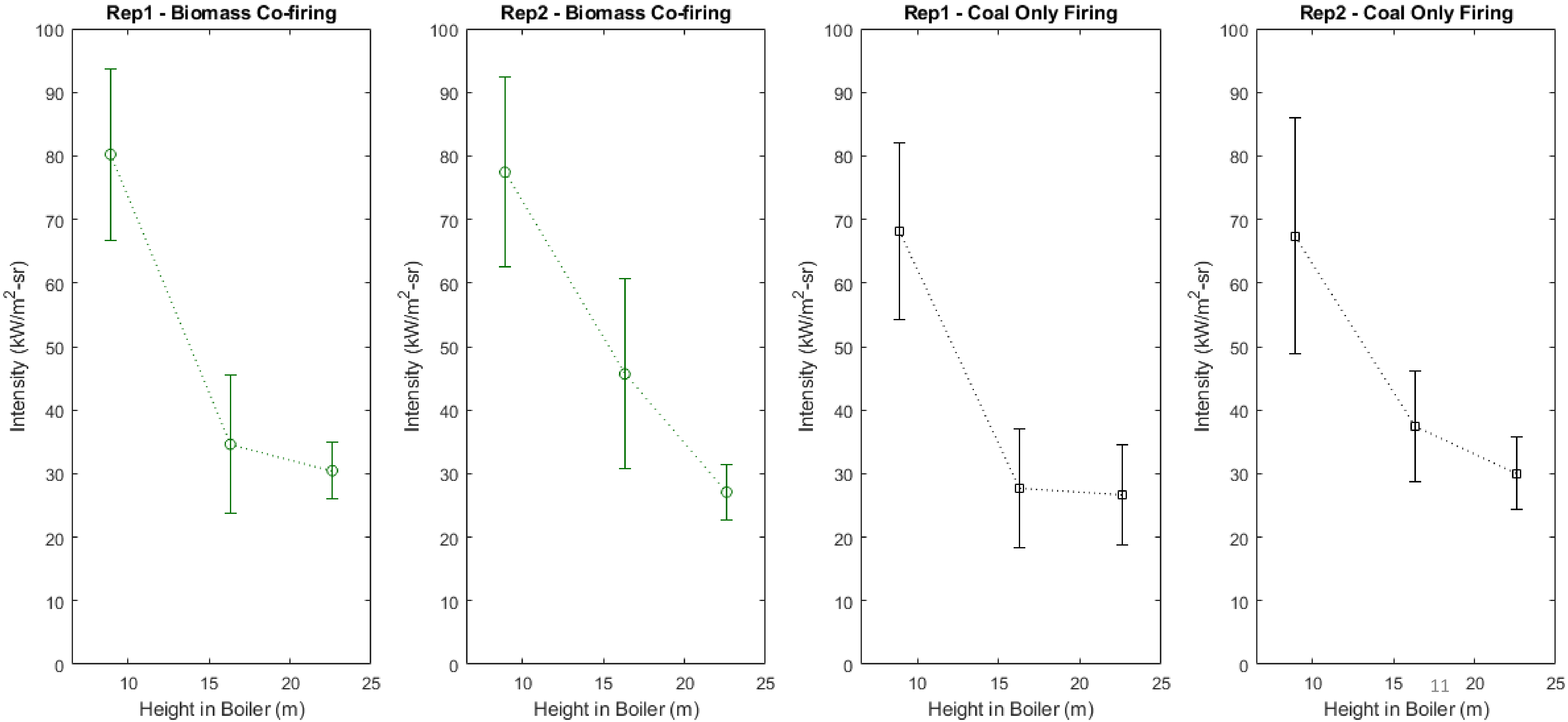

UofU Narrow-Angle Radiometer (UofU NAR)

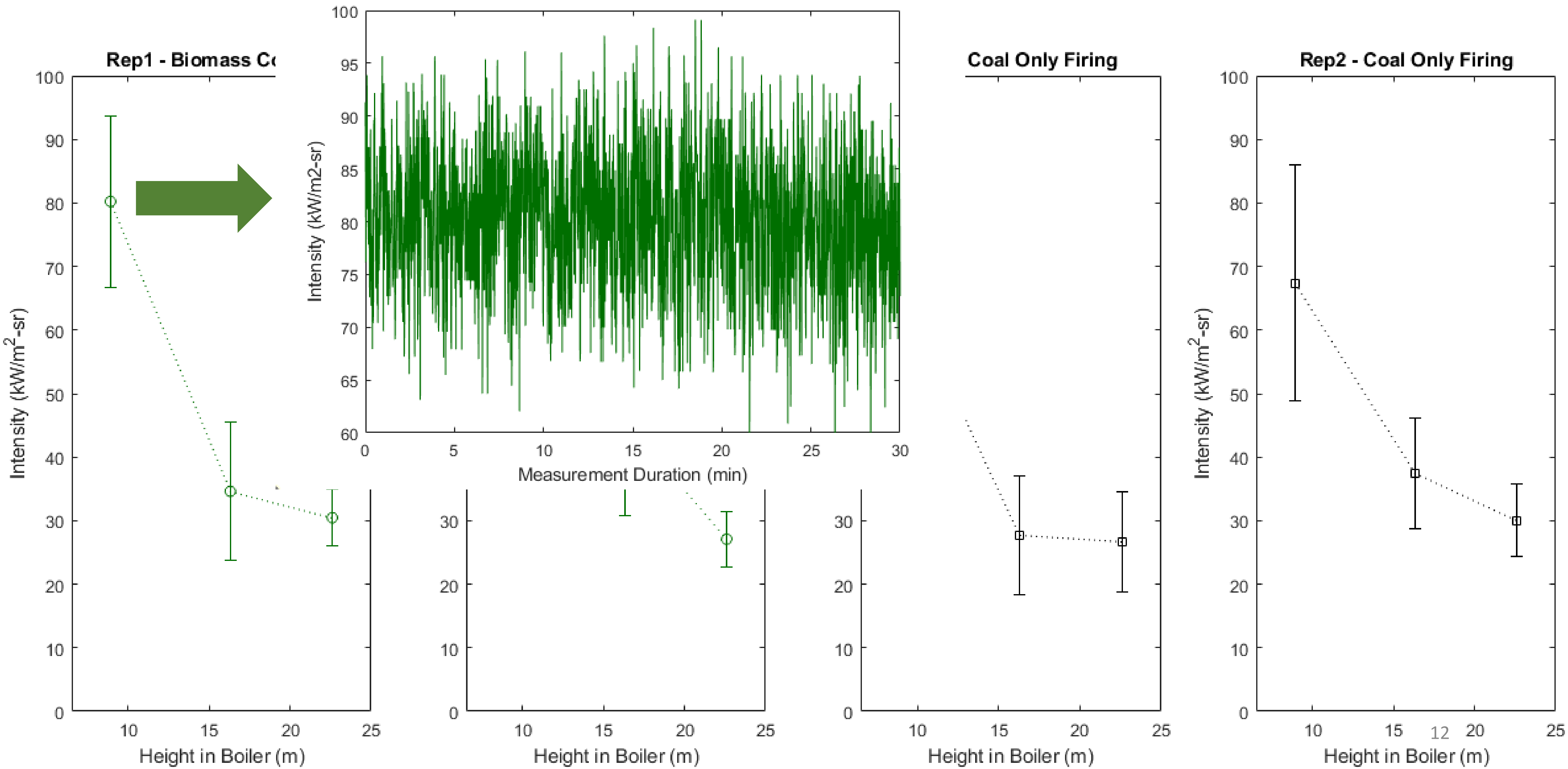

UofU Narrow-Angle Radiometer (UofU NAR)

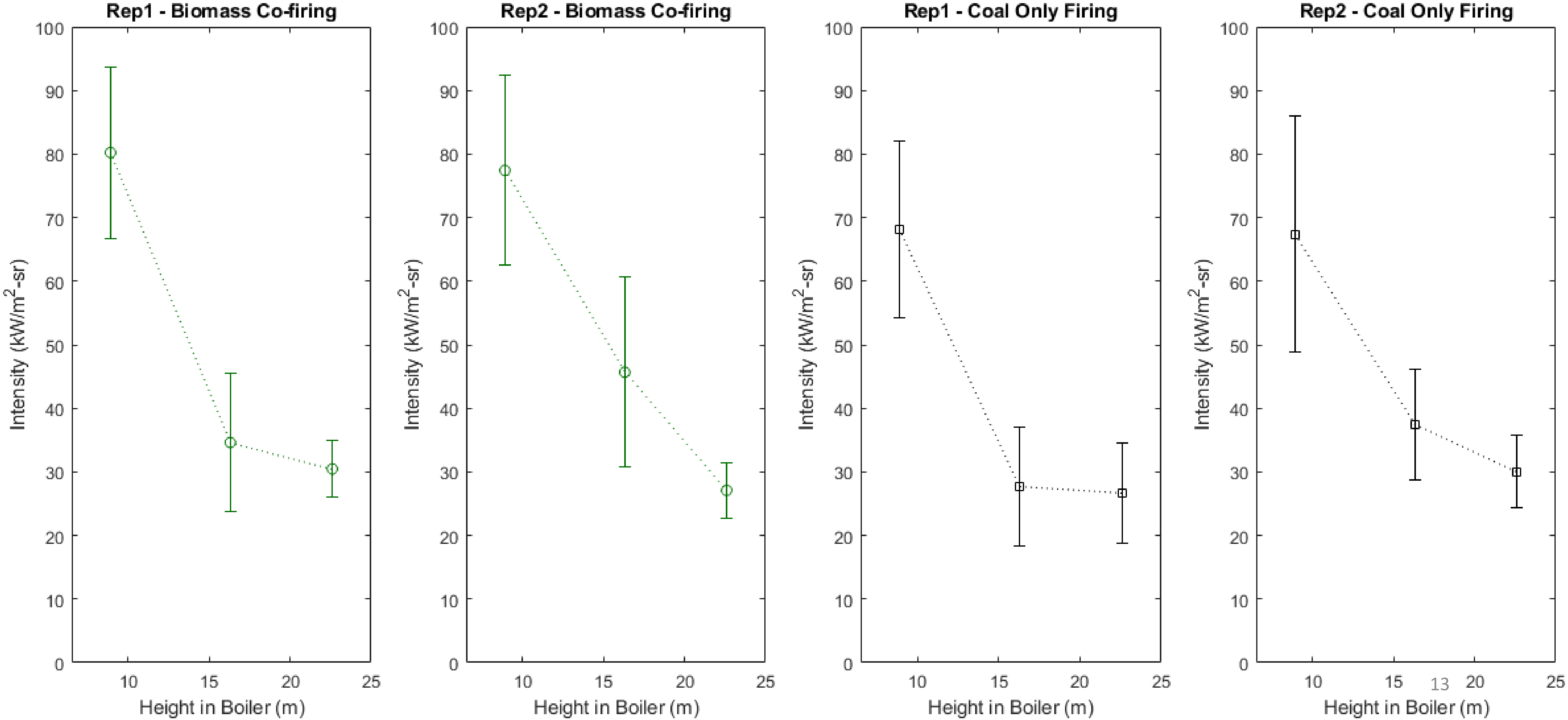

Chalmers Narrow-Angle Radiometer (CTH NAR)

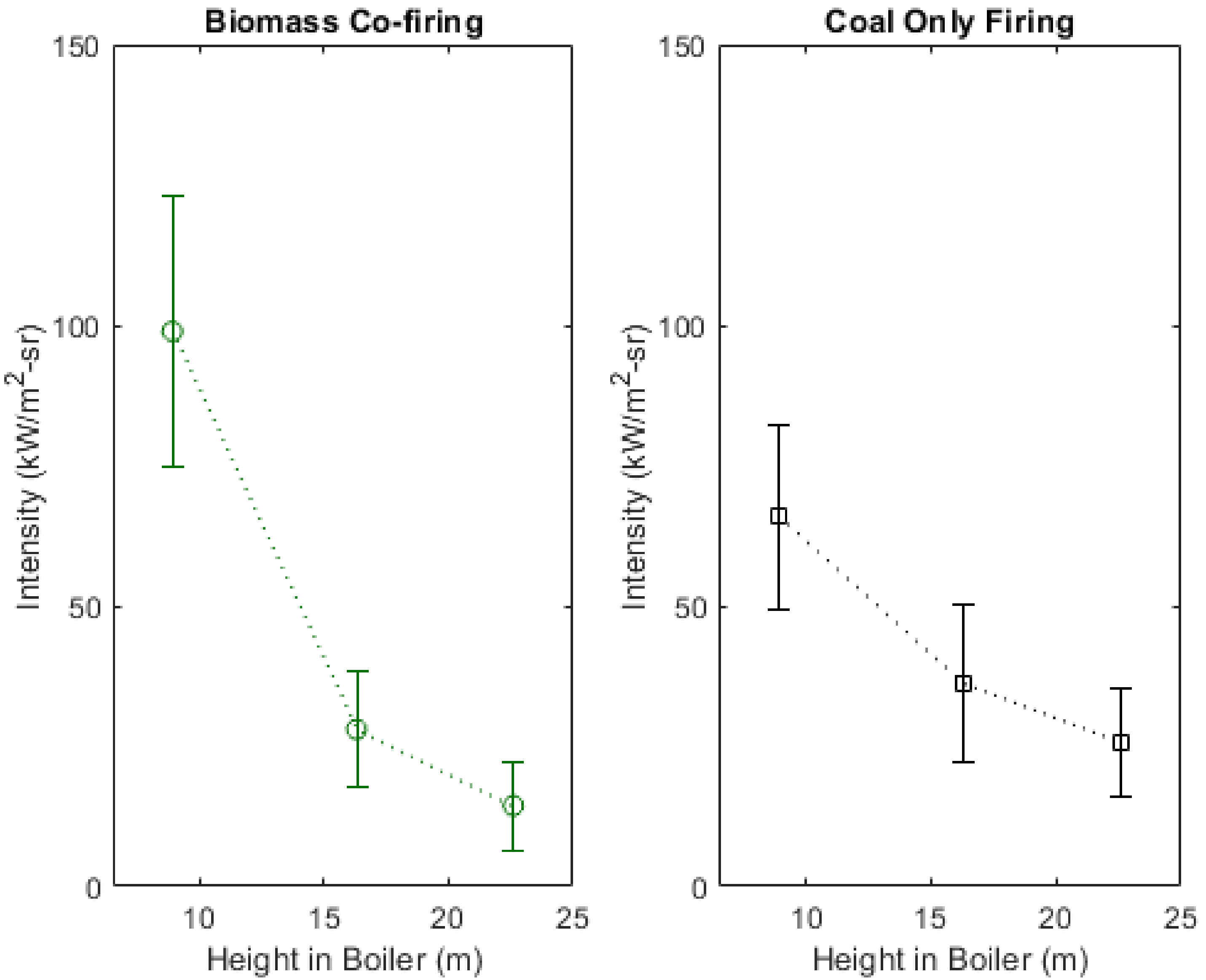

Chalmers Narrow-Angle Radiometer (CTH NAR)

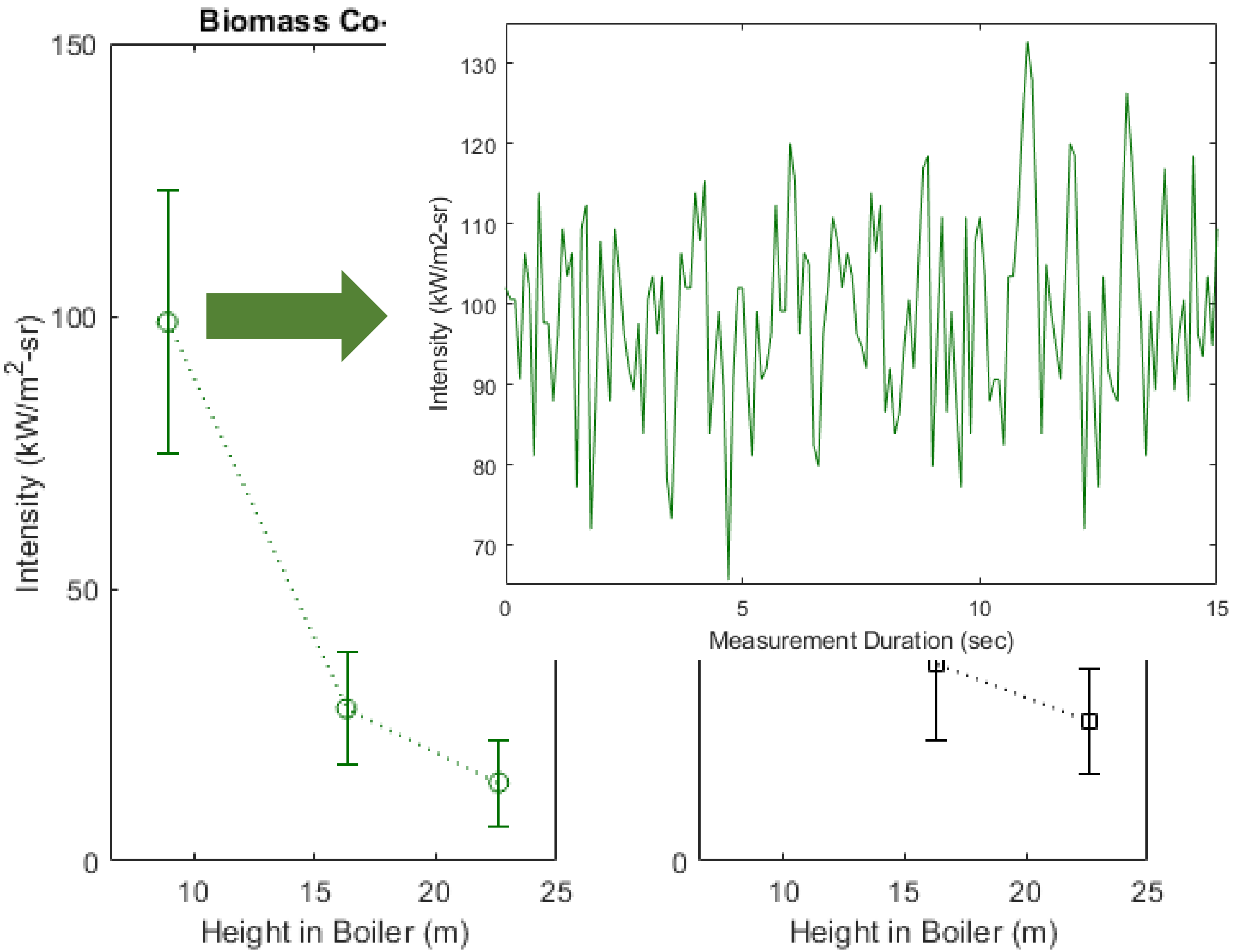

Chalmers Narrow-Angle Radiometer (CTH NAR)

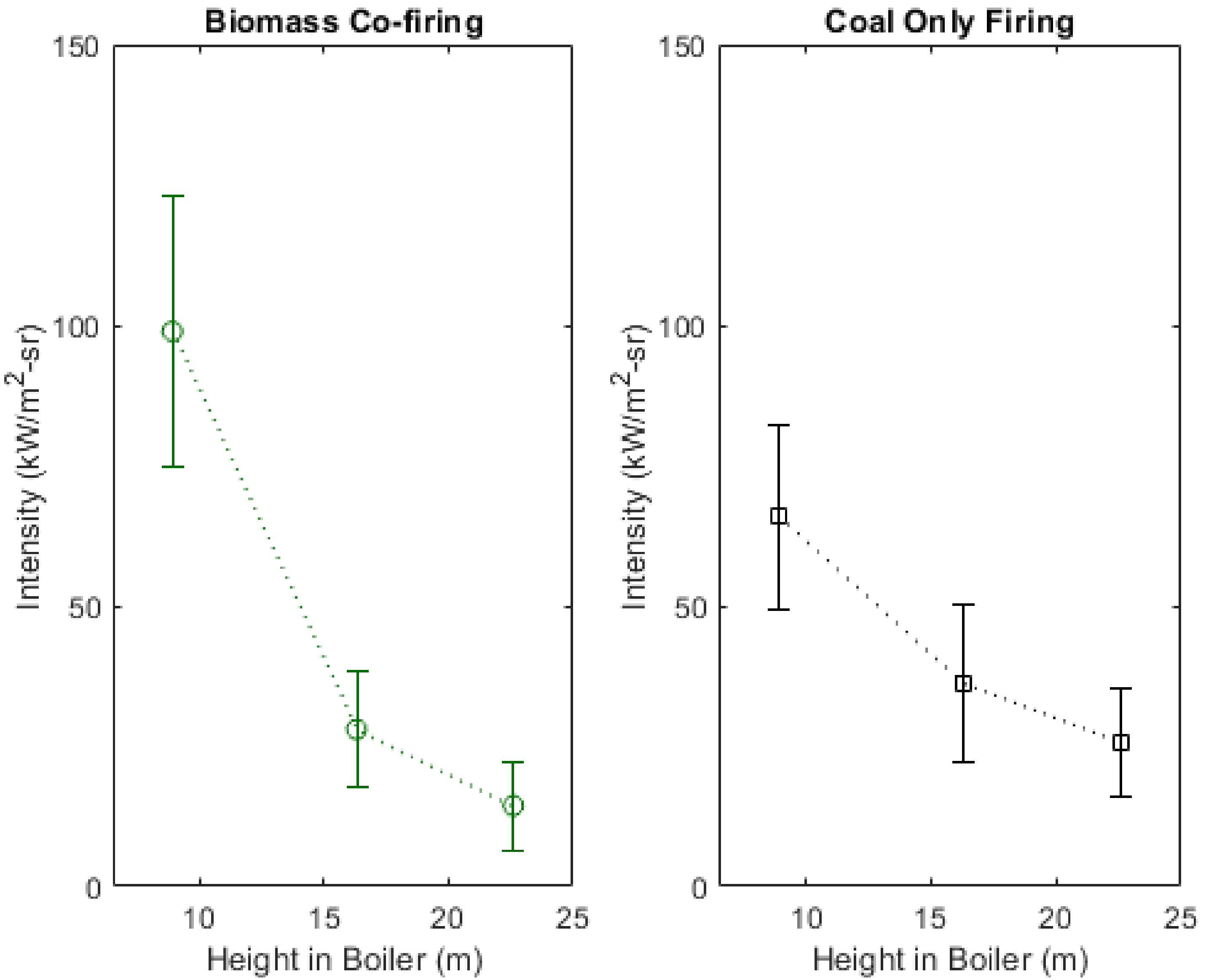

Chalmers Ellipsoidal Radiometer (CTH ER)

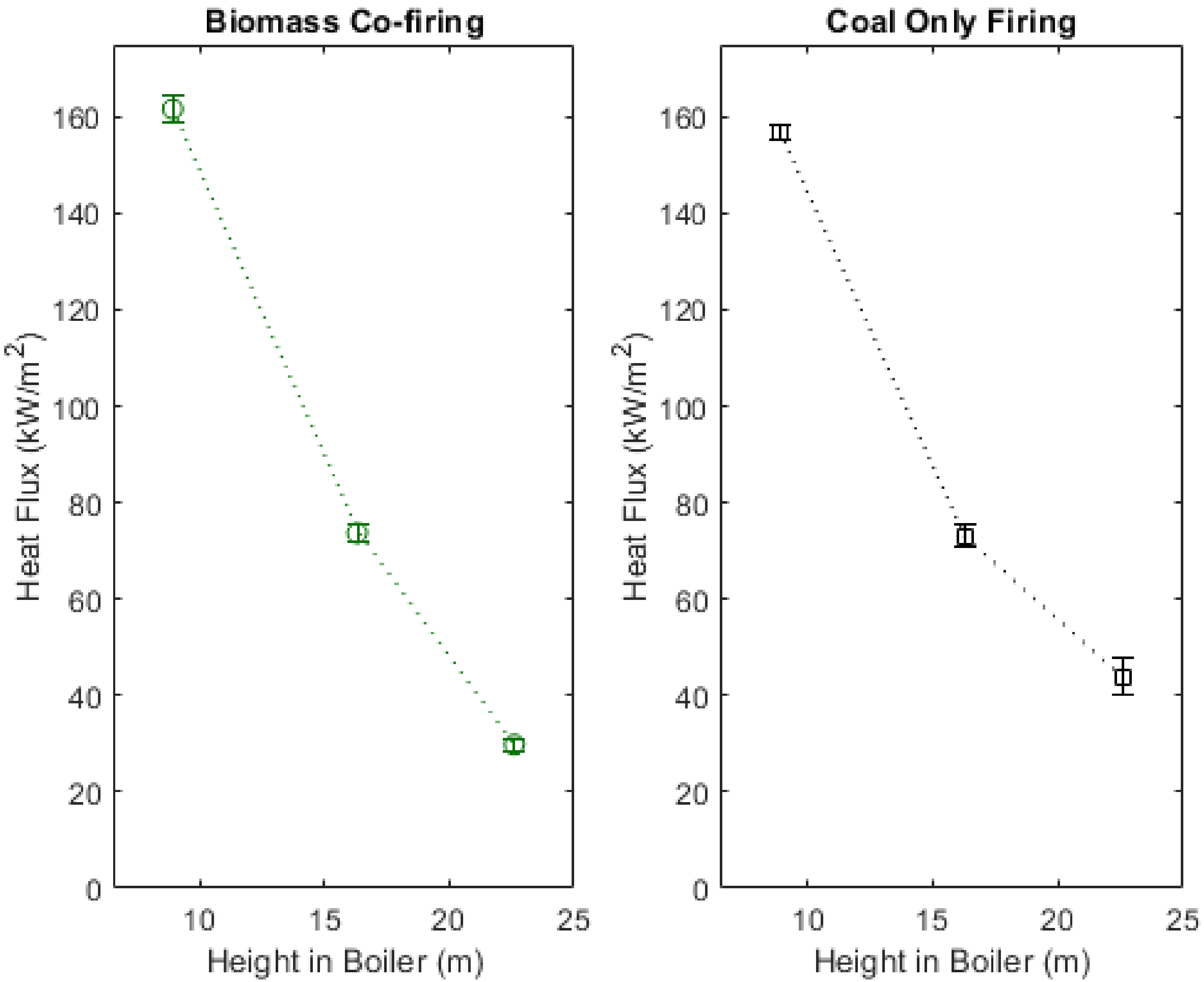

Chalmers Ellips R)

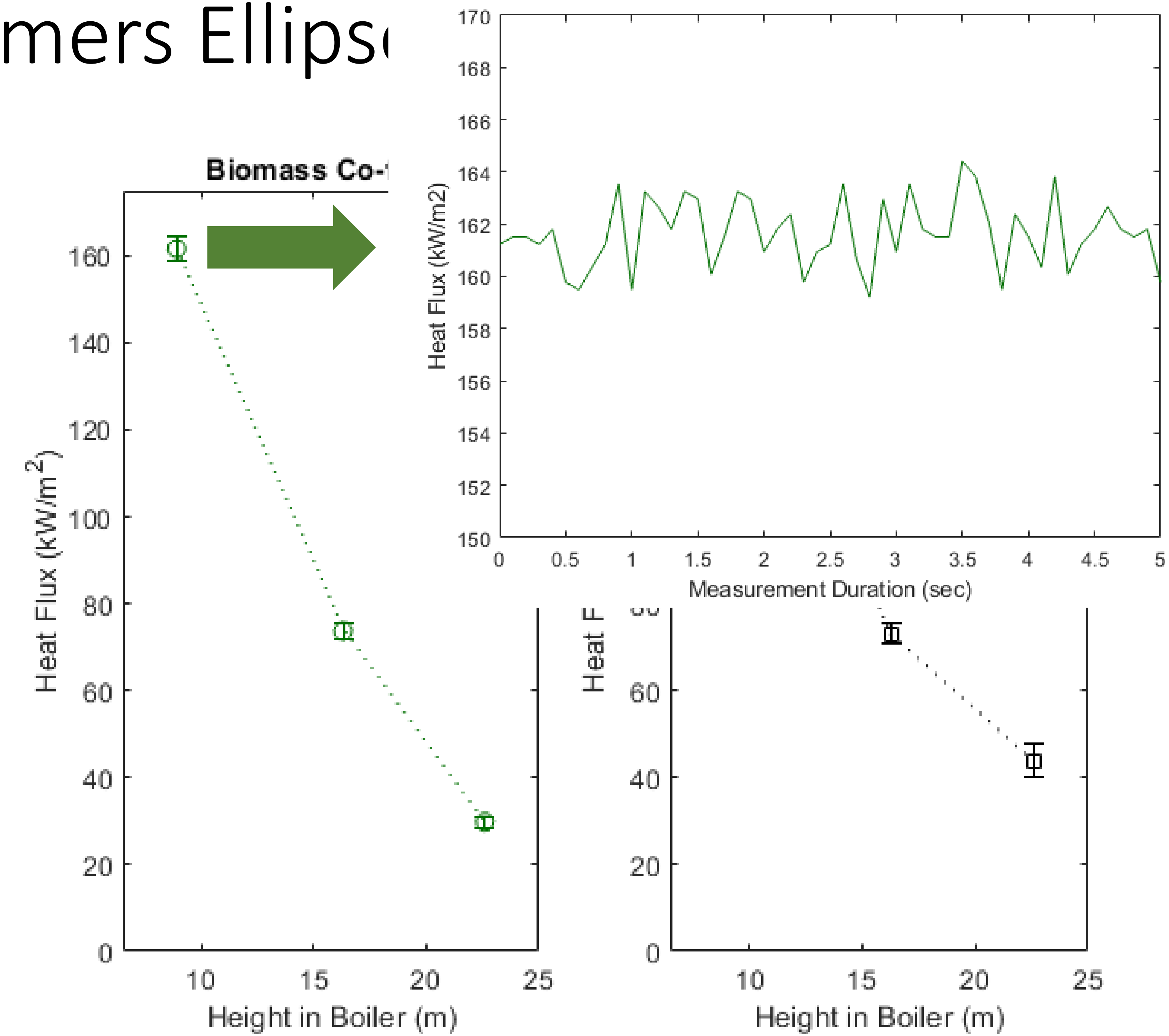

Chalmers Ellipsoidal Radiometer (CTH ER)

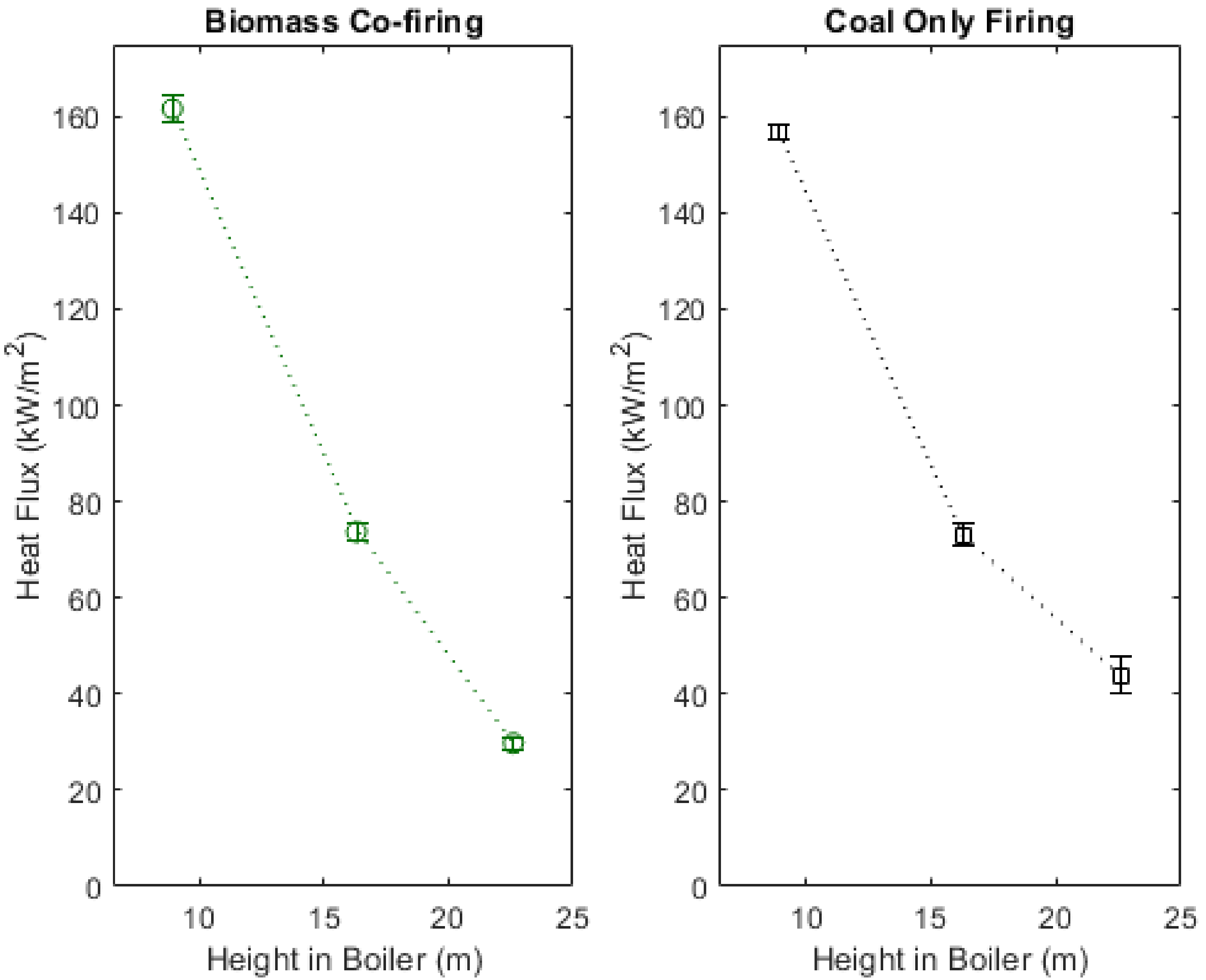

Comparing Instruments

- Instruments appear to do quite well comparing between replicates and fuel conditions
- How well do they compare against each other?
- The two NARs can be compared directly, but to compare the ER, we must make some assumptions
- If we assume the radiation from the flame is diffuse, we can convert the intensity from the NARs to heat flux:

$$E_f = \pi I_f$$

  - Not a great assumption for this application, but the comparison is still useful

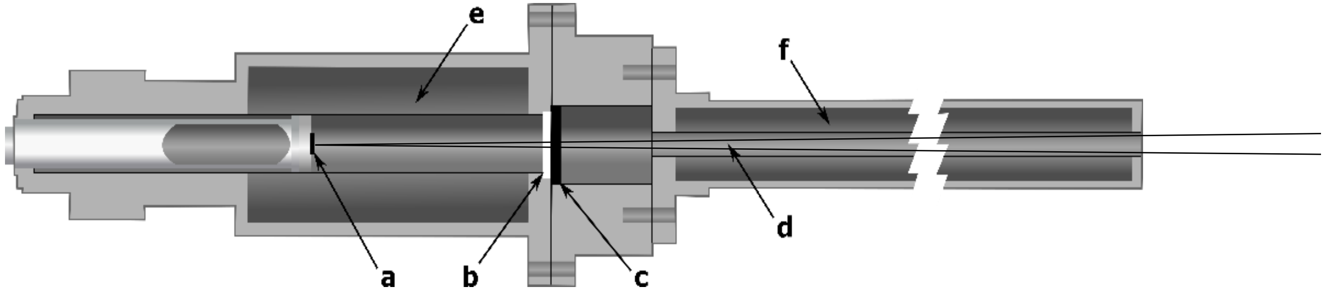

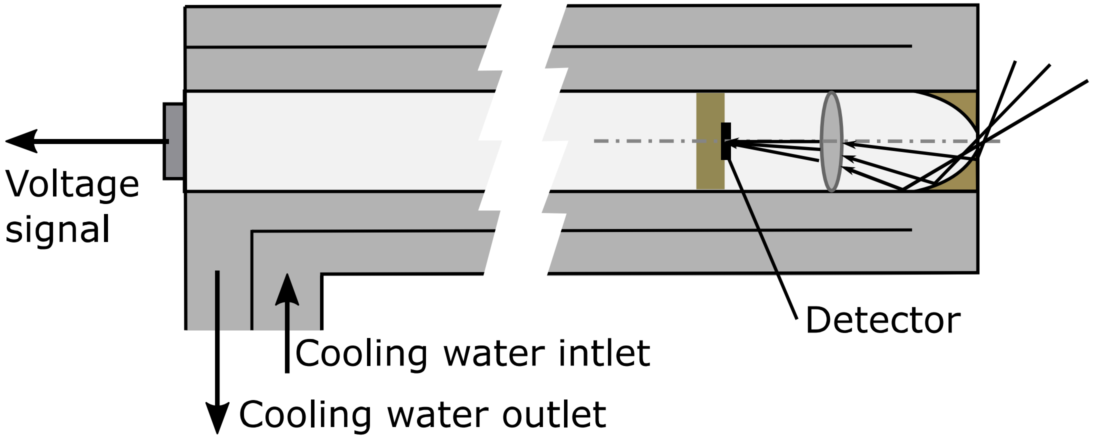

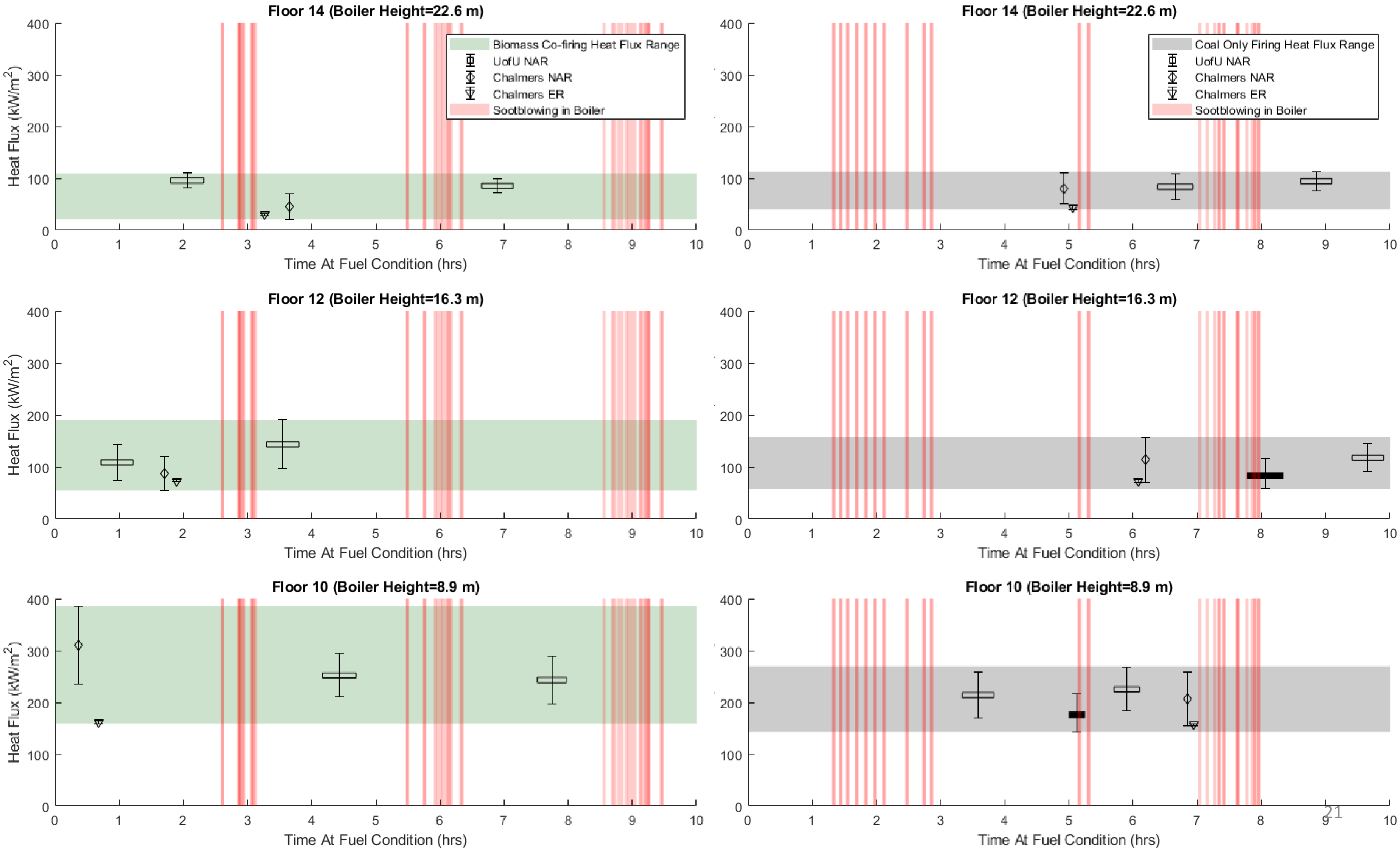
Floor 14 (Boiler Height=22.6 m)
Floor 12 (Boiler Height=16.3 m)
Floor 10 (Boiler Height=8.9 m)
Heat Flux (kW/m^2)
Time At Fuel Condition (hrs)
0
100
200
300
400
0
1
2
3
4
5
6
7
8
9
10
Biomass Co-firing Heat Flux Range
Coal Only Firing Heat Flux Range
UofU NAR
Chalmers NAR
Chalmers ER
Sootblowing in Boiler

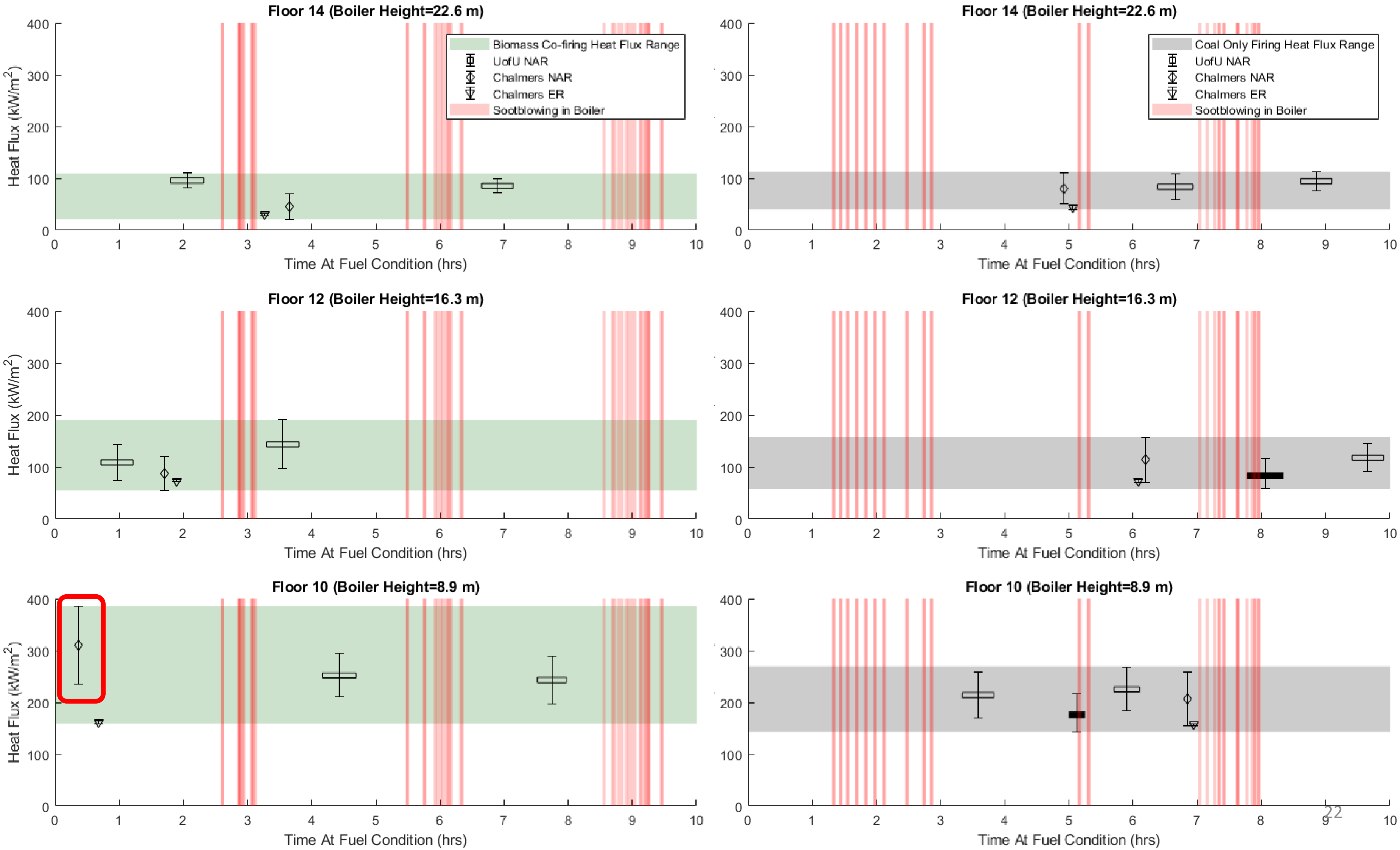
Floor 14 (Boiler Height=22.6 m)
Floor 12 (Boiler Height=16.3 m)
Floor 10 (Boiler Height=8.9 m)
Heat Flux (kW/m²)
Time At Fuel Condition (hrs)
Biomass Co-firing Heat Flux Range
Coal Only Firing Heat Flux Range
UofU NAR
Chalmers NAR
Chalmers ER
Sootblowing in Boiler
0
100
200
300
400
0
1
2
3
4
5
6
7
8
9
10

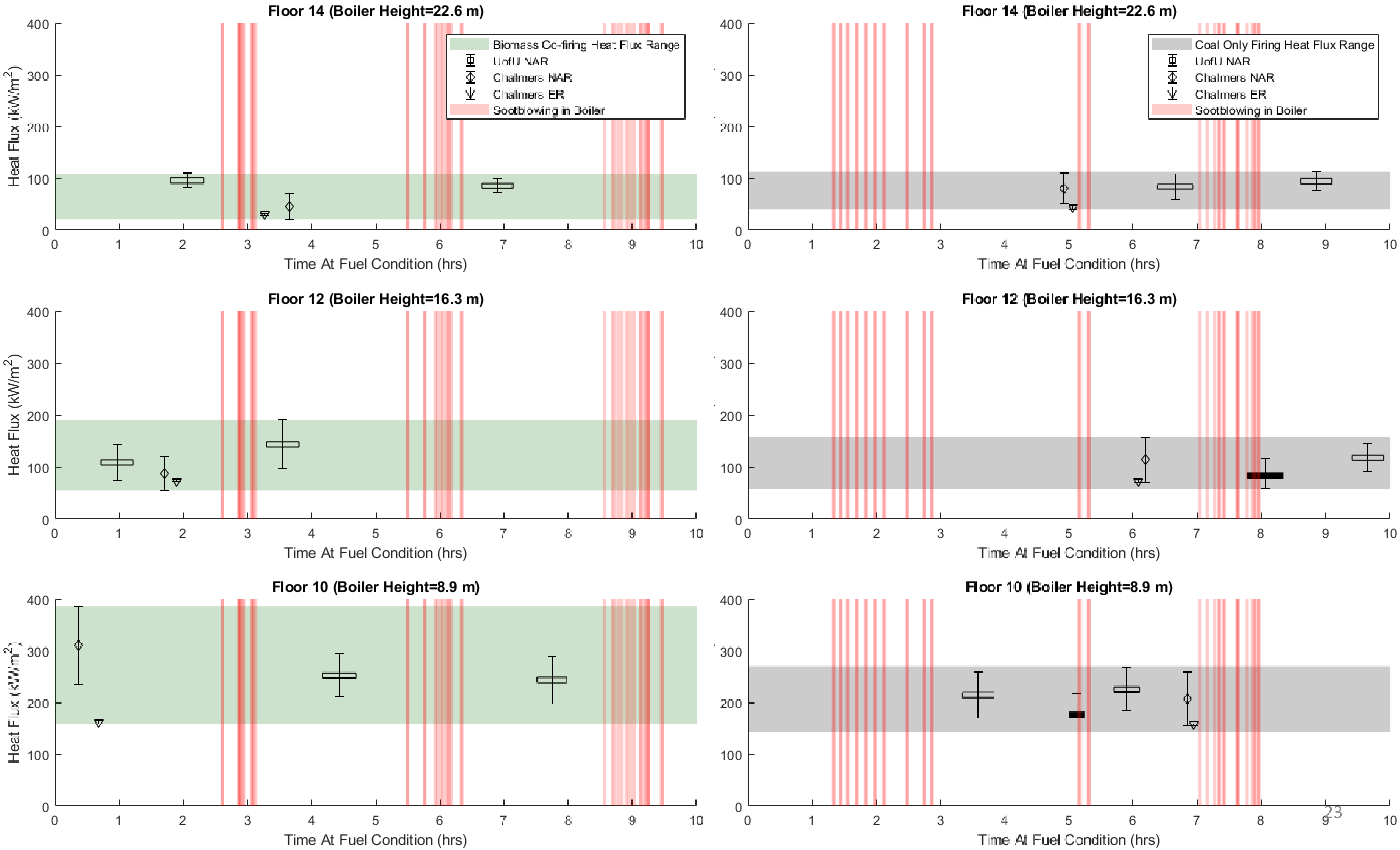
Floor 14 (Boiler Height=22.6 m)
Floor 14 (Boiler Height=22.6 m)
Biomass Co-firing Heat Flux Range
Coal Only Firing Heat Flux Range
UofU NAR
Chalmers NAR
Chalmers ER
Sootblowing in Boiler
Floor 12 (Boiler Height=16.3 m)
Floor 12 (Boiler Height=16.3 m)
Floor 10 (Boiler Height=8.9 m)
Floor 10 (Boiler Height=8.9 m)
Heat Flux (kW/m²)
0
100
200
300
400
Time At Fuel Condition (hrs)
0
1
2
3
4
5
6
7
8
9
10

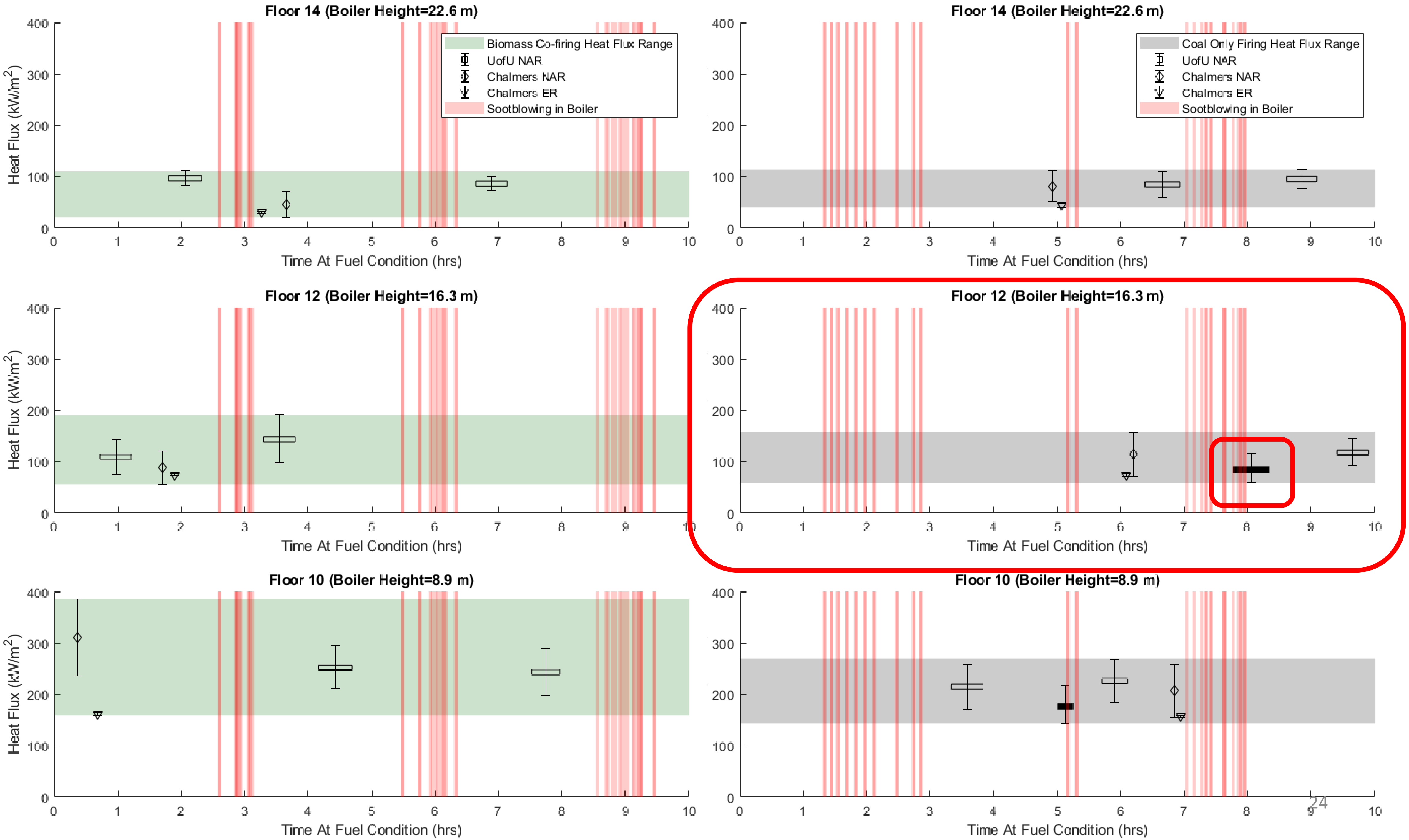
Floor 14 (Boiler Height=22.6 m)
Floor 12 (Boiler Height=16.3 m)
Floor 10 (Boiler Height=8.9 m)
Biomass Co-firing Heat Flux Range
Coal Only Firing Heat Flux Range
UofU NAR
Chalmers NAR
Chalmers ER
Sootblowing in Boiler
Heat Flux (kW/m²)
Time At Fuel Condition (hrs)
0
100
200
300
400
0
1
2
3
4
5
6
7
8
9
10

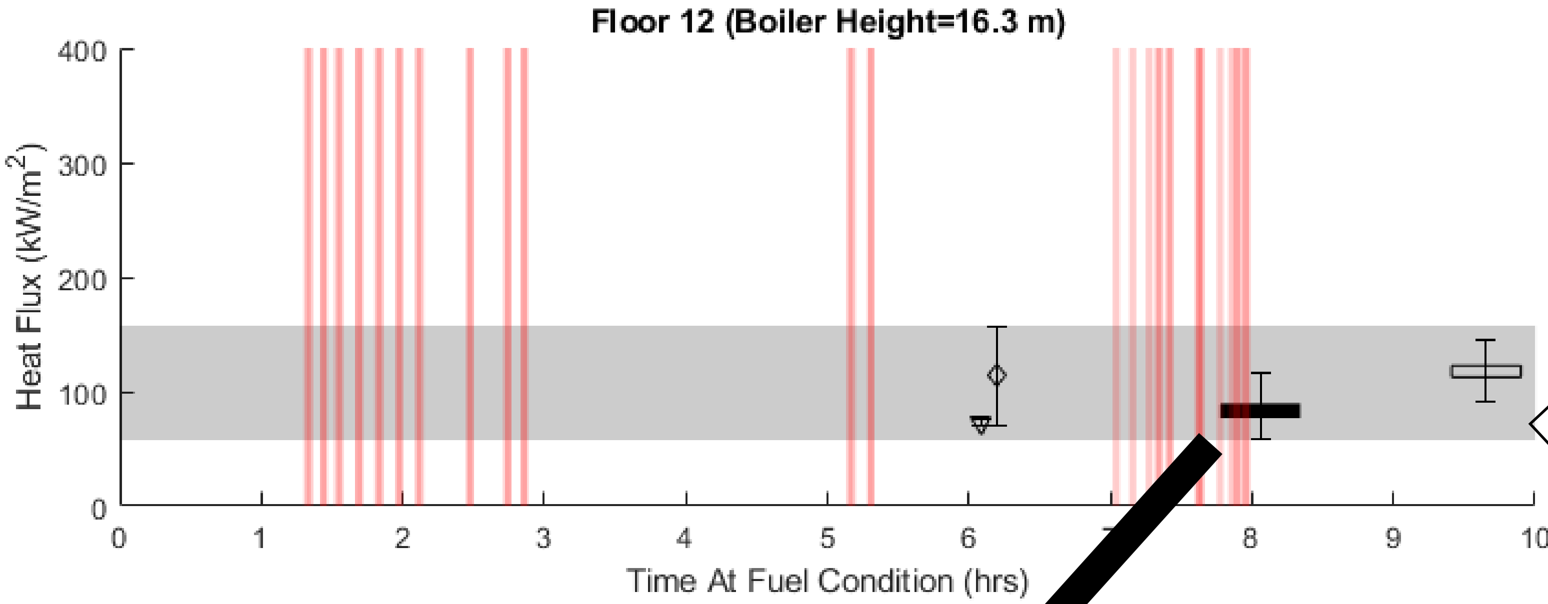

Trend is as expected, heat flux increases with time from soot blowing

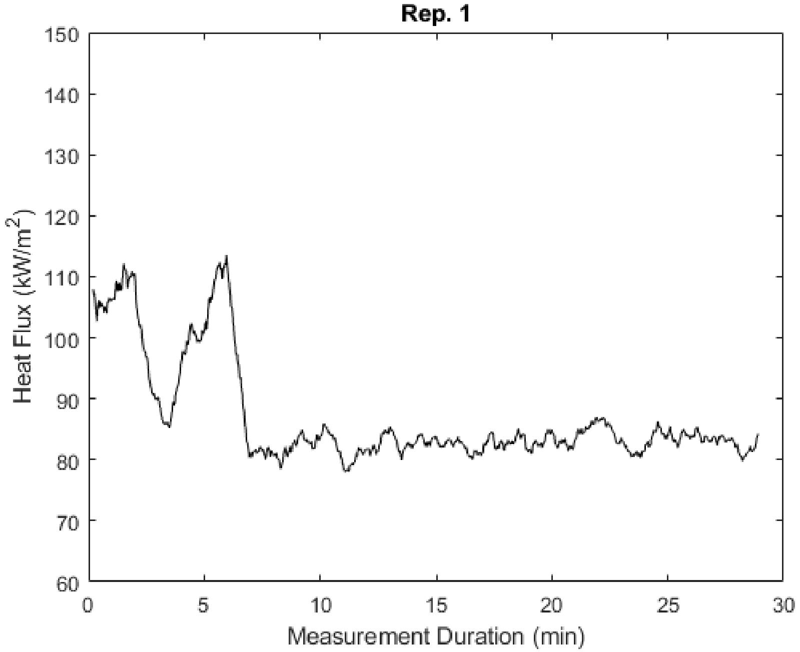

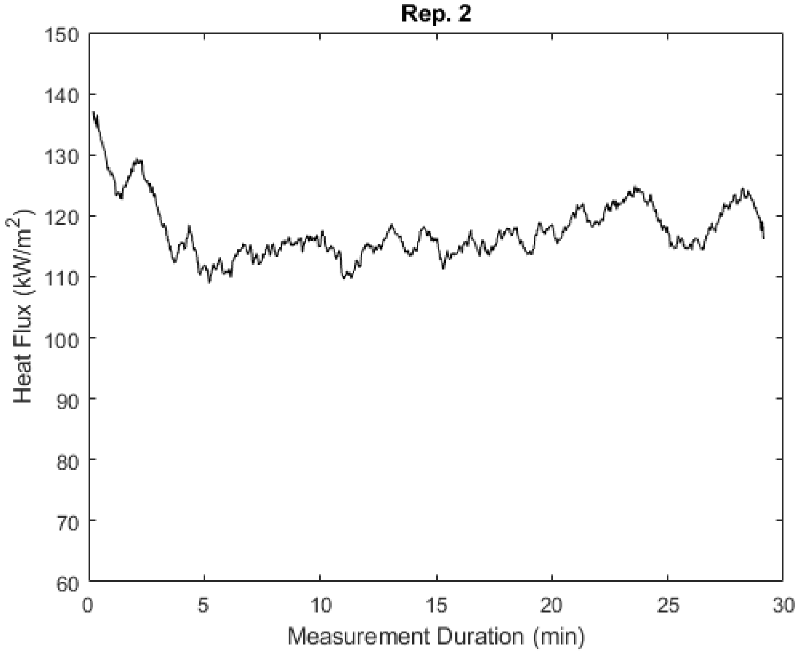

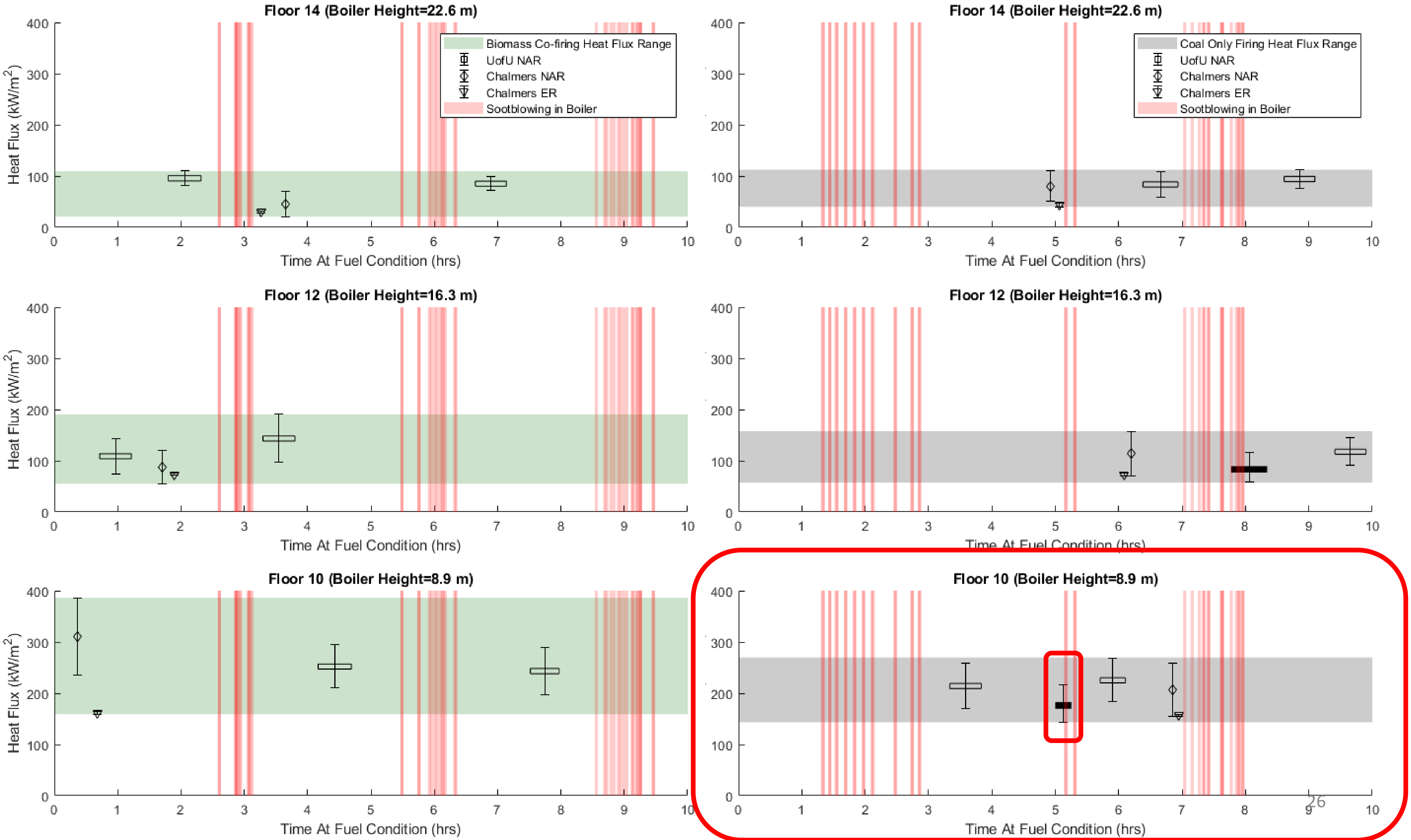
Floor 14 (Boiler Height=22.6 m)
Floor 12 (Boiler Height=16.3 m)
Floor 10 (Boiler Height=8.9 m)
Heat Flux (kW/m^2)
Time At Fuel Condition (hrs)
Biomass Co-firing Heat Flux Range
Coal Only Firing Heat Flux Range
UofU NAR
Chalmers NAR
Chalmers ER
Sootblowing in Boiler
0
100
200
300
400
0
1
2
3
4
5
6
7
8
9
10

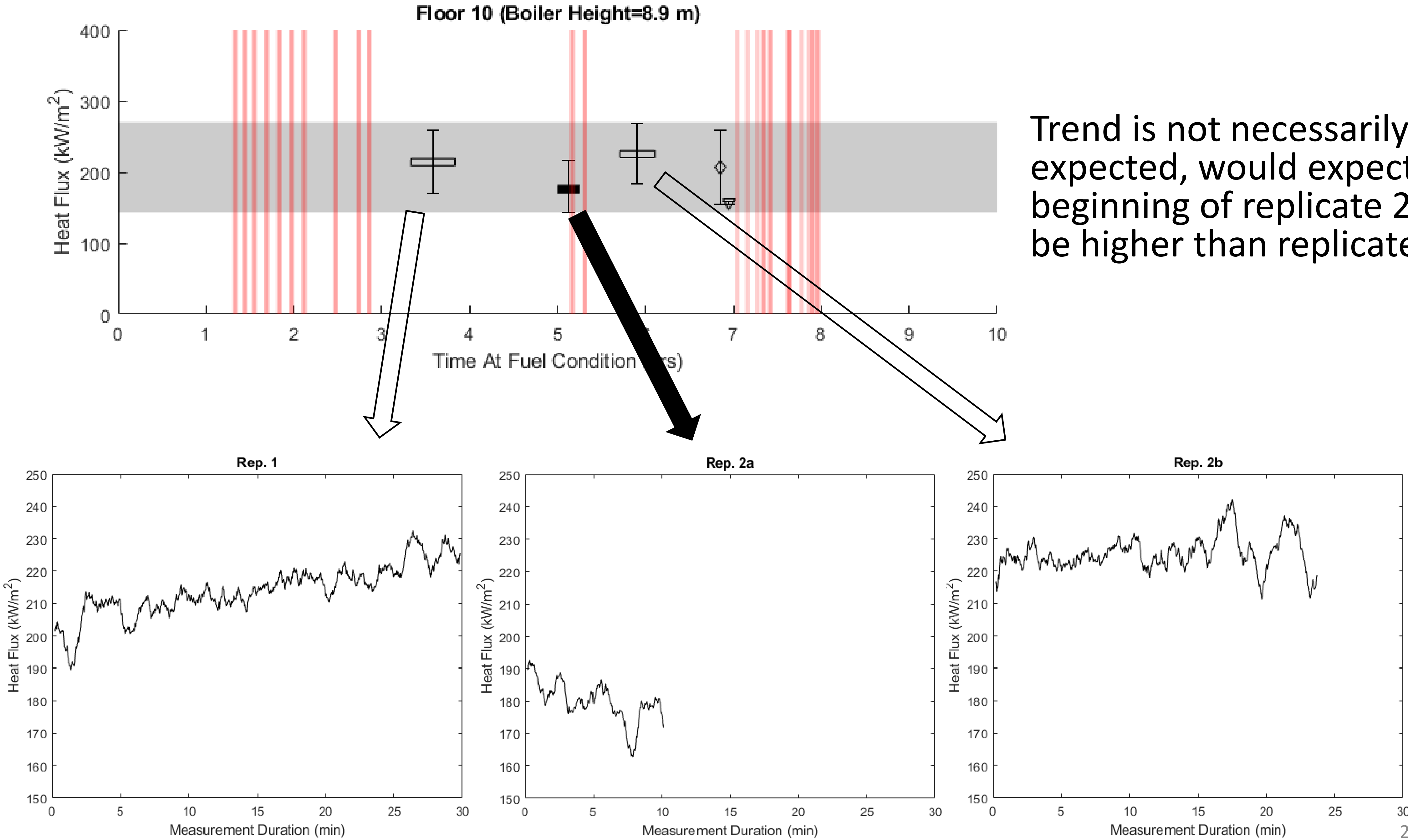

Trend is not necessarily as expected, would expect the beginning of replicate 2a to be higher than replicate 1

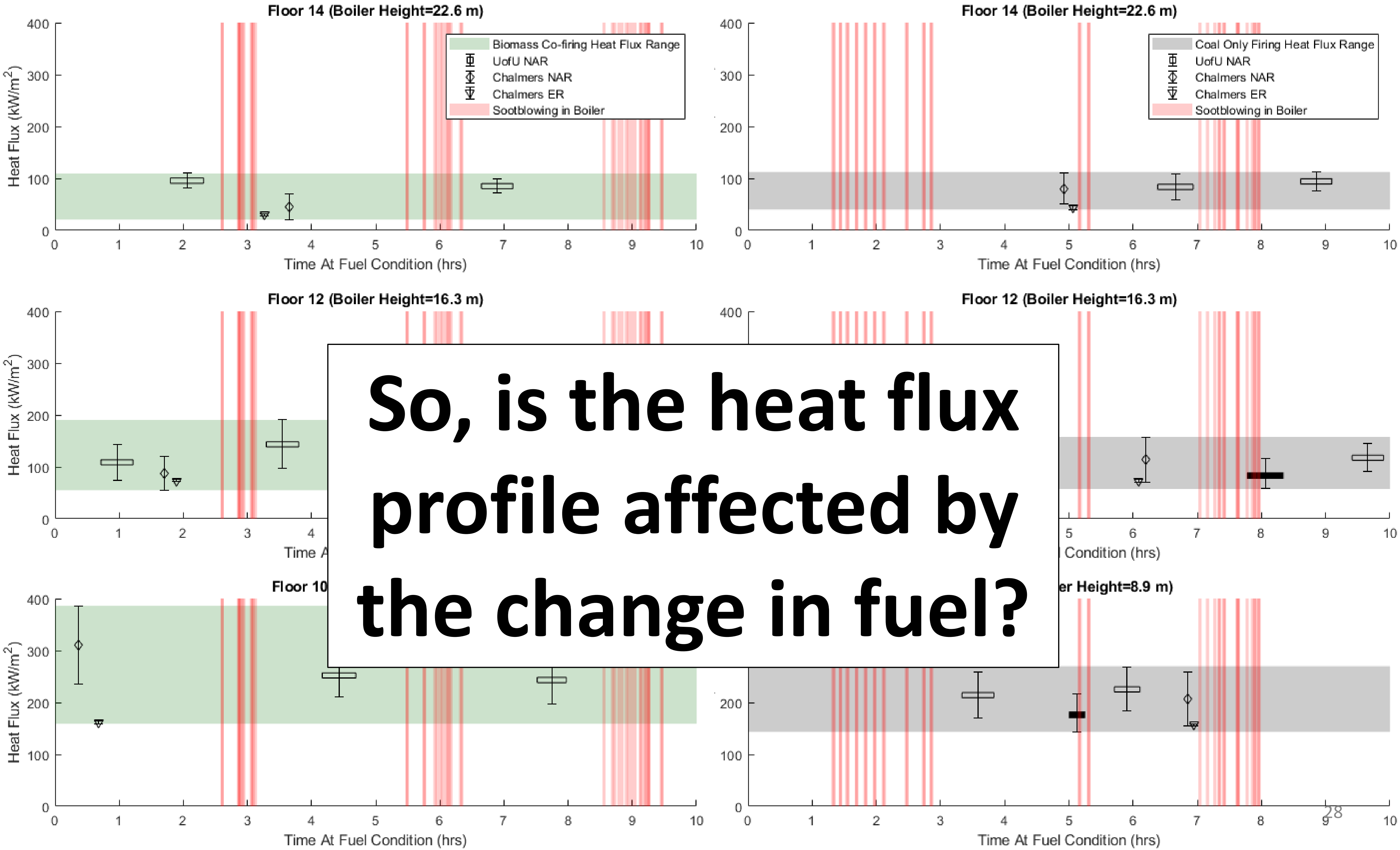

So, is the heat flux profile affected by the change in fuel?

Student’s T-test

- Null hypothesis: At a given floor, the mean heat flux is the same for either coal only or biomass co-firing.
  - $\mu_{biomass\ cofiring} = \mu_{coal\ firing}$
- Alternative hypothesis: the two means at each floor are different (thus, the heat flux profile is changed by the switching the fuel blend))
  - $\mu_{biomass\ cofiring} \neq \mu_{coal\ firing}$
- P-values can be calculated for each floor for both fuel conditions:
  - If $p < 0.05$, reject the null hypothesis
  - If $p > 0.05$, cannot reject the null hypothesis

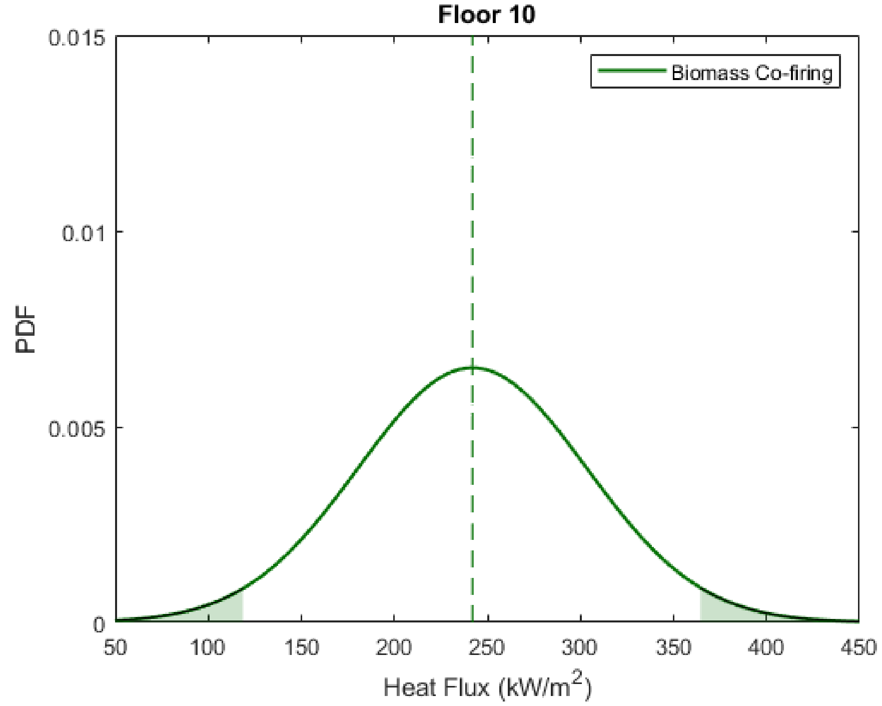

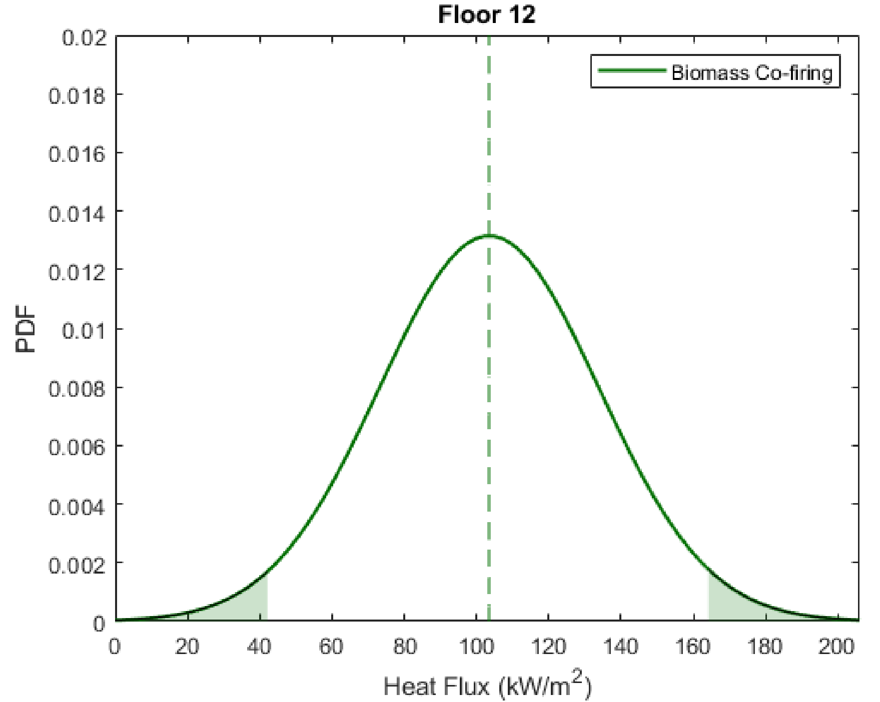

Student’s T-test

- Null hypothesis: At a given floor, the mean heat flux is the same for either coal only or biomass co-firing.
  - $\mu_{biomass\ cofiring} = \mu_{coal\ firing}$
- Alternative hypothesis: the two means at each floor are different (thus, the heat flux profile is changed by the switching the fuel blend))
  - $\mu_{biomass\ cofiring} \neq \mu_{coal\ firing}$
- P-values can be calculated for each floor for both fuel conditions:
  - If $p < 0.05$, reject the null hypothesis
  - If $p > 0.05$, cannot reject the null hypothesis

Floor	P-value
10	0.254
12	0.773
14	0.572

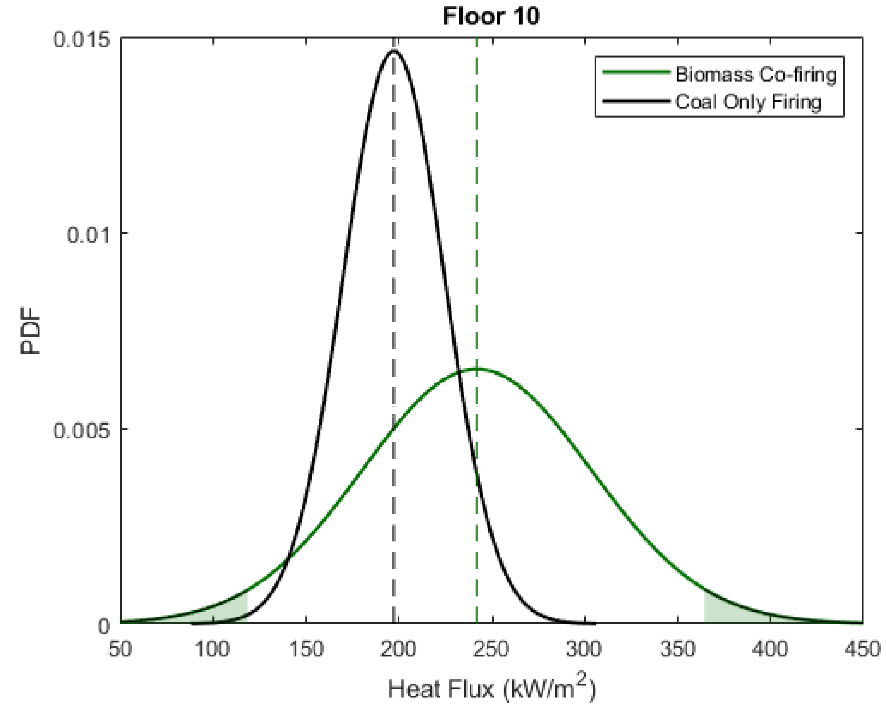

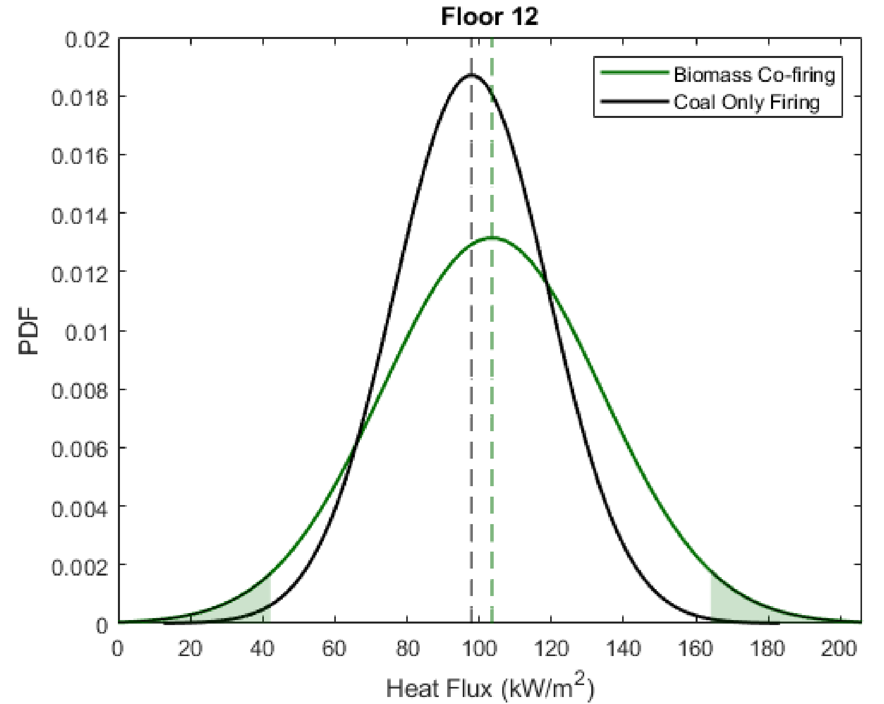

Student’s T-test

- Null hypothesis: At a given floor, the mean heat flux is the same for either coal only or biomass co-firing.
  - $\mu_{biomass\ cofiring} = \mu_{coal\ firing}$
- Alternative hypothesis: the two means at each floor are different (thus, the heat flux profile is changed by the switching the fuel blend))
  - $\mu_{biomass\ cofiring} \neq \mu_{coal\ firing}$
- P-values can be calculated for each floor for both fuel conditions:
  - If $p < 0.05$, reject the null hypothesis
  - If $p > 0.05$, cannot reject the null hypothesis

Floor	P-value
10	0.254
12	0.773
14	0.572

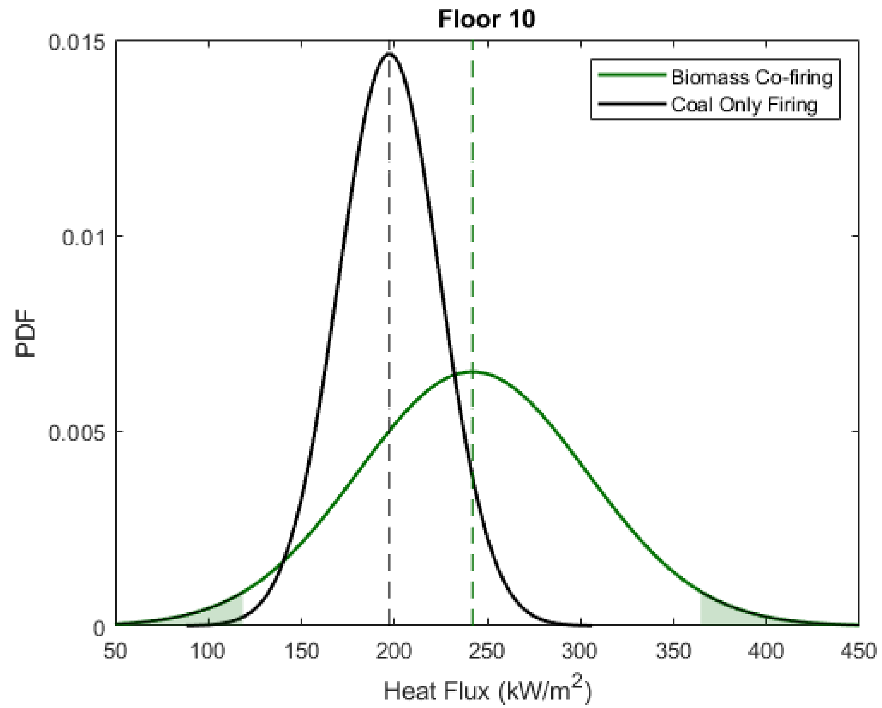

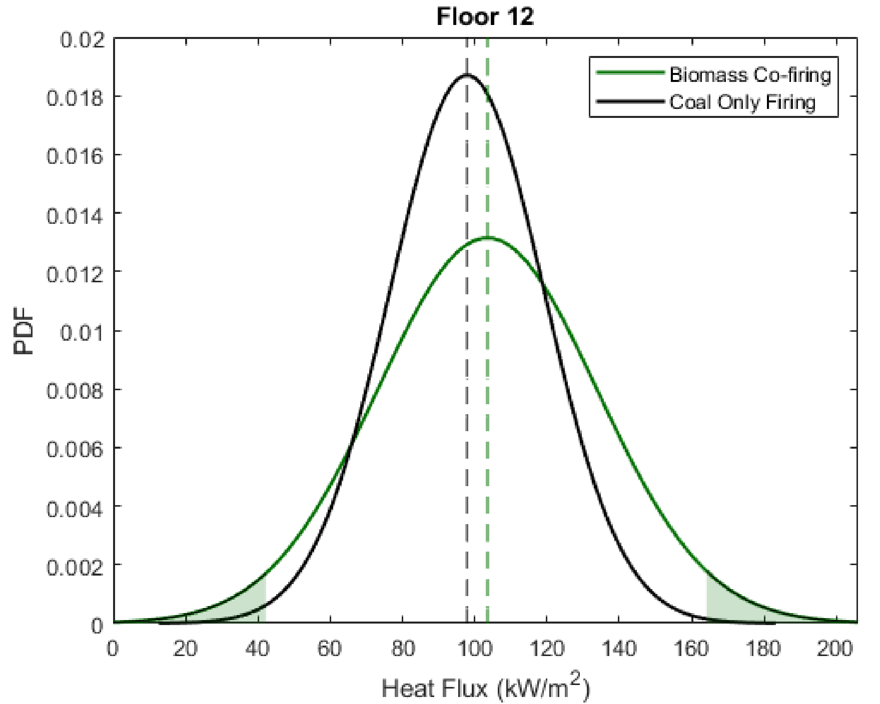

Student’s T-test

- Null hypothesis: At a given floor, the mean heat flux is the same for either coal only or biomass co-firing.
  - $\mu_{biomass\,cofiring} = \mu_{coal\,firing}$
- Alternative hypothesis: the two means at each floor are different (thus, the heat flux profile is changed by the switching the fuel blend))
  - $\mu_{biomass\,cofiring} \neq \mu_{coal\,firing}$
- P-values can be calculated for each floor for both fuel conditions:
  - If $p < 0.05$, reject the null hypothesis
  - If $p > 0.05$, cannot reject the null hypothesis

Floor	P-value
10	0.254
12	0.773
14	0.572

NOTE: Sparse data (only 4 replicates to calculate each p-value) means that even though we have evidence that we cannot reject null hypothesis (high p-values), the null hypothesis is not proven true.

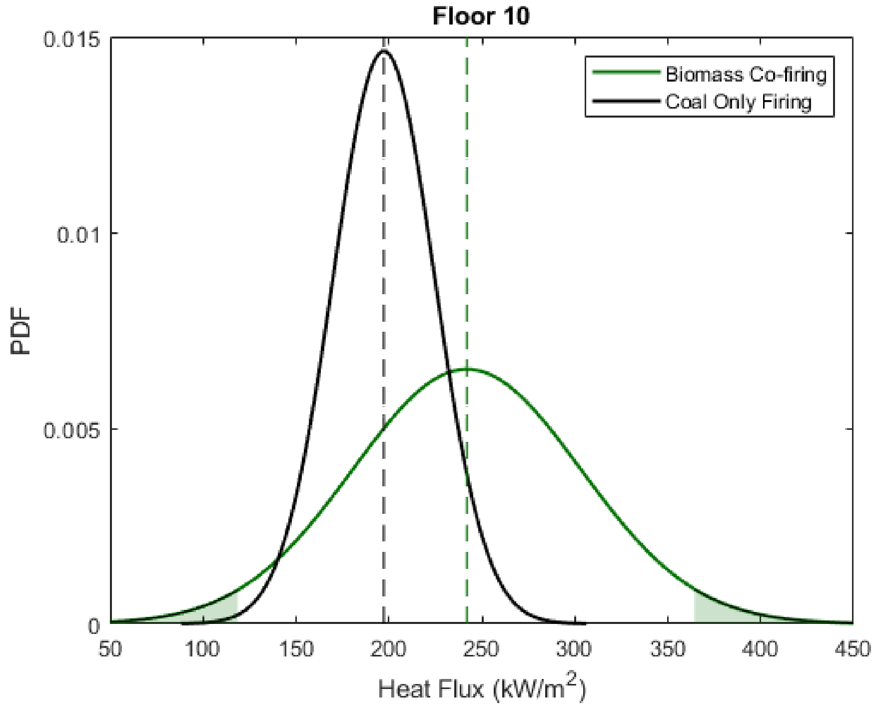

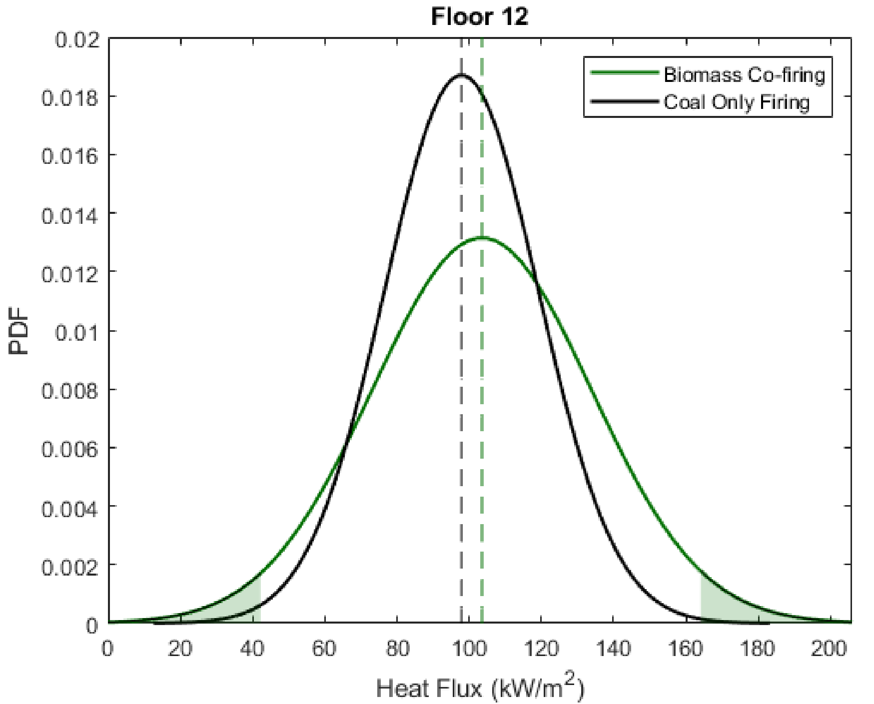

Conclusions

- Intensity/heat flux decreased substantially with boiler height
- Between a single instrument:
  - good repeatability between replicates
- Between all instruments:
  - large difference as a function of time – but similar between fuel conditions
  - Potential causes: instrument bias error, temporal boiler fluctuations, soot blowing, instrument repeatability…
- T-test: data did not point to heat flux profile changing with biomass co-firing
  - This is promising for implementing co-firing in the future.

Future Work

- More replicates!
  - Constraints: ~10.5-hour window for biomass co-firing
  - Suggestion: streamline setup at each location
  - Consider: use of multiple radiometers at different ports simultaneously
- Better setup repeatability:
  - More precise alignment mechanisms at each location
  - Even more care to ensure ambient temperatures of radiometers are kept stable
- Timing of soot blowing:
  - Better communication to avoid soot blowing during measurements
  - Consider: examining heat flux periodically at a single location between two local soot blowing events

Acknowledgements

The authors gratefully acknowledge financial support provided by Rocky Mountain Power/ PacifiCorp and the State of Utah through the Utah Sustainable Transportation and Energy Plan (STEP). We are grateful to Ken Clark, Program Manager for this project for Rocky Mountain Power/PacifiCorp.

Conclusions

- Intensity/heat flux decreased substantially with boiler height
- Between a single instrument:
  - good repeatability between replicates
- Between all instruments:
  - large difference as a function of time – but similar between fuel conditions
  - Potential causes: instrument bias error, temporal boiler fluctuations, soot blowing,…
- T-test: data did not point to heat flux profile changing with biomass co-firing
  - This is promising for implementing co-firing in the future.

Future Work

- More replicates!
  - Constraints: ~10.5-hour window for biomass co-firing
  - Suggestion: streamline setup at each location
  - Consider: use of multiple radiometers at different ports simultaneously
- Better setup repeatability:
  - More precise alignment mechanisms at each location
  - Even more care to ensure ambient temperatures of radiometers are kept stable
- Timing of soot blowing:
  - Better communication to avoid soot blowing during measurements
  - Consider: examining heat flux periodically at a single location between two soot blowing events

Fuel Processing Technology 182 (2018) 95–103

Contents lists available at ScienceDirect

Fuel Processing Technology

journal homepage: www.elsevier.com/locate/fuproc

Research article

Analysis of particle behavior inside the classifier of a Raymond Bowl Mill while co-milling woody biomass with coal

Seyedhassan Fakourian*, Andrew Fry, Tanner Jasperson

Brigham Young University, Department of Chemical Engineering, 84602 Provo, UT, USA

ARTICLE INFO

Keywords:
Co-milling
Biomass
Coal
Classifier
Swirl

ABSTRACT

Woody biomass cofiring with coal at existing pulverized-coal boilers is known to be a green energy source and is a low-expense alternative for pure coal combustion. Co-milling woody biomass particles (15 wt%) with coal particles (85 wt%) before burning at a boiler is a complex problem because large woody biomass particles (> 300 µm) exit the milling system along with the fine particles. A Computational Particle Fluid Dynamics (CPFD) is used in this paper to present a novel analysis about the behavior of woody biomass particles as they are mixed with coal particles inside the classifier. To meet this objective, a model of SolidWorks of the milling system is defined using the Barracuda VR 17.1.0 software package. We made a C# programming code to analyze the post processing files of this simulation (base simulation); it showed that approximately none of the large particles of woody biomass nor any of the coal particles that exit along with fine particles swirl inside the classifier, and they exit the system in the product stream immediately after getting through the vanes. More importantly, only a few numbers of the exiting particles, regardless of their size, swirl inside the classifier. Manipulation of hardware can improve the classifier performance and leads to changes in the behavior of particles inside the classifier. However, changes in operating conditions cannot improve it significantly. Particle size distribution and the average flow rate of the product stream of the experiment and the base simulation match well.

1. Introduction

Coal will continue to be an important source for electricity generation in the United States [1]. However, coal combustion has been identified as a major contributor to the rise in atmospheric greenhouse gas concentrations, intensifying focus on carbon abatement technologies. One such technology, co-firing woody biomass with coal, can result in a carbon-neutral or even a carbon-negative emission profile [2]. In addition, co-firing of beetle-kill woody biomass can significantly reduce risk of wildfires and increase the overall health of forests [3].

One of the key hurdles for this technology is the behavior of the pre-combustion fuel milling equipment when operating on a blend of prepared woody biomass and coal. Prior studies have shown that unprepared or raw woody biomass will build up over time in coal mills, increase the power requirement, and eventually plug the mill [4]. Therefore, co-firing of woody biomass with coal in electricity generating utility boilers requires either significant upgrades to fuel handling and combustion hardware or a pre-treatment process to convert the biomass into a more “coal-like” fuel. Typical pre-treatment processes implemented to avoid this issue are torrefaction and steam explosion. Each of these processes removes inherent moisture, increase the energy density and degrade the lignin structure, which is important to render the fuel grindable. Even though the resulting pre-treated biomass fuel is more “coal-like” there are differences in particle density and aspect ratio resulting asymmetric behavior in the mill classifier. Combustion kinetics of woody biomass and coal are different, and large biomass particles would be expected to burn out in utility boiler conditions and they are not necessarily ground as fine as the coal particles [5]. However, operators of utility boilers prefer to feed the boiler by biomass particles as small as coal particles. Therefore, if the simple changes can make the grind similar to that a pure coal, we should do it.

The objective of this research is to model the behavior of a blend of prepared biomass and coal particles in a Raymond Bowl Mill and to evaluate the expected performance change of the mill classifier when implementing simple hardware modifications. There have been few studies where milling systems have been modeled. Afolabi et al. [6] designed a laboratory scale static classifier and a Computational Fluid Dynamics (CFD) model of that hardware. They showed the importance of using proper cyclone dimensions to allow large particles residence time in the classifier cone where they are captured and returned to the

---

[*] Corresponding author.
E-mail addresses: sh.fakourian@gmail.com (S. Fakourian), afry@byu.edu (A. Fry).

https://doi.org/10.1016/j.fuproc.2018.10.023
Received 10 August 2018; Received in revised form 26 September 2018; Accepted 25 October 2018

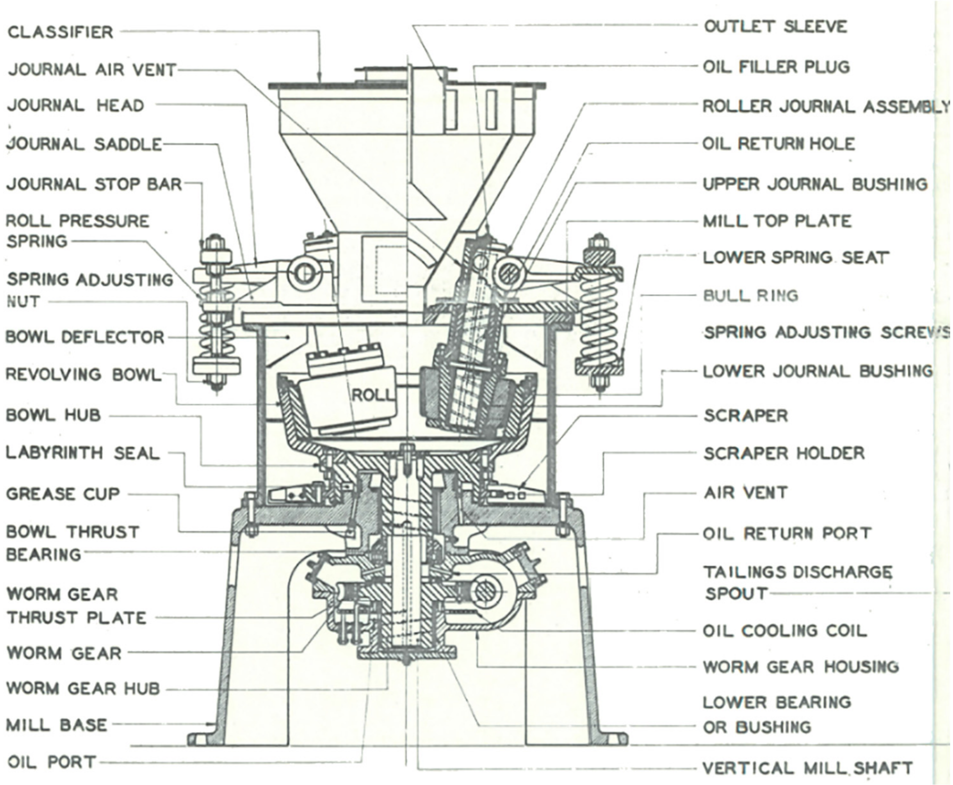

Fig. 1. Schematic side view of the physical milling system.

bowl for size reduction. Foster et al. [7] studied modifications to the classifier to reduce the cut size, resulting in a smaller particle size distribution (PSD) from the milled product. Neither of these studies investigated multiple particle types with differing physical properties, representative of co-firing of prepared woody biomass with coal. Because the specific grinding energy can be determined elsewhere [8], we feel it is outside the scope of this manuscript.

2. Materials and methods

Coal is typically received from the mine with a size distribution with a large diameter limit of about 2 in. Before it is combusted, the coal particles must be reduced in size so that 70 mass % of the particles are smaller than 200 mesh (74 μm) with < 1 mass % larger than 50 mesh (297 μm). This usually results in a mass mean particle size distribution of around 50 μm. A mill is a device that is used to pulverize coal into the desired size distribution. A diagram detailing the components of a mill is included in Fig. 1. The as received coal is loaded into the mill, using a gravimetric coal feeder. Upon entering the mill, the coal falls into a large steel bowl which is mounted to a drive system causing it to rotate. Large steel rollers, or rolls, are mounted on arms, or journals, that position them near the inside surface of the bowl wall. As the bowl rotates, the coal is forced between the bowl and rolls, crushing the coal. Simultaneously, warm air, is introduced through a tangential port below the bowl and swirls around the bowl as it rises and exits through the classifier at the top of the mill. Coal particles remain in the bowl until they become small enough to become entrained in the air and are carried into the classifier.

Coarse particles cause problems in the combustion system. They may not have enough residence time to completely combust, reducing combustion efficiency, and they can promote deposition near the burner. Classifiers are a hardware component of the mill which separates large particles from the entrained flow and returns them to the milling system so that they can be reduced in size [6,9,10]. This objective is achieved using a cyclone. The entrained particles enter the cyclone at the top through adjustable vanes which induce a tangential component to the air velocity. The tangential velocity causes the particles to migrate in an outward radial direction toward the cyclone walls. Larger particles move more quickly due to this centrifugal force and are more likely to impact the surface where they are pulled out of entrainment. The large particles then move down the wall of the cyclone and are reintroduced into the bowl for further milling. The outlet for the air and small particles is at the top of the classifier through a cylindrical tube, or vortex finder, which extends down into the cyclone. The geometry of the vortex finder relative to the cyclone forces the air and entrained particles to make rotations down through the cyclone before entering the vortex finder. This provides enough residence time for large particles to be captured by the surface of the cyclone. The fine particles which remain entrained in the air are carried to the boiler through the burners. The majority of power plants use static classifiers, which are less efficient than dynamic classifiers, leaving significant room for modifications to improve performance [6]. Dynamic classifiers utilize rotating vane blades to control the cut size, whereas adjustable and stationary vanes control the cut size in static classifiers [6]. The work in this research deals with a static classifier. A simple diagram indicating the movement of particles through a static classifier is included as Fig. 2 with: (1) entrained particles move from the bowl toward the cyclone, (2) entering the cyclone through vanes, (3) exiting the classifier through the vortex finder as the product stream and (4) coarse particles returning to the bowl.

2.1. Experimental work

In a study by Zsolt [8], the performance of a CE 312 Raymond Bowl Mill was investigated while milling a Bituminous Coal and blends of prepared woody biomass with Bituminous Coal. Results from this study were used to provide hardware configuration, operational data and performance data for model validation and parametric studies. Of

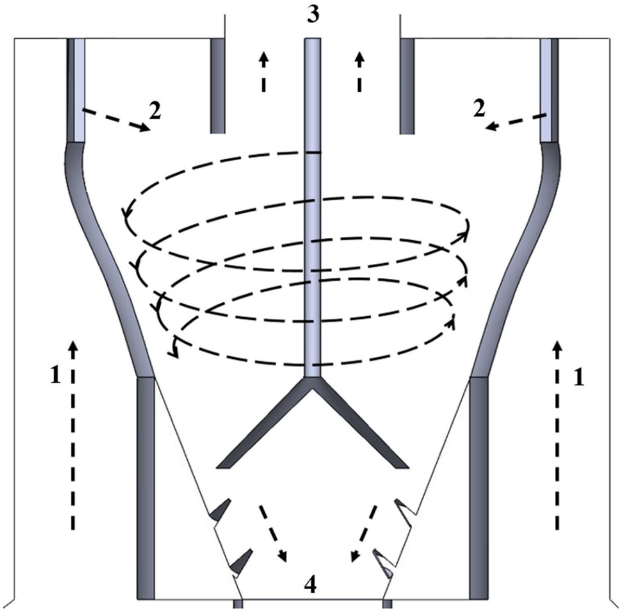

Fig. 2. A schematic diagram of a static classifier indicating typical movement of particles.

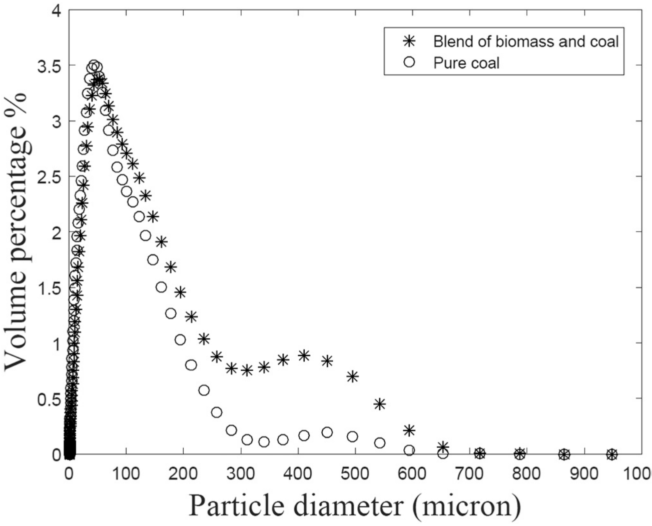

Fig. 3. Beckman Coulter analysis of particle size distribution for coal-woody biomass blend [8].

particular interest are the experimentally measured product PSD, as shown in Fig. 3, and product flowrate (0.189 kg/s) when milling a 15% wt% blend of torrefied pellets produced at a process temperature of 325 °C with 85% Bituminous Coal. Fig. 3 indicates that the blended fuel produces a bimodal distribution with the mode centered at about 400 μm unique to the blend when compared with pure coal. It is reasonable to assume that the particles in this mode are dominated by the prepared biomass. This suggests that physical properties of the biomass, presumably density and aspect ratio, allow larger biomass particles to escape from the classifier than corresponding coal particles.

2.2. Model description

A computational fluid dynamic (CFD) simulation of the CE 312 Raymond Bowl Mill was produced using Computational Particle Fluid Dynamics (CPFD) Barracuda Virtual Reactor 17.1.0 software package. This computational package was developed to represent dense particle phase systems and is based on the Multiphase Particle-in-Cell (MP-PIC) method which uses a particle probability distribution function [11].

Complete engineering drawings were not available for creation of the geometry and mesh. Missing dimensions were scaled from available drawings, assumed, or directly measured. Fig. 4 shows the SolidWorks model of the mill void space as it was imported into Barracuda VR as a stereolithographic (STL) file and the fully meshed geometry in Barracuda VR with locations of interest identified.

Since it is not possible to represent the rotation of the bowl and rolls or to represent the mechanical process of particle size reduction in the CFD model, and because experimental data are not available, we assume the location, size distribution, and rate that particles are generated for entrainment near the bowl. These parameters were discussed with experts in the field including engineers at: General Electric (formerly Alstom), Arvos Group (the holder of the Raymond Bowl Mill technology) and at a utility operating these mills. Reasonable ranges of values were determined for each parameter and their modeled values were varied in order to accurately reproduce the validation data with the model.

Locations for the model inlet and outlet boundaries have been identified in Fig. 4 as: (1) warm air inlet, (2) milled particle injection locations and (3) milled product and air outlet. The conditions at these boundaries are summarized in Table 1.

The main assumptions considered in the Barracuda base simulation are:

- The physical process of particle size reduction occurring in the bowl cannot be represented. Instead, the resulting size distribution of ground particles (both coal and wood) and the location of their injection into the model are assumed. The size distribution is a parameter that was adjusted in order to match the product size distribution to measured values. The injection locations were placed along the rim of the bowl, concentrated near the rolls.
- In the mill, large particles collected by the classifier are recycled to the bowl for further size reduction. In the model, large particles captured by the classifier are removed from the simulation by capturing them in a cavity at the bottom of the classifier cyclone. The assumed ground particle size distribution and rate of injection account for these recycled particles. The injection rate is the sum of the rates of milled product, particles captured by the classifier and particles captured at other locations in the system. The injection rate is a parameter adjusted until the rate of milled product matches the value measured in experiment.
- The recycle ratio (RR) is defined as the ratio of the flowrate of particles entering the classifier to the flowrate of the product stream. Experts tell us that RR should be close to 4, although this is a value that has not been reportedly measured. The RR can also be influenced by the assumed PSD of ground particles.
- Values of unknown or unmeasured operating conditions are assumed and adjusted within a reasonable range of values until the behavior of the model closely matches observed experimental behavior. For example, pressure at the inlet and the outlet of the mill has been assumed.
- Experimental PSD is volume base whereas the generated PSD by Barracuda is in terms of mass. Particle density and spherical particles have been used to convert mass-based PSD to volume-based PSD for comparison.
- The thickness of pulverizer surfaces has been slightly altered in the model to reduce stair stepping caused by meshing.

In order to tune the baseline model to match experimental data the following model parameters were adjusted: the PSD of milled particles, the number and the position of the injection locations of milled particles, the angle of expansion and the velocity of the injected particles, the drag model, particle density, particle sphericity, the position of the cone at the bottom of the classifier, air pressure, and air velocity. The

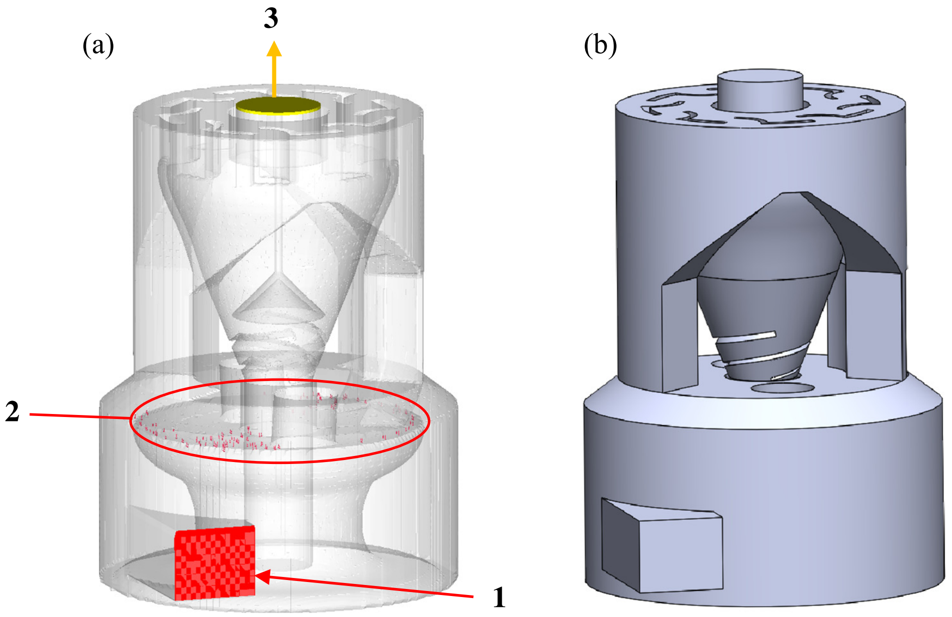

Fig. 4. (a) Translucent representation of meshed model in Barracuda VR, (b) SolidWorks model of void space.

Table 1
Summary of model boundary conditions identified in Fig. 4.

Boundary	1	2	3
Description	Air inlet	Particle injection	Milled product
Temperature (K)	394	366	338
Pressure (kPa)	95		82
Flow (m/s)	15		

Table 2
Final values of parameters that were adjusted to match the baseline model with experimental measurements.

Parameter	Value	
	Coal	Woody biomass
Density (kg/m^3)	1250 [12]	985
Sphericity[a]	0.85	0.75
Emissivity	1.0	1.0
Drag model	Ergun	
Multiplier constant of drag model	1.0	
Close pack volume fraction	0.66	
Maximum momentum redirection from collision	40%	
Normal-to-wall momentum retention	0.8	
Tangent-to-wall momentum retention	0.85	
Diffuse bounce	2.0	

[a] Shape factor.

value used for these parameters in the tuned baseline model is found in Table 2.

3. Results and discussion

The PSD of the mill product stream in the simulation is in good agreement with that of the experiment, which is shown in Fig. 5. In addition, the time averaged prediction of mass flow rate of the product stream matches well with the experiment at around 0.189 kg/s, which is presented in Fig. 6. It is worthy to note that this time dependent model has only come to a pseudo-steady state. A portion of the large particles injected near the rim of the bowl are not entrained and carried into the classifier. Instead, they deposit in locations within the cavity near the bowl. It is expected that eventually the rate of this deposition will become equal to the rate of re-entrainment resulting in steady state operation. It is not reasonable to extend a simulation out to times where this would occur. The recycle ratio in the baseline simulation is 4.2.

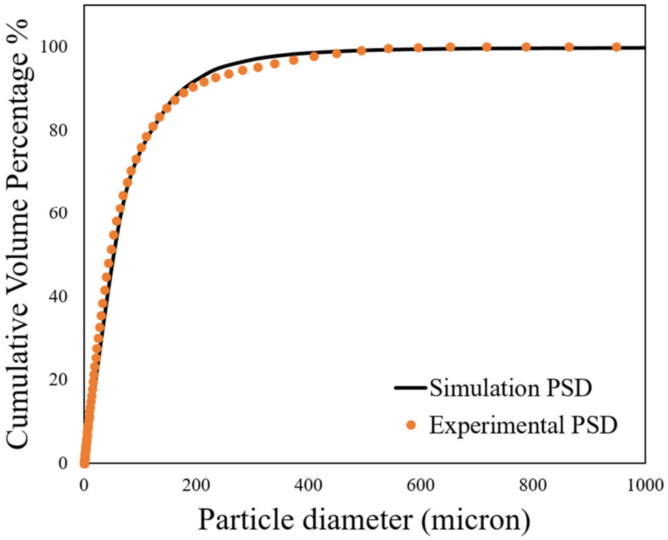

Fig. 5. Particle size distribution of blend product stream in simulation and experiment.

A comparison of the measured PSD of the pure coal product stream to the blended coal and biomass product stream shows that the blend produces a bimodal size distribution with a new mode of large particles with an average size of ~400 μm. This suggests that milling of the woody biomass produces many more large particles which exit the system than milling of coal. To capture this behavior, the assumed PSD of each of these materials have been adjusted accordingly in the model. The assumed PSD of input pulverized coal particles, which contains around nine mass percent particles larger than > 300 μm, and PSD of coal particles in the product stream are compared in Fig. 7. Similarly, the assumed PSD of input pulverized woody biomass, which contains around 33 mass percent particles larger than > 300 μm, and the PSD of woody biomass in the product stream are compared in Fig. 8. Fig. 9 is a comparison of the PSDs of the product material, the material collected

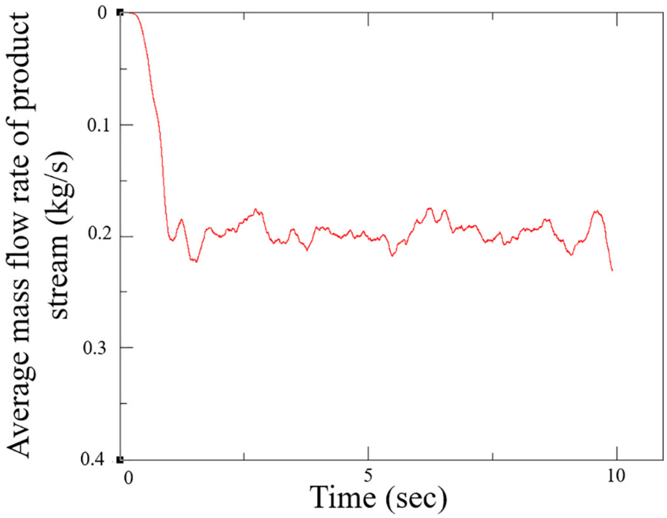

Fig. 6. Average mass flow rate of product stream (kg/s).

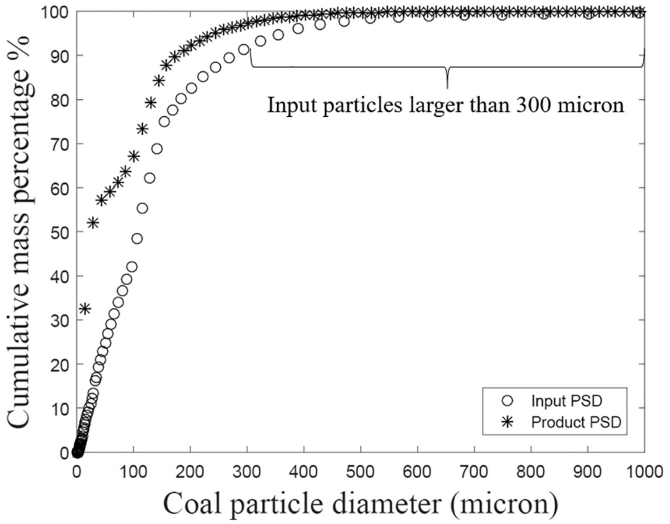

Fig. 7. Particle size distribution of coal particles at input (injectors) and product stream.

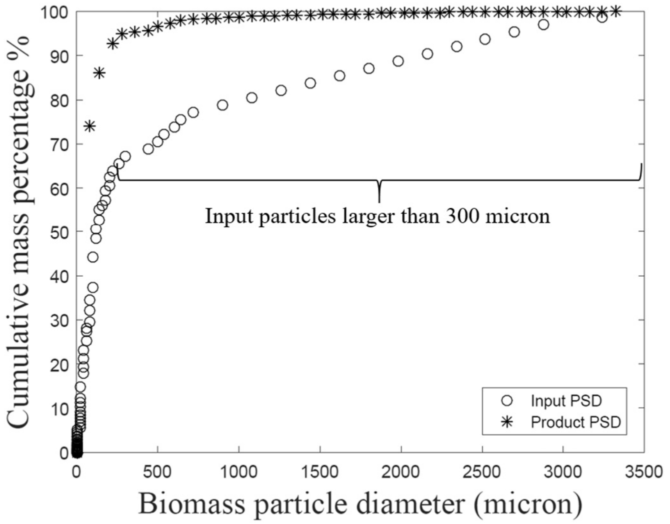

Fig. 8. Particle size distribution of woody biomass particles at input (injectors, which presented in Fig. 4) and product stream.

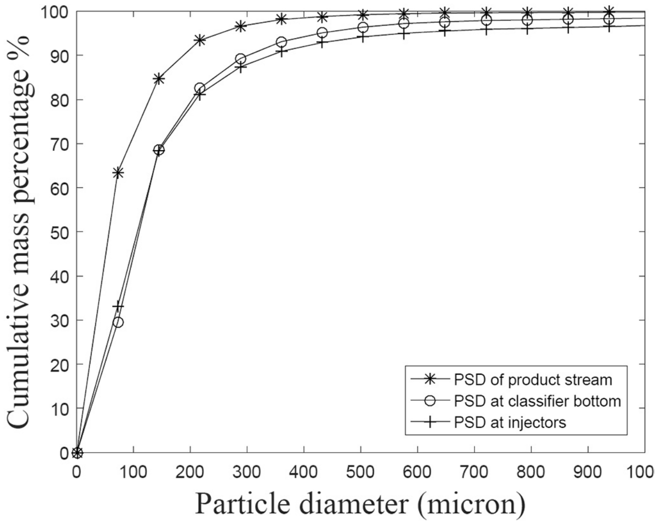

Fig. 9. PSD of product stream, bottom of classifier, and injectors.

in the classifier and the injected particles. This plot indicates that size distribution of the particles collected in the classifier is very similar to the injected material and the product stream includes only the small fraction of particles. This behavior suggests that there are many assumed PSDs for the injected milled particles that would satisfy the measured product PSD. Including the constraint of a RR of 4 limits the range of possible values for this assumption significantly. However, the assumptions made here for the baseline simulation are good enough to generate some understanding of the relative behavior of coal and biomass particles in the system and evaluate the impact of simple modifications to the classifier.

Barracuda software generates data files called general mesh viewers (GMV), which include information about the particles and cells at snapshots in time during the simulation; every particle in the simulation is tracked individually and has a unique identity number. For this simulation Barracuda was configured to generate a GMV file every 0.2 s. For our simulation of 10 s, 51 GMV files were generated. It was necessary to analyze the data of all 51 GMV files simultaneously to determine the pathway of individual wood and coal particles in order to understand the differences in their behavior in the classifier. To fulfill this purpose, all particles that exited the simulation in the product stream were identified and then their pathways were tracked and plotted using information in previous GMV files. A code was developed using C# to fulfill this purpose. The results of this analysis show that most large particles (> 300 μm) of coal and woody biomass that exit from the system bypass the cyclone in the classifier by moving directly from the vanes at the top of the classifier into the vortex finder. To demonstrate this behavior the pathway of a large (2 mm) woody biomass particle throughout the mill is plotted in Fig. 10 as: (1) injection of the particle into the system and subsequent swirling around the bowl, (2) entrainment in the gases moving toward the classifier, and (3) exiting from the system. It is possible that refining the simulation to smaller time steps would show that the particle entered the cyclone of the classifier, however it is unlikely that the particle traveled to an appreciable depth in the cyclone.

Quantitatively this analysis shows that < 5% of particles exiting as product make rotations inside cyclone of the classifier before entering the vortex finder and exiting the system, regardless of their type and size. This is an important result which may suggest 1) that particles which make rotations in the cyclone of the classifier are effectively captured and returend to the bowl and 2) that there are an appreciable number of large woody biomass particles which bypass the cyclone of the classifier completely. Small and simple modifications to the system operation and hardware were evaluated to determine if the latter

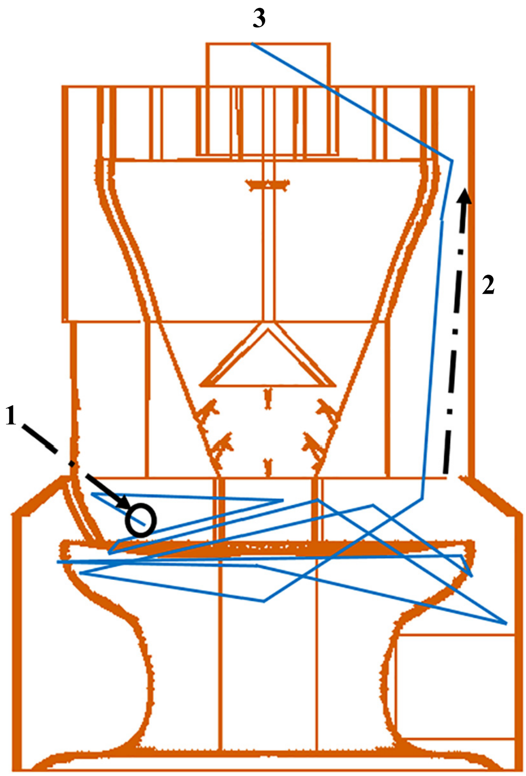

Fig. 10. An example pathway of a large woody biomass particle before exiting.

observation may easily be impacted or resolved.

3.1. Hardware manipulation scenarios

Three scenarios were defined and simulated to evaluate the effect of hardware manipulation on the classifier performance. The scenarios entitled Sc_{vane}, Sc_{vortex}, and $Sc_{vane\text{-}vortex}$ represent modifications of tightening the angle of the classifier inlet vanes, lengthening the vortex finder and a combination of changing the vane angle and lengthening the vortex finder, respectively. Fig. 11 shows the geometry configurations along with the modifications to the vane angle and vortex finder shape, which form our hardware scenarios.

Fig. 12 compares PSDs of three hardware scenarios with experimental PSD. It is apparent that each of these scenarios reduces significantly the amount of coarse particles in the product stream. Lengthening the vortex finder demonstrates a more favorable impact on PSD than adjustment of the vane angle. However, the impacts appear to be additive where the best results are obtained by lengthening the vortex and adjusting the vane angle.

The C# code was used to analyze the GMVs of the hardware scenarios by tracking how deep particles rotate in the classifier of the cyclone before entering the vortex finder and exiting with the product stream. Fig. 13 presents the geometry of the classifier in its baseline configuration with an indication of location of each component in the Y-axis (depth). Entrained particles enter the classifier through the vanes, at the height of 1.28–1.43 m. The depth to which the exiting particles penetrated into the cyclone were evaluated and discretized into four regions: between 1.1 and 1.0, between 1.0 and 0.9, between 0.9 and 0.8 m and finally < 0.8 m. Since the length of the vortex in the Sc_{vortex} and $Sc_{vane\text{-}vortex}$ scenarios extends down to 1.07 m the behavior of particles above 1.1 m was not evaluated.

Fig. 14 presents the ratio (in %) of the number of the product particles that swirl inside the classifier down to the indicated depth before exiting over the total number of particles exiting as product from the classifier. As discussed previously a low percentage of particles (< 5%) in the baseline simulation swirl inside the classifier before exiting, regardless of their type. In the case of Sc_{vortex}, there is no significant difference between coal and biomass, but the percentage of swirling particles increases up to around 13% at the 1.0 m. depth. In Sc_{vane} and $Sc_{vane\text{-}vortex}$, the percentages of swirling coals are higher than that of swirling woody biomass. The tighter vane angle induces high tangential velocity and ultimately impacts the swirl depth of particles more than the length of the vortex finder. In addition, the higher tangential velocity is expected to impact particles with a higher density more as demonstrated in the difference in behavior between the coal and biomass particles in the simulations. The combination of a modiftiation of the vortex finder and the vane angle, $Sc_{vane\text{-}vortex}$, pushes the exiting

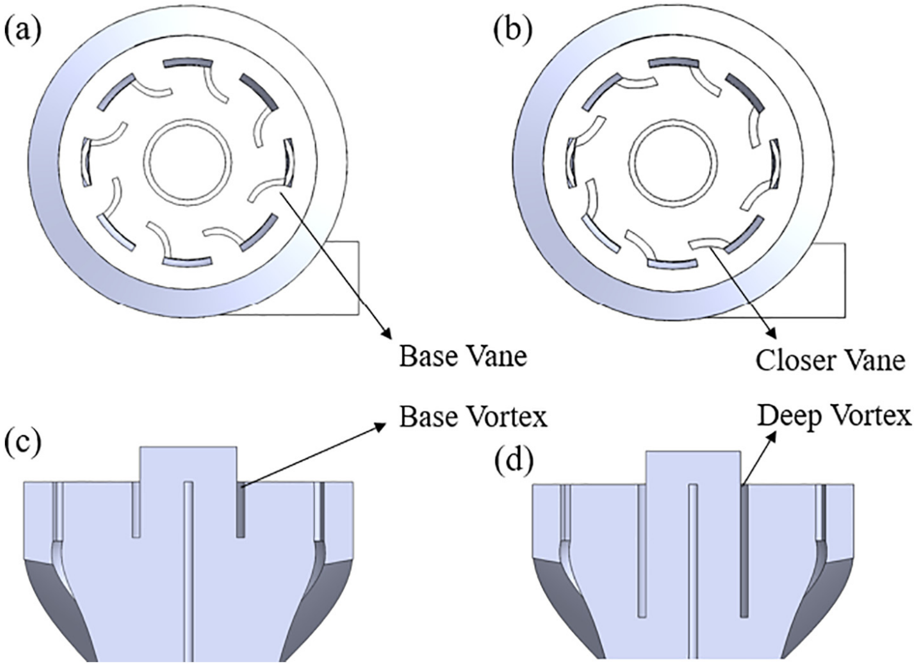

Fig. 11. Top view of (a) base vane angle (b) closer vane angle; cut side view of (c) base vortex (d) deep vortex.

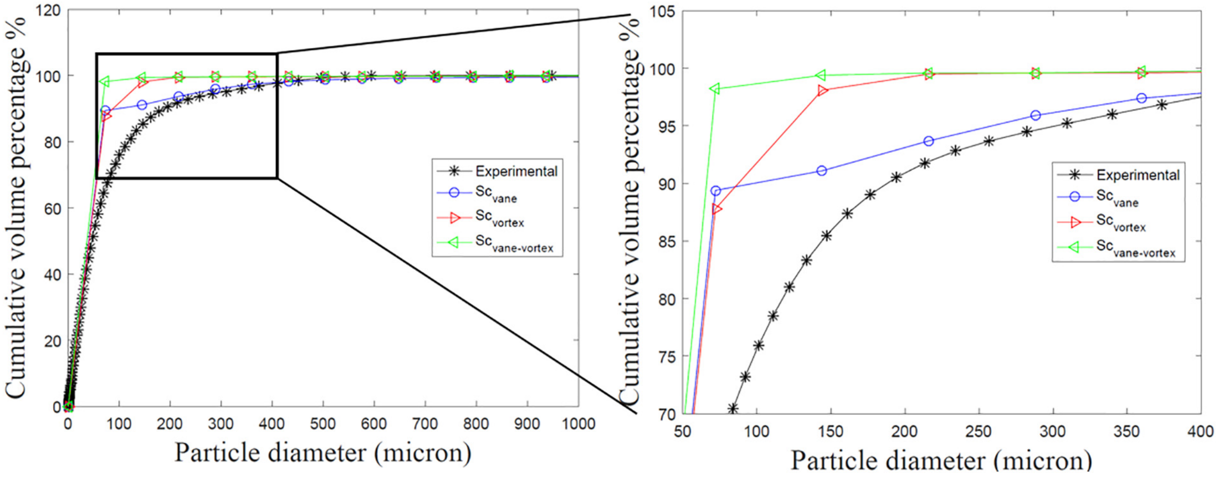

Fig. 12. Experimental PSD and generated PSD of scenarios Sc$_{\text{vane}}$, Sc$_{\text{vortex}}$, and Sc$_{\text{vane-vortex}}$.

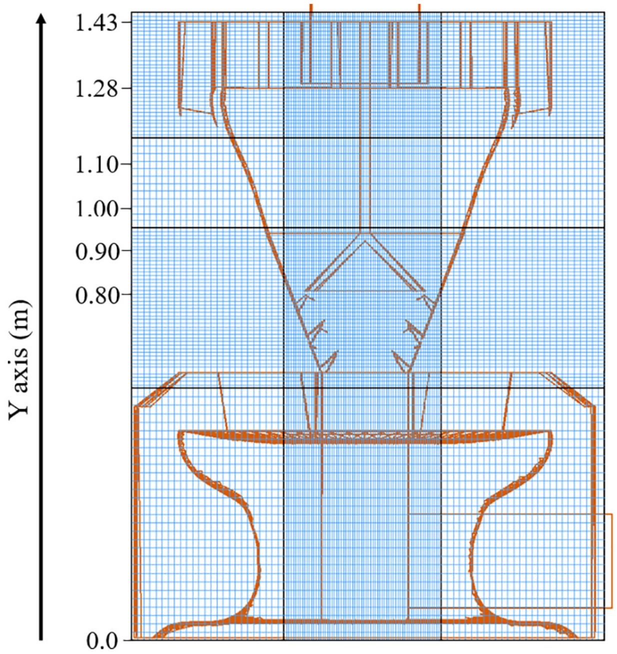

Fig. 13. Height of the pulverizer focusing on the classifier measurements in Y-axis (m).

particles deepest into the classifier, resulting in the highest likelyhood that large particles will be captured. The percentages of product particles that penetrate down below 0.8 m is zero in all scenarios. This is reasonable as it is not expected that particles reaching the bottom of the cyclone cone will capture by the classifier.

Fig. 15 shows the ratio (in %) of the number of particles > 300 μm that swirl inside the classifier to the indicated depth before exiting as product over the total number of particles > 300 μm that exit as product. It is demonstrated that no large exiting particles swirl inside the classifier before exiting in the base simulation and the condition where only the vane angle is adjusted. This shows that modification of the vane angle is not expected to have much effect on reducing the number of large biomass particles leaving with the product, which is suggested by the data presented in Fig. 12. Conversely, lengthening the vortex finder is expected to have a significant impact on pushing the large particles deep into the cyclone of the classifier where they are more likely to be captured. When combined with an adjustement of the vane angle, up to 80% of the particles reach a depth of Y = 1.0 m.

A secondary result of making small modifications to the vane angle

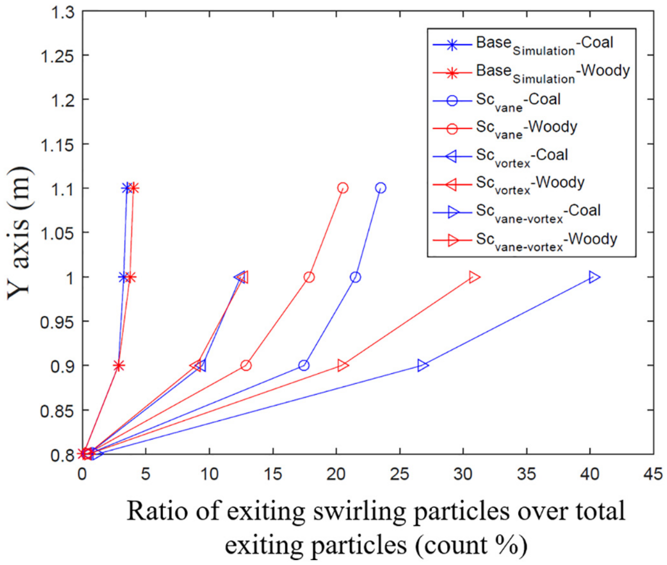

Fig. 14. Count percentages of exiting swirling particles over total exiting particles at various classifier depth.

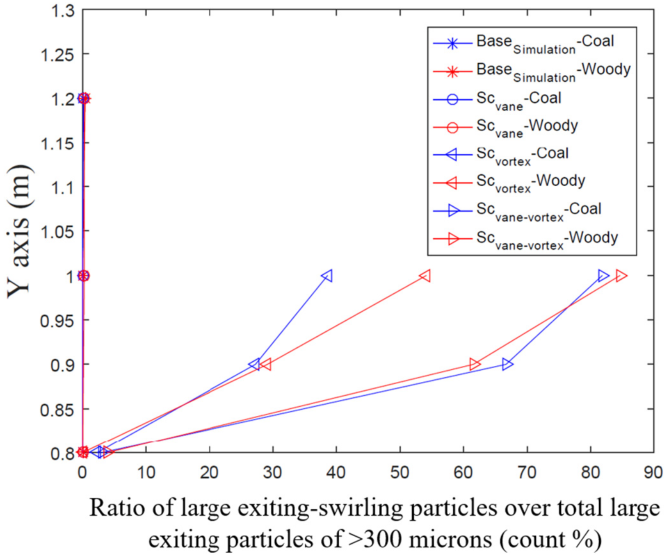

Fig. 15. Count percentages of large exiting swirling particles over total large exiting particles at the classifier.

Table 3
Primary results of analysis of running hardware scenarios.

Scenario	Flow rate of product stream (kg/s)	Recycle ratio
Sc_{vane}: Effect of closer vane angle	0.0834	9.9
Sc_{vortex}: Effect of deep vortex	0.122	7.0
$Sc_{vane\text{-}vortex}$: Effect of closer vane angle & deep vortex	0.0756	11.0
Base simulation	0.190	4.2

and the length of the vortex finder is that the overall pressure drop of the system increases and the flowrate of carrier gas may decrease, resulting in a decrease in product flowrate and an increase in RR. The impact of these modifications on product flowrate and RR without adjusting any other parameters was quantified in this study and is presented in Table 3. Maintaining the product flowrate at desired levels would require the adjustment of other operating parameters. This optimization was not included in this study as it would be more beneficial to perform on a mill that was being optimized for demonstration of biomass cofiring. However the sensitivity of performance to operating parameters was investigated and is presented in the next section.

3.2. Scenarios of operating parameters

The effect of air veocity and pressure drop on classifier performnace was investigated and the results are presented in Fig. 16. Two scenarios with air velocities of 12.0 m/s (for $Sc_{low\text{-}velocity}$) and 18.0 m/s (for $Sc_{high\text{-}velocity}$) were simulated, where air velocity of the base simulation is 15.0 m/s and two scenarios of low pressure drop ($Sc_{low\text{-}PD}$ = 92–85 kPa) and high pressure drop ($Sc_{high\text{-}PD}$ = 100–80 kPa) of air flow were simulated, where the air pressure drop in the base simulation is 95–82 kPa. The results of these simulations suggest that operating parameters have a much smaller impact on PSD than modifications to the mill geometry. PSDs of all of these four scenarios match relatively well with the experimental PSD. However the flow rate of the product stream is very sensitive to the velocity of the air, and it increases nearly linearly with increased air velocity as shown in Fig. 17. These results suggest that the air velocity can be used to maintain the product flowrate after making small modifications to the classifier geometry without significantly impacting the increased performance in particle size distribution.

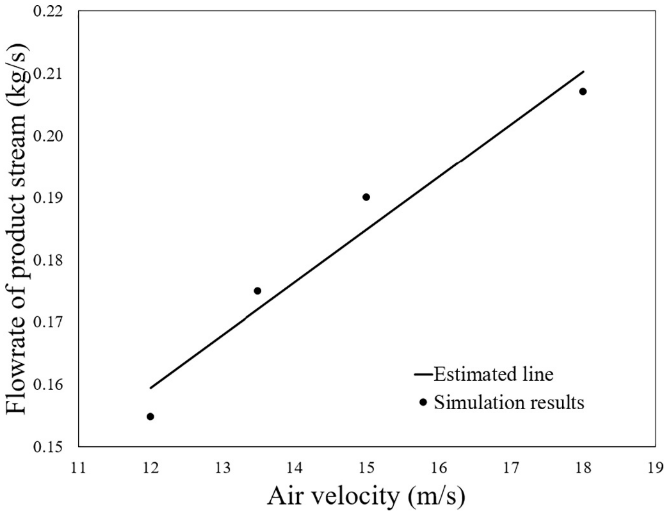

Fig. 17. Changes of flowrate of product stream versus air velocity.

4. Conclusion

Results from an experimental study on the behavior of a CE 312 Raymond Bowl Mill while processing pure coal and blends of coal and biomass were simulated using CFD to understand the differences in behavior between coal and biomass particles in the classifier and to evaluate the impact of geometry and operational changes on mill performance. The pulverizer was simulated using Barracuda VR 17.1.0 software package. Assumed parameters were varied within reasonable constraints in order to match PSD and the mass flow rate of the product stream with the experimental data. A C# code was produced to post process the results of the simulation in such a way to elucidate single particle behavior in the system. The main results of this study can be summarized as follows:

- Small changes in hardware configuration can improve PSD of the product stream, or in other words can reduce the number of large particles exiting the system with the product stream. Evaluated in this study were changes to the angle of the classifier inlet vanes and lengthening of the vortex finder in the cyclone. Each of these modifications decreased the amount of large particles exiting the system as product and the effects of the two modifications were additive. For example, the volume percentage of large particles (> 300 μm) in the product stream decreased from 5% to around 4% when comparing the vane case to the baseline simulation and reduced to < 0.5% for the other two hardware manipulations. However, hardware manipulations are expected to require additional operational changes to maintain product flowrate.

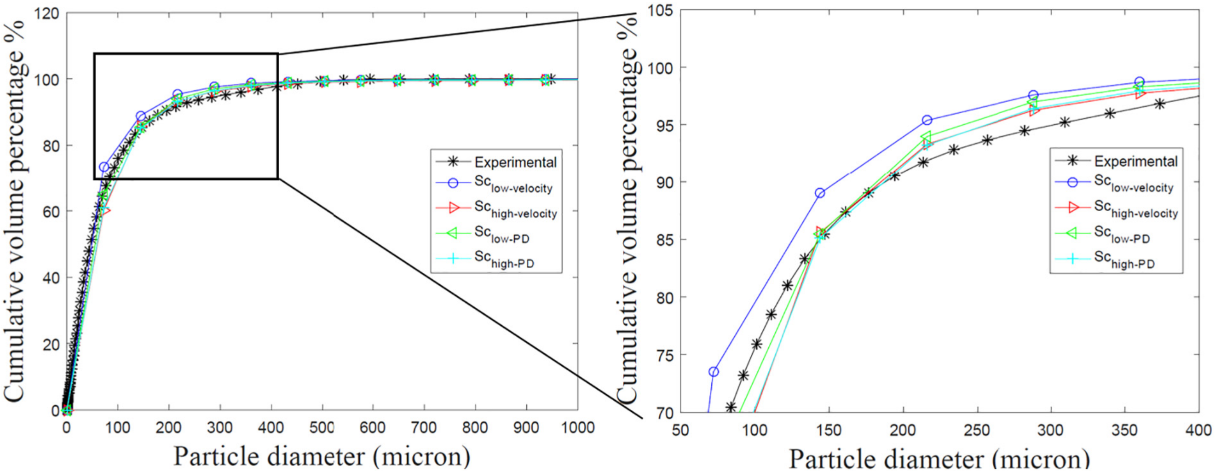

Fig. 16. Experimental PSD and generated PSD of scenarios $Sc_{low\text{-}velocity}$, $Sc_{high\text{-}velocity}$, $Sc_{low\text{-}PD}$, and $Sc_{high\text{-}PD}$.

- Tightening the vane angle will force particles to penetrate deeper into the classifier, where they are more likely to be collected and sent back to the bowl. However, the effect is expected to be greater on denser particles. Therefore, coal particles will be more impacted than biomass particles.
- Lengthening the vortex finder in the cyclone of the classifier was necessary in order to make large coal and biomass particles penetrate deep into the classifier before exiting. This may indicate that the classifier in the system that we evaluated was poorly designed. This also indicates that the length of the vortex finder should be evaluated when optimizing mill operation for coal and biomass cofiring.
- Changes in operating conditions do not significantly impact the PSD of the product stream, but changing the air velocity strongly influences the rate of product particle production. This suggests that a combination of simple modifications to hardware configuration and modifications to operating conditions can be used to optimize mill performance by reducing the number of large particles in the product stream while maintaining product flow rate and recycle ratio.

Acknowledgments

Authors would like to acknowledge Zsolt Dobó from University of Utah for his generous assistance.

References

[1] M. Sami, K. Annamalai, M. Wooldridge, Co-firing of coal and biomass fuel blends, Prog. Energy Combust. Sci. 27 (2) (2001) 171–214.
[2] L. Daniel, J.H.N. Sanchez, Josiah Johnston, Ana Mileva, Daniel M. Kammen, Biomass enables the transition to a carbon-negative power system across western North America, Nat. Clim. Chang. 5 (2015) 230–234.
[3] L. Baxter, Biomass-coal co-combustion: opportunity for affordable renewable energy, Fuel 84 (10) (2005) 1295–1302.
[4] K.R. Doug Boylan, Bill Zemo, Tom Johnson, Co-milling Green Wood Chips at Alabama Power Company's Plant Gadsden Unit 2, (2008).
[5] J. Li, M.C. Paul, K.M. Czajka, Studies of ignition behavior of biomass particles in a down-fire reactor for improving co-firing performance, Energy Fuel 30 (7) (2016) 5870–5877.
[6] J.L. Afolabi, The Performance of a Static Coal Classifier and Its Controlling Parameters, University of Leicester, 2012.
[7] D.J. Foster, W.R. Livingston, J. Wells, J. Williamson, W.H. Gibb, D. Bailey, Application of CFD Modelling to Mill Classifier Design, (2004).
[8] A.F. Zsolt Dobó, Investigation of co-milling Utah bituminous coal with prepared woody biomass materials in a Raymond Bowl Mill, Fuel 222 (2018) 343–349.
[9] C. Eswaraiah, S.I. Angadi, B.K. Mishra, Mechanism of particle separation and analysis of fish-hook phenomenon in a circulating air classifier, Powder Technol. 218 (2012) 57–63.
[10] Power, Dynamic classifiers improve pulverizer performance and more, Available from: http://www.powermag.com/dynamic-classifiers-improve-pulverizer-performance-and-more/.
[11] A.S. Berrouk, et al., Numerical simulation of a commercial FCC regenerator using Multiphase Particle-in-Cell methodology (MP-PIC), Adv. Powder Technol. 28 (11) (2017) 2947–2960.
[12] O.P. Mahajan, P.L. Walker Jr., Porosity of coals and coal products, Analytical methods for coal and coal products, 1978.

Fuel Processing Technology 217 (2021) 106777

Contents lists available at ScienceDirect

Fuel Processing Technology

journal homepage: www.elsevier.com/locate/fuproc

Research article

Modeling ash deposit growth rates for a wide range of solid fuels in a 100 kW combustor

Seyedhassan Fakourian [a,*], Zachary McAllister [a], Andrew Fry [a], Yueming Wang [b], Xiaolong Li [b], Jost O.L. Wendt [b], Jinze Dai [b]

[a] *Brigham Young University, Department of Chemical Engineering, 84602 Provo, UT, USA*
[b] *University of Utah, Department of Chemical Engineering and Institute for Clean and Secure Energy (ICSE), Salt Lake City, UT 84112, USA*

ARTICLE INFO

Keywords:
Biomass
Coal
Ash deposit model
Stickiness
Melt fraction
Kinetic energy

ABSTRACT

This work details a model for evaluating the relative ash deposition propensity of various solid fuels without the complicated spatial considerations included in CFD modeling. Four deposition mechanisms are included, namely: inertial impaction, thermophoresis, condensation, and eddy impaction. This model has been validated and shown to effectively predict ash deposit rates for a wide range of solid fuels including coal, biomass, and their blends, burned in a 100 kW rated downflow combustor. Specifically, this work presents and compares two separate models for the sticking efficiency of impacting ash particles on a coupon surface: the melt fraction stickiness model (MFSM), which is developed here and includes a novel approach to determine sticking efficiency, and the kinetic energy stickiness model (KESM), an existing model used for comparison. To apply the MFSM model, the equilibrium composition of vapor species are calculated by thermodynamic modeling using FactSage. By comparing the root-mean-square-errors of the MFSM and KESM over the wide variety of fuels, it is shown that the MFSM is more accurate than the KESM in predicting the ash deposit rate. This shows that NaCl and KCl are expected to be the main alkali vapor species in the flue gas, for the fuels evaluated.

1. Introduction

Extensive studies have been carried out to introduce alternative methods to reduce CO_2 pollution, believed to be driving global warming [1,2]. Partial replacement of coal in existing coal-fired power plants with biomass is one alternative to reduce CO_2 emissions [3,4]. Among the different types of biomass, woody biomass has attracted a great deal of attention because it is widely available, and removing unused woody residues can reduce the risk of wildland fires [5]. However, according to the proximate, ultimate, and ash composition analyses, the composition of woody biomass is different from that of coal [6]. Therefore, the formation and deposition of ash during the cofiring of biomass with coal can be different from that of pure coal combustion [7]. These differences can affect the deposition of solid particles on heat transfer surfaces and can lead to reduced efficiency and unscheduled plant shutdowns. It is therefore worthwhile to investigate how the properties of various fuels influence ash deposition rates in pilot and full-scale furnaces.

To understand the impact of inorganic elements, a knowledge of the mechanisms of deposition is required. Inorganic elements of solid fuels, are the greatest contributor to deposit growth on surfaces with a lower temperature than the flue gas [8]. Alkali contents of woody biomass, like sodium (Na) or potassium (K), vaporize during combustion and later condense with the other elements such as chlorine (Cl) and sulfur (S) to make alkali rich ash deposit. Such deposits have a low melting point and create a sticky layer on heat exchanger surfaces [9,10]. Alkali elements can additionally react with silicon (Si) to produce other compounds with low-melting points, further exacerbating ash deposition [11].

In addition to chemical composition of the ash, many physical properties affect the deposit mechanism and the ash deposition rate. These include ash particle properties such as particle size distribution (PSD), composition, velocity, density, and temperature as well as flue gas properties including temperature, viscosity, density, and velocity [12]. Slag deposition, which is a liquid-like ash deposition to the boiler walls in the radiation zone [13], is beyond the scope of this research. Our focus is on fouling, which occurs at gas and particle temperatures below the ash fusion temperature.

Modeling may be utilized to further our understanding of how the factors discussed above may affect systems where woody biomass is

---

* Corresponding author.
E-mail addresses: sh.fakourian@gmail.com (S. Fakourian), afry@byu.edu (A. Fry), jost@chemeng.utah.edu (J.O.L. Wendt), jinze.dai@utah.edu (J. Dai).

https://doi.org/10.1016/j.fuproc.2021.106777
Received 4 December 2020; Received in revised form 5 February 2021; Accepted 8 February 2021

cofired with coal [14]. There are many publications concerning the modeling of the ash deposition rate, although there is not yet a complete understanding of ash transformations and deposition [15]. Most of the published models are based upon Computational Fluid Dynamics (CFD) and include complex sub-models describing gas and particle phases [14,16–26]. In addition, some of them ignore the contributions of condensation and eddy impaction, which is addressed in this study. Other researchers have developed models to predict the fly ash formation [27,28]; however, this is beyond of the scope of this study. Recently, X. Yang et al. [29,30] developed a CFD model using ANSYS Fluent to predict the formation of ash deposit during the combustion of a lignite based fuel on inertial impaction, thermophoresis, and condensation mechanisms. Additionally, S. S. Lokare et al. [31] developed an ash deposition model using Fluent and C++ to predict the rates and mechanisms of ash deposition while cofiring straw and coal. Their model assumed that the total deposition rate is dependent on inertial impaction, condensation, and eddy impaction; however, their ash deposition rate was not time dependent. Further reviews of ash deposition models have also been published [14,16,32–34].

Despite these advances, there are few modeling studies that address the effect of various biomass compositions and blends of biomass with coal [35]. The objective of this paper is to generate a model to help operators of utility boilers readily predict the ash deposit propensity on the heat exchanger surfaces for a wide range of solid fuels including coal, biomass, and their blends. Therefore, this model is simply applied, is not based on CFD and accounts for only simple tube in cross flow geometry. Alternatively, it includes details about fuel chemistry and deposition mechanisms including four ash deposit mechanisms: inertial impaction, thermophoresis, condensation, and eddy impaction [9,30,36–39]. The stickiness of impacting ash particles in the model is evaluated using two separate stickiness models. The predicted ash deposition rates of a 100-kW boiler are then compared with the corresponding experimental data and the dominant ash deposit mechanisms for all surfaces of our probe are determined.

2. Materials and methods

2.1. Experimental Work

The following section details the various materials necessary to conduct the trials in this study. This includes the, combustor, fuels, and probe.

2.1.1. Combustor description

The experimental work was conducted in a down-fired 100 kW refractory-lined furnace, which is called an oxy-fuel combustor (OFC). The combustor, shown in Fig. 1, was designed to have three zones: ignition, radiation, and convection. There are nine pairs of ports in the vertical section of the OFC for sampling and observation. The ignition zone extends from ports 1 to 3 of the OFC and has an inner diameter of 0.37 m and a total length of 1.22 m. After a transition zone, the radiation zone extends from ports 5 to 9 (0.27 m × 2.60 m / internal diameter x length). The radiation zone is followed by a horizontal convection zone (0.15 m × 0.15 m × 3.66 m / width x height x length) which is comprised of eight heat exchangers [7]. The burner used for the experiments was a one register swirl burner which facilitates the mixing of the fuel and oxidant (which was air for all of the tests evaluated in this study) [40]. Deposition rate data were collected using a temperature-controlled deposit probe installed in port 6. It is also important to note that the peak temperatures for the reactor occur in the ignition zone occurs around port 2, which is difficult to measure [7]. More details about OFC can be found elsewhere [7,38].

2.1.2. Fuel description

Eleven solid fuels were combusted in OFC including a) rice husks (RH), b) Utah bituminous Sufco coal #1 (Sufco#1), c) Utah bituminous Sufco coal #2 (Sufco#2), d) a blend of 20 wt% rice husks with 80 wt% Sufco coal #1 (20RH-80Sufco#1), e) Powder River Basin sub-bituminous coal (PRB), f) a blend of 13 wt% rice husks with 87 wt% PRB (13RH-87PRB), g) petroleum coke (Petcoke), h) Illinois bituminous coal (Illinois), i) a blend of 60 wt% Illinois bituminous coal with 40 wt% PRB (60Illinois-40PRB), j) torrefied woody biomass (Torrefied), and k) a blend of 50 wt% torrefied woody biomass with 50 wt% Sufco coal #2 (50Torrefied-50Sufco#2). The fuel analysis and mineral ash analysis are presented in Table 1 and Table 2, respectively.

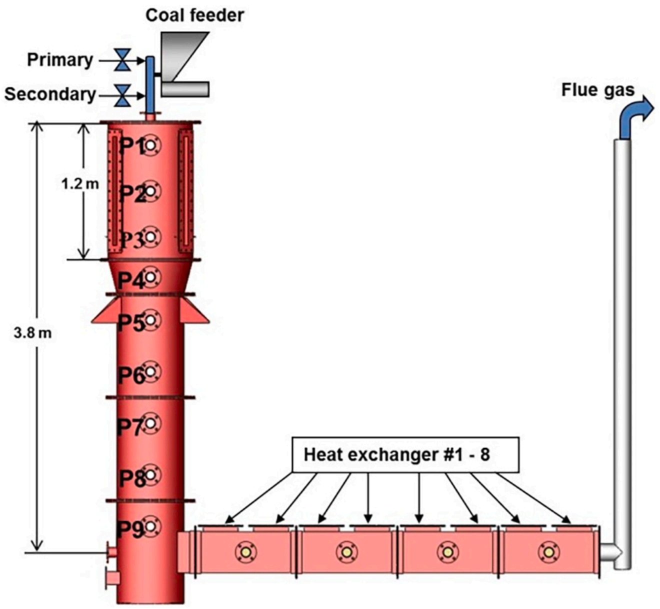

Fig. 1. Configuration of 100 kW oxy-fuel combustor (OFC).

2.1.3. Ash deposition probe description

A temperature-controlled ash deposit probe was used to determine deposition rate and profile for various fuels and operating conditions. The ash deposit collected from the horizontal surface of the probe, which is perpendicular to the flow direction of flue gas, includes inside (initial) deposit, outside deposit, and side deposit. The inside layer comprises the initial ash deposit, which is sticky, and must be scraped off to be collected. The outside deposit, which is formed by large fly ash particles, is different in composition than the inside layer and can be collected by vigorously shaking the probe until it falls off [7]. The length and the diameter of the coupon are 7.37 and 6.03 cm, respectively. More detailed information about the ash deposit probe can be found elsewhere [7,38]. The probe was installed in the OFC for durations of 30, 60, and 120 min for each fuel condition. The calculated ash deposit mass is the of the sum of the collected ash deposit on the outside, inside, and sides of the coupon surface (see Fig. 2) and the rate is the mass divided by the duration of installation.

2.2. Model description

This section provides: a list of assumptions that were made in order to apply the model, a detailed description of the deposition mechanisms and their mathematical representation and a discussion of intermediate calculated values including the ash deposit thickness, impact efficiency, heat energy balance, ash deposit thermal conductivity, and the sticking efficiency. In the latter section we will present a comparison of this model to an existing sticking efficiency model and their ability to estimate the ash deposit rate.

2.2.1. Model assumptions

The main assumptions of this model are:

Table 1
Ultimate and proximate fuel analysis.

Fuel	ASH (%)	C (%)	H (%)	N (%)	S (%)	O (diff) (%)	H_2O (%)	Volatile (%)	FC (%)	HHV (kJ/kg)	Cl (%)
a	33.67	28.47	4.15	1.05	0.10	24.42	8.16	48.96	9.22	11,551	0.071
b	8.36	67.87	4.77	1.09	0.36	11.44	6.11	38.49	47.04	27,677	0.047
c	13.96	62.41	4.52	1.10	0.46	11.04	6.52	37.36	42.16	27,319	[a]-
d	13.42	59.99	4.67	1.08	0.31	14.04	6.52	40.58	39.48	24,451	[a]-
e	4.94	53.72	3.59	0.78	0.23	13.05	23.69	33.36	38.01	21,115	[a]-
f	8.67	50.44	3.66	0.82	0.21	14.53	21.67	35.39	34.27	19,871	[a]-
g	2.99	82.51	6.02	1.71	5.65	0.49	0.57	10.18	86.26	35,720	[a]-
h	9.42	63.47	4.36	1.24	3.12	8.76	9.64	36.04	44.90	26,870	[a]-
i	7.63	59.57	4.05	1.06	1.96	10.48	15.26	34.97	42.14	24,567	[a]-
j	0.19	51.75	5.29	0.14	0.02	36.29	6.32	74.20	19.29	21,534	0.03
k	7.08	57.08	4.91	0.62	0.24	23.67	6.42	55.78	30.73	24,427	[a]-

[a] Cl either was not measured or was below the detection limit.

Table 2
Mineral ash analysis.

Fuel	Al_2O_3 (%)	CaO (%)	Fe_2O_3 (%)	MgO (%)	MnO (%)	P_2O_5 (%)	K_2O (%)	SiO_2 (%)	Na_2O (%)	SO_3 (%)	TiO_2 (%)	NiO (%)	V_2O_5 (%)
a	1.73	1.31	1.1	0.84	0.83	1.81	2.66	88.51	0.31	0.32	0.18	[a]-	[a]-
b	8.34	18.21	5.25	2.84	0.05	0.01	0.33	48.85	3.09	5.96	0.64	[a]-	[a]-
c	12.09	11.9	3.62	3.94	0.03	0.25	1.13	62.48	0.81	1.83	0.68	[a]-	[a]-
d	5.03	9.76	3.18	1.84	0.44	0.91	1.5	68.68	1.7	3.14	0.41	[a]-	[a]-
e	14.78	22.19	5.2	5.17	0.01	1.07	0.35	30.46	1.94	8.83	1.3	[a]-	[a]-
f	8.26	11.75	3.15	3.01	0.42	1.44	1.51	59.49	1.13	4.58	0.74	[a]-	[a]-
g	19.4	4.22	7.02	0.66	0.06	0.18	1.17	46.7	0.72	3.77	0.63	1.26	8.24
h	20.18	3.22	16.46	0.89	0.03	0.1	2.1	51.22	1.06	2.79	0.98	[a]-	[a]-
i	18.02	10.81	11.96	2.60	0.02	0.49	1.40	42.92	1.41	5.21	1.11	[a]-	[a]-
j	2.67	51.72	8.28	10.39	4.73	4.16	4.61	6.82	1.6	5.03	0	[a]-	[a]-
k	11.95	12.33	3.7	4.04	0.1	0.29	1.32	61.71	0.83	1.84	0.67	[a]-	[a]-

[a] Not measured.

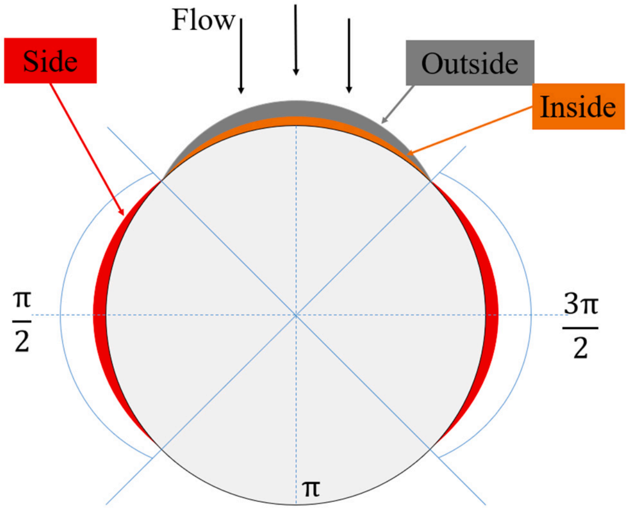

Fig. 2. Locations of ash deposit on the surface of heat exchanger tube depicted.

1. The temperature of the particle before impacting the probe surface is equal to the temperature of the surrounding flue gas [41].
2. The temperature gradient inside the ash particles is neglected [42].
3. The thermal boundary layer thickness is obtained from the average Nusselt number, which accounts for the average convective heat transfer coefficient. The empirical parameters of average Nusselt number are reported elsewhere [43].
4. The eroding effect of the high momentum solid large particles on deposit surface, which leads to either natural or artificial shedding, is neglected [44]. This is a reasonable assumption at short ash deposition times.
5. The geometry of the ash deposit surface may influence the deposition of ash particles on the probe surface. However, this level of detail requires CFD modeling, and is, therefore, neglected in this study.
6. The temperature of the downstream (π) side of the probe is assumed equal the probe surface temperature. This assumption is used for calculating thermophoresis and condensation on the π side.
7. The release fraction of Na and K from the fuel to the flue gas phase are the same. It is considering the fact that the potential chemical association of Na with other inorganic elements in fuel is similar to that of K. In addition, the volatilities of NaOH and NaCl are close to those of KOH and KCl, respectively.
8. The melt fractions of ash particles and the ash deposit are identical at the same temperatures and were obtained from thermodynamic modeling using FactSage 7.3 software.
9. The side ash deposits of some tests were not measured. However, since the inside and side ash deposit thicknesses are almost identical, it is assumed that the mass of side ash deposit is equal to the inside ash deposit [45].

2.2.2. Ash deposit mechanisms

In the present model, four essential mechanisms of ash deposition are considered including inertial impaction, thermophoresis, condensation, and eddy impaction. Particles above 10 μm, which do not follow the gas streamline, have enough force to contact with the heat exchanger surface and make inertial impaction ash deposit [36,37]. Thermophoresis causes ash deposit due to the induced force on the particles because of the temperature gradient. Furthermore, condensation of vapor species on the colder surfaces whose temperature is lower than the dew point of species in the flue gas also leads to ash deposit on the probe [36]. Lastly, eddy impaction caused ash deposits occur when turbulent flows provide enough momentum to the fine ash particles to impact π side of the heat exchanger surfaces [31,38]. A schematic diagram of ash deposit mechanisms for fouling formation is presented in Fig. 3. The definition and a mathematical representation of each of these mechanisms is presented in detail in this paper.

2.2.2.1. Inertial impaction. Inertial impaction is experienced predominately from large ash particles (typically $>10\ \mu m$) and is a strong function of velocity [46]. Particle velocity is governed by the momentum equation of a particle, which is determined by the balance of drag force, gravitational force, and the other forces as shown in the following equation [47]:

$$\frac{du_p}{dt} = \frac{18\mu_g}{\rho_p d_p^2}\frac{C_D Re_p}{24}\left(u_g - u_p\right) + \frac{g\left(\rho_p - \rho_g\right)}{\rho_p} + Force_{balance}, \tag{1}$$

where u, μ, ρ and d are the velocity, viscosity, density, and diameter. The subscripts of p and g mean particle and flue gas, respectively. The viscosity of flue gas is calculated using a simple equation by S.B. Hansen et al. [46]. C_D is the drag coefficient that is calculated elsewhere [48], $Force_{balance}$ is the balance of the other body forces, such as the thermophoretic force [29], and g is the gravitational constant (9.8 $\mathrm{m{\cdot}s^{-2}}$). Furthermore, Re_p refers to the particle Reynolds number ($Re_p = \rho_g d_p v_t / \mu_g$), where v_t is the terminal velocity of particle and is assumed to be identical to the flue gas velocity as both the particle and the fluid flow in the same direction and approximately at the same velocities. For other equations, it will be necessary to define the inertial impaction velocity of a particle (u_{in}), in which its time variation ($\frac{du_{in}}{dt}$) is assumed to be the balance of the first two terms of the right side of Eq. (1).

2.2.2.2. Thermophoresis. The thermophoresis mechanism is a phenomenon driven by the temperature gradient between the high-temperature small particles and the low-temperature probe surface. The flue gas molecules at the hot side of an ash aerosol particle, which are typically in the range of $0.1\mu m < d_p < 1.0\mu m$, impinge and carry the particle towards the cold side [33,49]. A thermophoretic force in the negative direction to such temperature gradient is the result [50]. Thermophoretic force (F_{th}), which is governed by the geometric relationship between the particle and the cold surface, is expressed by the following formula [51]:

$$F_{th} = \phi \frac{d_p \nabla T_{g-s}}{2T_g}\frac{\mu_g^2}{\rho_g} \tag{2}$$

where T_g is the flue gas temperature, and ∇T_{g-s} is temperature gradient between flue gas and the surface temperature. $\phi(\Lambda, Kn)$ is a function of the ratio of thermal conductivity of the particle to that of the flue gas ($\Lambda = k_p/k_g$) and Knudsen number (Kn) [50–54]. The particle thermal conductivity, k_p, is assumed constant at 2.0 W/m/K, and the flue gas thermal conductivity, k_g, can be estimated using the references [46, 51]. Later equations will refer to the thermophoretic velocity (u_{th}) which is the particle velocity due to thermophoresis and can be derived from the thermophoretic force elsewhere [52].

The effect of thermal conductivity ratio and Knudsen number on the thermophoretic force is presented in Fig. 4. As displayed in Fig. 4, the graphs of the expression $-\Phi/2\pi$ are a function of thermal conductivity ratio (Λ) and Knudsen number (Kn). The negative sign represents the direction of the thermophoretic force towards the cold surface. The expression $-\Phi/2\pi$ is smaller at the greater thermal conductivity ratios and the smaller Kn numbers, which indicates that the thermophoretic force declines. $-\Phi/2\pi$ is independent on the values of the conductivity ratios at $Kn > 1.0$.

2.2.2.3. Condensation. Ash deposition by condensation occurs when vapors species experience temperatuers lower than their dew point on colder surfaces inside the reactor and form aerosol in the boundary layer of the probe surface and precipitate [33]. The mass flux of vapor condensation, I_{cond}, is determined by the following expressions [55,56]:

$$I_{\mathrm{cond}} = Sh\left(T_g\right)\frac{\left(D_v\left(T_g\right)D_v\left(T_s\right)\right)^{1/2}}{D_h R_g}\left[\frac{p_v\left(T_g\right)}{T_g} - \frac{p_{v,s}\left(T_s\right)}{T_s}\right], \tag{3}$$

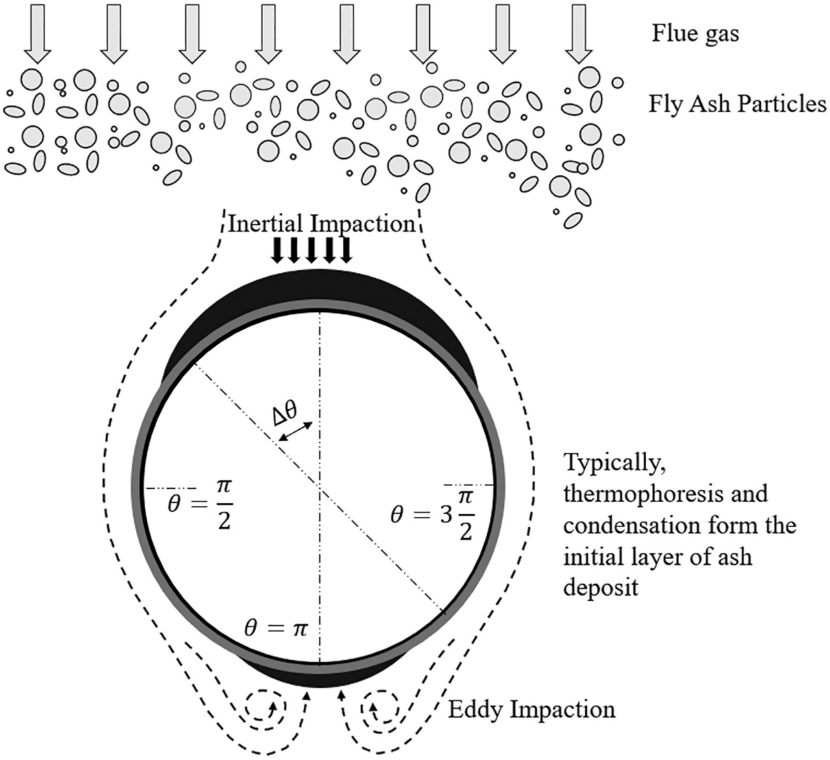

Fig. 3. Schematic diagram of fouling formation mechanisms.

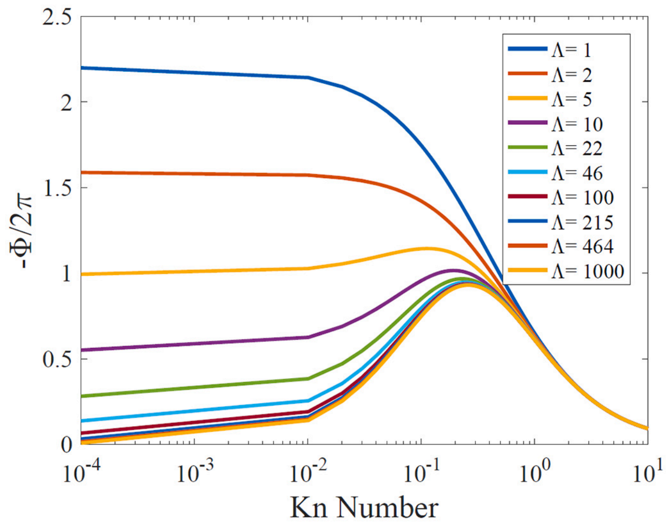

Fig. 4. Expression −ϕ/2π as a function of Knudsen number (Kn) and thermal conductivity ratio (Λ) [52].

$$Sh(T_g) = 0.023 \cdot Re^{0.8} \cdot Sc(T_g),^{0.4} \tag{4}$$

$$Sc(T_g) = \mu_g / (\rho_g D_v(T_g)), \tag{5}$$

where D_h is the hydraulic diameter of probe diameter and R_g is the universal gas constant. D_v, which was determined by S.B. Hansen et al. [46], is the diffusion coefficient of vapor at flue gas temperature, $D_v(T_g)$, or the deposit surface temperature, $D_v(T_s)$. Other variables include $p_v(T_g)$, which is the partial vapor pressure of the condensing components, and $p_{v,\,s}(T_s)$, which is the saturation vapor pressure at the deposit surface temperature. The Reynolds number for Eq. (4) is defined as $Re = \rho_g \overline{U} D_h / \mu_g$ where $\overline{U}$ is the magnitude of the flue gas velocity in this study.

2.2.2.4. Eddy impaction. Eddy impaction is a process by which the fine ash particles can impact the π side of the probe surface (see Fig. 3) once they obtain a high enough momentum to follow the eddy streams [41,57]. Circular vortices that cause the eddy streams form at Reynolds numbers of about 4.0 [58]. Only the particles with a diameter smaller than $d_{p\text{-}eddy}$, given by the following expression by W. D. Bachalo [59], may respond to eddy streams:

$$d_{p-eddy} \le \sqrt{D_h}\left[\frac{u_{rms}\cdot\rho_g}{\mu_g}\left(\frac{\rho_p}{\rho_g}+1\right)\right]^{-\frac{1}{2}} \tag{6}$$

where u_{rms} is root-mean-square speed of the flue gas. Particles with larger diameters may cross eddy streamlines and impact and stick on the upstream side of the probe surface due to their inertia [41].The flux of ash deposition by eddy impaction, I_{eddy}, can be expressed by the following equation [41]:

$$I_{eddy} = u_r C_{eddy} f_p, \tag{7}$$

where u_r is the maximum reverse flue gas velocity, assumed to be equal to the gas velocity [41], $\overline{U}$, in the present study, and C_{eddy} is the mass concentration of eddy particles. There is a lack of information in the literature about the definition of C_{eddy}. The authors of this study define it as a function of Re and the concentration of fly ash particles upstream from the probe (C_p) as follows:

$$C_{eddy} = 8 \times 10^{-6} \cdot Re \cdot C_p \tag{8}$$

Therefore, even at very high Re numbers ($Re \approx 10^5$), $C_{eddy}$is less than C_p. It should be noted that $Re < 1000$ for this study. Lastly, the probability of impacting and sticking the πside of probe surface (f_p) is determined elsewhere [41].

2.2.3. Ash deposit thickness

The ash deposit thickness on a coupon as a function of time is determined by X. Yang et al. [29] as follows:

$$\frac{dL_{deposit}}{dt} = \frac{\eta_{stick} A_{arrival} + I_{cond}}{\rho_p (1 - \varepsilon_{deposit})}, \tag{9}$$

where $L_{deposit}$, is the ash deposit thickness and η_{stick} is the sticking efficiency, or the ratio of the number of the particles that stick to the surface to the number of particles that impact the surface [60]. X. Yang et al. [29] defined $A_{arrival}$ as the flow flux of the arrival of ash particles due to the inertial impaction and thermophoresis in a CFD model. Since this study is not a CFD model, it is modified by replacing $A_{arrival}$ with $\eta_{imp} C_p (u_{in} + u_{th})$, in which η_{imp} is the impaction efficiency of fly ash particles surrounding the probe, and C_p is the concentration of fly ash particles also used in Eq. (8). The impaction efficiency (η_{imp}) is the ratio of the number of the impacted particles to the probe surface to the total number of the particles directed to the surface by the flue gas [31]. The inertial impaction velocity of a particle (u_{in}) and the thermophoretic velocity (u_{th}) were introduced previously. C_p, is obtained by the following equation:

$$C_p = \frac{x_{ash} \cdot \dot{m}_{fuel} \cdot \rho_g}{\dot{m}_g} \tag{10}$$

where x_{ash} is the ash mass fraction defined as the ratio of the mass of ash to the mass of fuel, $\dot{m}_{fuel}$ is the fuel rate defined as the ratio of the mass of fuel to time, ρ_g is the flue gas density, and $\dot{m}_g$ is the flue gas flow rate defined as the ratio of the mass of flue gas to time.

The ash deposit porosity is also an important factor in determining the ash deposit thickness. Ash deposit porosity ($\varepsilon_{deposit}$) varies according to the changing volume of liquid (V_l) and solid (V_s) phases of ash deposit as follows [61]:

$$\varepsilon_{deposit} = 1 - \left[(1-\varepsilon_0) + \frac{V_l}{V_s}(1-\varepsilon_0)\right], \tag{11}$$

where ε_0 is the initial ash deposit porosity, which is assumed at the range of 0.6–0.9 [46,61,62]. Volume of liquid phase (V_l) is calculated by using the melt fraction of ash deposit and estimating its density, which was obtained from the literature [63,64]. K. C. Mills and B. J. Keene [65] presented a review about the density of liquid phase of ash as a function of temperature and chemistry which can be used in connection with the volume of the liquid phase (V_l) mentioned previously.

2.2.4. Impaction efficiency

Impaction efficiency is expressed as a function of the effective Stokes number, St_{eff}, which is calculated by the correlation of R. Israel et al. [66], and is valid for $St_{eff} > 0.14$:

$$\eta_{imp} = \Big[1 + 1.25(St_{eff} - 0.125)^{-1} - 0.014(St_{eff} - 0.125)^{-2} + 0.0000508(St_{eff} - 0.125)^{-3}\Big]^{-1}, \tag{12}$$

The effective Stokes number is defined as follows [67]:

$$St_{eff} = \psi \cdot St, \tag{13}$$

where the Stokes number is expressed by $St = \frac{\rho_p d_p{}^2 \overline{U}}{9 \mu_g D_h}$ [67]. The Stokes correction factor (ψ) is a function of the particle Reynolds number (Re_p) [67]:

$$\psi = \frac{18}{Re_p}\left(Re_p^{\frac{1}{3}} - \sqrt{6}\,tan^{-1}\left(\frac{Re_p^{\frac{1}{3}}}{\sqrt{6}}\right)\right) \tag{14}$$

where all of the variables have been defined previously. The impaction efficiency increases with increasing particle size. Particles with $St < 0.1$ follow the flow streamlines and their impaction efficiencies cannot be predicted by available Eqs. [33]. Therefore, a constant impaction efficiency is assumed for such particles in this study [51].

2.2.5. Heat energy balance

The heat energy balance expresses the relationship between conduction, convection, and radiation heat transfer and is greatly affected by the ash deposit thickness. Heat transfer in the reactor occurs first from the flue gas to the ash deposit surface by convection and radiation; then, it transfers to the coupon surface by conduction [61]. Increasing ash deposit thickness leads to declining heat transfer from the flue gas to the heat exchanger surface. As a result, the deposit surface temperature, T_s, will increase due to the increasing thermal resistance. The deposit surface temperature, which is coupled with the ash deposit thickness calculation, is represented by the following energy balance that is organized from the components of references [41, 68]:

$$\frac{k_{deposit}}{L_{deposit}}\left(T_s - T_{coupon,s}\right) = h_g\left(T_g - T_s\right) + \sigma_r\left(\alpha_r T_g^4 - \varepsilon_r T_s^4\right), \tag{15}$$

where $T_{coupon,\ s}$ is the temperature of coupon surface, which is set at 922 K, a temperature representative of advanced power systems [7]. $L_{deposit}$ and $k_{deposit}$ are the thickness and the thermal conductivity of ash deposit layer, respectively. h_g is the forced crossflow convective heat transfer coefficient from the flue gas. ε_r is the emissivity of the ash deposit, and it declines with increasing temperature; the value of ε_r for ash is found in the literature [69,70]. σ_r is the Stefan-Boltzmann constant. Kirchhoff's law, which is assumed for this model, states that the absorbance thermal radiation, α_r, is equal to the emittance thermal radiation, ε_r, when they are in radiative thermodynamic equilibrium [68]. It should be noted that the heat flux to the probe surface is typically calculated by CFD calculations and can be affected by the fluid type [71]. Using an average Nusselt number ($\overline{Nu} = h_g D_h / k_g$), the convective heat coefficient is estimated. The reader is directed to the references [43,72,73,74] for more information about the forced convective heat transfer.

2.2.6. Ash deposit thermal conductivity

The ash deposit thermal conductivity is another essential input of the developed model. A simple equation to estimate the ash deposit thermal conductivity, $k_{deposit}$, is presented by G. H. Richards [61]:

$$k_{deposit} = (1 - \mathrm{F})k_s + Fk_{g-N_2}, \tag{16}$$

where k_s and $k_{g-N2}$are the thermal conductivity of the solid phase deposit and nitrogen gas, respectively. The thermal conductivity of nitrogen gas phase is approximated using a dataset [75]. k_s is assumed to be a constant value of 3 W/m/K by A. L. Robinson [76], which represents the thermal conductivity of silica-based materials at high temperatures. For the torrefied woody biomass ash, which is low in Si and high in Ca, k_s is assumed to be 0.4 W/m/K [77]. For more information about the thermal conductivities of materials, please refer to the following paper by Y. S. Touloukian [77]. Lastly, F is the weighting factor, which is a function of ash porosity and obtained elsewhere [61]. It is worthwhile to note that the thermal conductivities and the ash deposit porosities are calculated at the deposit surface temperatures. It should also be noted that the influence of radiation on thermal conductivity is neglected in this research.

2.2.7. Sticking efficiency

The sticking efficiency is a complex phenomenon that can be accurately represented by many parameters including the viscosity, kinetic energy, and melt fraction of ash particles [29,33,44,46,60,78,79]. Viscosity-based stickiness models imply that the sticking probability equals unity if the particle viscosity is lower than the critical viscosity [34,80]. While some sources disagree on the exact value for the critical viscosity of ash particles, J. R. Fan et al. [81] identified it as 1×10^5 (Pa·s). This value may be assumed or determined by experimentation [33]. Kinetic energy can also influence the sticking efficiency. If the kinetic energy of a particle is higher than the interfacial energy after the impaction, the particle bounces off the surface and it does not stick [34,82]. On the other hand, if the melt fraction of either impacting ash particle or ash deposit is in the range of 0.15–0.7, the stickiness of ash particle to the surface can be significant. M. U. Garba et al. [83] combined the sticking probabilities based on ash viscosity and melt fraction in a CFD model to predict the deposition rate of ash slag of coal/biomass cofiring. Similarly, M. Zhou et al. [84] integrated the three aforementioned stickiness models in a CFD model to predict the ash deposit rate in a pilot furnace. Traditionally, the complex stickiness models are solved by CFD packages; however, two stickiness models that do not require CFD are investigated independently in this study and their results are compared:

2.2.7.1. Melt fraction stickiness model (MFSM). The MFSM derives the sticking efficiency from the particle temperature, the ash deposit surface temperature, and the melt fraction of ash [44,81,85]. Neglecting ash shedding and the other deposit removing mechanisms such as erosion, melting, and debonding of ash deposit, the following equation for the sticking efficiency, η_{stick}, is presented [84]:

$$\eta_{stick} = P\left(T_p\right) + \left[1 - P\left(T_p\right)\right]P\left(T_s\right), \tag{17}$$

where $P(T_p)$ is the sticking probability of the impacting ash particles at the particle temperature and $P(T_s)$ is the sticking probability of the ash deposit at the deposit surface temperature [29]. The probabilities are needed as only part of an ash particle may stick whereas the remaining splashes [33]. The splash of impacting ash particles is ignored here. Typically, the stickiness probability is assumed to linearly increase from 0.0 to 1.0 for the melt fractions between 0.15 (at T_{15}) and 0.7 (at T_{70}), and it remains constant at a constant value of 1.0 for higher melt fractions [86,87]. The melt fraction is obtained through thermodynamic equilibrium calculations based on the minimization of the Gibbs free energy, which is performed using FactSage 7.3 thermochemical package [88–91]. The melt fractions that depend on the ash composition and designated temperature are tabulated in the Results and Discussion section. The MFSM considers the temperature and composition of ash as well as the velocity of ash particle influences the model through Reynolds numbers. It is generally assumed that the sticking probability of the particles and ash deposit are identical if they have the same temperature and composition. However, the sticking probability is also affected by the initial sticky condensation layer on the clean coupon surface (or the initial deposit surface). This sticky layer is one of the main contributors in building up the initial layer of ash deposit and it is a novel approach in estimating the stickiness in the MFSM. If the condensation of vapor species results in molten salt, the sticking efficiency will equal unity, and the ash deposit rate will rise significantly. This issue is clarified in the Results and Discussion section of this study.

2.2.7.2. Kinetic energy stickiness model (KESM). The KESM is based on several other factors distinct from the MFSM. The first of which is the velocity of impacting ash particles. The impacting particles will stick to the surface if their velocity is lower than the critical velocity [92]. The critical particle velocity ($u_{p,\ crit}$), which is a function of particle temperature and particle size, is defined according to the references [93, 94]. In addition to velocity, the viscosity of ash deposit on the surface also plays a role in the KESM as viscosity may decrease with increasing ash deposit surface temperature. The decrease in viscosity leads to the adhesion of the impacting ash particles even if they are non-sticky [46]. Likewise, the loss of kinetic energy also plays a substantial role in this model. This is because the ash particles may lose their kinetic energy upon impaction due to their penetration into the surface. This loss of kinetic energy also increases the particles' overall stickiness [95]. The critical velocity of surface capture ($u_{s,\ crit}$), which allows one to estimate the ability of the ash deposit surface to capture the kinetic energy of coming particles, is described by E. Raask [95]:

$$u_{s,crit} = \frac{\rho_p g^2 \left(d_p/2\right)^3 \mu_s}{\gamma^2} \tag{18}$$

where surface tension (γ) is calculated by a model of K.C. Mills [96], and the ash deposit surface viscosity, μ_s, is assumed as high as 10^{10} Pa·s [46].

In the KESM, the sticking probability of the impacting particle (P_p) at the stagnation point and the sticking probability caused by the surface (P_s) are defined using the following equations [33,46,94]:

$$P_p = \begin{cases} 0 \text{ for } u_p > u_{p,crit} \\ 1 \text{ for } u_p < u_{p,crit} \end{cases} \tag{19}$$

$$P_s = \begin{cases} 1 \text{ for } u_p > u_{s,crit} \\ 0 \text{ for } u_p < u_{s,crit} \end{cases} \tag{20}$$

Similar to MFSM, neglecting ash shedding and the other deposit removing mechanisms, the stickiness of kinetic-based model is defined as the following [46]:

$$\eta_{stick} = P_p + \left[1 - P_p\right] P_s \tag{21}$$

Fig. 5 shows the algorithm of our developed model using MATLAB R2016a. A total ash deposit thickness is guessed at the first step of the model. The dynamic ash deposit thickness is then calculated at the upstream stagnation point of the coupon surface for three bins of fly ash particle sizes. At this point, the ash deposit at the upstream stagnation point includes the inertial impaction, thermophoresis, and condensation, as previously discussed. Furthermore, the three bins are defined by 0–20%, 20–80%, and 80–100% of cumulative concentration of fly ash [92] by making an analogy with the data of Q. Gao et al. [27]. For as long as the model runs, the ash deposit thickness is calculated and the parameters of ash deposit such as porosity, thermal conductivity and deposit surface temperature are likewise calculated and updated. Eddy impaction, which builds up the eddy ash deposit, is also calculated at the stagnation point of the πside of the coupon, and its impaction efficiency is assumed to be unity.

The inertial ash deposit thickness at the angular position (θ) is estimated by multiplying the absolute value of cos(θ) with the inertial ash deposit thickness of the stagnation point (see Fig. 3). Other more complex estimations can be found elsewhere [97,98]. In a similar approach, the temperature gradient at the angle of θ is estimated by assuming that the ash deposit surface temperature of the π side of the coupon and $\theta = \pi/2$ and $\theta = 3\pi/2$ are equal to the coupon surface temperature (922 K). Therefore, the thermophoresis ash deposit and condensed ash deposit can be calculated at the circumference of the coupon at each angular position (θ) by estimating the temperature gradient between the ash deposit surface and the flue gas. It is assumed that the impaction efficiencies of the thermophoresis particles on the front and π sides are the same. The eddy impaction ash deposit, which can be maximum deposit at the stagnation point of the π side, is calculated at the angle of θ of the π side using the similar procedure that explained for calculating inertial ash deposit at the angle of θ of the upstream side. The initial guess for the model uses the results of the first step and is updated after each iteration until the new guess and the calculated total ash deposit thickness of the stagnation point converged (The error is less than 0.01%). Afterwards, the total mass of the ash deposit on the coupon surface is calculated and compared with the experimental data.

3. Results and discussion

The 11 fuels described in Table 1 and Table 2 were combusted in the OFC and ash deposits were collected on the temperature-controlled deposit probe in the manner described in the methods section. For each of the experiments the surface temperature of the deposit coupon was controlled at 922 K. The mass of deposit collected on the coupon for each condition is reported in Table 3 and have been previously reported in the literature.

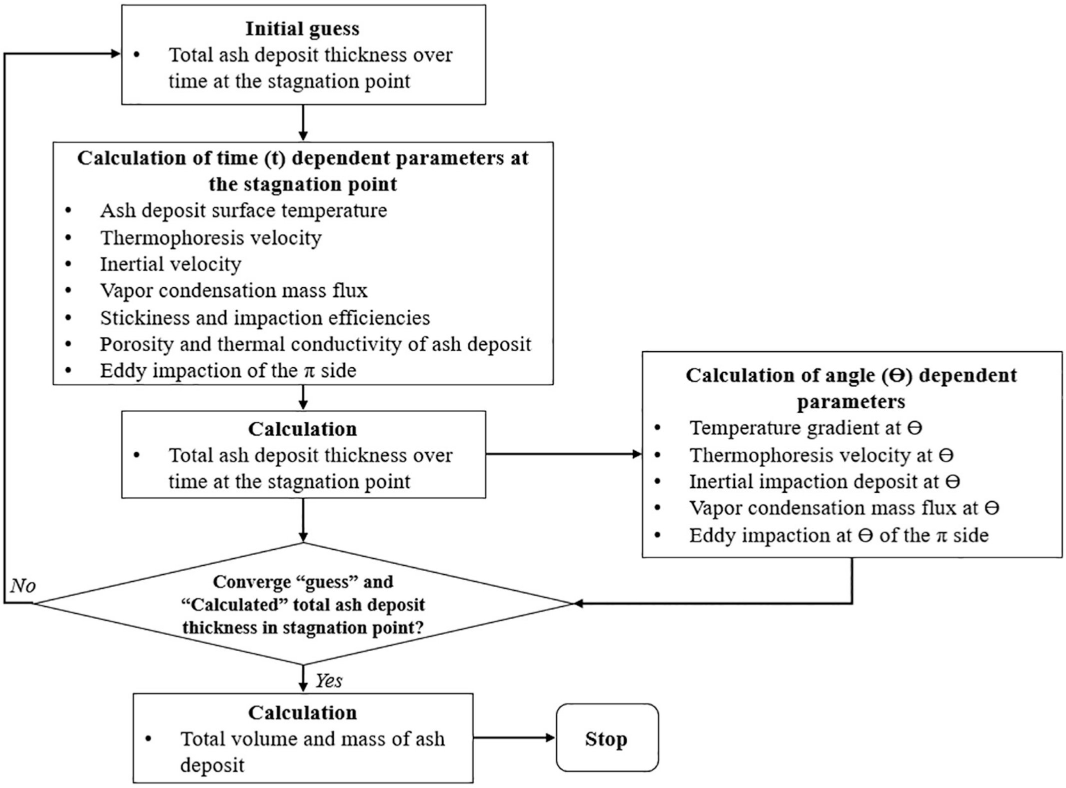

Fig. 5. Algorithm to carry out the simulation of ash deposition.

Table 3

Measured ash deposit accumulation (g/m^2) for 11 fuels and three different operation times (30,60 and 120 min) in the OFC. The fuels include: a) RH, b) Sufco#1, c) Sufco#2, d) 20RH-80Sufco#1, e) PRB, f) 13RH-87PRB, g) Petcoke, h) Illinois, i) 60Illinois-40PRB, j) Torrefied, k) 50Torrefied-50Sufco#2. Only one test was performed (60-min test) for fuels (e), (h), and (i) [99–101].

Operation time (min)	a	b	c	d	e	f	g	h	i	j	k
30	28.8	33.6	52.5	79.7	NA	31.7	24.1	NA	NA	0.9	7.9
60	61.0	77.1	116.8	112.1	36.5	77.0	69.5	53.3	36.2	1.5	23.0
120	130.2	148.3	237.5	295.0	NA	173.4	110.6	NA	NA	8.2	13.3

The following paragraphs compare the results of the MFSM and KESM approaches to modeling the experimental data to determine their effectiveness in predicting the sticking efficiency and, subsequently, the accuracy of our model is discussed. The effect of fuel type and time is then discussed for several important factors included the deposit surface temperature, deposit thickness, and thermal resistance. Lastly, the dominant mechanisms of ash deposition on each area of the coupon are presented.

The melt fraction temperature, which is distinct for each fuel type, is estimated by the simulation package FactSage 7.3. The values for this temperature depend heavily on the ash composition, presented in Table 4 for each of the eleven fuels. The common parameters in this table are shared for all the fuels in this study. FactSage 7.3 predicts the following four characteristic temperatures of the melt fractions of ash particles and ash deposits:

- T_0 (the temperature at which the melt fraction of ash particle, or deposit, is 0)
- T_{15} (the temperature at which the melt fraction of ash particle, or deposit, is 0.15)
- T_{70} (the temperature at which the melt fraction of ash particle, or deposit, is 0.7)
- T_{100} (the temperature at which the melt fraction of ash particle, or deposit, is 1.0)

The characteristic temperatures were determined via two steps. First, using the FToxid-SLAGA database with the ash components listed in Table 2 as the inputs, the melt fractions at various temperatures were calculated and tabulated. Second, the temperatures at which the melt fractions reach 0.15, 0.7, and 1.0 were determined using interpolation.

In order to calculate the characteristic temperatures, the mole fractions of the alkali vapor species need to be determined. This was also accomplished using FactSage, which showed that KCl and NaCl are the main alkali vapor species in the flue gas. S. B. Hansen et al. [46] provided a formula to obtain the amount of the K released from the fuel to the gas phase, which was used in this study. Due to their common properties, it was assumed that the release of K and Na to the gas phase is the same. Additionally, it is assumed that the K and Na of the ash analysis represent the K and Na of the fuel. Furthermore, it was assumed that both Cl and S are completely released [10,106]. These assumptions provide an accurate estimation of the amount of alkali vapor species and their condensation temperature ranges. The amount of Cl released is especially important as Cl facilitates the transfer of the alkali components from the fuel to the surface, forming sulfates and the sticky layer of ash deposit [9]. With NaCl and KCl identified as the major alkali species,

Table 4

Distinct and Common Parameters used in the model. The fuels include: a) RH, b) Sufco#1, c) Sufco#2, d) 20RH-80Sufco#1, e) PRB, f) 13RH-87PRB, g) Petcoke, h) Illinois, i) 60Illinois-40PRB, j) Torrefied, k) 50Torrefied-50Sufco#2.

			Fuels										
Distinct Parameters		Unit	a	b	c	d	e	f	g	h	i	j	k
Solid fuel rate		(kg/s) × 10^3	0.239	0.961	0.961	1.09	1.26	1.32	0.378	0.989	1.08	1.26	1.11
Flue gas density [46]		(kg/m^3)	0.28	0.286	0.304	0.288	0.298	0.289	0.291	0.29	0.287	0.306	0.302
Flue gas velocity		(m/s)	0.92	0.73	0.60	0.76	0.67	0.72	0.75	0.67	0.68	0.64	0.65
Flue gas temperature at port 6 (T_g)		(K)	1277	1247	1173	1241	1198	1235	1228	1232	1245	1166	1184
Viscosity of flue gas (μ_g) [46]		(Pa·s) × 10^5	4.87	4.80	4.61	4.78	4.67	4.76	4.75	4.76	4.79	4.59	4.64
Fly ash concentration (C_p)		(kg/m^3) × 10^3	1.56	1.96	3.99	3.45	1.65	2.84	0.269	2.50	2.16	0.0665	2.18
Melt fraction temperatures	T_0	(K)	1140	1160	1165	1175	1185	1180	1170	1180	1285	1180[b]	1180
	T_{15}		1165	1180	1185	1190	1285	1190	1180	1190	1320	1190[b]	1190
	T_{70}		1810	1495	1520	1530	1395	1380	1495	1415	1410	1410[b]	1410
	T_{100}		1850	1585	1575	1790	1465	1580	1575	1465	1460	1560[b]	1560
Common Parameters													
Coupon Surface Temperature		(K)	922										
Initial Porosity		–	0.6										
Fly ash particle density (ρ_p)[a]		(kg/m^3)	1300										
Bulk density of ash deposit[a]		(kg/m^3)	550										
Fly Ash PSD (three bins of beginning 20%, middle 60%, and end 20%)		(μm)	(1.6, 7.77, 95)										
Temperature range of alkali vapor condensation	Solid Sulfide	(K)	$800 < T \leq 850 \rightarrow$ Sticking efficiency of MFSM is calculated from Eq. (17)										
	Molten Salt		$851 \leq T \leq 1266 \rightarrow$ Sticking efficiency of MFSM is unity.										
	Alkali Vapor		$1266 < T \rightarrow$ Sticking efficiency of MFSM is calculated from Eq. (17)										
Alkali vapor species, estimated at flue gas temperature	NaCl	(Mole Fraction) × 10^5	5.59										
	KCl		5.4										

[a] Fly ash particle density and bulk density of ash deposit are assumed constant regarding the reported data in [102–104]. Due to the heavier minerals of Petcoke (g), its fly ash particle density and bulk density of ash deposit are assumed 2240 and 915 kg/m^3, respectively [105].

[b] The melt fraction temperatures of the Torrefied woody biomass are uncommon because of the fuel's unusual ash composition: low Si and Al content and very high Ca content (>50 wt%). FactSage predicts that there would be 10 wt% of molten salt but the melt fraction is not sensitive to the temperature. In addition, the ash content of this fuel is quite low (0.19 wt%). Therefore, the same melt fraction temperatures of fuel (k) (50Torrefied-50Sufco#2) are copied here. This assumption does not overestimate the stickiness model since $T_0 > T_g$, meaning that the melt fraction is zero.

the amount of the other mineral vapor species can be neglected when calculating the condensation ash deposit on the probe surface. It should be noted that the contribution of these alkali vapor species (forming submicron particles) to the ash deposit mass is small compared to that of the coarse ash particles [10]; however, their role in making sticky layer on the surfaces to build up ash deposit is significant because they might increase the sticking efficiency to unity as discussed in the model description.

The analysis of alkali vapor condensation was performed for the fuels whose Cl contents are available (see Table 1); however, Cl concentrations were not available for all of the fuels of this study. The mole fractions of NaCl and KCl in the flue gas vary from one fuel to another, as does their flue gas temperatures. Since the accurate amounts of the released Na and K to the gas phase are not known and Cl content data is not complete, the calculation of the temperature ranges of alkali vapor condensation and the amount of alkali vapor species by FactSage are estimated using literature compositions for similar fuels. Therefore, the constant mole fraction of NaCl and KCl, and a common range of temperatures of their condensation, which are calculated by FactSage, are assumed as displayed in Table 4. This assumption is reasonable and does not change the results significantly as the presence of a condensation deposition mechanism is more indicative of behavior than the amount of condensation deposition. Moreover, specifying the common parameters that are valid for a range of fuels would facilitate the understanding and application of this model by boiler operators. Careful analysis of the alkali vapor species and their condensation might be needed for longer operation times in which the ash deposit surface temperature may approach the flue gas temperature.

Alkali vapor species discussed above are important as they have been shown to condense on cooler surfaces, creating a sticky molten layer that acts like a glue, capturing further ash particles [107]. Thermodynamic modeling results confirm this and suggest that NaCl and KCl can condense partly on the colder external surfaces such as the clean coupon surface and the initial ash deposit surface. The resulting condensed phase reacts with S to make new compounds, which predominately consist of solid sulfates and molten salts. The solid sulfates are formed when S condenses at the lower surface temperatures of around 800 to 850 K. The molten salts are formed by the condensation of alkali vapor species at surface temperatures of around 851 to 1266 K and are sticky, efficiently capturing impacting particles. The upper limit of this temperature window (1266 K) is defined as the temperature at which 90% of the released K is in the vapor phase. Due to the stickiness of the molten salts, we assumed the sticking efficiency in this temperature range should be unity for the MFSM when there is an appropriate concentration of alkali and Cl in the gas phase. For this study, the molten salt deposits were predicted by the specific FTsalt database of FactSage, with the organic part of the fuel (C, H, O, N, and S), air, and the released K, Na, and Cl used as inputs. Meanwhile, as indicated in Table 4, it is reasonable to tabulate a common temperature range of alkali vapor condensation and their condensation temperature range for all the fuels of this study.

The ash aerosol particle size distribution (PSD) of the fuels, another important parameter for our model, was presented by Y. Wang [7]. The three bins of 0–20%, 20–80%, and 80–100% of cumulative fly ash PSD are defined by making an analogy with the data of Q. Gao et al. [27] For simplicity, it is assumed that the presented bin sizes in Table 4 are

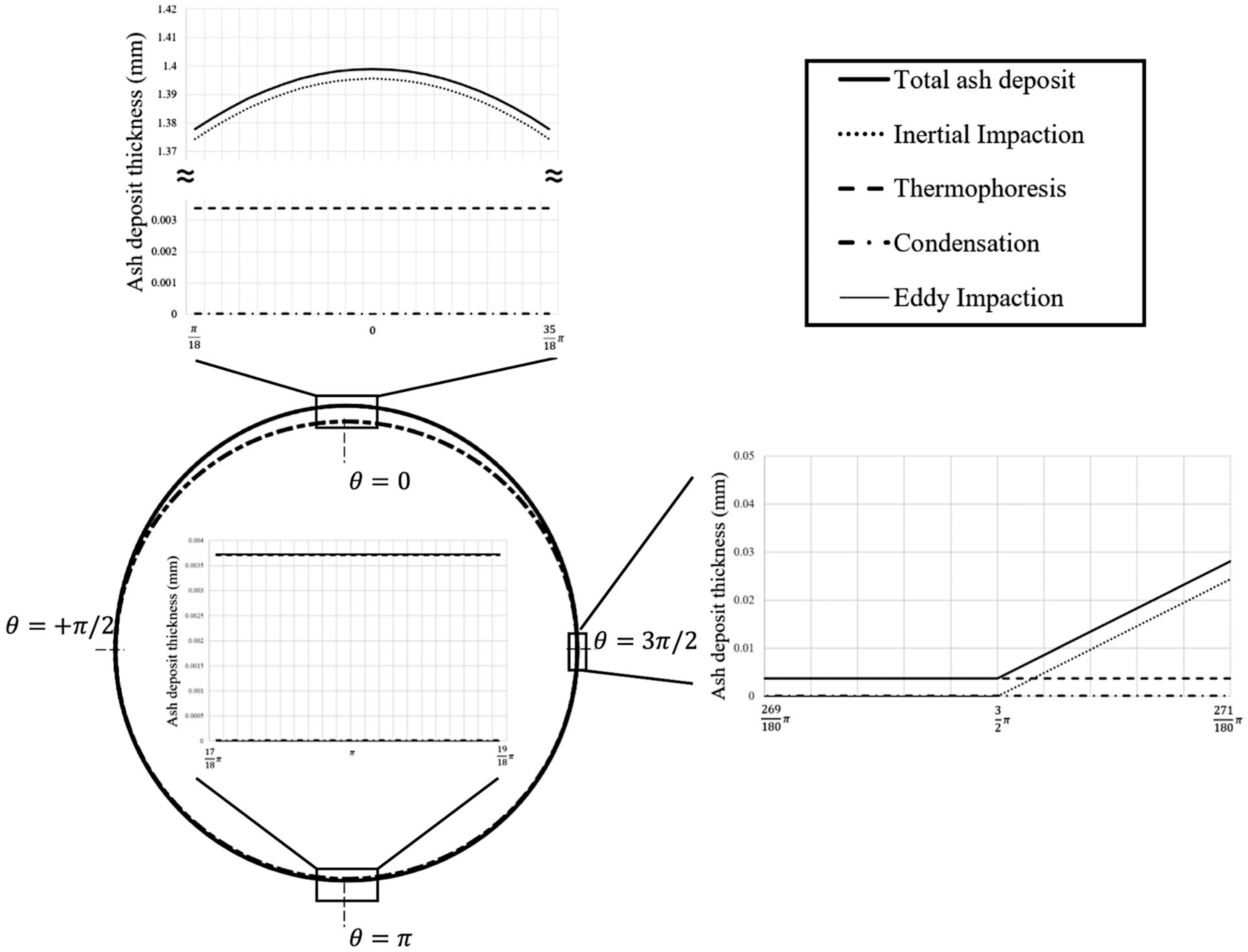

Fig. 6. Predicted ash deposit shape after 120-min of firing the 20/80 blend of rice husks and Sufco coal #1.

representative for all the fuels in this study.

3.1. *Predicted shape of ash deposit in cross view of the probe*

For visualization of the data of our model, Fig. 6 presents an approximate simulated shape of ash deposit on the coupon surface after 120 min of deposition time while firing the 20/80 blend of rice husks and Sufco coal #1. As expected, the largest ash deposit thickness is formed at the stagnation point of upstream ($\theta = 0$) with inertial impaction being the dominant mechanism of ash deposit formation. The contribution of thermophoresis and condensation can be significant as long as the temperature gradient between the surface and the flue gas is high enough; however, their general contributions in ash deposit growth are much lower than the inertial impaction. Eddy impaction does not contribute to the ash deposit on the π side of the coupon due to the high density of fly ash particles, meaning that the fly ash particles do not follow the eddy stream to impact the π side of the coupon. At angles $\theta = \pi/2$ and $3\pi/2$, inertial impaction contributes the least to ash deposit formation. Whereas thermophoresis is the dominant mechanism of ash deposit at such angles. Condensation in general contributes the least to ash deposit on the coupon surface; however, its contribution in making sticky layer is significant. Similar trends were observed for all 10 fuel types.

3.2. *Comparing the results of stickiness models*

The MFSM and KESM models were both used to predict the measured deposited mass for all of the conditions presented in Table 3. A comparison between prediction and experiment are presented in Fig. 7 for the KESM model and in Fig. 8 for the MFSM model. The error bars in both figures represents the standard error calculated from multiple measurements during experimentation. The KESM model significantly underpredicts the deposited mass for nearly all conditions and results in a root mean squared error of 84.6. The MFSM model tends to slightly overpredict the deposited mass. However, the fit is much better and results in a root mean squared error of 48.1.

It is reasonable to assume, based on the difference in mechanisms between the two models, that the KESM underpredicts deposited mass because ash particles bounce off instead of sticking to the surface. Both models underpredict the deposited mass for petcoke (Fuel g). Possibly this is because many additional volatile mineral components exist in petcoke, which may have been overlooked during the Fact Sage modeling. In addition, both models overestimate the ash deposit of 50/50 blend of torrefied wood and Sufco #2 (Fuel k), which is likely due to ash shedding occurring during the experiments, particularly for the 120-min test. The phenomenon of ash shedding is outside of the scope of this research and may be considered for future studies. For the other fuels and blends the MFSM model does a reasonable job of predicting deposited ash. Further improvement of model performance could be realized by individually defining additional model inputs, such as the initial porosity and the densities of ash. This approach could also be considered in future studies.

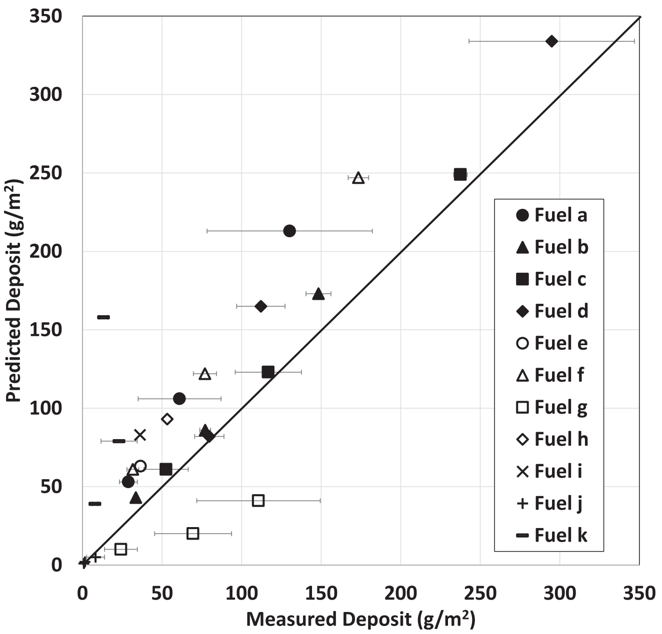

Fig. 8. Comparison of the MFSM model with experimental data, representing all of the data for 30, 60, and 120 min.

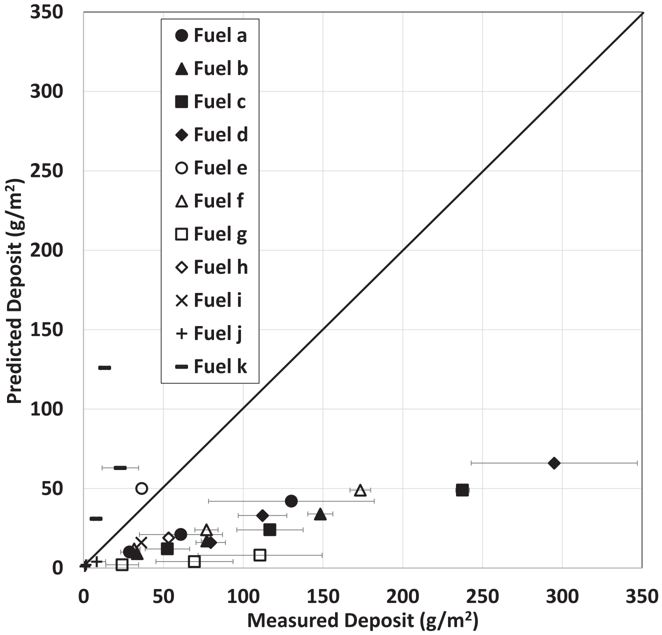

Fig. 7. Comparison of the KESM model with experimental data, representing all of the data for 30, 60, and 120 min.

3.3. *Dynamic changes of ash deposit properties*

The MFSM model also predicts ash deposit properties as the mass on the surface increases, including surface temperature, thickness, and thermal resistance. For all of the experimental conditions resulting in the measured deposits presented in Table 3 the predicted maximum surface temperature as a function of time is presented in Fig. 9, maximum deposit thickness as a function of time is presented in Fig. 10 and deposit thermal resistance (ratio of ash deposit thickness over its thermal conductivity) as a function of time is presented in Fig. 11. The ash deposit surface temperatures (Fig. 9) are predicted to increase with time relative to the coupon surface temperature (922 K). Given more time, the maximum value for these plots would eventually approach the flue gas temperature. The ash deposit thickness (Fig. 10) is predicted to increase over time, exhibiting a relatively linear trend until surface temperatures are reached where condensation/stickiness properties change. The condensed sticky layer, which forms in the temperature range of 851 to 1266 K, leads to the enhanced stickiness probability of the surface. While considering these plots it is important to remember that the thermal conductivity of the ash is lower for ashes containing more calcium (generated from torrefied biomass) than for ashes that are predominantly silicon (generated from coals). It is therefore preferable to present the plot of ash deposit thermal resistances instead of ash deposit thermal conductivities. In general, it is observed that thicker ash deposits contribute to a higher surface temperature and lower heat transfer

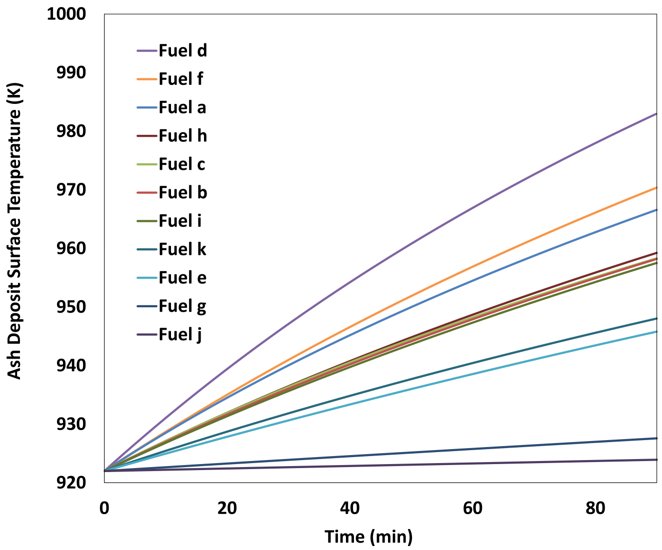

Fig. 9. Predicted outside surface temperature of the deposit as a function of time using the MFSM model. The order of the fuels presented in the legend indicates the order of temperatures in the plot.

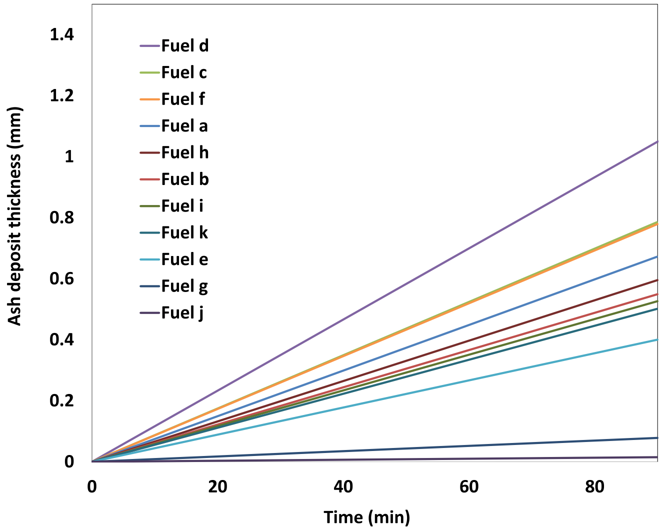

Fig. 10. Predicted maximum deposit thickness as a function of time using the MFSM model. The order of the fuels presented in the legend indicates the order of thickness in the plot.

due to the increased thermal resistance [107].

The MFSM model shows that the ash deposit rate, surface temperature, and thermal conductivity can vary depending upon the fuel type. The ash deposit surface temperature and the ash deposit thickness while firing the 20/80 fuel blend of rice husks and Sufco coal #1 (Fuel d) are high which is related to the high thermal resistance of the ash relative to the other fuels. In contrast, the ash deposit surface temperature and the thickness of petcoke (Fuel g) and torrefied wood (Fuel j) are relatively low, reflecting their low thermal resistances.

The MFSM model is able to determine the effect on the porosity of the ash deposit. As discussed in model description, the thermal conductivity of an ash deposit, which determines the ash deposit's ability to transfer heat [35], is a function of ash porosity (see Eq. (16) and refernce [61]). As mentioned above, the deposit surface temperature rises over time due to the increasing thermal resistance. Increasing the deposit surface temperature may cause the ash deposit porosity to decrease [33]. Neglecting the liquid volume of the condensed sticky layer, the model results show that the deposit porosity does not change since the liquid volume of ash deposit is not significant.

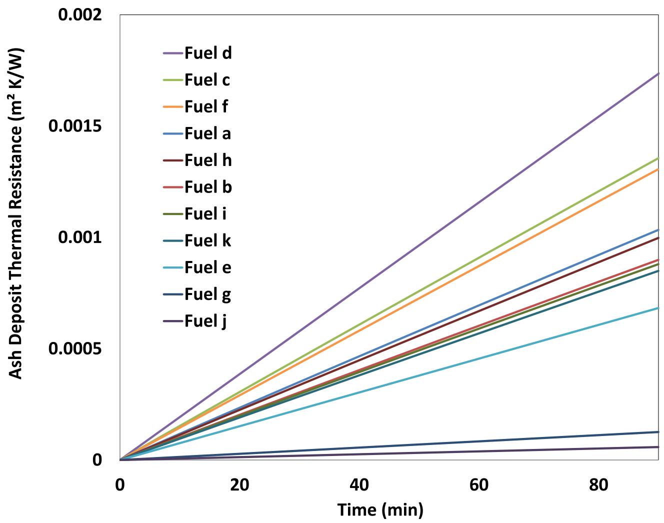

Fig. 11. Predicted thermal resistance of the deposit as a function of time using the MFSM model. The order of the fuels presented in the legend indicates the order of thermal resistance in the plot.

It is worthwhile to note that the effect of sintering—or the flow of the liquid phase on the surface of the bonded ash particles to the low potential energy surface—on the thermal conductivity during heating ash has been studied by other researchers [35,74,108–110]. For our study, however, we assume that the ash deposit never reaches the sintering point, and it is therefore not addressed.

4. Conclusion

A modeling methodology has been developed that can be used by utility boiler operators to evaluate relative deposition propensity of various solid fuels on heat transfer surfaces. This model has been validated against data sets where deposition on a temperature-controlled tube in cross flow was measured while firing 11 different fuels and fuel blends in a 100 kW down-fired combustor. The model incorporates mechanisms that describe ash deposition by inertial impaction, thermophoresis, condensation, and eddy impaction. The model does not require complicated CFD modeling of specific geometry and is generally applied to a tube in crossflow. Two ash deposit stickiness models were investigated: the melt fraction stickiness model (MFSM) and the kinetic energy stickiness model (KESM), which differ in the way that they predict sticking efficiency of particles that arrive at the deposit surface. In the MFSM, the sticking efficiency is calculated by accounting for the condensation of alkali vapor species as molten salts on the cooler surfaces (clean coupon surface and ash deposit surface). Thermodynamic modeling using FactSage was used to determine conditions where these salts would occur. In the KESM, the sticking efficiency is determined by analyzing the sticking or rebounding of impacting particles and depends on the critical velocities of the particle and surface and not the condensation of alkali vapor species. It was determined through a root mean squared error analysis that the MSFM model is much better at predicting deposit growth. Analysis of the results from the MFSM model demonstrate that the inertial impaction and thermophoresis are the dominant mechanisms in ash deposit formation on the upstream and the π side surface, respectively. It was also shown that thermophoresis is significant at the angles of $\theta = \pi/2$ and $3\pi/2$; and that thermophoretic forces have smaller values at larger thermal conductivity ratios and smaller Kn numbers. Likewise, the ash deposit surface temperature was shown to increase with the build up of ash deposit due to increasing thermal resistance. This validated model can be easily used by boiler operators to evaluate the relative propensity of deposition dependent on fuel characteristics. For ease of implementation of this model by plant operators, a table of sticking conditions (temperatures) should be developed using FactSage that apply to a broad range of fuel compositions.

Nomenclature

C_D	Drag coefficient
C_{eddy}	mass concentration of eddy particles (kg·m^{-3})
C_p	Mass concentration of fly ash particles surrounding the probe (kg·m^{-3})
d_p	Particle diameter (m)
$d_{p\text{-}eddy}$	Particle diameter of eddy impaction (m)
D_v	Diffusion coefficient of vapor (m^2·s^{-1})
D_h	Hydraulic diameter of probe (m)
F	Weighting factor
F_{th}	Thermophoretic force (N)
f_p	Probability of impacting and sticking the πside of probe surface in eddy impaction
g	Gravity (m·s^{-2})
h_g	Forced convective heat transfer coefficient (W·m^{-2}·K^{-1})
I_{cond}	Mass flux of vapor condensation (kg·m^{-2}·s^{-1})
I_{eddy}	Mass flux of eddy impaction (kg·m^{-2}·s^{-1})
KESM	Kinetic energy stickiness model
Kn	Knudsen number
$k_{deposit}$	Thermal conductivity of ash deposit (W·m^{-1}·K^{-1})
k_g	Thermal conductivity of flue gas (W·m^{-1}·K^{-1})
k_{g-N_2}	Thermal conductivity of nitrogen gas (W·m^{-1}·K^{-1})
k_p	Thermal conductivity of ash particle (W·m^{-1}·K^{-1})
k_s	Thermal conductivity of solid phase (W·m^{-1}·K^{-1})
$L_{deposit}$	Ash deposit thickness (m)
MFSM	Melt fraction stickiness model
$\overline{Nu}$	Nusselt number
PSD	Particle Size Distribution
$P(T_p)$	Sticking probability of the impacting particles at the particle temperature for melt fraction stickiness model
$P(T_s)$	Sticking probability of the ash deposit at the deposit surface temperature for melt fraction stickiness model
P_p	Sticking probability of the impacting particle for Kinetic energy stickiness model
P_s	Sticking probability caused by the surface for Kinetic energy stickiness model
$p_v(T_g)$	Partial vapor pressure of the condensing components (Pa)
$p_{v,\,s}(T_s)$	Saturation vapor pressure at the deposit surface temperature (Pa)
Re	Reynolds number around the probe
Re_p	Ash particle Reynolds number
R_g	Universal gas constant (J·kg^{-1}·K^{-1})
Sh	Sherwood number
Sc	Schmitt number
St	Stokes number
St_{eff}	Effective Stokes number
t	Time (s)
T	Temperature (K)
T_g	Flue gas temperature (K)
T_s	Deposit surface temperature (K)
$T_{coupon,s}$	Coupon surface Temperature (K)
T_X	The temperature at which melt fraction of ash particle or ash deposit is X/100
∇T_{g-s}	temperature gradient between flue gas and ash deposit surface temperature (K·m^{-1})
$\overline{U}$	Magnitude gas velocity (flue gas velocity) (m·s^{-1})
u_{in}	Inertial impaction velocity (m·s^{-1})
u_g	Flue gas velocity (m·s^{-1})
u_p	Ash particle velocity (m·s^{-1})
$u_{p,crit}$	Particle critical velocity (m·s^{-1})
u_r	Maximum reverse flue gas velocity (m·s^{-1})
u_{rms}	Root-mean-square speed (m·s^{-1})
$u_{s,crit}$	Critical velocity of surface capture (m·s^{-1})
u_{th}	Thermophoretic velocity (m·s^{-1})
V_l	Volume of liquid phase of ash deposit (m^3)
V_s	Volume of solid phase of ash deposit (m^3)
x_{ash}	Ash mass fraction

Greek symbols

η_{stick}	Sticking efficiency
η_{imp}	Impaction efficiency
$\varepsilon_{deposit}$	Ash deposit porosity
ε_0	Initial ash deposit porosity
ψ	Stokes correction factor
ρ_p	Ash particle density (kg·m^{-3})
ρ_g	Flue gas density (kg·m^{-3})
μ_g	Flue gas viscosity (kg·m^{-1}·s^{-1})
μ_s	Ash deposit surface viscosity (kg·m^{-1}·s^{-1})
Λ	Thermal conductivity ratio of ash particle over flue gas ($\Lambda = k_p/k_g$)
ϕ	Coefficient of thermophoretic force
λ	Mean free path length (m)
σ_r	Stefan-Boltzmann constant
α_r	Absorbance thermal radiation
ε_r	Emittance thermal radiation
π	Pi number
γ	Surface tension of ash deposit (N·m^{-1})
θ	Angle of impacting ash particle
$\dot{m}_{fuel}$	Fuel rate; defined as the ratio of the mass of fuel to time
$\dot{m}_g$	Flue gas flow rate; defined as the ratio of the mass of flue gas to time

Declaration of Competing Interest

None.

References

[1] S.N. Seo, Breakthrough technologies, in: The Behavioral Economics of Climate Change, 2017, pp. 139–183.

[2] S. Fakourian, A Theoretical Study on Overpotential and Photocurrent of a Photo fuel Cell, Theor. Found. Chem. Eng. 53 (2019) 147–150.

[3] A. Stroh, et al., 3-D numerical simulation for co-firing of torrefied biomass in a pulverized-fired 1 MWth combustion chamber, Energy 85 (2015) 105–116.

[4] S. Fakourian, A. Fry, T. Jasperson, Analysis of particle behavior inside the classifier of a Raymond Bowl Mill while co-milling woody biomass with coal, Fuel Process. Technol. 182 (2018) 95–103.

[5] U.S.E.P. Agency, Biofuels and the Environment: First Triennial Report to Congress, 2011.

[6] B.M. Jenkins, et al., Combustion properties of biomass, Fuel Process. Technol. 54 (1–3) (1998) 17–46.

[7] Y. Wang, Ash aerosol and ash deposit formation during high temperature OXY-combustion of various solid fuels, in: Department of Chemical Engineering, The University of Utah, 2019.

[8] N. Hare, A review on boiler deposition/foulage prevention and removal techniques for power plant, Rec. Adv. Energy Environ. (2010) 217–222.

[9] L.L. Baxter, et al., The behavior of inorganic material in biomass-fired power boilers: field and laboratory experiences, Fuel Process. Technol. 54 (1–3) (1998) 47–78.

[10] P.G. Stine Broholm Hansen, Flemming Jappe Frandsen, Peter Arendt Jensen, Model for Deposition Build-up in Biomass Boilers, in Department of Chemical and Biochemical Engineering, Technical University of Denmark, 2015.

[11] A. Moço, M. Costa, C. Casaca, Ash deposit formation during the combustion of pulverized grape pomace in a drop tube furnace, Energy Convers. Manag. 169 (2018) 383–389.

[12] A. Brink, et al., A temperature-history based model for the sticking probability of impacting pulverized coal ash particles, Fuel Process. Technol. 141 (2016) 210–215.

[13] Z. Zhan, et al., Ash formation and deposition during oxy-coal combustion in a 100 kW laboratory combustor with various flue gas recycle options, Fuel Process. Technol. 141 (2016) 249–257.

[14] A.A. Bhuiyan, A.S. Blicblau, J. Naser, Co-firing of biomass and slagging in industrial furnace: A review on modelling approach, J. Energy Inst. 90 (2016) 838–854.

[15] K. Jang, et al., Prediction of the Ash Deposition Characteristics of Blended Coals in a 500 MWe Tangentially Fired Boiler, Energy Fuel 32 (7) (2018) 7827–7840.

[16] F. Tabet, I. Gokalp, Review on CFD based models for co-firing coal and biomass, Renew. Sust. Energ. Rev. 51 (2015) 1101–1114.

[17] B.-H. Lee, et al., Numerical prediction of characteristics of ash deposition in heavy fuel oil heat recovery steam generator, J. Mech. Sci. Technol. 28 (7) (2014) 2889–2900.

[18] J. Tomeczek, K. Wacławiak, Two-dimensional modelling of deposits formation on platen superheaters in pulverized coal boilers, Fuel 88 (8) (2009) 1466–1471.

[19] J. Li, W. Du, L. Cheng, Numerical simulation and experiment of gas-solid two phase flow and ash deposition on a novel heat transfer surface, Appl. Therm. Eng. 113 (2017) 1033–1046.

[20] L.Y. Huang, M. Pourkashanian, A. Williams, Prediction of ash deposition on superheater tubes from pulverized coal combustion, Fuel 75 (1996) 271–279.

[21] S. Chapela, et al., Comprehensive CFD modeling of the ash deposition in a biomass packed bed burner, Fuel 234 (2018) 1099–1122.

[22] Z. Zheng, et al., Numerical investigation on ash deposition on the surface of tube bundle, Energy Procedia 143 (2017) 336–341.

[23] M.U. Degereji, et al., Prediction of ash slagging propensity in a pulverized coal combustion furnace, Fuel 101 (2012) 171–178.

[24] W.Y. Zhimin Zheng, Peng Yu, Yongtie Caia, Hao Zhou, Siah Keng Boon, Prabakaran Subbaiah, Simulating growth of ash deposit in boiler heat exchanger tube based on CFD dynamic mesh technique, Fuel 259 (2020).

[25] S.W. Lin Mu, Zhende Zhai, Yan Shang, Chen Zhao, Liang Zhao, Hongchao Yin, Unsteady CFD simulation on ash particle deposition and removal characteristics in tube banks: focusing on particle diameter, flow velocity, and temperature, J. Energy Inst. 93 (2020).

[26] L. Mu, H. Miao, C. Zhao, Z. Zhai, Y. Shang, H. Yin, Dynamic CFD modeling evaluation of ash deposition behavior and morphology evolution with different tube arrangements, Powder Technol. 379 (2020) 279–295.

[27] Q. Gao, et al., A general mechanistic model of fly ash formation during pulverized coal combustion, Combust. Flame 200 (2019) 374–386.

[28] H. Liu, Y. Wang, J.O.L. Wendt, Particle size distributions of fly ash arising from vaporized components of coal combustion: a comparison of theory and experiment, Energy Fuel 32 (2017) 4300–4307.

[29] X. Yang, et al., Understanding the ash deposition formation in Zhundong lignite combustion through dynamic CFD modelling analysis, Fuel 194 (2017) 533–543.

[30] X. Yang, et al., Predicting ash deposition behaviour for co-combustion of palm kernel with coal based on CFD modelling of particle impaction and sticking, Fuel 165 (2016) 41–49.

[31] S.S. Lokare, A Mechanistic investigation of ash deposition in pulverized-coal and biomass combustion, in: Chemical Engineering, Brigham Young University, 2008.

[32] Huafeng Wang, Modeling of deposition in large-scale combustion facilities building pulverized coal, Prog. Energy Combust. Sci. 23 (3) (1997).

[33] C.W. Ulrich Kleinhans, Flemming J. Frandsen, Hartmut Spliethoff, Ash formation and deposition in coal and biomass fired combustion systems: progress and challenges in the field of ash particle sticking and rebound behavior, Prog. Energy Combust. Sci. 68 (2018) 65–168.

[34] R. Weber, et al., On predicting the ash behaviour using computational fluid dynamics, Fuel Process. Technol. 105 (2013) 113–128.

[35] D. Zhang, Ash fouling, deposition and slagging in ultra-supercritical coal power plants, in: Ultra-Supercritical Coal Power Plants, Woodhead Publishing Limited, 2013.

[36] L.L. Baxter, Ash deposition during biomass and coal combustion - A mechanistic approach, Biomass Bioenergy 4 (2) (1993) 85–102.

[37] Z. Zheng, et al., Fly ash deposition during oxy-fuel combustion in a bench-scale fluidized-bed combustor, Energy Fuel 27 (8) (2013) 4609–4616.

[38] Z. Zhan, Ash deposition and ash aerosol formation mechanisms during oxy-coal combustion, in: Chemical Engineering, University of Utah, 2015.

[39] L.L. Baxter, Ash Deposit Formation and Deposit Properties: A Comprehensive Summary of Research Conducted at Sandia's Combustion Research Facility, 2000 (Sandia Report).

[40] Y. Wang, et al., Comparison study of ash partitioning and deposition behavior between two rice husk fuels under a 100 kW combustor, Energy Fuel 33 (11) (2019) 11968–11975.

[41] H. Zhou, P.A. Jensen, F.J. Frandsen, Dynamic mechanistic model of superheater deposit growth and shedding in a biomass fired grate boiler, Fuel 86 (10–11) (2007) 1519–1533.

[42] R. Johansson, B. Leckner, Influence of intraparticle gradients in modeling of fixed bed combustion, Combust. Flame 149 (2007) 49–62.

[43] P. Frank, D.P.D. Incropera, Theodore L. Bergman, S. Adrienne, Lavine, in: Fundamentals of Heat and Mass Transfer, S. edition, John Wiley & Sons, 2007.

[44] S. Kær, L. Rosendahl, L. Baxter, Towards a CFD-based mechanistic deposit formation model for straw-fired boilers, Fuel 85 (5–6) (2006) 833–848.

[45] Z. Zhan, et al., Novel temperature-controlled ash deposition probe system and its application to oxy-coal combustion with 50% inlet O2, Energy Fuel 28 (1) (2014) 146–154.

[46] S.B. Hansen, et al., Mechanistic model for ash deposit formation in biomass suspension firing. Part 1: model verification by use of entrained flow reactor experiments, Energy Fuel 31 (3) (2016) 2771–2789.

[47] L. Chen, A.F. Ghoniem, Development of a three-dimensional computational slag flow model for coal combustion and gasification, Fuel 113 (2013) 357–366.

[48] G.I. Kelbaliyev, Drag coefficients of variously shaped solid particles, drops, and bubbles, Theor. Found. Chem. Eng. 45 (3) (2011) 248–266.

[49] John H. Cameron, Role of thermophoresis in the deposition of fume particles resulting from the combustion of high inorganic containing fuels with reference to kraft black liquor, Fuel Process. Technol. 60 (1999) 49–68.

[50] L. Talbot, Thermophoresis of Particles in a Heated Boundary Layer, University of California, 1980.

[51] U.S. Kleinhans, S. Babat, C. Wieland, H. Spliethoff, The role of thermophoresis during deposit build-up on a superheater tube, in: International Conference on Heat Exchanger Fouling and Clean, 2015 (Enfield (Dublin), Irelan).

[52] H.F. Lutro, The effect of thermophoresis on the particle deposition on a cylinder, in: Physics, Norwegian University of Science and Technology, 2012.

[53] J.B. Young, Thermophoresis of a spherical particle: reassessment, clarification, and new analysis, Aerosol Sci. Technol. 45 (2011) 927–948.

[54] D.P. Healy, J.B. Young, An experimental and theoretical study of particle deposition due to thermophoresis and turbulence in an annular flow, Int. J. Multiphase Flow 36 (11–12) (2010) 870–881.

[55] J. Jokiniemi, J. Lyyränen, P. Mikkanen, E. Kauppinen, Modelling ash deposition during the combustion of low grade fuels, in: L. Baxter, R. DeSollar (Eds.), Applications of Advanced Technology to Ash-Related Problems in Boilers, Plenum Press, New York, 1996.

[56] A. Leppanen, et al., Numerical modeling of fine particle and deposit formation in a recovery boiler, Fuel 129 (2014) 45–53.

[57] M. Li, Eddy impaction as an ash deposition mechanism: a theoretical and experimental investigation, in: Chemical Engineering, Brigham Young University, 2011.

[58] N.D. Katopodes, Boundary-Layer Flow, 2019, pp. 652–708.

[59] W.D. Bachalo, Experimental methods in multiphase flows, Int. J. Multiphase Flow 20 (Supp1) (1994) 261–295.

[60] M. García Pérez, E. Vakkilainen, T. Hyppänen, 2D dynamic mesh model for deposit shape prediction in boiler banks of recovery boilers with different tube spacing arrangements, Fuel 158 (2015) 139–151.

[61] H. Galen, P.N.S. Richards, John N. Harb, Simulation of ash deposit growth in a pulverized coal-fired pilot scale reactor, Energy Fuel 7 (1993) 774–781.

[62] D.W. Anderson, F.P. Incropera, Effective thermal conductivity of coal ash deposits at moderate to high temperatures, J. Eng. Gas Turbines Power (1987) 109.

[63] A. Ilhan, J.A.P. Aksay, Densities of SiO2-Al2O3 melts, J. Am. Ceram. Soc. 76 (1979).

[64] J. Xin, et al., Accurate density Calculation for molten slags in SiO₂–Al₂O₃–CaO–MgO systems, ISIJ Int. 57 (8) (2017) 1340–1349.

[65] K.C. Mills, B.J. Keene, Physical properties of BOS slags, Int. Mater. Rev. 32 (1) (2013) 1–120.

[66] R. Israel, D.E. Rosner, Use of a generalized stokes number to determine the aerodynamic capture efficiency of non-stokesian particles from a compressible gas flow, Aerosol Sci. Technol. 2 (1) (1983) 45–51.

[67] R. Bradley, D.A.R.F. Adams, Constance L. Senior, Hong Shig Shim, Huafeng Wang, Jost Wendt, Christopher Shaddix, Characterization of Oxy-combustion Impacts in Existing Coal-fired Boilers, 2009.

[68] T.F. Wall, et al., The properties and thermal effects of ash deposits in coal-fired furnaces, Prog. Energy Combust. Sci. 19 (6) (1993) 487–504.

[69] P. Furmański, Thermal and Radiative Properties of Ash Deposits on Heat Transfer Surfaces of Boilers, Institute of Heat Engineering, Warsaw University of Technology, 1995.

[70] E.S. Morgan, Errors associated with radiant heat flux meters when used in boiler furnaces, J. Inst. Fuel 47 (1974).

[71] S. Sanitjai, R.J. Goldstein, Forced convection heat transfer from a circular cylinder in crossflow to air and liquids, Int. J. Heat Mass Transf. 47 (22) (2004) 4795–4805.

[72] A. Žkauskas, Heat transfer from tubes in crossflow, Adv. Heat Tran. 18 (1987) 87–159.

[73] T.L.M. Jakob, Experiments on Forced Convection and Their Correlation, in Heat Treansfer, John Wiley & Sons, Inc. Chapman & Hall, Limited, New York, London, 1949.

[74] A. Zbogar, et al., Heat transfer in ash deposits: a modelling tool-box, Prog. Energy Combust. Sci. 31 (5–6) (2005) 371–421.

[75] R.L. Rowley, J.L. Oscarson, T.A. Knotts, N.F. Giles, DIPPR ® Data Compilation of Pure Chemical Properties, Design Institute for Physical Properties, Brigham Young University, Provo, Utah, 2017.

[76] Allen L. Robinson, Larry L. Baxter, Experimental measurements of the thermal conductivity of ash deposits: part 1. Measurement technique, Energy Fuel 15 (2001) 66–74.

[77] Y.S. Touloukian, Thermophysical Properties of High Temperature Solid Materials, Vol. 4-Part I, The MacMillian Company, New York, 1967.

[78] Q.H. Yingqi Zhao, Qiang Yao, Shuiqing Li, Prediction and validation of ash sticking probability under fouling conditions in pulverized coal combustion, Proc. Combust. Inst. (2020). https://www.sciencedirect.com/science/article/abs/pii/S1540748920301073.

[79] S.H. Hao Zhou, Numerical simulation of ash deposition behavior with a novel erosion model using dynamic mesh, Fuel 286 (2021).

[80] F.C.C. Lee, Modelling ash deposition in pulverized coal-fired applications, Prog. Energy Combust. Sci. 25 (1999) 117–132.

[81] J.R. Fan, P. Sun, K.F. Cen, Simulation of ash deposit in a pulverized coal-fired boiler, Fuel 80 (2001) 645–654.

[82] C. Liu, et al., Numerical investigation on development of initial ash deposition layer for a high-alkali coal, Energy Fuel 31 (3) (2017) 2596–2606.

[83] M.U. Garba, et al., Modelling of deposit formation and sintering for the co-combustion of coal with biomass, Fuel 113 (2013) 863–872.

[84] M.-M. Zhou, et al., Large-eddy simulation of ash deposition in a large-scale laboratory furnace, Proc. Combust. Inst. 37 (4) (2019) 4409–4418.

[85] Peter M. Walsh, David O. Loehden, Larry S. Monroe, Janos M. Beer, Adel F. Sarofim, Deposition of bituminous coal ash on an isolated heat exchanger tube: effects of coal properties on deposit growth, Prog. Energy Combust. Sci. 16 (4) (1990) 327–346.

[86] Martin Forstner, Georg Hofmeister, Markus Braun, Stefan Kleditzsch, Robert Scharler, Lngwald Obernberger, CFD simulation of ash deposit formation in fixed bed biomass furnaces and boilers, Prog. Comput. Fluid Dyn. (2006) 6.

[87] K. Strandström, C. Mueller, M. Hupa, Development of an ash particle deposition model considering build-up and removal mechanisms, Fuel Process. Technol. 88 (11–12) (2007) 1053–1060.

[88] L. Fryda, et al., Study on ash deposition under oxyfuel combustion of coal/biomass blends, Fuel 89 (8) (2010) 1889–1902.

[89] C.W. Bale, et al., FactSage thermochemical software and databases — recent developments, Calphad 33 (2) (2009) 295–311.

[90] J. Dai, K. Whitty, Effects of coal ash on CuO as an oxygen carrier for chemical looping with oxygen uncoupling, Energy Fuel 32 (11) (2018) 11656–11665.

[91] J. Dai, K. Whitty, Predicting and alleviating coal ash-induced deactivation of CuO as an oxygen carrier for chemical looping with oxygen uncoupling, Fuel 241 (2019) 1214–1222.

[92] Y. Laxminarayan, et al., Biomass fly ash deposition in an entrained flow reactor, Proc. Combust. Inst. 37 (3) (2019) 2689–2696.

[93] R.M. Brach, P.F. Dunn, A mathematical model of the impact and adhesion of microsphers, Aerosol Sci. Technol. 16 (1) (1992) 51–64.

[94] W. Ai, J.M. Kuhlman, Simulation of coal ash particle deposition experiments†, Energy Fuel 25 (2) (2011) 708–718.

[95] E. Raask, Mineral Impurities in Coal Combustion, Hemisphere publishing corporation, 1985, pp. 198–199.

[96] K.C. Mills, Estimation of physico-chemical properties of coal slags and ashes, ACS Symp. Ser. 301 (1986) 195–214.

[97] R.A. Wessel, J. Righi, Generalized correlations for inertial impaction of particles on a circular cylinder, Aerosol Sci. Technol. 9 (1) (1988) 29–60.

[98] R.J. Brun, P.J. Perkins, J.S. Serafini, Impingement of Cloud Droplets on a Cylinder and Procedure for Measuring Liquid-Water Content and Droplet Sizes in Super-Cooled Clouds by Rotating Multicylinder Method, 1955.

[99] Y. Wang, X. Li, J.O.L. Wendt, Ash aerosol and deposition formation mechanisms during air/oxy-combustion of rice husks in a 100 kW combustor, Energy Fuel 32 (2018) 4391–4398.

[100] X.L. Yueming Wang, Jost Wendt, On ash deposition rates from air and oxy-combustion of pulverized coal, petroleum coke, and biomass, Energy Fuel 33 (7) (2019) 5849–5858.

[101] Y. Wang, J. Wu, X. Li, D. Yu, M. Xu, J.O. Wendt, Ash aerosol partitioning and ash deposition during the combustion of petroleum coke/natural gas mixtures, Fuel 256 (2019).

[102] Fly Ash, Slag, silica fume, and natural pozzolans, in: Design and Control of Concrete Mixtures, 2021.

[103] Adrian K. James, Steve Helle, Harpuneet S. Ghuman, Ash Management Review—Applications of Biomass Bottom Ash. Energies 5, 2012, pp. 3856–3873.

[104] C. Lanzerstorfer, Chemical composition and physical properties of filter fly ashes from eight grate-fired biomass combustion plants, J. Environ. Sci. 30 (2015).

[105] Wang Liang, Effect of solid waste-petroleum coke residue on the hydration reaction and property of concrete, Materials 12 (2019).

[106] Larry L. Baxter, The effects of fuel-bound chlorine and alkali on corrosion initiation, in: 214th American Chemical Society National Meeting, 1997, pp. 1089–1095. Las Vegas.

[107] Y. Cai, et al., Modeling of ash formation and deposition processes in coal and biomass fired boilers: a comprehensive review, Appl. Energy 230 (2018) 1447–1544.

[108] H.R. Rezaei, G.W. Bryant, J.T. Hart, G.S. Liu, C.W. Bailey, T.F. Wall, K.M. S. Miyamae, Y. Endo, Thernal conductivity of coal ash and slags and models used, Fuel 79 (2000) 1697–1710.

[109] D.P.K.A.M. Frank, in: V.K. Bryers RW (Ed.), An Effective Model of Viscosity for Ash Deposition Phenomena, in Mineral matter and Ash Deposition from Coal, 1988, pp. 89–101.

[110] R.P. Gupta, L. Baxter, The Thermal Conductivity of Ash Deposits, 1999.

CFD and Process Model Simulations of Woody Biomass/Coal Co-firing at Lab, Pilot and Industrial Scales

July 28, 2021

Hong-Shig Shim[1], Andrew Chiodo[1], Zhonghua Zhan[1], Kevin Davis[1], Jost Wendt[1,2], Andrew Fry[3]

[1]Reaction Engineering International
[2]University of Utah
[3]Brigham Young University

The 45th International Technical Conference on Clean Energy
July 26 - 29, 2021, Clearwater, Florida, USA

For Energy and Environmental Solutions

REACTION ENGINEERING INTERNATIONAL

189 E Fort Union Blvd., Suite 201
Midvale, UT 84047
U.S.A.

Predictive Technical Assessment

- Biomass co-firing can affect combustion and operation
- Application should be addressed on case-by-case basis due to variability of biomass and firing systems
- Combustion (CFD) modeling can be used to:
  - Characterize current system
  - Assess different biomass injection strategies and fuels
  - Track dispersion, reaction, deposition of coal and biomass
  - Predict combustion, emissions, and slagging/fouling

Overall Modeling Approach

- REI will leverage the existing CFD models for two pilot-scales and full-scale power plant
- Coal only and biomass (torrefied woody biomass) co-firing cases are simulated, and the results compared with the measurements available

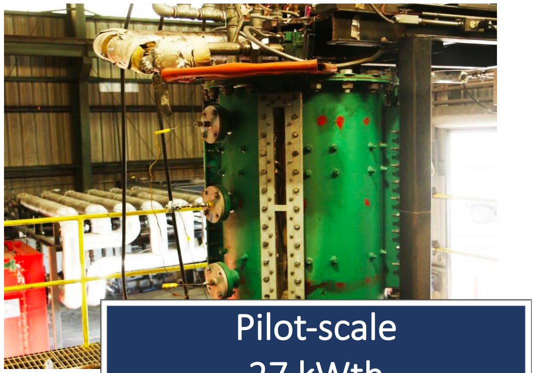

Pilot-scale
27 kWth

Pilot-scale
1,025 kWth

Full-scale Power Plant
1,200 MWth

OFC Pilot-scale Study

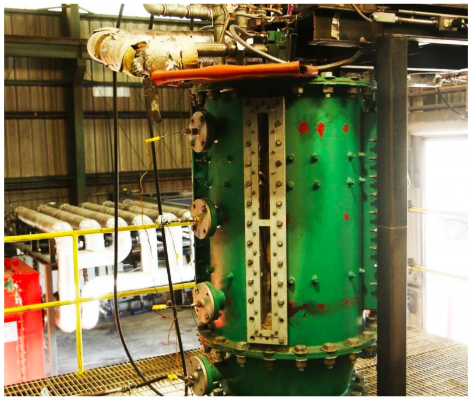

Pilot-scale

27 kWth

Pilot-scale

1,025 kWth

Full-scale Power Plant

1,200 MWth

OFC Geometry

Not to Scale
(unit: inch)

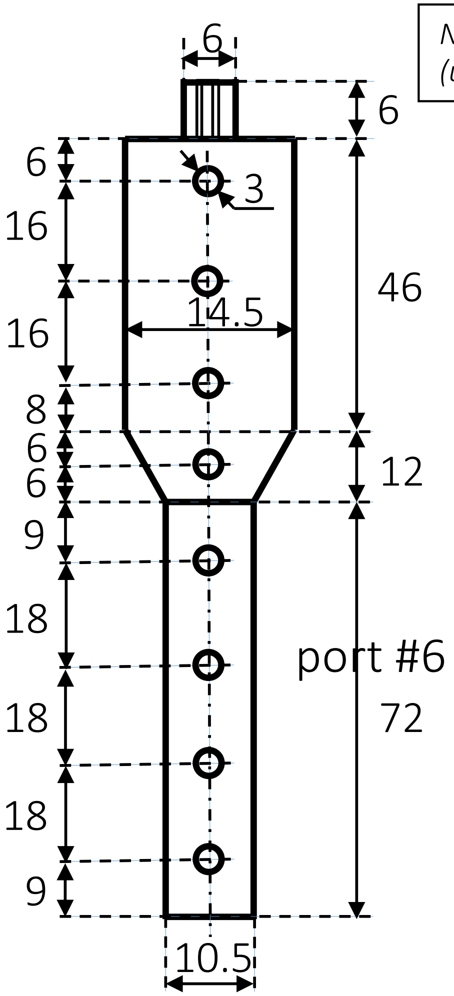

Front View

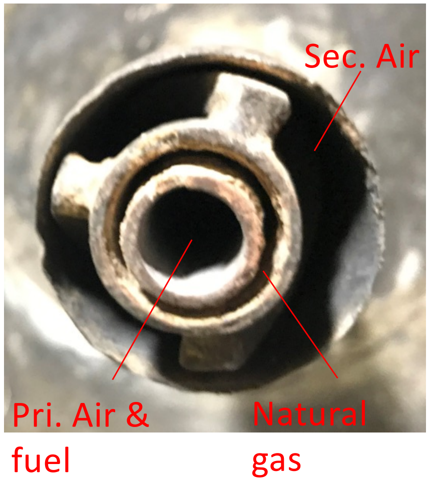

	OD (inch)	ID (inch)
Top Section	30	14.5
Bottom Section	24	10.5

Model Height: 11’4”

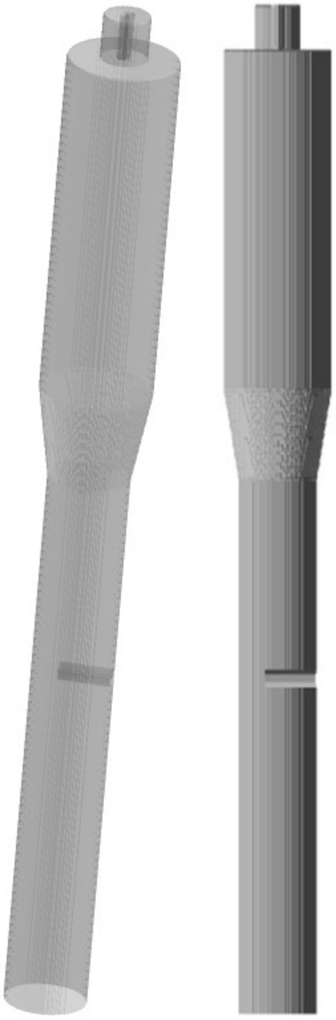

Grid size: 4.27M

Deposition Probe
@ port #6

Operating Conditions

Fuel	Coal	Blend (50% Coal, 50% Wood)
Fuel Feeding Rate (lb/hr)	7.53	8.72
Primary Air Rate (lb/hr)	13.70	15.55
Secondary Air Rate (lb/hr)	59.98	62.25
Primary Air Temperature (°F)	500	500
Secondary Air Temperature (°F)	109.64	117.41
Theoretical O_2 (%, dry)	3.3	4.0
Reactor Pressure (inH_2Og)	0.015	0.023
Exit Flue Gas Compositions		
CO_2 (%, dry)	11.75	15.17
CO (%, dry)	0.002	0.002
O_2 (%, dry)*	8.17	5.23

**High O2 due to air leakage in the flue gas sampling line*

Fuel Properties

Fuel	ASH	C	H	N	S	O	H2O	Volatile	FC	HHV
	(%)	(%)	(%)	(%)	(%)	(%)	(%)	(%)	(%)	(kJ/kg)
Sufco 2	13.96	62.41	4.52	1.1	0.46	11.04	6.52	37.36	42.16	27319
Torrefied wood	0.19	51.75	5.29	0.14	0.02	36.29	6.32	74.2	19.29	21534
50%/50% blend	7.08	57.08	4.91	0.62	0.24	23.67	6.42	55.78	30.73	24427

Fuel	Al2O3	CaO	Fe2O3	MgO	MnO	P2O5	K2O	SiO2	Na2O	SO3	TiO2
Sufco 2	12.09	11.9	3.62	3.94	0.03	0.25	1.13	62.48	0.81	1.83	0.68
Torrefied wood	2.67	51.72	8.28	10.39	4.73	4.16	4.61	6.82	1.6	5.03	0
50%/50% blend	11.95	12.33	3.7	4.04	0.1	0.29	1.32	61.71	0.83	1.84	0.67

Fuel Particle Size Distributions

Size #	Particle Size (μm)	Mass Fraction	
		Coal	Biomass
1	6.28	0.0250	0.0383
2	12.50	0.0500	0.0500
3	17.60	0.0750	0.0550
4	23.60	0.1000	0.0733
5	31.60	0.1500	0.0700
6	44.40	0.2000	0.1000
7	63.50	0.1500	0.1967
8	85.90	0.1000	0.1000
9	114.00	0.0750	0.1083
10	158.00	0.0500	0.1167
11	247.00	0.0250	0.0917

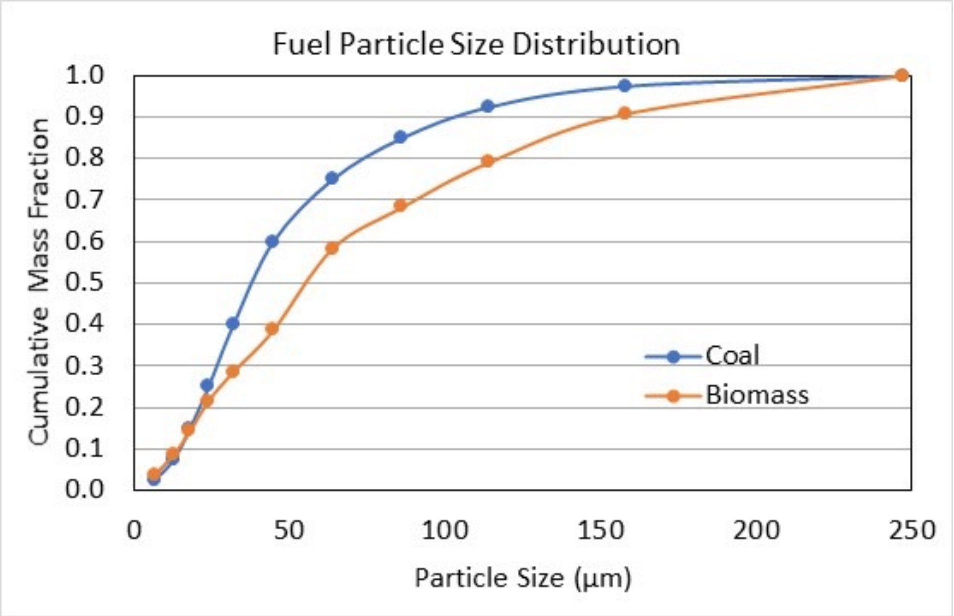

Flue Gas Temperature

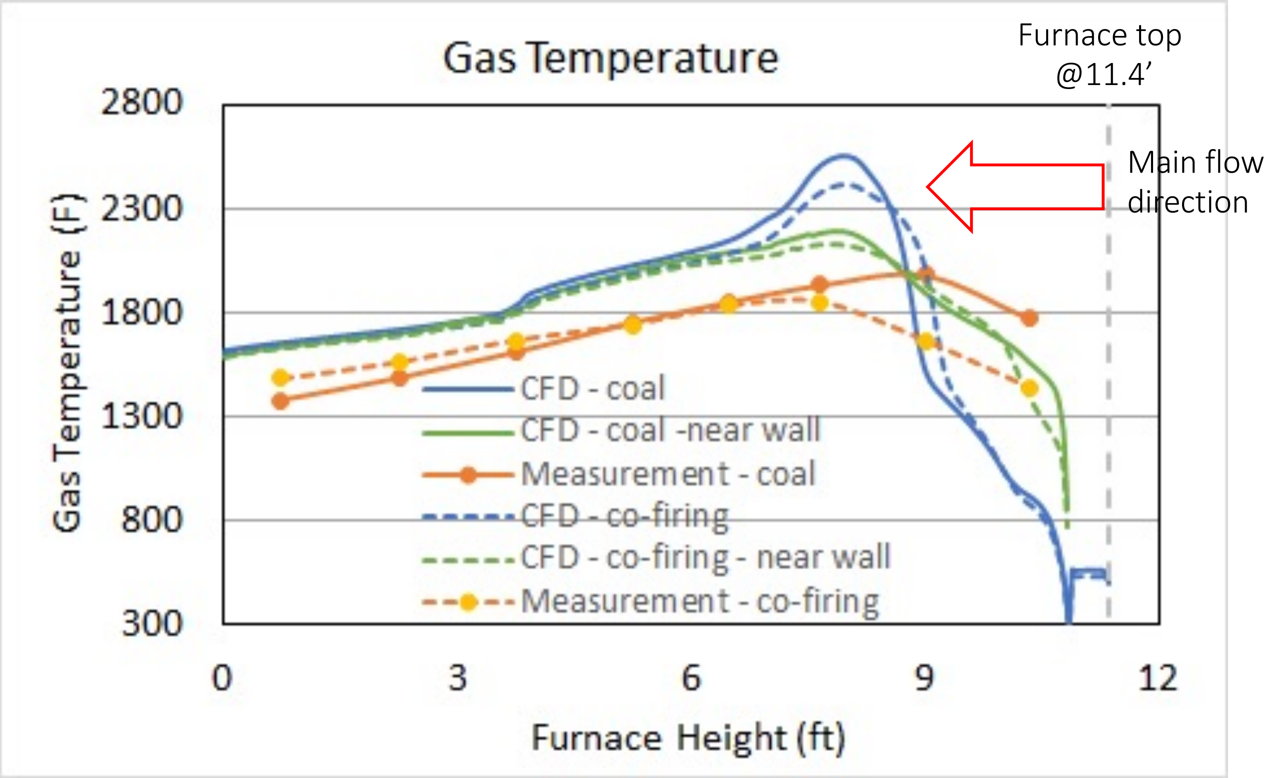

Ash Deposition Rate

	Deposition Rate	Ash Impaction Rate	Capture Efficiency
	g/h	g/h	
Coal	1.34	10.61	12.66%
Co-firing	0.23	6.63	3.45%

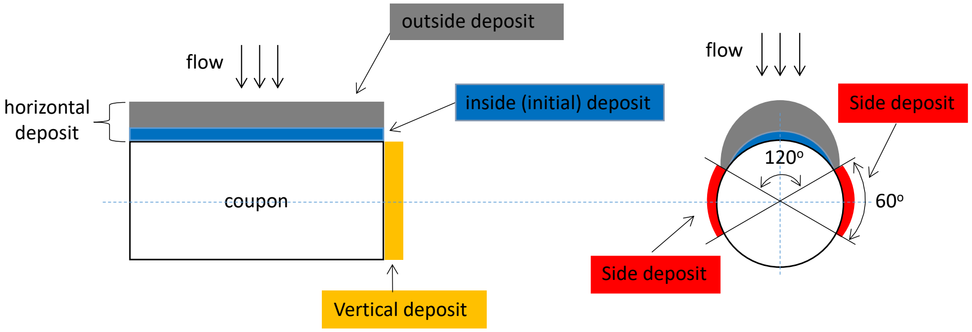

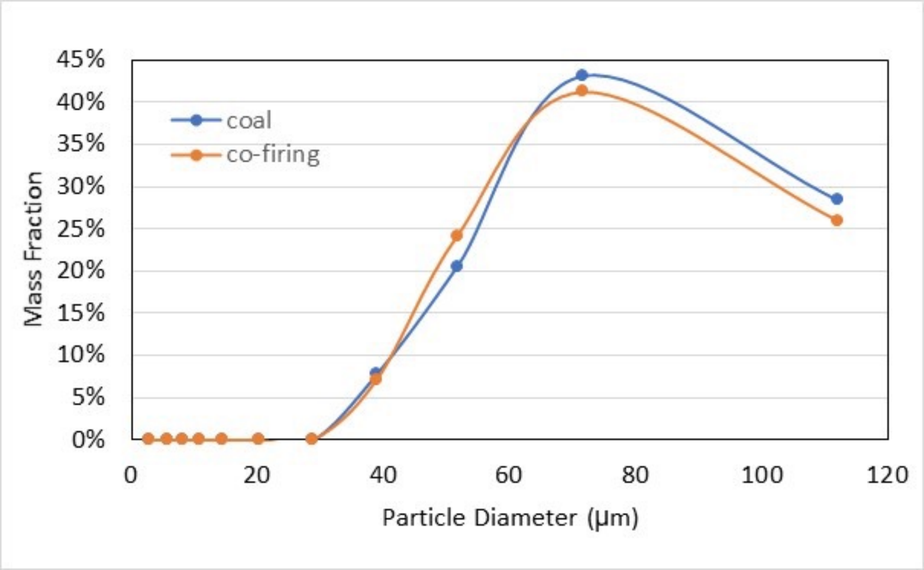

PSD of outside deposits

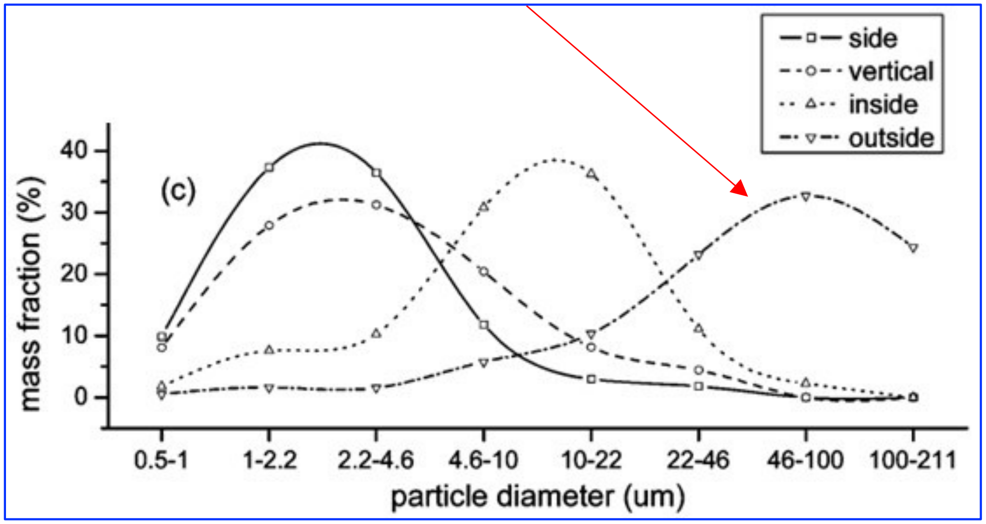

** Zhan et al, Energy Fuels 2014, 28, 146−154*

L1500 Pilot-scale Study

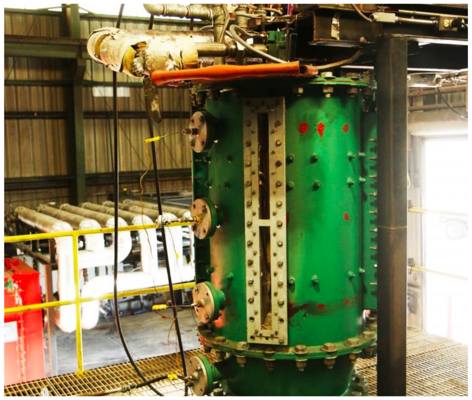
Pilot-scale

27 kWth


Pilot-scale

1,025 kWth


Full-scale Power Plant

1,200 MWth

Operating Conditions

Furnace Operational Data	Baseline	Blend
Firing Rate (MBtu/h)	3.0	2.96
Coal Flow Rate (lb/h)	269	281
Total Combustion Air Flow (lb/h)	2469	2389
Burner Operational Data		
Burner Air Flow (lb/h)	1879	1798
Primary Gas/Coal	1.93	1.93
Primary Air Flow (lb/h)	519	542
Primary Air Temperature (°F)	90.8	86.1
Burner Secondary Air Flow (lb/h)	1360	1256
Inner Secondary Air Flow (lb/h)	438	422
Outer Secondary Air Flow (lb/h)	922	834
Inner Secondary Air Temperature (°F)	485	484
Outer Secondary Air Temperature (°F)	499	490
Staging Air Operational Data		
Air Flow (kb/h)	590	591
Temperature (°F)	118	115
System Leakage		
Leakage Air (lb/h)	360	343

Gas Temperature Profiles

L1500: Coal vs. Blend

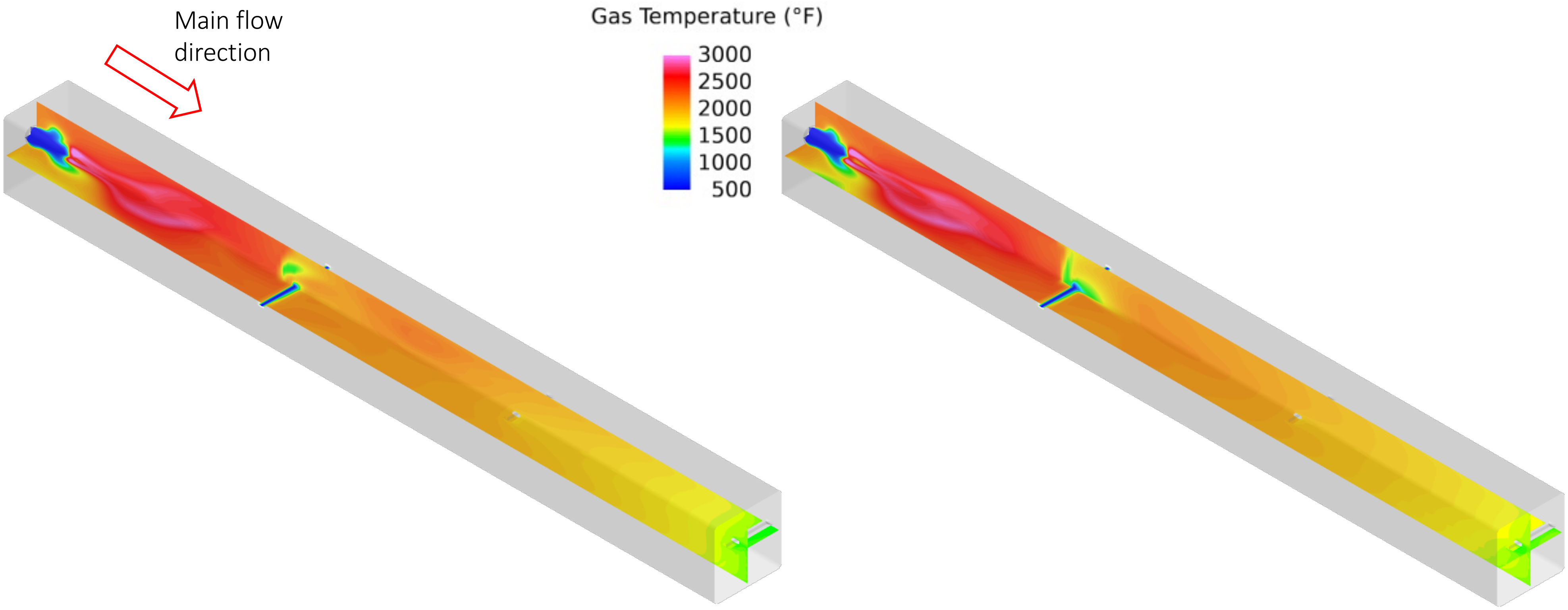

Sufco Coal Only

Coal/Torrefied Wood Blend (Coal-T)

CFD Model Predictions vs. Measurements

Gas Temperature in the L1500: Coal vs. Blend

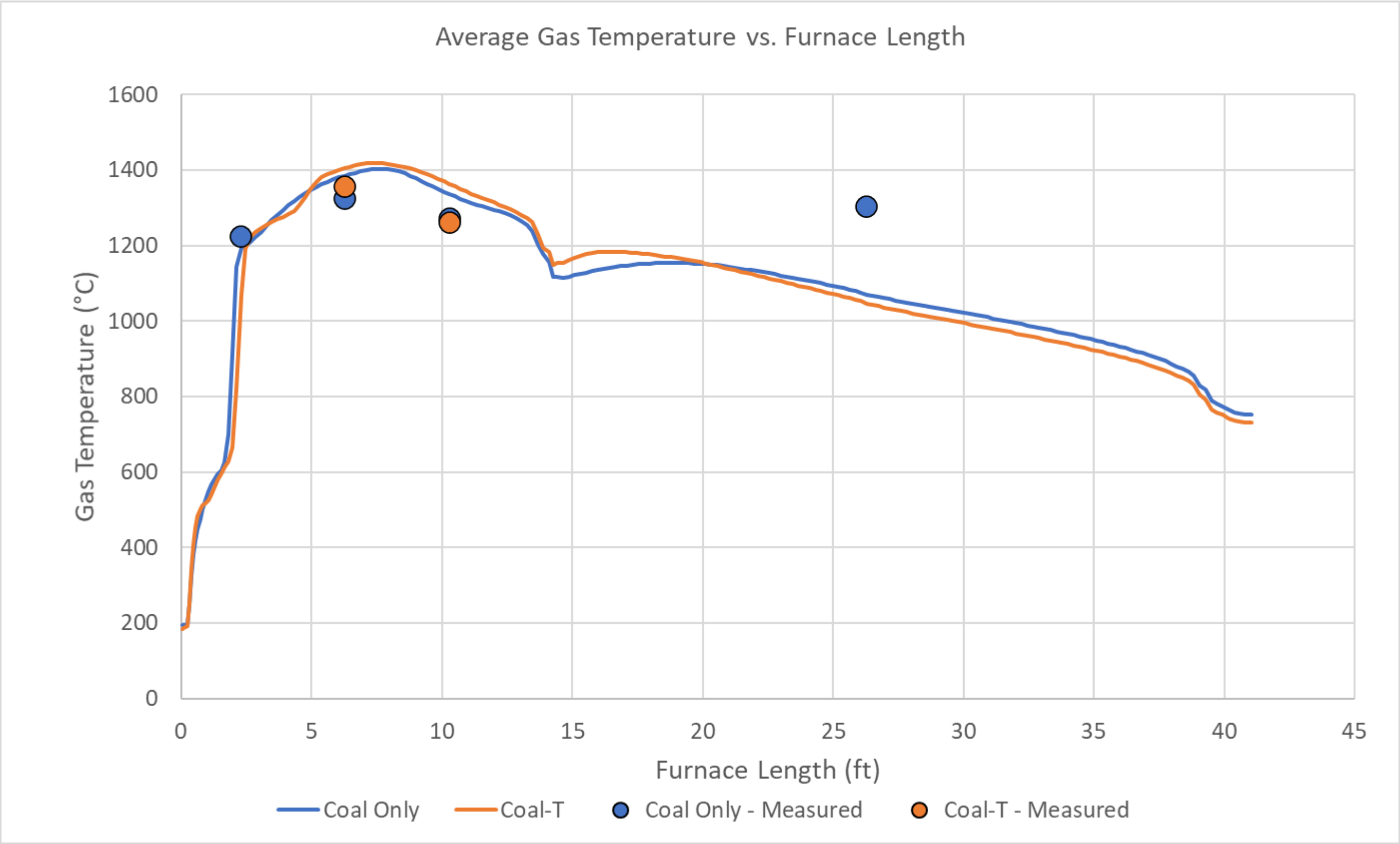

CFD Model Predictions vs. Measurements

O_2 in the L1500: Coal vs. Blend

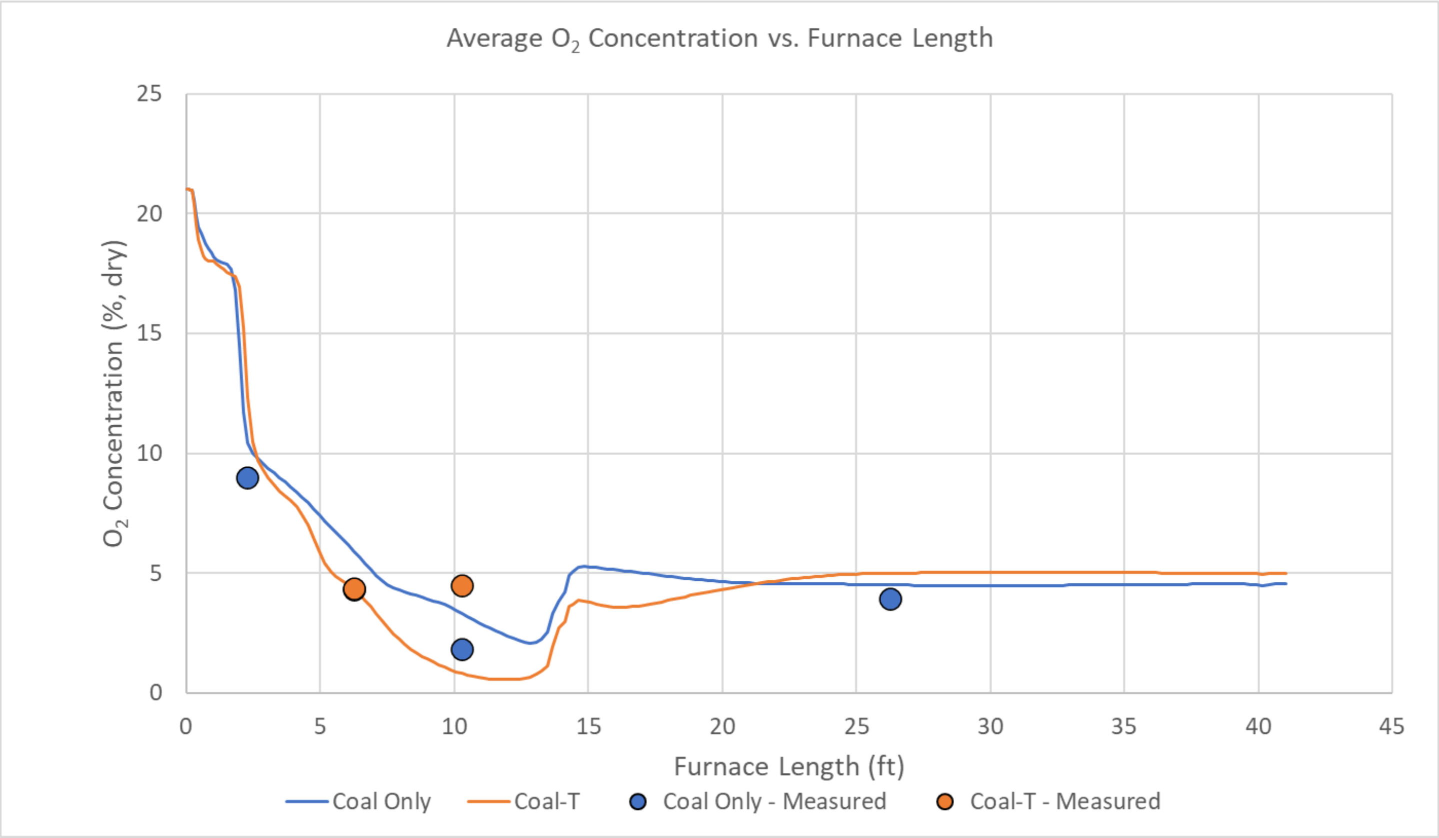

CFD Model Predictions vs. Measurements

CO in the L1500: Coal vs. Blend

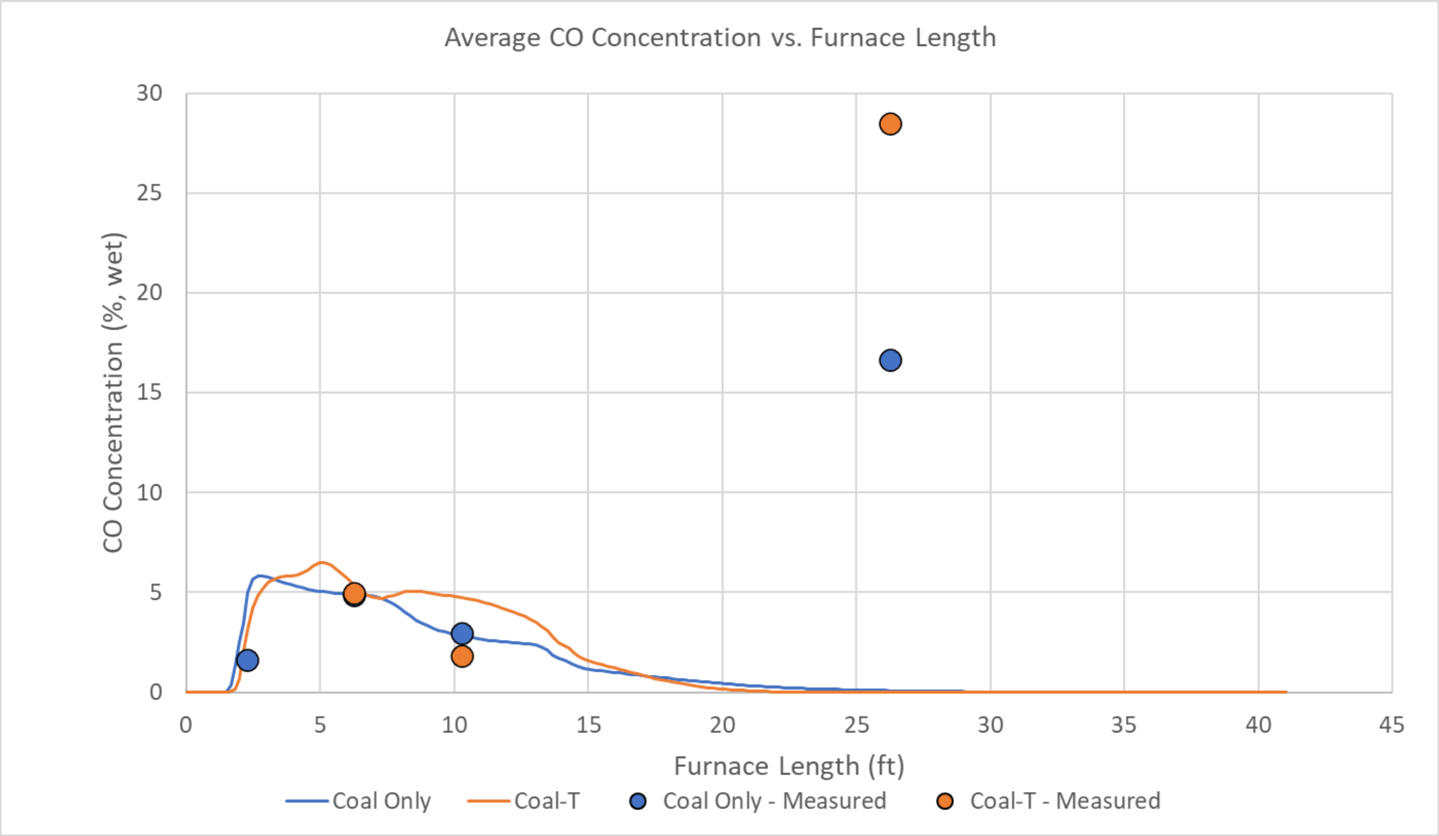

CFD Model Predictions vs. Measurements

Incident Heat Flux in L1500

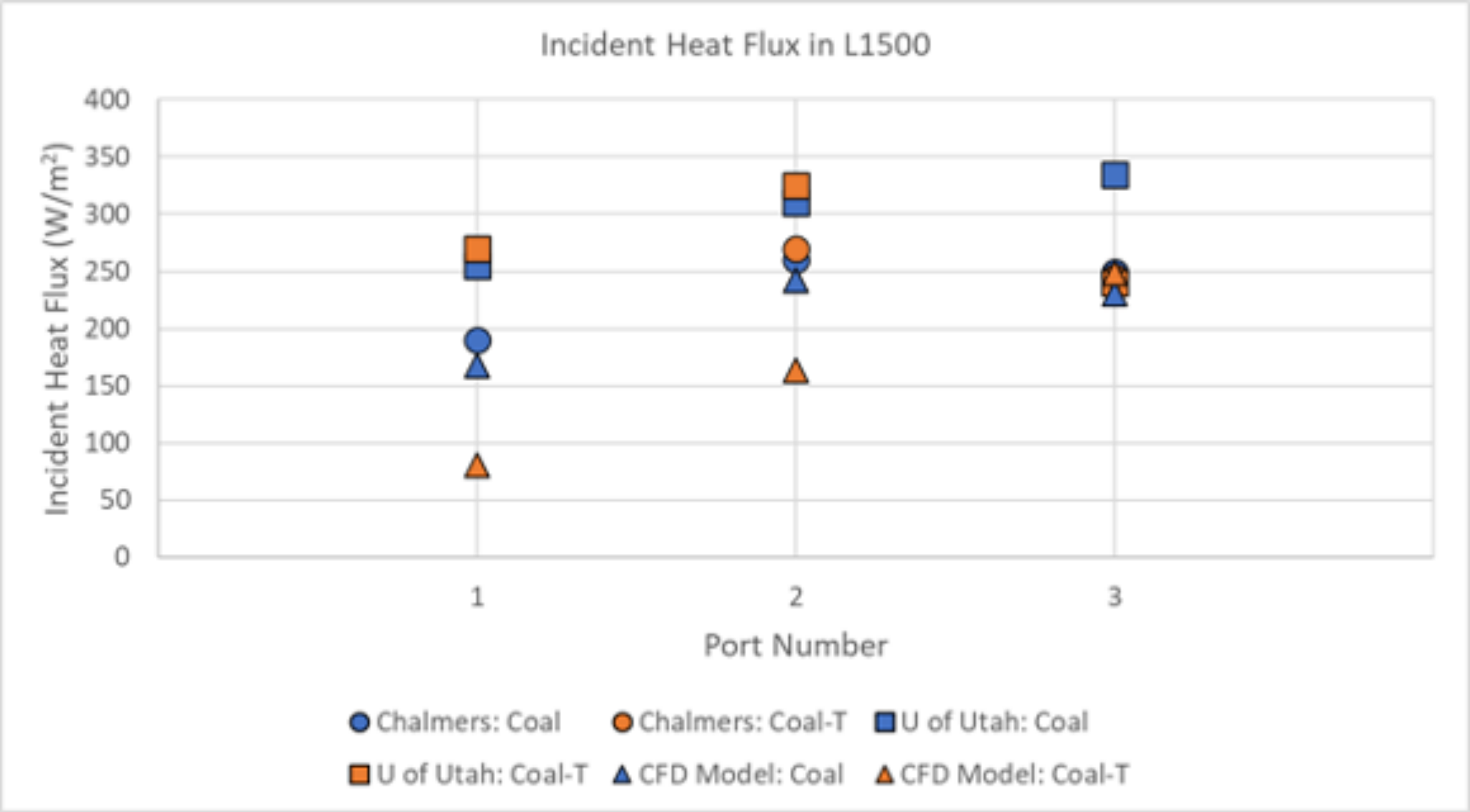

CFD Model Predictions vs. Measurements

Deposition Flux on Probe Coupons

		Model Predicted		Measured (90 min)	
Deposition Flux	Unit	Coal	Coal-T	Coal	Coal-T
Probe 7	g/m²h	2.2	4.4	105	115
Probe 10	g/m²h	0.3	0.6	66	64

Probe #7, 90 min

Probe #10, 90 min

Sufco Coal

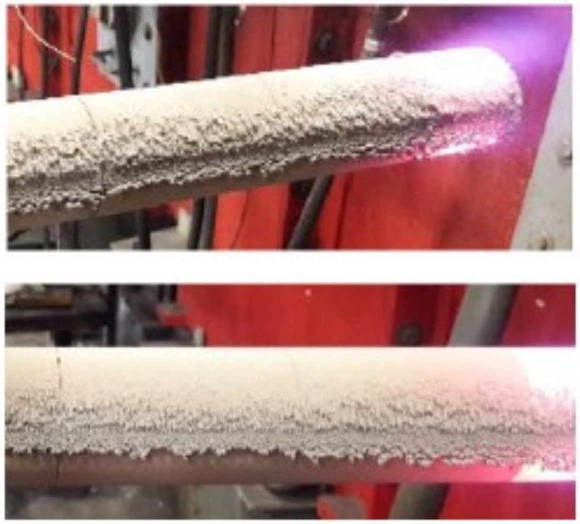

Coal/Torrefied Wood Blend (Coal-T)

Hunter Power Plant

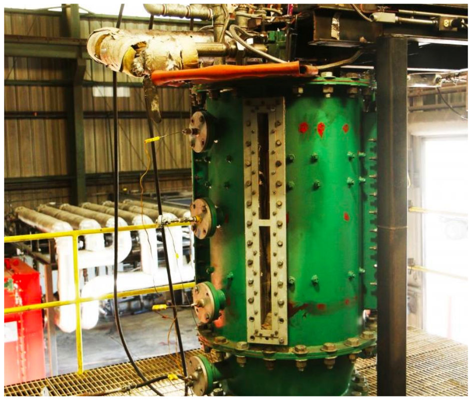

Pilot-scale

27 kWth

Pilot-scale

1,025 kWth

Full-scale Power Plant

1,200 MWth

Hunter Unit 3 Geometry

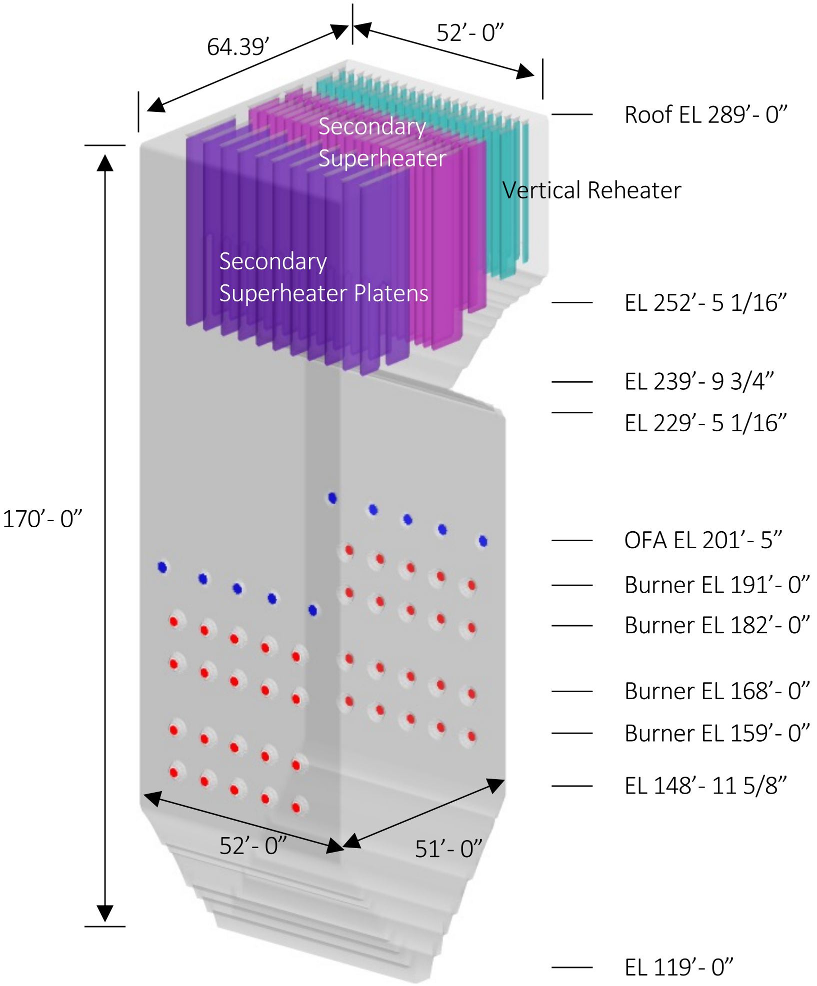

Equipped with 40 B&W DRB-4Z LNBs and 10 dual-register OFA ports

- 5 FW OFA Ports, 5 RW OFA Ports
- 20 FW Burners, 20 RW Burners

Geometry is extended from the existing model to include vertical reheater

Coal Properties

	Sufco	Amaron	Blend
C	63.14	47.74	60.83
H	4.36	5.20	4.49
N	1.13	0.23	0.99
S	0.45	0.02	0.39
O	11.63	35.55	15.22
Ash	12.76	0.85	10.97
H2O	6.53	10.40	7.11
HHV (Btu/lb)	11168	8219	10726

- Blend is Sufco/Amaron 85/15 by weight

Furnace Deposition Modeling

- Deposition initiation and growth
  - Inertial impaction of ash particles
  - Turbulent eddy diffusion and thermophoretic force
  - Ash viscosity and temperature relationship
- Fly ash viscosity = f(composition, temperature, local stoichiometry)
- Deposit sintering = f(deposit mass, composition, temperature)

Ash size & composition prediction

- Coal ash characterization (CCSEM, PCF)
- Mineral matter transformation

Transport (Inorganic vapors, liquids, & solids)

- State & size of ash species and system conditions such as gas flow patterns, gas velocity, & temperature
- Primary mode is inertial impaction

Deposition initiation & growth

- Effective stickiness (particle stickiness and deposit stickiness)
- Particle retention ~ f(surface tension, kinetic energy, viscosity)

Strength & removability

- Deposit characterization
- Boiler environment
- Composition

CCSEM+PCF & MMT

Coal (Sufco)

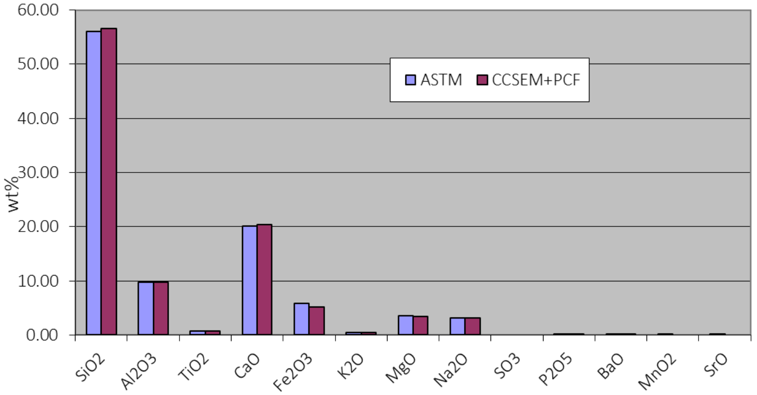

Woody Biomass

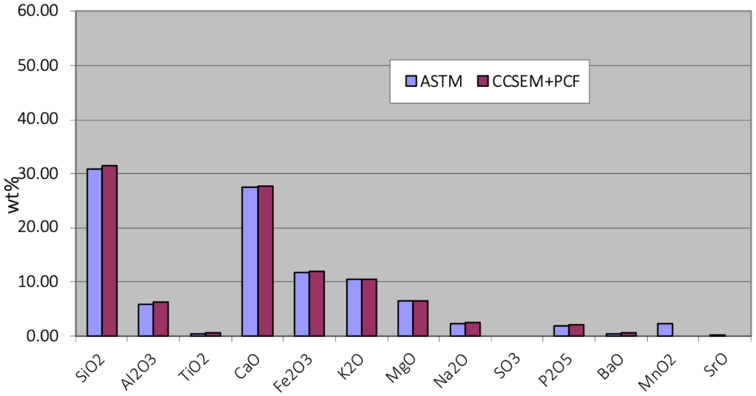

Fly ash composition by size predicted by MMT

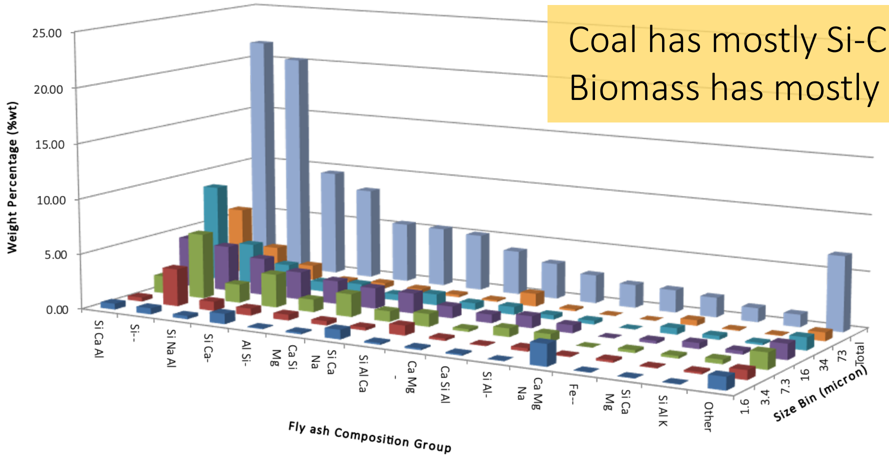

Coal has mostly Si-Ca-Al & Si- group

Biomass has mostly Ca-K-Mg group

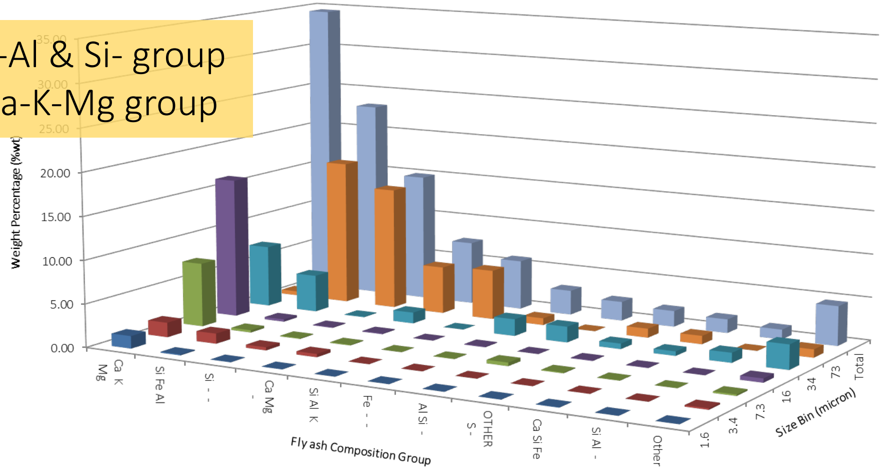

Fitted PSDs for Coal and Biomass

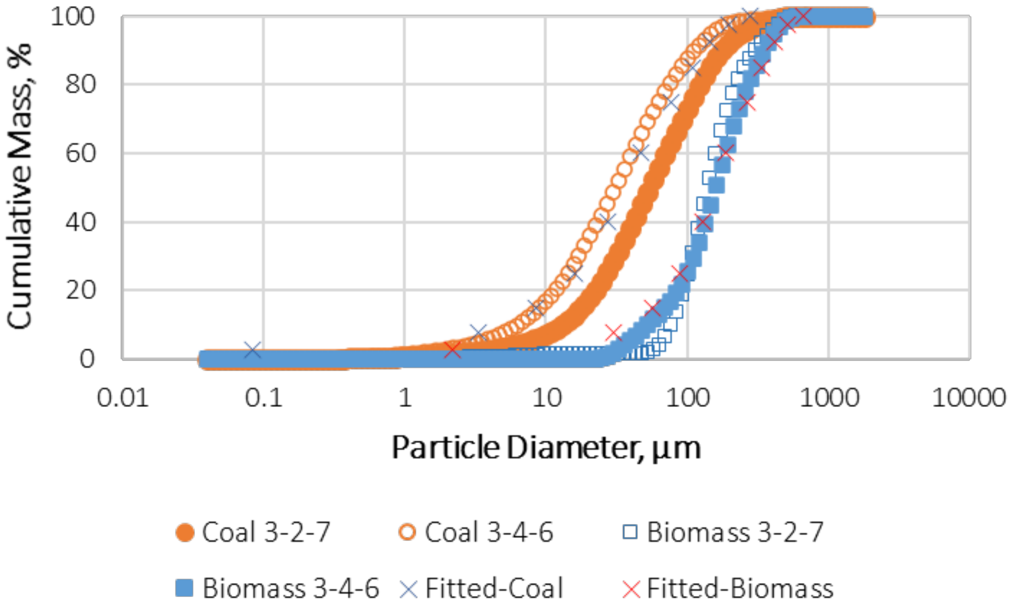

	Particle Diameter, um	
Mass Fraction	Coal	Biomass
0.025	0.08	2.20
0.05	3.36	30.51
0.075	8.50	57.34
0.1	15.99	88.81
0.15	27.35	129.56
0.2	46.90	189.29
0.15	76.30	265.21
0.1	108.47	338.88
0.075	145.20	415.95
0.05	196.03	514.00
0.025	281.82	666.78

- Biomass PSD estimated from the measured coal PSD and the blend PSD
- 3-2-7 and 3-4-6 show similar distribution and their average values were fitted with Rosin-Rammler distribution

Operating Conditions

Furnace Operational Data	Baseline	Blend
Firing Rate (MBtu/h)	4211	4313
Stoichiometric Ratio	1.182	1.176
Lower Furnace Stoichiometric Ratio	0.80	0.79
Theoretical Excess O_2, (%, dry)	3.30%	3.19%
Coal Flow Rate (klb/h)	377.1	402.1
Total Combustion Air Flow (klb/h)	3692.5	3735.7
Burner Zone Air Flow (klb/h)	2435.6	2422.8
OFA Flow Air (klb/h)	1159.4	1175.5
Leakage Air (klb/h)	97.5	138.8
Burner Operational Data (per burner)		
Coal Flow Rate (klb/h)	9.43	10.05
Primary Gas/Coal	2.32	2.19
Primary Air Flow (klb/h)	21.9	22.0
Primary Air Temperature (°F)	159	159
Burner Secondary Air Flow (klb/h)	40.7	40.9
Transition Air Flow (klb/h)	3.3	3.3
Inner Secondary Air Flow (klb/h)	11.2	11.3
Outer Secondary Air Flow (klb/h)	26.2	26.3
Secondary Air Temperature (°F)	520	519
OFA Port Operational Data (per port)		
Air Flow (klb/h)	119.1	122.1
Core Zone Air Flow (klb/h)	71.5	73.3
Core Zone Velocity (ft/s)	313	321
Outer Zone Air Flow (klb/h)	47.6	48.8
Outer Zone Velocity (ft/s)	140	143
Temperature (°F)	520	519

- Provided coal and primary air flow rates were used
- Total air flow rates were calculated to match the provided exit O_2 concentration assuming complete combustion
- Additional air required to match the exit O2 considered as leakage air
- Uniform distributions of fuel and air among the burners and OFA ports were assumed

Heat Duties

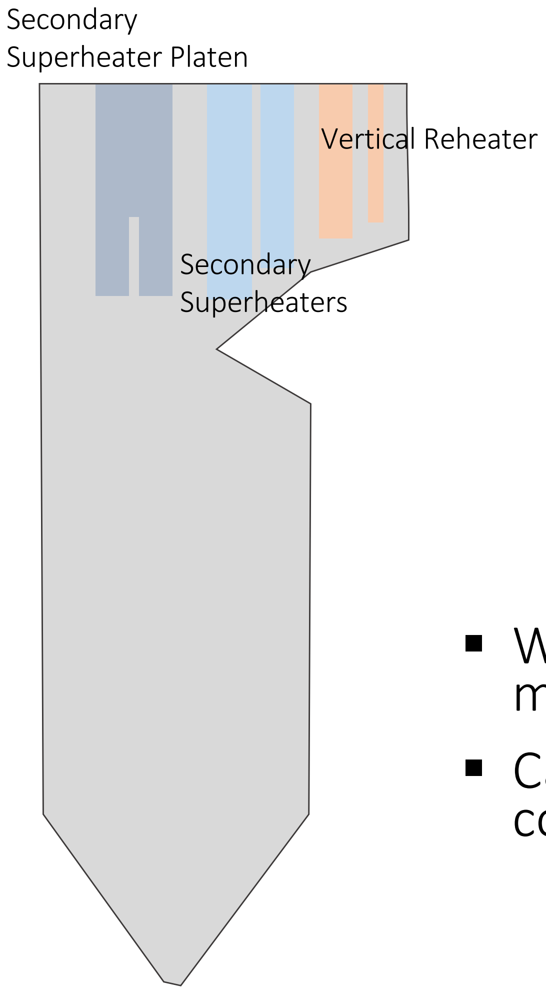

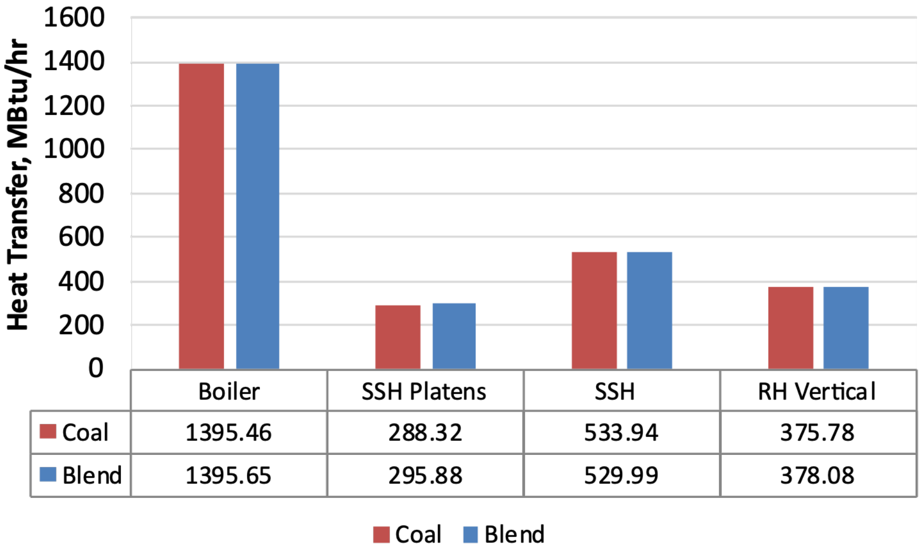

	Boiler	SSH Platens	SSH	RH Vertical
🟥 Coal	1395.46	288.32	533.94	375.78
🟦 Blend	1395.65	295.88	529.99	378.08

- Wall resistance and heat transfer factors are adjusted to match the provided heat duty shown in the bar chart
- Calculated furnace exit temperature assuming complete combustion
  - Baseline case: 1653 F (1174 K)
  - Blend case: 1688 F (1193 K)

Gas Temperature

Baseline

Blend

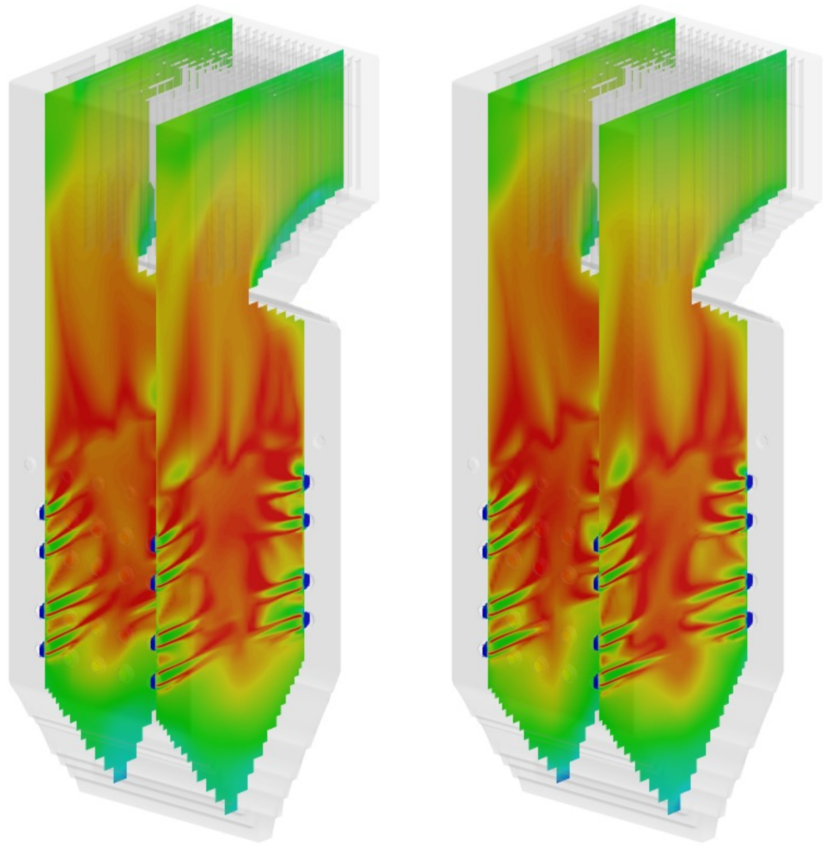

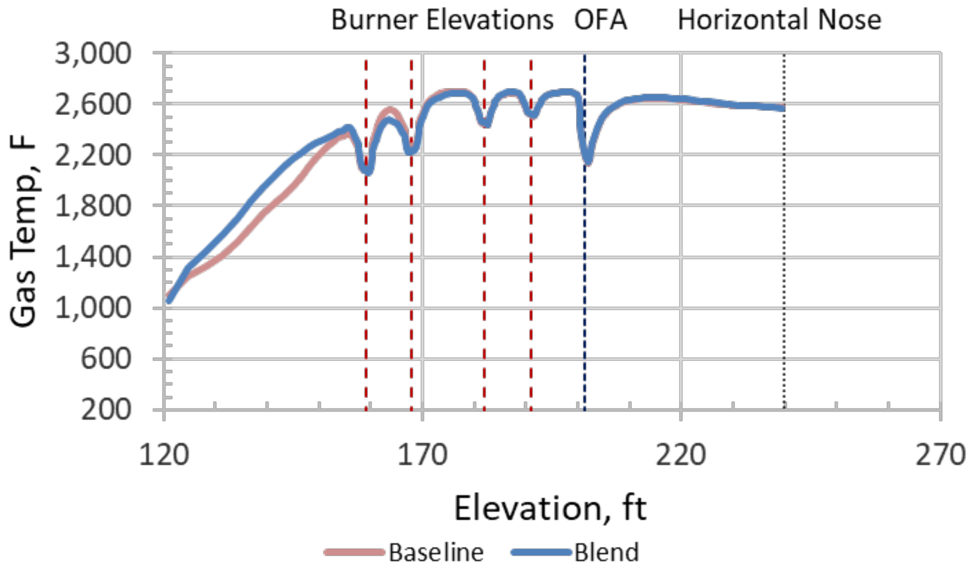

O_2 Distribution

3D Volumetric Rendering

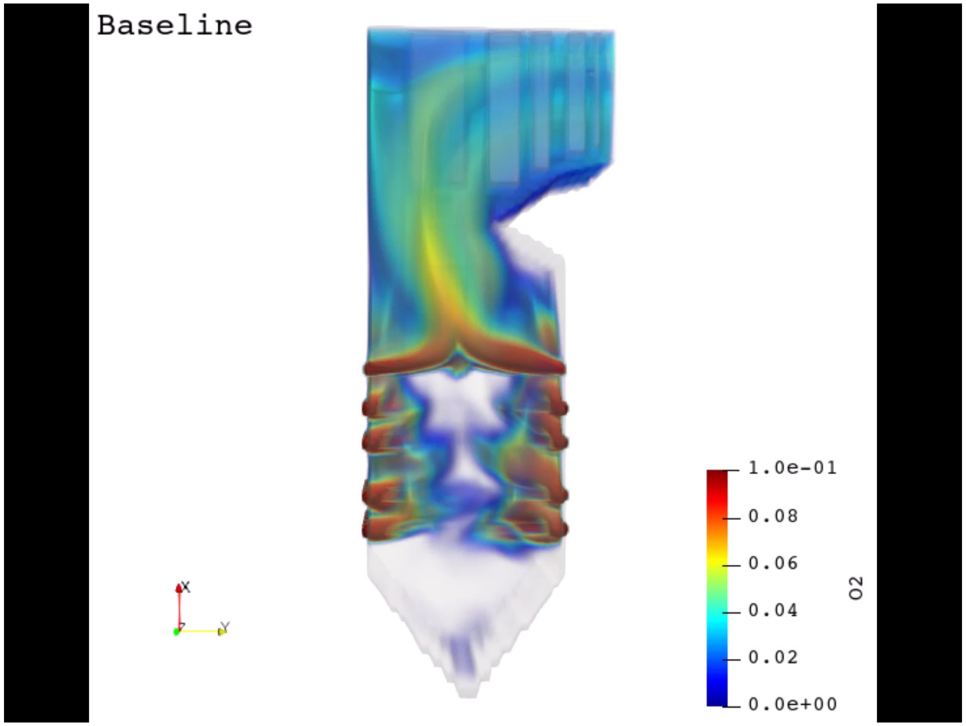

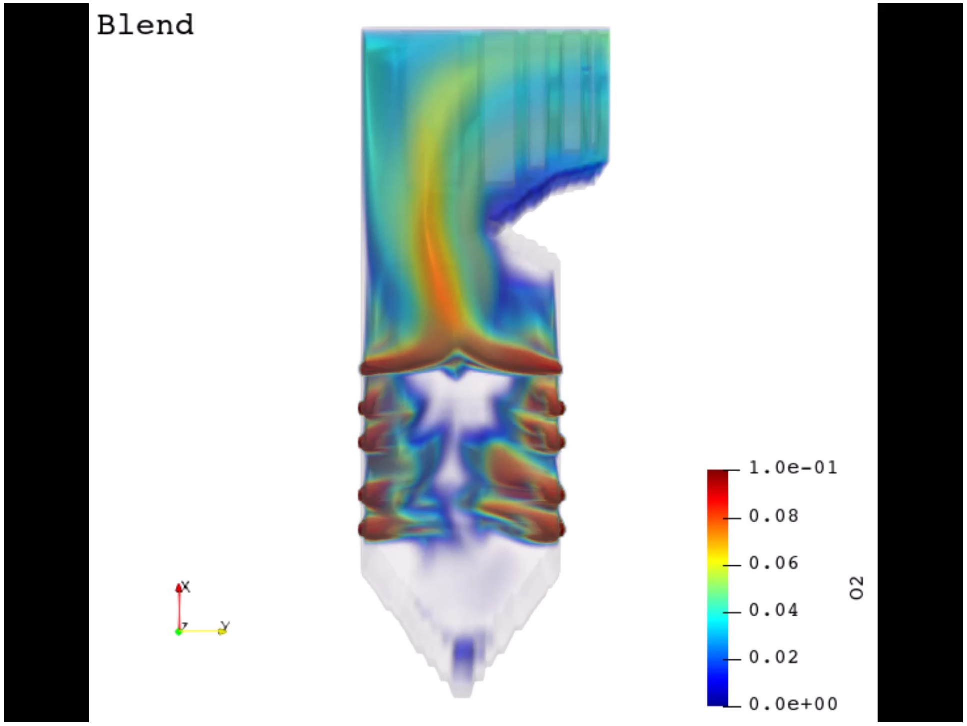

CO Distribution

3D Volumetric Rendering

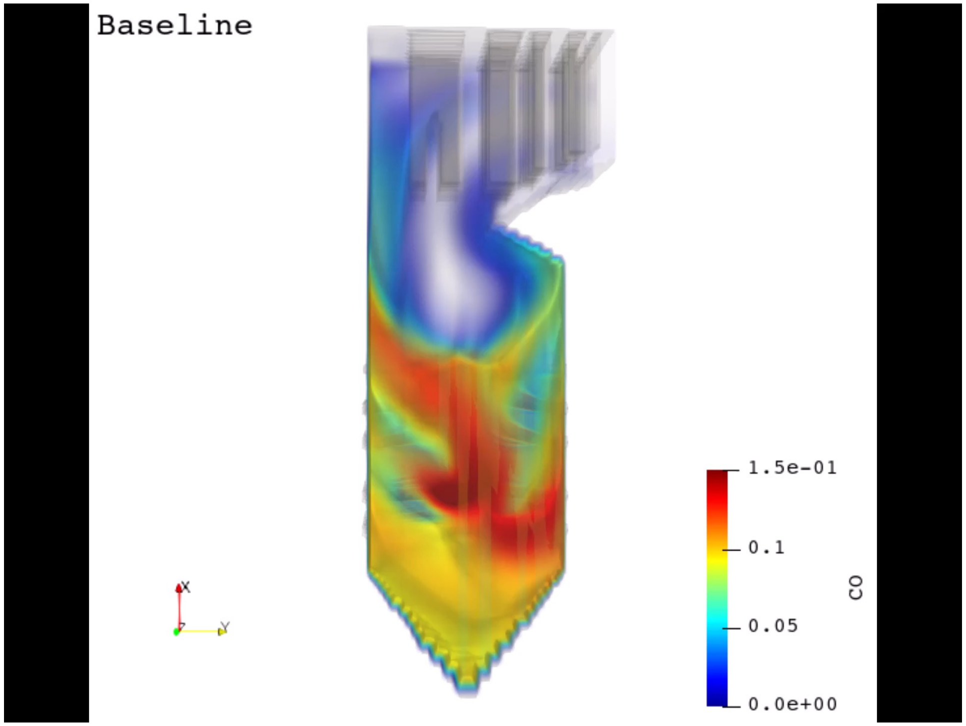

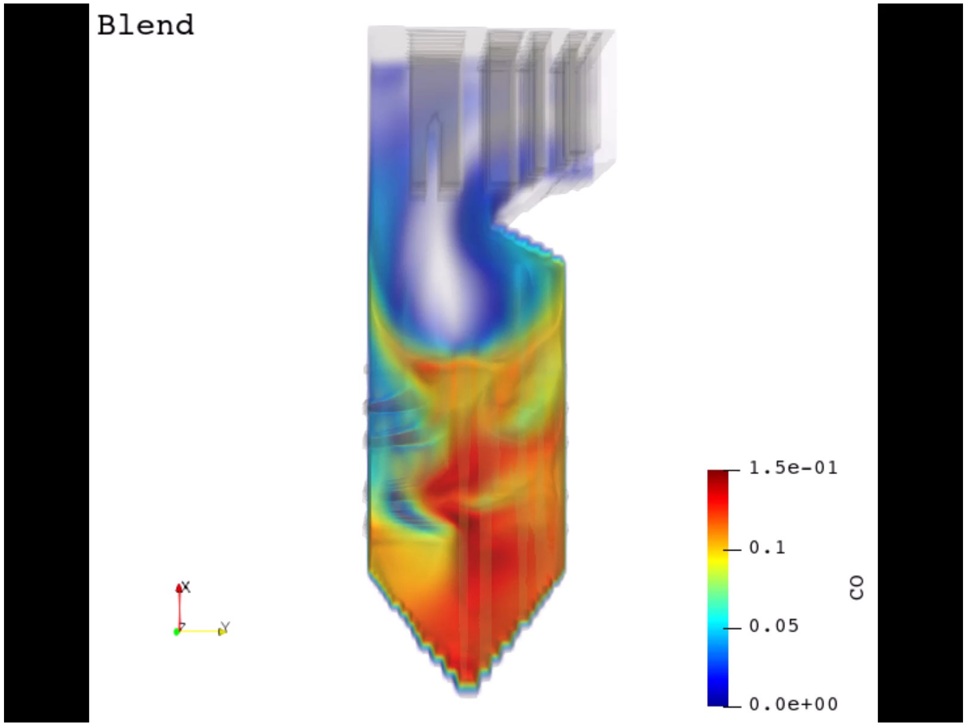

Particles: Baseline

LOI Contribution

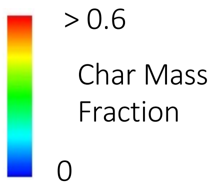

3.0%	20.6%	41.9%	34.5%

Overall LOI	2.9%

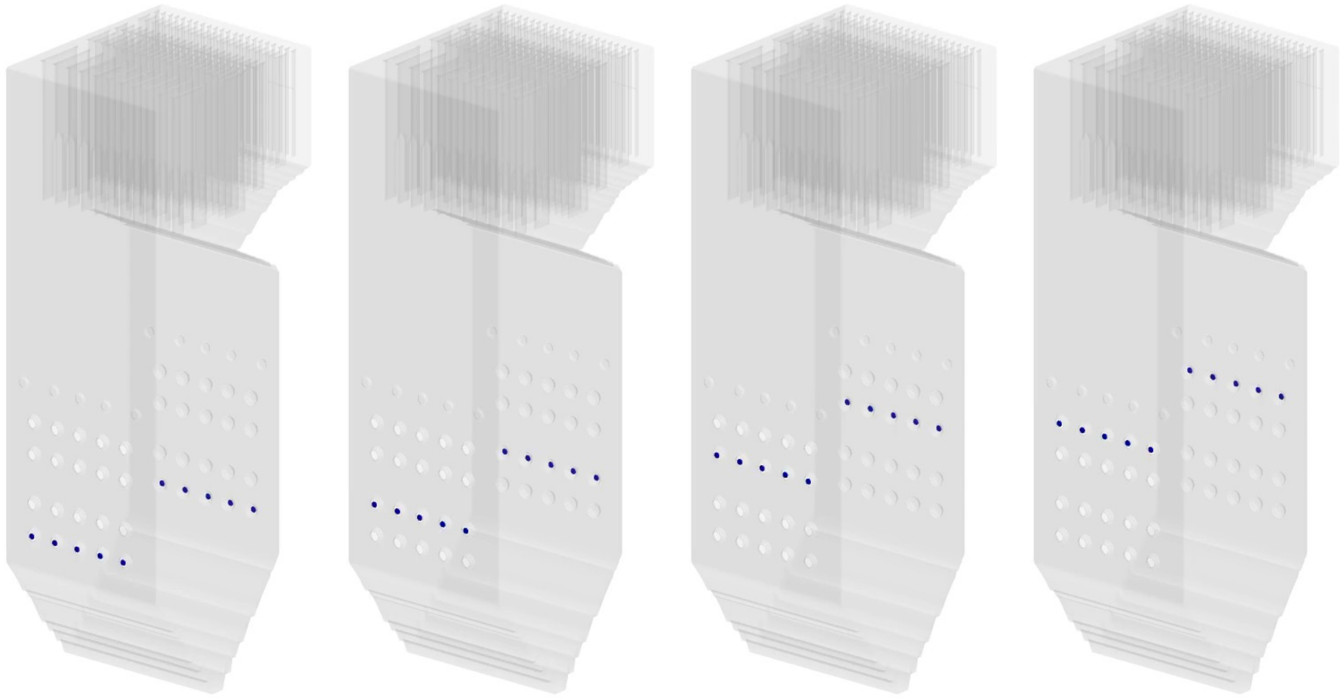

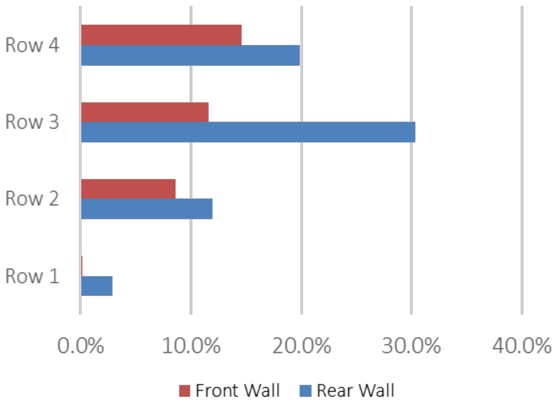

Particles: Blend

LOI Contribution

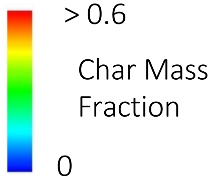

1.3%	33.9%	35.2%	29.6%

Overall LOI	3.2%

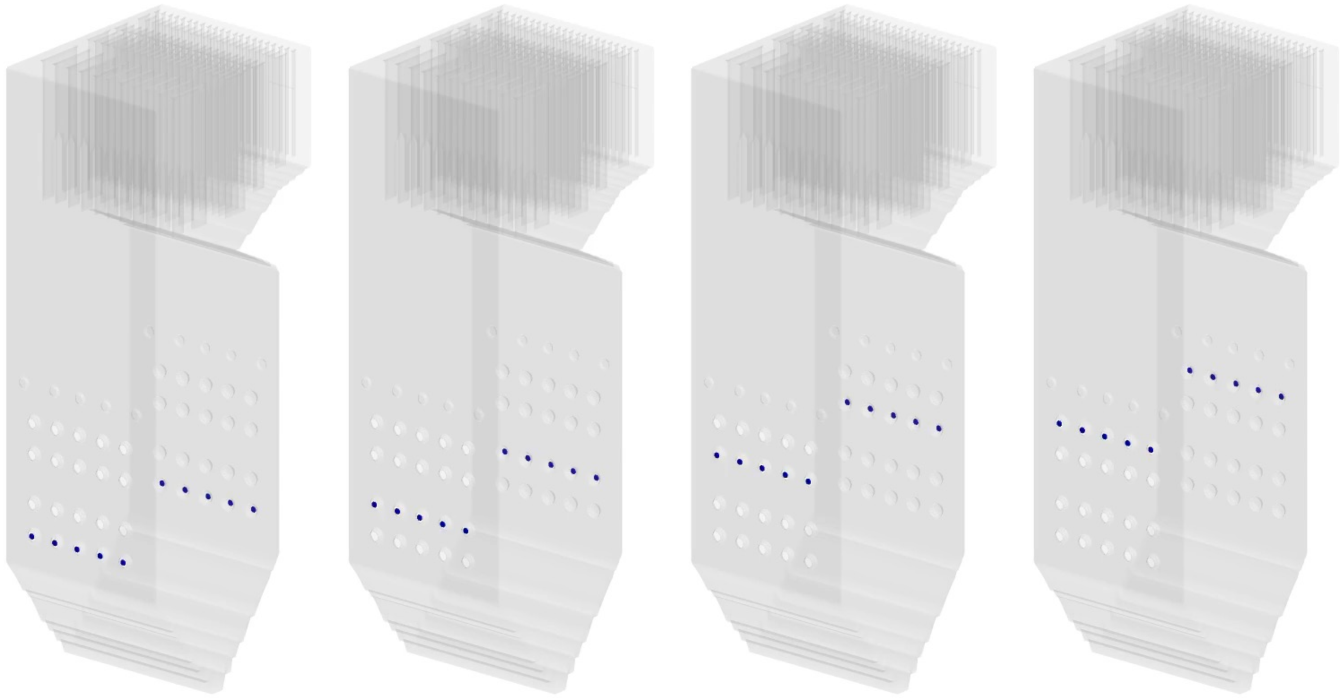

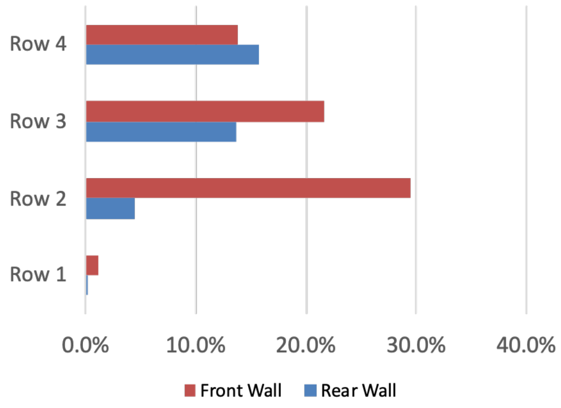

NOx Concentration and Rates

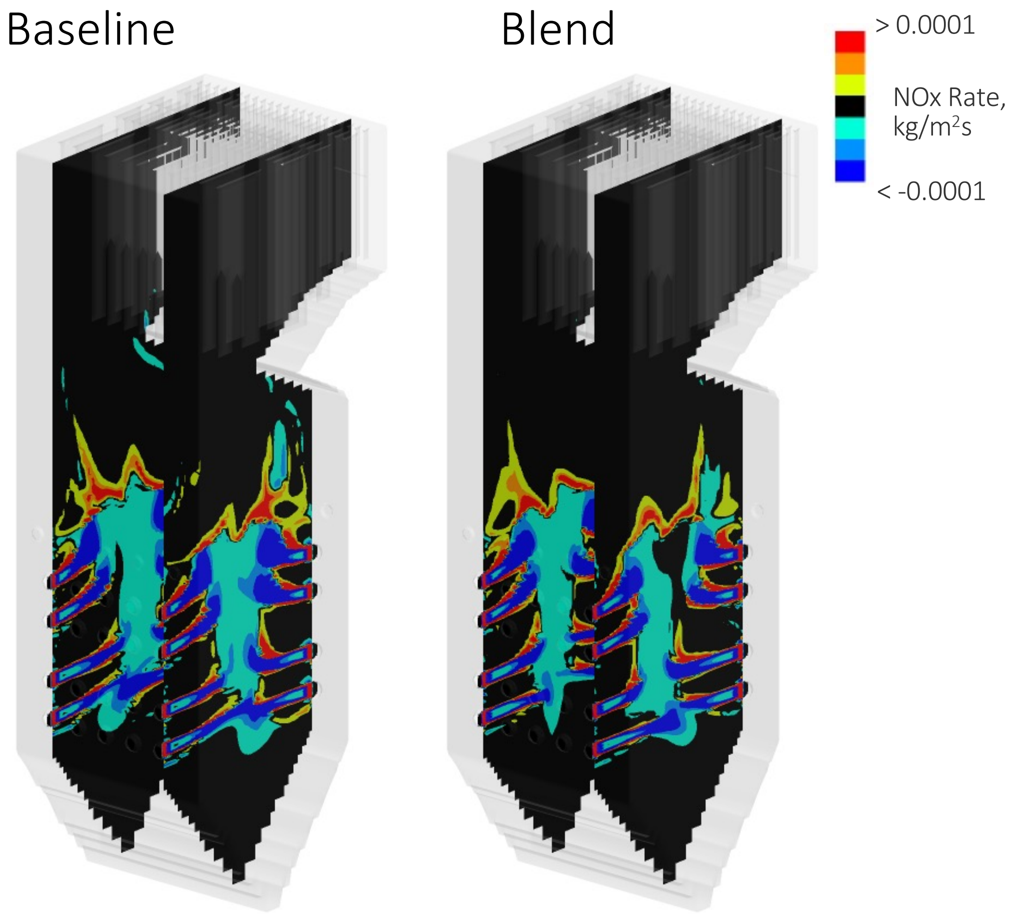
Baseline

Blend

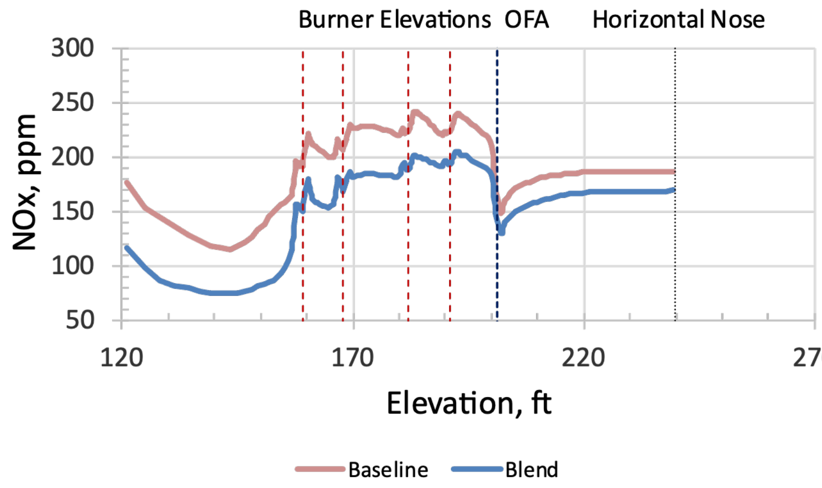

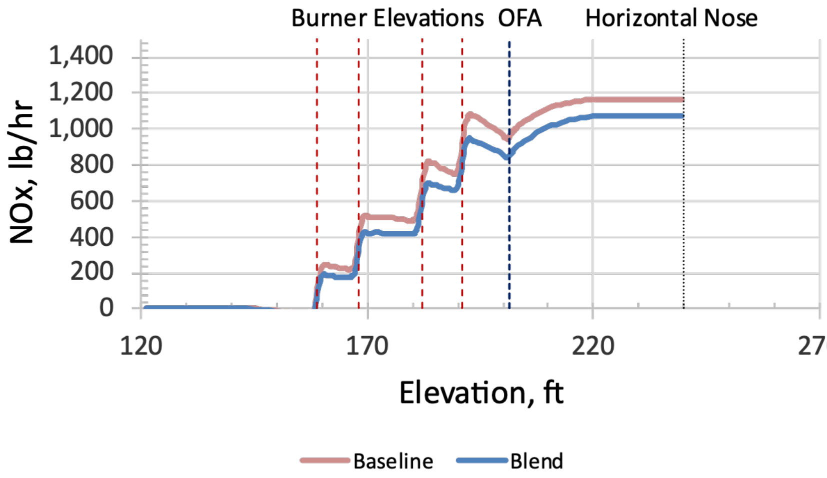

NOx Comparison

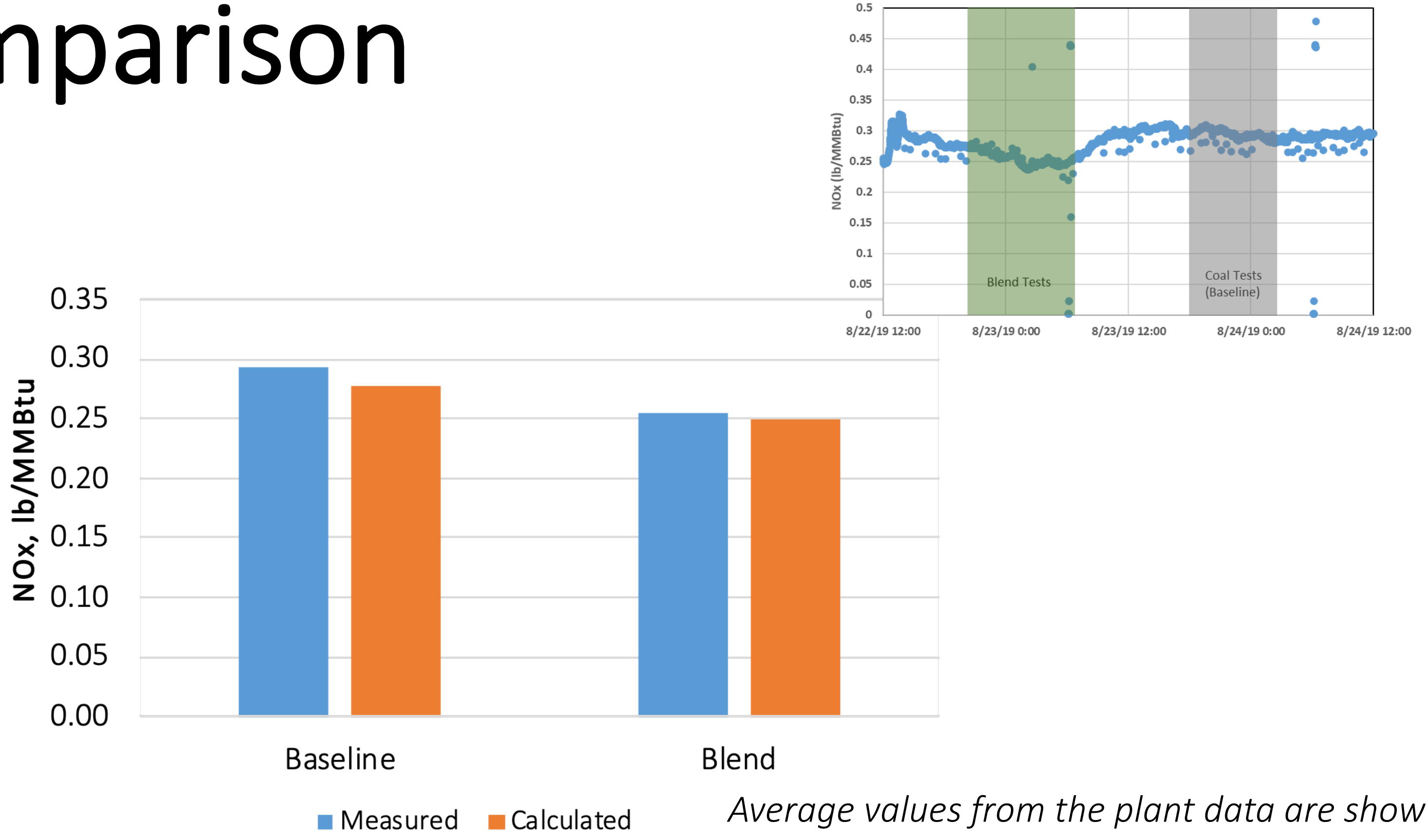

Average values from the plant data are shown

O_2 & CO Comparisons

Baseline

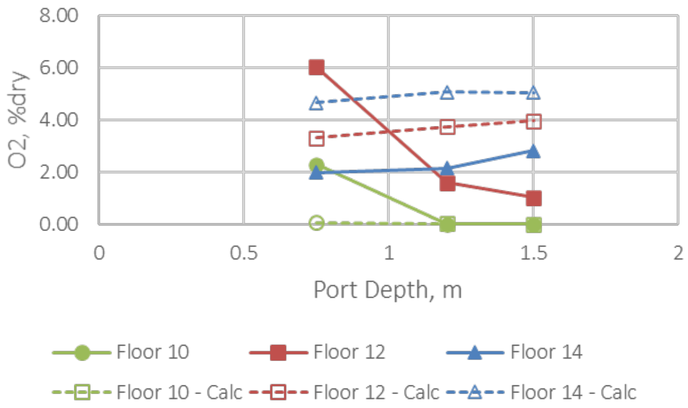

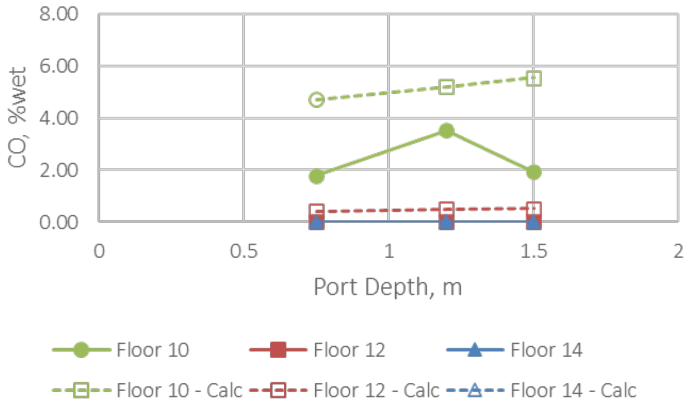

Blend

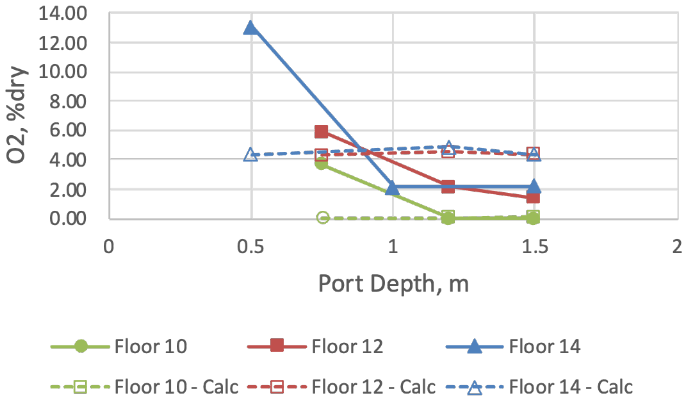

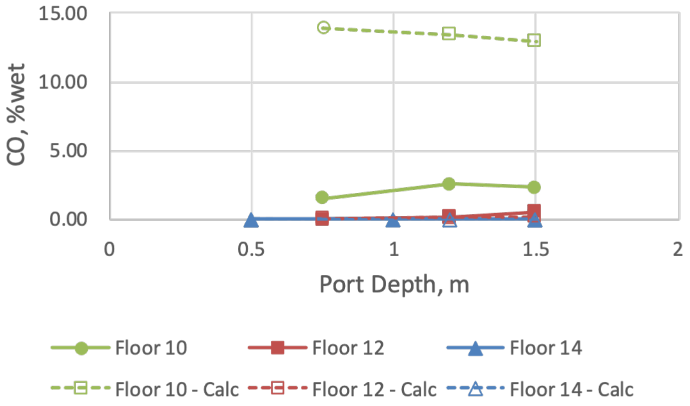

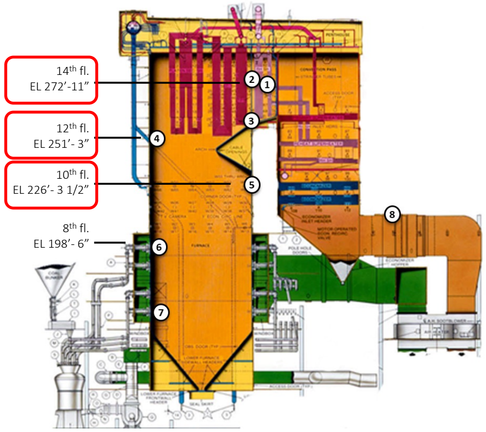

NOx and SO_2 Comparisons

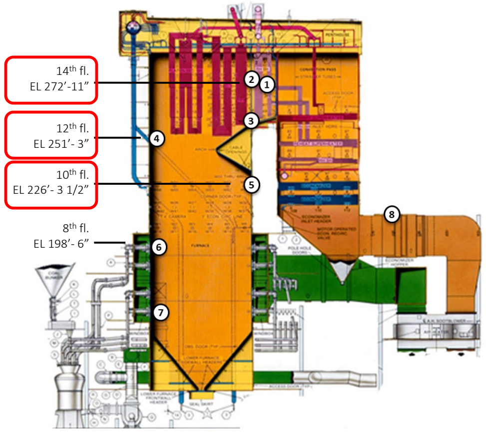

Baseline

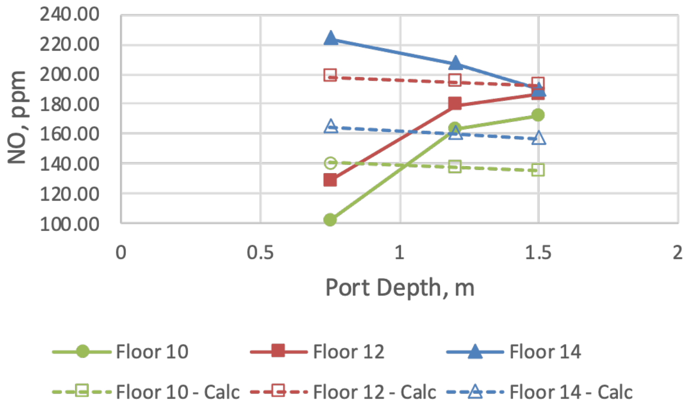

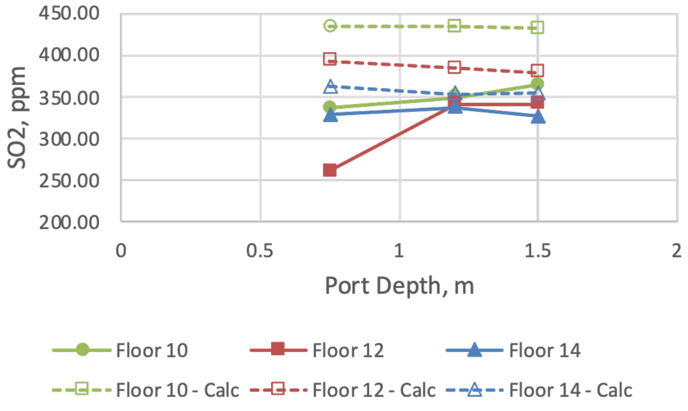

Blend

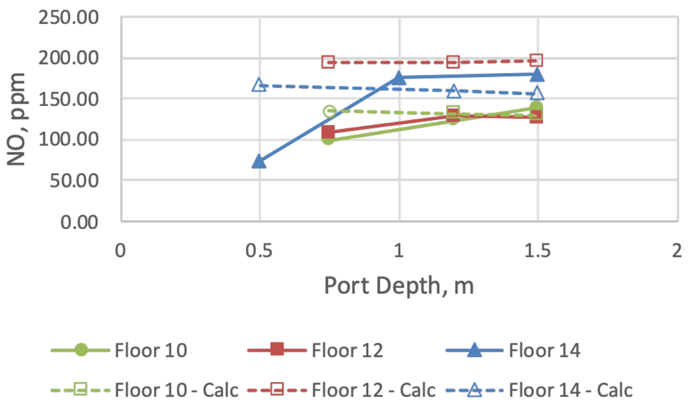

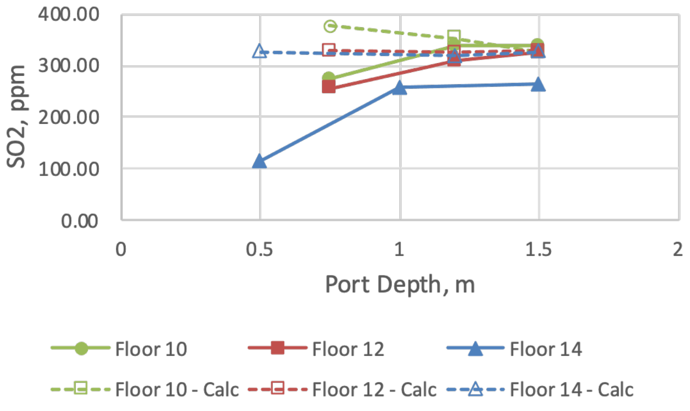

Gas Temperature

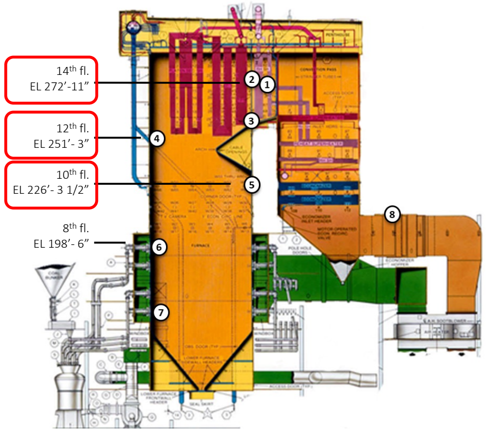

Baseline

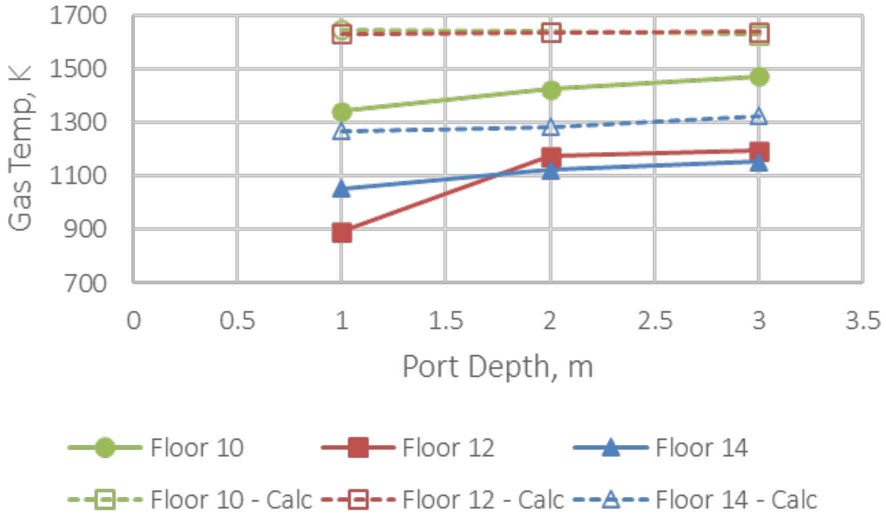

Blend

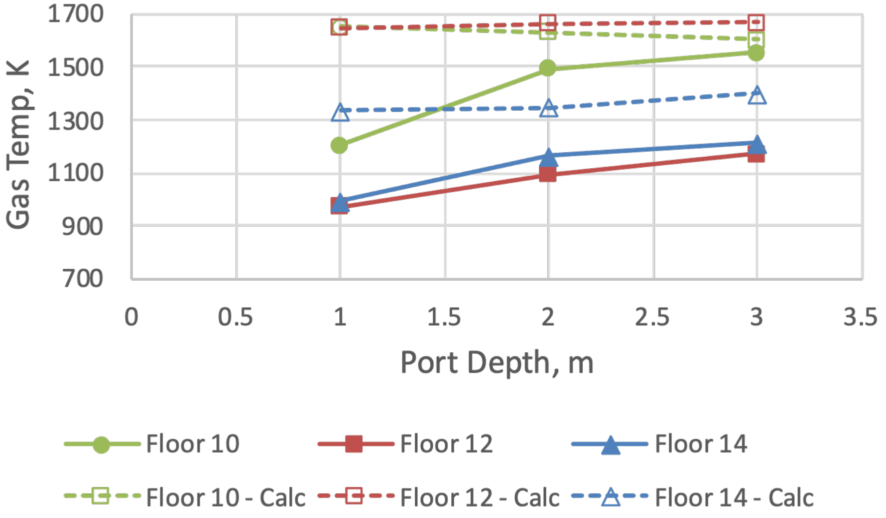

Deposition Flux

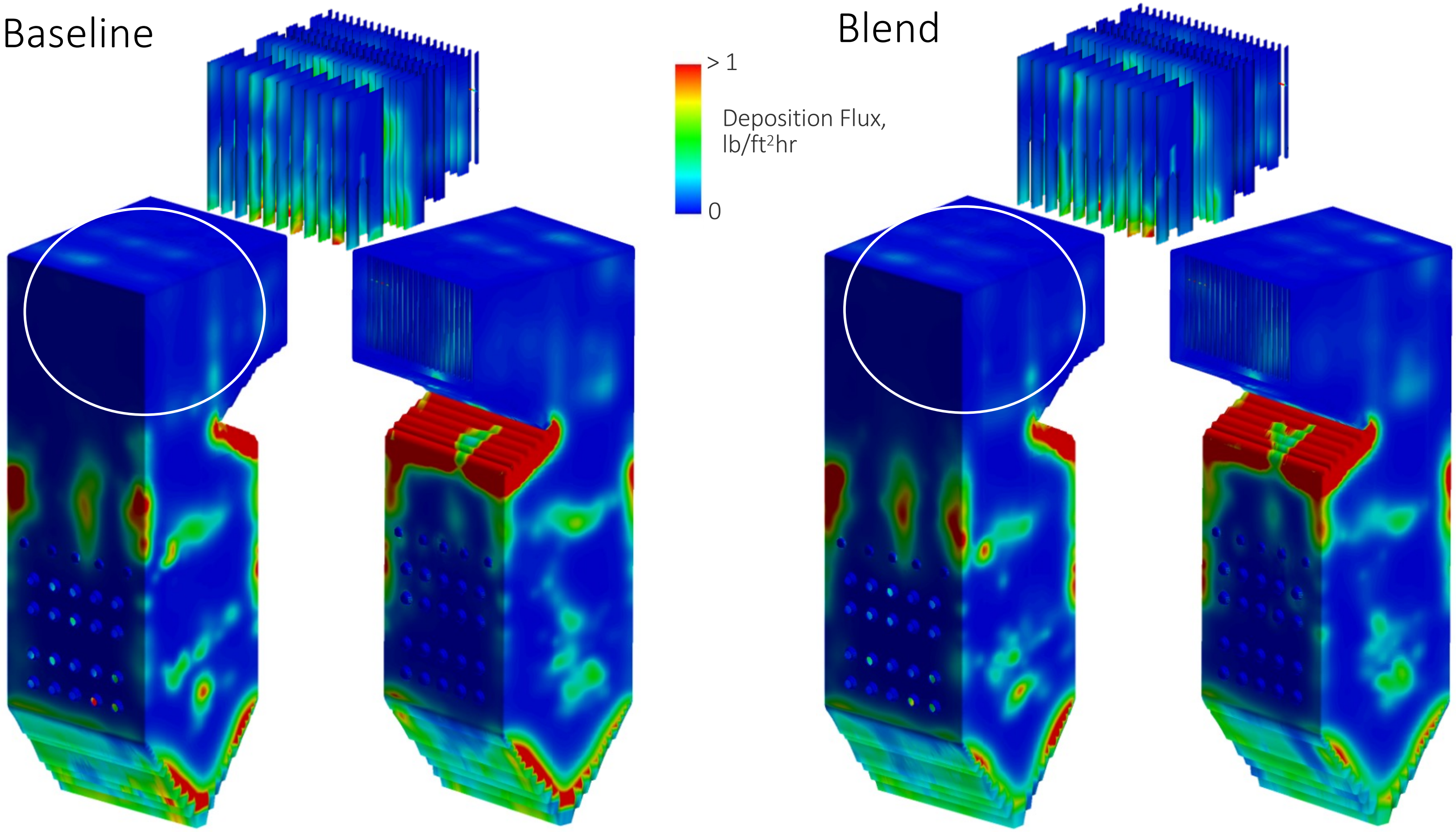

Deposition Rates by Zones

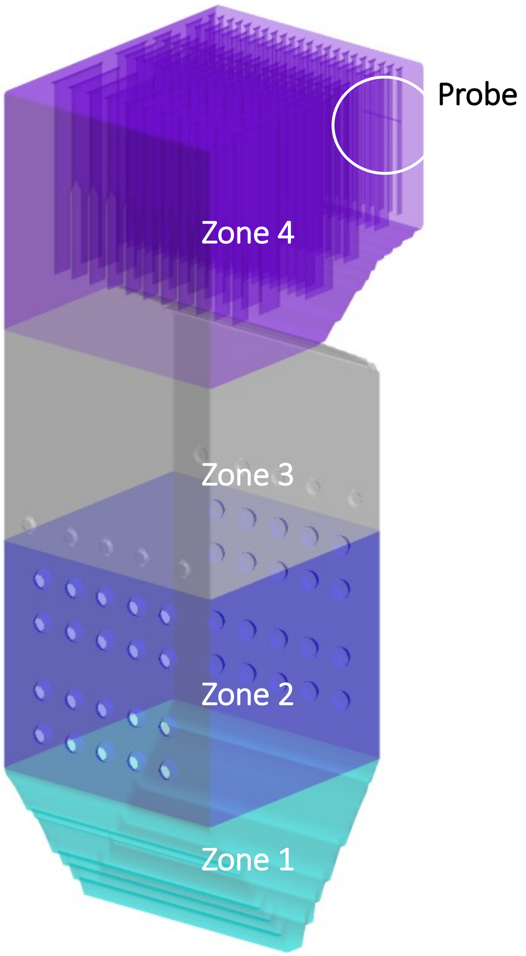

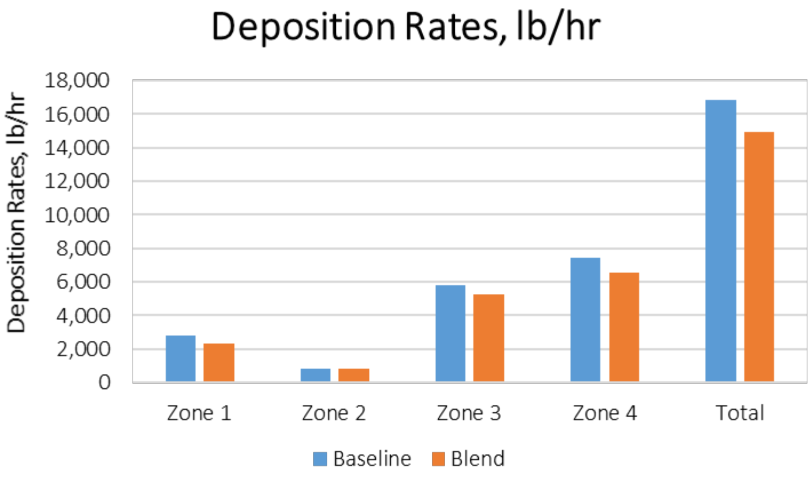

Total: 89% of Baseline

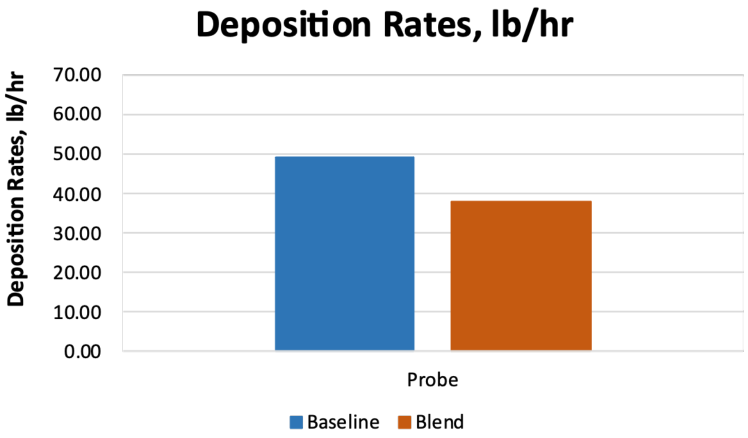

Probe: 77% of Baseline

Summary

- Coal and biomass co-firing cases are simulated for the furnaces with three different scales
- OFC 27 kWth
  - Predicted temperature profile show similar trends to the measurements
  - High burn out with low exit CO calculated consistent with the measurements
  - Lower capture efficiency is calculated for the co-firing case based on the measured deposition rates and predicted ash impaction rates
- L1500 1,025 kWth
  - Gas species calculation shows relatively good agreement with the measurements, but with some discrepancies that need to be further analyzed
  - Calculated radiant flux shows similar pattern to one set of the measurements, but lower values for the blend
- Hunter 3 1,200 MWth
  - Generally, the exit results show good agreement with the plant experiences
  - Predicted local gas compositions compare well with the measurements, but the comparison is sensitive to local fluid dynamics and flow stratification
  - Overall predicted deposition in the furnace reduces to 89% of the baseline (77% on the probe)
- CFD modeling results compare well with the measurements and can be used to analyze the testing data: further analysis is in progress

Acknowledgement

- PacifiCorp for financial support